MOLECULAR PHYSICS

VOLUME 2

1959

Printed and Published by
TAYLOR & FRANCIS LTD
RED LION COURT, FLEET STREET, LONDON, E.C.4

CONTENTS OF VOLUME 2

NUMBER 1—JANUARY 1959

Page

Zur Theorie der generalisierten Gesamtheiten. A. Münster 1

Pressure-dependent partition functions. R. A. Sack 8

On Mayer's ionic solution theory. H. L. Friedman 23

Rotational effect on the thermodynamic properties of isotopes. Agnessa Babloyantz 39

The structure of shock fronts in various gases. W. H. Andersen and D. F. Hornig 49

Relationship between proton shielding constants and electric dipole moments in the hydrogen halides. H. F. Hameka 64

Chemical shifts of thallium resonance spectra in solutions of thallous salts. R. Freeman, R. P. H. Gasser, R. E. Richards and D. H. Wheeler 75

Correlations between the electronic spectra of alternant hydrocarbon molecules and their mono- and di-valent ions. I. Benzene, coronene and triphenylene. G. J. Hoijtink 85

Absorption spectra of actinide compounds. C. K. Jørgensen 96

NUMBER 2—APRIL 1959

The colours of transition metal hexafluorides. W. Moffitt, G. L. Goodman, M. Fred and B. Weinstock 109

Intensities in inorganic complexes. III. Octahedral complexes of Ni(II) and V(III). C. J. Ballhausen and Andrew D. Liehr 123

Theory of anisotropic hyperfine interactions in π-electron radicals. Harden M. McConnell and John Strathdee 129

The electronic structure of hydrogen fluoride. R. A. Ballinger .. 139

Molecular-orbital treatment of a new type of heteroaromatic compound. R. D. Brown and B. A. W. Coller 158

Statistical mechanics of solid and liquid mixtures of ortho- and parahydrogen. A. Bellemans and Agnessa Babloyantz 169

Page

On the motion of a particle coupled to lattice vibrations. THOR A. BAK, M. GOCHE and F. HENIN 181

The singularities of the integrals in Mayer's ionic solution theory. HAROLD L. FRIEDMAN 190

Calculation of vibrational relaxation times in gaseous cyanogen. P. G. DICKENS 206

Thermodynamic properties of clathrates. I. The heat capacity and entropy of argon in the argon quinol clathrates. N. G. PARSONAGE and L. A. K. STAVELEY 212

RESEARCH NOTES

The signs of the valence bond wave functions in an alternant hydrocarbon. A. D. MCLACHLAN 223

A self-consistent field for the H_2 molecule. G. BERTHIER 225

Proton acceptor properties of lycopene. ALBERT WASSERMANN .. 226

NUMBER 3—JULY 1959

Long-range interaction of two ls-hydrogen atoms expressed in terms of natural spin-orbitals. J. O. HIRSCHFELDER and P. O. LÖWDIN .. 229

Efficiencies of third bodies in the reaction $H+O_2+M=HO_2+M$. P. G. DICKENS and J. W. LINNETT 259

Diffusion coefficients of gases from the rate of approach to the steady state in thermal diffusion. S. C. SAXENA and E. A. MASON 264

The pairing of electronic states in alternant hydrocarbons. A. D. MCLACHLAN 271

The electron spin resonance spectrum of a γ-irradiated single crystal of glycine. D. K. GHOSH and D. H. WHIFFEN 285

Thallium nuclear resonance spectra, Part II. R. FREEMAN, R. P. H. GASSER and R. E. RICHARDS 301

Electron transfer spectra of hexahalide complexes. C. K. JØRGENSEN 309

NUMBER 4—OCTOBER 1959

Paramagnetic resonance in phosphorescent aromatic hydrocarbons. I: Naphthalene. J. H. VAN DER WAALS and M. S. DE GROOT .. 333

Electron resonance studies on the kinetics of free radical formation and reaction in the solid phase. M. FUJIMOTO and D. J. E. INGRAM .. 341

Page

Nuclear resonance spectrum of ortho bromoaniline. S. CLOUGH .. 349

Ion-pair formation in thallous solutions: III. R. P. H. GASSER and R. E. RICHARDS 357

The Jahn–Teller effect in manganic acetylacetonate. A. FORMAN and L. E. ORGEL 362

A determination of the electronegativity parameter in molecular orbital calculations on heteronuclear molecules containing nitrogen. ALF LOFTHUS 367

Application of the principle of corresponding states to the viscosity and diffusion of pure liquids and mixtures. G. THOMAES and J. VAN ITTERBEEK 372

Thermal diffusion and the approach to the steady state in gases: II. S. C. SAXENA and E. A. MASON 379

Steric forces in halogen-substituted benzenes. C. A. COULSON and D. STOCKER 397

An analysis of the fluorescence spectrum of europium ethyl sulphate. B. R. JUDD 407

Environmental perturbations on foreign atoms and molecules in solid argon, krypton and xenon. MACLYN MCCARTY, Jr. and G. WILSE ROBINSON 415

RESEARCH NOTE

Photo-ionization of aromatic hydrocarbons in boric acid glasses. P. BENNEMA, G. J. HOIJTINK, J. H. LUPINSKI, L. J. OOSTERHOFF, P. SELIER and J. D. W. VAN VOORST 431

ERRATA

The singularities of the integrals in Mayer's ionic solution theory. HAROLD L. FRIEDMAN 436

Index of Authors (with the Titles of Papers) 437

Zur Theorie der generalisierten Gesamtheiten

von A. MÜNSTER
Physikalisch-chemisches Institut der Universität Frankfurt/Main

(*Received* 28 *October* 1958)

Es wird gezeigt, dass der Dichte-Operator einer generalisierten Gesamtheit gewisse Bedingungen erfüllen muss, wenn sie die Gleichungen der Thermodynamik und korrekte Schwankungsgleichungen ergeben soll. Die von Byers Brown vorgeschlagene Druckgesamtheit erfüllt die Bedingungen für die Gültigkeit der Thermodynamik, führt aber auf unrichtige Schwankungsgleichungen. Insbesondere ergibt sich eine falsche Formel für die Lichtstreuung eines Einkomponentensystems. Dies beruht darauf, dass in der Gesamtheit von Byers Brown die Schwankungen von vornherein teilweise unterdrückt werden.

1. EINLEITUNG

Die von Gibbs [1] untersuchten statistischen Gesamtheiten, die mikrokanonische, die kanonische und die grosse kanonische Gesamtheit, sind bekanntlich den Massieu–Planck'schen Funktionen S, $-F/T$, PV/T zugeordnet durch die allgemeine Formel

$$\phi_k = k \ln \Xi_k \tag{1}$$

wo Ξ_k die Verteilungsfunktion der betreffenden Gesamtheit und k die Boltzmann'sche Konstante ist. Da thermodynamisch

$$\phi_k = S - \sum_{i=1}^{k} X_i P_i \tag{2}$$

ist, wo X_i extensive und P_i die konjugierten intensiven Parameter sind, liegt der Gedanke nahe, die Definition (1) auf alle Funktionen des Satzes (2) auszudehnen und damit zu jeder Massieu–Planck'schen Funktion eine statistische Gesamtheit zu konstruieren. Dieser Gedanke ist zuerst von Guggenheim [2] und in neuerer Zeit ausführlicher von Hill [3] formuliert worden. Münster [4, 5] hat als axiomatischen Ausgangspunkt den Satz gewählt, dass die Messung eines intensiven Parameters P_i notwendig den konjugierten extensiven Parameter X_i unscharf macht und dass (im Falle der halbklassischen Näherung) das System dann durch die Laplace-Transformierte der ursprünglichen Verteilungsfunktion beschrieben wird. Für ein unendlich grosses System geht dieselbe in die Legendre-Transformation der thermodynamischen Potentiale über.

Zwischen den genannten Formulierungen bestehen keine grundsätzlichen Unterschiede†. In einer kürzlich an dieser Stelle erschienenen Arbeit hat jedoch Byers Brown [6] eine Theorie der 'Druckgesamtheiten' (d.h. der Gesamtheiten, in denen P als unabhängige Variable auftritt) entwickelt, deren Grundkonzept zu allen früheren Arbeiten in prinzipiellem Widerspruch steht. Im Folgenden sollen daher die wesentlichen Punkte dieser Theorie genauer untersucht werden. Zur Vereinfachung der Diskussion beginnen wir mit einigen allgemeinen Betrachtungen.

---

† Wir sehen hier ab von der Frage der T, P, μ-Gesamtheit, die wir in diesem Zusammenhang nicht diskutieren.

2. ALLGEMEINES ÜBER GENERALISIERTE VERTEILUNGSFUNKTIONEN

Die Einführung der generalisierten Gesamtheiten kann rein formal auf zwei Wegen erfolgen: Durch Betrachtung von Teilsystemen eines abgeschlossenen Gesamtsystems, das durch eine mikrokanonische Gesamtheit abgebildet wird [3] oder durch Ableitung aus gewissen Axiomen [4, 5]. Obwohl die Ergebnisse beider Methoden schon aus Konsistenzgründen übereinstimmen müssen, betrachten wir hier lediglich die zweite, die auch von Byers Brown [6] benutzt wird. Bezeichnen wir mit $\mathbf{H} \equiv \mathbf{X}_1$ den Hamilton-Operator des Systems, so ist

$$\mathbf{H} = \mathbf{H}(X_2, \ldots, X_r) \tag{3}$$

wo die X_i die Molekülzahlen und äusseren Parameter bezeichnen. Die generalisierten Kräfte werden dann durch die Operatoren

$$\mathbf{P}_i = -\frac{\partial \mathbf{H}}{\partial X_i} \tag{4}$$

dargestellt. Wenn beim Übergang zu einer generalisierten Gesamtheit der entsprechende intensive Parameter vorgegeben ist, muss im Dichteoperator ein Eigenwert des Operators (4) auftreten, während der entsprechende extensive Parameter jetzt als Operator erscheint. Der Dichteoperator habe die Form

$$\boldsymbol{\rho}_k = \exp\left[-\phi_k - P_1\mathbf{H} - \sum_{i=2}^{k} P_i \mathbf{X}_i\right]^{\dagger} \tag{5}$$

und es sei

$$\bar{X}_i = \operatorname{spur}(\boldsymbol{\rho}_k \mathbf{X}_i) \quad (i = 1 \text{ bis } k), \tag{6}$$

$$\bar{P}_j = \operatorname{spur}(\boldsymbol{\rho}_k \mathbf{P}_j) \quad (j = k+1 \text{ bis } r). \tag{7}$$

Wenn ρ_k eine Gesamtheit im Sinne der Gl. (1) darstellen soll, müssen offenbar folgende Bedingungen erfüllt sein:

(*a*) Alle in (5) auftretenden Operatoren müssen miteinander vertauschbar und es muss

$$\operatorname{spur} \boldsymbol{\rho}_k = 1 \tag{8}$$

sein.

(*b*) ϕ_k muss der Gleichung

$$d\phi_k = -\sum_{i=1}^{k} \bar{X}_i \, dP_i + \sum_{l=k+1}^{r} \bar{P}_l \, dX_l \tag{9}$$

genügen.

(*c*) Es seien X_{im} die Eigenwerte des Operators $\mathbf{X}_i$ und es sei

$$X_{im} - \bar{X}_i = \delta X_i, \quad \frac{\delta X_i}{\bar{X}_i} = \xi_i. \tag{10, 11}$$

Dann dürfen die Korrelationsmomente $\overline{\xi_i \xi_j}$ nur von den Analoga thermodynamischer Grössen abhängen.

---

† Der Einfachheit halber schreiben wir in den allgemeinen Formeln die Boltzmann-Konstante nicht explizit an. Wir verzichten hier auf eine Begründung dieser Formulierung ebenso wie auf die Erörterung der Frage, ob die Ausdehnung des Operator-Formalismus auf die generalisierten Gesamtheiten überhaupt notwendig oder zweckmässig ist.

(a) und (b) bedürfen keiner Erläuterung. (c) ist notwendig, weil nur unter dieser Voraussetzung die thermodynamischen Stabilitätsbedingungen statistisch zu begründen sind [4, 5] und die beobachtbaren Schwankungen (Lichtstreuung) durch die thermodynamischen Zustandsgrössen bestimmt werden.

Wir wollen nun zeigen, dass die notwendige und hinreichende Bedingung für (b) ist

$$\left.\begin{array}{ccc} \dfrac{\partial E_n}{\partial X_{im}} = -\dfrac{P_i}{P_1}(\alpha) & \text{oder} & \dfrac{\partial X_{im}}{\partial P_i} = 0(\beta) \\ (i=2 \text{ bis } k) & & (i=1 \text{ bis } k) \end{array}\right\} \tag{12}$$

die notwendige und hinreichende Bedingung für (c)

$$\frac{\partial X_{im}}{\partial P_i} = 0. \tag{13}$$

Wir wählen eine Darstellung, die ρ_k auf Diagonalform bringt und setzen der Einfachheit halber $k=2$. Dann wird

$$\exp(\phi_2) = \sum_m \sum_n \exp(-P_1 E_n - P_2 X_{2m}). \tag{14}$$

Daraus folgt mit

$$F_{nm} = P_1 E_n + P_2 X_{2m}, \tag{15}$$

$$d\phi_2 = -\bar{E}\,dP_1 - \overline{\frac{\partial F_{nm}}{\partial P_2}}\,dP_2 + \sum_{l=3}^{r} \bar{P}_l\,dX_l. \tag{16}$$

Wenn eine der Bedingungen (12) erfüllt ist, und nur dann, geht Gl. (16) in Gl. (9) über.

Differentiation von (14) nach P_2 ergibt

$$\sum_m \sum_n \left(-\frac{\partial \phi_2}{\partial P_2} - \frac{\partial F_{nm}}{\partial P_2}\right) \exp(-\phi_2 - P_1 E_n - P_2 X_{2m}) = 0. \tag{17}$$

Ist (12) erfüllt; so wird daraus

$$\bar{X}_2 = -\frac{\partial \phi_2}{\partial P_2}. \tag{18}$$

Nochmalige Differentiation von (17) nach P_2 ergibt

$$\sum_m \sum_n \left[-\frac{\partial^2 \phi_2}{\partial P_2^2} - \frac{\partial^2 F_{nm}}{\partial P_2^2} + \left(\frac{\partial \phi_2}{\partial P_2}\right)^2 + 2\frac{\partial \phi_2}{\partial P_2}\frac{\partial F_{nm}}{\partial P_2} + \left(\frac{\partial F_{nm}}{\partial P_2}\right)^2\right] \times \exp(-\phi_2 - P_1 E_n - P_2 X_{2m}) = 0. \tag{19}$$

Ist die Voraussetzung (12α) erfüllt; so folgt aus (19)

$$\overline{\xi_2^{\,2}} = -\bar{X}_2^{\,-2}\left[\frac{\partial \bar{X}_2}{\partial P_2} - \overline{\frac{\partial X_{2m}}{\partial P_2}}\right] \tag{20}$$

während aus (13) sich ergibt

$$\overline{\xi_2^{\,2}} = -\bar{X}_2^{\,-2}\frac{\partial \bar{X}_2}{\partial P_2}. \tag{21}$$

Da der zweite Term der rechten Seite von (20) kein thermodynamisches Analogon hat, ist damit die Behauptung bewiesen.

3. DAS GRUNDKONZEPT DER THEORIE VON BYERS BROWN

Die Theorie von Byers Brown [6] beruht auf dem Grundgedanken, dass jedes System der Gesamtheit sich im mechanischen Gleichgewicht mit seiner

Umgebung bei dem für alle Systeme gleichen Druck P befindet. Durch Vorgabe des Druckes wird dann jedem Eigenwert des Hamilton-Operators ein 'Eigenvolumen' V_n zugeordnet als Lösung der Gleichung

$$P = -\frac{dE_n}{dV_n}. \tag{22}$$

Für das ideale Gas der quantisierten Maxwell–Boltzmann-Statistik in einem kubischen Behälter wird

$$V_n = \left(\frac{h^2 n^2}{12mP}\right)^{3/5} \tag{23}$$

mit

$$n^2 = \sum_{i=1}^{3N} n_i^2. \tag{24}$$

Er ist dann

$$\exp\left(-\frac{G}{kT}\right) = \sum_n \exp\left(-\frac{H_n(P)}{kT}\right) \tag{25}$$

mit

$$H_n(P) = E_n[V_n(P)] + PV_n(P). \tag{26}$$

Dieses Konzept steht zunächst in Widerspruch zu dem Ergebnis, das man durch Betrachtung eines Teilsystems, welches mit dem 'Reservoir' Energie und Volumen austauschen kann, ableitet [3]. Der Druck (bzw. die Grösse P/kT) wird hier als Modul der Verteilung der Volumina (etwa mittels der Methode der unbestimmten Multiplikatoren) definiert. Der Einzelwert des Volumens muss daher notwendig von P unabhängig sein.

Man sieht weiter aus Gl. (22) und (23), dass hier

$$\frac{dV_n}{dP} \neq 0 \tag{27}$$

ist und somit zwar die Bedingung (12α), aber nicht (13) erfüllt ist. Der Formalismus von Byers Brown ergibt daher, wie am Beispiel des idealen Gases gezeigt wird, korrekte thermodynamische Funktionen, führt aber auf unrichtige Schwankungsgleichungen. Wir wollen dies noch etwas näher ausführen.

4. Lichtstreuung eines Einkomponentensystems

Die Lichtstreuung eines Einkomponentensystems ist bekanntlich in hinreichender Entfernung vom kritischen Punkt gegeben durch die Gleichhung

$$\tau = \frac{32\pi n^2}{3\lambda^4} V\overline{(\delta n)^2} \tag{28}$$

wo τ die sogenannte Trübung (turbidity), λ die Wellenlänge, n der Brechungsindex und $\overline{(\delta n)^2}$ dessen mittleres Schwankungsquadrat ist. V ist ein Volumen, dessen Lineardimension klein gegen die Lichtwellenlänge ist, das aber genügend Moleküle enthält, um die Schwankungstheorie anwenden zu können. Halten wir die Molekülzahl fest und betrachten die Schwankungen des Volumens bei konstantem Druck, so wird

$$\overline{(\delta n)^2} = \left(\rho\frac{\partial n}{\partial \rho}\right)^2 \bar{V}^{-2}\overline{(\delta V)^2}. \tag{29}$$

Aus Gl. (20) folgt, in Übereinstimmung mit Byers Brown [6],

$$\overline{(\delta V)^2} = kT\left(\bar{V}\kappa - \overline{\frac{\partial V_n}{\partial P}}\right) \tag{30}$$

wo κ die isotherme Kompressibilität ist. Es wird somit

$$\tau = \frac{32\pi n^2}{3\lambda^4}\left(\rho\frac{\partial n}{\partial \rho}\right)^2 kT\left(\kappa - \frac{1}{\bar{V}}\overline{\frac{\partial V_n}{\partial P}}\right) \tag{31}$$

im Widerspruch zu der Einstein'schen Formel

$$\tau = \frac{32\pi n^2}{3\lambda^4}\left(\rho\frac{\partial n}{\partial \rho}\right)^2 kT\kappa \tag{32}$$

deren Korrektheit (für verschwindenden Depolarisationsgrad) neuerdings von Fixman [7] nach der Methode der molekularen Verteilungsfunktionen bestätigt worden ist.

5. Der thermische Ausdehnungskoeffizient

Der isobare thermische Ausdehnungskoeffizient γ wird von Byers Brown in Zusammenhang gebracht mit dem Korrelationsmoment des Volumens und der durch Gl. (26) definierten Enthalpie. Es soll gelten

$$\overline{\delta V \delta H} = kT^2 V\gamma. \tag{33}$$

Auch diese Formel ist unrichtig. Wählt man nämlich in (14) als unabhängige Variable T und P (statt $1/T$ und P/T), so erhält man

$$\overline{\delta V \delta \eta} = TV\gamma \tag{34}$$

wo

$$\eta = \frac{G - E_n - PV_m}{kT} \tag{35}$$

der Wahrscheinlichkeitsindex der Druck-Gesamtheit ist. Der isobare Ausdehnungskoeffizient hat somit statistisch nur eine ziemlich abstrakte Bedeutung. Wesentlich anschaulicher ist die bei Verwendung der Variablen $1/T$ und P/T sich ergebende Gleichung

$$\overline{\delta E \delta V} = kT^2\left(\frac{\partial \bar{V}}{\partial T}\right)_{P/T}. \tag{36}$$

6. Die Methode von Rosenfeld. Die halbklassische Näherung

Byers Brown [6] gibt noch eine zweite Methode zur Einführung der Druck-Gesamtheit an, die auf einer Idee von Rosenfeld beruht. Diese Methode ist völlig korrekt, und die daraus abgeleitete Gl. (10.3) bei Byers Brown ist mit unserer Gl. (14) identisch. Es ist nach den obigen Überlegungen klar, dass diese Methode nicht der in Ziffer 2 besprochenen, von Byers Brown stammenden, aequivalent sein kann, weil man in beiden Fällen verschiedene Schwankungsgleichungen erhält. Die formale Beziehung zwischen den Gl. (14) und (25) besteht, wie Byers Brown [6] gezeigt hat, darin, dass in (25) für jedes E_n nur der in Bezug auf V maximale Term beibehalten ist. Dieser ist durch die Gleichung

$$\left(\frac{dE_n}{dV} + P\right)\delta V = 0 \tag{37}$$

definiert, woraus unmittelbar Gl. (22) folgt. Dieser Zusammenhang bestätigt die Richtigkeit der vorhergehenden Analyse, denn die Beschränkung auf den maximalen Term bedeutet nichts anderes, als dass die Schwankungen ganz oder (wie hier) teilweise unterdrückt werden, während die thermodynamischen Zusammenhänge erhalten bleiben. Man übersieht dies leicht an einem einfachen Beispiel. Wir schreiben die Gl. (14)

$$\exp(\phi_2) = \sum_m \exp(-P_2 X_2 + \phi_1) \tag{38}$$

mit

$$\exp(\phi_1) = \sum_n \exp(-P_1 E_n). \tag{39}$$

Die Funktion ϕ_1 entwickeln wir in eine Taylor'sche Reihe nach X_2 an der Stelle $X_2 = \bar{X}_2$. Wir haben dann

$$\phi_1 = \phi_{01} + \left(\frac{\partial\phi_1}{\partial X_2}\right)_0 \delta X_2 + \frac{1}{2}\left(\frac{\partial^2\phi_1}{\partial X_2{}^2}\right)(\delta X_2)^2 + \dots. \tag{40}$$

Damit wird

$$\exp(\phi_2) = \exp(-P_2\bar{X}_2 + \phi_{01}) \sum_m \exp\left\{\left[\left(\frac{\partial\phi_1}{\partial X_2}\right)_0 - P_2\right] \times \delta X_2 + \frac{1}{2}\left(\frac{\partial^2\phi_1}{\partial X_2{}^2}\right)_0 (\delta X_2)^2 + \dots\right\}. \tag{41}$$

Nun ist

$$P_2 = \left(\frac{\partial\phi_1}{\partial X_2}\right)_0 + \tfrac{1}{2}\bar{X}_2{}^2\left(\frac{\partial\phi_1}{\partial X_2}\right)_0 \overline{\xi_2{}^2} + \dots. \tag{42}$$

Beschränken wir jetzt die Summierung in (41) auf den Term $X_2 = \bar{X}$, so wird

$$\overline{\xi_2{}^2} = 0, \tag{43}$$

$$\left(\frac{\partial\phi_1}{\partial X_2}\right)_0 = P_2, \tag{44}$$

und

$$\phi_2 = -P_2\bar{X}_2 + \phi_{01} \tag{45}$$

in Übereinstimmung mit der thermodynamischen Formel.

Für die halbklassische Näherung setzt Byers Brown [6]

$$\exp\left(-\frac{G}{kT}\right) = \frac{1}{h^n N!}\int\int \exp\left(-\frac{H_p}{kT}\right) d\mathbf{q}\, d\mathbf{p} \tag{46}$$

wo H_p, die 'Hamilton-Funktion für konstanten Druck' durch

$$H_p = H(\mathbf{q}, \mathbf{p}) + P\mathscr{V} \tag{47}$$

gegeben ist. Die 'extension function' $\mathscr{V}$ ist

$$\mathscr{V} = \omega \ln\left[\sum_{i=1}^{N} \exp(v_i/\omega)\right] - \omega \ln \frac{P\omega}{W} \tag{48}$$

wo ω und W positive Parameter sind. Dabei wird angenommen, dass eine trägheitslose Wand der Bewegung jedes Moleküls, das sie berührt, folgt. $v_i(\mathbf{q}_i)$ ist das so durch das i-te Molekül bestimmte Volumen. Für $\omega \to 0$ (unendlich steiles Wandpotential) reduziert sich (48) auf das maximale v_i und wird vom Druck unanhängig. Die aus (46) abgeleitete Gleichung für die Volumenschwankung hat daher die korrekte Form. Es erscheint aber wenig sinnvoll, ein solches Resultat explizit an eine spezielle Annahme über das Wandpotential zu binden. Ausserdem ist gegen Gl. (46) einzuwenden, dass die Funktion H_p kein uniformes Integral der Bewegungsgleichungen ist. Nach dem

Liouville'schen Satz kann daher eine durch (46) dargestellte Gesamtheit nicht im statistischen Gleichgewicht sein.

Der letztere Einwand beantwortet zugleich für den klassischen Fall die Bemerkung von Byers Brown [6], dass weder Guggenheim [2], noch Hill [3], noch Münster [4, 5] eine 'mikrokanonische Druck-Gesamtheit' einführen. Eine klassische Gesamtheit dieser Art könnte nämlich unter keinen Umständen stationär sein. Im quantenstatistischen Fall bringt diese Gesamtheit überhaupt nicht Neues. Da hier alle Systeme der Gesamtheit das gleiche Volumen haben, ist es gleichgültig, ob dies von vornherein vorgegeben oder nach Gl. (22) aus dem Druck bestimmt wird. Das Analogon der Grösse $\ln \Omega$ ist aber trotzdem $S(E, V, N)$. Eine Funktion von H, P, N kann kein direktes statistisches Analogon haben, weil die Enthalpie keine primäre Zustandsvariable ist. Die Funktion

$$S = S(H, P, N) \tag{49}$$

ist die Inverse der Funktion

$$H = H(S, P, N) \tag{50}$$

die aus

$$E = E(S, V, N) \tag{51}$$

durch Legendre-Transformation hervorgeht.

It is shown that the density operator of a generalized ensemble has to satisfy certain conditions if one wants to derive the equations of thermodynamics and correct fluctuation formulae. The pressure ensemble proposed by Byers Brown is consistent with thermodynamics but it leads to wrong fluctuation formulae, especially to a wrong formula for the light scattering of a one-component system. This is explained by the fact, that in the Byers Brown ensemble the fluctuations have been partially discarded from the very beginning.

On étudie les conditions auxquelles l'opérateur de densité doit satisfaire si l'on veut déduire les équations de la thermodynamique et les formules correctes pour les fluctuations. 'L'ensemble de pression' proposé par Byers Brown est consistent pour la thermodynamique mais il conduit à des formules fausses pour les fluctuations. Pour la diffusion de la lumière on déduit une équation différente de la formule bien connue d'Einstein. Ceci s'explique par le fait que l'on élimine une partie des fluctuations en construisant l'ensemble de Byers Brown.

REFERENCES

[1] Gibbs, J. W., 1948, *Elementary Principles in Statistical Mechanics*, Collected Works Vol. II (New York: Longmans, Green & Co.).
[2] Guggenheim, E. A., 1939, *J. chem. Phys.*, **7**, 103.
[3] Hill, T. L., 1956, *Statistical Mechanics* (New York: McGraw-Hill).
[4] Münster, A., 1953, *Z. Phys.*, **136**, 179.
[5] Münster, A., 1956, *Statistische Thermodynamik* (Berlin: Springer).
[6] Byers Brown, W., 1958, *Mol. Phys.*, **1**, 68.
[7] Fixman, M., 1955, *J. chem. Phys.*, **23**, 2074.

Pressure-dependent partition functions

by R. A. SACK†
Department of Theoretical Chemistry, University of Cambridge
and
British Rayon Research Association, Wythenshawe, Manchester

(*Received* 10 *August* 1958)

It is shown that the partition functions relating to statistical ensembles can be classified as cumulative, distributive or differential with regard to any of the extensive thermodynamic variables. The Laplace transforms involved in the general formulation of transformed partition functions, when extensive parameters are replaced by their conjugate intensive variables, are two-sided and appear in different forms according to the classification mentioned.

The petit partition function at constant pressure can be defined for both classical and quantal systems as a Stieltjes integral or dimensionless Laplace transform over the volume-dependent partition function. This expression contains no arbitrary external parameters and satisfies all the conditions formulated by Münster; it can be interpreted as the ratio of two partition functions, the one relating jointly to the system and a macroscopic boundary, and the second to the boundary alone.

It is known that the constant pressure grand partition function as defined by Guggenheim diverges for all thermodynamically compatible values of its independent variables. It is shown that the Gibbs–Duhem relation, and hence all the statistical properties of the system, except its size, can be derived by differentiating the reciprocal of this, or a similarly defined, function, not its logarithm as with other partition functions.

The mathematical differences arising out of the various proposed definitions are illustrated in a number of simple examples.

1. INTRODUCTION

The suggestion of generalizing Gibbs' [1] concept of statistical ensembles to represent systems subject to a prescribed pressure was first made by Guggenheim [2]. His approach involves the use of vaguely described ' eigenvolumes ', and its development by Hill [3] necessitates the introduction of an arbitrarily chosen elementary volume. Recently Brown [4] has proposed a definition of pressure dependent (isobaric) quantal ensembles for which the partition function (P.F.)

$$W = W[T, P, N\,;\, \mathscr{H}(V, N)] \tag{1.1}$$

is a unique function of the pressure P, temperature T, number of particles N and the eigenvalues of the Hamiltonian $\mathscr{H}$ for a given V and N, and does not depend on any additional, arbitrary, constants. However, as shown by Münster [5], Brown's formalism violates some of the principles underlying the transformation of statistical ensembles [6, 7]; although the thermodynamic properties of isobaric systems are correctly rendered in Brown's theory, the fluctuation terms are in error. Following a suggestion due to Rosenfeld, Brown [4] has developed an alternative definition of W which he considered of less importance as it involves the arbitrary masses of macroscopic pistons; on the other hand, Münster [5] has shown that this definition is compatible with the postulates of statistical thermodynamics.

---

† Present address: Laboratory for Molecular Structure and Spectra, Department of Physics, University of Chicago.

It is clear that any consistent definition of a generalized ensemble must lead to a dimensionless P.F., which, like W in (1.1), may depend only on the form of the Hamiltonian and the specifying extensive and intensive thermodynamic parameters. According to Münster [6, 7] such P.F.'s can be derived (in the semi-classical approximation) on an axiomatic basis by an appropriate Laplace transform whenever an extensive variable is replaced by its intensive thermodynamic conjugate. However, the term ' Laplace transform ' may denote two different functionals according to whether the integral is, or is not, multiplied by the transformation variable:

$$L_1[f(X)]=p\int_0^\infty f(X)\exp(-pX)dX, \tag{1.2}$$

$$L_2[f(X)]=\int_0^\infty f(X)\exp(-pX)dX. \tag{1.3}$$

In addition cases may have to be considered where X can only assume discrete values; in such cases a simple generalization of (1.2), (1.3) leads to

$$L_3[f(X)]=\sum_m f(X_m)\exp(-pX_m), \tag{1.4}$$

the summation being taken over all allowed values of X. The form L_1 is usually known as the dimensionless (or proper) Laplace transform; in the following L_2 will be referred to as the normal, and L_3 as the discrete form. It is not obvious from Münster's axiomatic approach which form of the transformation has to be applied in any given case; moreover, Münster's definition is inadequate whenever any of the external parameters may take either sign, as in the case of electric charges or deflections.

In § 2 Münster's formalism [6, 7] will be refined by reference to the properties of microcanonical ensembles and general criteria will be established which determine the choice of the various Laplace transforms in the definition of generalized P.F.'s. On the basis of these results the isobaric ensemble will be discussed in § 3 and a consistent definition derived for the P.F. W as a Stieltjes integral or dimensionless Laplace transform over the canonical P.F. $Z(T, V, N)$. This definition agrees with that given by Wilson [8] and, for classical systems only, by Brown [4].

There has been considerable discussion in the literature whether any meaning can be attached to a constant pressure grand partition function (G.P.F.), or more generally to a P.F. depending on intensive variables only, since these variables are related by an equation (the Gibbs-Duhem relation) which causes the G.P.F. Y to diverge [2, 9]. Attempts have been made to enforce convergence by ascribing an upper bound to one of the extensive variables (the volume) [3]; on the other hand, for several classical models correct results have been obtained with the use of an unrestricted, divergent, G.P.F. [10, 11]. The problem will be re-examined in § 4, and it will be shown that a function Y can always be defined either as the Laplace transform of the constant volume G.P.F. or as the generating function of the isobaric petit P.F.'s. For values of the variables corresponding to a macroscopic equilibrium Y has, in general, a simple pole; higher singularities occur in the case of phase transitions. All the information about the system, except for its absolute size, can be derived from a differentiation of the inverse of Y, not the logarithm as with other P.F.'s.

In § 5, the isobaric P.F.'s will be compared according to the various definitions for several simple examples.

2. General theory of generalized partition functions

The theory of statistical mechanics is essentially based on the concept of the microcanonical ensemble [1] which represents systems with given V, N and energy E, or more generally, with given extensive thermodynamic parameters $X_1 \ldots, X_R$ ($X_1 = E$). The link between statistics and thermodynamics is provided by the Gibbs relation between the entropy S and the volume Ω in the $2s$-dimensional phase space (or Γ-space), s being the number of degrees of freedom,

$$S = k \log \Omega(E, V, N), \tag{2.1}$$

or more generally

$$S = k \log \Omega(X_1 \ldots . X_R). \tag{2.2}$$

The density function or probability of finding the system within a given unit volume of the accessible phase space is a constant for this ensemble

$$\rho_0 = \Omega^{-1}. \tag{2.3}$$

As already pointed out by Gibbs [1], the definition of Ω differs according to whether the Hamiltonian $\mathscr{H}$ may take values *less than* or (within prescribed limits ΔE) *equal to* E; the phase integrals can be written in the two cases

$$\Omega_c(E, V, N) = \int_{H=-\infty}^{H=E} d\Omega, \tag{2.4}$$

$$\Omega_d(E, V, N; \Delta E) = \int_{H=E-\Delta E/2}^{H=E+\Delta E/2} d\Omega, \tag{2.5}$$

where for semi-classical systems

$$d\Omega = (h^s N!)^{-1} dp_1 \ldots dp_s dq_1 \ldots dq_s. \tag{2.6}$$

The denominator $N!$ arises from the indistinguishability of the particles which is ignored in the integration. With the definition (2.5) each point in Γ-space belongs to a well-defined energy shell with volume Ω_d. For systems of non-interacting particles the thickness of the shells ΔE can be interpreted as the distance between energy levels and Ω_d as the degree of degeneracy of each level as in the work of Darwin and Fowler (c.f. [12]); in other cases ΔE may be prescribed arbitrarily. With classical or semi-classical ensembles, for which Ω_c is a continuous, differentiable function of E, a third definition Ω' can be used

$$\Omega' = \partial \Omega_c / \partial E, \quad \Omega_d \approx \Omega' . \Delta E, \tag{2.7}$$

but whereas Ω_c and Ω_d are dimensionless quantities for both quantal and semi-classical ensembles, Ω' has the inverse dimensions of energy; it represents the area of a hyper-surface in Γ-space, not a volume.

Although the statistical properties derived with the use of Ω_c and Ω_d (or Ω') are essentially similar, provided s is large [1, 13], it is important to distinguish between the various definitions. In the following we shall denote the phase integrals Ω_c, Ω_d and Ω' as being cumulative, distributive and differential respectively with regard to the variable E.

The same distinctions must be made for all phase integrals with regard to any independent extensive variable. Thus Ω_c, Ω_d and Ω' are all distributive with regard to N (the number of particles is kept fixed), but cumulative with regard to V (the particles may, but need not, fill the whole available volume).

The properties of generalized ensembles in which K of the R extensive thermodynamic parameters X_i are replaced by their intensive conjugates are most easily derived by considering a large number Λ of identical systems which are weakly coupled so that the values $X_{i_\nu}(i=1\ldots K)$ for the individual systems ν may vary and only their sum is prescribed:

$$\sum_\nu X_{i_\nu}=\Lambda\langle X_i\rangle, \quad (i=1,2\ldots K). \tag{2.8}$$

If we define a probability w_n of finding a single system in a given cell n of a hyperspace (τ_K-space) involving the $2s$ coordinates of the Γ-space and the K extensive variables $X_1\ldots X_K$, the most probable distribution for the ensemble of Λ systems is given by the condition

$$\prod_n(\Lambda w_n)!=\max \tag{2.9}$$

with the subsidiary conditions

$$\sum_n X_i w_n=\langle X_i\rangle, \quad (i=1\ldots K) \tag{2.10}$$

$$\sum_n w_n=1. \tag{2.11}$$

As Λ tends to infinity, Stirling's formula can be applied to the factorials in (2.9), and on taking logarithms the formula becomes

$$\sum_n \Lambda w_n\log(\Lambda w_n-1)=\max, \tag{2.12}$$

and since Λ is assumed to be prescribed, this becomes in the limit

$$\sum_n w_n\log w_n=\max. \tag{2.13}$$

If we can express w_n by a density function ρ in τ_K -space

$$w_n=\rho d\tau_K \tag{2.14}$$

(2.13), (2.10) and (2.11) become respectively

$$\int\rho\log\rho\, d\tau_K=\max, \tag{2.15}$$

$$\int X_i\rho\, d\tau_K=\langle X_i\rangle, \tag{2.16}$$

$$\int\rho\, d\tau_K=1. \tag{2.17}$$

On choosing indeterminate Lagrangian multipliers p_i and $\eta_K(=\log\xi_K)$ for (2.16) and (2.17) and adding to (2.15) the condition becomes

$$\delta\int\rho\left(\log\rho+\sum_{i=1}^{K}p_iX_i+\eta_K\right)=0, \tag{2.18}$$

the solution of which is

$$\rho=\exp(-\sum p_iX_i-\eta_K). \tag{2.19}$$

Substitution of (2.19) in (2.17) and (2.16) leads to

$$\xi_K=\exp\eta_K=\int\exp(-\sum p_iX_i)\, d\tau_K \tag{2.20}$$

and

$$\langle X_i\rangle=-\partial\log\xi_K/\partial p_i. \tag{2.21}$$

Corresponding expressions can be derived for a model with discrete cells from (2.13), (2.10) and (2.11), the solution being

$$w_n = \exp\Bigl(-\sum_i p_i X_i - \eta_K\Bigr) \tag{2.22}$$

with

$$\xi_K = \sum_n \exp\Bigl(-\sum_i p_i X_i\Bigr) \tag{2.23}$$

and (2.21) being unaffected. Identification of p_i with the intensive conjugates of the X_i connects the P.F. ξ_K with the Massieu–Planck function Φ_K for the ensemble [5, 6, 7]

$$\Phi_K = S - \sum_{i=1}^{K} p_i X_i = k \log \xi_K. \tag{2.24}$$

In the above, somewhat sketchy, treatment no clear indication has been given as to the relation of the τ_K-space to the Γ-space, in particular as to which of the X_i can be treated as independent variables in τ_K-space and which are functions of the coordinates in Γ-space. To some extent this question can be decided by the consideration that P.F. ξ_K of (2.20) and (2.23) must be a dimensionless expression for (2.20) and (2.24) to have any meaning. On replacement of a given X_K by p_K, the ratio of ξ_K to ξ_{K-1} has the same dimensions as X_K if this appears as an independent variable in (2.20). Thus in the definition of a generalized P.F. the only extensive thermodynamic parameters which may be taken as independent integration variables are dimensionless quantities, e.g. the number of particles N, whereas all dimensional variables, such as volume, energy, elongation, must be treated as functions of the coordinates in the usual phase space.

This is in agreement with the standard derivation of the properties of the canonical ensemble from those of the microcanonical ensemble. In this case the τ- and Γ-spaces are identical and if the integrations in (2.20) are first performed over all parts of phase space compatible with a given energy $X_1 = E$ and the prescribed values of $X_2, \ldots, X_R$, the result is in view of (2.4) and (2.7)

$$\xi_1(p_1, V, N) = \int_{\infty}^{\infty} \Omega' \exp(-p_1 E)\, dE = \int_{\infty}^{\infty} (\partial\Omega_c/\partial E) \exp(-p_1 E)\, dE. \tag{2.25}$$

For discrete energy states (2.23) and (2.5) yield

$$\xi_1(p_1, V, N) = \sum_m \Omega_d(E_m, V, N) \exp(-p_1 E_m). \tag{2.26}$$

In each case

$$p_1 = 1/kT, \tag{2.27}$$

so that

$$\xi_1(p_1, V, N) = Z(T, V, N) \tag{2.28}$$

is the usual canonical P.F. The expression (2.25) can be re-written as a Stieltjes integral over the cumulative phase volume Ω_c

$$Z(T, V, N) = \int_{E=-\infty}^{E=\infty} \exp(-E/kT)\, d_E[\Omega_c(E, V, N)], \tag{2.29}$$

and integration by parts leads to a dimensionless Laplace transform of Ω_c

$$\begin{aligned} Z(T, V, N) &= p_1 \int_{-\infty}^{\infty} \Omega_c(E, V, N) \exp(-p_1 E)\, dE \\ &= (kT)^{-1} \int_{-\infty}^{\infty} \Omega_c \exp(-E/kT)\, dE. \end{aligned} \tag{2.30}$$

The lower limit of the integrals in (2.25), (2.29) and (2.30), as also in (2.4), has been chosen as $-\infty$ instead of the more conventional value 0; this does not affect the result if negative energy states are absent since $\Omega_c \equiv 0$ for all values of E lower than the lowest eigenvalue of the Hamiltonian, and consideration of possible negative energy levels is thus included in a consistent formalism. The Laplace transform should therefore always be considered as two-sided [14].

If the energy levels of the system are discrete, Ω_c increases stepwise, but this does not affect the validity of (2.29) or (2.30). The only condition imposed in the Stieltjes integral is that Ω_c should be a monotonically non-decreasing function of E; this is always satisfied since Ω_d can never be negative. If the energy levels E_n are counted individually, as in (2.23), (2.29) can be expressed in the more familiar form

$$Z(T, V, N) = \sum_{n} \exp(-E_n/kT). \tag{2.31}$$

It should be pointed out that (2.26)–(2.28) are equivalent to (2.31) only in the case that ΔE defined in (2.5) is taken to be the difference between successive degenerate energy levels. For all other choices of ΔE some of the terms occurring in (2.31) will be differently weighted, leading to an expression (2.26) which, though perfectly consistent according to the criteria stated by Münster [5], is more complicated than (2.31).

A completely analogous treatment can be applied to any generalized ensemble and its corresponding P.F. ξ_K. If all the $X_i (1 \ldots K)$ have non-vanishing dimensions, the τ- and Γ-spaces must be identical; integration of (2.20) first over all parts of phase space compatible with prescribed values of $X_K, X_{K+1} \ldots X_R$ and then over X_K yields

$$\xi_K(p_1 \ldots p_K, X_{K+1} \ldots X_R) = \int_{-\infty}^{\infty} \xi_{K-1}(\ldots X_K \ldots) \exp(-p_K X_K)\, dX_K \tag{2.32}$$

if ξ_{K-1} is defined as a differential P.F. with regard to X_K and, if ξ_{K-1} is distributive in X_K,

$$\xi_K(\ldots p_K \ldots) = \sum \xi_{K-1}(\ldots X_K \ldots) \exp(-p_K X_K), \tag{2.33}$$

the sum being taken over all possible values of X_K. If, however, ξ_{K-1} is taken to be cumulative with regard to X_K, reinterpretation of both (2.32) and (2.33) leads to the expressions

$$\xi_K(\ldots p_K \ldots) = \int_{X_K=-\infty}^{X_K=\infty} \exp(-p_K X_K)\, d[\xi_{K-1}(\ldots X_K \ldots)] \tag{2.34}$$

$$= p_K \int_{-\infty}^{\infty} \exp(-p_K X_K) \xi_{K-1}(\ldots X_K \ldots)\, dX_K. \tag{2.35}$$

The formulae (2.32)–(2.35) are meaningful only if an unambiguous definition can be given to the differential dX_K (cf. § 3 for the case of $X_2 = V$); in addition the cumulative P.F. ξ_{K-1} must be a monotonically non-decreasing function X_K for the Stieltjes integral (2.34) to have any meaning [15]. The derivation of (2.32)–(2.35) is in accordance with the principle stated by Münster [5] that the values which X_K can take must be independent of p_K, and only the probability of finding the system in a state with a prescribed value of X_K may be weighted as a function of p_K. The definitions (2.32)–(2.35) form thus a consistent scheme for the formation of P.F.'s satisfying the relation (2.24); this consistency remains unimpaired if X_K is a dimensionless variable. We can thus formulate the following general principle.

The P.F. ξ_K relating to a generalized ensemble depending on an intensive thermodynamic parameter p_K is defined as the two-sided Laplace transform of the P.F. ξ_{K-1} depending on the conjugate extensive parameter X_K, all other independent parameters being kept the same. The Laplace transform is to be taken in its discrete, normal or dimensionless form according to whether ξ_{K-1} is defined as the distributive, differential or cumulative P.F. with regard to X_K.

Though the above definitions lead to a consistent set of generalized P.F.'s, it is not claimed that these are the only possible ones. The functions thus obtained may have to be interpreted in each individual case; this will be done in the next section for the isothermal–isobaric ensemble.

3. THE CONSTANT PRESSURE PETIT PARTITION FUNCTION

To apply the general theorems of the preceding section to the derivation of the constant pressure P.F. for a given N, the simplest procedure is to assume the canonical P.F. $Z(T, V, N)$ as given and to replace $X_2 = V$ by its intensive conjugate

$$p_2 = P/kT. \tag{3.1}$$

It is irrelevant whether Z is given in any of the forms (2.25)–(2.30) or in its more usual formulation (2.31) for quantal ensembles or

$$Z(T, V, N) = (h^s N!)^{-1} \int \exp[-E(\mathbf{p}, \mathbf{q})/kT]\, dp_1 \ldots dp_s\, dq_1 \ldots dq_s \tag{3.2}$$

for classical systems where the q_i are compatible with the value of V. As stated in § 2, Ω_c and Ω_d are cumulative phase integrals with regard to the variable V; this relation is unaffected by integration over E and therefore applies equally to Z. Application of (2.34) and (2.35) with the use of (3.1) and (2.28) yields formally

$$\xi_2(p_1, p_2, N) = W(T, P, N) = \int_{V=0}^{V=\infty} \exp(-PV/kT) d_V[Z(T, V, N)] \tag{3.3}$$

$$= (P/kT) \int_0^\infty Z(T, V, N) \exp(-PV/kT)\, dV. \tag{3.4}$$

The lower limit of integration can be chosen as 0, instead of $-\infty$ since configurations with $V < 0$ do not exist. The way in which V is allowed to vary from 0 to ∞ is subject to certain restrictions, connected with the fact that the analytic theory of integration requires a definite ordering of the integration variable or variables [15]. Such an ordering can be achieved by selecting a family of closed surfaces in three-dimensional space, specified by one or several continuously variable parameters. For a one-parameter family of boundaries the envelopes must be chosen in such a way that for any two non-identical volumes one is wholly contained within the other, e.g. if a single piston can move between rigid walls; this is the same condition as that specified by Brown [4] for the surfaces defining an extension function $\mathscr{V}$ in his formulation of classical isobaric ensembles. The two treatments are entirely equivalent if $\mathscr{V}$ is identified with V in (3.3), (3.4): Brown's formula

$$W = (h^s N!)^{-1} \int \exp\{-[E(\mathbf{p}, \mathbf{q}) + P\mathscr{V}(\mathbf{q})]/kT\}\, dp_1 \ldots dp_s\, dq_1 \ldots dq_s \tag{3.5}$$

can be derived immediately from (3.2) and (3.3); and the Stieltjes integral formulation (3.3) has, in fact, been used by Brown in the special case of the perfect gas [4]. The main difference between the present treatment and Brown's [4] is that here V (or $\mathscr{V}$) appears as a purely geometric or analytic concept whereas Brown derives it from mechanical arguments. Brown's approach has been criticized by Münster [5], but the resulting equation (3.5) for classical systems satisfies all the requirements of generalized P.F.'s.

The definitions (3.3)–(3.5) are thus not new, as far as classical ensembles are concerned; in addition to Brown's work [4], equation (3.4) has been given explicitly by Wilson [8] and the expression (3.5) is closely paralleled in more specific theories making use of classical ensembles with constant forces, in particular the statistical theory of molecular chains [16, 17, 18]. The Stieltjes integral formulation (3.3) has the advantage that it applies equally for systems in which the volume can assume discrete values only, e.g. an integer number of lattice sites; it further remains valid if the allowed variations of the boundaries of the volume depend on several parameters, provided V or ($\mathscr{V}$) is a monotonically non-decreasing function of the parameters singly and jointly (for a definition see Young [15]). Such multiple integrations are always necessary if the system is inherently anisotropic; this question will not be further developed here.

We shall next discuss the applicability of (3.3) and (3.4) to quantal systems. It may be argued that $Z(T, V, N)$ defined by (2.31) is not a cumulative P.F. with regard to V, since the eigenvalues E_n depend on the actual value, and not on any prescribed upper boundary of V, and the Laplace transform should therefore not take its dimensionless form. Interpretation of Z as a distributive P.F. with regard to V would lead, by the theorems of § 2 to the expression

$$W_{\mathrm{G}} = \sum_{n,l} \exp\{-[E_n(V_l) + PV_l]/kT\}, \tag{3.6}$$

the sum to be taken over all permissible volumes V_l and all energy levels E_n. If Z is taken as differential with regard to V, the resultant normal Laplace transform would have the dimensions of a volume, but could be rendered dimensionless on division by an elementary volume v^*

$$W_{\mathrm{H}} = (v^*)^{-1} \int_0^\infty \sum_n \exp[-E_n(V)/kT] \exp(-PV/kT)\, dV. \tag{3.7}$$

The definition (3.6) has been proposed by Guggenheim [2] and is used by Münster [5], but it suffers from the drawback that there is no known way of determining the permissible 'eigenvolumes' V_l, whereas (3.7), the definition given by Hill [3], involves the use of the arbitrary volume v^*.

Brown [4], in addition to the formulation critized by Münster, has given a definition for a quantal ensemble based on a suggestion by Rosenfeld; in this the system is considered separated from its reservoir by heavy movable walls; Brown discusses the case of three pistons, but the argument is independent of the number of degrees of freedom of the boundary. A P.F. can be set up for the combined system of the envelope and its contents; the latter are treated quantally with the use of the Born–Oppenheimer approximation; the movement of the former is described macroscopically. The resulting P.F. agrees with (3.7) where the unknown v^* is now determined by the properties of the envelope. Thus for a single moving rigid piston of mass M and cross section A

$$v^* = Ah(2\pi MkT)^{-1/2}, \tag{3.8}$$

and for the model of three pistons with variable effective cross sections discussed by Brown

$$v^* = h^3(2\pi MkT)^{-3/2}; \tag{3.9}$$

more complicated expressions are obtained for flexible enclosures.

The expression (3.7) thus represents a well-defined P.F., which is derived by integration over a phase space involving momenta and configuration coordinates of the enclosure as well as those of the original system. The impossibility of deriving directly a constant pressure petit P.F. for a general system is connected with the fact that such a closed system, if gaseous, can be maintained only if surrounded by solid, though movable, walls. On the other hand it is possible to evaluate a P.F. in the phase space of the degrees of freedom of the envelope alone, taking the external pressure to be the same; a P.F. for the enclosed system can alone then be defined by inference†:

$$W\,(\text{system}) = \frac{W(\text{system} + \text{envelope})}{W\,(\text{envelope})}. \tag{3.10}$$

For a single piston with coordinate and momentum denoted by p_w and x_w

$$\begin{aligned} W(\text{envelope}) &= h^{-1}\iint \exp\left(-p_w^2/2MkT - PAx_w/kT\right) dx_w\, dp_w \\ &= (2\pi MkT)^{1/2}(kT/PAh) \end{aligned} \tag{3.11}$$

or with the use of (3.8)

$$W(\text{envelope}) = kT/Pv^*. \tag{3.12}$$

The same expression (3.12) is found regardless of the number of degrees of freedom, v^* in each case agreeing with the denominator in (3.7) according to the Rosenfeld–Brown formalism. Substitution of (3.7) and (3.12) in (3.10) yields

$$W(T, P, N) = (P/kT)\int_0^\infty \sum_n \exp\left(-E_n(V)/kT\right)\exp\left(-PV/kT\right) dV \tag{3.13}$$

which is one of the ways in which (3.4) can be written for quantal ensembles. Each term in this series can be expressed as a Stieltjes integral so that the fomula (3.3) becomes

$$W(T, P, N) = \int \exp\left(-PV/kT\right) d_V\left\{\sum_n \exp\left[-E_n(V)/kT\right]\right\}. \tag{3.14}$$

As each eigenvalue $E_n(V)$ is a monotonically non-increasing function of V (cf. [19]), the integrator in (3.14) is a sum of monotonically non-decreasing functions; therefore (3.14) and (3.3) are always meaningful expressions.

The definitions (3.3) and (3.4), originally developed from the general considerations of § 2, have thus been shown to be valid for all ensembles, directly for classical systems and indirectly for quantal systems. An indirect approach, analogous to (3.7)–(3.13) can also be used for classical ensembles; in this case the variable V does not correspond to Brown's extension function $\mathscr{V}$, but denotes the volume enclosed by the envelope.

4. GRAND PARTITION FUNCTIONS

The discussion of the constant pressure G.P.F. will be facilitated by a brief recapitulation of the properties of the constant volume G.P.F. In the concept of the grand ensemble at constant volume, first introduced by Gibbs [1], it is assumed that the system and its reservoir can exchange not only energy, but also particles. The corresponding G.P.F. Ξ is defined in terms of the petit P.F. $Z(T, V, N)$ (cf. (2.25)–(2.31), (3.2)) as

---

† I am indebted to Professor H. C. Longuet-Higgins for suggesting this approach.

$$\Xi(T, V, \lambda) = \sum_{N=0}^{\infty} Z(T, V, N)\lambda^N \tag{4.1}$$

for systems with a single component and as

$$\Xi(T, V, \lambda_i) = \sum_{N_1=0}^{\infty} \sum_{N_2=0}^{\infty} \dots \sum_{N_u=0}^{\infty} Z(T, V, N_i)\lambda_1^{N_1}\lambda_2^{N_2}\dots\lambda_u^{N_u} \tag{4.2}$$

for u-component systems. The petit P.F. $Z(T, V, N_i)$ is defined in an analogous way to $Z(T, V, N)$, the denominator $N!$ in (2.6) and (3.2) for classical systems being replaced by

$$N! \rightarrow N_1!\, N_2! \dots N_u!. \tag{4.3}$$

The expressions (4.1) and (4.2) can be interpreted in two different ways (cf. [7]). On the one hand we can regard $\Xi(\lambda)$ in (4.1) merely as a generating function of the $Z(N)$ for arbitrary argument λ, such that $Z(N)$ appears as the coefficient of λ^N in the power series expansion of $\Xi(\lambda)$ and can be evaluated by a contour integration similar to the procedure due to Darwin and Fowler [12]; analogous considerations apply to (4.2). Alternatively we can equate λ_i to the absolute activity of the ith species, defined by the chemical potential μ_i per molecule

$$\lambda_i = \exp(\mu_i/kT). \tag{4.4}$$

In this case Ξ has the thermodynamic significance

$$\log[\Xi(T, V, \lambda_i)] = P_e(T, \lambda_i)V/kT, \tag{4.5}$$

and the mean number of particles N_i, the entropy S and the pressure $P = P_e$ can be derived in the usual way:

$$N_i = \lambda_i \partial(\log \Xi)/\partial\lambda_i, \qquad S = kT\partial(\log \Xi)/\partial T, \qquad P = kT\partial(\log \Xi)/\partial V \tag{4.6}$$

which, provided V is not too small, is equivalent to

$$N_i/V = \lambda_i \partial(P_e/kT)/\partial\lambda_i, \qquad S/V = kT\partial(P_e/kT)/\partial T, \tag{4.7}$$

$$P_e(\lambda_i, T) = (kT/V)\log \Xi. \tag{4.8}$$

The definition (4.5) with (4.1) or (4.2) is consistent with the general development of §2 if we bear in mind that all the petit P.F.'s are distributive with regard to the number of particles, so that the corresponding Laplace transform appears as a weighted sum with $p_3 = -\log\lambda$.

(For quantal systems ter Haar (20) suggests that the N_i in (4.1), (4.2) should be treated not as numbers, but as number operators. This procedure is entirely equivalent to the simpler, classical, summation over N of quantal P.F.'s $Z(N)$ (cf. (2.31)), provided the particles are not actually created and destroyed within the system, but only interchanged between this system and the reservoir.)

Guggenheim [2] was the first to introduce the concept of an isobaric G.P.F. Y as a weighted integral over the G.P.F. (4.1), (4.2); Prigogine [9] has shown that the resulting expression diverges for physically consistent values of the arguments, and hence concludes that no meaning can be attached to Y (cf. also Münster [7]). Hill [3] has tried to overcome this difficulty by either keeping one extensive variable fixed or limiting the integration over the last extensive variable to a finite range. Brown [4] has left open the question of an unrestricted (T, P, λ) P.F., and Rushbrooke's [21] treatment of G.P.F.'s referring to specific volumes does not fully describe their properties. Since, however, unrestricted P.F.'s depending on intensive variables only, have been successfully used in the theory of linear chains by Rushbrooke and Ursell [10] and of one-dimensional gases by Longuet-Higgins [11], it is of interest to re-examine their usefulness in the light of Prigogine's criticism.

In a thermodynamic u-component system the $u+2$ intensive variables μ_i (or λ_i), P and T cannot be varied independently, but only in accordance with the Gibbs–Duhem relation

$$S\delta T - V\delta P + kT\sum N_i\delta\lambda_i/\lambda_i = 0. \tag{4.9}$$

One can thus postulate a thermodynamic function per unit volume $L(T, P, \lambda_i)$ defined through its derivatives

$$\partial L/\partial T = S/V, \qquad \partial L/\partial P = -1, \qquad \lambda_i\partial L/\partial\lambda_i = kTN_i/V, \tag{4.10}$$

for arbitrary values of T, P and λ_i, but this only corresponds to a macroscopic system when L has an arbitrarily chosen constant value, say 0. On the other hand when the intensive variables satisfy the relation (4.9), they provide no information whatever as to the size of the resulting system; only the ratios of the thermodynamic function can be determined. The reason for this is that it is impossible to draw a distinct boundary between the system and the reservoir since they are specified by the same intensive variables†; properly speaking the reservoir must be taken to be not only very large, but unlimited.

As regards the corresponding G.P.F., it can be defined purely mathematically as the dimensionless Laplace transform of $\Xi(T, V, \lambda_i)$ of (4.1), (4.2) over $V = X_2$:

$$\Upsilon(T, P, \lambda_i) = p_2\int dV \exp(-p_2 V)\Xi(T, V, \lambda_i) \tag{4.11}$$

with the identification (3.1). This function converges for sufficiently large positive values of p_2 or P; its value is, in view of (4.7) and (4.8)

$$\Upsilon(T, P, \lambda_i) = P[P - P_e(T, \lambda_i)]^{-1}. \tag{4.12}$$

Here P has to be treated as an independent variable and P_e as the equilibrium pressure depending on λ_i and T. These two quantities must be equal if the expression is to have any meaning, but as far as derivatives are concerned, this identification may be made only after the differentiations have been carried out [11]. Thus when $P = P_e$, Υ has a simple pole as a function of P and also as function of λ_i or T, as long as the derivatives $\partial P_e/\partial T$ and $\partial P_e/\partial\lambda_i$ exist and do not vanish. Finite results are thus obtained on differentiating the function

$$\Delta(T, P, \lambda_i) = -[\Upsilon(T, P, \lambda_i)]^{-1}. \tag{4.13}$$

From (4.6), (4.7) and (4.12) we obtain

$$P\partial\Delta/\partial P = -1, \tag{4.14}$$

$$P(\partial\Delta/\partial T) = S/V, \qquad P\lambda_i(\partial\Delta/\partial\lambda_i) = kTN_i/V, \tag{4.15}$$

or

$$N_i : V : S = (\lambda_i/kT)\partial\Delta/\partial\lambda_i : -\partial\Delta/\partial P : \partial\Delta/\partial T. \tag{4.16}$$

---

† Münster [7] concludes that for this reason such an ensemble is not definable at all; the writer does not agree with this conclusion.

Equation (4.16), with the condition that for a macroscopic system Δ must remain 0, leads to the Gibbs–Duhem relation (4.9). The P.F. Y and the postulated thermodynamic function L are therefore not related by equation (2.24) which applies to all other P.F.'s, since L is essentially equal to P/Y.

An alternative, but entirely equivalent, definition of the isobaric G.P.F. is that of the moment generating function of the isobaric petit P.F.'s W in (3.3) and (3.4). Thus in analogy to (4.1) we can put

$$Y(T,P,\lambda)=\sum_{N=0} W(T,P,N)\lambda^N \tag{4.17}$$

with a corresponding expression for $Y(T,P,\lambda_i)$ in analogy to (4.2). The resulting sum converges for sufficiently small values of λ_i, its value being given by the expression (4.12); the relations (4.14)–(4.16) follow equally from the definition (4.17).

If in (4.17) the $W(T,P,N)$ are given the values (3.6) or (3.7) in accordance with Guggenheim's or Hill's definitions (2.3), a value of Y is obtained which differs from (4.11), (4.12) by a factor of the order of kT/Pv^*. Any such factor with slowly varying logarithm leaves the ratios (4.16) unaltered. Similarly the relations (4.13)–(4.16) are not affected by any finite additive corrections to Y in (4.12) which may arise from the fact that the right-hand side of (4.8) is constant only in the limit of large V. For particles with long-range interaction (e.g. space charges), (4.8) may not even be asymptotically constant; the arguments of this section do not apply to such cases.

As mentioned above, the nature of the singularity of Y depends on the analytic behaviour of $\partial P_e/\partial T$ and $\partial P_e/\partial\lambda_i$. When these quantities become infinite, discontinuous or vanish, as they do at phase transitions, the singularity of Y becomes of higher order than that of a simple pole.

The condition that the system is stable (except for its absolute size) corresponds to the largest positive value of P or the smallest positive value of one of the λ_i for which $Y(T,P,\lambda_i)$ has a pole. Other poles may occur, but have no physical significance, since they could only correspond to unstable phases which according to Münster [6] cannot be described by statistical ensembles.

Other divergent P.F.'s arise whenever an ensemble is specified by intensive variables only, e.g. by λ, T and the density $\rho=N/V$. Several such systems have been indicated by Rushbrooke [21] in the table on p. 296, marked by asterisks. They all exhibit poles; the relative constitution of each system, but not its size, can be determined for a differentiation of their inverses. Rushbrooke defines these G.P.F.'s in a manner analogous to (4.17) and suggests taking the largest term in the series (p. 295). However, in equilibrium, all the terms (for large N) are equal; thus Rushbrooke's procedure is incorrect. It is possible, however, to break off the series after a finite number of terms, as suggested by Hill [3], or to take a single term of the series for large N, which takes us back to the P.F. W of § 3.

5. APPLICATIONS

In this section we shall compare the values for the isobaric P.F.'s W and Y according to the various definitions for a number of simple systems. Most of the results are well known and are only quoted for the sake of completeness; in each case the P.F.'s Z and Ξ will be taken as known.

5.1. *The perfect classical gas*

$$Z(N,V,T)=(BV)^N/N!,\qquad \Xi(T,V,\lambda)=\exp(\lambda BV) \tag{5.1}$$

where

$$B=\phi(2\pi mkT)^{3/2}h^{-3}, \tag{5.2}$$

m being the mass of the molecules and ϕ the P.F. per molecule over its internal degrees of freedom. With the definitions (3.4) and (4.11) this yields

$$W(T,P,N)=(BkT/P)^N,\qquad Y(T,P,\lambda)=P/(P-kTB\lambda). \tag{5.3}$$

This should be compared with Hill's results [3] based on the definition (3.7) for W (denoted by Hill as Δ) and a restricted integration over a volume V_m for Y

$$W_{\mathrm{H}}=(kT/Pv^*)(BkT/P)^N,\qquad Y_{\mathrm{H}}=\alpha^{-1}[1-\exp(-\alpha u_m)] \tag{5.4}$$

where

$$u_m=V_m/v^*,\qquad \alpha=Pv^*/kT-Bv^*\lambda. \tag{5.5}$$

5.2. *Mixture of two perfect classical gases*

$$Z=(B_1V)^{N_1}(B_2V)^{N_2}/(N_1!\,N_2!);\quad \Xi=\exp[(\lambda_1B_1+\lambda_2B_2)V] \tag{5.6}$$

This yields in analogy to (5.3)

$$W=\frac{(N_1+N_2)!}{N_1!N_2!}\left(\frac{B_1kT}{P}\right)^{N_1}\left(\frac{B_2kT}{P}\right)^{N_2};\quad Y=\frac{P}{P-kT(\lambda_1B_1+\lambda_2B_2)}. \tag{5.7}$$

Hill's expression for W differs from this by the same factor (kT/Pv^*) and for Y is given by (5.4) where now

$$u_m=V_m/v^*;\qquad \alpha=Pv^*/kT-(B_1\lambda_1+B_2\lambda_2)v^*. \tag{5.8}$$

5.3. *The imperfect classical gas*

We shall only discuss the G.P.F.'s since the virial expansion in terms of N/V and T is always obtained by a series inversion of Ξ [22]. The G.P.F. involves the Ursell–Mayer reducible cluster integrals b_l

$$\Xi=\exp\left[V\sum_l b_l(B\lambda)^l\right] \tag{5.9}$$

from which Y can be calculated by means of (4.12)

$$Y=P/[P-kT\sum b_l(B\lambda)^l]. \tag{5.10}$$

Brown [4] has, in fact, been led to this expression as the generating function for the corresponding W's; he states that the derivation of the relation

$$P=kT\sum b_l(B\lambda)^l \tag{5.11}$$

from (5.10) requires careful discussion; here we see that it is the immediate consequence of the asymptotic constancy of P_e in (4.8) and the divergence of Y.

The writer wishes to thank Professor H. C. Longuet-Higgins, Mr. W. Byers Brown, and Professor A. Münster for stimulating discussions and criticism; in particular, he wishes to thank Professor A. Münster for showing him his paper [5] before publication.

On montre que lës fonctions de partition correspondant aux divers ensembles statistiques peuvent entre classifiées en cumulatives, distributives ou différentielles par rapport à chacune de leurs variables thermodynamiques extensives. Les transformations de Laplace utilisées dans la définition générale des fonctions de partition transformées, quand on remplace des variables extensives par leurs conjuguées intensives, sont bilatérales et se présentent sous des formes différentes selon la classification indiquée.

La fonction de partition petit-canonique à pression constante peut se définir pour tous les systèmes, classiques ou quantiques, par une intégrale de Stieltjes, ou une transformée de Laplace sans dimensions, de la fonction de partition dépendant du volume. Cette expression ne contient point de paramètres externes arbitraires et obéit à toutes les conditions établies par Münster; elle est égale au rapport de deux fonctions de partition, l'une relative à l'ensemble du système et de son enveloppe macroscopique, l'autre relative à l'enveloppe seule.

Il est bien connu que la fonction de partition grand-canonique à pression constante, telle qu'elle est définie par Guggenheim, diverge pour toutes les valeurs thermodynamiquement compatibles de ses variables indépendantes. L'auteur montre que la relation de Duhem–Gibbs, et du même coup toutes les propriétés statistiques du système, à l'exception de l'étendue, peuvent s'obtenir en différentiant, non pas le logarithme commes pour les autres fonctions de partition, mais la réciproque de la fonction en question (ou d'une fonction définie de façon semblable).

Les différences mathématiques qui proviennent des diverses définitions proposées sont exposées dans quelques exemples simples.

Es wird gezeigt, dass die zu statistischen Gesamtheiten gehörigen Zustandsintegrale in bezug auf ihre unabhängigen äusseren thermodynamischen Variabeln in kumulative, distributive und differentielle einzuteilen sind. Die in der allgemeinen Formulierung transformierter Verteilungsfunktionen (wenn extensive Parameter durch ihre konjugierten intensiven Veränderlichen ersetzt werden) auftretenden Laplace-Transformationen sind beiderseitig und nehmen entsprechend der genannten Einteilung verschiedene Gestalt an.

Die kleine Verteilungsfunktion bei konstantem Druck kann für klassische wie für quantenmechanische Systeme als ein Stieltjessches Integral oder eine dimensionslose Laplace-Transformierte des volumenbestimmten Zustandsintegrals definiert werden. Dieser Ausdruck enthält keine willkürlichen äusseren Parameter und genügt den von Münster aufgestellten Bedingungen; er kann als Quotient zweier Zustandsintegrale aufgefasst werden, von denen sich das eine auf das System einschliesslich seiner makroskopischen Hülle und das zweite auf die Hülle allein bezieht.

Es ist bekannt, dass die von Guggenheim definierte grosse Verteilungsfunktion bei konstantem Druck für alle thermodynamisch verträglichen Werte der unabhängigen Variabeln divergiert. Es wird hier gezeigt, dass die Gibbs–Duhemsche Beziehung und damit alle statistischen Eigenschaften des Systems mit Ausnahme seiner Ausdehnung abgeleitet werden können durch Differenzieren der Reziproken dieser oder einer ähnlich definierten Funktion, und nicht des Logarithmus wie bei andern Zustandsintegralen.

Die durch die verschiedene Definitionen bedingten mathematischen Unterschiede werden an einigen einfachen Beispielen erörtert.

REFERENCES

[1] GIBBS, J. W., 1928, *Elementary Principles in Statistical Mechanics*, Collected Works, Vol. II (New York: Longmans, Green and Co.).

[2] GUGGENHEIM, E. A., 1939, *J. chem. Phys.*, **7**, 103.

[3] HILL, T. L., 1956, *Statistical Mechanics* (New York: McGraw-Hill).

[4] BROWN, W. B., 1958, *Mol. Phys.*, **1**, 68.

[5] MÜNSTER, A., 1959, *Mol. Phys.*, **2**, 1.

[6] MÜNSTER, A., 1953, *Z. Phys.*, **136**, 179.

[7] MÜNSTER, A., 1956, *Statistische Thermodynamik*, Chapter 7 (Berlin: Springer).

[8] WILSON, A. H., 1957, *Thermodynamics and Statistical Mechanics* (Cambridge: University Press).

[9] PRIGOGINE, I., 1950, *Physica*, **16**, 133.

[10] Rushbrooke, G. S., and Ursell, H. D., 1947, *Proc. Camb. phil. Soc.*, **44**, 263.

[11] Longuet-Higgins, H. C., 1958, *Mol. Phys.*, **1**, 83.

[12] Fowler, R. H., 1936, *Statistical Mechanics* (Cambridge: University Press).

[13] Münster, A., 1954, *Z. Phys.*, **137**, 386.

[14] van der Pol, B., and Bremmer, H., 1950, *Operational Calculus based on the Two-sided Laplace Integral* (Cambridge: University Press).

[15] Young, L. C., 1927, *The theory of Integration*, Chapters 3 and 4 (Cambridge: University Press).

[16] James, H. M., and Guth, E., 1943, *J. chem. Phys.*, **11**, 455.

[17] Wang, M. C., and Guth, E., 1952, *J. chem. Phys.*, **20**, 1144.

[18] Kubo, R., 1947, *J. phys. Soc. Japan*, **2**, 47.

[19] Brown, W. B., 1958, *Proc. Camb. phil. Soc.*, **54**, 251.

[20] ter Haar, D., 1954, *Elements of Statistical Mechanics* (New York: Rinehart and Co.).

[21] Rushbrooke, G. S., 1949, *Introduction to Statistical Mechanics* (Oxford: Clarendon Press).

[22] Mayer, J. E., and Mayer, M. G., 1940, *Statistical Mechanics* (New York: John Wiley and Sons).

On Mayer's ionic solution theory

by HAROLD L. FRIEDMAN†
Faculté des Sciences, Université Libre de Bruxelles

(*Received* 17 *July* 1958)

This theory, which is based upon McMillan and Mayer's cluster expansion of the grand partition function, is extended to include all of the components of the potentials of average force between sets of solute molecules or ions in the solvent at infinite dilution. The resulting cluster integral sum, which is a sum of integrals over an infinite number of infinite series of Mayer prototype graphs, is transformed into the sum of a single infinite series of integrals on graphs involving new types of bonds. These bonds are defined in a way first suggested by Meeron. There results a compact expression for the cluster integral sum.

1. Introduction

The theory of electrolyte solutions which has been developed by Mayer [1] is based upon the cluster expansion of the grand partition function and relates the thermodynamic properties of the solution to the *pairwise* components of the potentials of average force between sets of ions in the pure solvent (i.e. potentials of average force at infinite dilution). Poirier [2] and Haga [3] have compared the lowest order terms of the theory with experiment on the basis of the primitive model in which the ions are represented by hard spheres and the solvent by a structureless dielectric whose properties are independent of electric field strength. Meeron [4] has shown how the simplest infinite series of prototype graphs resulting from Mayer's theory can be summed.

The potential of average force of a set of ions in the pure solvent is a sum of only pairwise contributions when the primitive model is used to derive the potential because (1), the average over coordinates of solvent molecules is replaced by the dielectric constant [5] and (2), the short-range interaction of the ions is replaced by a hard-sphere cut-off potential. In a real electrolyte solution, on the other hand, the potential of average force of a set of ions in the solvent differs from the sum of pairwise contributions for two reasons. First, the average over the coordinates of solvent molecules depends upon the contributions to the electric field from all of the ions of the set as well as from the solvent molecules. The use of the dielectric constant can give a good approximation to this average only if the electric field from the ions is relatively small, and the use of any better approximation must take into account the positions of all of the ions of the set. The second reason is that the potential of average force which is used here is an average over the internal coordinates of the solute molecules. This average may also be affected by the proximity of other ions, especially in the case of non-spherical ions.

---

† On leave from the Department of Chemistry, University of Southern California, Los Angeles 7, Calif.

One can expect, therefore, that more elaborate models of electrolyte solutions than the primitive model will yield non-vanishing higher components of the potentials of average force at infinite dilution and for this reason it is of interest to extend Mayer's theory to include *all* of the components of the potentials of average force.

In § 2 we give a statement of the part of the McMillan–Mayer theory [6] which pertains to this problem. The extension of Mayer's theory is developed in § 3. A further result in § 4 is the manipulation of the final expression of the extended Mayer theory to give a compact expression for the cluster integral sum. Some aspects of the results of this paper are briefly discussed in § 5.

2. THE MCMILLAN–MAYER THEORY

In this section we describe certain concepts of cluster theories, particularly of the McMillan–Mayer theory of multicomponent systems [6], in terms which are particularly appropriate to the present problem. A good introductory account of these theories has been given by Hill [7]. The notation used by Meeron [8] is adopted here with only minor changes.

We consider a solution consisting of unspecified solvent species and of solute species which are designated 1, 2, . . . s, . . . σ. These may be either ions or neutral molecules; the term 'molecule' will be used in either case. A set of numbers of solute molecules is

$$\mathbf{n}=n_1,\, n_2,\, \ldots\, n_s,\, \ldots\, n_\sigma, \tag{2.1}$$

and in order to have distinguishable sets we also use $\mathbf{k}$ and $\mathbf{u}$ for this purpose. Any such set is a subset of all of the solute particles in the system. The set of macroscopic concentrations of the solute molecules in the system (particle number densities) is

$$\mathbf{c}=c_1,\, c_2,\, \ldots\, c_s,\, \ldots\, c_\sigma. \tag{2.2}$$

The symbol $\{\mathbf{n}\}$ represents the spatial coordinates of the particles of the set $\mathbf{n}$. Round parentheses will be used in mathematical expressions only to indicate functional dependence, as $f(x)$ or $f(\{\mathbf{n}\})$. We also make the following conventions:

$$\mathbf{n}!=n_1!\, n_2!\, \ldots\, n_s!\, \ldots\, n_\sigma! \qquad \text{[product]}, \tag{2.3}$$

$$\mathbf{c}^{\mathbf{n}}=c_1^{\,n_1}\, c_2^{\,n_2}\, \ldots\, c_s^{\,n_s}\, \ldots\, c_\sigma^{\,n_\sigma} \qquad \text{[product]}, \tag{2.4}$$

$$n=n_1+n_2+\, \ldots\, +n_s+\, \ldots\, +n_\sigma. \tag{2.5}$$

The spatial distribution function at infinite dilution is [6, 7]

$$g_{\mathbf{k}}(\{\mathbf{k}\})=\lim_{c\to 0}\left[\frac{\text{Probability of observing } \mathbf{k} \text{ at } \{\mathbf{k}\}}{\mathbf{c}^{\mathbf{k}}}\right], \tag{2.6}$$

and is a measure of the mutual interaction of a set, $\mathbf{k}$, of solute molecules at coordinates, $\{\mathbf{k}\}$, averaged over the coordinates of the solvent molecules and the internal coordinates of the molecules of the set $\mathbf{k}$. The potential of average force at infinite dilution is

$$W_{\mathbf{k}}(\{\mathbf{k}\})=-kT\log(g_{\mathbf{k}}(\{\mathbf{k}\})). \tag{2.7}$$

This potential of average force is considered as a sum over component potentials (see Mayer [9], eqn. (24)):

$$W_{\mathbf{k}}(\{\mathbf{k}\})=\sum_{i,j\subset\mathbf{k}} w^{(2)}{}_{i,\,j}(\{i,j\})+\sum_{i,j,x\subset\mathbf{k}} w^{(3)}{}_{i,\,j,\,x}(\{i,j,x\})+\sum_{i,j,x,y\subset\mathbf{k}} w^{(4)}{}_{i,\,j,\,x,\,y}(\{i,j,x,y\})+\ldots \tag{2.8}$$

The first sum is over all pairs, i, j, which comprise a subset of $\mathbf{k}$, and $\{i,j\}$ are the coordinates of this pair in $\mathbf{k}$. The same relations apply between the larger subsets and $\mathbf{k}$. The last term in the series is $w_{\mathbf{k}}{}^{(k)}(\{\mathbf{k}\})$, but $w^{(k)}$ must be negligible for large k for the cluster method to succeed [9]. Given a model for the solution, one can in principle calculate $W_{i,j}(\{i,j\}) = w^{(2)}{}_{i,j}(\{i,j\})$ from the model for every kind of pair of solute molecules. Then $W_{i,j,x}(\{i,j,x\})$ can be calculated from the model and combined with three appropriate $w^{(2)}$ components according to equation (2.8) to obtain $w^{(3)}{}_{i,j,x}(\{i,j,x\})$. All of the $w^{(3)}$ components, corresponding to every different group of three solute molecules, can be calculated, and then a calculation of $W_{\mathbf{k}}$ for sets of four solute molecules leads to the $\omega^{(4)}$ component potentials. In the sequel we assume that all of the component potentials have been calculated from the model and we relate them to the thermodynamic properties.

Each component potential corresponds to a cluster function, $\gamma_{\mathbf{n}}{}^{(n)}(\{\mathbf{n}\})$:

$$\gamma_{\mathbf{n}}{}^{(n)} = \exp(-w_{\mathbf{n}}{}^{(n)}/kT) - 1. \tag{2.9}$$

Then, by equations 2.7, 2.8, and 2.9, $g_{\mathbf{k}}$ can be represented as a sum of terms such as

$$1 + \gamma^{(2)}{}_{i,j} + \gamma^{(2)}{}_{i,j}\gamma^{(2)}{}_{x,y} + \gamma^{(3)}{}_{i,j,x}\gamma^{(2)}{}_{i,x}\gamma^{(2)}{}_{j,x} + \gamma^{(2)}{}_{i,y}\gamma^{(2)}{}_{j,x} + \cdots,$$

where each subscript must be a subset of $\mathbf{k}$, a given cluster function never appears more than once in the same term, and, if all of the molecules in $\mathbf{k}$ are regarded as distinguishable, then every product of cluster functions which meets the first two conditions appears exactly once as a term in $g_{\mathbf{k}}$.

Each term of the cluster expansion of $g_{\mathbf{k}}$ may be represented as a topological graph on a *skeleton* consisting of a set of vertices, each of which corresponds to a molecule of the set, $\mathbf{k}$. A $\gamma^{(2)}{}_{i,j}$ cluster function is represented as a line connecting the vertices which correspond to the molecules, i,j of the set, $\mathbf{k}$. A $\gamma^{(3)}{}_{i,j,x}$ cluster function is represented as a triangle connecting the vertices which correspond to the molecules, i, j, x, of the set, $\mathbf{k}$. The extension to higher cluster functions is obvious and, although the graphs become harder to visualize, the topological description of the terms of the cluster expansion of $g_{\mathbf{k}}$ remains valid and convenient. The topological representation of a $\gamma^{(n)}$ cluster function is called a $\gamma^{(n)}$ *bond*. The representation of several terms is illustrated in figure 1.

If two vertices of a skeleton are directly connected by any $\gamma^{(n)}$ bond we say that there is an *edge* connecting these vertices. A *sequence* of edges joining two vertices, a, b, is an indirect connection by a chain: a, edge, vertex, edge, . . . edge, b; which contains at least one vertex in addition to a and b. Two vertices are said to be *at least doubly connected* if they are connected by at least one edge and one sequence of edges, or if they are connected by at least two sequences of edges which do not intersect at any third vertex. A graph on the skeleton of $\mathbf{k}$ is at least doubly connected if every pair of vertices of the skeleton of $\mathbf{k}$ is at least doubly connected by bonds of the graph.

Each term of the cluster expansion of $g_{\mathbf{k}}$ which corresponds to an at least doubly connected graph on the skeleton of $\mathbf{k}$ is now integrated over the $\{\mathbf{k}\}$ space, that is, over an infinite range of the spatial coordinates of all of the molecules in the set $\mathbf{k}$ but one. The sum of the resulting integrals is defined as $B_{\mathbf{k}}\mathbf{k}!$, with $B_{\mathbf{k}}$ called the irreducible cluster integral. If $k=2$, then $B_{\mathbf{k}}$ is exceptional and corresponds to the graph of two vertices and a $\gamma^{(2)}$ bond.

These formalities give a topological representation of the irreducible cluster integrals for multicomponent systems with higher components of the potentials of average force. The integral, $B_{\mathbf{k}}$, will include contributions from all of the doubly or more connected graphs on the skeleton of **k** which can be generated by the cluster expansion of $g_{\mathbf{k}}$, namely all such graphs in which there are no two $\gamma^{(n)}$ bonds joining exactly the same n vertices. The topological description of $B_{\mathbf{k}}$ is completed by noting that if the vertices of the skeleton of **k** correspond to k distinguishable molecules, then the terms of the cluster expansion are all distinguishable from each other. Each of these appears once in the integrand of $B_{\mathbf{k}}$, and then $B_{\mathbf{k}}$ corresponds to the sum of the integrals on all of the distinguishable graphs (subject to the two conditions just mentioned) on a skeleton of k distinguishable vertices. In the more general case in which some or all of the molecules of the set **k** are of the same species, some of the graphs become degenerate, but the multiplicity of their contribution to $B_{\mathbf{k}}$ is correspondingly increased. This combinatorial aspect is discussed in detail in § 3.2. Some of the graphs in the first few $B_{\mathbf{k}}$ are shown in figure 2.

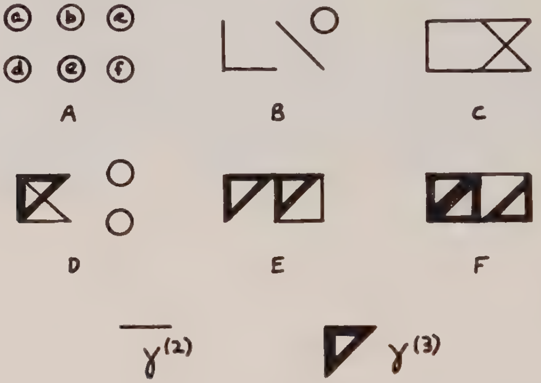

Figure 1. The topological representation of some terms of the cluster expansion of $g_{\mathbf{k}}$. In this example the set **k** is $1_a, 1_b, 1_c, 1_d, 1_e, 1_f$. The vertices of the skeleton of **k** which are not connected by any bonds are represented by circles. The correspondence of the vertices to the molecules of **k** is shown only in A. The correspondence to products of cluster functions is: $A=1$. $B=\gamma^{(2)}{}_{a,d}\gamma^{(2)}{}_{d,e}\gamma^{(2)}{}_{b,f}$. $C=\gamma^{(2)}{}_{a,b}\gamma^{(2)}{}_{b,c}\gamma^{(2)}{}_{c,e}\gamma^{(2)}{}_{a,d}\gamma^{(2)}{}_{d,e}\gamma^{(2)}{}_{e,f}\gamma^{(2)}{}_{b,f}$. $D=\gamma^{(2)}{}_{d,e}\gamma^{(2)}{}_{a,e}\gamma^{(3)}{}_{a,b,d}$. $E=\gamma^{(2)}{}_{c,f}\gamma^{(2)}{}_{e,f}\gamma^{(3)}{}_{a,b,d}\gamma^{(3)}{}_{b,e,c}$. $F=\gamma^{(2)}{}_{b,c}\gamma^{(3)}{}_{a,b,d}\gamma^{(3)}{}_{b,d,e}\gamma^{(3)}{}_{c,e,f}$. Only C and F are at least doubly connected graphs on the skeleton of **k**.

It seems worthwhile to also point out that in the case of a one component system,

$$B_{\mathbf{k}} \rightarrow B_k = \beta_{k-1}/k, \tag{2.11}$$

where β_k is the irreducible cluster integral as usually defined for one-component systems [7].

McMillan and Mayer [6] have shown that the cluster integral sum,

$$\mathbf{S} = \textstyle\sum_{\mathbf{k}} B_{\mathbf{k}} \mathbf{c}^{\mathbf{k}}, \tag{2.12}$$

is simply related to the osmotic pressure of the solution and this is the basis of the calculation of the thermodynamic properties of the solution from the potentials of average force at infinite dilution. The summation in equation (2.12) is over all sets, **k**, of solute particles such that $k \geqslant 2$. However, in the case that some or all of the solute molecules are ions, many of the $B_{\mathbf{k}}$ are divergent as a result of the long range character of the $\gamma^{(2)}$ bonds [1]. In order to get a useful expression for **S** it is then necessary to regroup the contributions to this sum.

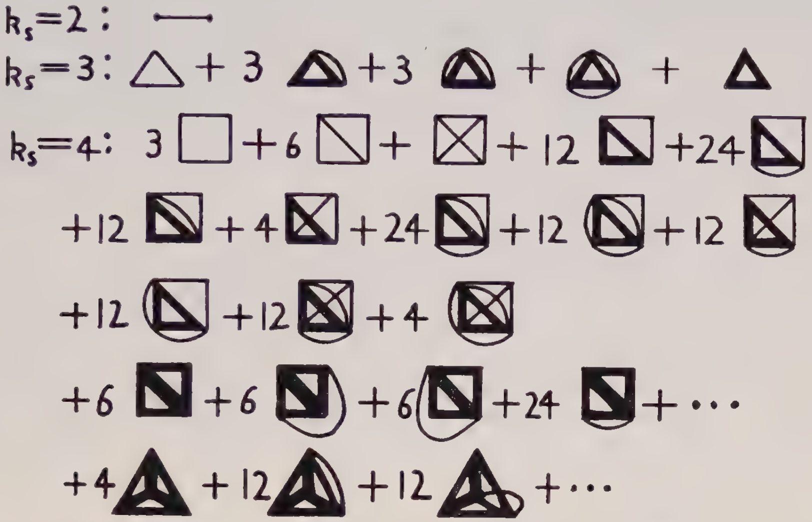

Figure 2. The topological representation of the terms in the integrands of the first few irreducible cluster integrals for clusters of only one species of solute ($\mathbf{k} = k_s$). The graphs in the bottom row each represent three $\gamma^{(3)}$ bonds. The terms with four $\gamma^{(3)}$ bonds or one $\gamma^{(4)}$ bond are omitted. $\gamma^{(2)}$ bonds are represented by straight or curved lines in this figure.

3. THE EXTENSION OF MAYER'S THEORY

The $\gamma^{(2)}$ bonds appearing in **S** may be expanded by the method divised by Mayer ([1], equations (8), (11)–(14)), who there considered *only* $\gamma^{(2)}$ bonds.

The first step is to expand the pairwise component potential into an ideal Coulomb part and a short range part:

$$w^{(2)}_{i,j}(R_{ij}) = w^*_{i,j}(R_{i,j}) + z_i z_j \epsilon^2/DR_{ij}. \tag{3.1}$$

Here R_{ij} is the separation of the molecules and D is the macroscopic dielectric constant of the pure solvent in the reference state. Because $w^{(2)}_{i,j}$ is to be calculated from the model and the Coulomb term is completely defined, equation (3.1) serves as the definition of $w^*_{i,j}$. The only property of $w^*_{i,j}$ which is of importance in this section is that, unlike the Coulomb potential, it is short range, i.e. it does not contribute to the divergence of the $B_{\mathbf{k}}$ integrals.

Now it is necessary to expand the cluster function for two particles in the following way:

$$\begin{aligned}\gamma^{(2)}_{i,j} &= \exp(-w^*_{i,j}/kT)exp(-z_i z_j \lambda g_{ij}) - 1 \\ &= k_{i,j} + [k_{i,j}+1]\textstyle\sum_{p\geq 1}[-z_i z_j \lambda g_{ij}]^p/p\,!,\end{aligned} \tag{3.2}$$

where

$$k_{i,j} = \exp(-w^*_{i,j}(R_{ij})/kT) - 1, \tag{3.3}$$

$$\lambda = 4\pi\epsilon^2/DkT, \tag{3.4}$$

$$g_{ij} = 1/4\pi R_{ij}. \tag{3.5}$$

This expansion of $\gamma^{(2)}{}_{i,j}$ in terms of k_{ij} and g_{ij} corresponds to replacing each graph in which there is a $\gamma^{(2)}$ bond by an infinity of graphs with zero or one k bond and any number of g bonds in place of the $\gamma^{(2)}$ bond. This expansion of the graphs corresponding to terms of the $B_{\mathbf{k}}$ is illustrated for two examples in figure 3. The coefficients (numerical and powers of λ and z_iz_j) which result from the expansion are not shown in the figure. Each of the graphs resulting from the expansion contributes to the same irreducible cluster integral as the parent graph.

In the expanded graphs those vertices which lie at the junction of exactly two g bonds are called *g-bond nodes.* A sequence of g bonds connected by g-bond nodes is said to be a *g-bond chain.* Just two of the graphs in figure 3 have any g-bond chains.

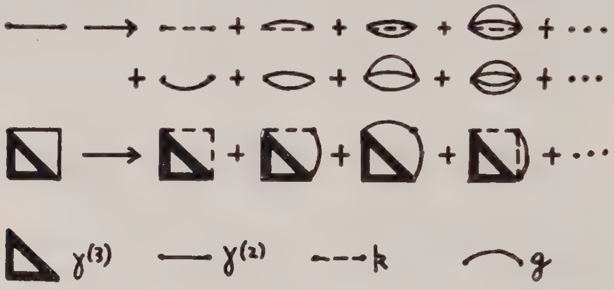

Figure 3. The expansion of graphs corresponding to the exponential expansion of equation (3.2).

For a given graph on the skeleton of $\mathbf{k}$ the vertices of the skeleton which are g-bond nodes correspond to the subset $\mathbf{n}$ of $\mathbf{k}$. The remainder of $\mathbf{k}$ is designated $\mathbf{u}$. Thus $\mathbf{k}=\mathbf{n}+\mathbf{u}$. Now the cluster integral sum is rewritten as

$$\mathbf{S}=\mathbf{S}_l+\mathbf{S}_c+\textstyle\sum_{u\geqslant 2}\mathbf{S}_u. \tag{3.6}$$

The sum, $\mathbf{S}_l$, is the sum over all integrals corresponding to graphs which consist of two vertices connected by a single g bond. Mayer [1] has shown that

$$\mathbf{S}_l=0. \tag{3.7}$$

The sum over all of the integrals corresponding to graphs in which $u=0$ is $\mathbf{S}_c$. Such graphs are simple cycles of g bonds, and as Mayer [1] has shown,

$$\mathbf{S}_c=\kappa^3/12\pi, \tag{3.8}$$

where

$$\kappa^2=\lambda\textstyle\sum_s c_s z^2{}_s. \tag{3.9}$$

The sum, $\mathbf{S}_u$, is the sum over all integrals corresponding to graphs in which there are u vertices which are not g-bond nodes, except that those graphs in which $u=2$ and which have been included in $\mathbf{S}_l$ are not included in $\mathbf{S}_2$ as well. Mayer has calculated some of the terms of $\mathbf{S}_u$, namely those terms which he designates as $S^{(l,m)}$ [1], and his calculation forms the basis of the following development.

3.1. *Classification of the terms of* $\mathbf{S}_u$

The terms of the integrand of $\mathbf{S}_u$ correspond to a wide variety of graphs which we now proceed to classify in detail. We write

$$\mathbf{S}_u=\textstyle\sum_{\mathbf{u}}\mathbf{c}^{\mathbf{u}}\sum_{\tau}\sum_{\boldsymbol{\nu}}\sum_{\langle n_{si}\rangle}\mathbf{c}^{\mathbf{n}}K(\mathbf{u},\tau_i,\boldsymbol{\nu},\langle n_{si}\rangle)I(\mathbf{u},\tau_i,\boldsymbol{\nu},\langle n_{si}\rangle), \tag{3.10}$$

the expansion of $\mathbf{S}_u$ as a sum of integrals, I, over specified graphs. These integrals and the combinatorial factor, K, are discussed in later sections of this paper. The summation over $\mathbf{u}$ in equation (3.10) is over all compositions, $\mathbf{u}$, of those vertices of the graphs which are not g-bond nodes. This set of vertices will be called the skeleton of $\mathbf{u}$. Because $\mathbf{u}$ is only the set of the numbers of molecules of each species, it gives only the overall composition of its skeleton and does not specify which species occupies a given vertex. This is only sufficient if the vertices are all equivalent to the molecules, so the summation over τ is defined in such a way as to satisfy this condition.

The symbol, τ, represents a partial topological description of the graph. It specifies the number and interconnections of k, $\gamma^{(3)}$, $\gamma^{(4)}$, ... bonds, but *not* g bonds, on the skeleton of $\mathbf{u}$. There will be some topological descriptions of this sort, say τ_1, τ_2, τ_3, ... which are distinguishable from each other if and only if the vertices of the skeleton of $\mathbf{u}$ are distinguishable, e.g. if these vertices are numbered from 1 to u. A complete set of all of the topological descriptions which are related to each other in this way is said to comprise a *protograph*, $\boldsymbol{\tau}$. Protographs are not necessarily at least doubly connected, the reason being that (usually multiple) g-bonds between the vertices of the skeleton of $\mathbf{u}$ are by definition omitted and are considered later. These relations are illustrated in figure 4.

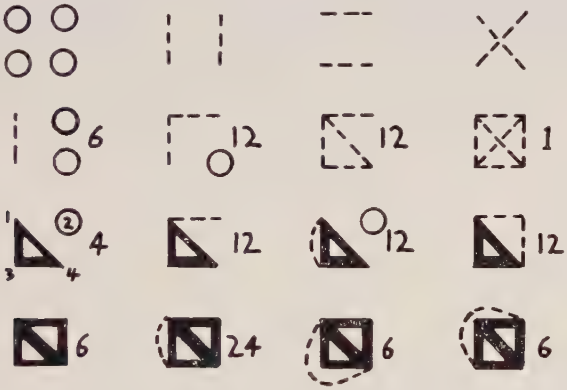

Figure 4. Some protographs on a skeleton of four vertices. In the top row there are two protographs, one having one element and the other having three. In the remaining rows the number of elements in each protograph is given by the number to the right of the graph. The bonds are represented in the same way as in figure 3. Vertices which are not connected by any bonds are represented as circles. The protograph with numbered vertices is referred to in the text.

In order to make the vertices of the skeleton of $\mathbf{u}$ all equivalent to the molecules it is necessary to sum over all of the elements of each protograph, or in other words, over all of the permutations of each protograph on the skeleton of $\mathbf{u}$. In order to include all of the graphs which contribute to $\mathbf{S}_u$ it is also necessary to sum over all possible protographs. The simplest of these is the skeleton of $\mathbf{u}$ itself, and we may proceed to develop more complicated protographs by adding k, $\gamma^{(3)}$, $\gamma^{(4)}$, ... bonds until we attain the most complicated protograph on the given skeleton, in which every pair of vertices is connected by a k bond, every three vertices by a $\gamma^{(3)}$ bond, ... and the u vertices are also connected by a $\gamma^{(u)}$ bond. (However the success of the cluster expansion method depends upon

$\gamma^{(n)}$ being negligible for n large enough [9].) Thus the second summation in equation (3.10) is really a double summation,

$$\textstyle\sum_{\boldsymbol{\tau}}=\sum_{\boldsymbol{\tau}}\sum_{\tau_i}, \qquad (3.11)$$

first over all possible protographs and then over all of the elements of each protograph. In some cases, for instance the simplest and most complicated protographs just described, $\boldsymbol{\tau}$ has only one element, but in general it has many, up to a limit of $u!$ elements.

The protographs may be thought of as derived from the graphs by removing all of the g bonds and the skeleton of $\mathbf{n}$ from the latter. The remaining two summations in equation (3.10) are summations over classes of graphs which reduce to the same protograph.

We next attach the g bonds to the protographs. For a given element of a protograph, τ_i, we number the vertices of the skeleton of $\mathbf{u}$, as $1, 2, \ldots j, \ldots u$. A general pair of vertices is now designated as j, j'. The summation over $\boldsymbol{\nu}$ is over all sets,

$$\boldsymbol{\nu}=\nu_{1,2}, \nu_{1,3}, \ldots \nu_{2,3}, \nu_{2,4}, \ldots$$

of numbers, $\nu_{j,j'}$, of g bonds connecting the pairs of vertices of the skeleton of $\mathbf{u}$, subject to two conditions. The first condition on $\boldsymbol{\nu}$ is that the graph described by τ_i, $\boldsymbol{\nu}$, be an at least doubly connected graph on the skeleton of $\mathbf{u}$, and the second condition is that this graph have no g-bond nodes. For example, referring to the graph with numbered vertices in figure 4, these conditions are met by only the following:

$$\nu_{3,4}\geqslant 0,\ \nu_{1,4}\geqslant 0,\ \nu_{1,3}\geqslant 0, \text{ together with either}$$

$$\nu_{1,2}\nu_{2,4}\nu_{2,3}\geqslant 1,$$

$$\nu_{1,2}=0,\ \nu_{2,4}\nu_{2,3}\geqslant 2,$$

$$\nu_{2,4}=0,\ \nu_{2,3}\nu_{1,2}\geqslant 2,$$

or

$$\nu_{2,3}=0,\ \nu_{1,2}\nu_{2,4}\geqslant 2.$$

Therefore the smallest set, $\boldsymbol{\nu}$, in this sum is not in general the empty set, $\boldsymbol{\nu}=0$. This observation is of importance in §4. A graph which is defined by the characteristics, $\mathbf{u}$, τ_i, $\boldsymbol{\nu}$, is called a *prototype* by Mayer [1].

The summation over $\langle n_{si}\rangle$ in equation (3.10) is over all of the graphs which may be obtained from a given prototype by replacing some or all of the g bonds in the prototype by g-bond chains. We number the g bonds of the prototype $1, 2, \ldots i, \ldots \nu$. The composition of the g-bond chains in the graph is given by $\langle n_{si}\rangle$, which may be thought of as a two-dimensional array of numbers, n_{si}. Each of these is the number of molecules of species s in the ith g-bond chain. The ith g-bond chain is derived from the ith bond of the prototype by inserting

$$n_i=\textstyle\sum_s n_{si}$$

g-bond nodes. The smallest set, $\langle n_{si}\rangle$, is the empty set, $\langle n_{si}\rangle=0$, because the prototype graphs themselves represent integrals which contribute to $\mathbf{S}_u$. It is also true that for any graph summed in $\mathbf{S}_u$,

$$\mathbf{n}=\textstyle\sum_i n_{1i}, \sum_i n_{2i}, \ldots \sum_i n_{si}, \ldots \sum_i n_{\sigma i}, \qquad (3.12)$$

is the set of molecules occupying the g-bond nodes, and that a graph which is classified as $\mathbf{u}$, τ_i, $\boldsymbol{\nu}$, $\langle n_{si}\rangle$ here is found in that $B_{\mathbf{k}}$ of equation (2.12) for which $\mathbf{k}$ is given by

$$\mathbf{k}=\mathbf{n}+\mathbf{u}. \qquad (3.13)$$

This completes our classification of the graphs corresponding to terms in the irreducible cluster integrals. The classification, $\mathbf{u}$, τ_i, $\boldsymbol{\nu}$, $\langle n_{si}\rangle$, does not, however, completely specify a graph, for all graphs which differ only in the order of molecules of various species within the individual g-bond chains will have the same classification. They will be said to comprise a *class of graphs*. A more detailed classification is not required in this problem because, as one may deduce directly from the convolution theorem, the integration over the g-bond chains gives the same result for all graphs belonging to the same class. The application of the convolution theorem to these problems has been considered by Montroll and Mayer [10] and by Meeron [11]. We return to this in §3.3.

We recapitulate the hierarchy of the present classification of graphs:

protograph: $\mathbf{u}$, $\boldsymbol{\tau}$;

element of a protograph: $\mathbf{u}$, τ_i;

prototype: $\mathbf{u}$, τ_i, $\boldsymbol{\nu}$;

class of graphs; $\mathbf{u}$, τ_i, $\boldsymbol{\nu}$, $\langle n_{si}\rangle$;

graph of a term of $B_{\mathbf{k}}$; $\mathbf{u}$, τ_i, $\boldsymbol{\nu}$, $\langle n_{si}\rangle$, specified order of molecules in each chain.

In the protographs all of the vertices of the skeleton of $\mathbf{u}$ are equivalent. Likewise, if one considers the infinity of graphs which may be derived from a given protograph, all of the vertices of the skeleton of $\mathbf{u}$ are again equivalent because this infinity of graphs includes all permutations of all of the graphs on the skeleton of $\mathbf{u}$, the vertices of this skeleton being considered as numbered from 1 to u in order to define these permutations.

3.2. *The combinatorial factor*, $K(\mathbf{u}, \tau_i, \boldsymbol{\nu}, \langle n_{si}\rangle)$

One contribution to this factor is $1/\mathbf{k}!$ from the definition of the cluster integrals, $B_{\mathbf{k}}$. The remaining contributions stem from the number of terms in the cluster expansion of $g_{\mathbf{k}}$ represented by each graph, the number of graphs in the class of graphs, the factorials generated by the exponential expansion in equation (3.2), and certain corrections associated with the arbitrary assignment of numbers to the g bonds in the prototype graphs.

In the following discussion we give 'distinguishable' the special meaning that 'distinguishable' graphs on the skeleton of $\mathbf{k}$ can be distinguished from each other by topological criteria if the vertices of the skeleton are themselves considered to be distinguishable, for example if they are numbered from 1 to k. Then the multiplicative process leading to the cluster expansion of $g_{\mathbf{k}}$ can be described by saying that there results one term in the cluster expansion corresponding to each possible 'distinguishable' graph on the skeleton of $\mathbf{k}$. By reference to §2 we conclude that those graphs are possible which have no two k bonds joining the same two vertices and no two $\gamma^{(n)}$ bond joining the same n vertices. Finally it follows that there is one term in the integrand of $B_{\mathbf{k}}$ corresponding to every possible, 'distinguishable', at least doubly connected graph on the skeleton of $\mathbf{k}$, and this is the basis of our calculation of K.

The number of ways of dividing the molecules of the set $\mathbf{k}$ into the subsets $\mathbf{u}$ and $\langle n_{si}\rangle$ is

$$N_a = \mathbf{k}!/\mathbf{u}!\textstyle\prod_s\prod_i n_{si}!.$$

This corresponds to the number of distinguishable subdivisions only in the hypothetical case that the molecules of each species are distinguishable from each other. We group the elements of the two-dimensional array, $\langle n_{si} \rangle$, into sets corresponding to the nodes of the g-bond chains:

$$\mathbf{n}_i = n_{1i},\ n_{2i},\ \ldots\ n_{si},\ \ldots\ n_{\sigma i}. \tag{3.14}$$

Then the number of arrangements of the molecules corresponding to different orders within the individual g-bond chains of a graph is

$$N_b = \prod_i \mathbf{n}_i!,$$

and again this is a number of distinguishable arrangements only in the hypothetical case that the molecules of each species are distinguishable from each other. The number of arrangements of the molecules corresponding to rearrangements on the skeleton of $\mathbf{u}$ is not considered here because this factor, which depends upon the topology, is taken into account by the summation ever elements of protographs and the summation over $\boldsymbol{\nu}$.

If the molecules of each species were distinguishable from each other, then the number of distinguishable graphs on the skeleton of $\mathbf{k}$ with the same number and connections of bonds of the various kinds would be the same as the number of ‘ distinguishable ’ graphs with these characteristics. Therefore, apart from the correction factor to be considered, $N_a N_b$ is the number of ‘ distinguishable ’ graphs corresponding to a class of graphs and it is the contribution to K corresponding to the number of terms in $\mathbf{S}$ represented by a single class of graphs.

The correction factor is based upon the fact that there are different sets, $\langle n_{si} \rangle$, which do not correspond to ‘ distinguishable ’ graphs if they have the same remaining characteristics: $\mathbf{u}$, τ_i, $\boldsymbol{\nu}$, order of molecules in chains. For example, if i_1 and i_2 are two g-bond chains with the same endpoints on the skeleton of $\mathbf{u}$, and there are two sets, $\langle n_{si} \rangle$ and $\langle n_{si} \rangle'$, which are identical except that $\mathbf{n}_{i_1}$ and $\mathbf{n}_{i_2}$ in one are replaced, respectively, by $\mathbf{n}_{i_2}$ and $\mathbf{n}_{i_1}$ in the other, then these two sets do not correspond to ‘ distinguishable ’ graphs. In order to calculate the correction factor we divide $\nu_{j,j'}$, the total number of direct g bonds and of g-bond chains from j to j' of the skeleton of $\mathbf{u}$, into two parts,

$$\nu_{j,j'} = \bar{\nu}_{j,j'} + \nu_{j,j'},$$

where $\bar{\nu}$ is the number of direct g bonds and $\tilde{\nu}$ is the number of g-bond chains The correction factor in K to account for the fact that the interchange of g-bond chains with the same endpoints does not correspond to making distinguishable graphs, even when all of the molecules in each chain are considered to be distinguishable, is then

$$1/\prod_{j,j'} \tilde{\nu}_{j,j'}!.$$

There is also a factor in K given by

$$1/\prod_{j,j'} \bar{\nu}_{j,j'}!,$$

which comes from the exponential expansion, equation (3.2), which generates the multiple g bonds. Finally, we recognize that the interchange of a g bond and a g-bond chain with the same endpoints, although corresponding to a change from one $\langle n_{si} \rangle$ to another, does not correspond to making a different ‘ distinguishable ’ graph. For each pair of vertices of the skeleton of $\mathbf{u}$ the number of such interchanges is

$$\nu!/\bar{\nu}!\tilde{\nu}!$$

and the reciprocal of this number is also a factor in K. All of these factors related to $\mathbf{v}$ combine to give a factor in K of $1/\mathbf{v}!$.

The final result of this section is

$$K(\mathbf{u}, \tau_i, \mathbf{v}, \langle n_{si}\rangle) = \prod_i[n_i!]/\mathbf{u}!\mathbf{v}!\prod_s\prod_i[n_{si}!]. \tag{3.15}$$

3.3. *Integration over g-bond chains*

The integral in equation (3.10) is a multiple integral over the coordinates of $k-1$ molecules, one of the molecules of the set $\mathbf{u}$ being arbitrarily chosen as the origin of coordinates. Now consider, for a given graph, the integration over the coordinates of the molecules in the g-bond chains, the molecules of the skeleton of $\mathbf{u}$ being in an arbitrary, fixed configuration. The lengths of the bonds in each g-bond chain are then independent of the lengths of the bonds in the other g-bond chains. Then we may write,

$$I(\mathbf{u}, \tau_i, \mathbf{v}, \langle n_{si}\rangle) = \int f(\mathbf{u}, \tau_i)\, d\{\mathbf{u}\}\prod_i[I_i(j, j', \mathbf{n}_i)], \tag{3.16}$$

where $f(\mathbf{u}, \tau_i)$ is a product of cluster functions corresponding to the element of the protograph and I_i is the integral over the ith g-bond chain or g bond. This integral depends upon the charges and coordinates of the molecules at j and j', the vertices of the skeleton of $\mathbf{u}$ which are the endpoints of the particular chain, and it depends upon the composition of the chain, $\mathbf{n}_i$.

In the case that $\mathbf{n}_i$ is an empty set, then $I_i(j, j', \mathbf{n}_i)$ is simply a g bond,

$$-\lambda z_j z_{j'} g(R_{jj'}).$$

In the general case it is

$$I_i = -\lambda z_j z_{j'} \prod_s[-\lambda z_s{}^2]^{n_{si}}\, q_{n_i}(R_{jj'}), \tag{3.17}$$

where

$$q_{n_i}(R_{jj'}) = \int g(\{j, 1\})g(\{1, 2\})g(\{2, 3\}) \ldots g(\{n_i, j'\})\, d\{1, 2, \ldots n_i\}, \tag{3.18}$$

is an integral depending only upon the number of particles in the chain and upon its length, $R_{jj'}$. These equations are now combined with equation (3.10), using the fact that $\sum_{\langle n_{si}\rangle} = \prod_i \sum_{n_i}$ if the summand is factorable, as in the present case. We obtain,

$$\mathbf{S}_u = \sum_{\mathbf{u}}[\mathbf{c}^{\mathbf{u}}/\mathbf{u}!]\sum_\tau \int f(\mathbf{u}, \tau_i)\, d\{\mathbf{u}\}\sum_{\mathbf{v}}[1/\mathbf{v}!]\prod_i q_i, \tag{3.19}$$

where

$$\begin{aligned} q_i &= \sum_{\mathbf{n}_i}\{\mathbf{c}^{\mathbf{n}_i}\, n_i![-\lambda z_j z_{j'}]\prod_s[-\lambda z_s{}^2]^{n_{si}}\, q_{n_i}(R_{jj'})/\prod_s n_{si}!\} \\ &= -\lambda z_j z_{j'} \sum_{n_i=0}[-\kappa^2]^{n_i}\, q_{n_i}(R_{jj'}). \end{aligned} \tag{3.20}$$

In equation (3.20) the third member is obtained from the second by the use of the multinomial theorem and κ is defined by,

$$\kappa^2 = \lambda \sum_s [c_s z_s{}^2]. \tag{3.21}$$

Mayer [1] has evaluated q_{n_i} by a convolution method and has shown that

$$q_i = -\lambda z_j z_{j'} \exp(-\kappa R_{jj'})/4\pi R_{jj'}. \tag{3.22}$$

We note from this equation that all q bonds that join two given vertices, j and j', are the same function of $R_{jj'}$ and may be designated as $q_{jj'}$. We also note that the product over g-bond chains in equation (3.19) is simply related to the product over pairs of vertices of the skeleton of $\mathbf{u}$, and then we have

$$[1/\boldsymbol{\nu}\,!]\textstyle\prod_i q_i = \prod_{j,j'}\{[q_{j,j'}]^{\nu_{j,j'}}/\nu_{j,j'}\,!\}. \tag{3.23}$$

The final result of this section is obtained by combining equations (3.19) and (3.23):

$$\mathbf{S}_u = \textstyle\sum_{\mathbf{u}}[\mathbf{c}^{\mathbf{u}}/\mathbf{u}\,!]\sum_\tau \displaystyle\int f(\mathbf{u},\tau_i)\,d\{\mathbf{u}\}\textstyle\sum_{\boldsymbol{\nu}}\prod_{j,j'}\{[q_{jj'}]^{\nu_{j,j'}}/\nu_{j,j'}\,!\}. \tag{3.24}$$

4. SUMMATION OVER SERIES OF PROTOTYPES

The summation over $\boldsymbol{\nu}$ in equation (3.24) is *almost* the expansion of a product of exponential functions (Meeron [4, 12]):

$$\textstyle\prod_{j,j'}\exp(q_{j,j'}).$$

The inaccuracy arises because for some $\boldsymbol{\tau}$ the smallest set in the summation is not the empty set, $\boldsymbol{\nu}=0$. This happens because every prototype formed by introducing g bonds into a protograph must be an at least doubly connected graph on the skeleton of $\mathbf{u}$ with no g-bond chains. However it is possible to use the exponential to sum the infinite series in $\boldsymbol{\nu}$ and then to correct for the 'error' made in including the lowest terms of the series if these terms do not correspond to protoypte graphs.

There is one other difficulty in this summation, namely that the function, $\exp(q_{j,j'})$ has an essential singularity at the origin ($R_{jj'}=0$) if $z_j z_{j'}<0$ and therefore any graph with such a 'bond' corresponds to a divergent integral. This difficulty may be surmounted by combining certain prototypes derived from different protographs.

We proceed by reference to figure 5, where parts of several series of prototypes are illustrated. The composition, $\mathbf{u}$, of the skeletons makes no difference in the following procedure except that we will only combine prototoypes in which the corresponding vertices have the same composition. The graphs to the left of the bar in each series correspond to false prototypes, which are introduced by the expansion of a product of exponentials but which are not terms in $\mathbf{S}_u$. We observe that for every prototype with g bonds but no k bonds between some pairs of points of the skeleton, there is another prototype which is the same in every respect except that it also has k bonds connecting these vertices. Note that the reverse of this statement is not true. However the first observation enables us to combine prototypes additively to produce integrands of convergent integrals because as $R_{ij} >0$, $1+k_{ij} >0$ sufficiently fast so that $[1+k_{ij}]\exp(q_{ij})$ also goes to zero. As a result, the summations may be performed as desired by combining every series having a pair of vertices of the skeleton of $\mathbf{u}$ with no k bond with another series having a k bond in this place.

We first consider $\mathbf{S}_2$, for which these relations are obvious.

$$\mathbf{S}_2 = \textstyle\sum_{\mathbf{u}}[\mathbf{c}^{\mathbf{u}}/\mathbf{u}\,!]\sum_\tau \displaystyle\int f(\mathbf{u},\tau_i)\,d\{\mathbf{u}\}\textstyle\sum_{\boldsymbol{\nu}}[q^{\nu}/\boldsymbol{\nu}\,!]. \tag{4.1}$$

There are only two possibilities for $f(\mathbf{u},\tau_i)$ in this case:

$$f(\mathbf{u},\tau_i)=1\ \ldots\ \text{no } k \text{ bond}$$

$$\text{or } =k(\mathbf{u})\ \ldots\ k \text{ bond}.$$

In the former case the lowest value of ν is 3†, in the latter it is zero. Thus we have

$$\mathbf{S}_2 = \sum_{\mathbf{u}} [\mathbf{c}^{\mathbf{u}}/\mathbf{u}\,!] \int d\{\mathbf{u}\} [e^q - 1 - q - q^2/2\,! + ke^q]. \tag{4.2}$$

In this case $\{\mathbf{u}\}$ is simply the vector from one molecule of $\mathbf{u}$ to the other and q and k are functions of the length of this vector and of the composition, $\mathbf{u}$.

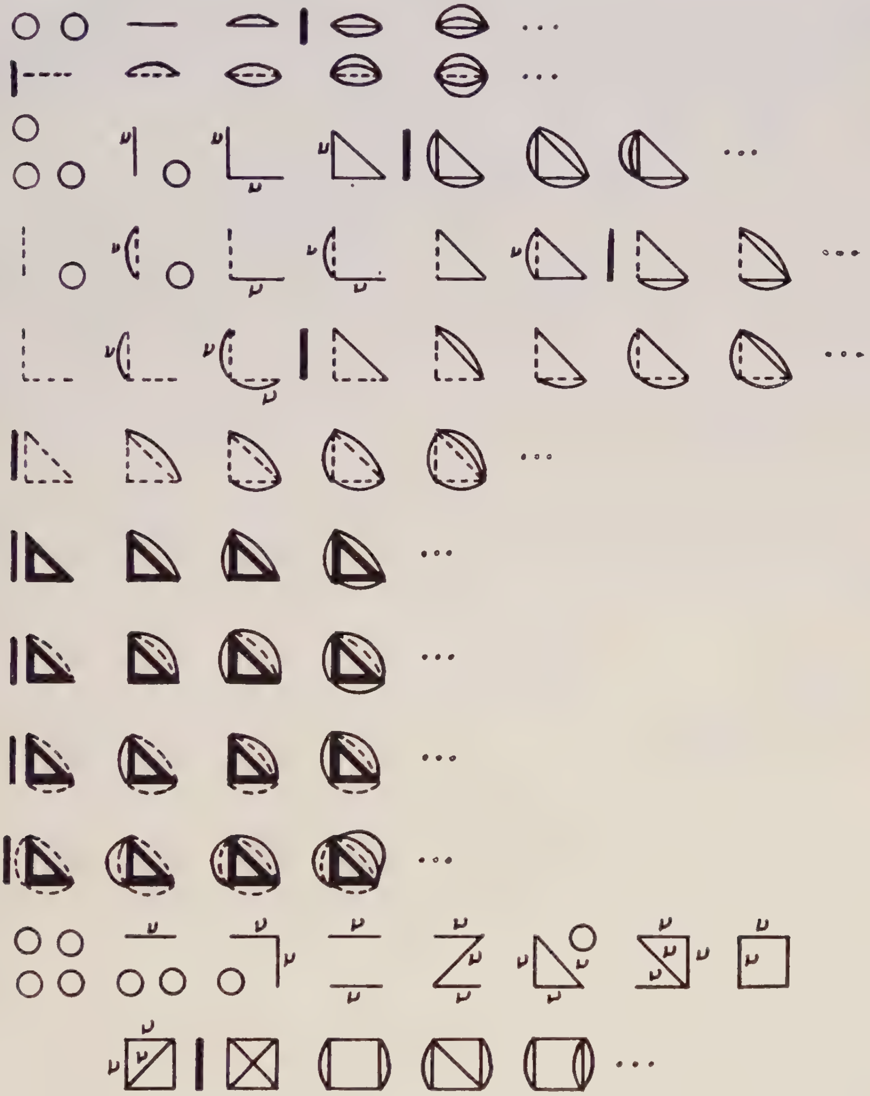

Figure 5. Some series of prototype graphs. The vertical bar in each series divides false prototypes on the left from true prototypes on the right. A ν next to a g bond indicates that the graph remains a false prototype for any multiplicity of this bond from 1 to ∞. The bonds are represented in the same way as in figure 3 except that here the g bonds may be either straight or curved lines. There are no $\gamma^{(2)}$ bonds in this figure.

---

† The case, $\nu = 2$, has been included in $\mathbf{S}_c$.

It is convenient to define a new class of bonds as follows (see Meeron [12] for another example of this procedure):

$$\left.\begin{aligned}\Phi &= [1+k]e^{q} = \exp(q - w^*/kT),\\ \Phi' &= \Phi - 1\\ \Phi'' &= \Phi - 1 - q\\ \Phi''' &= \Phi - 1 - q - q^2/2.\end{aligned}\right\} \tag{4.3}$$

These pairwise bonds are all functions of the charges and short-range interactions of the molecules they connect and of the distance between them. The integral in $\mathbf{S}_2$ is an integral over a Φ''' bond. It is sometimes useful to represent $\mathbf{S}_2$ in another way:

$$\mathbf{S}_2 = [\textstyle\sum_s c_s]^2 \tfrac{1}{2} I^{(2)}. \tag{4.4}$$

Here $I^{(2)}$ is the integral of a Φ''' bond on the *empty* skeleton of $\mathbf{u}$, and the operation in the right-hand member is not simply multiplicative, but involves instructions from $[\sum c_s]^2$ as to the composition of the skeleton of $\mathbf{u}$. The instructions are obtained by making the multinomial expansion of $[\sum c_s]^2$, after which each term of the expansion multiplies an integral having the functional form of $I^{(2)}$ on a skeleton of the same composition as the term itself. Thus $\frac{1}{2}c_s c_t$ multiplies an integral in which a Φ''' bond connects a molecule of species s to one of species t. This is simply a procedure for recovering equation (4.2) from the more compact form, equation (4.4).

In the case of the prototypes related to $\mathbf{S}_3$ there is an infinite number of false prototypes. The procedure of collecting the terms in the proper way becomes very tedious but it is easy to verify that the answer, once obtained, correctly expands to yield all of the prototypes and none of the false prototypes. The correct result is

$$\mathbf{S}_3 = [1/3\,!][\textstyle\sum c_s]^3 I^{(3)}. \tag{4.5}$$

The integral, $I^{(3)}$, has terms in its integrand corresponding to the three protographs:

$A = \Phi''_{1,2}\Phi''_{2,3}\Phi''_{1,3}$,

$B = \Phi''_{1,2}\Phi''_{2,3}q_{1,3}$ (threefold, but only one element shown here),

$C = \gamma^{(3)}_{1,2,3}\Phi_{1,3}\Phi_{2,3}\Phi_{1,2}$.

This is a slightly different use of the term 'protograph' than that in §3 but the difference merely corresponds to the change from k and g bonds to q and Φ bonds. It is clear that in A, B, and C the vertices are all equivalent to the molecules (one must consider the three elements of B), so it is sufficient to specify the overall composition of the skeleton. This is done by considering the multinomial expansion of $[\sum_s c_s]^3$ and multiplying each term of the expansion by an $I^{(3)}$ on a skeleton of the same composition as the term itself.

Now we expand the function corresponding to the first protograph,

$$\begin{aligned}A = {}&[k_{1,2}\exp(q_{1,2}) + \exp(q_{1,2}) - 1 - q_{1,2}][k_{2,3}\exp(q_{2,3}) + \exp(q_{2,3}) - 1 - q_{2,3}]\\ &\times [k_{1,3}\exp(q_{1,3}) + \exp(q_{1,3}) - 1 - q_{1,3}].\end{aligned} \tag{4.6}$$

This corresponds to all possible graphs on a skeleton of three vertices in which each pair of vertices is connected by either (i) a k bond with any number of q bonds or (ii) two or more q bonds.

The prototypes in which a pair of vertices is connected by a single q bond are all produced by the expansion of B. It is clear that in this case the other two pairs of vertices will be connected by either (i) or (ii) as described above. Finally, in the prototypes with a $\gamma^{(3)}$ bond, the empty set, $\mathbf{v}=0$, is the lower limit of summation over $\mathbf{v}$ in equation (3.24) (with $u=3$) and correspondingly the expansion of C produces prototypes in which every pair of points is connected by an edge of a $\gamma^{(3)}$ bond plus zero or one k bond and plus any number, $\geqslant 0$, of q bonds.

In the general case, $u \geqslant 3$, we write

$$\mathbf{S}_u = [1/u!][\sum c_s]^u I^{(u)}, \tag{4.7}$$

and then consider the protographs which contribute to $I^{(u)}$. These may be constructed by the following procedure:

(*a*) Form all possible configurations of $\gamma^{(3)}$, $\gamma^{(4)}$, . . . bonds on the skeleton of $\mathbf{u}$, beginning with the skeleton itself as the first such configuration.

(*b*) In each distinguishable graph produced in (*a*), every pair of vertices which is at least doubly connected by sequences of edges on $\gamma^{(3)}$, $\gamma^{(4)}$, . . . bonds must also be connected by a Φ bond.

(*c*) In each graph produced by the steps, (*a*, *b*), the pairs of vertices which remain not directly connected may be connected by Φ'' and q bonds to form an at least doubly connected graph on the skeleton of $\mathbf{u}$ with no q-bond chains. Every way of doing this which is topologically distinguishable from the others when the vertices of the skeleton of $\mathbf{u}$ are unlabelled is a protograph.

The elements of each protograph are then obtained by numbering the vertices of the skeleton of $\mathbf{u}$ and representing all distinguishable permutations of the numbers on the skeleton of each protograph. The criterion of distinguishability must be topological and not merely geometrical. Finally, for a more detailed calculation, the composition of the skeleton is obtained by making the multinomial expansion of $[\sum c_s]^u$ and multiplying each term of this expansion by an $I^{(u)}$ on a skeleton of the same composition as the term itself.

The final result for the cluster integral sum is

$$\mathbf{S} = \kappa^3/12\pi + \sum_{u\geqslant 2}[1/u!][\sum c_s]^u I^{(u)} \tag{4.8}$$

together with the instructions that have just been given for interpreting the $I^{(u)}$.

5. DISCUSSION

It is not obvious that the regrouping of the terms of equation (2.12) which occurs in the derivation of equation (4.8) must lead to a useful expression for $\mathbf{S}$. In particular, we ask whether the terms of the expansion are arranged in order of increasing power of the solute concentration. The answer to this is not at once clear because all of the $I^{(u)}$ are concentration dependent. This problem has been partially investigated by Mayer [1] and Haga [3] and we have made a more complete, but as yet unpublished, investigation of the order of the terms. It seems quite clear, although it has not yet been proven conclusively, that at the limit of low concentration the terms of equation (4.8) are arranged in order of decreasing magnitude, although this is certainly not an ordinary power series. The important question of the rapidity of convergence of the series at finite concentrations can, unfortunately, only be answered by numerical calculation from a specific model.

Another question is whether the compact form of equation (4.8) is advantageous in more than a mnemonic way. This depends upon the extent to which the equation can be used without first reversing the summation processes which lead to the compact form. Meeron [4] has indicated that it is most convenient to evaluate the $I^{(2)}$ integrals in the summed form and we have found that this is also the case with some $I^{(3)}$ integrals. Furthermore, in the case of solutions of mixtures of electrolytes, advantage may be taken of the fact that the $I^{(u)}$ integrals depend upon concentration only through κ. In this way the properties of the mixed electrolyte solution may be related to the properties of solutions of single electrolytes at the same κ without at first evaluating any integrals at all, and a further analysis only involves some of the integrals. Our preliminary investigation along these lines indicates that this is a promising approach to mixed electrolyte solutions even at high concentrations.

I am obliged to Professors I. Prigogine and S. Ono for the benefit of many discussions during the course of this research. I also wish to thank the John Simon Guggenheim Memorial Foundation for the fellowship which made this work possible.

Cette théorie, qui est basée sur le développement de la fonction de répartition grand-canonique en intégrales d'essaim par McMillan et Mayer, est étendue pour tenir compte de toutes les composantes des potentiels de force moyenne entre des ensembles de molécules, ou ions, du soluté dans le solvant à dilution infinie. La somme d'intégrales d'essaim résultante, qui est une somme d'intégrales sur un nombre infini de séries infinies de diagrammes-prototypes de Mayer, est transformée en la somme d'une seule série infinie d'intégrales sur des diagrammes comportant des nouveaux types de liaisons. Les liaisons sont définies d'une manière proposée pour la première fois par Meeron. Il en résulte une expression compacte pour la somme d'intégrales d'essaim.

Diese Theorie, die auf der Entwicklung der grossen Verteilungsfunktion nach Clusters entsprechend McMillan und Mayer beruht, wird weiter ausgebaut, so dass sie nunmehr alle Komponenten der Potentiale der Durchschnittskraft einschliesst, die zwischen den Gruppen von gelösten Molekeln oder Ionen bei unendlicher Verdünnung herrschen. Die sich ergebende Cluster-Integralsumme besteht zunächst aus einer Summe von Integralen über unendlich viele unendliche Reihen Mayerscher Prototyp-Diagramme. Sie wird in die Summe einzelner unendlicher Reihen von Integralen über Diagramme umgewandelt, die neue Typen von ' Bindungen ' mit sich bringt. Diese ' Bindungen ' sind nach dem Vorschlag von Meeron definiert, dabei ergibt sich ein kompakter Ausdruck für die Cluster-Integralsumme.

REFERENCES

[1] MAYER, J. E., 1950, *J. chem. Phys.*, **18,** 1426.
[2] POIRIER, J., 1953, *J. chem. Phys.*, **21,** 965, 972.
[3] HAGA, E., 1953, *J. phys. Soc. Japan*, **8,** 714.
[4] MEERON, E., 1957, *J. chem. Phys.*, **26,** 804.
[5] FOWLER, R., and GUGGENHEIM, E. A., 1939, *Statistical Thermodynamics* (Cambridge).
[6] MCMILLAN, W. G., and MAYER, J. E., 1945, *J. chem. Phys.*, **13,** 276.
[7] HILL, T., 1956, *Statistical Mechanics* (New York: McGraw Hill).
[8] MEERON, E., 1957, *J. chem. Phys.*, **27,** 1238.
[9] MAYER, J. E., 1942, *J. chem. Phys.*, **10,** 629.
[10] MONTROLL, E., and MAYER, J., 1941, *J. chem. Phys.*, **9,** 626.
[11] MEERON, E., 1958, *J. chem. Phys.*, **28,** 630.
[12] MEERON, E., 1958, *Physics of Fluids*, **1,** 139.

Rotational effect on the thermodynamic properties of isotopes

by AGNESSA BABLOYANTZ

Faculté des sciences de l'Université Libre de Bruxelles, Belgique

(*Received* 16 *June* 1958)

It is shown that the differences in the thermodynamic properties of HT and D_2 is due to the fact that, for the same total mass, the distribution of mass between the two atoms is not the same. This fact introduces for the heteronuclear molecules a correlation between translational and rotational degrees of freedom. This is a pure quantal effect. A quantum-mechanical perturbation calculation shows that the energy of the ground state is higher for assemblies of heteronuclear molecules than for assemblies of homonuclear ones. On account of this the equation of state of heteronuclear hydrogen molecules is different from that of homonuclear hydrogen molecules. This permits an understanding, for example, of the higher vapour pressure of HT compared to D_2 and the anomalous behaviour of HD.

1. INTRODUCTION

The differences in the thermodynamic properties of the light isotopes can be explained by the quantum-mechanical version of the theorem of corresponding states developed by de Boer [1]. In this theorem the intermolecular potential between two isotopes

$$\epsilon(r)=\epsilon^*\phi(r^*/\sigma) \tag{1.1}$$

is a universal function and ϵ, σ are the same for all isotopic species of a given chemical compound. The quantum effects are measured by the parameter

$$\Lambda^2=\hbar^2/M\epsilon^*\sigma^2 \tag{1.2}$$

where M is the molecular mass.

This theory however fails in some cases. Measurements of J. Bigeleisen and E. C. Kerr [2] have shown that at 20·3 K the vapour pressure of HT is about 36 per cent higher than that of D_2, although both molecules have the same Λ: (it appears the value of Λ should be decreased by a few per cent from that given by Bigeleisen and Kerr because they neglected the non-ideality of the liquid and gaseous phases in their experiments).

Figures 1 and 2 show that the vapour pressure and the molar volume of HD are larger than the expected values interpolated from H_2, D_2 and T_2.

These examples suggest that one has to take account of the distribution of the total mass among the constituent atoms, as was pointed out by Bigeleisen and Kerr.

The deviation from the theorem of corresponding states may be due to: (1) intermolecular forces slightly varying with isotopic substitution; (2) quantum rotational corrections.

This second effect is considered in this paper and it is of two kinds: (*a*) an effect related to the angular dependence of the intermolecular potential; this effect depends on $2I/\hbar^2$ where I is the moment of inertia; (*b*) a coupling effect between translational and rotational degrees of freedom present only for asymmetrical molecules such as HT, HD.

In this paper we discuss the effect (*b*). We consider a system of N interacting molecules and show that the quantum rotational effect can explain the differences in thermodynamic properties of two isotopes of the same total mass. This effect disappears in the classical case†. The quantum effect is computed by a simple perturbation calculation assuming that the molecules are in their lowest translational and rotational states. (This approximation is legitimate because if n_0 is the number of molecules of D_2 in their rotational ground state and n_1 in the first excited level,

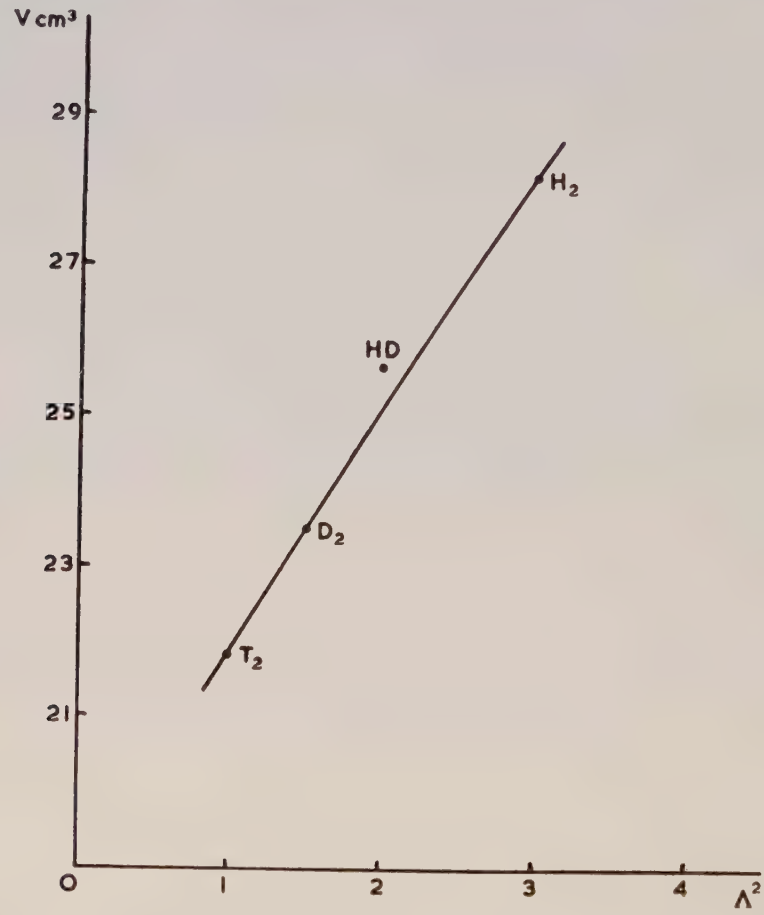

Figure 1. Molar volumes of H_2, HD, D_2, and T_2 in function of Λ^2 at 20°K.

$$\frac{n_1}{n_0} = 2 \times 10^{-2}$$

for $T = 20$°K.) These perturbation calculations lead to an increase of the energy of the first level of the heteronuclear isotopes.

---

† A preliminary communication has been given at Varenna (Italy) by A. Bellemans in September 1957, to appear in *Nuovo Cimento*, Supplemento al Vol. VII serie X (1958).

We compute the vapour pressure and molar volume of HT, D_2 and $H_2^{3/2}$ (a fictitious molecule of the same mass as HD) by the smoothed potential and harmonic oscillator models.

In an appendix we shall discuss the effect (*a*) above and show that it is small compared with (*b*) and goes in the same direction.

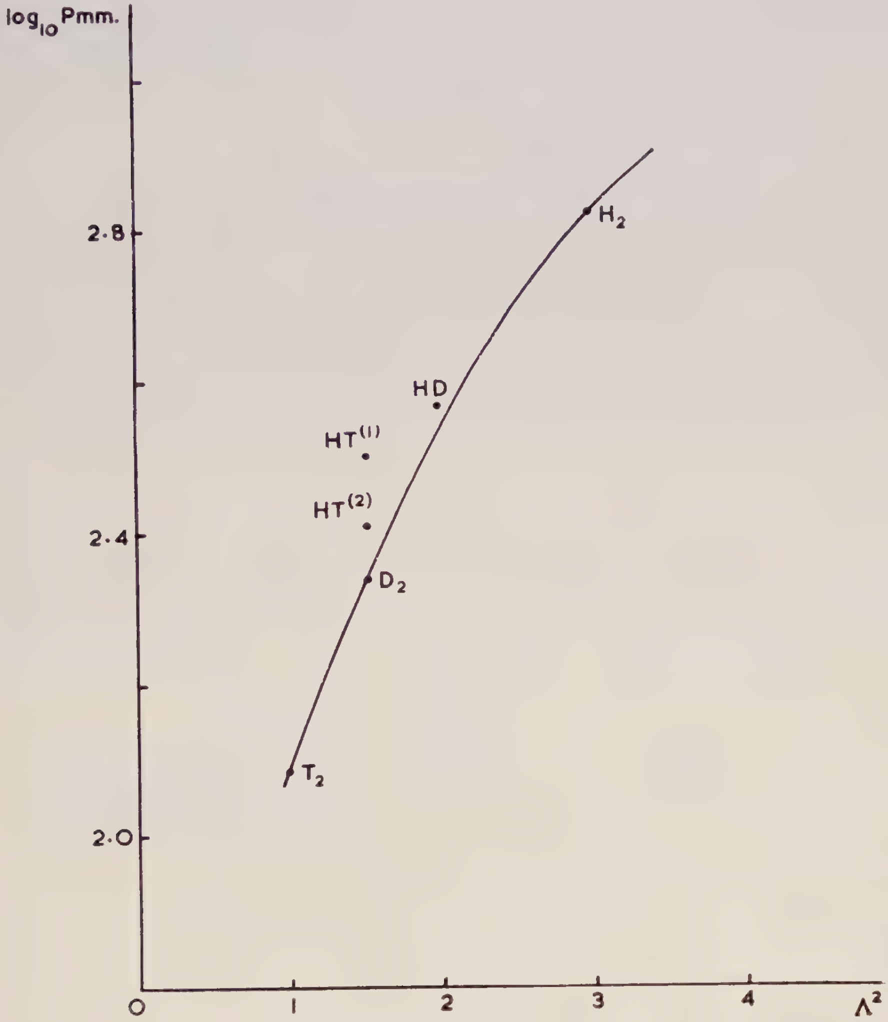

Figure 2. Vapour pressures of H_2, HD, D_2, HT and T_2 in function of Λ^2 at 20°K.

2. Classical case

Consider a system of N mutually interacting diatomic molecules. Let A and B be two isotopic molecules identical from the 'chemical' point of view; A is homonuclear and B heteronuclear, their molecular masses being equal (e.g. $A = D_2$, $B = HT$). We assume that the intermolecular potential is the same for a pair of molecules A and a pair of molecules B. On account of the symmetry of nuclear charges and electronic density of A and B it will be most conveniently expressed in terms of the distance between the mid-points of the molecules (which will be called hereafter their centres of interaction, C) and their relative orientations.

Two systems of coordinates can be used to fix the position of the ith molecule in space: (a) the coordinates of its centre of mass G_i, denoted by $\mathbf{r}_{G_i}$, and two angles θ_i, ϕ_i; (b) the coordinates of its centre of interaction C_i, denoted by $\mathbf{r}_{C_i}$, and the same two angles as in (a).

System (a) leads to the simpler expression for the kinetic energy, while (b) is more convenient for the potential energy. Of course for homonuclear molecules A, (a) and (b) systems are the same.

The partition function of the N molecules expressed in coordinates (a) is, after integration over the momenta

$$Z_N = \left(\frac{2\pi M}{h^2\beta}\right)^{3N/2} \left(\frac{2\pi I}{h^2\beta}\right)^N j^N \frac{1}{N!} \int \exp\left[-\beta V(\mathbf{r}_G{}^N, \Omega^N)\right] d\mathbf{r}_G{}^N \, d\Omega^N \tag{2.1}$$

where M is the molecular mass $\beta = +1/kT$, I the moment of inertia (about an axis through G perpendicular to the molecule), j the internal partition function, V the potential energy and Ω_N stands for the angular coordinates of the molecules. We now focus attention on the last term of the right-hand side of (2.1) which determines the equation of state.

For homonuclear molecules A,

$$\mathbf{r}_{G_i} \equiv \mathbf{r}_{C_i}$$

and

$$\int \exp\left[-\beta V(\mathbf{r}_G{}^N, \Omega^N)\right] d\mathbf{r}_G{}^N \, d\Omega^N = \int \exp\left[-\beta V(\mathbf{r}_C{}^N, \Omega^N)\right] d\mathbf{r}_C{}^N \, d\Omega^N. \tag{2.2}$$

We now prove the same relation to hold for heteronuclear molecules B although in this case

$$\mathbf{r}_{G_i} \neq \mathbf{r}_{C_i}.$$

Changing from coordinates (a) to coordinates (b) we have

$$\int \exp\left[-\beta V(\mathbf{r}_G{}^N, \Omega^N)\right] d\mathbf{r}_G{}^N \, d\Omega^N = \int \exp\left[-\beta V(\mathbf{r}_C{}^N, \Omega^N)\right] \frac{\partial(\mathbf{r}_G{}^N)}{\partial(\mathbf{r}_C{}^N)} \, d\mathbf{r}_C{}^N \, d\Omega^N. \tag{2.3}$$

Furthermore, the systems of coordinates (a) and (b) are related by

$$\mathbf{r}_{G_i} = \mathbf{r}_{C_i} + \alpha \mathbf{1}_{\Omega_i} \tag{2.4}$$

where $\alpha \mathbf{1}_\Omega$ is a vector pointing from G_i to C_i; $\mathbf{1}_\Omega$ is the unit vector determining the orientation of the ith molecule in space and

$$\alpha = \frac{d}{2} \frac{M_1 - M_2}{M_1 + M_2} \tag{2.5}$$

(d is the internuclear distance; M_1, M_2 are atomic masses).

From (2.4), clearly

$$\frac{\partial(\mathbf{r}_G{}^N)}{\partial(\mathbf{r}_C{}^N)} \equiv 1. \tag{2.6}$$

This proves relationship (2.2) in the case of heteronuclear molecules B. Hence assemblies of homo- and heteronuclear molecules have the same equation of state in classical mechanics.

3. QUANTUM CASE

We start from the same system of N molecules considered in the preceding section. The Hamiltonian operator is

$$H=\sum_{i=1}^{N} H_i+V \tag{3.1}$$

where

$$H_i=-\frac{\hbar^2}{2M}\nabla_{G_i}^{\ 2}-\frac{\hbar^2}{2I}\left\{\frac{1}{\sin\theta_i}\frac{\partial}{\partial\theta_i}\left(\sin\theta_i\frac{\partial}{\partial\theta_i}\right)+\frac{1}{\sin^2\theta_i}\frac{\partial^2}{\partial^2\phi_i}\right\} \tag{3.2}$$

and V is the potential energy. H_i is naturally expressed in the system of coordinates (a) while V takes a simpler form with system (b). It will be more convenient here to adopt this last coordinate system because in that case we need not specify the analytical form of V. Thus changing from system (a) to system (b) according to (2.4), which in algebraic form reads

$$\left.\begin{aligned} x_{G_i}&=x_{C_i}+\alpha\sin\theta_i\cos\phi_i,\\ y_{G_i}&=y_{C_i}+\alpha\sin\theta_i\sin\phi_i,\\ z_{G_i}&=z_{C_i}+\alpha\cos\theta_i,\end{aligned}\right\} \tag{3.3}$$

we get after tedious manipulations

$$H_i=H_i^0+\alpha H_i^{(1)}+\alpha^2H_i^{(2)} \tag{3.4}$$

with

$$\begin{aligned} H_i^{(1)}=&-\frac{h^2}{I}\left(\sin\theta_i\cos\phi_i\frac{\partial}{\partial x_i}+\sin\theta_i\cos\phi_i\frac{\partial}{\partial y_i}+\cos\theta_i\frac{\partial}{\partial z_i}\right)\\ &-\frac{h^2}{I}\left(-\cos\theta_i\cos\phi_i\frac{\partial}{\partial x_i}-\cos\theta_i\sin\phi_i\frac{\partial}{\partial \phi_i}+\sin\theta_i\frac{\partial}{\partial z_i}\right)\frac{\partial}{\partial\theta_i}\\ &-\frac{\hbar^2}{2I}\left(\frac{\sin\phi_i}{\sin\theta_i}\frac{\partial}{\partial x_i}-\frac{\cos\phi_i}{\sin\theta_i}\frac{\partial}{\partial y_i}\right)\frac{\partial}{\partial\phi_i},\end{aligned} \tag{3.5}$$

$$\begin{aligned} H_i^{(2)}=&-\frac{\hbar^2}{2I}\Bigg[\frac{\partial^2}{\partial^2x_i}(1-\sin\theta_i^2\cos\phi_i^2)+\frac{\partial^2}{\partial^2y_i}(1-\sin\theta_i^2\sin\phi_i^2)\\ &\frac{\partial^2}{\partial^2z_i}\sin\theta_i^2-\frac{\partial^2}{\partial x_i\partial y_i}\sin\theta_i^2\sin 2\phi_i-\frac{\partial^2}{\partial x_i\partial z_i}\sin 2\theta_i\cos\phi_i\\ &-\frac{\partial^2}{\partial x_i\partial z_i}\sin 2\theta_i\sin\phi_i\Bigg].\end{aligned} \tag{3.6}$$

The potential energy itself may be divided in two terms

$$V=V^0+V^{(1)}, \tag{3.6$'$}$$

V^0 and $V^{(1)}$ being respectively angular independent and angular dependent parts. We shall assume throughout this paper that $V^{(1)}=0$. In the appendix we discuss briefly the case $V^{(1)}\neq 0$.

Let terms in α and α^2 of (3.4) be taken as perturbation terms. The unperturbed Hamiltonian is then

$$H^0=\sum_i H_i^0+V^0. \tag{3.7}$$

As V^0 is angular independent H^0 can be split into a translational part for the N interacting molecules (each molecule behaves like a point-centre of interaction) and N independent rotational parts.

The eigenfunctions of the unperturbed system are

$$\Psi_{n,\mathbf{lm}}(\mathbf{r}^N, \Omega^N) = \psi(\mathbf{r}^N) \prod_{1}^{N} Y_{l_i m_i}(\theta_i, \phi_i), \qquad (3.8)$$

where $\mathbf{l} = \{l_i\}$, $\mathbf{m} = \{m_i\}$; Y_{lm} is the normalized spherical harmonic. Clearly the unperturbed problem corresponds to homonuclear molecules of mass M and moment of inertia I. We now wish to evaluate the perturbation energy related to α and α^2. We limit calculations to the first energy level.

The unperturbed wave function of the lowest level is

$$\Psi_{0,\mathbf{00}} = \psi_0 \cdot \left(\frac{1}{4\pi}\right)^{N/2}. \qquad (3.9)$$

The first-order perturbation energy is easily found to be

$$\Delta E_0^{(1)} = -\frac{1}{3}\frac{N\alpha^2}{I}\hbar^2 \left\{ \left(\psi_0^* \left| \frac{\partial^2}{\partial^2 x_i} \right| \psi_0\right) + \left(\psi_0^* \left| \frac{\partial^2}{\partial^2 y_i} \right| \psi_0\right) + \left(\psi_0^* \left| \frac{\partial^2}{\partial^2 z_i} \right| \psi_0\right) \right\}. \qquad (3.10)$$

It is related to terms in α^2 of (3.4).

The second-order perturbation, limited to α^2, will include only wave functions of the form

$$\psi_n \prod_{1}^{N} y_{1m}(\theta_i, \phi_i).$$

The perturbation calculation leads to

$$\Delta E_0^{(2)} = \frac{1}{3} N \frac{\hbar^2 \alpha^2}{I} \sum_n \frac{\left(\psi_n^* \left| \frac{\partial}{\partial x_i} \right| \psi_0\right)\left(\psi_0^* \left| \frac{\partial}{\partial x_i} \right| \psi_n\right) + \ldots + \ldots}{1 + I(E_n - E_0)/\hbar^2}. \qquad (3.11)$$

$\Delta E_0^{(1)}$ and $\Delta E_0^{(2)}$ can be combined in a single expression by means of the relation:

$$\left(\psi_n^* \left| \frac{\partial}{\partial x} \right| \psi_0\right) = X_{n0}$$

$$\left(\psi_0^* \left| \frac{\partial^2}{\partial^2 x} \right| \psi_0\right) = \sum_n X_{n0} X_{0n}$$

and we get

$$\Delta E = \alpha^2 \frac{1}{3} N \frac{\hbar^2}{I} \sum_n \frac{|X_{n0}|^2 + |Y_{n0}|^2 + |Z_{n0}|^2}{1 + \hbar^2/I(E_n - E_0)} > 0. \qquad (3.12)$$

This shows in a quite general way that the lowest energy level of an assembly of heteronuclear molecules is higher than that of an assembly of homonuclear molecules.

For evaluation of the matrix elements X_{n0}, Y_{n0}, . . . we need the explicit form of the translational wave functions. For doing this we consider two cell models for which the wave-functions are known; the harmonic oscillator model and the smoothed potential model [3, 4].

3.1. *Smoothed potential cell model*

We assume that the centre of interaction of each molecule is enclosed in a cubic cell of side L. The wave function is

$$\psi_{rst} = \left(\frac{2}{L}\right)^{3/2} \sin\frac{\pi r x}{L} \sin\frac{\pi s y}{L} \sin\frac{\pi t z}{L}. \qquad (3.13)$$

With this wave function the matrix element $|X_{r0}|^2$ is

$$4\frac{[1+(-1)^r]^2}{L^2}\left(\frac{r}{r^2-1}\right)^2. \tag{3.14}$$

and (3.12) becomes

$$\frac{\Delta E}{N}=\frac{1}{6}\frac{(M_1-M_2)^2}{M_1M_2}\left(\frac{2}{\pi}\right)^2\sum_r\frac{[1+(-1)^r]^2(r/r^2-1)^2e^0}{1+(3\hbar^2/Ie^0)(1/r^2-1)}; \tag{3.15}$$

e^0 is the lowest energy level of the unperturbed system.

3.2. *Harmonic oscillator cell model*

In this model each molecule moves in an harmonic field due to its neighbours. The wave functions are the Hermite functions. The form of the perturbation and the orthonormality condition of Hermite polynomials shows that the only matrix elements which contribute to ΔE are

$$|X_{100,000}|=|Y_{010,000}|=|Z_{001,000}|=\frac{M\pi\nu}{\hbar}=\frac{\beta}{2},$$

where

$$|X_{100,000}|=\left\langle\left(\frac{1\ (\beta\ \pi)}{2}\right)^{1\ 2}\sqrt{\left(\frac{\beta}{\pi}\right)}\exp\left[-(\beta/2)(x^2+y^2+z^2)\right]\ 2x\left|\frac{\partial}{\partial x}\right|\sqrt{\left(\frac{\beta}{\pi}\right)^{3/2}}\right.$$
$$\left.\times\exp\left[-(\beta/2)(x^2+y+z^2)\right]\right\rangle$$

and ν is the vibration frequency. ΔE is

$$\frac{\Delta E}{N}=\frac{1}{12}\frac{(M_1-M_2)^2}{M_1M_2}\frac{e^0}{1+3\hbar^2/2Ie^0}.$$

4. RESULTS

In this section we use the relations (3.15) and (3.16) to compute some thermodynamic properties of isotopes and compare them with experimental data. As this quantum rotational effect is proportional to $(M_1-M_2)^2/M_1M_2$ it contributes only to the equation of state of light molecules such as HT (compared with D_2) and HD (compared with a fictitious homonuclear molecule of the same mass).

Here we calculate the vapour pressure and molar volume of HT–D_2 and HT-H_2[32] systems for the smoothed potential cell models described above (3.4). We define reduced variables by

$$\tilde{v}=\frac{v}{\sigma^3},\quad \tilde{p}=p\left(\frac{\sigma^3}{\epsilon^*}\right),\quad \tilde{e}=\frac{e}{\epsilon^*},$$

with $r^*=\sigma 2^{1/6}$ where ϵ^* and r^* are the coordinates of the minimum of the curve representing the intermolecular interaction as a function of the intermolecular distance.

Then the reduced energy at absolute zero is supposed to be the sum of two contributions : the reduced lattice energy and the reduced energy of the ground state e^0.

$$\tilde{e}=w+e^0. \tag{4.1}$$

The $\tilde{e}$ versus $\tilde{v}$ curve shows a minimum corresponding to the vaporization energy.

The explicit form of e^0 is:

$$e^0 = \frac{3}{8}\frac{\Lambda^2}{L^2} = \frac{3}{8\gamma^2}\frac{\Lambda^2}{[2^{1/6}\tilde{v}^{1/3}-1]}$$

where $\gamma^2 = 2{\cdot}4$. It has been calculated from experimental data on the energy of D_2.

We suppose w to be of the form

$$w = 6[\tilde{v}^{-4} - 2{\cdot}4\tilde{v}^{-2}]\,;$$

$\tilde{v}$ is the reduced molar volume.

The equation of state is

$$\frac{\partial\tilde{e}}{\partial\tilde{v}} + \tilde{p} = \frac{\partial w}{\partial\tilde{v}} + \frac{\partial e^0}{\partial\tilde{v}} + \tilde{p} = 0 \qquad (4.2)$$

and we take $\tilde{p} = 0$.

As the analytical form of e^0 and w is known it is easy to compute the reduced molar volume by the relation (4.2) (graphically): putting this value of $\tilde{v}$ in (4.1) we get the reduced energy. The ratio of the vapour pressures for two substances is approximately given by

$$\ln\frac{p_A}{p_B} = \frac{\tilde{f}_A - \tilde{f}_B}{\tilde{T}}, \qquad (4.3)$$

where $\tilde{f}$ is the reduced Helmholtz free energy. Near the absolute zero this can be written

$$\ln\frac{p_A}{p_B} = \frac{\tilde{e}_A - \tilde{e}_B}{\tilde{T}}$$

where $\tilde{e}_A - \tilde{e}_B$ is the difference of the energy of vaporization of the two isotopes. The numerical results are given in tables 1 and 2.

	$\Delta \ln p$ (exp.)	$\Delta \ln p$ (calc.)	
		harm. oscil.	smoothed pot.
HT/D_2	0·37(*a*) 0·16(*b*)	0·14	0·50
$HD/H^{3/2}$	0·08	0·04	0·14

Table 1. ($T = 20$°K).

(*a*) Bigeleisen and Kerr [2].

(*b*) Corrected value for non-ideality of the solution and the gas phase†.

---

† The original value of the ratio p_{HT}/p_{D_2} quoted by Bigeleisen and Kerr was deduced from the measured ratio y_{HT}/x_{HT} of an infinitely dilute solution of HT in H_2 in equilibrium with a gaseous phase (y_{HT}: mole fraction of HT in gas; x_{HT}: mole fraction of HT in liquid). They assumed the gas to be perfect and the solution to be ideal, obtaining

$$\frac{p_{HT}}{p_{D_2}} = 1{\cdot}45.$$

However, from analogous liquid mixtures such as H_2–D_2 and H_2–HD it is expected that H_2–HT solutions present an excess free energy of the order of 1·0 to 2·0 cal/mole at 20°K (for $x = 0{\cdot}5$). Assuming an excess free energy of 1·5 cal (for $x = 0{\cdot}5$) and taking account of gas imperfections we find an appreciably lower value, namely

$$\frac{p_{HT}}{p_{D_2}} = 1{\cdot}17.$$

Δv (exp.)		Δv (cal.)	
		harm. oscil.	smout. pot.
HT	—	—	0·07
HD	0·03	0·3	0·03

Table 2.

5. Conclusion

The quantum rotational coupling effect between translational and rotational degrees of freedom may be one of the main effects underlying the departure of homonuclear and heteronuclear isotopes of the same mass from the quantum theorem of corresponding states.

For the reduced volume of HD the agreement between the calculated values and experimental data is quite satisfactory.

Table 1 shows that the experimental value for the differences of the vapour pressure of the $HT–D_2$ and $HD–H_2^{3.2}$ systems lie between our calculated values. Both harmonic oscillator and smoothed potential models are very rough approximations to reality; they give only an order of magnitude. The main point is that this effect is positive and large.

In the appendix we discuss the quantum rotational effect due to angular dependent forces. Our calculations show that this effect is small compared to the first one, and goes in the same direction.

We would like to express our gratitude to Professor I. Prigogine, who suggested this work, for constant interest and helpful advice. We are also indebted to Dr. A. Bellemans and Dr. J. Philippot for their valuable help, and to Dr. J. Jeener for interesting discussions. The research reported in this publication has been made possible through the support of the General Electric Research Laboratory, Schenectady, N.Y., through its European Office.

Appendix

In this section we briefly discuss the quantum rotational effect related to the angular dependence of the intermolecular forces. We discuss elsewhere [5] this kind of effect and show that the differences in the thermodynamic functions of the ortho and para-H_2 can be explained by these forces. In a similar way the calculations can be carried out for the $HT–D_2$ problem. $F_{\text{pert.}}$ (perturbation due to angular forces) for HT can be computed as we did for para-H_2. For D_2 the experimental data is relative to D_2–*e* at 20 with 1·998 per cent para-D_2. So we can compare HT to pure ortho-D_2.

The decrease of the Helmholtz free energy due to the orientational forces is of the form

$$\Delta F \sim -\frac{2I}{\hbar^2}.$$

Then if one considers two isotopic molecules A and B with $I_A < I_B$, their molecular masses being identical the vapour pressure of A is higher than that of B.

Applying this to the case of HT–D_2 with the help of (4.3) we find

$$\ln\frac{p_{\mathrm{HT}}}{p_{\mathrm{D}_2}} = 0{\cdot}003.$$

This effect is in the same direction as the one considered above, but its order of magnitude is much smaller.

On montre que les différences de propriétés thermodynamiques de HT et D_2 sont dues au fait que, pour une même masse moléculaire totale, la répartition de la masse entre les deux atomes n'est pas la même. Ce fait introduit pour les molécules hétéronucléaires une corrélation entre les degrés de liberté translationnels et rotationnels. Ceci est un effet purement quantique. Un calcul de perturbation par la mécanique quantique montre que l'énergie de l'état fondamental est plus haute pour des assemblées de molécules hétéronucléaires que pour des assemblées de molécules homonucléaires. Il en résulte que les équations d'état des molécules d'hydrogène hétéronucléaires sont différentes de celles des molécules d'hydrogène homonucléaires. Ceci nous permet de comprendre, par exemple, la haute pression de vapeur de HT comparée à celle de D_2, et le comportement anormal de HD.

Es wird gezeigt, dass die Unterschiede zwischen den thermodynamischen Eigenschaften von HT und D_2 aus der Tatsache folgen, dass die Massenverteilung der beiden Atome in der Molekel bei gleicher Gesamtmasse verschieden ist. Für verschiedenkernige Molekeln wird hierdurch eine Beziehung zwischen den Translations- und den Rotationsfreiheitsgraden aufgezeigt. Dies ist ein reiner Quanteneffekt. Eine quantenmechanische Störungsrechnung zeigt, dass die Energie des Grundzustandes für eine Gesamtheit verschiedenkerniger Molekeln höher ist als für eine Gesamtheit gleichkerniger Molekeln. Infolgedessen sind die Zustandsgleichungen für verschiedenkernige Wasserstoffmolekeln verschieden von denjenigen für gleichkernige Wasserstoffmolekeln. Hierdurch lassen sich z.B. die hohe Dampfspannung von HT im Vergleich zu D_2, sowie das aussergewöhnliche Verhalten von HD verstehen.

REFERENCES

[1] Boer, J. de, 1948, *Physica*, **14,** 149; 1948, *Ibid.*, **14,** 139.
[2] Bigeleisen, J., and Kerr, E. C., 1955, *J. chem. Phys.*, **23,** 2442.
[3] Prigogine, I., 1957, *The Molecular Theory of Solutions* (Amsterdam: North-Holland Publishing Co.).
[4] Prigogine, I., Bingen, R., and Bellemans, A., 1954, *Physica*, **20,** 633.
[5] Bellemans, A., and Babloyantz, A., 1959, *Mol. Phys.* (in the press).

The structure of shock fronts in various gases

by W. H. ANDERSEN† and D. F. HORNIG‡
Metcalf Research Laboratory, Brown University, Providence, Rhode Island

(*Received* 1 *September* 1958)

The optical reflectivity of shock fronts in A, N_2, O_2, CO, CO_2, N_2O, CH_4, Cl_2 and HCl have been studied. The thickness of shock fronts in A up to the Mach number $M=1{\cdot}55$ is in agreement with the theory of Gilbarg and Paolucci. The rotational relaxation time is about 5·5 collisions in N_2 and equal to or less than that in the other gases. However, for stronger shocks N_2 does not appear to reach rotational equilibrium in the shock front and a qualitative theoretical discussion of this phenomenon is presented. In HCl there appears to be over-excitation of rotation in the shock front. There is no vibrational excitation of any of the gases.

1. Introduction

The structure of shock fronts in a number of gases has been investigated experimentally by the light reflectivity method and a limited amount of experimental information regarding weak shock fronts has been obtained [1–5]. In the case of monatomic gases, particularly argon, the experimental data could be compared with various theoretical treatments which have been given, both from the hydrodynamic and kinetic theory points of view [6].

The thickness of shock fronts in argon, determined both by the light reflectivity method and by the wire probe method, agrees [7, 8] within experimental error with the theoretical values obtained by Gilbarg and Paolucci from the Navier–Stokes equations, at least for fairly weak shocks [6, 7, 8]. Similar results have been obtained for He [7]. However, the precision was not high in any of the work reported to date.

The presence of rotational relaxation in polyatomic gases has also been demonstrated [3–5, 7]. In hydrogen the rotational degrees of freedom are not excited in the shock front at all; in oxygen and nitrogen the shock front data were originally interpreted to indicate that rotational relaxation took place in 20 to 30 collisions. More recently Sherman has shown [7] that the results for nitrogen could be well represented by a bulk viscosity, κ, if $\kappa/\mu=\frac{2}{3}$. A bulk viscosity results, according to Tisza [9], from a relaxation process which occurs in a time which is short compared to the time of measurement. His expression for the bulk viscosity can be rearranged to the equation

$$\kappa=\frac{nk^2T}{C_v^{\,2}}C_i\tau_i, \tag{1}$$

where τ_i is the relaxation time and C_i is the heat capacity contribution by the relaxing degree of freedom. This same expression has been obtained from statistical considerations by Wang-Chang and Uhlenbeck [10] in the limit $T_{\text{internal}}\to T_{\text{translation}}$. This condition is fulfilled in weak shocks but not in strong ones.

---

† Present address : Aerojet-General Corporation, Azuza, California.

‡ Present address : Frick Chemical Laboratory, Princeton University, Princeton, N.J.

If equation (1) is compared with those for the viscosity and collision number of Maxwellian molecules, it can also be rewritten

$$\tau' = 8\kappa/\mu \tag{2}$$

where τ' is the number of collisions required for relaxation to $1/e$ of equilibrium. For nitrogen, then, $\tau' = 5{\cdot}3$ collisions.

The work of Andersen and Hornig showed that in N_2O and CO_2 vibrational excitation was negligible in weak shock fronts and must appear as a relatively slow relaxation region behind the shock front.

The work reported in this paper is a continuation of the previous studies. We have reinvestigated argon in order to make better comparisons with theoretical expressions for the shock front process. In addition, it seemed important to extend the studies to as many gases and shock strengths as practicable in the hope of gaining further information on the variables involved in fast energy transfer processes. Finally, it seemed important to look into the previous conclusion that equilibrium densities were not obtained behind the front in nitrogen, which had suggested that the fast rotational relaxation did not go to rotational equilibrium.

2. EXPERIMENTAL

The apparatus and technique employed in this study were nearly the same as in the earlier studies [4, 5]. In brief, the method consists of measuring the optical reflectivity of the shock front as a function of the parameter $(\rho_1\lambda/\rho_0 \cos\theta)$, where λ is the wavelength of the light, θ the angle of incidence, ρ_1 the initial density and ρ_0 the density under standard conditions (1 atm, 296°K). Details of the theory have been described by Cowan and Hornig. All of our measurements were made with a cobalt glass filter which, together with the emission from the tungsten source and the response of the photomultiplier, defined a band falling to half the maximum at 3750 Å and 4850 Å. The effective λ was 4250 Å. The angle of reflection was usually 82° but some measurements were made down to as little as 67°. The gases studied were chosen to obtain different symmetry numbers, moments of inertia and intermolecular potentials.

The reflectivities of shock fronts in argon, nitrogen, oxygen, carbon monoxide, carbon dioxide, nitrous oxide, methane, ammonia, hydrogen, chlorine and hydrogen chloride gases were measured at various shock strengths and the results are shown in figures 1–10. In these figures the reduced reflectivity, R', is plotted logarithmically as a function of $\rho_1\lambda/\rho_0 \cos\theta$, the reduced reflectivity being defined by the relation

$$R = \left(\frac{\rho_1}{\rho_0}\right)^2 \frac{(1+\tan^4\theta)}{4} R'\left(\frac{\rho_1\lambda}{\rho_0\cos\theta}\right), \tag{3}$$

where R is the measured reflectivity. The thickness of the shock front, defined by the equation

$$L = \frac{n_2 - n_1}{(dn/dx)_{\max}} = \frac{\rho_2 - \rho_1}{(d\rho/dx)_{\max}}, \tag{4}$$

where ρ is the density, and the suffixes 1 and 2 refer to the initial and final states, is determined by comparing the experimental reflectivities with the theoretical curve for a suitable shock front model. That used was

$$\rho = \rho_1 + \frac{\rho_2 - \rho_1}{1 + \exp(-4x/L)} \tag{5}$$

which approximates all of the existing theories very closely.

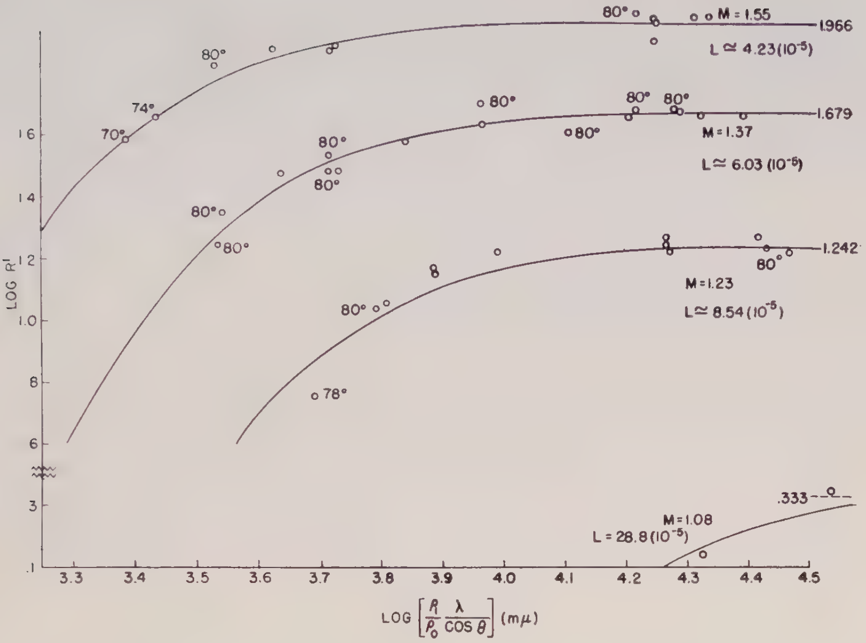

Figure 1. Reduced reflectivity of shock fronts in argon.

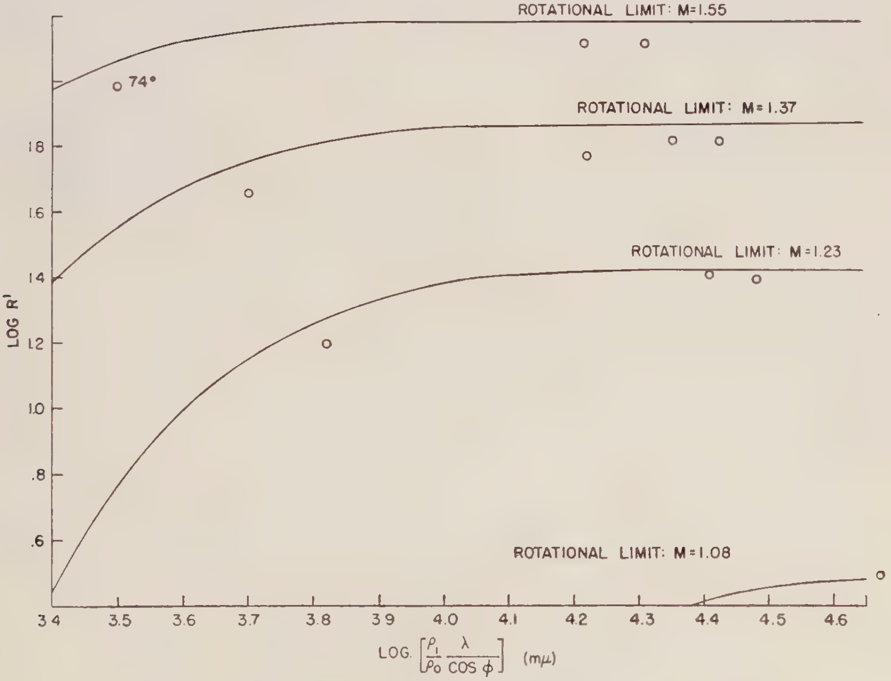

Figure 2. Reduced reflectivity of shock fronts in nitrogen.

It has sometimes been stated that the reflectivity method measures the 'maximum slope thickness' defined by equation (4). This is not true and in comparing our results with profiles other than that of equation (5) one ought not to compare our L with the maximum slope thickness of the theory; rather our L should be compared with the best fit of the form of equation (5) to the theoretical profile.

The reduced reflectivity for the profile expressed by equation (5) is given by the equation

$$R' = \frac{(\pi^2 \rho_0 L_0 \cos\theta/\rho_1\lambda)\,(\Delta n)_0{}^2}{\sinh^2(\pi^2 \rho_0 L_0 \cos\theta/\rho_1\lambda)}\,. \tag{6}$$

This function is included in each of the figures as a solid black line. L_0 is the shock front thickness when the initial pressure is one atmosphere and $(\Delta n)_0$ the change in index of refraction under the same conditions. The various terms in ρ_1 reflect the scaling laws which have been discussed previously [2–4]. ρ_1 is in fact the best quantity to vary accurately over a wide range. For perfect gases ρ_1/ρ_0 is simply the pressure p_1 in atmospheres, but for many of the gases studied imperfection had to be taken into account.

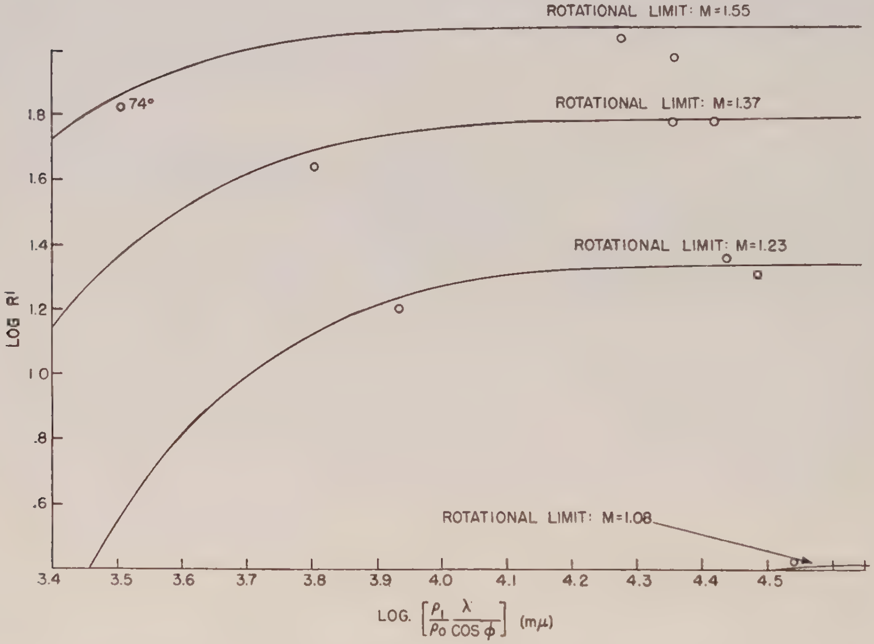

Figure 3. Reduced reflectivity of shock fronts in oxygen.

The apparatus was not suited for measuring velocities and reflectivities simultaneously, so velocities were obtained from separate runs under the same conditions as those used to obtain reflectivities. In general two runs were sufficient to obtain the velocity for a given point on the curves whereas the reflectivity is the average from three or more identical runs, sometimes as many as twelve. The sources of scatter in the measured reflectivities have been discussed previously; it is believed that small fluctuations in the angle between the shock front and the axis of the shock tube are the principal cause.

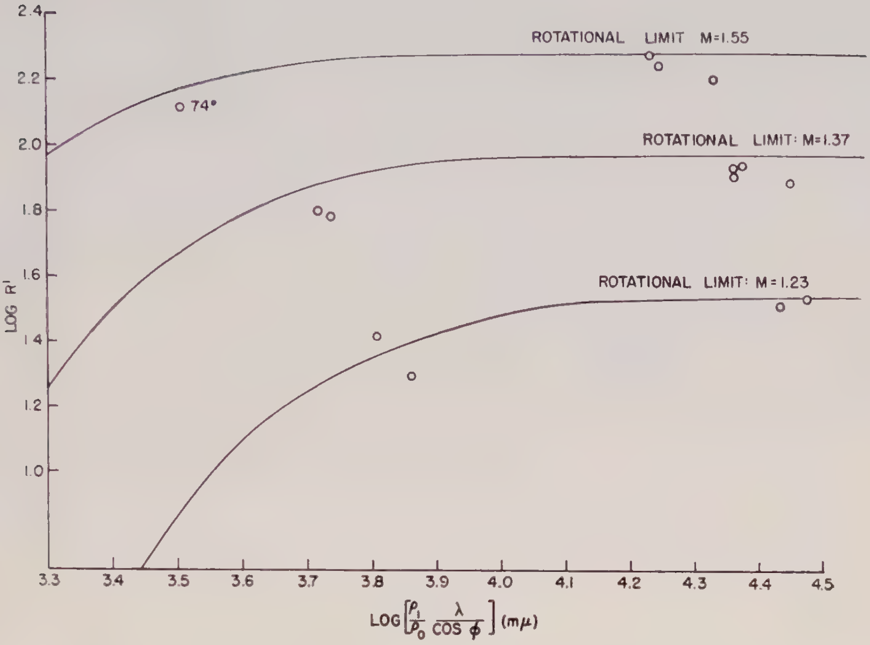

Figure 4. Reduced reflectivity of shock fronts in carbon monoxide.

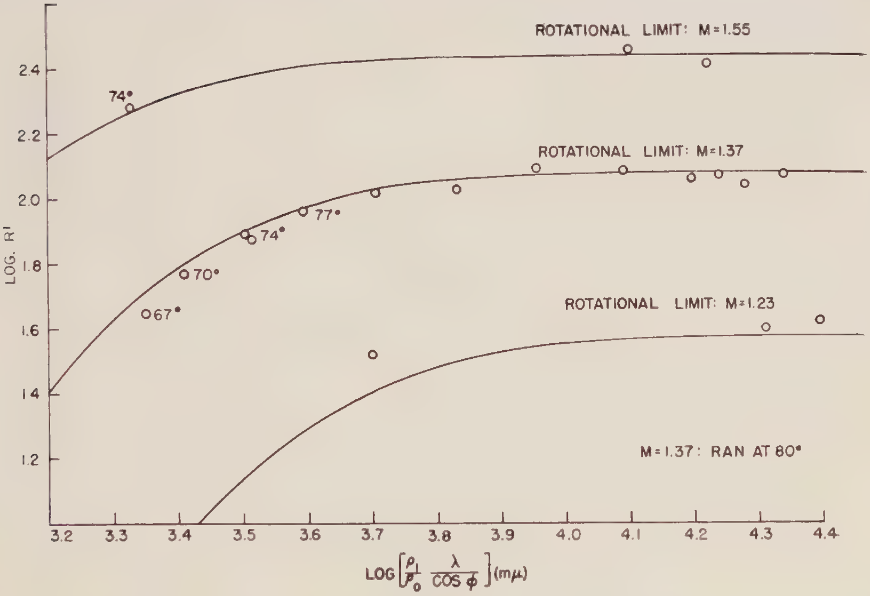

Figure 5. Reduced reflectivity of shock fronts in carbon dioxide.

Because the apparatus was not capable of measuring absolute reflectivities the measurements were all made relative to the reflectivity of argon (figure 1) at the limiting (asymptotic) reflectivity. The three argon curves were not fitted independently; rather an average value for b in the expression $R_A(\infty) = b(\Delta\rho)^2$ was found and used for all three shock strengths. By means of the relation

$$\frac{R_x(\infty)}{R_A(\infty)} = \frac{[(\Delta\rho/\rho_1)(n-1)]^2_X}{[(\Delta\rho/\rho_1)(n-1)]^2_A} \tag{7}$$

it was therefore possible to determine $\Delta\rho$, and hence the absolute reflectivity scale, for each gas X. On each figure the theoretical reflectivity curve if equilibrium is maintained between translation and rotation is drawn as a solid line. The thickness, L_{eqm}, employed in the theoretical curves is based on the ratio of the absolute thickness to that of argon predicted by the Wang-Chang expression for Maxwell molecules [10], multiplied by the experimental value for argon found from figure 1.

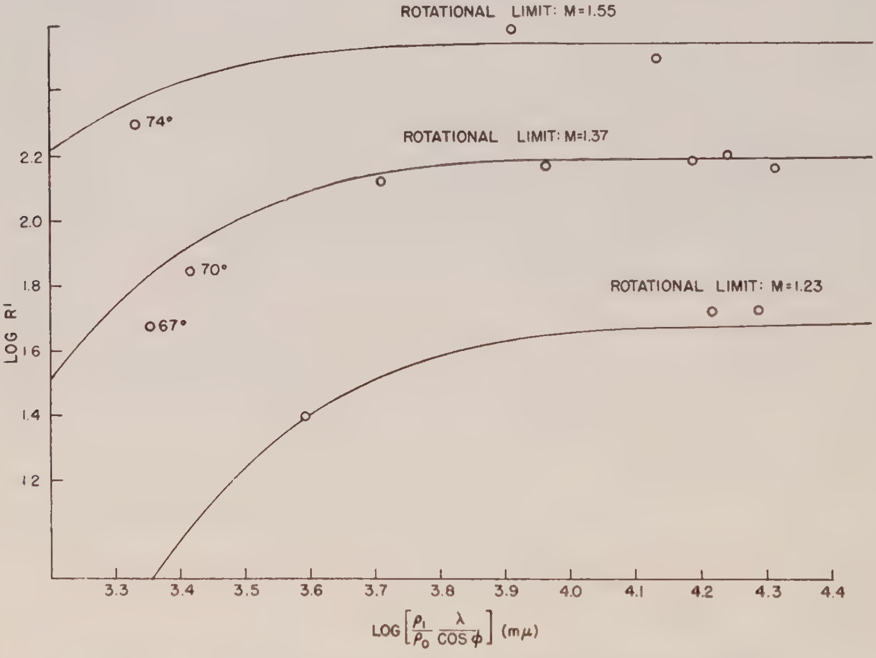

Figure 6. Reduced reflectivity of shock fronts in nitrous oxide.

The gases CO_2, N_2O, CH_4, NH_3, Cl_2 and HCl are all imperfect and the observed reflectivities had to be corrected to take this into account. The procedure used, based on the Berthelot equation of state, has been described in detail previously [5].

The properties of shock fronts in the various gases (considered ideal) at an initial pressure of one atmosphere and an initial temperature of 23 °c are shown in table 1. ρ_T, ρ_R and ρ_V are the theoretical densities behind the shock front if translational, translational plus rotational, or both of these plus vibrational degrees of freedom are brought to equilibrium. ρ_2 is the measured final density and C_2/C_R is the apparent fraction of the rotational energy which is equilibrated immediately behind the front. T_R is the equilibrium temperature behind the front. L_0 is the thickness which gives the best fit to equation (5) and $L_{\mathrm{eq.}}$ is the Wang-Chang thickness for equilibrated translation and rotation.

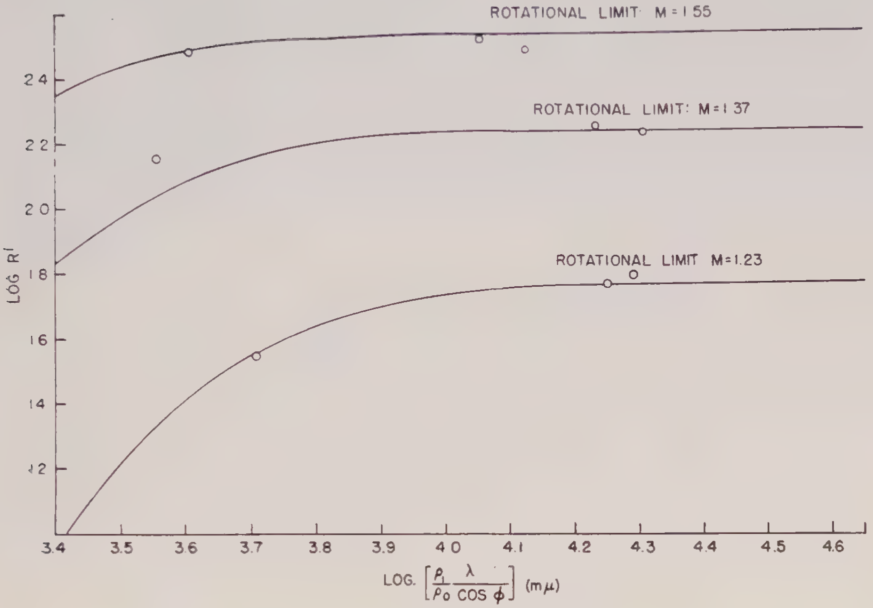

Figure 7. Reduced reflectivity of shock fronts in methane.

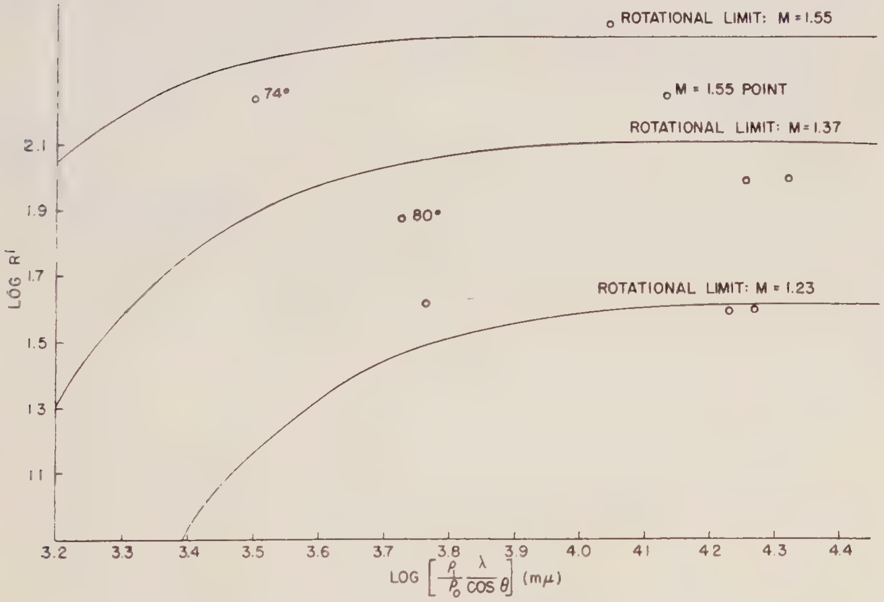

Figure 8. Reduced reflectivity of shock fronts in ammonia.

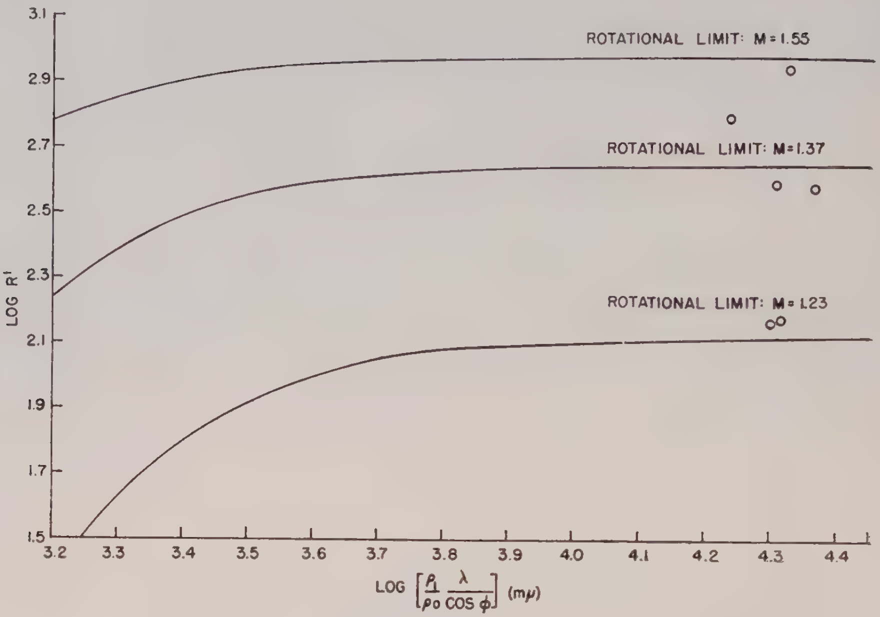

Figure 9. Reduced reflectivity of shock fronts in chlorine.

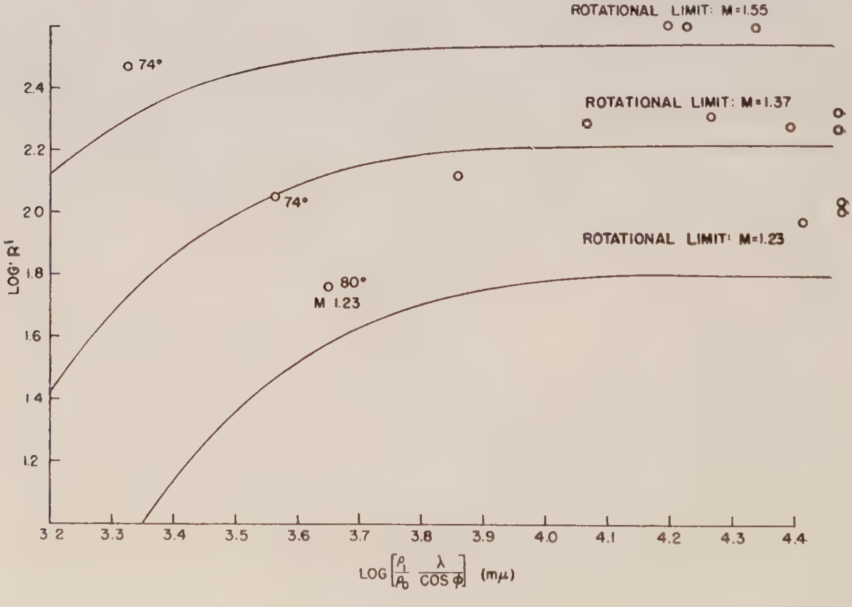

Figure 10. Reduced reflectivity of shock fronts in hydrogen chloride.

The number of collisions a molecule undergoes in a shock front is given to a good approximation by the expression

$$N_L = N_{\rho_1,\bar{T}} \int \left(\frac{\rho}{\rho_1}\right) dt = \frac{N_{\rho_1,\bar{T}}}{\rho_1{}^2 D} \int_{-L/2}^{L/2} \rho^2\, dx; \tag{8}$$

D is the shock velocity and the integration is carried from $x=-\frac{1}{2}L$ to $x=\frac{1}{2}L$. $N_{\rho_1,\bar{T}}$ is the number of collisions a single molecule makes per second at a density ρ_1 and a temperature $\bar{T}$, which we take as the mean of the initial temperature and that after rotational equilibration in the shock. Substituting equation (5) into (8) and integrating,

$$N_L = N_{\rho_1,\bar{T}} \frac{L}{D}\left\{0{\cdot}38\frac{\rho_2}{\rho_1} + 0{\cdot}31\left[\left(\frac{\rho_2}{\rho_1}\right)^2 + 1\right]\right\}. \tag{9}$$

The purity of the gases used in the study was usually better than 99·5 per cent. However, some of the carbon monoxide contained 1·4 per cent hydrogen and the remainder 3·5 per cent hydrogen. The reflectivity calculations were corrected for this impurity but no allowance was made for diffusion effects.

3. The effect of shock strength on thickness

Previous studies had shown that the measured shock thicknesses were systematically greater than given by the available theoretical expressions and the question arose whether the Navier–Stokes equations, without additional terms from higher

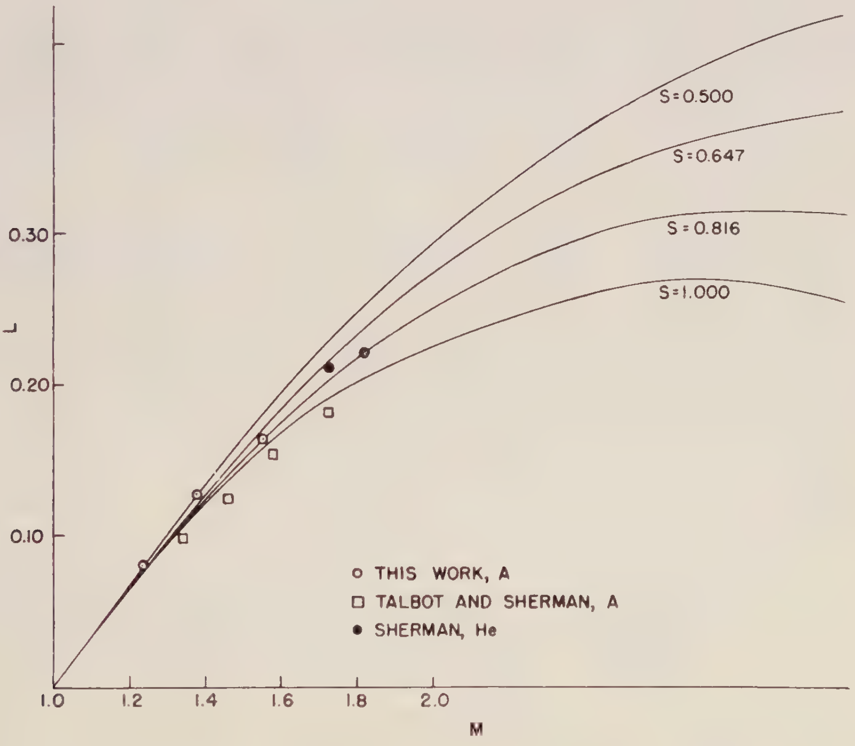

Figure 11. The thickness (L) of shock fronts in argon and helium, measured in Maxwell mean free paths (Λ), as a function of Mach number. The theoretical curves are those of Gilbarg and Paolucci or $\mu=\mu'(T/300)^s$. $s=0{\cdot}816$ for A and $0{\cdot}647$ for He.

Gas and shock strength	ρ_V g/cm³ (10^{-3})	ρ_T g/cm³ (10^{-3})	ρ_R g/cm³ (10^{-3})	T_R °K	L_0 cm (10^{-5})	L_{eq} cm (10^{-5})	Collisions through the front† N	ρ_2 (exptl.) g/cm³ (10^{-3})	$\frac{C_2}{C_R}$
Nitrogen $\rho_0=1\cdot151\ (10^{-3})$ g/cm³ Mach 1·08	1·306	1·132	1·306	312	—	21·5	45	1·31	1·00
1·23	1·606	1·370	1·606	339	8·5	7·4	18	1·59	0·97
1·37	1·884	1·582	1·884	365	5·7	5·0	13	1·86	0·97
1·55	2·238	1·849	2·238	401	3·3	3·1	10	2·17	0·93
Oxygen $\rho_0=1\cdot319\ (10^{-3})$ Mach 1·08	1·497	1·299	1·497	311	—	22·9	46	1·50	1·00
1·23	1·838	1·569	1·838	339	9·9	8·2	19	1·84	1·00
1·37	2·158	1·814	2·158	365	7·0	5·8	15	2·16	1·00
1·55	2·520	2·084	2·520	406	4·1	4·0	12	2·44	0·93
Carbon Monoxide $\rho_0=1\cdot151\ (10^{-3})$ Mach 1·23	1·605	1·370	1·605	339	7·4	7·4	18	1·60	1·00
1·37	1·885	1·582	1·885	365	6·0	5·0	13	1·85	0·96
1·55	2·238	1·849	2·238	401	3·7	3·1	10	2·19	0·95
Nitrous Oxide $\rho_0=1\cdot811\ (10^{-3})$ Mach 1·23	2·635	2·036	2·377	330	6·2	5·9	21	2·40	1·03
1·37	3·136	2·365	2·796	356	4·5	3·8	15	2·80	1·00
1·55	3·814	2·770	3·332	389	2·9	2·5	12	3·33	1·00
Carbon Dioxide $\rho_0=1\cdot811\ (10^{-3})$ Mach 1·23	2·600	2·042	2·382	330	5·0	5·9	21	2·40	1·02
1·37	3·095	2·372	2·794	355	4·2	3·8	15	2·79	1·00
1·55	3·791	2·789	3·355	388	2·5	2·5	12	3·36	1·00

Methane									
$\rho_0=0{\cdot}66$ (10^{-3})									
Mach 1·23	0·965	0·775	0·925	332	6·8	6·7	18	0·93	1·00
1·37	1·139	0·881	1·099	354	3·6	4·6	15	1·10	1·00
1·55	1·369	1·021	1·301	382	3·1	3·2	12	1·30	1·00
Ammonia									
$\rho_0=0{\cdot}7$ (10^{-3})									
Mach 1·23	0·993	0·790	0·965	331	2·5	6·0	19	0·95	0·97
1·37	1·187	0·922	1·150	353	5·3	4·1	15	1·10	0·93
1·55	1·434	1·078	1·379	382	2·2	2·8	12	1·32	0·94
Hydrogen Chloride									
$\rho_0=1{\cdot}503$ (10^{-3})									
Mach 1·23	2·116	1·799	2·116	341	6·2	5·9	19	2·28	1·22
1·37	2·456	2·058	2·456	366	5·0	4·1	15	2·59	1·13
1·55	2·935	2·416	2·935	402	2·0	2·9	12	3·04	1·07
Chlorine									
$\rho_0=2{\cdot}917$ (10^{-3})									
Mach 1·23	4·215	3·330	3·890	333	—	3·9	18	3·95	1·05
1·37	4·935	3·900	4·620	359	—	2·8	14	4·58	0·98
1·55	5·975	4·550	5·500	393	—	1·9	10	5·23	0·99
Hydrogen									
$\rho_0=0{\cdot}082$ (10^{-3})									
Mach 1·772	0·191	0·154	0·191	447	—	6·9	13	—	—
Argon									
$\rho_0=1{\cdot}642$ (10^{-3})									
Mach 1·08	—	1·838	—	322	28·8	—	55	—	—
1·23	—	2·200	—	362	8·5	—	18	—	—
1·37	—	2·529	—	402	6·0	—	14	—	—
1·55	—	2·920	—	458	4·2	—	11	—	—

† Calculated from theoretical thickness.

Table 1. Properties of shock waves in various gases at an initial pressure of one-atmosphere and an initial temperature of 296°K.

order kinetic theory, were adequate to describe a shock front. Since that time Gilbarg and Paolucci have shown how to integrate the Navier–Stokes equations when empirical viscosity temperature and thermal conductivity temperature relations are employed. Our results for argon are compared with their calculated curves, using $\mu=\mu_0(T/T_0)^s$, in figure 11. The viscosity of argon is best fitted experimentally for $s=0{\cdot}816$. For comparison the results obtained for He ($s=0{\cdot}647$) by Sherman and those for A by Talbot and Sherman are also included.

All of the results agree better with the Gilbarg and Paolucci calculations than with any previous theoretical curve. It must be concluded, therefore, that despite the enormous pressure, temperature and velocity gradients in the shock front the Navier–Stokes equations yield a reasonably good representation of a shock front in a monatomic gas if $M<1{\cdot}8$ and higher order kinetic theory effects are not important in this region. Consequently, it is most important that shock front measurements be extended to stronger shocks where the kinetic theory effects resulting from deviations from local equilibrium become more marked.

4. ROTATIONAL RELAXATION

In the polyatomic gases it is clear that there are at least two different kinds of process involved. For weak shocks one might anticipate that rotational relaxation would affect the shock as a bulk viscosity since the number of collisions involved in the shock is great compared to the rotational relaxation time. In that case, since L is essentially proportional to the effective viscosity

$$(\tfrac{4}{3})\mu_{\text{eff}}=(\tfrac{4}{3})\mu+\kappa,$$

we have

$$\frac{L_{\text{exp}}}{L_{\text{eqm}}}=\frac{(\frac{4}{3})\mu+\kappa}{(\frac{4}{3})\mu}=1+\frac{3\kappa}{4\mu}, \tag{10}$$

so that

$$\tau'=\frac{32}{3}\left(\frac{L_{\text{exp}}}{L_{\text{eqm}}}-1\right).$$

Using this equation, the data of Greene and Hornig yield $\tau'=5{\cdot}5$ collisions for the mean of shocks up to $M=1{\cdot}287$, agreeing with the conclusion of Sherman, but the present results give $\tau'=1{\cdot}5$ collisions. The careful data on N_2O and CO_2 at $M=1{\cdot}37$ yield $\tau'<1{\cdot}5$ collisions in all cases. Inspection of figures 2–10 and of table 1 makes it very clear that the measured thicknesses are so close to the calculated ones that the rotation must be regarded as very close to equilibrium as far as the thicknesses of the fronts are concerned. The small differences cannot be taken very seriously since there is considerable uncertainty in the theoretical thickness.

Although the shocks show no evidence of slow relaxation in the front, it can be seen readily from the figures and from table 1 that in the stronger shocks ($M=1{\cdot}55$) there is a consistent deviation of the final density from the equilibrium value. In N_2, for example, the final density is about 5 per cent low. In terms of the rotational heat capacity, one can note that

$$\frac{C_R-C_2}{C_R}=\frac{C_T(\rho_R-\rho_2)M^2\gamma_e}{C_R\rho_2(M^2\gamma_e-\rho_2/\rho_R)}; \tag{11}$$

where C_2 is the effective rotational heat capacity, C_R is the equilibrium rotational and C_T the translational heat capacity, M the Mach number and γ_e is C_p/C_v when equilibrium rotational and translational heat capacities are considered. In these terms then, the effective rotational heat capacity in N_2 is about 93 per cent of the equilibrium value at $M = 1{\cdot}55$.

The same is approximately true for the other gases, although in the gases CO_2 and N_2O where the moment of inertia is large the effect is smaller. Although we have not reproduced the data, we have also extended the measurements on hydrogen to $M = 1{\cdot}77$ and there is no rotational excitation at all. The most surprising case, though, is hydrogen chloride in which the final density is higher than the equilibrium value. This corresponds to over-excitation of rotation in the front, presumably followed later by a slow relaxation back to equilibrium.

5. Discussion

We have not yet been able to account for these observations theoretically but some qualitative observations are possible. The basic process we observe is the conversion of the kinetic energy of flow, $D^2/2$ per g. of gas, into thermal energy. This process occurs in the shock front in approximately 10 collisions for all but the weakest shocks. In a frame of reference in which the shock front is stationary there is then an incoming gas stream with a velocity greater than that of sound. In passing through the front region where there are N collisions, the kinetic energy lost per mole of gas is

$$\Delta H = \frac{M^2 \gamma R T}{2}\left(1 - \frac{\rho_1{}^2}{\rho_2{}^2}\right). \tag{12}$$

In the case of a gas like hydrogen, the spacing between the level $J = 0$ and $J = 2$ is 360 cm^{-1} or more than $\frac{3}{2}kT$. Consequently, for $M < 1{\cdot}5$ this excitation could not take place, even if all of the ΔH were dissipated in a single collision. As a consequence there is no rotational excitation in the front and equilibrium is reached by a subsequent slow thermal relaxation.

On the other hand, in N_2 for example, the rotational level spacing is $4BJ$ and $B = 2\,\mathrm{cm}^{-1}$. For $M = 1{\cdot}4$, the kinetic energy dissipated in the shock front is about 165 cm^{-1} or 470 cal/mol, sufficient to bring about rotational transitions when J is not too large. We suggest therefore that the repopulation of the low J states occurs readily in the front. On the other hand, the $J = 20 \rightarrow J = 22$ transition has a spacing of 176 cm^{-1} and, just as in H_2, could not be brought about by the loss of the flow kinetic energy in the shock front. We suggest, therefore, that the decrease in the effective heat capacity occurs because the repopulation of the high J levels does not occur in the shock front but in a slow subsequent equilibration.

This point is perhaps made clearer in figures 12 and 13 in which the distribution of energy and of population among the rotational states of N_2 is shown at 300 °K and at 450 °K. It is seen from figure 12 that the increase of 300 cal/mol in the rotational energy when the gas is heated to 450 °K is distributed mostly among states between $J = 12$ and $J = 32$. About 38 cal/mol, or over 10 per cent, goes into states $J \geqslant 28$ and half of the increase is in states $J > 20$. It is clear, therefore, that these very high J states play a major role at $M = 1{\cdot}4$ and above.

From figure 13 it seems that repopulation is primarily from states $J \leqslant 10$ to states $J \geqslant 12$. When $J \geqslant 18$, not only are the energy level spacings large but there is still another effect which should slow down rotational equilibration. For each

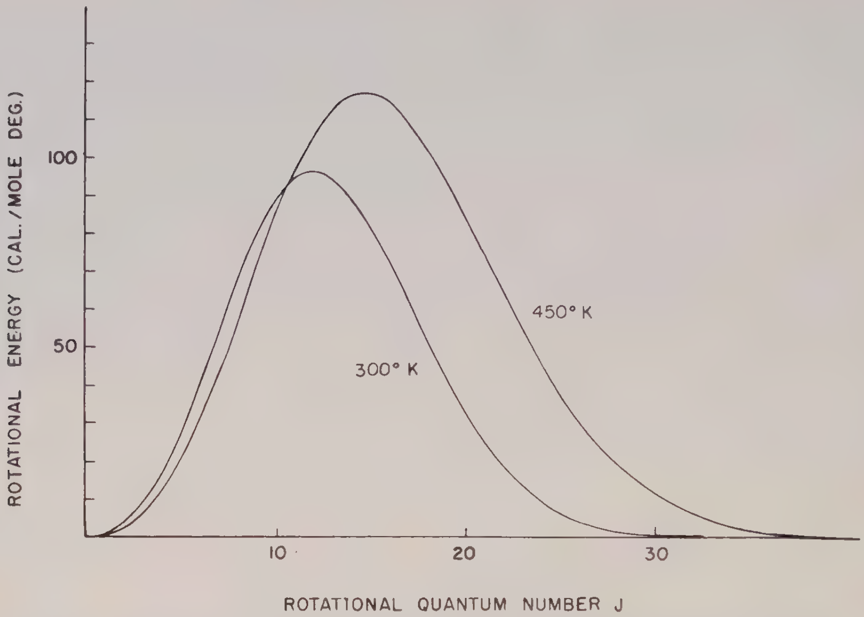

Figure 12. Distribution of rotational energy among quantum states for N_2 at 300°K and 450°K.

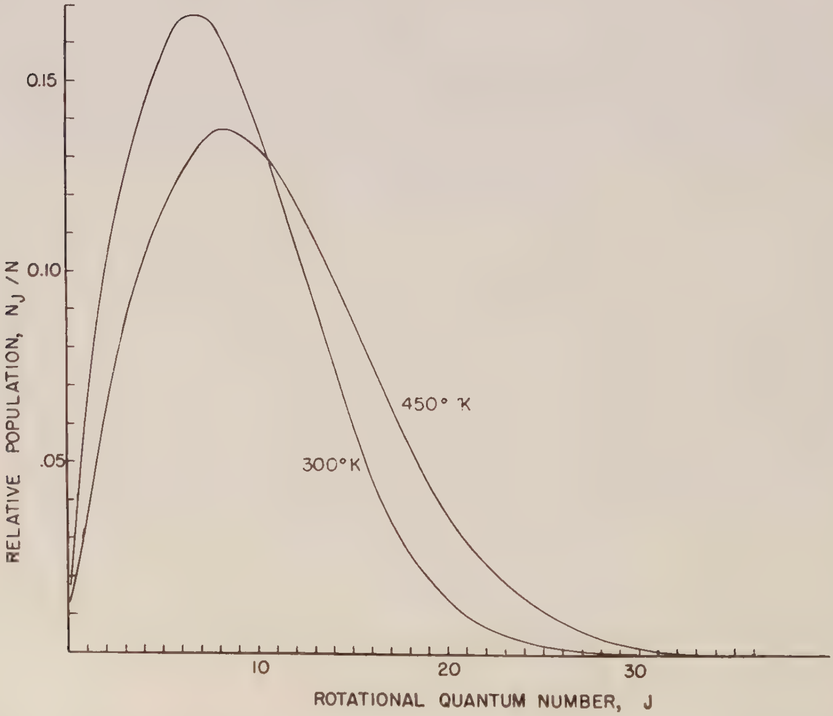

Figure 13. Distribution of molecules among rotational energy states for N_2 at 300°K and 450°K.

of these states the population in $J-2$ at 300°K is less than that in J at 450°K. Therefore, the repopulation must either take place in several steps or $\Delta J > 2$, either of which may be expected to be slow.

The rapid initial equilibration seems, therefore, to be concerned with the low J states. The spacing between high J states makes equilibration in the front impossible and it must come about in a subsequent slow thermal process. This effect should become still more marked in stronger shocks and at high temperatures may lead to very long equilibration times for the states of still higher J which would be encountered.

Our view, then, of the problem of over-excitation is that in the shock front the flow kinetic energy is converted into rotation and translation in proportions which are determined by the dynamics of the collisions, i.e. by the relative cross sections for the processes. This may result in either under- or over-excitaton In either case equilibrium is restored by a relaxation process after the gas has passed through the shock front.

These views are still very tenuous but it is hoped that further theoretical and experimental work will clarify them.

We should like to acknowledge the continued advice and assistance of Professor E. R. Greene as well as the support of the Office of Naval Research.

On a étudié la réflexibilité optique des fronts de choc dans A, N_2, O_2, CO, CO_2, N_2O, CH_4, Cl_2, et HCl. Dans l'Argon, l'épaisseur des fronts de choc, jusqu'au nombre de Mach $M = 1{,}55$, est en accord avec la théorie de Gilbarg et Paolucci. Le temps de relaxation de rotation est d'environ 5,5 collisions dans N_2, et est égal ou inférieur à cette quantité dans les autres gaz. Cependant, pour des chocs plus violents, N_2 ne semble pas atteindre l'equilibre rotationnel dans le front de choc et une discussion théorique qualitative du phénomène est présentée. Dans HCl il semble y avoir une surexcitation de rotation dans le front de choc. Il n'y a d'excitation de vibration pour aucun gaz.

Das optische Reflexionsvermögen von Stosswellenfronten wurde in A, N_2, O_2, CO, CO_2, N_2O, CH_4, Cl_2 und HCl untersucht. Die Dicke der Wellenfronten stimmt für Argon bis zu einer Machzahl von 1,55 mit der Theorie von Gilbarg und Paolucci überein. Die Rotationsrelaxationszeit entspricht für N_2 etwa 5,5 Zusammenstössen; in den anderen Gasen ist sie von der gleichen Grösse oder kleiner. Indessen scheint sich für stärkere Stösse das Rotationsgleichgewicht in der Wellenfront bei N_2 nicht einzustellen; diese Erscheinung wird qualitativ theoretisch diskutiert. In HCl scheint eine Ueber-Anregung der Rotation in der Wellenfront aufzutreten. Keines der Gase zeigt eine Schwingungsanregung.

References

[1] Hornig, D. F., 1947, *Phys. Rev.*, **72,** 179.
[2] Cowan, G. R., and Hornig, D. F., 1950, *J. chem. Phys.*, **17,** 1008.
[3[Greene, E. F., Cowan, G. R., and Hornig, D. F., 1951, *J. chem. Phys.*, **19,** 427.
[4] Greene, E. F., and Hornig, D. F., 1953, *J. chem. Phys.*, **21,** 617.
[5] Andersen, W. H., and Hornig, D. F., 1956, *J. chem. Phys.*, **24,** 767.
[6] Gilbarg, D., and Paolucci, D., 1953, *J. Rat. Mech. Anal.*, **2,** 617.
[7] Sherman, F. S., 1955, *NACA Tech. Note* 3298.
[8] Talbot, L., and Sherman, F. S., 1956, Report No. He–150–137, *Inst. of Eng. Res., University of California.*
[9] Tisza, L., 1932, *Phys. Rev.*, **61,** 531.
[10] Wang-Chang, C. S., and Uhlenbeck, G. E., 1951, Report No. CM–681, *Eng. Res. Inst., University of Michigan.*

Relationship between proton shielding constants and electric dipole moments in the hydrogen halides†

by H. F. HAMEKA

Department of Chemistry, Carnegie Institute of Technology,
Pittsburgh, Pennsylvania

(*Received* 17 *June* 1958)

The proton shielding constants of the hydrogen halides have been calculated employing a molecular wave function built from gauge-invariant atomic orbitals. Each of the molecular wave functions contains a single parameter which is determined from the observed dipole moment. Calculated and experimental values of the shielding constants for HF, HCl, HBr and HI agree to within approximately 10 per cent.

1. INTRODUCTION

The small differences between an applied external magnetic field and the local fields at the positions of the various nuclei of a molecule, which have been observed for many compounds by means of nuclear magnetic resonance measurements, present a useful aid for the understanding of some aspects of the electronic structures of molecules. Usually this phenomenon is described by reporting a chemical shift constant σ. If $\mathbf{H}_e$ is the external field and $\mathbf{H}_A$ is the magnetic field at the position of nucleus A, then σ_A is defined by means of the relation

$$\mathbf{H}_A=(1-\sigma_A)\mathbf{H}_e. \qquad (1)$$

In this paper we will discuss only the shielding of hydrogen nuclei, in particular the proton shift in the hydrogen halides.

The problem of calculating chemical shift constants has been discussed rather elaborately by Ramsay [1], and fairly precise determinations of the proton shift in the hydrogen molecule have been reported; in particular one may mention the considerations of Ramsay [1] and Ishiguro and Koide [2]. As we have discussed previously [3], Ramsay's theoretical expression for σ consists of two terms: the first depends on the wave function of the ground state; the second is an infinite series, which depends on the wave functions of all excited states. Although the total expression is independent of the origin for the vector potential, in cases where an inadequate choice for this origin is made the second term is relatively large and very slowly convergent, which may render a calculation of σ very difficult. For the hydrogen molecule, this difficulty has been overcome by Ramsay [1] and by Ishiguro and Koide [2] in different ways. Taking a special choice for the origin for the vector potential, Ramsay connected the second term with the spin–rotational coupling constant of the molecule; then by using the value of the first term which had been calculated by others [4, 5], he obtained a reliable value for the proton shielding. Ishiguro and Koide obtained an equally satisfactory result for this molecule by means of a variational treatment in which the variational function depends on the magnetic field $\mathbf{H}$ and the nuclear magnetic moments $\boldsymbol{\mu}$. In this calculation an 11-term James Coolidge wave function was used; unfortunately it is hardly possible to extend this method to more complicated systems without great computational difficulties.

---

† Research supported by a grant from the Alfred P. Sloan Foundation to Carnegie Institute of Technology.

An attempt has been made by McGarvey [6] to apply Ramsay's method to a calculation of proton shifts in the hydrogen halides. In this work it was not fully recognized that Ramsay's formula was specially constructed for making use of experimental data on rotational magnetism in molecules and may not be very adequate for complete calculations in more complicated molecules (where such experimental data are not available). There is some confusion about the choice of origin for the vector potential in this paper, and also the omission of the contributions of certain electrons of the halogen atoms does not seem wholly justified.

In order to overcome these difficulties we have made some slight alterations in Ramsay's formulation. In our description [3] use is made of gauge invariant atomic orbitals; as a consequence not only the total expression for σ, but also each term of it, is independent of the choice of origin for the vector potential. In the modified formula the second-order perturbation term is more rapidly convergent than in Ramsay's formula, which has practical advantages. In the present paper applications of this method to the hydrogen halides will be reported.

2. PROTON SHIFT AND ELECTRIC DIPOLE MOMENTS

It has been observed that in some cases there is a very clear connection between the measured σ values and the electronegativities of the corresponding and adjacent nuclei [7, 8]. This seems to confirm that the proton shielding constant depends mainly on the part of the total charge which is centred on the proton and on the overlap charge between the proton and the adjacent nuclei, whereas the contribution of the charges on the other nuclei is either small or not affected by interatomic variations of charge distribution. This property of shielding contants may enable us to calculate them from simple but rather crude wave functions in which only one feature of the molecule is clearly described, namely which parts of the charge distributions belong to the hydrogen and halogen atoms respectively. The wave functions which have been suggested by Mulliken [9] seem to fulfill these requirements. Here the molecular wave function is written as a product of one-electron wave functions, each of which is either an atomic orbital or a linear combination of two atomic orbitals belonging to adjacent nuclei. In this way the ground state of the HF molecule is represented by the properly anti-symmetrized form of the following product

$$\begin{aligned} F &= 1s_F(1)1s_F(2)t_{1F}(4)t_{2F}(5)t_{2F}(6)t_{3F}(7)t_{3F}(8)u_F(9)u_F(10), \\ u_F &= (1+2\lambda_F\Delta_F+\lambda_F{}^2)^{-1/2}(s_H+\lambda_F t_{4F}), \\ t_{4F} &= a_F(2s_F)+b_F(2p_{zF}) \end{aligned} \qquad (2)$$

where $1s_F$, $2s_F$ etc. are atomic orbitals of the F atom, t_{iF} are hybridized (sp^3) orbitals (t_{4F} directed from the F to the H nucleus), Δ_F is the overlap integral between s_H and t_{4F}, λ_F is a charge transfer parameter, and a_F and b_F are hybridization constants.

For symmetrical tetragonal molecules a and b are $\frac{1}{2}$ and $\frac{1}{2}\sqrt{3}$ respectively. It has been shown [10] that in non-symmetrical molecules these values are slightly different. In many cases a and b may be connected with the bond angles [11] but unfortunately this is not possible for the hydrogen halides. There actually are no reliable a and b values available for the hydrogen halides so we have set them equal to $\frac{1}{2}$ and $\frac{1}{2}\sqrt{3}$, although this may not be entirely correct.

The description (2) of the hydrogen halides is rather rough, but on the other hand, the overall charge distribution of the molecule may be made to resemble the real charge distribution fairly well by variating λ. From our considerations it will turn out that the shielding constants depend in the main on the total charge distribution only; because this is also true for the electrical dipole moments we were inclined to believe that, by adjusting λ a relationship might be established between both quantities. In fact, our procedure will be to determine both electric dipole moments and magnetic shielding constants as functions of λ, then adjust λ in such a way as to give the correct dipole moments, and finally calculate the shielding constants from these λ values. It should be realized that the λ values which are thus found will tend to make the exterior parts of the theoretical charge distribution resemble the real charge distribution. For a description of other quantities, which depend mainly on the form of interior parts of the wave functions, completely different λ values might be appropriate; in fact, there could be rather great differences between our λ values and those which result from energy considerations. We do not believe, however, that this would form a serious objection against our considerations.

It may be profitable to make some remarks about the explicit form of the atomic orbitals which appear in our calculations. We have decided to make use of atomic Hartree functions. For F^- and Cl^- the Hartree functions have been calculated and reported [12, 13], but unfortunately there are no such data available for Br^- and I^-. On the other hand, Rb^+ and Cs^+ have been calculated [12, 14] and an attempt may be made to derive the functions for Br^- and I from those of Rb^+ and Cs^+ respectively. A difficulty in doing so is that the usual extrapolation procedures, as reported by Hartree [15], are designed to give correct values for the energies, which are mainly determined by the parts of the wave functions in the vicinity of the nucleus, whereas our results depend mainly on the outer parts of the wave function. Therefore, without intending to contest the validity of Hartree's extrapolation method, we decided to obtain the Br^- and I functions from the Rb^+ and Cs^+ functions by means of pure scaling with the ratios between the ionic radii [16, 17] of Br^- and Rb^+ or I^- and Cs^+ respectively as scaling factors. The results are listed in table 1. It should be pointed out that the wave functions of the inner shell electrons, as well as the exact form of the wave functions near the nuclei, will not be needed in our calculations.

3. CALCULATION OF THE ELECTRIC DIPOLE MOMENTS

For a calculation of the electric dipole moments it is convenient to write the total electronic charge distribution as a sum of three parts:

$$\rho_{\mathrm{X}}(\mathbf{r}) = g_{\mathrm{X}}(r) - \frac{(2\lambda_{\mathrm{X}}\Delta_{\mathrm{X}}+1)\{\mathrm{s}_{\mathrm{X}}^2(r) + 6\mathrm{s}_{\mathrm{X}}(r)\mathrm{p}_{\mathrm{X}}(r)\cos\theta + g\mathrm{p}_{\mathrm{X}}^2(r)\cos^2\theta\}}{8\pi(1+2\lambda_{\mathrm{X}}\Delta_{\mathrm{X}}+\lambda_{\mathrm{X}}^2)},$$

$$\rho_{\mathrm{H}}(\mathbf{r}) = \frac{2\mathrm{s}_{\mathrm{H}}^2(r,\theta)}{1+2\lambda_{\mathrm{X}}\Delta_{\mathrm{X}}+\lambda_{\mathrm{X}}^2},$$

$$\rho_{\mathrm{HX}}(\mathbf{r}) = \frac{2\lambda_{\mathrm{X}}\,\mathrm{s}_{\mathrm{H}}(r,\theta)\{\mathrm{s}_{\mathrm{X}}(r)+3\mathrm{p}_{\mathrm{X}}(r)\cos\theta\}}{(4\pi)^{1/2}(1+2\lambda_{\mathrm{X}}\Delta_{\mathrm{X}}+\lambda_{\mathrm{X}}^2)} \qquad (3)$$

where $g_{\mathrm{X}}(r)$ is the total charge distribution of the halogen ion, $\mathrm{s}_{\mathrm{X}}(r)$ and $\mathrm{p}_{\mathrm{X}}(r)$ are the radial parts of the outer shell s and p orbitals of the halogen and $\mathrm{s}_{\mathrm{H}}(r,\theta)$ is the (1s) orbital of the hydrogen. Use is made of polar coordinates with the halogen nucleus as origin.

r	F		Cl		Br		I	
	2s	2p	3s	3p	4s	4p	5s	5p
0	0·0000	0·0000	0·0000	0·0000	0·0000	0·0000	0·0000	0·0000
0·1	0·4430	0·1140	0·1022	0·1630	−0·1302	0·1982	−0·1750	0·1270
0·2	0·2028	0·3137	−0·2835	0·3032	−0·2270	0·1225	0·0668	−0·1309
0·3	−0·1743	0·4994	−0·4400	0·3120	0·0354	−0·1003	0·2591	−0·2130
0·4	−0·5081	0·6401	−0·3782	0·2304	0·2948	−0·2720	0·1646	−0·1172
0·5	−0·7495	0·7330	−0·1969	0·1038	0·4046	−0·3377	−0·0502	0·0532
0·6	−0·8991	0·7854	−0·0280	−0·0378	0·3876	−0·3125	−0·2540	0·2078
0·7	−0·9739	0·8069	0·2506	−0·1761	0·2742	−0·2383	−0·3720	0·3000
0·8	−0·9937	0·8067	0·4458	−0·3010	0·1120	−0·1236	−0·3912	0·3268
0·9	−0·9758	0·7920	0·6027	−0·4073	−0·0604	−0·0091	−0·3324	0·2998
1·0	−0·9334	0·7679	0·7190	−0·4934	−0·2396	0·1438	−0·2294	0·2326
1·1	−0·8765	0·7384	0·7975	−0·5601	−0·3840	0·2422	−0·0898	0·1400
1·2	−0·8123	0·7057	0·8430	−0·6090	−0·5182	0·3534	0·0580	0·0392
1·4	−0·6787	0·6381	0·8588	−0·6636	−0·6954	0·5162	0·3012	−0·1654
1·6	−0·5538	0·5728	0·8100	−0·6761	−0·7822	0·6256	0·5252	−0·3466
1·8	−0·4453	0·5129	0·7289	−0·6622	−0·7992	0·6820	0·6566	−0·4826
2·0	−0·3547	0·4592	0·6364	−0·6331	−0·7686	0·7000	0·7282	−0·5744
2·2	−0·2809	0·4114	0·5447	−0·5963	−0·7070	0·6882	0·7442	−0·6320
2·4	−0·2216	0·3693	0·4597	−0·5561	−0·6365	0·6612	0·7280	−0·6556
2·6	−0·1743	0·3323	0·3844	−0·5156	−0·5618	0·6222	0·6888	−0·6554
2·8	−0·1367	0·2995	0·3189	−0·4761	−0·4880	0·5760	0·6314	−0·6400
3·0	−0·1070	0·2705	0·2634	−0·4386	−0·4164	0·5300	0·5692	−0·6132
3·2	—	—	0·2166	−0·4036	−0·3544	0·4800	0·5054	−0·5782
3·4	—	—	0·1777	−0·3709	−0·2989	0·4348	0·4462	−0·5398
3·5	−0·0501	0·2112	—	—	—	—	—	—
3·6	—	—	0·1454	−0·3409	−0·2517	0·3916	0·3878	−0·5020
3·8	—	—	0·1188	−0·3133	−0·2127	0·3472	0·3384	−0·4574
4·0	−0·0313	0·1666	0·0970	−0·2880	−0·1774	0·3110	0·2926	−0·4197
4·5	−0·0169	0·1324	0·0581	−0·2340	−0·1083	0·2287	0·1952	−0·3274
5·0	−0·0092	0·1059	0·0347	−0·1908	−0·0664	0·1653	0·1288	−0·2509
5·5	−0·0049	0·0850	0·0208	−0·1562	−0·0398	0·1172	0·0811	−0·1882
6·0	−0·0026	0·0687	0·0124	−0·1281	−0·0239	0·0826	0·0629	−0·1411
6·5	—	—	—	—	−0·0131	0·0558	0·0461	−0·1021
7·0	−0·0007	0·0453	0·0044	−0·0871	−0·0077	0·0382	0·0220	−0·0745
8·0	−0·0002	0·0300	0·0016	−0·0597	−0·0023	0·0191	0·0084	−0·0381
9·0	—	0·0201	0·0005	−0·0412	−0·0009	0·0086	0·0030	−0·0189
10·0	—	0·0135	0·0002	−0·0286	−0·0005	0·0044	0·0010	−0·0100
11·0	—	—	—	—	−0·0001	0·0016	0·0005	−0·0042
12·0	—	0·0064	—	−0·0139	—	0·0008	0·0002	−0·0024
13·0	—	—	—	—	—	—	—	−0·0009
14·0	—	0·0029	—	−0·0068	—	0·0002	—	−0·0005
16·0	—	0·0014	—	−0·0034	—	—	—	−0·0001
18·0	—	0·0007	—	−0·0017	—	—	—	—
20·0	—	0·0003	—	−0·0008	—	—	—	—
22·0	—	0·0002	—	−0·0004	—	—	—	—
24·0	—	—	—	−0·0002	—	—	—	—
26·0	—	—	—	−0·0001	—	—	—	—

Table 1. Reported and extrapolated Hartree functions of outer shell electrons.

The dipole moment may now be expressed as

$$\mu_X = \frac{(2\lambda_X\Delta_X+1)\alpha_X - 4\lambda_X\beta_X + R_X(\lambda_X^2+2\lambda_X\Delta_X-1)}{1+2\lambda_X\Delta_X+\lambda_X^2} \tag{4}$$

where

$$\alpha_X = \int s_X(r)p_X(r)r\,dr$$

$$\beta_X = (4\pi)^{-1/2}\left\{\int s_X(r)r\cos\theta\, s_H(r,\theta)\,dt + 3\int p_X(r)r\cos^2\theta\, s_H(r,\theta)\,dt\right\}. \tag{5}$$

The integrals α_X have been calculated exactly from the Hartree functions, but in the integrals β_X the orbitals s_X and p_X have been approximated by Slater functions and the results have been obtained from the tables of Mulliken *et al.* [18]. The few integrals which were not listed were obtained by either interpolating or extrapolating the tables with respect to the quantum numbers. The integrals α_X, γ_X, Δ_X and $\beta_X = R_X\Delta_X - \gamma_X$, together with the internuclear distances R_X [19] are listed in table 2; values obtained by interpolation or extrapolation are marked by asterisks.

	Δ	α	γ	R/a_0	β
F	0·634	1·101	0·311	1·733	0·788
Cl	0·650	1·681	0·408	2·409	1·158
Br	0·666*	2·132	0·428*	2·672	1·352*
I	0·601	2·593	0·458*	3·031	1·364*

Table 2. Quantities which are required for the calculation of dipole moments.

In this way the following expressions for the dipole moments are obtained

$$\left.\begin{aligned}
\mu_F &= (1{\cdot}733\,\lambda_F^2 + 0{\cdot}441\,\lambda_F - 0{\cdot}632)\,ea_0/(\lambda_F^2 + 1{\cdot}268\,\lambda_F + 1),\\
\mu_{Cl} &= (2{\cdot}409\,\lambda_{Cl}^2 + 0{\cdot}686\,\lambda_{Cl} - 0{\cdot}728)\,ea_0/(\lambda_{Cl}^2 + 1{\cdot}300\,\lambda_{Cl} + 1),\\
\mu_{Br} &= (2{\cdot}672\,\lambda_{Br}^2 + 0{\cdot}991\,\lambda_{Br} - 0{\cdot}540)\,ea_0/(\lambda_{Br}^2 + 1{\cdot}332\,\lambda_{Br} + 1),\\
\mu_I &= (3{\cdot}031\,\lambda_I^2 + 1{\cdot}304\,\lambda_I - 0{\cdot}438)\,ea_0/(\lambda_I^2 + 1{\cdot}202\,\lambda_I + 1).
\end{aligned}\right\} \tag{6}$$

The values $\mu_{Cl} = 1{\cdot}03D$, $\mu_{Br} = 0{\cdot}79D$ and $\mu_I = 0{\cdot}38D$ have been reported by Zahn [20]. For HF a vast variety of different values have been reported; we have followed Syrkin and Dyatkina [21] in choosing $\mu_F = 2{\cdot}00D$. In order to obtain these values from (6) the following λ values have to be taken: $\lambda_F = 1{\cdot}5440$, $\lambda_{Cl} = 0{\cdot}7127$, $\lambda_{Br} = 0{\cdot}4904$ and $\lambda_I = 0{\cdot}2970$. Although there seem to exist rather great discrepancies between these results and λ values which result from energy considerations [22] we believe that the exterior part of the charge distribution is best represented by our λ values.

4. CALCULATION OF THE PROTON SHIFT

As has been discussed previously [3] the vector potential acting on electron i will be

$$\mathbf{A}_i(\mathbf{q}) = \tfrac{1}{2}[\mathbf{H}, \mathbf{r}_i - \mathbf{q}] + \frac{[\boldsymbol{\mu}_H\,\mathbf{r}_{Hi}]}{r_{Hi}^3}. \tag{7}$$

With the function $\phi(\mathbf{q})$ defined by

$$\phi_j(\mathbf{q}) = \tfrac{1}{2}([\mathbf{H}\mathbf{q}]\mathbf{r}_j) \tag{8}$$

use is made in our calculations of the following gauge invariant atomic orbitals

$$\tilde{\psi}_{nlm} = \psi_{nlm} \exp\left[ie\{\phi(\mathbf{q}) - \phi(\mathbf{a})\}/\hbar c\right] \tag{9}$$

where $\mathbf{a}$ is the position of the nucleus and ψ_{nlm} is the atomic orbital in the absence of a magnetic field. The orbitals $\tilde{\psi}_{nlm}$ are now in accord with the choice of origin $\mathbf{q}$ for the vector potential. The Hamiltonian is then

$$\mathscr{H}_2 = \sum_{i=1}^{N} \frac{1}{2m_i}\left(\mathbf{p}_i - \frac{e}{c}\mathbf{A}_i(\mathbf{q})\right)^2 + V(\mathbf{r}_1, \mathbf{r}_2, \ldots \mathbf{r}_N). \tag{10}$$

It has been shown [3] that the proton shielding constant may then be obtained from

$$\sigma_i = \left(\frac{\partial^2}{\partial\mu_i\,\partial H_i}\left[\mathscr{H}_{0,0} - \sum_{n\neq 0}\frac{\mathscr{H}_{n,0}\mathscr{H}_{0,n}}{E_n - E_0}\right]\right)_{\boldsymbol{\mu}=\mathbf{H}=0} \tag{11}$$

where

$$\mathscr{H}_{k,l} = \langle\Psi_k|\mathscr{H}_{0p}|\Psi_l\rangle. \tag{12}$$

It should be noticed that the matrix elements $\mathscr{H}_{k,l}$ are independent of the choice of origin for the vector potential. For the sake of mathematical simplicity the first and second terms of (11) have been named first- and second-order perturbation term respectively.

It may easily be seen that in the case of the hydrogen halides, if the molecular wave function is written as a product of mono-electronic wave functions $\psi_1'(1)$, $\psi_2'(2)$, $\psi_N'(N)$, the first-order perturbation term is given by

$$\mathscr{H}_{0,0} = \sum_{i=1}^{N}\frac{1}{2m}\left\langle \psi_i'(i)\left|\left(\mathbf{p}_i - \frac{e}{c}\mathbf{A}_i\right)^2\right|\psi_i'(i)\right\rangle. \tag{13}$$

This expression will now be divided into three parts: (1) the part which contains only wave functions which are centred on the halogen nucleus, (2) the part which contains only wave functions which are centred on the hydrogen and (3), the part which contains both halogen and hydrogen atomic orbitals. Because each term is independent of the choice of origin for the vector potential, this origin may now be chosen in such a way as to facilitate the calculations. Therefore, in the first part it will be chosen as the halogen nucleus; in the second and third parts as the hydrogen nucleus. It may then easily be verified that the matrix elements $\langle\tilde{\psi}_i^{(0)}|\mathscr{H}^{(2)}|\tilde{\psi}_i^{(0)}\rangle_1$ will all be zero (see [3] for nomenclature.). Then, if the first order perturbation terms of σ are called σ_x', σ_y' and σ_z' and if σ' is the average

$$\sigma' = \tfrac{1}{3}(\sigma_x' + \sigma_y' + \sigma_z'), \tag{14}$$

σ' may be written as (cf. (3))

$$\sigma' = \frac{e^2}{3mc^2a_0}\left[\int \rho_{\mathrm{X}}(\mathbf{r})\left(\frac{1}{r_{\mathrm{H}}} - \frac{R_{\mathrm{X}}z}{r_{\mathrm{H}}{}^3}\right)d\tau + \int\frac{\rho_{\mathrm{H}}(\mathbf{r})}{r_{\mathrm{H}}}\,d\tau + \int\frac{\rho_{\mathrm{HX}}(\mathbf{r})}{r_{\mathrm{H}}}\,d\tau\right] \tag{15}$$

where use has been made of a coordinate system with the origin on the halogen nucleus and the Z-axis along the line XH and R_{X} is the distance HX.

From (3), (15) and the results of Appendix A follows that

$$\begin{aligned}\sigma' = \frac{e^2}{3mc^2a_0}\Bigg[\int_R^\infty \frac{2\mathrm{s}^2+6\mathrm{p}^2}{r}\,dr + \frac{2\lambda\Delta+1}{2(1+2\lambda\Delta+\lambda^2)}\Bigg\{-\int_R^\infty \frac{\mathrm{s}^2}{r}\,dr \\ +2\int_0^R \frac{r\mathrm{sp}}{R^2}\,dr - 4\int_R^\infty \frac{R\mathrm{sp}}{r^2}\,dr + \frac{12}{5}\int_0^R \frac{r^3\mathrm{p}^2}{R^2}\,dr - \int_R^\infty\left(\frac{18R^2}{5r^3}+\frac{3}{r}\right) \\ \times\,\mathrm{p}^2\,dr\Bigg\} + \frac{2}{1+2\lambda\Delta+\lambda^2} + \frac{2\lambda}{1+2\lambda\Delta+\lambda^2}\Bigg\{\frac{2e^{-R}}{R}\int_0^R \mathrm{s}\sinh r\,dr \\ + \frac{2\sinh R}{R}\int_R^\infty \mathrm{s}\,e^{-r}\,dr + \frac{3(R+1)\,e^{-R}}{R^2}\int_0^R \frac{(r-1)\,e^r+(r+1)\,e^{-r}}{r^2}\,\mathrm{p}\,dr \\ + \frac{3\{(R-1)\,e^R+(R+1)e^{-R}\}}{R^2}\int_R^\infty \frac{(r+1)\,e^{-r}}{r^2}\,\mathrm{p}\,dr\Bigg\}\Bigg],\end{aligned} \tag{16}$$

where for clarity the subscripts in s_X, p_X, λ_X, Δ_X and R_X have been omitted. It may easily be seen that the contribution of the inner shell electrons to I_1 is negligible.

	g	s^2	sp	p^2	$\mathrm{s}\,\mathrm{s}_H$	$\mathrm{p}\,\mathrm{s}_H$
F	0·8792	−0·0483	0·2871	−0·2907	0·3981	0·8387
Cl	0·7562	−0·0387	0·1763	−0·3222	0·3071	0·8044
Br	0·7494	−0·0563	0·1137	−0·2849	0·3035	0·7911
I	0·8152	−0·0657	0·0594	−0·3593	0·2791	0·7413

Table 3. Integrals which occur in the formulae of the first-order perturbation term of the proton shielding constant.

The various integrals which occur in (16) have been calculated numerically, making use of the Hartree functions of table 1. The values are listed in table 3. It is then found that

$$\begin{aligned}\sigma_F' &= \left[0{\cdot}8792 + \frac{1{\cdot}9720+(2{\cdot}4737-0{\cdot}0519\,\Delta_F)\lambda_F}{1+2\lambda_F\Delta_F+\lambda_F^2}\right]\times 1{\cdot}7748\times 10^{-5} \\ \sigma_{Cl}' &= \left[0{\cdot}7562 + \frac{1{\cdot}9077+(2{\cdot}2231-0{\cdot}1846\,\Delta_{Cl})\lambda_{Cl}}{1+2\lambda_{Cl}\Delta_{Cl}+\lambda_{Cl}^2}\right]\times 1{\cdot}7748\times 10^{-5} \\ \sigma_{Br}' &= \left[0{\cdot}7494 + \frac{1{\cdot}8862+(2{\cdot}1892-0{\cdot}2275\,\Delta_{Br})\lambda_{Br}}{1+2\lambda_{Br}\Delta_{Br}+\lambda_{Br}^2}\right]\times 1{\cdot}7748\times 10^{-5} \\ \sigma_I' &= \left[0{\cdot}8152 + \frac{1{\cdot}81272+(2{\cdot}0409-0{\cdot}3656\,\Delta_I)\lambda_I}{1+2\lambda_I\Delta_I+\lambda_I^2}\right]\times 1{\cdot}7748\times 10^{-5}.\end{aligned} \tag{17}$$

For a calculation of the second-order perturbation term use will be made of the method which has been derived for the hydrogen molecule. There are, however, some minor differences between the cases of the hydrogen molecule and of the hydrogen halides. The terms which result from an excitation of an electron into an anti-bonding excited π orbital will be much smaller for the halides than for the hydrogen molecule, whereas in the case of the hydrogen halides there will be a contribution of an anti-bonding σ orbital which will appear to be the predominant term. This anti-bonding σ orbital may be represented by

$$\begin{aligned} \mathrm{v}_\mathrm{X} &= (1-2\lambda_\mathrm{X}'\Delta_\mathrm{X}+\lambda_\mathrm{X}'^2)^{-1/2}(\mathrm{s}_\mathrm{H}-\lambda_\mathrm{X}'\mathrm{t}_{4\mathrm{X}}) \\ \lambda_\mathrm{X}' &= (1+\lambda_\mathrm{X}\Delta_\mathrm{X})/(\lambda_\mathrm{X}+\Delta_\mathrm{X}). \end{aligned} \tag{18}$$

Now all cases in which either one of the valence or lone-pair electrons is excited into the orbital v_X ought to be considered, but for the sake of simplicity we will assume that either an $n\mathrm{p}_\mathrm{X}$ or an $n\mathrm{p}_y$ electron is excited. (This will not affect the final result.) By analogy with our considerations for the hydrogen molecule [3] it is found that the contribution of this state to the shielding constant σ'' is

$$\begin{aligned} \sigma'' = -[\{\lambda_\mathrm{X}'\epsilon_0\hbar^2\}/\{2mc^2a_0(1-2\lambda_\mathrm{X}'\Delta_\mathrm{X}+\lambda_\mathrm{X}'^2)\Delta E\}]\{(\lambda_\mathrm{X}'\langle \mathrm{p}_y|\mathrm{p}_y\rangle \\ +R_\mathrm{X}\langle \mathrm{p}_y|y|\mathrm{s}_\mathrm{H}\rangle)(\langle \mathrm{p}_y|r_\mathrm{H}^{-3}|\mathrm{p}_y\rangle+\tfrac{1}{3}R_\mathrm{X}\sqrt{(3)}\langle \mathrm{p}_y|(y/rr_\mathrm{H}^3)|(\partial \mathrm{s}_\mathrm{X}/\partial r)\rangle)\} \end{aligned} \tag{19}$$

where $\Delta E/\epsilon_0$ is the excitation energy in units e^2/a_0 which results from the excitation of a lone pair electron into an anti-bonding σ orbital. The first two integrals may, to a first approximation, be found in the tables of Mulliken *et al.* [18]. According to the method which has been discussed in Appendix A, the third integral may be reduced to

$$\begin{aligned} \langle \mathrm{p}_y|r_\mathrm{H}^{-3}|\mathrm{p}_y\rangle &= \int_0^R \frac{\rho^2(r)}{R^3}\,dr+\int_R^\infty \frac{\rho^2(r)}{r^3}\,dr \\ \mathrm{p}_y &= (3/4\pi)^{1/2}\sin\theta\cos\phi\, r^{-1}\,\mathrm{p}(r). \end{aligned} \tag{20}$$

It may be suspected that the fourth integral may be neglected with respect to the third one. In fact, a calculation with hydrogen-like functions reveals that it is very small. Therefore this term has been neglected. All quantities which are required for a calculation of σ'' are listed in table 4. It should be observed that these numbers are not very accurate, but, especially for the heavier halogens, σ'' is relatively small so that no very accurate determinations are required. For this reason it has been assumed that the two integrals which are missing in table 4 may both be approximated by 0·35. Then it is found that

	$\Delta E/\epsilon_0$	$\langle \mathrm{p}_y\|y\|\mathrm{s}\rangle$	$\langle \mathrm{p}_{y\mathrm{H}}\|r_\mathrm{H}^{-3}\|\mathrm{p}_y\rangle$
F	1·34†	0·302‡	0·16148
Cl	1·01†	0·439‡	0·05646
Br	0·97†	—	0·04369
I	0·94†	—	0·02835

† See Mulliken [23]. ‡ See Mulliken *et al.* [18].

Table 4. Quantities that occur in the formulae of the second-order perturbation term of the proton shielding constant.

$$\begin{aligned} \sigma_\mathrm{F}'' &= \{-0{\cdot}321\lambda_\mathrm{F}'(\lambda_\mathrm{F}'+0{\cdot}523)\times 10^{-5}\}/\{1-2\lambda_\mathrm{F}'\Delta_\mathrm{F}+\lambda_\mathrm{F}'^2\} \\ \sigma_\mathrm{Cl}'' &= \{-0{\cdot}149\lambda_\mathrm{Cl}'(\lambda_\mathrm{Cl}'+1{\cdot}058)\times 10^{-5}\}/\{1-2\lambda_\mathrm{Cl}'\Delta_\mathrm{Cl}+\lambda_\mathrm{Cl}'^2\} \\ \sigma_\mathrm{Br}'' &= \{-0{\cdot}120\lambda_\mathrm{Br}'(\lambda_\mathrm{Br}'+0{\cdot}935)\times 10^{-5}\}/\{1-2\lambda_\mathrm{Br}'\Delta_\mathrm{Br}+\lambda_\mathrm{Br}'^2\} \\ \sigma_\mathrm{I}'' &= \{-0{\cdot}080\lambda_\mathrm{I}'(\lambda_\mathrm{I}'+1{\cdot}061)\times 10^{-5}\}/\{1-2\lambda_\mathrm{I}'\Delta_\mathrm{I}+\lambda_\mathrm{I}'^2\}. \end{aligned} \tag{21}$$

For an estimation of the order of magnitude of the other terms which occur in the second-order perturbation term it may be useful to consider again our results for the hydrogen molecule [3]. Here the terms which result from the first anti-bonding orbital were relatively great, but this was mainly due to the fact that the overlap integral between two 2p orbitals was almost unity. In the case of the halogen halides the corresponding overlap integral, for example in the case of HF, between a $3p_\pi$ and a $2p_\pi$ orbital of F and H respectively is smaller than 0·4, which causes the corresponding σ'' term to become smaller by a factor of ten. Furthermore it is to be expected that all integrals in the case of the hydrogen halides will be much smaller than the corresponding quantities for hydrogen. (In the case of hydrogen these integrals contained overlap charges of identical orbitals separated by a relatively small internuclear distance, whereas in the case of the hydrogen halides the atomic orbitals are non-identical and the internuclear distances much greater.) Consequently the contribution of the higher excited states to σ'' have been neglected.

	$10^5\sigma'$	$10^5\sigma''$	theor.	exp. [24]
F	3·468	−0·682	2·79	2·78
Cl	3·826	−0·420	3·41	3·08
Br	4·034	−0·317	3·72	3·47
I	4·343	−0·166	4·18	4·36

Table 5. Calculated and experimental proton shielding constants for the hydrogen halides; σ' and σ'' are respectively the calculated first- and second-order perturbation terms.

By making use of the λ values which have been derived in § 3 from the dipole moments, the proton shielding constants may easily be found from the equations (17), (18) and (21). The results, together with the experimental values, are listed in table 5.

5. Discussion

In view of the many approximations which have been used some deviations between theoretical and experimental shielding constants should be expected. On considering the results of table 5 one may conclude that our calculations of the proton shielding constants for the hydrogen halides reproduce the experimental values to within approximately 10 per cent. It should be observed that the excellent agreement for HF is fortuitous, especially since the experimental shielding constant is not more accurate than within $0{\cdot}2\times10^{-5}$. Our method seems to be more successful for an application to the hydrogen halides than in the case of the hydrogen molecule [3]. This is probably due to the fact that for the hydrogen halides the second-order perturbation terms are relatively smaller and may be calculated with greater accuracy.

There are not many data available which enable us to check the λ values which we obtained. Only in the case of HF Duncan [25] has performed a self-consistent field calculation; it appears that our corresponding λ value is roughly in agreement with his results.

A calculation of proton shielding constants has some pleasant features which might explain the fairly accurate results which we have obtained. First it has become clear that the calculated values are not very sensitive to changes in the wave functions and secondly it seems that the parameters λ amply account for the various aspects of the wave functions which are important in determining σ.

I wish to express my gratitude to Dr. Robert G. Parr for many inspiring discussions and some valuable suggestions and to Dr. W. G. Schneider for sending me his experimental data before they were published.

APPENDIX A

The first-order perturbation term may be expressed in terms of the following integrals:

$$I_1=\int h(r)\,t^{-3}\{r^2-Rr\cos\theta\}\sin\theta\,dr\,d\theta\,d\phi \tag{A1}$$

$$I_2=\int h(r)\,t^{-3}\{r^2-Rr\cos\theta\}\cos\theta\sin\theta\,dr\,d\theta\,d\phi \tag{A2}$$

$$I_3=\int h(r)\,t^{-3}\{r^2-Rr\cos\theta\}\cos^2\theta\sin\theta\,dr\,d\theta\,d\phi \tag{A3}$$

$$I_4=\int h(r)\,t^{-1}e^{-t}\sin\theta\,dr\,d\theta\,d\phi \tag{A4}$$

$$I_5=\int h(r)\,t^{-1}e^{-t}\cos\theta\sin\theta\,dr\,d\theta\,d\phi \tag{A5}$$

where t indicates a distance with respect to a point at the Z-axis at a distance R from the origin:

$$t=(R^2+r^2-2Rr\cos\theta)^{1/2}. \tag{A6}$$

When r is kept constant the integration over θ may be replaced by an integration over t. It is then found that

$$I_1=4\pi\int_R^\infty\frac{h(r)}{r}\,dr \tag{A7}$$

$$I_2=\frac{4\pi}{3}\left\{-\int_0^R\frac{rh(r)}{R^2}\,dr+2\int_R^\infty\frac{Rh(r)}{r^2}\,dr\right\} \tag{A8}$$

$$I_3=-\frac{16\pi}{15}\int_0^R\frac{r^2h(r)}{R^3}\,dr+4\pi\int_R^\infty\left(\frac{2R^2}{5r^3}+\frac{1}{3r}\right)h(r)\,dr \tag{A9}$$

$$I_4=\frac{4\pi e^{-R}}{R}\int_0^R\frac{\sinh r}{r}\,h(r)\,dr+\frac{4\pi\sinh R}{R}\int_R^\infty\frac{e^{-r}}{r}\,h(r)\,dr \tag{A10}$$

$$I_5=\frac{2\pi(R+1)e^{-R}}{R^2}\int_0^R\frac{(r-1)\,e^{r}+(r+1)\,e^{-r}}{r^2}\,h(r)\,dr+\frac{2\pi\{(R-1)\,e^{R}+(R+1)\,e^{-R}\}}{R^2}\int_R^\infty\frac{(r+1)\,e^{-r}}{r^2}\,h(r)\,dr. \tag{A11}$$

On a calculé les constantes d'écran protoniques pour les hydracides halogénés en utilisant une fonction d'onde moléculaire construite à partir d'orbitales atomiques gauges-invariantes. Chacune des fonctions d'onde moléculaires contient un seul paramètre qui est déterminé par le moment dipolaire observé. Les valeurs calculées et expérimentales des constantes d'écran, pour HF, HCl, HBr, et HI, sont en accord à dix pour cent près environ.

Die Proton-Abschirmungskonstanten der HalogenWasserstoffe werden mit Hilfe einer molekularen Wellenfunktion berechnet, die aus eichinvarianten atomic orbitals aufgebaut ist. Jede der molekularen Wellenfunktionen enthält einen einzigen Parameter, der aus dem beobachteten Dipolmoment bestimmt wird. Die berechneten und die gemessenen Werte der Abschirmkonstanten stimmen für HF, HCl, HBr und HJ etwa innerhalb 10 Prozent überein.

REFERENCES

[1] RAMSAY, N. F., 1950, *Phys. Rev.*, **78,** 699.
[2] ISHIGURO, E., and KOIDE, S., 1954, *Phys. Rev.*, **94,** 350.
[3] HAMEKA, H. F., 1958, *Mol. Phys.*, **1,** 203.
[4] ANDERSON, H. L., 1949, *Phys. Rev.*, **76,** 1460.
[5] NEWELL, G. F., 1950, *Phys. Rev.*, **80,** 476.
[6] McGARVEY, B. R., 1957, *J. chem. Phys.*, **27,** 68.
[7] SHOOLERY, J. N., 1953, *J. chem. Phys.*, **21,** 1899.
[8] GUTOWSKY, H. S., McCALL, D. W., McGARVEY, B. R., and MEYER, L. H., 1952, *J. Amer. chem. Soc.*, **74,** 4809.
[9] MULLIKEN, R. S., 1935, *J. chem. Phys.*, **3,** 373.
[10] DUNCAN, A. B. F., and POPLE, J. A., 1953, *Trans. Faraday Soc.*, **49,** 217.
[11] HAMEKA, H. F., and LIQUORI, A. M., 1956, *Proc. Kon. Ak. Wet.*, Ser. B, **59,** 242.
[12] HARTREE, D. R., 1935, *Proc. roy. Soc.* A, **151,** 96.
[13] HARTREE, D. R., 1933, *Proc. roy. Soc.* A, **141,** 282.
[14] HARTREE, D. R. 1934, *Proc. roy. Soc.* A, **143,** 506.
[15] HARTREE, D. R., 1957, *The Calculation of Atomic Structures* (London: Chapman & Hall).
[16] PAULING, L., 1927, *J. Amer. chem. Soc.*, **49,** 765.
[17] GOLDSCHMIDT, M., 1926, *Skr. norske VidenskAkad.*, No. 2, 117.
[18] MULLIKEN, R. S., RICHE, C. A., ORLOFF, D., and ORLOFF, H., 1949, *J. chem. Phys.*, **17,** 1248.
[19] HERZBERG, G., 1950, *Spectra of Diatomic Molecules* (New York : van Nostrand), p. 358.
[20] ZAHN, C. T., 1924, *Phys. Rev.*, **24**, 400.
[21] SYRKIN, Y. K., and DYATKINA, M. E., 1950, *Structure of Molecules* (London: Butterworths).
[22] DUNCAN, A. B. F., 1955, *J. Amer. chem. Soc.*, **77,** 2107.
[23] MULLIKEN, R. S., 1934, *Phys. Rev.*, **46,** 549.
[24] SCHNEIDER, W. G., BERNSTEIN, H. J., and POPLE, J. A., 1958, *J. chem. Phys.*, **28,** 601.
[25] DUNCAN, A. B. F., 1955, *J. Amer. chem. Soc.*, **77,** 2107.

Chemical shifts of thallium resonance spectra in solutions of thallous salts

by R. FREEMAN, R. P. H. GASSER, R. E. RICHARDS
and D. H. WHEELER
Physical Chemistry Laboratory, South Parks Road, Oxford

(*Received* 10 *September* 1958)

Chemical shifts of the thallium nuclear resonance have been measured in solutions of thallous hydroxide, fluoride, acetate, formate, nitrate, and perchlorate of varying concentrations and in the presence of added substances. At low concentrations the chemical shift varies non-linearly with concentration of anion and can be correlated with the formation of ion-pairs. In stronger solutions the variation of chemical shift becomes linear, and is attributed to interactions between the ion-pairs and the added substances.

1. Introduction

Gutowsky and McGarvey [1] found that solutions of two thallous salts show a marked concentration dependence of the chemical shift of the thallium nuclear resonance. Furthermore, the shifts varied in a closely linear manner with anion concentration and it appeared that these results were inconsistent with the formation of ion pairs even at concentrations as high as 6 molar.

There is, however, considerable evidence from other sources [2–6] that there is appreciable association of the ions in thallous solutions at high concentrations and so the following experiments were undertaken to study these and other solutions in greater detail. A considerable range of solutions and concentrations has been studied. The nature of concentrated electrolyte solutions is imperfectly understood and so in order to explain the NMR results in detail certain assumptions have been necessary. However, some conclusions about the nature of these solutions are strongly indicated by the NMR results.

2. Experimental

2.1. *Compounds*

Thallous acetate, formate and nitrate were obtained from Messrs. B. D. H. and recrystallized from water. Thallous hydroxide was prepared by mixing strong solutions of the acetate and of potassium hydroxide. The yellow solid was recrystallized, dissolved immediately in water and the solution standardized by titration. Care was taken to exclude atmospheric carbon dioxide.

The fluoride was prepared by neutralizing the carbonate with aqueous hydrofluoric acid in a platinum vessel and the product was recrystallized from water. Thallous perchlorate was obtained similarly by the action of perchloric acid on thallous carbonate.

The other salts and acids used were 'analar' reagents.

2.2. *Apparatus*

The variable frequency spectrometer described by Freeman *et al.* (1957) was used, with a magnetic field of 4370·9 gauss.

3. Results

All the solutions studied showed a single thallium resonance line for each of the two naturally occurring thallium isotopes. The resonance from ^{205}Tl gave the strongest signals and so most of the measurements were made on this isotope. The line widths were usually approximately $\frac{1}{2}$ gauss or 500 c/s.

The chemical shift of the thallium resonance was measured for each solution with respect to 0·3 M aqueous thallous nitrate solution and is expressed as

$$\sigma = \frac{\nu_s - \nu_r}{\nu_r} \times 10^4$$

where ν_s and ν_r are the resonance frequencies of the sample and reference respectively at constant magnetic field, so that positive shifts imply decreased magnetic shielding.

The measurements may be grouped under five headings.

3.1. *Addition of salts*

Aqueous solutions of TlX, each 0·3 M in TlX, contained different molar concentrations of KX, where X is hydroxide, acetate, formate and fluoride. The results are shown in figure 1, in which the chemical shift of the thallium resonance is plotted against the molar concentration of the added salt, KX.

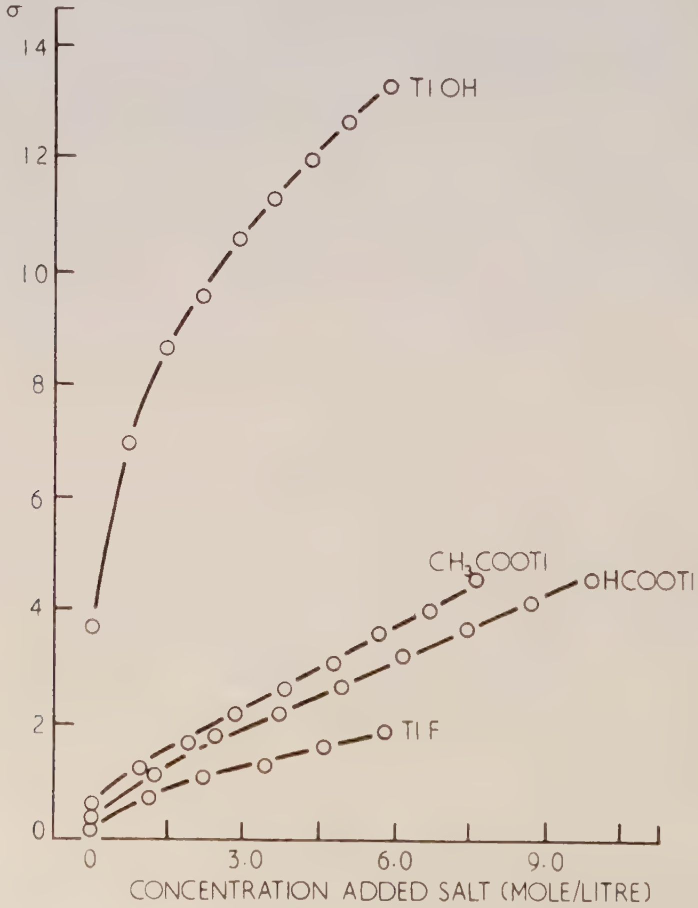

Figure 1.

The curves are linear at high concentrations of KX, but at low concentrations a curvature occurs which is particularly marked for the hydroxide. This curvature occurs with the acetate, formate and fluoride at lower concentrations. Measurements on more dilute solutions of thallous acetate are shown in figure 2. Addition of sodium acetate instead of the potassium salt was found by Gutowsky and McGarvey to produce similar results.

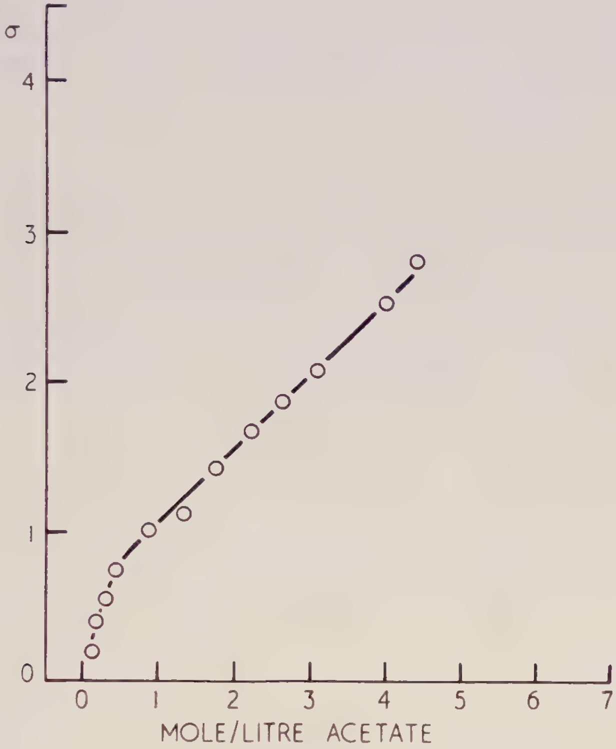

Figure 2.

3.2. *Addition of acids*

Aqueous solutions of TlX, each 0·3 M in TlX, contained different molar concentrations of HX, where HX is acetic acid, formic acid, and nitric acid. The solutions of thallous perchlorate contained only 0·2 M thallous ion, because of the limited solubility of the salt. Many of the thallous nitrate solutions were super-saturated. The results are summarized in figure 3, from which it is clear that closely linear variation is observed; no curvature at low concentrations could be detected.

3.3. *Methanol/water mixtures as solvent*

Solutions of thallous acetate were made up, in which the mole fraction of thallous acetate compared with (methanol + water) was constant. The thallium shift is plotted in figure 4 as a function of the ratio (moles of methanol)/(moles of water + methanol).

3.4. *Solutions of constant anion concentration*

Aqueous solutions of thallous and potassium acetate were studied in which the relative concentrations of thallous and potassium ions were varied, but in which the acetate concentration remained constant. Two series of experiments were carried out with acetate concentrations of 1·5 M and 4·0 M. In each case the thallium resonance showed no shifts as the ratio of Tl/K was varied, the shift depending only on the acetate concentration.

3.5. *Effect of bulk susceptibility*

This was studied experimentally by measuring the shifts in a series of twelve solutions containing thallous, nickel and potassium nitrates, of constant total nitrate concentration but varying paramagnetism. No change in the resonance frequency was detected up to a concentration of 0·3 g ions of nickel per litre.

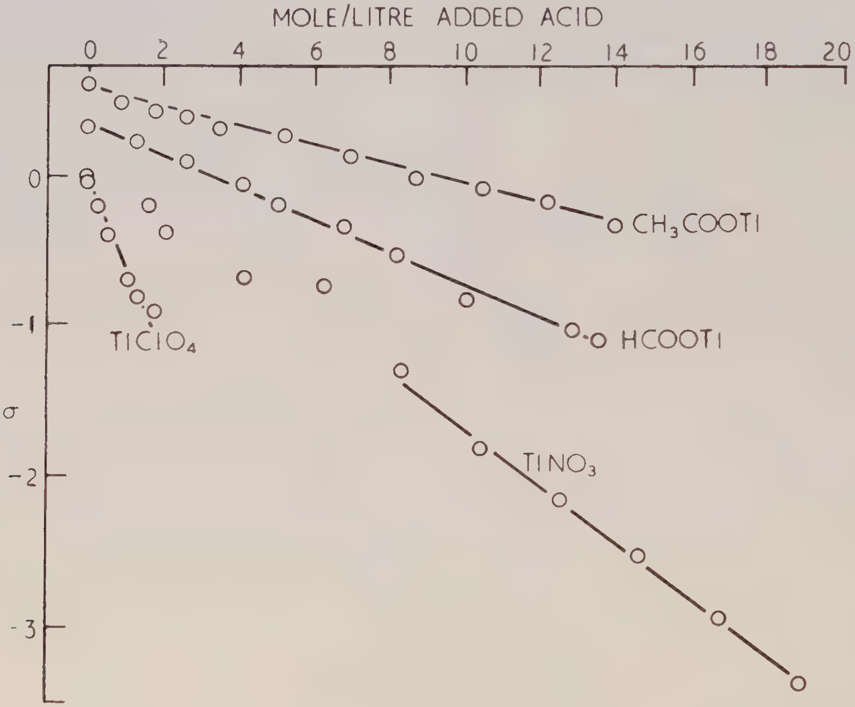

Figure 3.

4. Discussion

These experiments show a more complicated behaviour than the simple linear curves observed by Gutowsky and McGarvey [1], over limited concentration ranges, and it is clear that the explanations given by them are incomplete.

The chemical shifts are far too large to be accounted for by variation of the bulk susceptibility of the solutions which are diamagnetic, and this is confirmed by the experiments in the presence of paramagnetic salts. No attempt has been made to apply the very small correction for diamagnetism to the shifts discussed below.

The results of figures 1 and 2 show that on addition of salts there are at least two processes to be considered. At low concentrations the chemical shift varies non-linearly with anion concentration, but at high concentrations the variation becomes closely linear.

It is convenient to consider first the behaviour of the solutions at low concentrations. We shall assume that the linear variation of chemical shift with anion concentration arises from a process which occurs in all the solutions and this assumption will be examined later on page 82. This assumption allows the linear portion to be extrapolated to low concentrations and subtracted from the experimental curve, leaving only the curved portion, describing the effect which disappears at high concentrations. This subtraction has been done for thallous hydroxide and thallous acetate, and the results are shown in figures 5 and 6.

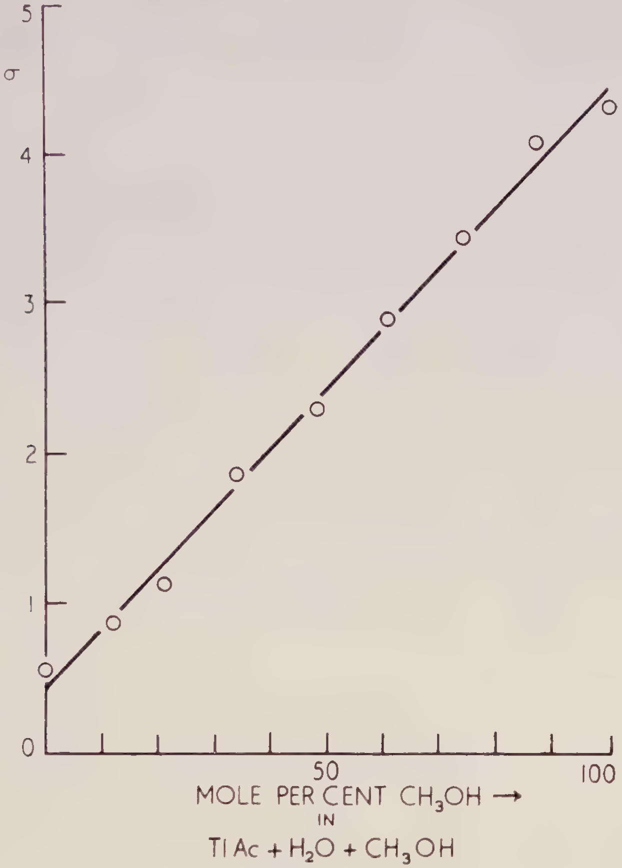

Figure 4.

4.1. *The low concentration effect* (*figure* 5)

At these concentrations, thallous salts frequently form ion-pairs according to an equilibrium, e.g.

$$\underset{\substack{\text{ion}\\\text{pair}\\(1-x)a}}{\text{TlOH}} \rightleftharpoons \underset{ax}{\text{Tl}^+} + \underset{(ax+b).}{\text{OH}'}$$

This implies that there are present two types of thallium atom, and if these have different magnetic shielding constants we might expect to observe two thallium resonances. However, in these experiments we observe only a single thallium line and so the two species must be undergoing rapid chemical exchange. The chemical shifts range over about 15 kc/s at the magnetic fields used, so that the exchange rate must considerably exceed a frequency of this order. If there were *a* moles/litre of thallous hydroxide with added amounts of potassium hydroxide (*b* moles/litre) and if the degree of dissociation of the thallous hydroxide is *x* then

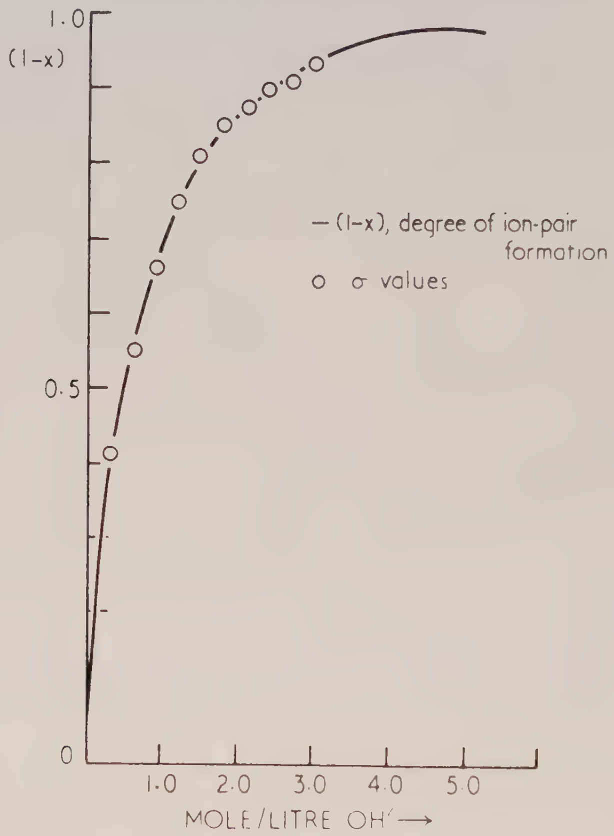

Figure 5. Variation of chemical shift with hydroxide concentration compared with degree of ion-pair formation in TlOH.

$$K_a = \frac{x(b+ax)}{(1-x)} \cdot \frac{f_{\mathrm{Tl}^+} \cdot f_{\mathrm{OH}'}}{f_{\mathrm{TlOH}}}$$

where f is the appropriate activity coefficient.

Now $f(\mathrm{TlOH})$, the activity coefficient of the ion pair, may be assumed not to change very much with ionic strength, and can be taken as unity to a fairly good approximation, while $f(\mathrm{Tl}^+).f(\mathrm{OH}')$ may be replaced by $f_\pm^2$, the square of the mean activity coefficient. Thus

$$K_a = \frac{x(b+xa)}{1-x} \cdot f_\pm^2.$$

If s_1 is the chemical shift of hydrated thallous ions with respect to some arbitrary reference point, and s_2 that of undissociated thallous hydroxide, then for rapid chemical exchange,

$$\text{observed shift} = xs_1 + (1-x)s_2.$$

Taking the reference point as the frequency of the hydrated thallous ion,

$$\text{observed shift} = (1-x)s_2.$$

The thermodynamic dissociation constant, K_a, has been estimated as about 0·2 from kinetic and spectrophotometric studies [3, 5, 6]. Activity coefficients measured for thallous salts are anomalously low as a result of incomplete dissociation, but for an approximate treatment those given for potassium hydroxide [8] may be used. Since the ionic strength of a thallous hydroxide solution depends on x, the degree of dissociation, x must be calculated by successive approximations, until the result is consistent with the ionic strength used in the calculation. The results for the degree of association, $(1-x)$, when a is kept constant at 0·3 M, and b varied, are shown plotted against total hydroxide concentration $(a+b)$ in figure 5. The observed chemical shift should vary in exactly the same way with a proportionality constant s_2. If s_2 is taken arbitrarily as 8·4, to give the correct scale along the Y axis, then the points shown in figure 5 are obtained. They fit the curve calculated for a dissociation equilibrium with

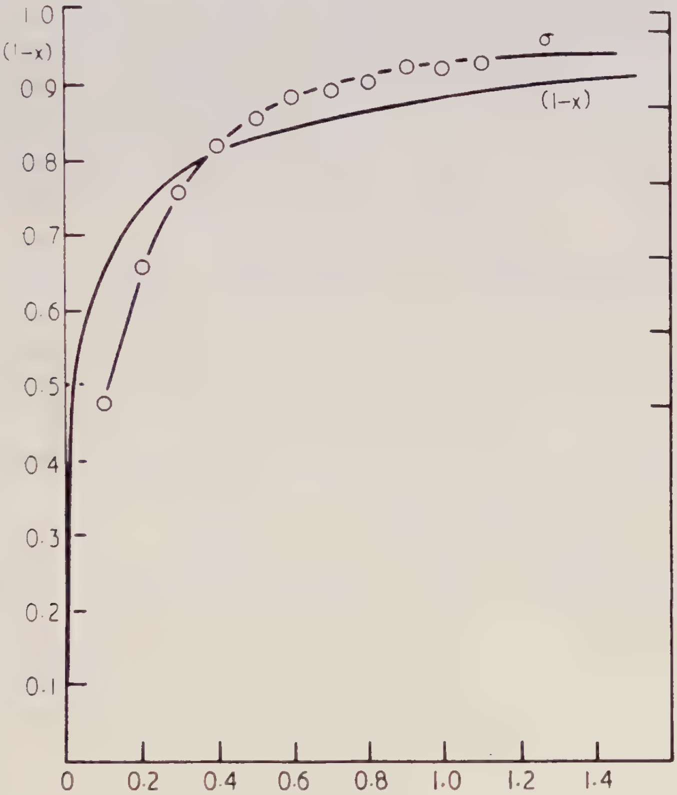

Figure 6. Chemical shifts compared with degree of ion-pair formation in thallous acetate.

$K_a = 0{\cdot}2$, surprisingly well, indicating that at least the shape of the chemical shift curve is consistent with the theory. In the light of evidence from other methods of investigation therefore, the initial curved portions may be fairly confidently attributed to an association equilibrium.

This interpretation can also be applied to the low concentration measurements on thallous acetate solutions. If plausible values for the activity coefficients are used, then the shape of the curve of chemical shift against acetate concentration (figure 6) can be used to obtain an approximate value of K for the equilibrium

$$Tl^+Ac^- \rightleftharpoons Tl^+ + Ac^-.$$

This would lead to a value for the equilibrium constant of about 0·01. This value of K cannot be checked by spectrophotometric methods because of the absorption of the acetate ions. However, Robinson and Davies [9] found a value of 1·3 from conductance measurements, but this figure is larger than the one they found for the dissociation of thallous perchlorate. However, when the value obtained above of 0·01 is used to calculate the curve for figure 6, the agreement is seen to be much less satisfactory than for thallous hydroxide.

4.2. *The linear portion*

At high anion concentrations, when the formation of ion pairs can be regarded as complete, the variation of chemical shift with concentration becomes closely linear.

Of the processes which could be responsible for chemical shifts in these solutions, one of the mechanisms considered by Gutowsky and McGarvey provides the only plausible explanation of the experimental results. The model they proposed considered interaction between thallous ions and anions, but we have seen that at these concentrations virtually all the thallous atoms must be in ion pairs. The explanation which follows is similar to that of Gutowsky and McGarvey, except that the interactions concern *ion pairs* instead of thallous ions. The most detailed experiments are made on thallous acetate solutions and so the discussion will refer to this compound, but the general argument can be applied also to the hydroxide, formate and fluoride.

In a strong solution of thallous acetate, the thallium is present as Tl^+Ac^- ion pairs, which must possess a hydration atmosphere. This atmosphere will consist largely of water molecules, but there will also, on the average, be a certain proportion of any other species which may be in the solution. It is the change in this atmosphere which is probably responsible for the linear variation in chemical shift.

Let us consider first the addition of acetate ions to a solution of thallous acetate ion-pairs. The hypothesis which follows requires that interactions between anion and ion pair are such that no appreciable concentration of species such as $Ac^-Tl^+Ac^-$ can be built up, but that these interactions modify the electronic environment of the thallium nucleus. The possible origin of the chemical shifts produced by these interactions will be considered later.

The probability that an acetate ion is included in the environment of an ion pair increases linearly with the acetate concentration, and is not significantly dependent on the ionic strength of the solution, because the ion pair has a zero net charge. The chemical shift is then linearly proportional to the average number of anions and water molecules surrounding the ion pair. This is proportional to the mole fraction of anions. At the concentrations used in these experiments, the mole fraction is a closely linear function of the molar concentration, and so the linear portion of the curves can be explained.

If, on the other hand, thallous acetate is added to a solution of thallous acetate of sufficient concentration to be on the linear portion of the curve, the effect is just to increase the concentration of thallous acetate ion pairs. However, the experimental results show that the chemical shift depends only on the acetate concentration and is independent of the ratio of the concentrations of thallous ion to potassium ion, and this implies that the collision of an ion pair with an acetate ion produces the same effect as collision with another ion pair. The acetate ion of the ion pair must therefore be closely similar to an ordinary acetate ion. In other words the ion pair is very ionic. This would imply that the interaction between an acetate ion and the thallium atom of a thallous acetate ion pair would probably be similar to that in a similar collision between an acetate ion and a thallous ion. The chemical shift produced by these collisions would then be expected to remain approximately linear even at low concentrations when ion pair formation is incomplete, and so the linear extrapolation used above in the discussion of the curved portion may be justified.

4.3. *Addition of neutral molecules*

Addition of the slightly ionized acetic and formic acids or of methanol, to a solution of constant thallium mole fraction, produces chemical shifts which vary linearly with the mole fraction of added substance. In this case the concentration of thallium used was such that most of the thallium was present as ion pairs, and so the change of medium did not significantly affect the ion pair equilibrium. The chemical shift therefore arises only from the change in the solvation environment of the thallium atoms.

4.4. *Addition of nitric and perchloric acids*

Thallous perchlorate is probably fully dissociated, and the addition of further perchlorate ions as perchloric acid must provide a change in the environment of the thallium atom and hence a chemical shift which varies linearly with perchlorate ion concentration.

The addition of nitric acid causes small chemical shifts which appear to vary approximately linearly at high concentrations, where the acid is ionized only to a small extent.

5. MAGNETIC SHIELDING OF THE THALLIUM NUCLEUS

The effect of the various solvation environments on the shielding of the thallium nucleus can be obtained from the slopes of the chemical shift curves. The greatest magnetic shielding is caused by the perchlorate ion and the shielding falls in the order perchlorate ion, nitric acid, acetic acid, formic acid, water, fluoride ion, formate ion, acetate ion, hydroxide ion. The change in the magnetic shielding is probably due mainly to a change in the temperature independent paramagnetism induced in the electrons of the thallium atom. This term is most effective when chemical interactions are strongest, and so it appears that these interactions are most important with hydroxide ions and weakest with perchlorate ions. It is significant that the tendency to accept a proton increases from perchlorate ions in the same order as the chemical shifts described above. The very powerful effect of the hydroxide ion may be associated with the particularly easy mechanism by which it can penetrate a hydration sphere.

It appears [10] that the electric field set up at the thallium atom by an adjacent ion could also induce a paramagnetic term in the chemical shielding which is not averaged to zero by molecular motion in the liquid, and this may well be a contributory factor in these results.

6. Conclusion

From these measurements the following conclusions may be drawn:

(*a*) Solutions of thallous ions and other anions may often contain 'ion-pairs' in which the thallous ion and anion are associated for long enough to be treated in terms of an equilibrium. The equilibrium constant obtained for thallous hydroxide ion pairs by other methods can be used to interpret the NMR results quantitatively.

(*b*) The chemical shift of the thallium resonance is also affected by collisions with other species which can modify the electron distribution about the thallium atom. The interaction is greatest for hydroxide ions and least for perchlorate ions, and is similar for acetate ions and thallous acetate ion pairs. This implies that the 'ion-pair' is highly ionic.

We are grateful to the Department of Scientific and Industrial Research for a Maintenance Grant to R. F. and R. G. We also thank the Hydrocarbon Research Group of the Institute of Petroleum and the Coal Board for Grants in aid of apparatus.

On a mesuré les déplacements chimiques dans la résonance nucléaire du thallium pour des solutions d'hydroxyde, fluorure, acétate, formiate, nitrate, et perchlorate thalleux, à des concentrations variées, et en présence de substances ajoutées. Aux faibles concentrations le déplacement chimique varie de façon non-linéaire en fonction de la concentration de l'anion, et on peut le mettre en corrélation avec la formation de paires d'ions. Dans les solutions plus concentrées la variation du déplacement chimique devient linéaire et on l'attribue aux interactions entre les paires d'ions et les substances ajoutées.

Chemische Verschiebungen der Kernresonanz von Thallium wurden in Lösungen von Thallohydroxyd, -fluorid, -azetat, -formiat, -nitrat und -perchlorat bei verschiedenen Konzentrationen, sowie in Anwesenheit von Fremdsubstanzen gemessen. Bei niedrigen Konzentrationen nimmt die Chemische Verschiebung nicht-linear mit der Anionenkonzentration zu und lässt sich zu der Bildung von Ionenpaaren in Beziehung setzen. In stärkeren Lösungen wird die Änderung der Chemischen Verschiebung linear und lässt sich auf Wechselwirkungen zwischen den Ionenpaaren und den zugesetzten Substanzen zurückführen.

References

[1] Gutowsky, H. S., and McGarvey, B. R., 1953, *Phys. Rev.*, **91**, 81.
[2] Bell, R. P., and George, J. H. B., 1953, *Trans. Faraday Soc.*, **49**, 619.
[3] Bell, R. P., and Prue, J. E., 1949, *J. chem. Soc.*, 362.
[4] Robinson, R. A., 1937, *J. Amer. chem. Soc.*, **59**, 84.
[5] Bell, R. P., and Panckhurst, M. H., 1956, *J. chem. Soc.*, 2836.
[6] Bell, R. P., and Panckhurst, M. H., 1956, *Rec. Trav. chim. Pays-Bas*, **75**, 725.
[7] Freeman, R., Murray, G., and Richards, R. E., 1957, *Proc. roy. Soc.* A, **242**, 455.
[8] Robinson, R. A., and Stokes, R. H., 1949, *Trans. Faraday Soc.*, **45**, 612.
[9] Robinson, R. A., and Davies, C. W., 1937, *J. chem. Soc.*, 574.
[10] Marshall, T. W., and Pople, J. A., 1958, *Mol. Phys.*, **1**, 199.

Correlations between the electronic spectra of alternant hydrocarbon molecules and their mono- and di-valent ions†

I. Benzene, coronene and triphenylene

by G. J. HOIJTINK

Chemical Laboratory of the Free University, Amsterdam

(*Received* 7 *November* 1958)

A comparison is made between the π-electron transitions in the benzene molecule and its mono- and di-valent ions following the A.S.M.O.-treatment of Pariser and Parr. Starting from this theoretical treatment the experimental spectra of the molecules and negative ions of coronene and triphenylene have been interpreted. The locations of the absorption bands are in good agreement with the theoretical expectations; the intensity rules, however, are strongly violated. This divergence between theory and experiment is probably due to a Jahn–Teller distortion.

1. INTRODUCTION

Hydrocarbon mono- and di-negative ions are formed by the reaction of conjugated hydrocarbons with alkali metal in active ethers, such as 1, 2-dimethoxyethane or tetrahydrofuran [1, 2].

In a previous paper the absorption spectra in the 5–30 kilo-Kayser ($1\,\mathrm{kK} = 10^3\,\mathrm{cm}^{-1}$) region of various alternant hydrocarbon negative ions have been reported [3]. These spectra could be satisfactorily interpreted by means of a simplified A.S.M.O.-treatment [4, 5].

Very recently it has been found that the mono- and di-positive ions of conjugated hydrocarbons are formed when these compounds react with strong electron acceptors such as sulphur trioxide (sulphuric acid) boron trifluoride, antimony pentachloride, etc. [6, 7, 8, 9].

The spectral measurements have now been extended into the 30–40 kK region. Since the hydrocarbon molecules absorb in this region a comparison can be made between the spectra of alternant hydrocarbon molecules and ions.

In the present paper such a comparison will be made for benzene, coronene and triphenylene. These hydrocarbons have in common that the highest bonding and lowest anti-bonding π-electronic levels are two-fold degenerate. The π-electronic transitions in the benzene molecule and ions will be treated quantitatively following the A.S.M.O.-procedure of Pariser and Parr [10]. Starting from these calculations the spectra of the molecules and ions of coronene and triphenylene will be interpreted qualitatively.

2. EXPERIMENTAL PART

(in collaboration with Mr. R. van Hardeveld)

The purity of the hydrocarbon samples, the preparation of the positive and negative ions and the techniques of the spectral measurements have been

---

† These investigations form part of a research programme supported by the Netherlands Organization for the Advancement of Pure Research.

described in previous papers [3, 9]. In the figures shown in this paper ϵ/σ (ϵ = molar extinction) has been plotted against the wave number σ. According to the formula [11]

$$D = 3{\cdot}99 \times 10^{-20} \int \frac{\epsilon}{\sigma}\, d\sigma \quad (\text{in Å}^2) \tag{1}$$

the areas under the 'absorption' bands become directly proportional to the dipole strengths D of the corresponding transitions.

3. THEORETICAL PART

In the scope of the A.S.M.O.-treatment of Pariser and Parr [10] (differential overlap neglected) the π-electrons in benzene may be described by the L.C.A.O.–M.O.'s [12]:

$$\phi_k = \frac{1}{\sqrt{6}} \sum_{s=0}^{5} \varphi_s(\nu) \exp\left(\frac{2\pi}{6} isk\right); \; k = 0, \; \pm 1, \; \pm 2, \; 3 \tag{2}$$

in which $\varphi_s(\nu)$ describes the π-electron ν in the $2p_z$-orbital at the sth carbon atom.

The M.O.'s (2) are completely determined by symmetry; because of the neglect of overlap they hold both for the benzene molecule and its positive and negative ions. The symmetry notations are the same as those used by Moffitt [12]; for a detailed outlay of the symmetry properties of the spatial symmetry group D_{6h} we refer to this author.

Throughout this paper the nuclear framework is assumed to be the same for the molecule and its positive and negative ions, so that the same values of the bond integral β and the electron correlation integrals hold for all species.

3.1. *The benzene molecule*

In the ground state of the benzene molecule all bonding orbitals are doubly occupied, so that the lower excited configurations are due to π-electron excitations from the highest bonding to the lowest anti-bonding level. As has been discussed in detail by various authors [10, 12, 13] the singlet ground and excited configurations are described by the antisymmetrized wave functions†:

$$^1A_{1,g}: \qquad {}^1\psi_0 = |\phi_1\bar{\phi}_1\phi_{-1}\bar{\phi}_{-1}| \tag{3}$$

$$\begin{aligned} ^1B_{1,2u}: \qquad {}^1\psi_{1,2} = \tfrac{1}{2}[\{|\phi_1\bar{\phi}_{-2}\phi_{-1}\bar{\phi}_{-1}| + |\phi_{-2}\bar{\phi}_1\phi_{-1}\bar{\phi}_{-1}|\} \\ \pm\{|\phi_1\bar{\phi}_1\phi_{-1}\bar{\phi}_2| + |\phi_1\bar{\phi}_1\phi_2\bar{\phi}_{-1}|\}] \end{aligned} \tag{4}$$

$$^1E_{1,u}: \qquad {}^1\psi_3 = \frac{1}{\sqrt{2}}\{|\phi_1\bar{\phi}_2\phi_{-1}\bar{\phi}_{-1}| + |\phi_2\bar{\phi}_1\phi_{-1}\bar{\phi}_{-1}|\} \text{ and its complex conjugate } {}^1\psi_3^*. \tag{5}$$

In (4) the + and – sign refer to $B_{1,u}$ and $B_{2,u}$ respectively.

The energies of the excited configurations relative to the ground state and the corresponding dipole strengths become:

$$^1B_{1,u}: \qquad {}^1E_1 = 2\beta - K_{1,-2} + K_{1,-1}; \qquad D = 0, \tag{6}$$

$$^1B_{2,u}: \qquad {}^1E_2 = 2\beta + 3K_{1,-2} - K_{1,-1}; \qquad D = 0, \tag{7}$$

$$^1E_{1,u}: \qquad {}^1E_3 = 2\beta + 2K_{1,2} - K_{1,-2}; \qquad D = 8\mathscr{D}_{1,2} \tag{8}$$

in which

$$\begin{aligned} K_{1,2} &= \iint \phi_1(\mu)\phi_2^*(\mu)\frac{e^2}{r_{\mu\nu}}\phi_2(\nu)\phi_1^*(\nu)\, d\tau_\mu\, d\tau_\nu \\ &= \iint \phi_1(\mu)\phi_{-2}(\mu)\frac{e^2}{r_{\mu\nu}}\phi_2(\nu)\phi_{-1}(\nu)\, d\tau_\mu\, d\tau_\nu, \end{aligned} \tag{9}$$

---

† The two electrons in the closed shell $k = 0$ have been omitted.

$$|\mathscr{D}_{1,2}^{1/2}| = \int \phi_1(\mu) r \phi_2^*(\mu)\, d\tau_\mu = \int \phi_1(\mu) r \phi_{-2}(\mu)\, d\tau_\mu \tag{10}$$

and β denotes the bond integral for neighbouring carbon atoms.

3.2. *The mono-negative ion*

In the ground state of the mono-negative ion the lowest anti-bonding level is occupied by one electron, so that the ground state is doubly degenerate. Moreover the ground and excited states are spin degenerate: $S_z = \pm \frac{1}{2}$. The doublet ground and excited configurations ($S^2 = \frac{3}{4}$) are described by:

$$^2E_{2,u}:\quad {}^2\psi_0 = |\phi_1\bar{\phi}_1\phi_{-1}\bar{\phi}_{-1}\phi_2| \text{ and } {}^2\psi_0^* \tag{11}$$

$$^2E_{1,g}:\quad \left\{\begin{array}{ll} {}^2\psi_1 = |\phi_1\bar{\phi}_1\phi_{-1}\bar{\phi}_2\phi_2| \text{ and } {}^2\psi_1^*, & (12) \\ {}^2\psi_2 = \dfrac{1}{\sqrt{6}}\{2|\phi_1\bar{\phi}_{-2}\phi_{-1}\bar{\phi}_{-1}\phi_2| + |\phi_1\bar{\phi}_2\phi_{-1}\bar{\phi}_{-1}\phi_{-2}| & \\ \qquad\qquad - |\phi_2\bar{\phi}_1\phi_{-1}\bar{\phi}_{-1}\phi_{-2}|\} \text{ and } {}^2\psi_2^* & (13) \\ {}^2\psi_3 = \dfrac{1}{\sqrt{2}}\{|\phi_1\bar{\phi}_2\phi_{-1}\bar{\phi}_{-1}\phi_{-2}| + |\phi_2\bar{\phi}_1\phi_{-1}\bar{\phi}_{-1}\phi_{-2}|\} \text{ and } {}^2\psi_3^*, & (14) \end{array}\right.$$

$$^2B_{1,2g}:\quad {}^2\psi_{4,5} = \frac{1}{\sqrt{2}}\{|\phi_1\bar{\phi}_1\phi_{-1}\bar{\phi}_{-2}\phi_{-2}| \pm |\phi_1\bar{\phi}_2\phi_{-1}\bar{\phi}_{-1}\phi_2|\}. \tag{15}$$

The lowest quartet state ($S^2 = 15/4$) is described by:

$$^4E_{1,g}:\quad {}^4\psi = \frac{1}{\sqrt{3}}\{|\phi_1\bar{\phi}_2\phi_{-1}\bar{\phi}_{-1}\phi_2| + |\phi_2\bar{\phi}_1\phi_{-1}\bar{\phi}_{-1}\phi_{-2}| - |\phi_1\bar{\phi}_{-2}\phi_{-1}\bar{\phi}_{-1}\phi_2|\} \text{ and } {}^4\psi^*. \tag{16}$$

The excitation of a π-electron from the lowest anti-bonding to the vacant π-electron level ($k = 3$) gives rise to the doublet configuration

$$^2B_{1,g}:\quad {}^2\psi_6 = |\phi_1\bar{\phi}_1\phi_{-1}\bar{\phi}_{-1}\phi_3|. \tag{17}$$

The transition energies and dipole strengths here become:

$$\begin{array}{lllr} {}^2E_{1,g}: & \left\{\begin{array}{l} {}^2E_1 = 2\beta + K_{1,-1} - K_{1,-2}; \\ {}^2E_2 = 2\beta + \frac{1}{2}K_{1,-1} + \frac{1}{2}K_{1,-2}; \\ {}^2E_3 = 2\beta + 2K_{1,2} - \frac{1}{2}K_{1,-1} - \frac{1}{2}K_{1,-2}; \end{array}\right. & \begin{array}{l} D = 0, \\ D = 0, \\ D = 4\mathscr{D}_{1,2}, \end{array} & \begin{array}{r} (18) \\ (19) \\ (20) \end{array} \\ {}^2B_{1,2g}: & {}^2E_4 = {}^2E_5 = 2\beta + K_{1,2} + K_{1,-1} - 2K_{1,-2}; & D = 2\mathscr{D}_{1,2}, & (21) \\ {}^2B_{1,g}: & {}^2E_6 = \beta + K_{1,-2} - K_{1,-1}; & D = \mathscr{D}_{2,3}, & (22) \\ {}^4E_{1,g}: & {}^4E = 2\beta - K_{1,-2} - K_{1,-1}; & \text{spin forbidden.} & (23) \end{array}$$

Contrary to the benzene molecule the mono-negative ion does not possess a closed shell ground state. This implies that though the M.O.'s are completely determined by symmetry the ground state described by (11) will interact with doublet excited configurations with the same symmetry. Because of the high symmetry, however, the energies of these excited configurations are considerably higher than the energy of the ground state, so that the effect of configuration interaction on the energy of the ground state will be small.

The degeneracy of the excited state $B_{1,2g}$ is removed by the interaction between the two $B_{1,g}$ configurations.

3.3. *The di-negative ion*

For systems in which the lowest anti-bonding level is two-fold degenerate the ground state of the di-negative ion may be either a triplet or a singlet state.

If the ground state of the benzene di-negative ion is a triplet the wave functions for the triplet ground and excited configurations are:

$$^3A_{1,g}: \qquad {}^3\psi_0 = |\phi_1\bar{\phi}_1\phi_{-1}\bar{\phi}_{-1}\phi_2\phi_{-2}|, \tag{24}$$

$$^3B_{1,2u}: \qquad {}^3\psi_{1,2} = \frac{1}{\sqrt{2}}\{|\phi_1\bar{\phi}_{-2}\phi_{-1}\bar{\phi}_{-1}\phi_2\phi_{-2}| \pm |\phi_1\bar{\phi}_1\phi_{-1}\bar{\phi}_2\phi_2\phi_{-2}|\}, \tag{25}$$

$$^3E_{1,u}: \qquad {}^3\psi_3 = |\phi_1\bar{\phi}_2\phi_{-1}\bar{\phi}_{-1}\phi_2\phi_{-2}| \quad \text{and } {}^3\psi_3{}^*. \tag{26}$$

$$^3E_{1,u}: \qquad {}^3\psi_4 = |\phi_1\bar{\phi}_1\phi_{-1}\bar{\phi}_{-1}\phi_2\phi_3| \quad \text{and } {}^3\psi_4{}^*. \tag{27}$$

The lowest singlet excited configuration is described by:

$$^1E_{2,g}: \qquad {}^1\psi_0 = |\phi_1\bar{\phi}_1\phi_{-1}\bar{\phi}_{-1}\phi_2\bar{\phi}_2| \quad \text{and } {}^1\psi_0{}^*. \tag{28}$$

The corresponding configurational energies relative to the triplet ground state and the dipole strengths are:

$$^1E_{2,g}: \qquad {}^1E_0 = +K_{1,-1}; \qquad \text{spin forbidden,} \tag{29}$$

$$^3B_{1,u}: \qquad {}^3E_1 = 2\beta; \qquad D=0, \tag{30}$$

$$^3B_{2,u}: \qquad {}^3E_2 = 2\beta + 2K_{1,-1} - 2K_{1,-2}; \qquad D=0, \tag{31}$$

$$^3E_{1,u}: \qquad \left\{ \begin{array}{lll} {}^3E_3 = 2\beta + K_{1,2} + K_{1,-1} - 2K_{1,-2}; & D=4\mathscr{D}_{1,2}, & (32) \\ {}^3E_4 = \beta + K_{1,-2} - K_{1,2}; & D=2\mathscr{D}_{2,3}. & (33) \end{array} \right.$$

The ground state of the di-negative ion is not a closed shell state, so that the energy of this state will become lower by configuration interaction. Since the matrix elements for the interaction between the lowest singlet state $^1E_{2,g}$ and higher singlet configurations are larger than those for the interaction between the triplet ground state and triplet excited configurations it is even possible that the lowest singlet comes down below the triplet 'ground' state. For the benzene di-negative ion however, the effect of configuration interaction on the energies of the lowest singlet and triplet configurations is small and consequently the ground state will be a triplet state.

In the present calculations configuration interaction is neglected except for the two excited configurations $^3E_{1,u}$.

3.4. *The mono- and di-positive ion*

In the scope of the A.S.M.O.-treatment of Pariser and Parr [10] the results of the calculations of the transition energies and dipole strengths are exactly the same for positive and negative ions of the same valency.

The proof of this equality goes along the same lines as the more general proof given by Weijland [14]. As this author has shown in the scope of the S.C.F.M.O.-treatment the spectra of the mono- and di-positive ions of alternant hydrocarbons are identical with those of the corresponding negative ions.

In figure 1 the results of the calculations on benzene have been drawn schematically. If in the equations (6)–(8), (18)–(21) and (30)–(33), 2β is replaced by the appropriate Hückel excitation energy these transition energies (corresponding to $n > n+1$ in figures 3 and 7) hold in general for alternant hydrocarbons of symmetry D_{3h} or higher, in which the highest bonding and lowest anti-bonding π-electronic levels are doubly degenerate. Accordingly the calculated spectra may also serve as a basis for the interpretation of the experimental spectra of the molecules and ions of coronene (symmetry D_{6h}) and triphenylene (symmetry D_{3h}), reported in this paper.

The main conclusions to be inferred from the calculated spectra are:

(1) A strong band $^2E_{1,g}$ occurs in the spectrum of the mono-valent ion at practically the same wave number as the strong band $^1E_{1,u}$ in the spectrum of the molecule and with half the intensity of the latter.

(2) The first bands in the spectra of the mono-valent and di-valent ion are located at about the same wave number. It is worthwhile noticing that if the ground state of the di-valent ion is a singlet state the first band in the spectrum of the di-valent ion will be located far more to the ultraviolet than the corresponding band for the mono-valent ion. In those cases in which it is difficult to decide from the theory whether the ion has a triplet or singlet ground state this criterion may be helpful.

(3) The strong band $^3E_{1,u}$ of the di-valent ion is nearer to the red than the strong absorption band $^2E_{1,g}$ of the mono-valent ion.

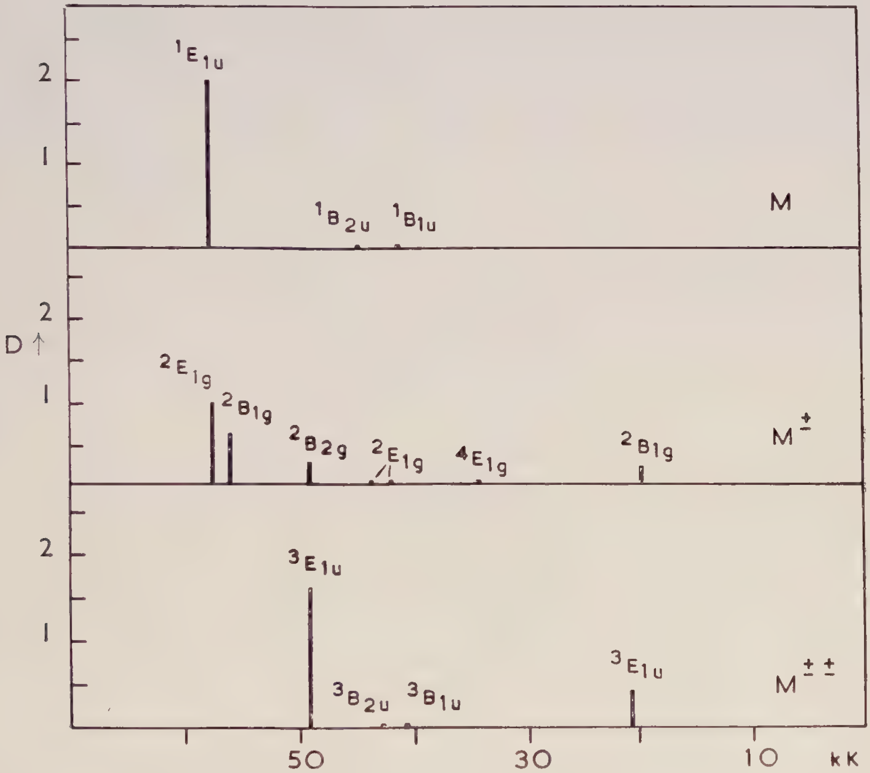

Figure 1. Electronic spectra of the benzene molecule and its mono- and di-valent ions calculated according to the A.S.M.O.-treatment of Pariser and Parr ($\beta = 20 \cdot 5$ kK).

4. INTERPRETATION OF THE SPECTRA

Since the reduction potential of benzene lies much lower than the standard potentials of sodium and potassium the mono-negative ion is formed only in the presence of a very large excess of hydrocarbon molecules. Owing to the absorption of the benzene molecule in the near ultraviolet one may therefore expect from figure 1 that only the lowest absorption band of the mono-negative ion will be observable. Unfortunately attempts to prepare a solution of the mononegative ion remained unsuccessful until now, since at room temperature the negative ion is rapidly decomposed by the solvent. Both the preparation of the ion and the spectral measurements should therefore be carried out at lower temperature.

4.1. *Coronene*

This hydrocarbon belongs to the same spatial symmetry group as benzene. The Hückel level scheme shown in figure 3 leads to the following ground and excited configurations:

π-electronic excitation	M	M^-	M^{--}
$n \rightarrow n+1$	${}^1E_{1,u}$ ${}^1B_{2,u}$ forb. ${}^1B_{1,u}$ forb.	${}^2E_{2,u}$ ${}^2A_{1,2u}$ ${}^2E_{2,u}$ ${}^2E_{2,u}$	${}^3E_{1,u}$ ${}^3B_{2,u}$ forb. ${}^3B_{1,u}$ forb.
$n+1 \rightarrow n+3$	—	${}^2A_{1,u}$	${}^3E_{1,u}$
$n+1 \rightarrow n+2$	— —	${}^2A_{2,u}$ ${}^2E_{2,u}$	${}^3E_{1,u}$ $\left\{\begin{array}{l}{}^3E_{1,u}\\ {}^3B_{1,2u}\ \text{forb.}\end{array}\right.$
Ground state	${}^1A_{1,g}$	${}^2E_{1,g}$	${}^3A_{1,g}$

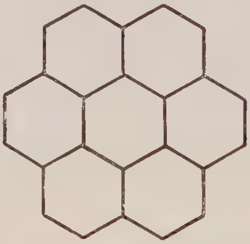

Figure 2. Carbon skeleton of coronene.

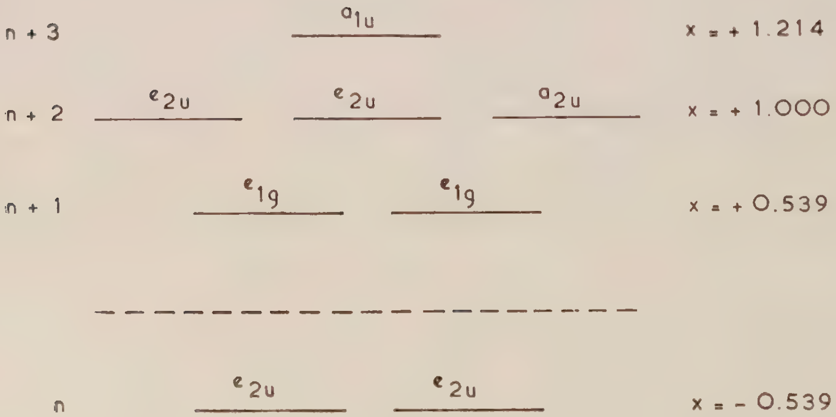

Figure 3. Part of the Hückel level scheme of coronene.

The experimental spectra of the coronene molecule and its mono- and di-negative ion are shown in figure 4. Following the simplified A.S.M.O.-treatment discussed in a previous paper [4] we obtain the spectrum of the coronene mono-valent ion given in figure 5. From the quantitative treatment of benzene it appeared that the strong absorption band of the molecule should be repeated at practically the same wave number and with half the intensity in the spectrum of the mono-valent ion.

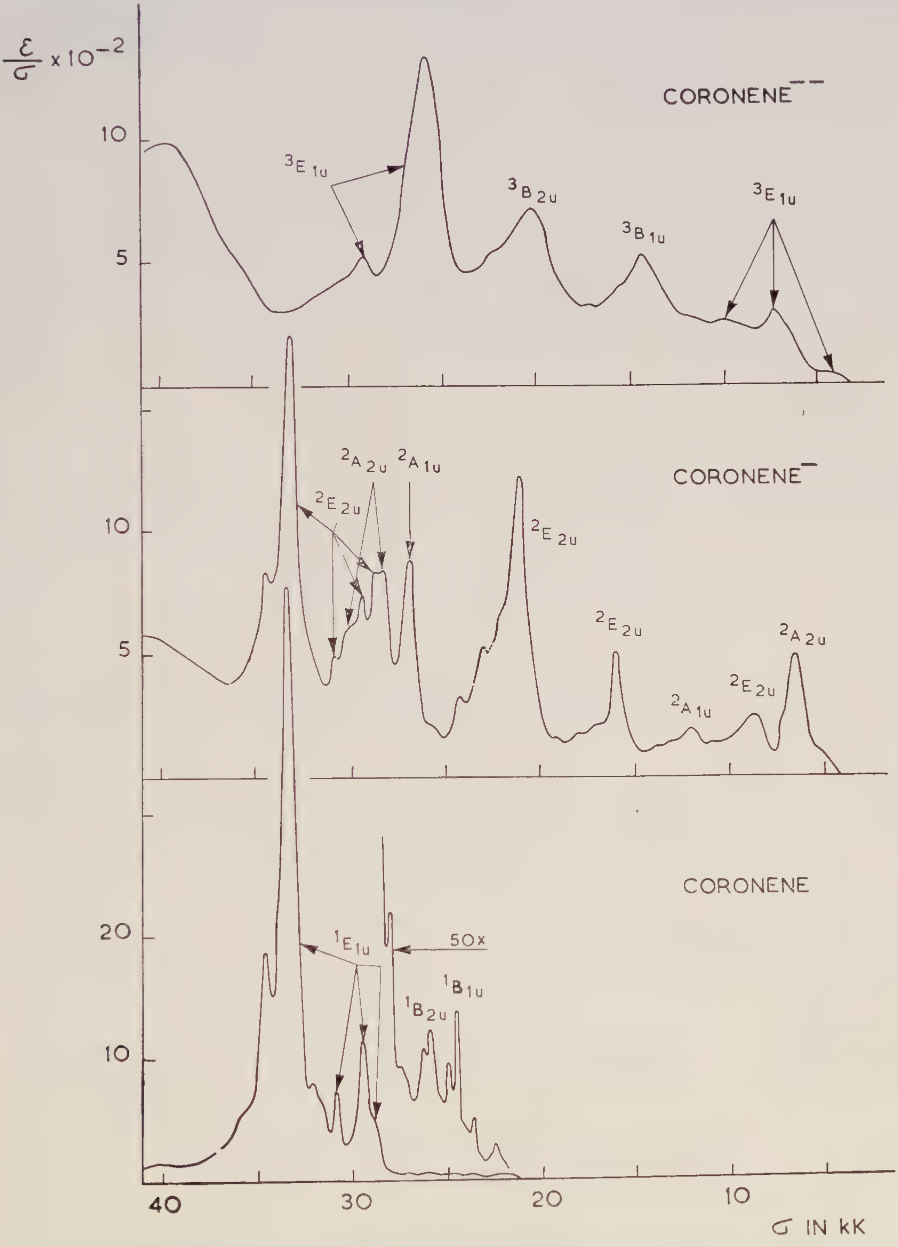

Figure 4. Electronic absorption spectra of the coronene molecule and its mono- and di-negative ion.

A comparison between the experimental spectra of the coronene molecule and its mono-negative ion indicates that not only the strong absorption band in the 33–35 kK region but also the absorption peaks in the 28–32 kK region of the spectrum of the molecule occur at practically the same wave number and with half the intensity in the spectrum of the mono-negative ion. In previous assignments [12, 15] the absorption by the molecule in the 28–32 kK region was ascribed to the $^1A_{1,g} \rightarrow {}^1B_{2,u}$ transition. In view of the above correspondence between the spectra of the coronene molecule and its mono-negative ion both the absorptions in the 28–32 kK and 33–35 kK regions are probably due to one and the same electronic transition, viz. $^1A_{1,g} \rightarrow {}^1E_{1,u}$ in the molecule and $^2E_{1,g} \rightarrow {}^2E_{2,u}$ in the mono-valent ion.

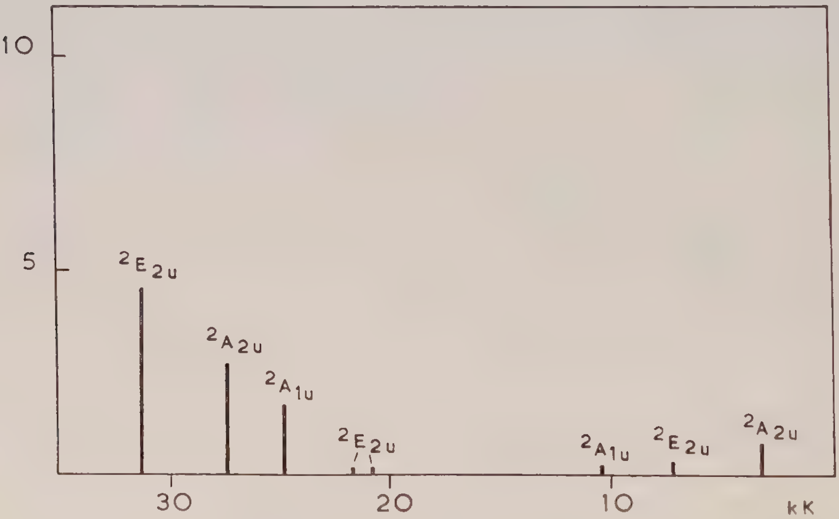

Figure 5. Electronic spectrum of the coronene monovalent ion calculated according to a simplified A.S.M.O.-treatment [4].

If this interpretation is correct the degeneracy of these doubly degenerate excited states is removed by some distortion, reducing the symmetry from D_{6h} to D_{2h}. Under this assumption the divergence between the observed and calculated intensity distribution in the spectra of the mono- and di-valent ions also becomes understandable. According to the foregoing theoretical treatment one expects the transitions to the $^3B_{1,u}$ and $^3B_{2,u}$ states of the di-valent ion to be forbidden and the transitions to the lower excited $^2E_{2,u}$ states of the mono-valent ion to be very weak, whereas actually strong absorption bands are observed for the di-negative and the mono-negative ion. Under the influence of a distortion of the symmetry one may expect indeed that the intensities are distributed more equally over the absorption spectra. In the light of recent studies [16, 17] it becomes probable that such a distortion is due to the coupling between the electronic and nuclear motions known as a Jahn–Teller distortion.

This supposition is supported by the behaviour of the coronene mono-negative ion in electron spin resonance absorption. According to de Boer and Weissman [18] the E.S.R. spectrum of this ion exhibits no hyperfine structure. For the undistorted ion one would expect 13 equidistant hyperfine structure lines owing to the magnetic interaction of the electron with the 12 equivalent protons. Since in the ground state the ion is doubly degenerate (apart from the spin degeneracy) this denegeracy may be removed by a Jahn–Teller distortion [18]. Under this distortion the 12 protons are no longer equivalent so that the hyperfine structure of the E.S.R. spectrum may become blurred.

The spectra of the coronene mono- and di-negative ions exhibit strong absorption at 40 kK, which appears to be absent in the spectrum of the molecule. This absorption is very likely due to the excitation of an electron from the lowest anti-bonding to one of the higher π-electronic levels. Since the di-negative ion has a triplet ground state one may expect the energy of this transition to be nearly the same for both ions. In accordance with the theory the dipole strength of the absorption band of the di-negative ion is about twice as large as for the corresponding band of the mono-negative ion.

4.2. *Triphenylene*

Owing to the relatively low reduction potential of the triphenylene mono-negative ion the di-negative ion can be prepared only in the presence of a large excess of the mono-negative ion. Under this condition the spectrum of the di-negative ion is completely masked by the absorption of the mono-negative ion.

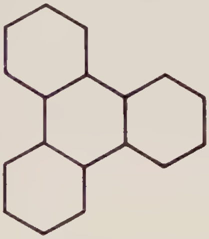

Figure 6. Carbon skeleton of triphenylene.

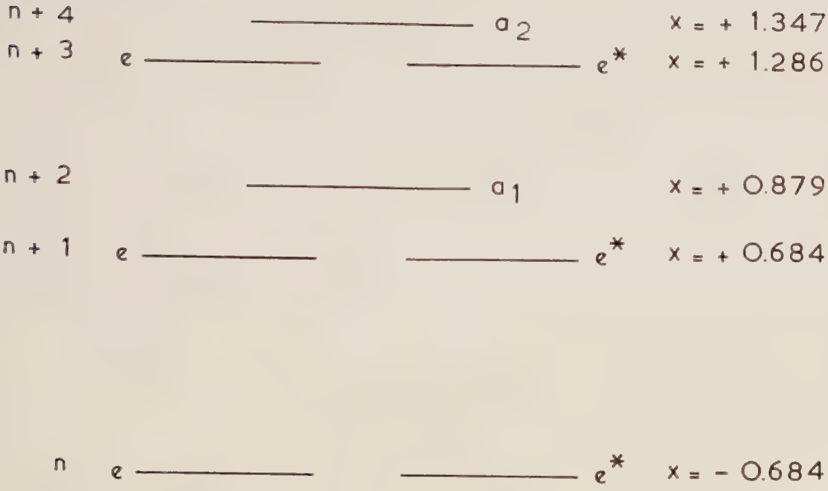

Figure 7. Part of the Hückel level scheme of triphenylene.

From the Hückel level scheme of triphenylene (figure 7) and coronene one may expect the spectra of the molecules and ions of these hydrocarbons to be very similar. The interpretation of the spectrum of the triphenylene mono-negative ion shown in figure 8 is not quite as convincing as for the coronene mono-negative ion. The absorption peaks in the 30–40 kK region of the spectrum of the molecule are indeed located at about the same wave numbers in the spectrum of the mono-negative ion, but in the latter case the intensities are lower than half the intensities of the corresponding bands in the spectrum of the molecule.

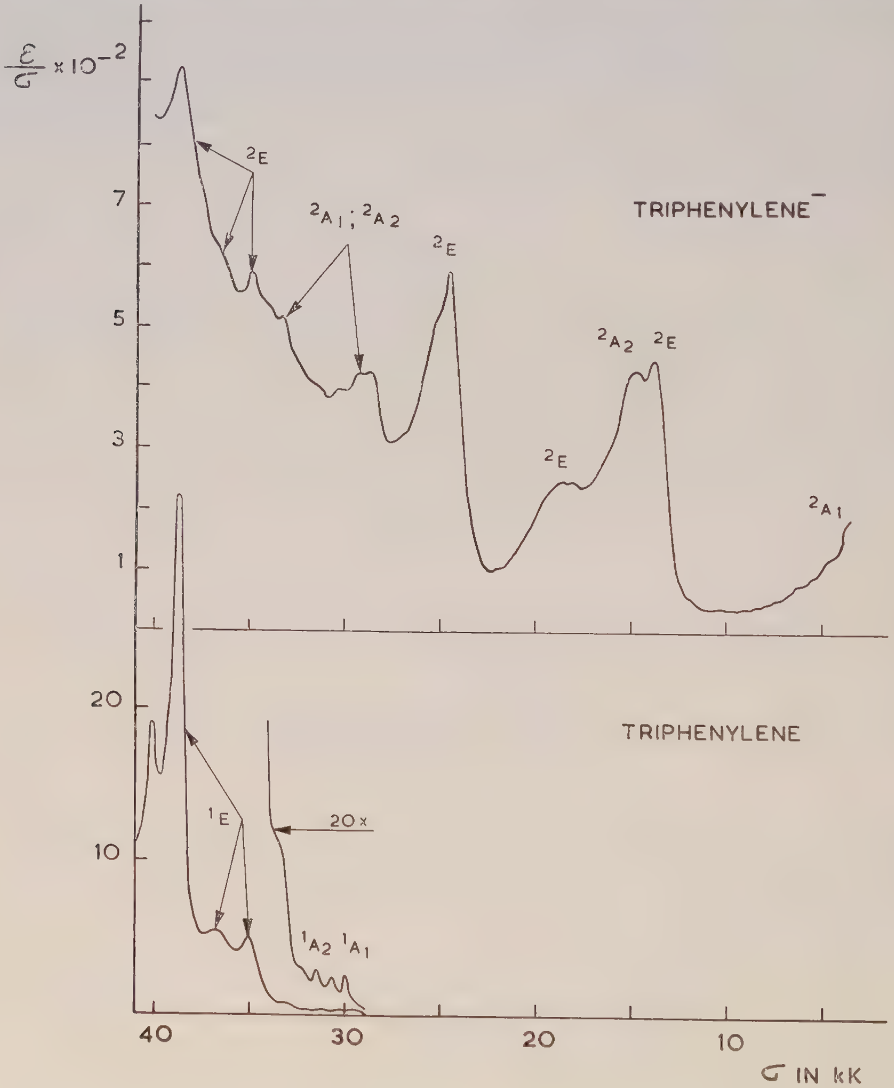

Figure 8. Electronic absorption spectra of the triphenylene molecule and its mono-negative ion.

In accordance with the Hückel level scheme the first absorption band due to the excitation $n+1 \rightarrow n+2$ lies far in the infra-red.

The spectral behaviour of the triphenylene molecule and its mono-negative ion as well as the fact that the hyperfine structures in the electron spin resonance spectra of the mono-negative ion is practically blurred again are thought to point to a Jahn–Teller distortion [18].

On compare les transitions des électrons π pour la molécule du benzène et pour ses ions mono- et bivalents en suivant la méthode A.S.M.O. de Pariser et Parr. A partir de ce traitement théorique, on a interprété les spectres expérimentaux des molécules et des ions négatifs du coronène et du triphenylène. La position des bandes d'absorption est en bon accord avec les prévisions théoriques; cependant les règles pour les intensités sont fortement violées. Cet écart entre la théorie et l'expérience est probablement dû à une distorsion de Jahn–Teller.

Entsprechend der A.S.M.O.-Behandlung von Pariser und Parr wird ein Vergleich zwischen den π-Elektronenübergängen in der Benzolmolekel, sowie in ihren ein- und zweiwertigen Ionen durchgeführt. Von dieser theoretischen Behandlung ausgehend, werden die gefundenen Spektren der Molekeln und Anionen von Coronen und Triphenylen gedeutet. Die Lage der Absorptionsbanden stimmt mit der theoretischen Erwartung gut überein; Unstimmigkeiten treten jedoch hinsichtlich der Intensitäten auf. Diese Diskrepanz zwischen Theorie und Experiment wird wahrscheinlich durch eine Jahn–Teller-Verformung verursacht.

REFERENCES

[1] LIPKIN, D., PAUL, D. E., TOWNSEND, J., and WEISSMAN, S. I., 1953, *Science*, **117**, 534; 1956, *J. Amer. chem. Soc.*, **78**, 119.
[2] HOIJTINK, G. J., BOER, E. DE, MEIJ, P. H. VAN DER, and WEIJLAND, W. P., 1955, *Rec. Trav. chim. Pays-Bas*, **74**, 255; 1956, *Ibid.*, **75**, 487.
[3] BALK, P., HOIJTINK, G. J., and SCHREURS, J. W. H., 1957, *Rec. Trav. chim. Pays-Bas*, **76**, 813.
[4] BALK, P., BRUYN, S. DE, and HOIJTINK, G. J., 1957, *Rec. Trav. chim. Pays-Bas*, **76**, 907.
[5] BALK, P., BRUYN, S. DE, and HOIJTINK, G. J., 1958, *Mol. Phys.*, **1**, 151.
[6] WEISSMAN, S. I., BOER, E. DE, and CONRADI, J. J., 1957, *J. chem. Phys.*, **26**, 963.
[7] HOIJTINK, G. J., and WEIJLAND, W. P., 1957, *Rec. Trav. chim. Pays-Bas*, **76**, 836.
[8] KON, H., and BLOIS, M. S., JR., 1958, *J. chem. Phys.*, **28**, 743.
[9] AALBERSBERG, W. IJ., HOIJTINK, G. J., MACKOR, E. L.. WEIJLAND, W. P. (in the press).
[10] PARISER, R., and PARR, R. G., 1953, *J. chem. Phys.*, **21**, 466, 767; PARISER, R., 1956, *Ibid.*, **24**, 50.
[11] MULLIKEN, R. S., and RIEKE, C. A., 1941, *Rep. Progr. Phys.*, **8**, 231.
[12] MOFFITT, W., 1954, *J. chem. Phys.*, **22**, 320, 1820.
[13] GOEPPERT-MEYER, M., and SKLAR, A. L., 1938, *J. chem. Phys.*, **6**, 645.
[14] WEIJLAND, W. P., 1958, *Thesis*, Free University, Amsterdam.
[15] PLATT, J. R., 1950, *J. chem. Phys.*, **18**, 1168.
[16] LONGUET-HIGGINS, H. C., ÖPIK, U., PRYCE, M. H. L., and SACK, R. A., 1958, *Proc. roy. Soc.* A, **244**, 1.
[17] LIEHR, A. D., and MOFFITT, W., 1956, *J. chem. Phys.*, **25**, 1074; 1957, *Phys. Rev.*, **106**, 1195.
[18] BOER, E. DE, and WEISSMAN, S. I., 1958, *J. Amer. chem. Soc.*, **80**, 4549.

Absorption spectra of actinide compounds†

by CHR. KLIXBÜLL JØRGENSEN
Chemistry Department A, Technical University of Denmark,
Copenhagen, Denmark

(*Received* 27 *August* 1958)

From the energy levels of the gaseous ions Ac^{++}, Th^{+++}, and Th^{++}, it can safely be extrapolated that the ground electron configuration of all actinide ions with ionic charges at least +3 contains only 5f-electrons outside the emanation shells. This is further supported by the $5f^n \rightarrow 5f^{n-1}6d$ transitions observed in Pa(IV), U(III), Np(III) (though their wave numbers are too high to be measured in U(IV) and Np(IV)). The configuration f^2 has a very characteristic distribution of energy levels between $^3H_4$ and $^3P_2$ with $^1S_0$ as much higher, isolated level. The absorption spectra of U(IV) complexes and of PuF_6 suggest interelectronic repulsion parameters ~60 per cent of the values in the corresponding lanthanides, while the Landé factors are about twice as large. This would also explain the recent measurements of Cm(III) complexes, compared to Gd(III). The larger average radius of the 5f-shell causes larger perturbation effects from the ligands than in the lanthanides. The J-values will therefore be distributed between several adjacent, observed energy levels without making the general treatment of the f^n-configurations impossible. The variation with oxidation numbers in isoelectronic series are discussed, e.g. U(III) and Np(IV); Pu(III) and AmF_4; and Am(III) and CmF_4. Band positions are predicted in Bk(III) and BkF_4. Finally, the chemical properties of the actinide elements are discussed, and it is emphasized that no necessary connections exist between the presence of f-electrons and constant trivalency.

Seaborg's actinide hypothesis [1–3] contains as the most important assumption that the electron configurations of actinides and lanthanides are similar in containing 5f- and 4f-electrons, respectively. It must be realized that the electron configurations of transition group elements do not have a simple connection with the chemical properties, e.g. the differences between iron and ruthenium cannot be simply explained by electron configurations. Thus, the notorious differences between the chemical properties of the series Th, Pa, U, Np, Pu and of Ce, Pr, Nd, Pm, Sm cannot disprove that the electron configurations may be analogous. It has been argued by some chemists that the 5f-electrons, if present in the actinides, are so easily removed by ionization and so perturbed by the influences of the ligands, the neighbour molecules, that they resemble d-electrons more than 4f. However, the definition of d ($l=2$) and f ($l=3$) electrons does not depend on chemical behaviour, but on the separability of the one-electron wave function into the product of a radial function, determined by the central field of spherical symmetry, and a hydrogenic angular function, characterizing l. Two effects may make the distinction between l-values impossible: the intermixing of electron configurations, occurring also in the gaseous ions; and the deviation of the chemical compounds from spherical symmetry, corresponding to formation of molecular orbitals with γ_n rather than l as quantum number. However, the present author believes that these two effects are rather unimportant in the actinides, and that it is a good approximation to talk about integral numbers of 5f- and 6d-electrons in the partly filled shell of the actinide compounds [38].

---

† This paper was presented 14 April 1958 for the Symposium on the Chemistry of the Less Familiar Elements in connection with the 133rd national meeting of American Chemical Society in San Francisco.

In systems with one electron outside the emanation shell (radon is for the present author the name of an isotope, just as deuterium), Ra^+ does not show any sign of low energy of the 5f-electron [4]. In Ac^{++}, this electron has still higher energy [5] than 6d or 7s, while it has the lowest energy [6] in Th^{+++}. For a single electron with $l > 0$, two values of J $(= l \pm 1/2)$ are possible. The energy of these two levels is separated by $(l+1/2)\zeta_{nl}$, where ζ_{nl} is the Landé multiplet splitting factor. The energy levels are, in K $(= cm^{-1})$, with the ground state at zero:

		Ra^{++}	Ac^{++}	Th^{+++}
5f	$J = 5/2$	48988	23454	0
	7/2	49272	26080	4325
6d	3/2	12085	801	9193
	5/2	13743	4204	14486
7s	1/2	0	0	23130
7p	1/2	21351	29466	60239
	3/2	26209	38063	73056

Thus, the energy difference between the means of 5f and 6d changes sign from Ac^{++} to Th^{+++}, being -23 kK and $+10$ kK $(1\,kK = 1000\,cm^{-1})$, respectively. When compared to the behaviour of similar energy differences in the beginning of the other transition groups, it can safely be concluded that the $5f \rightarrow 6d$ energy difference will be at least $+43$ kK in Pa^{+4} and $+76$ kK in U^{+5}. While the line spectra of these gaseous ions are not known at present, it is very interesting to note that Fried and Hindman [7] actually observe broad, intense (Laporte-allowed) absorption bands of Pa(IV) in 1 M HCl at 36·3, 39·2, and 44·8 kK. Just as is the case in the lanthanides Ce(III), Sm(II), Eu(II), and Tb(III), it seems possible to identify such $f \rightarrow d$ transitions in actinide complexes [8–10]. In the case of Ce(III), they seem [11] to have lower wave numbers in anion complexes (with ethylenediaminetetraacetate, tartrate, citrate, etc.) than in the hydrate, which further has lower wave numbers than gaseous Ce^{+++}. Similar evidence is presented by chloro complexes of U(III), compared to the hydrates [12].

A closer analysis [10, 13] shows that the variation of the 5f–6d distance within different isoelectronic series is more an increase with the ionic charge $Z_0 - 1$ than an increase with the atomic number Z. It only has meaning to discuss the value of Z at which the two orbital energies cross, if the ionic charge is specified. In the neutral actinide atoms, two 7s- and in some cases one 6d-electron occur; but they are removed first by ionization, leaving the $[Em]\,5f^n$ for Z_0 above 3. The number of 'valence' electrons in the neutral atom is not necessarily equal to the most common oxidation number. Thus, most neutral lanthanide atoms have only two valence electrons, $[Xe]\,4f^n\,6s^2$, in their ground state. Only one gaseous ion with two electrons [14, 15] outside the emanation shells, viz. Th^{++}, is well-known from atomic spectroscopy, if we except [5] Ac^+, where the 5f-electrons are very excited. For two valence electrons, several multiplet terms, characterized by the quantum numbers L and S, occur for each configuration. And each multiplet term may be divided into energy levels, characterized by J.

For discussing the relative energy of different configurations, it may be useful to consider the baricenters, i.e. the average after weighting with the degeneracy numbers $2J+1$. These baricenters occur (assuming [14] that $6d^2\ ^3F_2$ is 810·6 K below $5f\ 6d\ ^3H_4$) in Th^{++} at:

5f 7s	+5·436 kK
$6d^2$	6·630
6d 7s	7·212
5f 6d	9·531
$7s^2$	11·898
$5f^2$	24·356
5f 7p	43·923
6d 7p	46·365
7s 7p	54 121

It is seen that the three orbitals 5f, 6d, and 7s have nearly the same energy. The total energies of the baricenters are not a simple linear combination of the single orbital energies (which seem smaller for 5f than 6d); thus, the distance from 5f 6d to $5f^2$ is five times as large as the distance from $6d^2$ to 5f 6d. This is explained by the more effective repulsion between two 5f-electrons, expressed by the Slater–Condon–Shortley [16] integral F^0 (5f, 5f) than between one 5f- and one 6d-electron G^k (5f, 6d) with k = 1, 3, 5. By the arguments given above, the baricenter of $5f^2$ of gaseous U^{+4} would be expected to represent the lowest configuration, some 50 kK below 5f 6d. Actually, no Laporte-allowed absorption maxima are observed in uranium (IV) aquo ions in the experimentally accessible range below 50 kK, and the present author has previously [17] considered this fact as a strong argument for Seaborg's actinide hypothesis, insofar as electronic configurations are concerned. In U(III) aquo ions with $5f^3$ groundstate and lower ionic charge, the transitions to those states which are $5f^2\ 6d$ to a good approximation, are situated [9, 10, 12] at 25·5, 26·8, and 31·2 kK.

Twelve of the 13 possible J-levels of $5f^2$ in Th^{++} are situated [14, 15] within a comparatively narrow range of 17 717 K with $^3H_4$ at lowest and $^3P_2$ at highest energy. Only $^1S_0$ occurs as an isolated top level of $5f^2$, 17 799 K higher than $^3P_2$. This is exactly as predicted [16]. If we may describe the actinide complexes mainly as problems in atomic spectroscopy, we must use three different types of parameter:

(1) The orbital energies of 5f, 6d, etc.

(2) The interelectronic repulsion energy parameters F^2, F^4, and F^6 (or Racah's linear combinations E^1, E^2, and E^3), separating the L, S-multiplet terms within a given $5f^n$-configuration.

(3) The Landé multiplet splitting parameter ζ_{5f}, separating the J-energy levels within the terms and intermixing L and S (for constant J) by intermediate coupling.

Racah's linear combination E^3 is especially important for the effect (2), in complexes, since it gives an expression for the distances between the terms with the maximum value of S, and thus, for the wave numbers of the spin-allowed bands. In the lanthanides [10, 18, 19], the values are, in K:

	E^3	ζ_{4f}
$4f^2$ Pr(III)	460	740
$4f^3$ Nd(III)	480	860
$4f^5$ Sm(III)	480	1180
$4f^7$ Gd(III)	520	—
$4f^9$ Dy(III)	570	1920
$4f^{12}$ Tm(III)	630	2700

The gaseous ions Ac^{++}, Th^{++} and Th^{+++} suggest considerably higher values of ζ_{5f} (750, 1035, and 1236 K, respectively) than $\zeta_{4f} = 644$ K in Ce^{+++}. Therefore, the influence of intermediate coupling must be larger in the actinides than in the lanthanides.

Originally, the present author could not estimate the relative size of the interelectronic repulsion integrals, viz. E^3, in the 5f- and 4f-shells. However, in the following, arguments will be presented for these quantities being 50–65 per cent as large in the actinides as in the corresponding lanthanides. Since the interelectronic repulsion integrals [11, 18] are roughly inversely proportional to the average radius of the partly filled shell, and since actinides and lanthanides have nearly the same crystallographic radii [3], this will explain the much larger perturbations from the ligands in the former ions.

The absorption bands of U(IV) aquo ions all occur [17] below 23·4 kK, except a narrow, weak band at 40·8 kK. It is at the present time natural to assume the whole range of $5f^2$-energy levels from $^3H_4$ to $^3P_2$ to be concentrated in the range 0–24 kK with the exception of $^1S_0$ at 40·8 kK. It is not argued that every observed energy level in the former range belongs to exactly one J-level of the gaseous ion. Even though the ligand perturbations may be so strong as to intermix several levels of a given J-value extending over a range of perhaps 2 kK, it will still be valid to consider the large-scale distribution of J-values in the $5f^2$-configuration of the complex.

Since the distance $^3H_4$–$^3P_2$ is composed of $(7/2)\zeta_{5f} + 42E^3$ + second-order energies from the intermediate coupling (in this case necessarily positive), the observed value 23·4 kK sets serious limits to the two quantities. If it is assumed that ζ_{5f} is about 1600 K, then E^3 is at most 400 K and is more probably 350 K. The latter value is rather low, since $E^3 = 300$ K can be estimated from Th^{++}, and since these quantities ordinarily increase proportionally to Z_0 + a small constant [20]. However, since $(U\ ox_4)^{-4}$ and other complexes have E^3 some 2 per cent smaller than the aquo ion, it may be assumed that gaseous U^{+4} has E^3 some 3–5 per cent higher than the aquo ion.

The comparison with the observed energy levels can be made by Gruen's plot of $5f^2$ in intermediate coupling [21] (which must be slightly corrected in the case of the two curves $^3P_2$ and $^1D_2$, which intersect on the drawing). Two essentially different possibilities for the identification of the excited states of the U(IV) aquo ion bands subsist:

Band at	Oscillator strength $P(\times 10^{-5})$	$\zeta_{5f} \sim 1600$	$\zeta_{5f} \sim 2000$
6550, (6900)	—	$^3F_3$, $^3F_4$	$^3H_5$
(8750), 9300	22	$^3H_6$	$^3F_3$, $^3F_4$
11200, 12000	5·6	?	$^3H_6$
14850, 15350, (15800)	21	$^1D_2$, $^1G_4$	$^1D_2$, $^3P_0$, $^1G_4$
18200, (18350)	5	$^3P_0$	$^3P_1$
20150, 20500, (21300)	15·5	$^3P_1$, $^1I_6$	$^1I_6$
(23000), 23350	6·5	$^3P_2$	$^3P_2$
40800	~4	$^1S_0$	$^1S_0$

The unusual feature of the second possibility is that the transition to $^3H_6$ has such a relatively low intensity. The levels $^1D_2$ and $^1G_4$ have a very large amount of triplet character, due to intermediate coupling [17].

Gruen and Fred [22] studied the absorption spectra of UF_4, $NaUF_5$, and Na_2UF_6 at very low temperatures and measured many sharp lines. However, it cannot be concluded that the number of sub-levels at most is $2J+1$ and thus can be used for determination of J for the levels. Rather, vibrations are also excited, as is often the case in the ordinary transition groups.

Weinstock *et al.* [23, 24] studied the gaseous compounds NpF_6 and PuF_6. The former has bands at 7299, 7604, 7888, 8197, 9191, 9367, and 9523 K, and they may be identified [23, 24] with the transition from $^2F_{5/2}$ to $^2F_{7/2}$, implying $\zeta_{5f} \sim 2400$ K and a splitting from the ligand fields amounting to some 2000 K. PuF_6 has a very complicated absorption spectrum [24] with weak band groups at 3780–6604 K, six very sharp lines at 9583–10 678 K with the highest peak at 9926 K, two band groups at 12 260 and 12 720 K with a prominent fine structure, and finally three bands at 17 260, 17 817, and 18 448 K before the strong electron transfer band. There seems to be a correspondence between the bands of U(IV) aquo ions and PuF_6, the wave numbers being some 10 per cent larger in the latter case.

If the ligand field splittings are not larger than 2000 K in PuF_6, it is an interesting question, whether the transitions such as $^3H_4$–$^3H_6$ can be found in the dioxo ions NpO_2^+ and PuO_2^{++}. The very high, narrow bands at 10 170 and 12 000 K, respectively, have been identified in this way [17, 21]. In particular, the transitions within the same multiplet might be caused by magnetic dipole radiation [18]. Eisenstein and Pryce [25] assumed that the splitting of the 5f-shell by the linear ligand field from the two oxygen atoms is so large that the distance between $\lambda=3$ and $\lambda=2$ is 17 000 K. However, the present author [26] assumes that the weak bands with vibrational structure in UO_2^{++}, NpO_2^{++}, PuO_2^{++}, and AmO_2^{++} have a common cause, and that the λ-splitting cannot be estimated from these bands. It cannot be excluded that the excited states of the narrow bands of dioxo ions still have fairly well-defined J-values, even though the linear field has a large influence on the distribution of sub-levels and on the intensity of the transitions.

Thus, it is rather remarkable that the last visible band of U(IV) is not very strong, compared to Pr(III), where the transition $^3H_4$ $^3P_2$ gives the strongest band observed, as also $^3H_6$–$^3P_2$ in Tm(III) [27]. However, if the J-levels are mixed to some extent, the cross-products $C_{n1}C_{n2}\Psi_{nJ1}\Psi_{nJ2}$ may interfere seriously with the size of a matrix element of the type

$$\int \Psi_1 \mathbf{r}\, \Psi_2 \, d\tau \quad \text{with } \Psi_1 = \sum C_{n1}\Psi_{nJ1} \quad \text{and } \Psi_2 = \sum C_{n2}\Psi_{nJ2}$$

determining the oscillator strength of the transition from the ground state Ψ_1 to an excited state Ψ_2, written as linear combinations of states with particular J-values. Curious things happen to the distribution of intensities, as one passes continuously from Russell–Saunders' coupling to pure j, j-coupling. In the former case, the intensities vanish for transitions between states with different S, while in the latter case, at most one electron changes its j-value. In all the intermediate cases, both rules are applicable, if the wave functions are expanded in terms of the pure S, J- or the pure $j_1^a j_2^b$, J-states. However, it must be realized that the calculation of oscillator strengths of Laporte-forbidden transitions is a much more difficult task than the calculation of Laporte-allowed transitions, which essentially arise from the matrix elements given above. The Laporte-forbidden transitions obtain their intensities from so many sources (e.g. vibrational intermixing with states of the opposite parity), that the present author doubts that any reliable results can be obtained, in view of our ignorance of the actual wave functions (whose radial parts certainly are not hydrogenic), of the admixed functions of the opposite parity and their energy, and of the vibrational mechanism of this admixing.

It was seen [p. 98] that the interelectronic repulsion parameter E^3 is proportional to $(Z-35)$ in the trivalent lanthanides. This dependence on the atomic number Z might seduce some spectroscopists, thinking in terms of X-ray energies, into assuming a very 'internal' nature for the 4f-electrons, corresponding to the krypton shell. However, if the behaviour of the 4f-electrons as a function of the ionic charge Z_0-1 is considered, E^3 (e.g. in Sm(II): Eu(III) or Eu(II): Gd(III) [19]) is rather proportional to Z_0+2 than to Z_0+25. Previously, the present author [10, 17] has noted the proportionality to $\sim Z_0+1$ occurring in the wave numbers of corresponding pair of bands in U(III): Np(IV) and Np(III): Pu(IV). In the following, similar relations will be discussed for Pu(III): AmF_4 and Am(III): CmF_4. Several American chemists and physicists have been so kind as to inform me about such absorption spectra before their publication.

We may begin to compare also the lanthanide $4f^7$ Gd(III) with the actinide $5f^7$ Cm(III). Previously, the existing measurements have been criticized [10], because only broad, large bands of impurities, induced by the strong α-radioactivity of Cm 242 (162 days half-life) were reported. With the longer lived isotope Cm 244 (18 years), it has become possible to recognize the narrow $5f^7$-bands, and it may be hoped that one of the isotopes Cm 245, 246, 247, or 248, which all have half-lives of many thousand years, will be available in substantial amounts in the future.

The most conspicuous band group of Cm(III) is placed [28] at 396 mμ in an aqueous solution of 0·017 M $Cm(ClO_4)_3$ in 1·3 M $HClO_4$ ($\epsilon=53$), at 399, 399·5, 400·1 mμ of Cm(III) imbedded [29] in anhydrous $LaCl_3$, and at 395 mμ in solid [30] CmF_3. The excited level of this band group [29] has $J=7/2$. According to Dieke *et al.* [31, 39] $^6P_{7/2}$ of Gd(III) does not correspond to the strong band group at 273–279 mμ, but rather to the weak groups at 311 mμ (311·5 mμ $^6P_{7/2}$ and 305·7 mμ $^6P_{5/2}$ in $GdCl_3$, 6 H_2O, while $^6P_{3/2}$ has slightly higher energy).

The decrease of the wave-number of Cm(III), compared to Gd(III), supports further the conclusions arrived at above for U(IV), that the interelectronic repulsion parameters are considerably smaller in the actinides than in the lanthanides. The non-diagonal element of intermediate coupling [32] between the ground state ^8S and ^6P, both levels having $J=7/2$, is $\sqrt{(14)}\,\zeta_{nf}$. Since $\zeta_{5f}\sim 3000$ K or more in Cm(III), these two levels will be intermixed ~20 per cent in the squares of the wave functions. The distance between the two levels will be increased ~8000 K by their mutual interaction. Even though the upper level may be heavily depressed by further levels with $J=7/2$, it may thus be argued that the distance between the baricenters of ^8S and ^6P, when corrected for intermediate coupling, is only half as large in Cm(III) as in Gd(III). The excited states with J different from 7/2 correspond to smaller band intensities. Thus, a weaker band group at 458·8, 460·3, 460·6 mμ of Cm(III) in $LaCl_3$ (the excited state has $J=5/2$ according to Conway *et al.* [29]) or at 449 mμ [30] of CmF_3 corresponds to the weaker bands of Gd(III) at lower wave numbers, while Carnall, Fields, and Keenan [28] indicate a much weaker band at 590 mμ (ϵ below 1) of aqueous Cm(III). Since f^7 is a half-filled shell, no first-order L, S-coupling splitting is produced, and the spreading of such energy levels, belonging to the same multiplet term in Russell–Saunders' approximation, will be proportional to ζ_{nf}^2 and thus, roughly four times larger in Cm(III) than in Gd(III).

It is seen from the results cited above that the position in the nephelauxetic series [33], i.e. the order of decreasing interelectronic repulsion parameters, is

$$CmF_3 > Cm(H_2O)_n^{+++} > Cm(III) \text{ in } LaCl_3$$

with a variation slightly above 1 per cent. Similar variation was found by Ephraim [11]

$$RF_3 > RCl_3 > RBr_3 > R_2O_3$$

with R = Pr(III) or Nd(III). In the three ordinary transition groups, the nephelauxetic series is, as a function of the ligands for a given central ion [33]:

$$\text{gaseous ion} > F^- > H_2O > NH_3 > C_2O_4^{--} > SCN^- > Cl^- \gtrsim CN^- > Br^-$$

The chemical shifts in Cm(III) are not more than thrice those encountered in Gd(III) [11]. The perturbations from the ligands for a partly filled shell seem to increase in the order

$$4f < 5f < 3d < 4d < 5d$$

if the nephelauxetic effects are considered, while the direct splittings, caused by the ligand fields, have the same order, but with a stronger unequality sign between 5f and 3d, and probably also between 4f and 5f.

In the treatment of lanthanide spectra, it is often assumed that the ligand field can be treated as a first-order perturbation (i.e. that the wave functions are not changed from $4f^n$ in the gaseous ion). However, the relative importance of the nephelauxetic (= ‘ cloud-expanding ’) effect and the ligand field splittings seems rather to show that the second-order perturbations (i.e. the covalent bonding, where molecular orbitals are formed by changing the wave function of the partly filled shell) are just as important in the f- as in the d-groups. Thus, the ligand field parameters of the ‘ electrostatic ’ first-order model are only descriptive quantities, which cannot be theoretically predicted. The present author does not believe that the ratio R between the second-order and the first-order ligand effects goes towards zero when we go from the three ordinary transition groups to the actinides and further to the lanthanides, though the effects themselves decrease. Rather, the strong decrease of the interelectronic repulsion parameters by complex formation might be taken to indicate that the ratio R is strongly increasing in the lanthanides. However, it may be explained by the difference between ‘ symmetry-restricted ’ and ‘ central field ’ covalent bonding [40]. In symmetry-restricted covalent bonding, the partly filled shell directly participates in formation of molecular orbitals, while the central field covalent bonding only acts on the partly filled shell as a changed central field, corresponding to a smaller effective charge than in the gaseous ion. This change of the central field of spherical symmetry can be produced by the donation of any type of electrons from the ligands, e.g. in combination with empty s- and p-orbitals of the central ion. Recently, the very weak ligand field perturbations on cooled, trapped nitrogen atoms have been observed [41], and the distance ^4S ^2D is observed to decrease by about 1 per cent.

It is, of course, rather interesting to study whether the spatial extension of the d- and f-radial wave functions correspond to the observed F^k-integrals. Actually, in the first transition group, Hartree-Fock's self-consistent 3d-radial functions give 15–30 per cent larger parameters of interelectronic repulsion than estimated from atomic spectroscopy. This may be explained by a general form of configuration intermixing, expressing the internal electronic correlation in each electron pair. Even though Löwdin and Fröman have demonstrated that e.g. a neon atom is 250 kcal/mole stabilized by not having the pure configuration $1s^2\,2s^2\,2p^6$, it is not believed that these correlation effects will be extremely important for the semi-empirical description of energy differences in the transition groups. The variation of the value of E^3 will probably correspond fairly well to the average value of the reciprocal distance of the f-electron from the nucleus [18]. However, the absolute value will be dependent on the ratio between the F^k-integral and W, which actually expresses the latter average $\overline{r^{-1}}$. For hydrogenic radial functions, W/F^2 is 2·84 for 2p, 2·45 for 3d, and 2·22 for 4f, while $W/F^2 = 3{\cdot}01$ for the Hartree–Fock 3d of Mn^{++}, according to Dr. Klaus Appel, Uppsala. Thus, the average radii of the f-shells may be somewhat smaller than previously given by the author [11, 18] when the correlation effects and the large values possible of W/F^2 are considered. Probably, $\bar{r}$ varies between 0·5 Å in Pr(III) and 0·35 Å in Tm(III), while $\bar{r} \sim 0{\cdot}65$ Å in U(IV) and 0·7 Å in Cm(III). Since the crystallographic radii [3] vary between 1·1 and 0·9 Å, it is understood why 5f-electrons in actinide compounds are more influenced by the ligands than 4f-electrons in the lanthanides.

The oxidation number +4 is not known in aqueous solution of Am and Cm. Therefore, it is very valuable that Asprey and Keenan [30] have measured the spectra of solid AmF_4 and CmF_4. The former compound exhibits a number of relatively broad bands, which seem to have from 18 to 22 per cent larger wave numbers than the corresponding bands of Pu(III) aquo ion. Even though this treatment can be criticized as long as the J-values have not been established in the two systems, the general form of the band groups is very similar, and the behaviour is in accord with a change of Z_0 for this $5f^5$-system from 4 to 5. It is surprising that no band is observed [30] between 5000 and 11 000 K of AmF_4, since the transitions to levels of ^6H with $J = 9/2$ or $11/2$ should have a fair chance of being present in that range.

Asprey, Ellinger, Fried, and Zachariasen [34], who first prepared CmF_4, noticed a narrow band at 450·4 mμ, analogous to the band at 503 mμ of Am(III) and thus giving a reasonable ratio 1·11 for the increase of the wave number. However, many more bands are observed by Asprey and Keenan [30] of CmF_4. Weak bands occur in the neighbourhood of 1612 and 1098 mμ, while a band group with three sharp maxima at 856, 696, and 673 mμ have invaded the visible range. It can be compared with Am(III), which [9] have weak bands at 1050 and 815 mμ. The $5f^6$-systems seem to display strong effects of intermediate coupling, and it is not yet known, what has exactly happened to the two lowest multiplet terms ^7F and ^5D.

Of the following actinide elements, several have isotopes of sufficiently large half-life to be produced in weighable amounts in the future (Bk 247 7000 years, Cf 249 400 years); the big problem is to add enough neutrons to make a reasonable mass number A for a given Z. The most stable isotopes (against α-emission and spontaneous fission) have A-values slightly above the β-stability line, which at this point has a slope $dA/dZ \sim 2{\cdot}8$. The absorption spectra of berkelium seem within reach now. Bk(III) is predicted to have the prominent, broad bands caused by $5f^8 \rightarrow 5f^7\,6d$ at a lower wave number than the previous actinides, since the half-filled f^7-shell of the excited state is so stable. This stabilization can be expressed in interelectronic repulsion parameters [35] and is expected to produce a shift of the first large band to about 30 kK. Analogously, Stewart and Kato [46] and Onstott and Brown [37] have found a band of Tb(III) at 219 mμ, while the $4f^{n-1}5d$ bands cannot be observed of the other trivalent lanthanides, except of Ce(III) and some features near the limiting wavelength of Pr(III) and Eu(III).

It would be interesting to find the narrow $5f^7$-bands of aqueous Bk(IV) or BkF_4 near 350 mμ.

It may be concluded that the distribution of energy levels in the actinide compounds can be largely explained by the theory of atomic spectra [16], if the following assumptions are made:

1. The lowest electron configuration is [Em] $5f^n$, followed by [Em] $5f^{n-1}$ 6d at a distance 25–50 kK, dependent on the ionic charge $Z_0 - 1$ and the atomic number Z.

2. Within $5f^n$, the multiplet terms are separated by parameters of interelectronic repulsion, which are about 60 per cent as large as in $4f^n$ of the corresponding lanthanides. In particular, Racah's linear combination E^3 is about 300 K in the trivalent actinides and about 360 K in the quadrivalent actinides.

3. Within the multiplet terms, the J-levels are separated by Lande's parameter ζ_{5f}, which is about twice as large as ζ_{4f} in the lanthanides, and thus at least 1600 K. Therefore, the intermediate coupling is very pronounced.

4. The ligand fields (electrostatic first-order and covalent second-order perturbation energies) split the J-levels by amounts of some 1000 K and may produce some intermixing of J-levels. However, this influence is much smaller than in any d^n-transition group complexes.

In the actinides, electron transfer spectra also occur, just as in the other parts of the periodic system. Oxidizing central ions and reducing ligands produce these bands at relatively low wave numbers—cf. U(IV) and Pu(IV) in concentrated HCl, forming chloro complexes. The ions RO_2^{++} have much more pronounced electron transfer bands than RO_2^+, among those Laporte-forbidden, weak bands with vibrational structure.

The conclusion drawn above, that the electron configurations of trivalent and tetravalent actinides are [Em] $5f^n$ to a very good approximation both in their ground states and excited states below about 25 kK, probably will surprise some chemists who will argue that, nevertheless, the chemistry of uranium does not resemble the chemistry of neodymium. It may be answered that the two aspects, the electron configurations and the chemical properties, are not as contradictory as many text-book writers might guess. For the present author, it is no more remarkable that uranium with three 'valency electrons' ($6d\,7s^2$) in the neutral, gaseous atom is mainly hexavalent and tetravalent, than that neodymium with two 'valency' electrons ($6s^2$) is always trivalent. There is no necessary connection between the presence of f-electrons and constant trivalency. In this way, the name 'actinides' obscures to some extent Seaborg's great idea that the elements Th, Pa, U, . . . , 103 have f-electrons in some of the oxidation states to the same extent that Ce, Pr, . . . , Lu have f-electrons. Whether in their chemistry these elements turn out to resemble most Ac and thus the rare earths, or Th, or U, could not easily be predicted *a priori*. The name 'uranides' proposed by Haissinsky [42, 43] for expressing the common chemical properties of the series U, Np, Pu, Am . . . (which does not seem to terminate at a definite element) is reasonable from a chemical point of view, but cannot alter the fact that gaseous Th^{+3} and Pa(IV) compounds have been shown to have the ground state [Em] 5f.

The discussion between partisans of 'actinides' and 'uranides' reflects two different conceptions of the periodical system of elements. After Moseley established the atomic numbers, any classification could only be connected with a periodicity in Z. Chemical analogies of the type Ba–Pb, Sn–Pt, or In–Bi, which would be proposed by a chemist without a knowledge of Z, cannot have any influence now. However, the sub-classification into 'inner groups' of the periodic system may be made according to one of two criteria:

1. Analogy between the electron configuration of the ground states (and we may add, the other low states) of the corresponding elements (the neutral atoms and their ions in gaseous state).

2. Analogy between the chemical properties of the corresponding elements. Of these, (1) derived from atomic spectroscopy is by far the more objective and consistent, while (2) is often ambiguous and liable to subjective feelings. However, (1) offends the chemist by several anomalies. By far the most serious is that helium is irreparably placed in the same group as Be, Mg, Ca, Sr, Ba, Ra and not in the groups of the other inert gases Ne, A, Kr, X, Em. But other exceptions of the same type is that the chemistry of Pa and U does not resemble that of Pr and Nd. In the author's opinion, Seaborg's actinide hypothesis is entirely a truth of type (1). On the other hand, (2) often produces ambiguous decisions. It is in the spirit of (2) that N. Bohr introduced the dashed lines in his periodical table, many elements having two homologues in the following period. From the point of view of (2), both Sc and Ga are homologues of Al, and Hf has *both* Th and 104 as homologues. If electron configurations (1) are considered. Ga is the only legitimate homologue of Al, while chemists argue that Sc, only existing in trivalent compounds, is not a typical transition group element. In all transition groups, the first elements have a tendency to have the maximum value of the oxidation state, while later on, the oxidation state is somewhat stabilized at a rather low and slowly decreasing value. This stabilization occurs at a higher average oxidation state in the 4d-, 5d-, and 5f-groups than in the 3d- and the 4f-groups. It has previously been discussed [18] whether this phenomenon and the larger variability of oxidation states in the former class is caused by the presence of several maxima of the radial function of the partly filled shell, as contrasted with 3d and 4f. Our family names '-ides' are derived from the first element, where this stabilization begins. Thus, the first transition group might very well be said to contain a family of mainly di- and trivalent 'chromides', while Sc, Ti, V still have the evolutionary tendency of an ordinary group 3, 4, 5. It is interesting to note that the stabilization occurs later on in the second transition group, where we rather have 'ruthenides', while Y, Zr, Nb, Mo and perhaps Tc prefer their maximum values of the oxidation state. In close analogy to this evolution of the d-elements, nobody can wonder that a chemist, following the best advice of his conscience, may prefer to call the 4f-elements lanthanides and the 5f-elements uranides. However, according to atomic spectroscopy and the absorption spectra of the compounds, 5f-electrons appear before the state of maximum oxidation is achieved, and the name 'actinides' is derived from two sources: that an extrapolation of [Em] $5f^n$ 6d $7s^2$ backwards to $n=0$ hits Ac, and that the late 5f-elements have a strong preference for +3,

two somewhat accidentally connected facts, since Am has the configuration [Em] $5f^7$ $7s^2$ in its groundstate [44]. Most of the actinide versus uranide discussion is caused by the fact that atomic spectroscopists and chemists do not take account of all the results of each others' subjects and that it is often assumed that either (1) or (2) is the only valid form of the periodical classification. Finally, much confusion has been produced by the formal applications of theoretical equations, related to special cases of the behaviour of d^n- or f^n-configurations, to magneto-chemical measurements on actinide compounds [3, 45]. Since the ligand field perturbations of the $5f^n$-ground levels are large compared to kT, nearly any form of magnetochemical behaviour can be encountered (e.g. the near diamagnetism of PuF_6), and it is impossible from macroscopic measurements (as contrasted to paramagnetic resonance results) to deduce the electron configuration, as was once done for $6d^2$ rather than $5f^2$ of uranium(IV) compounds from 10 per cent difference in the magnetic susceptibility.

I would like to thank Professor Glenn T. Seaborg, Professor B. B. Cunningham, Dr. J. C. Conway, Dr. J. C. Wallmann, and the other members of the Radiation Laboratory, University of California, and Professor J. C. Hindman, Professor B. Weinstock, Dr. M. Fred, Dr. D. Gruen, and Dr. W. T. Carnall of the Argonne National Laboratory and Professor L. B. Asprey of the Los Alamos National Laboratory much for interesting discussions and valuable, private communications. I thank Professor I. Perlman, University of California, and Professor J. W. Cobble, Lafayette, Indiana, for their kind invitation to participate in the Symposium on the Chemistry of the Less Familiar Elements, San Francisco, April 1958, and the Chemistry Division, U.S. Air Force Office of Scientific Research, for having made my travel possible. Finally, I thank Professor M. Haissinsky, Laboratoire Curie, Institut du Radium, Université de Paris, for many interesting discussions about the chemical properties of the actinide elements as compared with their electron configurations.

Il est possible, à partir de l'extrapolation des niveaux d'énergie des ions gazeux Ac^{++}, Th^{+++}, et Th^{++}, de conclure de façon sûre que la configuration électronique de l'état fondamental de tous les ions des actinides, possédant une charge ionique +3 au moins, contient seulement des électrons 5f en dehors des couches complètes du Radon. Ceci est confirmé par les transitions $5f^n \rightarrow 5f^{n-1}$ 6d que l'on observe dans Pa(IV), U(III), Np(III) (mais les nombres d'onde sont trop grands pour être mesurés dans U(IV) et Np(IV)). La configuration f^2 possède une distribution très caractéristique des niveaux d'énergie entre $^3H_4$ et $^3P_2$, avec $^1S_0$ en niveau isolé, beaucoup plus haut. Les spectres d'absorption des complexes de U(IV), et de PuF_6, suggèrent des paramètres de répulsion interélectronique de l'ordre de 60 pour cent des valeurs pour les lanthanides correspondants, tandis que les facteurs de Landé sont environ deux fois plus grands. Ceci expliquerait aussi les mesures récentes faites sur des complexes de Cm(III), comparé à Gd(III). Les effets de perturbation dûs aux groupes coordonnés (" ligands ") sont plus larges que dans les lanthanides à cause de la plus grande valeur du rayon moyen de la couche 5f. Les valeurs de J seront en conséquence réparties entre plusieurs niveaux d'énergie observés adjacents, sans que pour celà une étude générale des configurations f^n soit impossible. On discute la variation de la répartition des niveaux d'énergie en fonction du nombre d'oxydation pour des séries isoélectroniques, c'est-à-dire U(III) et Np(IV); Pu(III) et AmF_4; et Am(III) et CmF_4. Des positions de bandes sont prédites pour Bk(III) et BkF_4. Enfin les propriétés chimiques des éléments de la série des actinides sont discutées, et on souligne le fait qu'il n'y a pas nécessairement de rapport entre la présence d'électrons f et une trivalence constante.

Aus den Energieniveaus der gasförmigen Ionen Ac^{++}, Th^{+++} und Th^{++} lässt sich mit beträchtlicher Sicherheit schliessen, dass die Elektronenkonfiguration des Grundzustandes aller Aktiniden-Ionen mit Ionenladungen +3 oder höher ausschliesslich 5f-Elektronen ausserhalb der Radon-Schalen enthält. Dieser Schluss wird weiter erhärtet durch die Übergänge $5f^n \rightarrow 5f^{n-1}6d$, die in Pa(IV), U(III), Np(III) beobachtet wurden, (während in U(IV) und Np(IV) die Wellenzahlen für eine Messung zu hoch liegen). Die Konfiguration f^2 zeichnet sich durch eine sehr charakteristische Verteilung der Energieniveaus zwischen $^3H_4$ und $^3P_2$ aus, wobei $^1S_0$ ein viel höher liegendes isoliertes Niveau ist. Die Absorptionsspektren von U(IV)-Komplexen, sowie von PuF_6 deuten auf interelektronische Abstossungsparameter von etwa 60 Prozent der Werte der entsprechenden Lanthaniden, während die Landé-Faktoren etwa doppelt so gross sind. Hiermit würden sich auch die neueren Messungen von Cm(III)-Komplexen deuten lassen, insbesondere im Vergleich zu Gd(III). Der grössere mittlere Radius der 5f-Schale bedingt stärkere Störeffekte durch die Liganden als bei den Lanthaniden. Die J-Werte werden sich daher über verschiedene benachbarte Energieniveaus verteilen, ohne dass hierdurch die allgemeine Behandlung der f^n-Konfigurationen unmöglich würde. Die Änderung mit der Oxydationszahl in isoelektronischen Reihen wird diskutiert, z.B. bei U(III) und Np(IV); Pu(III) und AmF_4; Am(III) und CmF_4. Die Lagen der Banden in Bk(III) und BkF_4 werden vorausgesagt. Schliesslich werden die chemischen Eigenschaften der Aktiniden erörtert; hierbei wird betont, dass zwischen der Anwesenheit von f-Elektronen und einer konstanten Dreiwertigkeit kein notwendiger Zusammenhang zu bestehen braucht.

REFERENCES

[1] SEABORG, G. T., KATZ, J. J., and MANNING, W. M., 1949, *Nat. Nucl. Energy Series IV*, **14A**.

[2] SEABORG, G. T. and KATZ, J. J., 1954, *Nat. Nucl. Energy Series IV*, **14B**.

[3] KATZ, J. J., and SEABORG, G. T., 1957, *The Chemistry of the Actinide Elements* (London: Methuen).

[4] RASMUSSEN, E., 1933, *Z. Phys.*, **86**, 24.

[5] MEGGERS, W. F., FRED, M., and TOMKINS, F. S., 1957, *J. Res. nat. Bur. Stand.*, **58**, 297.

[6] KLINKENBERG, P. F. A., 1949, *Physica*, **15**, 774.

[7] FRIED, S., and HINDMAN, J. C., 1954, *J. Amer. chem. Soc.*, **76**, 4863.

[8] SJOBLOM, R., and HINDMAN, J. C., 1951, *J. Amer. chem. Soc.*, **73**, 1744.

[9] STEWART, D. C., 1952, *Absorption Spectra* (ANL 4812, Argonne Nat. Lab., Chicago).

[10] JØRGENSEN, C. KLIXBÜLL, 1955, *Math.-fys. Medd.*, **29**, No. 11.

[11] JØRGENSEN, C. KLIXBÜLL, 1956, *Math.-fys. Medd.*, **30**, No. 22.

[12] JØRGENSEN, C. KLIXBÜLL, 1956, *Acta chem. Scand.*, **10**, 1503.

[13] JØRGENSEN, C. KLIXBÜLL, *J. inorg. nucl. Chem.*, **1**, 301.

[14] KLINKENBERG, P. F. A., 1950, *Physica*, **16**, 618.

[15] RACAH, G., 1950, *Physica*, **16**, 651.

[16] CONDON, E. U., and SHORTLEY, G. H., 1953, *Theory of Atomic Spectra* (Cambridge : University Press).

[17] JØRGENSEN, C. KLIXBÜLL, 1955, *Math.-fys. Medd.*, **29**, No. 7.

[18] JØRGENSEN, C. KLIXBÜLL, 1957, *Energy Levels of Complexes and Gaseous Ions* (Copenhagen: Gjellerups Forlag).

[19] JØRGENSEN, C. KLIXBÜLL, 1957, *Acta chem. Scand.*, **11**, 981.

[20] JØRGENSEN, C. KLIXBÜLL, 1957, *J. inorg. nucl. Chem.*, **4**, 369.

[21] GRUEN, D. M., 1952, *J. chem. Phys.*, **20**, 1818.

[22] GRUEN, D. M., and FRED, M., 1954, *J. Amer. chem. Soc.*, **76**, 3850.

[23] WEINSTOCK, B., and MALM, J. G., 1956, *J. inorg. nucl. Chem.*, **2**, 380.

[24] WEINSTOCK, B., and FRED, M., private communication.

[25] EISENSTEIN, J. C., and PRYCE, M. H. L., 1955, *Proc. roy. Soc.* A, **229**, 20.

[26] JØRGENSEN, C. KLIXBÜLL, 1957, *Acta chem. Scand.*, **11**, 166.

[27] JØRGENSEN, C. KLIXBÜLL, 1955, *Acta chem. Scand.*, **9**, 540.

[28] CARNALL, W. T., FIELDS, P. R., STEWART, D. C., and KEENAN, T. K., 1958, *J. inorg. nucl. Chem.*, **6**, 213.

[29] CONWAY, J. C., WALLMANN, J. C., CUNNINGHAM, B. B., and SHALIMOFF, G. V., 1957, *J. chem. Phys.*, **27**, 1416.

[30] Asprey, L. B., and Keenan, T. K, 1958, *J. inorg nucl. Chem.*, **7,** 27.
[31] Cook, S. P., and Dieke, G. H., 1957, *J. chem. Phys.*, **27,** 1213.
[32] Judd, B. R., 1955, *Proc. roy. Soc.* A, **228,** 120.
[33] Schäffer, C. E., and Jørgensen, C. Klixbüll, 1958, International Symposium on the Chemistry of the coordination compounds. *Suppl. Ricerca Scientifica*, **28,** 143; 1958, *J. inorg. nucl. Chem.*, **8,** 143; and *Acta chem. Scand.*, to be published.
[34] Asprey, L. P., Elliner, F. H., Fried, S., and Zachariasen, W. H., 1957, *J. Amer. chem. Soc.*, **79,** 5825.
[35] Jørgensen, C. Klixbüll, 1956, *Acta chem. Scand.*, **10,** 1505.
[36] Stewart, D. C., and Kato, D., 1958, *Analyt. Chem.*, **30,** 164.
[37] Onstott, E. I., and Brown, C. J., 1958, *Analyt. Chem.*, **30,** 172.
[38] Jørgensen, C. Klixbüll, 1957, Proceedings of the Inorganic Chemistry section of the International Chemical Congress, Paris, July (Paris: Sedes), p. 313.
[39] Dieke, G. H., and Leopold, L., 1957, *J. opt. Soc. Amer.*, **47,** 944.
[40] Jørgensen, C. Klixbüll, 1958, *Disc. Faraday Soc.*, **26.**
[41] Herzfeld, C. M., 1957, *Phys. Rev.*, **107,** 1239.
[42] Haissinsky, M., 1949, *J. chem. Soc.*, (supplement) 241.
[43] Haissinsky, M., 1950, *J. Chim. phys.*, **47,** 415; 1953, *Experientia*, **9,** 117.
[44] Fred, M., and Tomkins, F. S., 1957, *J. opt. Soc. Amer.*, **47,** 1076.
[45] Haissinsky, M., 1958, *Traité de Chimie Minérale* (Paris).

The colours of transition metal hexafluorides†

by the late W. MOFFITT, G. L. GOODMAN‡
Chemistry Department, Harvard University

M. FRED and B. WEINSTOCK
Argonne National Laboratory, Lemont, Illinois

(*Received* 10 *January* 1959)

The absorption spectra of ReF_6, OsF_6, IrF_6 and PtF_6 have been obtained between 2500 and 40 000 cm^{-1} in the gas phase. The interesting band systems have been assigned on the basis of ligand field theory, and some predictions have been made as to magnetic properties.

1. Introduction

The recent preparation of platinum hexafluoride [27], extends the number of elements in the third transition group which are known to form hexafluorides. The others are tungsten (cf. [3]), rhenium (cf. [3]), osmium [28] and iridium (cf. [3]). Since all of these compounds are quite volatile and several of the gases are coloured, it was decided to investigate their absorption spectra in the vapour phase from just below 4000 cm^{-1} through 40 000 cm^{-1}.

These compounds are of considerable theoretical interest, largely as a result of their volatility. In the past, the interpretation of certain structural, magnetic and spectroscopic features of the complex ions formed by transition metals has always suffered from some ambiguity, inasmuch as these properties have been studied in condensed phases: whether a departure from high, say, octahedral symmetry about a particular centre, or an equivalent magnetic anisotropy, is due to an intrinsic instability of the complex ion itself or to packing considerations is difficult to determine [26]; similarly, the vibrational structure of electronic transitions within a complex is very largely unresolved, even in crystals (cf. [10]), so that these spectra are incompletely characterized. Although the electronic structure of transition-metal complexes has been elucidated in considerable detail, certain of its nicer predictions have not been amenable to direct experimental proof. For this reason, the opportunity of studying a series of such compounds in the vapour phase offers most interesting possibilities.

As a prerequisite for more sophisticated work, it is necessary to determine the electronic structure of these hexafluorides and, in particular, to assign the observed spectra to specific electronic transitions. Ligand field theory was therefore used in the analysis, as a result of which two interesting features emerged. In the first place, it was discovered that the lower electronic states of these complexes are to be described in terms of an unusual coupling scheme, which is very simple to work out. In the second, an apparently satisfactory assignment of the observed band systems led to a prediction of an additional system, farther out into the infra-red, for platinum hexafluoride. Additional measurements, extending to longer wavelengths, did indeed reveal the missing band.

---

† The work described here was performed, in part, under the auspices of the Atomic Energy Commission.

‡ National Science Foundation Predoctoral Fellow.

Although the spectra which were obtained are rich in vibrational structure, and in many respects rather unusual, no vibrational assignments are reported at present. The concomitant analysis is complicated by a peculiar coupling between electronic and vibrational modes to which attention has recently been directed [13, 16, 17]; it presents quite different problems and has therefore been postponed.

2. EXPERIMENTAL

The experimental work to be described in this section was carried out at the Argonne National Laboratory in close association with Messrs. B. Weinstock, H. H. Claassen, J. G. Malm and E. Weaver.

The hexafluorides were prepared by heating the metals in an atmosphere of fluorine, the most difficult procedure being that for obtaining PtF_6 [27]. The products were repeatedly distilled in order to remove most of the hydrogen fluoride, which occurred as an impurity. The absorption cells were first carefully dried and then filled with purified samples; these samples were then withdrawn, redistilled and, finally, readmitted in the required amounts. Quartz cells, some 10 cm. long, were used for studies in the near infra-red through the ultra-violet. In the region below $3800\,cm^{-1}$, a nickel cell of the same length, which had been fitted with calcium fluoride windows, was used. Platinum hexafluoride is sensitive to light and cells containing it gradually became coated with photodecomposition products. However, in quartz cells containing the remaining hexafluorides no visible changes were detected over several months.

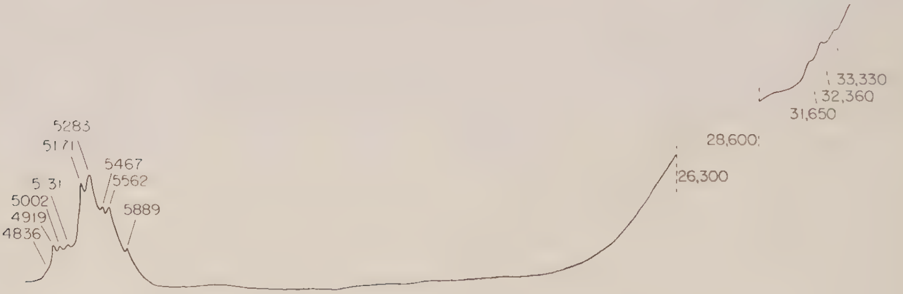

Figure 1. The absorption spectrum of rhenium hexafluoride.
——— Peak frequencies (grating measurement) in wavenumbers.
– – – – Peak frequencies (prism measurement) in wavenumbers.
(Scale of absorption arbitrary.)

The absorption spectra between $2500\,cm^{-1}$ and $40\,000\,cm^{-1}$ are reported for the hexafluorides of rhenium, osmium, iridium and platinum in figures 1, 2, 3 and 4 respectively. Tungsten hexafluoride is transparent throughout this frequency range, and no figure is therefore given for this compound. A Perkin–Elmer Spectrocord was used to make the measurements above about $27\,000\,cm^{-1}$ and the absorption maxima obtained in this region are located in cm^{-1} and indicated by broken lines in the diagrams. A prism spectrometer, namely the

Perkin–Elmer Model 21 with a calcium fluoride prism, was also used in the far infra-red and the corresponding frequencies are similarly listed—only PtF_6 absorbs in this region. The intermediate frequency range, between 3800 cm^{-1} and about 26 000 cm^{-1}, was covered using the Cary Model 14, a grating spectrophotometer; absorption maxima so obtained are indicated by solid lines in the diagrams. However, the reported spectral profiles in this intermediate range were also obtained with the Spectrocord.

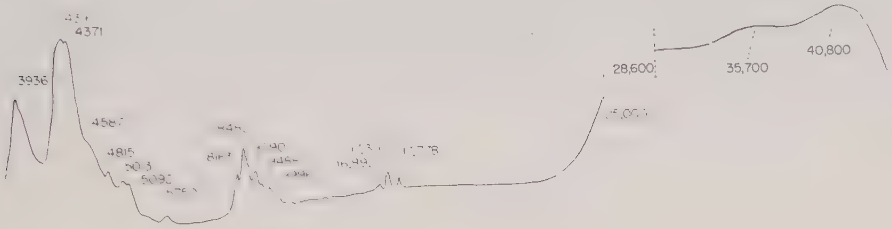

Figure 2. The absorption spectrum of osmium hexafluoride.
——— Peak frequencies (grating measurement) in wavenumbers.
– – – – Peak frequencies (prism measurement) in wavenumbers.
(Scale of absorption arbitrary.)

The absorption scales used in figures 1–4 are for the most part arbitrary. As has already been remarked, the present studies are directed more towards the location of excited states than to the complete characterization of the corresponding band systems. Consequently, no great pains were taken to overcome the problems associated with the precise determination of absorption coefficients over so diverse a frequency range. The relative intensities depicted in a single curve below about 25 000 cm^{-1} are approximately consistent, as are those appearing at higher frequencies. But a comparison between absorptions in these two regions should not be made: extinctions on the right-hand sides of figures 1–4 are very much higher than those on the left-hand sides.

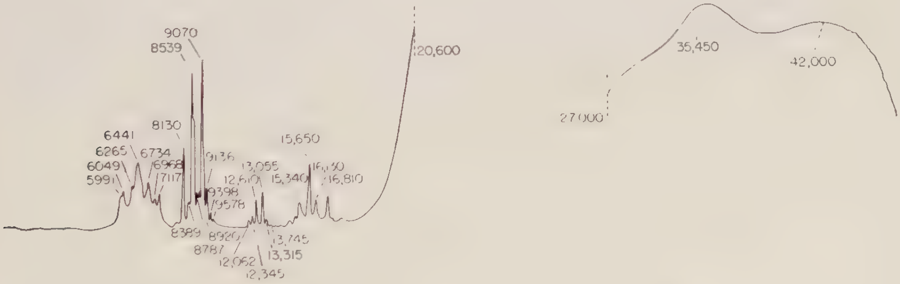

Figure 3. The absorption spectrum of iridium hexafluoride.
——— Peak frequencies (grating measurement) in wavenumbers.
– – – – Peak frequencies (prism measurement) in wavenumbers.
(Scale of absorption arbitrary.)

On a purely phenomenological basis, three distinct types of band systems may be distinguished in these figures. The first, which we call the A systems, are characterized by a half-width of approximately 1000 cm^{-1}, a rich but irregular structure and a rather low total intensity. The region of absorption around 5200 cm^{-1} in rhenium hexafluoride typifies our A systems. The second type of absorption, which we call B systems, are associated with half-widths of several thousand wavenumbers and show either no structure at all, or have the rather regular appearance associated with a totally symmetric progression; although not as strong as the continua on which they are superposed, the B systems are appreciably more intense than the A systems. A typical B system may be recognized in the spectrum of platinum hexafluoride around 32 000 cm^{-1}. Finally, the intense continua, beginning at progressively longer wavelengths as we go across the periodic table from ReF_6 to PtF_6, are called C systems. They appear to have no structure and extend over tens of thousands of wavenumbers.

For convenience, we have enumerated the various types of band systems in the table, together with the frequencies about which they are centred or at which the broad C continua begin.

Compound	System	Location (cm^{-1})
ReF_6	A	5200
	B	32500
	C	24000
OsF_6	A	3900
	A	4300
	A	8500
	A	17300
	B	35700
	B	40800
	C	22500
IrF_6	A	6400
	A	9000
	A	13000
	A	16000
	B	35500
	B	42000
	C	18500
PtF_6	A	3300
	A	5500
	A	12000
	A	16000
	B	32000
	C	14000

Observed absorption bands

3. LIGAND FIELD THEORY

As customary in ligand field theory (cf. [15]), the hexafluorides MF_6 are regarded as 'ionic', so that the central M^{6+} ion is surrounded octahedrally by six F^- ions, with M equal in turn to W, Re, Os, Ir and Pt†. The metallic ion itself has the structure $(Lu^{+++})(5d)^n$, with $n=0$, 1, 2, 3 and 4 respectively, where the Lu^{+++}-core has the closed shell configuration $(K)(L)(M)(N)(5s)^2(5p)^6$.

---

† That any departures from octahedral symmetry are small in this series seems clear from infra-red (W: [4]; Re: [7]; Os: [5]; Ir: [14]; Pt: [5]), Raman (W: [23]; Re: [7]; Os: [5]) and electron diffraction [21] studies.

As was first shown by Van Vleck [25], this description, however convenient, is unnecessarily crude since the subsequent analysis in fact automatically allows for a large measure of 'covalent' bonding as well. We ascribe the observed A and B systems to excitations within the incompleted $(5d)^n$ shell, supposing the electronic structure of the Lu^{+++} core and of the surrounding anions to be unaffected by such motions, and therefore to be separable from them. Throughout the spectral region of interest, WF_6 is transparent, which is consistent with our model since this molecule has no $5d$ electrons $(n=0)$; moreover, for the other molecules, these band systems are very weak, confirming at least that the associated transitions are most likely to be forbidden on parity grounds.

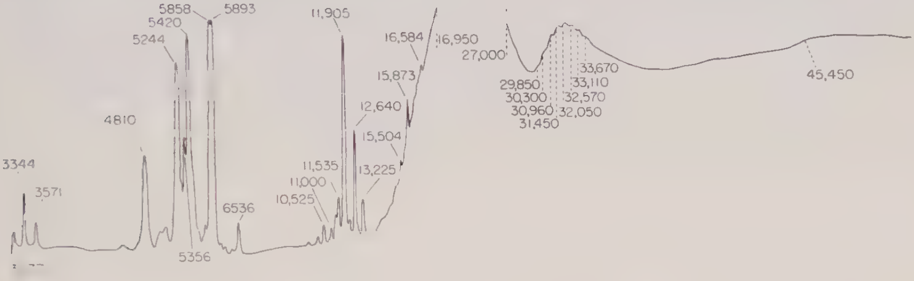

Figure 4. The absorption spectrum of platinum hexafluoride.
——— Peak frequencies (grating measurement) in wavenumbers.
– – – – Peak frequencies (prism measurement) in wavenumbers.
(Scale of absorption arbitrary.)

The behaviour of the n non-bonding $5d$ electrons is governed by a Hamiltonian

$$H=H_0+H_C+H_S+H_F,$$

where H_0 contains their kinetic energy and the spherically symmetric part of all potentials, due to their interaction with the metallic core and with the ligands as well as to the average interaction of these $5d$ electrons with themselves; H_C represents the specifically correlative interaction of the $5d$ electrons with themselves; H_S represents their spin-orbit coupling; and H_F represents the stereospecific potentials due to the octahedral ligand field. These terms are more completely defined below (note 1). The eigenvalue problem associated with H is formidable but, as we shall see, it becomes more tractable owing to the special features of our systems.

It is convenient first to consider the case of a single $5d$ electron, as exemplified by ReF_6. Here the term H_C is absent, of course, so that we can get some idea of the relative magnitudes of H_S and H_F. In the absence of either term, the $5d$ level is ten-fold degenerate, owing to the five-fold orbital and two-fold spin degeneracies. The effect of the spin–orbit coupling H_S, alone, is to split this level into an upper sextet $d_{5/2}$ (or $^2D_{5/2}$) and a lower quartet $d_{3/2}$ (or $^2D_{3/2}$); their respective energies are $+\zeta_d$ and $-(3/2)\zeta_d$, where ζ_d is a constant with the dimensions of energy (left-hand side of figure 5). Conversely, the effect of the octahedral field H_F, alone, is to split the orbital degeneracy into an upper orbital doublet, the so-called de_g level, and a lower orbital triplet, the so-called dt_{2g} level; their respective energies are $+6Dq$ and $-4Dq$, where the constant Dq represents the strength of the ligand field, and their total respective degeneracies are four and six (right-hand side of figure 5). When the spin–orbit splitting $(5/2)\zeta_d$ is much larger than the ligand field splitting $10Dq$, we may continue to speak of $d_{5/2}$ and $d_{3/2}$ electrons, recognizing that the former six-fold level $d_{5/2}$ is now split into a lower doublet, of energy $-4Dq$, and an upper quartet, of energy $+2Dq$, whereas the latter $d_{3/2}$ level is unaffected. On the other hand, when the ligand field splitting greatly exceeds the spin–orbit interaction, we may continue to speak of de_g and dt_{2g} electrons: the six-fold level dt_{2g} is now split into a lower quartet of energy $-(1/2)\zeta_d$, which we call $t_{3/2}$, and an upper doublet of energy $+\zeta_d$, which we call $t_{1/2}$. These two extremes of behaviour, together with the intermediate case where $(5/2)\zeta_d$ and $10Dq$ are of comparable magnitude, are shown in figure 5. It will be noticed that the degeneracies of the two quartet states, as of the doublet state, are never removed: their representatives span irreducible representations (Γ_8 and Γ_7) of the double octahedral group O_h^r [2,11].

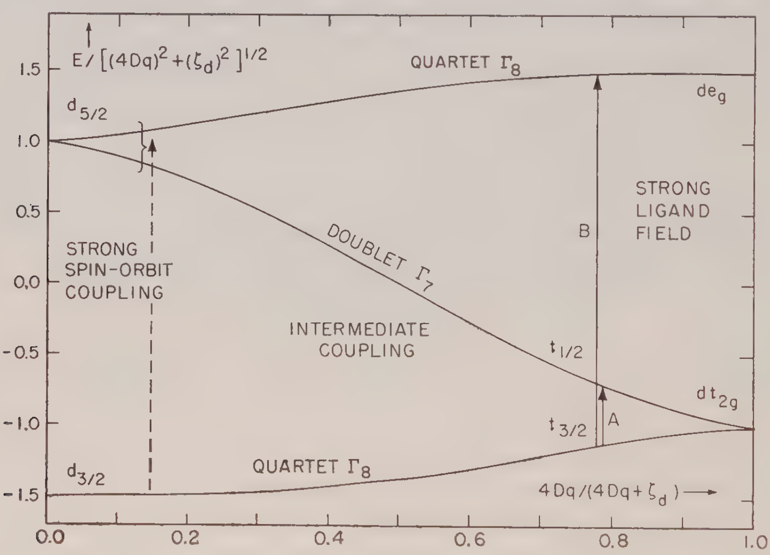

Figure 5. The coupling scheme for a single d electron in an octahedral field.

Now, as we have seen, rhenium hexafluoride has an A system centred at 5200 cm^{-1} and a B system centred at 32 500 cm^{-1}, which may be discerned as underlying a rising C continuum. We attribute the A system to an electronic transition within the dt_{2g} level, namely $t_{1/2} \rightarrow t_{3/2}$, and the B system to a transition from the lower dt_{2g} multiplet of the de_g level. These assignments are shown as solid arrows on the right of figure 5. This implies that the ligand field is very strong—more specifically, that $10Dq \approx 32\,000$ cm^{-1} and $(3/2)\zeta_d \approx 5200$ cm^{-1}. These values are most reasonable: both ζ_d and Dq are known to be much greater (cf. [6]) and greater [9, 18] respectively than their counterparts in the first transition period, where ζ_d ranges from 100 to 800 cm^{-1} and $10Dq$, for F or H_2O ligands, ranges from 10 000 to 20 000 cm^{-1}. (The alternative assignment, that system A is due to the weak field transition $d_{5/2} \rightarrow d_{3/2}$, shown as an interrupted arrow on the left of figure 5, must be excluded since it would imply that $6Dq$ is smaller than the width (~ 1200 cm^{-1}) of the band system.)

These considerations suggest an immediate simplification of the many-electron problems which confront us when $n > 1$. Since the ligand field H_F is so very strong, it will outweigh not only the spin–orbit coupling H_S but also the correlative interactions in determining the coupling scheme. A similar situation has already been encountered in connection with the magnetic properties of other complexes in the second and third transition periods [9]. On this basis, we may first assign electrons individually to the de_g and dt_{2g} levels, subject only to the restrictions imposed by the Pauli exclusion principle. Any such assignment determines a configuration $(dt_{2g})^{n-x}(de_g)^x$ of energy $(-4n+10x)Dq$, where the occupation number x is integral and an effective constant of the motion; interactions between different configurations may be neglected. The spin–orbit and correlative interactions are now only operative within one and the same configuration. Since the configurations themselves are still highly degenerate, H_S and H_C will cause splittings within each of these. Indeed, since $10Dq$ is considerably greater than the excitation energies of all the A band systems, both the associated ground and excited states of these arise from the same configuration, namely the lowest, $(dt_{2g})^n$. The B systems, which are unfortunately only incompletely characterized, then arise from the inter-configurational excitations $(dt_{2g})^{n-1}(de_g) \leftarrow (dt_{2g})^n$.

These generic assignments are the more plausible since they offer a rationalization of the different vibrational structure of the A and B band systems. The former are narrow, with a width of about 1000 cm^{-1}, and show no pronounced progressions in the totally symmetric vibrational mode α_{1g}. Correspondingly, by the Franck–Condon principle, the overall dimensions of their excited states do not differ greatly from those in their ground states; they appear to show evidence for asymmetric Jahn–Teller distortions, but clearly the octahedron is not appreciably expanded. The interaction of the central ion with the ligands differs only subtly in the ground and excited states of the A systems, suggesting that both have much the same energy under the strong ligand field—that is, they arise from the same configuration $(dt_{2g})^n$. By contrast, the B systems are apparently much broader and, in PtF_6 at least, have the very regular appearance consistent with a strong progression in the α_{1g} vibrational mode: their upper states must correspond to considerably expanded octahedra and therefore show strong evidence of $(dt_{2g})^{-1}(de_g)$ promotions which alter the aspect of the electrons to the ligand field. (Similar arguments were first advanced by Santen and Wieringen [20] and particularly by Orgel [19].)

For the remainder of this section, we shall solve the energy problem concerned with the single configuration $(dt_{2g})^n$, on the basis of which all A band systems are assigned. This calculation is remarkably simple since, 'accidentally', it has full spherical rather than only octahedral symmetry: the separations between the various levels associated with the configuration $(dt_{2g})^n$ are formally identical with those of the atomic configuration p^{6-n}. As a result of this equivalence—which is established in note 2, below—we may associate with each state a total angular momentum $\mathbf{J}'$, which is a constant of the motion. The correlative interaction H_C may now be assessed by a single energy parameter G, whose magnitude relative to that of the spin–orbit parameter ζ_d determines the coupling scheme.

When $\zeta_d \ll G$, we encounter Russell–Saunders coupling and may meaningfully associate with each state total orbital and total spin angular momenta, $\mathbf{L}'$ and $\mathbf{S}$ respectively, with $\mathbf{J}' = \mathbf{L}' + \mathbf{S}$. Thus for $(dt_{2g})^2 \equiv p^1$, the ground state is $^3P'$ with an inverted multiplet structure: $^3P'_2(J'=2)$, lying below $^3P'_1(J'=1)$, which lies below $^3P'_0(J'=0)$. This case is shown on the right-hand sides of figures 6, 7 and 8.

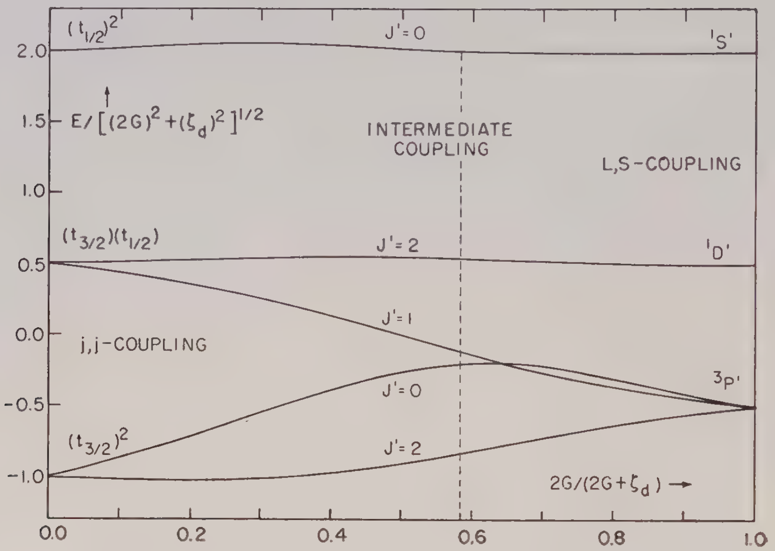

Figure 6. The coupling scheme for the configuration $(dt_{2g})^2$.

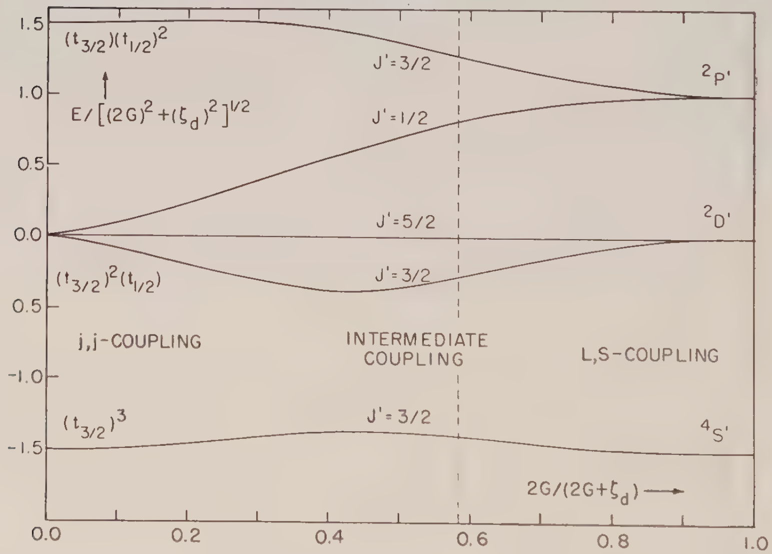

Figure 7. The coupling scheme for the configuration $(dt_{2g})^3$.

On the other hand, when $\zeta_d \gg G$, we encounter j, j-coupling. In the p^{6-n} problem, we assign (6 n) electrons individually to the lower $p_{1/2}$ and the upper $p_{3/2}$ levels, subject only to the restrictions imposed by the Pauli exclusion principle. This is equivalent to assigning n electrons individually to the lower $t_{3/2}$ and upper $t_{1/2}$ levels. The occupation numbers, in either case, serve to classify the different states. When $n=1$, we encounter the already familiar case of the lower $t_{3/2}(J'=3/2)$ state, which is equivalent to $(p_{1/2})^2(p_{3/2})^3(J=3/2)$, and the upper $t_{1/2}(J'=1/2)$ state, which is equivalent to $(p_{1/2})(p_{3/2})^4(J=1/2)$. Similarly, when $n=4$, we have as the ground state $(t_{3/2})^4(J'=0)$, which is equivalent to $(p_{1/2})^2(J=0)$. This coupling case is shown on the left-hand sides of figures 6, 7 and 8.

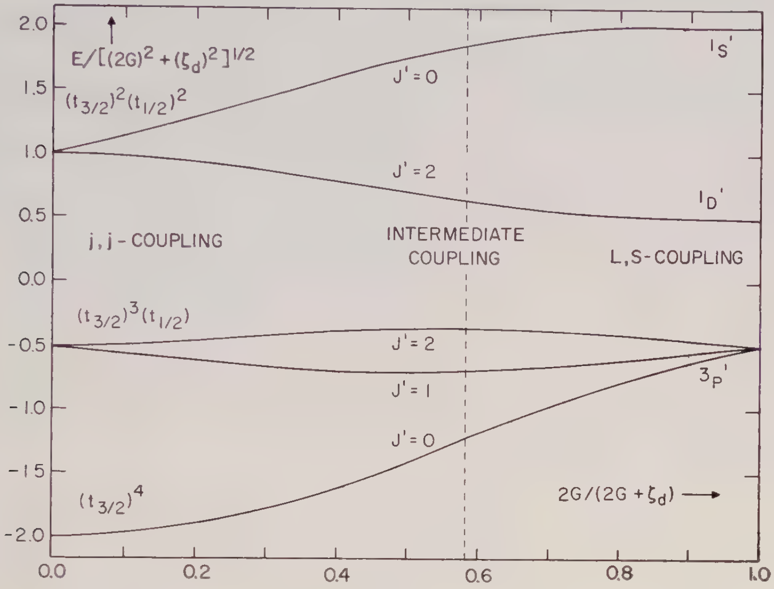

Figure 8. The coupling scheme for the configuration $(dt_{2g})^4$.

More generally, when $\zeta_d \sim G$, the occupation numbers on the one hand and the angular momenta L', S on the other lose their meaning, and only J' remains to classify the various states. This intermediate coupling scheme is illustrated in the centres of figures 6, 7 and 8.

4. ASSIGNMENTS

Comparing figures 6–8 with the absorption spectra of figures 2–4, it is seen that a satisfactory assignment of the A band systems may be made on the basis of transitions within the respective $(dt_{2g})^n$ configurations. Since we should expect ζ_d and G to be much the same for all these compounds, we have chosen the same set of values,

$$\zeta_d = 3400\,\text{cm}^{-1}, \quad G = 2400\,\text{cm}^{-1}$$

for each. The corresponding ratios of energy intervals are indicated by the broken vertical lines in figures 6–8. Observed and predicted spectra are compared in figure 9, together with the J' values for the respective ground and excited states. Calculated excitation energies are indicated by bars beneath the corresponding absorption curves. (The lengths of these bars are chosen to be proportional to the degeneracies of the upper states; since the absorption intensities have neither been measured nor ascribed to particular sources, this choice is arbitrary.) It is seen that almost quantitative agreement has been attained. The first absorption system $(0 \to 1)$ in platinum hexafluoride lay outside the spectral region originally covered, and it was on the basis of the theory that measurements were extended to longer wavelengths and that this system was located.

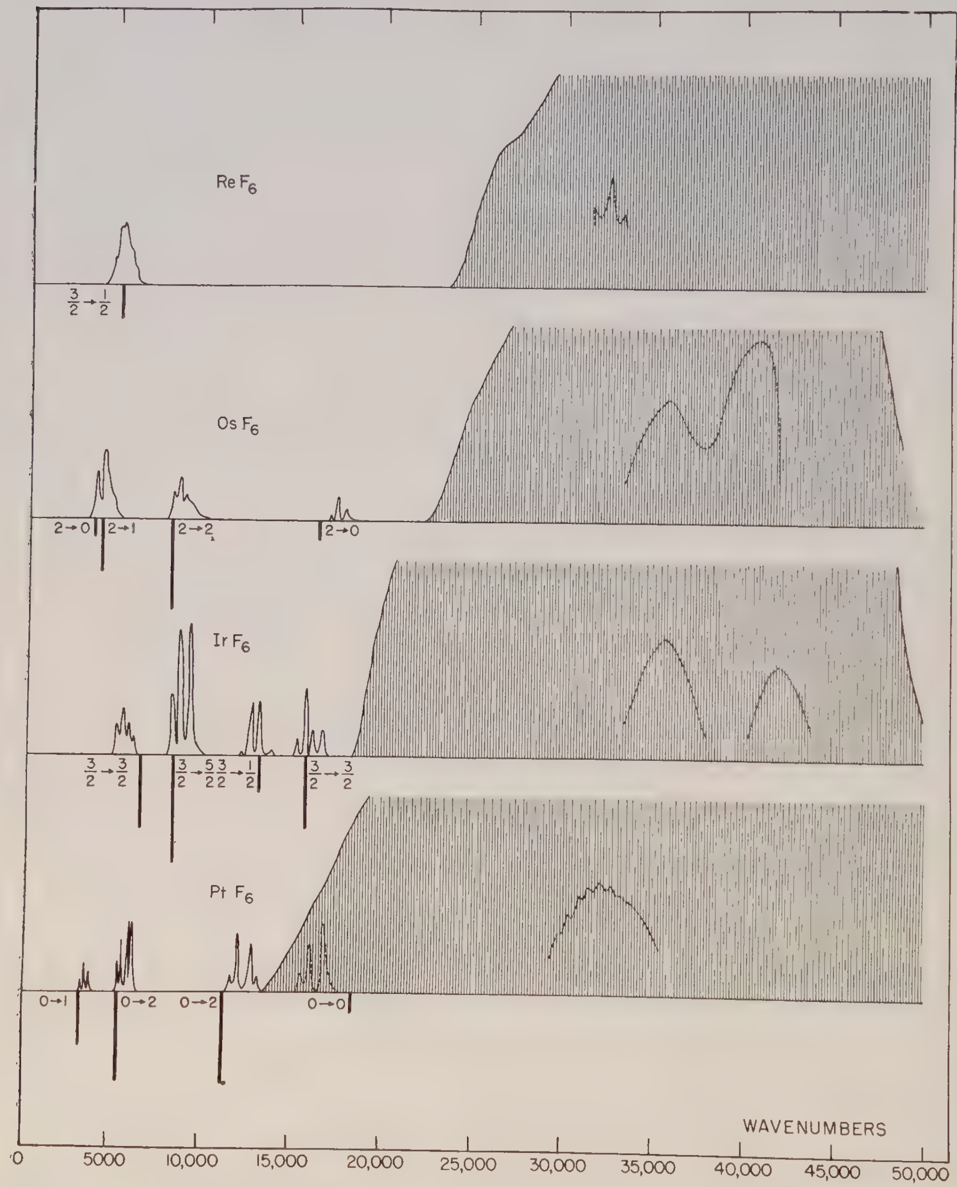

Figure 9. A comparison of the observed and calculated spectra for the transition metal hexafluorides.

It is a tribute to the power and simplicity of ligand field theory that all thirteen A band systems for these four hexafluorides can be assigned with such relative ease using only two parameters.

5. Magnetic properties

Just as the energy levels arising from configurations $(dt_{2g})^n$ are easily evaluated because of the 'accidental' spherical symmetry, so the magnetic properties of these states may also be determined with little difficulty. It should be recalled, however, that second-order errors in the energy become first-order errors in the value of an observable which is not a function of the Hamiltonian. That interactions with other configurations, arising from $(dt_{2g})^{-1}(de_g)$ excitations, say, are ignored, is therefore a serious limitation on the reliability of magnetic predictions (*vide infra*).

In the presence of an external magnetic field $\mathbf{H}$, the term

$$H_M = \beta \mathbf{H} \,.\, (\mathbf{L} + 2\mathbf{S})$$

must be added to the Hamiltonian, β being the Bohr magneton. Following note 2, we replace $\mathbf{L}$ by $-\mathbf{L}'$, so that

$$H_M = \beta \mathbf{H} \,.\, (-\mathbf{L}' + 2\mathbf{S}).$$

Choosing the direction of $\mathbf{H}$ as our axis of quantization, the Zeeman energies for state E, say, take the form $\beta|\mathbf{H}|g(E, J')M_{J'}$, where $g(E, J')$ is the spectroscopic splitting factor. In the Russell–Saunders limit, where L', S are good quantum numbers, we find

$$g(J', L', S) = (1/2)\{1 + 3[S(S+1) - L'(L'+1)][J'(J'+1)]^{-1}\}$$

by the usual cosine law [6], which is of course very similar to the Landé g-factor. On the other hand, in the limit of j, j-coupling, we find that

$$g[(t_{3/2})^n, J'] = 0$$

for all values of J', and $n = 1, \ldots, 4$, so that the ground states would all have vanishing g-factors.

In the intermediate coupling which we actually encounter, it is convenient to adopt a Russell–Saunders representation, writing

$$\psi(E, J') = \sum_{L'} \sum_S \phi(J', L', S) C(E, J', L', S),$$

to find

$$g(E, J') = \sum_{L'} \sum_S |C(E, J', L', S)|^2 g(J', L', S).$$

For the ground state of rhenium hexafluoride, of which more later, this yields

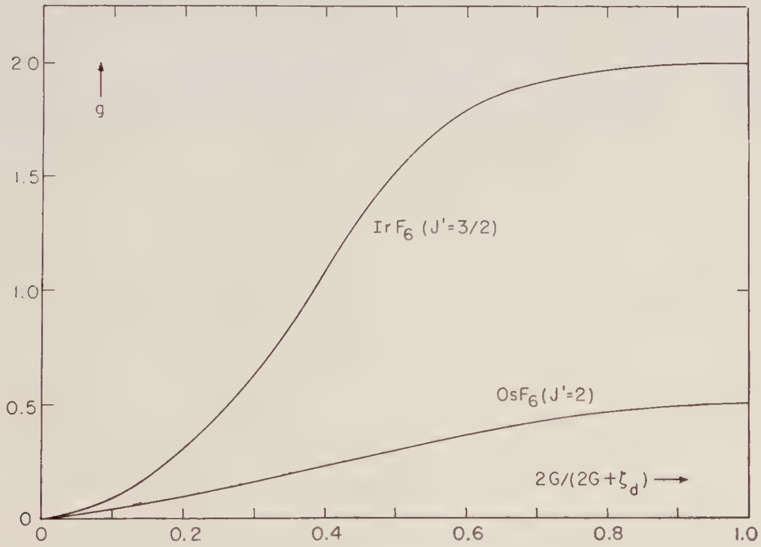

Figure 10. The spectroscopic splitting factors for the ground states of configurations $(dt_{2g})^2$, $(dt_{2g})^3$.

$g=0$, as it does for the ground state of platinum hexafluoride (for which $J'=0$). For the ground states of the $(dt_{2g})^2$ and $(dt_{2g})^3$ configurations, namely the hexafluorides of osmium ($J'=2$) and iridium ($J'=3/2$) respectively, we plot $g(E, J')$ as a function of the ratio $2G/(2G+\zeta_d)$ in figure 10; these yield the specific values 0·35 and 1·76 with our choice of parameters. That the susceptibility of PtF_6 in the vapour phase should be independent of temperature is a reliable prediction. No great store should be set by the remaining figures, however; they do little more than predict a trend in the g-factors.

To understand more clearly the limitations of our treatment, and to obtain a more trustworthy description of rhenium hexafluoride, we may include interaction between the configurations dt_{2g} and de_g for a single d electron (cf. [12]). At present it seems premature to evaluate more than the temperature-dependent part of the molar susceptibility of the vapour, which may be written in the form

$$\chi_T = N_0\beta^2\langle J'(J'+1)g^2\rangle/3\,kT,$$

provided that kT is much larger than the Zeeman splitting in the ground state and appreciably smaller than $5200\,\mathrm{cm}^{-1}$, the location of the first excited electronic state. It is then easily shown that

$$\langle J'(J'+1)g^2\rangle = (1/4)(1+\cos\theta)(19-13\cos\theta-4\sqrt{6}\sin\theta),$$

where $\pi/2<\theta<\pi$ and

$$\tan\theta = -\sqrt{6}\zeta_d/[10Dq+(\tfrac{1}{2})\zeta_d].$$

Using the spectroscopic values $10Dq=30\,000\,\mathrm{cm}^{-1}$, $\zeta_d=3400\,\mathrm{cm}^{-1}$, this leads to $\langle J'(J'+1)g^2\rangle=0{\cdot}24$ for ReF_6. Although $10Dq$ is so much larger than ζ_d, the correction to $\langle J'(J'+1)g^2\rangle$ is seen to be appreciable. Similar calculations are not offered for OsF_6 and IrF_6, but it may be anticipated that the g-factors which were estimated on the basis of the single $(dt_{2g})^n$ configurations are subject to corrections of comparable magnitude.

APPENDIX

Note 1. The interaction of the $5d$ electrons with themselves is represented in the Hamiltonian by the term $\sum_{j>i}(e^2/r_{ij})$. Making use of the relation

$$(1/r_{ij}) = \sum_{k=0}^{\infty}(r_a{}^k/r_b{}^{k+1})P_k(\cos\omega_{ij}),$$

where r_a is the lesser and r_b the greater of r_i and r_j, we may split $\sum_{j>i}(e^2/r_{ij})$ up into two terms: the former contains only those terms with $k=0$ and is subsumed in H_0, whereas the latter becomes

$$H'_C = \sum_{k=1}^{\infty} e^2(r_a{}^k/r_b{}^{k+1})P_k(\cos\omega_{ij})$$

and contains all the angular correlations between the electronic motions. Owing to the constraints imposed by the Pauli exclusion principle, the expectation value $\langle H'_C\rangle$, averaged over all states arising from a configuration $(5d)^n$, does not vanish identically, as might otherwise have been expected. For this reason, we also subsume $\langle H'_C\rangle$ in H_0, writing $H_C=H'_C-\langle H'_C\rangle$.

The potentials due to the ligand field may also be expanded in a series of spherical harmonics. Owing to the octahedral symmetry, only the 0, 4, 6, ...th order harmonics appear; of these, the zeroth-order are subsumed in H_0 and the remainder yield H_F.

H_0 is by far the largest term in H and dominates the motion. However, since each $\mathbf{l}_i$ and $\mathbf{s}_i$ commutes with H_0, its eigenvalues are highly degenerate;

here $\mathbf{l}_i$, $\mathbf{s}_i$ are respectively the orbital and spin angular momenta of electron i, in units of $\hbar$. Accordingly the radial parts of the $5d$ orbitals are determined by a self-consistent field solution of H_0 (which is then treated as a constant, and dropped), and first-order perturbation theory is used to evaluate the combined effect of H_C, H_S and H_F. In this representation, H_S and H_F may be simplified immediately to give

$$H_S = \zeta_d \textstyle\sum_i \mathbf{l}_i \,.\, \mathbf{s}_i,$$

$$H_F = (5/3) Dq \textstyle\sum_i [l_{xi}^4 + l_{yi}^4 + l_{zi}^4 - (102/5)],$$

where ζ_d is a constant with the dimensions of energy which assesses the spin–orbit coupling strength (cf. [6]), and Dq similarly gauges the strength of the octahedral field. (We have given H_F in terms of its operator equivalent—cf. [22].) H_C, which of course consists of two-electron terms, is rather more complicated; however, it too may be expressed in terms of angular and spin variables together with two constants of energy dimensions, namely F_2 and F_4, the Slater–Condon parameters [6]:

$$\begin{aligned} H_C = \textstyle\sum_{j>i} \{ & F_2[-(58/9) + (\lambda_{ij}/3)(2\lambda_{ij} + 1)] \\ & + F_4[40 - 140\sigma_{ij} + (5\lambda_{ij}/18)(99 - 26\lambda_{ij} - 7\lambda_{ij}^2)]\}, \end{aligned}$$

where $\lambda_{ij} = \mathbf{l}_i \,.\, \mathbf{l}_j$ and $\sigma_{ij} = \mathbf{s}_i \,.\, \mathbf{s}_j$. (This form for H_C may be derived by the methods of Van Vleck [24].)

Note 2. The demonstration of the equivalence of the octahedral $(dt_{2g})^n$ and the atomic p^{6-n} problems takes two parts, dealing separately with H_S and with H_C.

The three-dimensional matrix representation of $\mathbf{l}$, referred to the dt_{2g} orbitals as basis, is identical with $-\mathbf{l}'$, where $\mathbf{l}'$ is the matrix of $\mathbf{l}$, referred to three atomic p orbitals as basis; in particular, $\mathbf{l}'^2 = 2$. Accordingly H_S becomes

$$-\zeta_d \textstyle\sum_i \mathbf{l}'_i \,.\, \mathbf{s}_i,$$

which is identical in form, but opposite in sign, to the spin–orbit coupling term $\zeta_p \sum_i \mathbf{l}'_i \,.\, \mathbf{s}_i$ for the same number of p electrons; or, better, H_S is identical in form and equal in sign, to the spin–orbit coupling term $-\zeta_p \sum_i \mathbf{l}'_i \,.\, \mathbf{s}_i$ associated with n positive holes in the completed p^6 shell—that is, with the p^{6-n} configuration. This trick has been used to good advantage by Griffith [8] as well as by Abragam and Pryce [1].

The latter part consists in showing that, apart from a constant of proportionality, the matrix representation of H_C, referred to states of the configuration $(dt_{2g})^n$ as basis, is the same as the representation of the correlative interactions, referred to states of the p^n configuration as basis. By the familiar Hund equivalence, p^n and p^{6-n} are identical in this respect. It is readily shown that, for $(dt_{2g})^n$,

$$H_C = -G \textstyle\sum_{j>i} (1 + \mathbf{l}'_i \,.\, \mathbf{l}'_j + 4\mathbf{s}_i \,.\, \mathbf{s}_j),$$

where $G = 3F_2 + 20F_4$. This is to be compared with the analogous term for p^n, namely

$$-3F_2^p \textstyle\sum_{j>i} (1 + \mathbf{l}'_i \,.\, \mathbf{l}'_j + 4\mathbf{s}_i \,.\, \mathbf{s}_j),$$

where F_2^p is the familiar Slater–Condon parameter for p electrons, and establishes the second part of the equivalence.

It will be noticed that H_S commutes with each $\mathbf{j}'_i = \mathbf{l}'_i + \mathbf{s}_i$, and may be written

$$H_S = -\tfrac{1}{2}\zeta_d \textstyle\sum_i (\mathbf{j}'^2_i - \mathbf{l}'^2_i - \mathbf{s}_i^2);$$

in j, j-coupling this part becomes

$$H_S = -\tfrac{1}{2}\zeta_d \textstyle\sum_i [j'_i(j'_i + 1) - (11/4)].$$

Similarly, H_C commutes with both $\mathbf{L}' = \sum_i \mathbf{l}'_i$ and $\mathbf{S} = \sum_i \mathbf{s}_i$, and may be written

$$H_C = -\tfrac{1}{2}G[n(n-1) + \mathbf{L}'^2 + 4\mathbf{S}^2 - \textstyle\sum_i(\mathbf{l}'^2_i + 4\mathbf{s}_i^2)];$$

in LS coupling this just becomes

$$H_C = -\tfrac{1}{2}G[n(n-6) + L'(L'+1) + 4S(S+1)].$$

In intermediate coupling, of course, only $\mathbf{J}' = \mathbf{L}' + \mathbf{S}$ commutes with both H_S and H_C. The treatment for p^n is exhaustively covered in Condon and Shortley's treatise [6].

On a obtenu les spectres d'absorption entre 2500 et 40 000 cm^{-1} de ReF_6, OsF_6, IrF_6, et PtF_6, en phase gazeuse. L'attribution des systèmes de bandes intéressants a été faite à partir de la théorie du champ des ligands et quelques prévisions ont été avancées quant aux propriétés magnétiques.

Die Absorptionsspektren von ReF_6, OsF_6, IrF_6 und PtF_6 wurden im Gaszustand zwischen 2500 und 40 000 cm^{-1} vermessen. Die interessierenden Bandensysteme wurden unter Zugrundelegung der Ligandenfeldtheorie zugeordnet; hinsichtlich der magnetischen Eigenschaften wurden einige Voraussagen gemacht.

REFERENCES

[1] ABRAGAM, A., and PRYCE, M. H. L., 1951, *Proc. roy. Soc.* A, **205,** 135.
[2] BETHE, H., 1929, *Ann. Phys.*, **3,** 133.
[3] BURG, A. B., 1950, *Fluorine Chemistry*, ed. J. H. Simons, I (New York: Academic Press), pp. 113–7.
[4] BURKE, T. G., SMITH, D. F., and NIELSEN, A. H., 1952, *J. chem. Phys.*, **20,** 447.
[5] CLAASSEN, H. H., MALM, J. G., and WEINSTOCK, B., 1959 (to be published).
[6] CONDON, E. U., and SHORTLEY, G. H., 1935, *Theory of Atomic Spectra* (Cambridge: University Press).
[7] GAUNT, J., 1954, *Trans. Faraday Soc.*, **50,** 209.
[8] GRIFFITH, J. S., 1958, *Trans. Faraday Soc.*, **54,** 1109.
[9] GRIFFITHS, J. H. E., OWEN, J., and WARD, I. M., 1953, *Proc. roy. Soc.* A, **219,** 526.
[10] HOLMES, O. G., and MCCLURE, D. S., 1957, *J. chem. Phys.*, **26,** 1686.
[11] JAHN, H. A., 1938, *Proc. roy. Soc.* A, **164,** 117.
[12] JORDAHL, O. M., 1934, *Phys. Rev.*, **45,** 87.
[13] LONGUET-HIGGINS, H. C., ÖPIK, U., PRYCE, M. H. L., and SACK, R. A., 1958, *Proc. roy. Soc.*, A, **244,** 1.
[14] MATTRAW, H. C., HAWKINS, N. J., CARPENTER, D. R., and SABOL, W. W., 1955, *J. chem. Phys.*, **23,** 985.
[15] MOFFITT, W., and BALLHAUSEN, C. J., 1956, *Ann. Rev. phys. Chem.*, **7,** 107.
[16] MOFFITT, W., and LIEHR, A. D., 1957, *Phys. Rev.*, **106,** 1195.
[17] MOFFITT, W., and THORSON, W., 1957, *Phys. Rev.*, **108,** 1251.
[18] ORGEL, L. E., 1955, *J. chem. Phys.*, **23,** 1819.
[19] ORGEL, L. E., 1955, *J. chem. Phys.*, **23,** 1824.
[20] SANTEN, J. H., and WIERINGEN, J. S., 1952, *Rec. Trav. chim. Pays-Bas*, **71,** 420.
[21] SCHOMAKER, V., *et al.* (to be published).
[22] STEVENS, K. W. H., 1952, *Proc. phys. Soc. Lond.*, A, **65**, 209.
[23] TANNER, K. N., and DUNCAN, A. B. F., 1951, *J. Amer. chem. Soc.*, **73,** 1164.
[24] VAN VLECK, J. H., 1934, *Phys. Rev.*, **45,** 405.
[25] VAN VLECK, J. H., 1935, *J. chem. Phys.*, **3,** 803, 807.
[26] VAN VLECK, J. H., 1939, *J. chem. Phys.*, **7,** 61, 72.
[27] WEINSTOCK, B., CLAASSEN, H. H., and MALM, J. G., 1957, *J. Amer. chem. Soc.*, **79,** 5832.
[28] WEINSTOCK, B., and MALM, J. G., 1958, *J. Amer. chem. Soc.*, **80,** 4466.

Intensities in inorganic complexes
III. Octahedral complexes of Ni(II) and V(III)

by C. J. BALLHAUSEN† and ANDREW D. LIEHR
Bell Telephone Laboratories, Incorporated,
Murray Hill, New Jersey

(*Received* 5 *December* 1958)

The method, previously developed by the authors, for calculating the intensity of d^n electronic transitions in inorganic complexes is extended to include electronic systems which exhibit configuration interaction. The oscillator strengths of both the spin-allowed and spin-forbidden spectral transitions of divalent nickel and trivalent vanadium complex salts are computed and compared with experiment. Fair agreement is found. Some critical comments concerning the relative merit of such calculations are presented. The envelope of the Ni(II) red band is elucidated in terms of the spin–orbit fine structure of the $^3T_{1g}$ electronic state.

1. Introduction

The symptomatic features of the spectral intensity patterns expected for interconfigurational electronic transitions of inorganic complexes were delineated by Van Vleck [1] in 1937. Since then the theory has been embellished both qualitatively [2–11] and quantitatively [9–11] by many authors‡. For octahedral complexes the quantitative calculations have been thus far confined to electronic states which do not undergo configurational interaction via the potential field of the surrounding ligands. In this note we shall show that this limitation was more a matter of convenience than of necessity, at least in so far as complexes of divalent nickel and trivalent vanadium are concerned. Indeed, we shall demonstrate that the simultaneous consideration of the spin–orbit coupling, the electronic correlation, and the vibronic interaction terms leads to a fair comprehension of the sundry tints displayed by Ni(II) and V(III) complex salts.

2. Theory

The general principles of symmetry and mechanics which govern the appearance of vibronically allowed bands were laid down by Herzberg and Teller [13] as early as 1933. However, not until recent years has this theory been rigorized [14, 15] and applied in a semiquantitative fashion to problems in the physics and chemistry of inorganic complexes [9, 11]. In dealing with the detailed interpretation of the observed optical intensity distribution in (normal) nickel and vanadium salts, we shall adopt the same general computation scheme as in our initial paper [9]. An alternative mode of calculation has recently been given by Koide and Pryce [11].

---

† Visiting scholar 1957–8. Now at the Technical University of Denmark, Chemical Laboratory A, Copenhagen, Denmark.

‡ A review of work prior to 1956 may be found in ref. [12].

The requisite wave functions for the d^n, $(n=2, 8)$, electronic systems here under consideration have been determined by standard techniques and the details of this reckoning have been published elsewhere [16]. Suffice it to say that these functions were acquired by an exact crystalline field treatment, inclusive of spin–orbit interaction terms, for various numerical values of: (i) the cubic crystalline field parameter, Dq; (ii) the spin–orbit coupling parameter, λ; and (iii) the Slater–Condon–Shortley [17] electron correlation parameters, F_k, $(k=2, 4)$. The functions were evaluated numerically on an IBM 704 electronic data processing machine†.

3. RESULTS

3.1. *Divalent nickel systems*

With the exception of the necessary modification of the crystalline field wave functions by configuration interaction, the detailed intensity calculation is essentially the same as that outlined in our previous paper on divalent copper and trivalent titanium [9] and we shall hence only comment briefly on the algebra required. For the electronic configurations d^n, $(n=1, 9)$, the strong crystalline field representation, in the absence of spin–orbit coupling, completely diagonalizes the energy matrix. This is not so for the systems d^n, $(n=2, 8)$: here the γth wave function, $|\gamma\Gamma_j\rangle$, of spin–orbit symmetry Γ_j, is given by

$$|\gamma\Gamma_j\rangle = \sum |t_{2g}{}^n e_g{}^m, \Gamma_j\rangle\langle t_{2g}{}^n e_g{}^m, \Gamma_j|\gamma\Gamma_j\rangle. \tag{1}$$

In equation (1), t_{2g} and e_g are the Mulliken [18] symmetry designations of the (d_{xy}, d_{xz}, d_{yz}) and $(d_{x^2-y^2}, d_{z^2})$ orbitals, respectively; n and m are their occupation numbers; and Γ_j are the Bethe [19] overall symmetry appellations. The mixing coefficients, $\langle t_{2g}{}^n e_g{}^m, \Gamma_j|\gamma\Gamma_j\rangle$, were obtained from the solution of the appropriate secular equations.

As only broadband absorption is experimentally observed for the spin-allowed optical transitions, we shall not explicitly compute the individual spin–orbit component oscillator strengths. This procedure is made feasible by the fact that the mixing coefficients, $\langle t_{2g}{}^n e_g{}^m, \Gamma_j|\gamma\Gamma_j\rangle$, are of numerical significance only for those Γ_j which arise from the two ${}^3T_{1g}$ electronic states, $t_{2g}{}^5 e_g{}^3$ and $t_{2g}{}^4 e_g{}^4$; and for these two states these coefficients have numerical values which are essentially independent of Γ_j‡. Since the ground electronic state is nearly a pure $t_{2g}{}^6 e_g{}^2$ configuration, in equation (1) only the terms $t_{2g}{}^5 e_g{}^3$ can contribute to the characteristic intensity of a particular transition. The vibronic scrambling of these latter states with p configurations, as described in our first communication [9], then leads to the calculated triplet triplet oscillator strengths displayed in Table 1.

The computation of the intensity of the corresponding triplet–singlet transitions is slightly more complicated as only certain of the 'triplet' spin–orbit symmetry species Γ_j interact with the relevant singlet species. Since the intensity calculations are at best semiquantitative, we have not felt it worth while to reckon the singlet–triplet mixing for each triplet Γ_j species. Instead,

---

† The necessary programme was written by Victor A. Vyssotsky.

‡ For example, the average (over Γ_j) ${}^3T_{1g}$ wave functions of the hexaquo and hexammino nickel ions are, in the 'hole' formalism [16],

$$\mathrm{Ni(H_2O)_6^{++}}: \quad 0{\cdot}75 t_{2g}e_g + 0{\cdot}64 t_{2g}{}^2 \text{ and } -0{\cdot}63 t_{2g}e_g + 0{\cdot}74 t_{2g}{}^2,$$

$$\mathrm{Ni(NH_3)_6^{++}}: \quad 0{\cdot}82 t_{2g}e_g + 0{\cdot}56 t_{2g}{}^2 \text{ and } -0{\cdot}56 t_{2g}e_g + 0{\cdot}82 t_{2g}{}^2.$$

we shall adopt a reasonable dodge and assume that the intensity of a given triplet–triplet transition is uniformly distributed over its spin-orbit fine structure components, Γ_j. Hence, for example, we suppose that the singlet level $\Gamma_3(^1E_g)$ interacts intensity-wise with 2/9 of the triplet levels $\Gamma_j(^3T_{2g})$, $(j=2, 3, 4, 5)$, and $\Gamma_j(^3T_{1g})$, $(j=1, 3, 4, 5)$, respectively†. This simplification yields the predicted triplet–singlet oscillator strengths of table 1.

	$Ni(H_2O)_6^{++}$: $Dq=850$, $\lambda=-275$, $F_4=90\ \text{cm}^{-1}$, $F_2=14F_4$		$Ni(NH_3)_6^{++}$: $Dq=1080$, $\lambda=-200$, $F_4=90\ \text{cm}^{-1}$, $F_2=14F_4$	
Transition	Calculated $f\times10^5$	Observed [21] $f\times10^5$	Calculated $f\times10^5$	Observed [21] $f\times10^5$
$^3A_{2g}\to{}^3T_{2g}$	3·1	2·2	6·2	5·3
$^3T_{1g}$	4·3	3·5	10·0	7·0
$^3T_{1g}$*	5·4	7·2	7·9	9·8
^1E_g	0·1	—	0·2	0·2
$^1T_{2g}$	0·1	—	—	—
$^1T_{2g}$*	0·008	—	—	—
$^1T_{1g}$	0·2	—	—	—
^1E_g*	0·008	—	—	—
$^1A_{1g}$	0·002	—	—	—
$^1A_{1g}$*	0·004	—	—	—

Table 1. Computed and observed oscillator strengths, f, for the hexaquo and hexammino Ni(II) complexes at room temperature. The effective charge of the 3d orbitals Z_{3d}, was taken to be 7·20 and that of the 4p orbitals, Z_{4p}, to be 4·25. A metal–ligand distance of 2 Å was also assumed. The necessary integrals were taken from ref. [23]. The corresponding computed transition frequencies are given in ref. [16].

Before terminating this section, we wish to make a few comments pertaining to the absorption band envelope expected for the Ni(II) hexaquo and hexammino 'red band'. In figures 1 and 2 we give the computed absorption spectrum of these complex ions [16]. As there exist no vibrational frequencies large enough (or small enough) [9, 11, 20] to fill the $612\ \text{cm}^{-1}$ gap appearing in the $\Gamma_j(^3T_{1g}, t_{2g}e_g)$, $(j=1, 3, 4, 5)$, spin–orbit structure, the hexaquo complex of divalent nickel should exhibit a double-peaked red band. On the other hand, as there do exist vibrations [9, 11, 20] which may close the $372\ \text{cm}^{-1}$ cleft in the appositive spin–orbit structure of the hexammino complex, the ion $Ni(NH_3)_6^{++}$ should possess a single-peaked red band, at least at room temperatures. This is exactly what is observed [21, 22]. *It is to be emphasized that the doublet structure of the hexaquo* Ni(II) *red band is thus due to the spin-orbit fine structure of the* $^3T_{1g}$ *level* [16] *and not to a superimposed* ^1E_g, *as has been heretofore postulated* [21, 22].

---

† Of course, in actuality the $\Gamma_3(^1E_g)$ level may interact configurationally only with the levels $\Gamma_3(^3T_{2g})$ and $\Gamma_3(^3T_{1g})$; that is, solely with levels which have the same spin–orbit pedigree. As an instance, the exact hexaquo and hexammino nickel 'singlet' Γ_3 wave functions are

$$\begin{aligned} Ni(H_2O)_6^{++}:\ & 0{\cdot}942\,^1E_g(e_g^2)-0{\cdot}124\,^3T_{2g}(t_{2g}e_g)+0{\cdot}232\,^3T_{1g}(t_{2g}e_g) \\ & +0{\cdot}145\,^3T_{1g}(t_{2g}^2)-0{\cdot}149\,^1E_g(t_{2g}^2), \\ Ni(NH_3)_6^{++}:\ & 0{\cdot}953\,^1E_g(e_g^2)-0{\cdot}250\,^3T_{2g}(t_{2g}e_g)+0{\cdot}108\,^3T_{1g}(t_{2g}e_g) \\ & +0{\cdot}056\,^3T_{1g}(t_{2g}^2)-0{\cdot}119\,^1E_g(t_{2g}^2). \end{aligned}$$

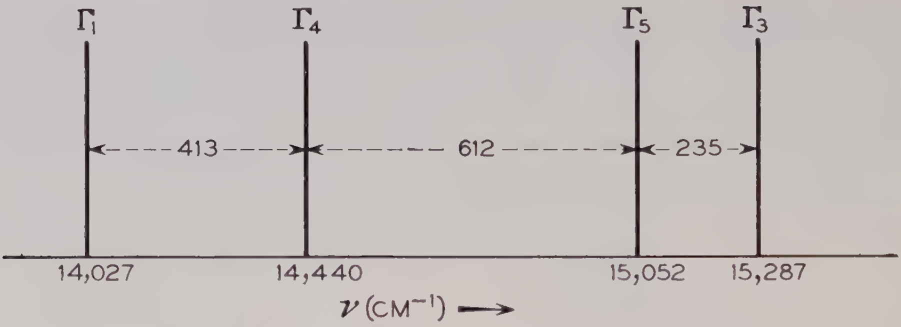

Figure 1. Predicted spin–orbit fine structure [16] of the Ni(II) hexaquo red band ($Dq=900$, $\lambda=-275$, $F_4=90$ cm^{-1}, $F_2=14F_4$).

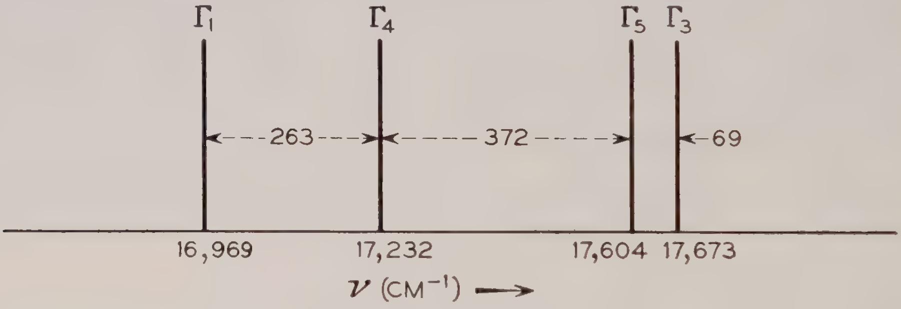

Figure 2. Predicted spin–orbit fine structure [16] of the Ni(II) hexammino red band ($Dq=1100$, $\lambda=-200$, $F_4=90$ cm^{-1}, $F_2=14F_4$).

3.2. *Trivalent vanadium systems*

The determination of the various oscillator strengths characteristic of V(III) complex ions is quite analogous to that of the parallel Ni(II) systems. We shall therefore omit a minute discussion of the algebra involved and content ourselves with a tabulation of the relevant results (see table 2). It is interesting to note

Transition	Predicted frequency [16]	Calculated $f\times10^5$	Observed [24] $f\times10^5$
$\Gamma_3(^3T_{1g})\rightarrow\Gamma_5(^3T_{1g})$	$1{\cdot}64+\nu_{\text{vibrational}}$ cm^{-1}	$\sim1\times10^{-2}$	—
$\Gamma_4(^3T_{1g})$	$168\ +\nu_{\text{vibrational}}$	$\sim1\times10^{-2}$	—
$\Gamma_1(^3T_{1g})$	$250\ +\nu_{\text{vibrational}}$	$\sim1\times10^{-2}$	—
$^3T_{1g}\rightarrow{}^3T_{2g}$	~16800	1·9	9·3
$^3T_{1g}$*	~24900	3·5	18
$^3A_{2g}$	34790	0·05	—
$^1T_{2g}$	9082	1×10^{-4}	—
^1E_g	9221	1×10^{-5}	—
$^1A_{1g}$	19991	1×10^{-4}	—
$^1T_{2g}$*	26998	1×10^{-3}	—
$^1T_{1g}$	29247	1×10^{-5}	—

Table 2. Computed and observed oscillator strengths, f, for the hexaquo V(III) complex ($Dq=1800$, $\lambda=65$, and $F_4=70$ cm^{-1}, $F_2=14F_4$) at room temperature. The effective charge of the 3d orbitals, Z_{3d}, was taken to be 4·30 and that of the 4p orbitals, Z_{4p}, to be 4·00. A metal–ligand distance of 2 Å was also assumed. The necessary integrals were taken from ref. [23].

that the predicted electric dipole intensity of the interconfigurational transitions $\Gamma_j(^3\mathrm{T}_{1g}, t_{2g}^2)$, $(j=1, 3, 4, 5)$, is less than that expected for magnetic dipole or electric quadrupole radiation [1, 2, 5].

4. DISCUSSION

From Tables 1 and 2 we see that the agreement of the calculated and observed oscillator strengths is fair. Of course, the numerical accord could be improved by judicious juggling of the various semi-empirical parameters which arise during the calculation (see ref. [9]), but such manipulations would defeat the very purpose of the computation—the justification of the Van Vleck [1] intensity mechanism. It is worth underscoring, however, that the rigid choice of one half Rydberg for the 3d–4p crystalline energy difference, ΔE_{pd}, for *all* levels is not realistic. As this quantity occurs to the minus third power in the intensity formulae, a slight decrease in its magnitude will produce a sizeable increase in the predicted oscillator strengths. Thus, the discrepancies in the predicted oscillator strengths of some of the higher lying bands are not to be taken too seriously.

The vanadium calculation is only correct for V^{+++} ions immersed in fields of cubic symmetry and thus cannot be compared too critically with experiment [24–26]. If the hexacoordinated complex is also subject to fields of lower symmetry, complications due to further configuration interaction arise. The spectral transition whose oscillator strength is most sensitive to such perturbing fields is the $^3\mathrm{T}_{1g} \rightarrow {}^3\mathrm{A}_{2g}$ [26].

Our vibronic calculation has glossed over completely questions concerning the detailed nature of the potential energy surfaces which govern the vibrational and electronic motions. Such queries would lead us far afield into the intricate problems of molecular stability [20, 27–32] and would not contribute anything new, as long as we confined our attention to gross band intensities. However, even for electronic states in which stability posers are not of paramount importance, there is grave doubt as to whether as crude a model as utilized both here and elsewhere [11] can yield significant results for *individual* vibronic transitions. Indeed, if one is allowed to extrapolate from the results of the moderately precise vibronic calculations performed for organic molecular systems [33] this doubt is replaced by a fair degree of certainty that such models cannot hope to accurately predict individual vibronic oscillator strengths. Thus one must view the detailed vibronic analysis of hexacoordinated Mn(II) complexes by Koide and Pryce [11] with some degree of reservation†.

We are deeply indebted to Victor A. Vyssotsky for the machine solution of the secular equations.

On généralise la méthode de calcul de l'intensité des transitions électroniques d^n dans les complexes organiques, développée précédemment par les auteurs, afin d'y inclure les systèmes électroniques qui présentent une interaction de configuration. On calcule les forces d'oscillateur de l'une et l'autre des transitions spectrales, spin-permises et spin-défendues, pour les sels complexes du nickel divalent et du vanadium trivalent, et on les compare aux données expérimentales. L'accord est assez bon. On présente de façon

---

† The success of some of the semi-empirical vibronic intensity calculations [33–36] in the prediction of intensity distributions for organic systems does not allow a completely negative attitude to be taken.

critique quelques commentaires sur la valeur relative de tels calculs. On explique l'enveloppe de la bande rouge de Ni(II) en fonction de la structure fine spin–orbite de l'état électronique ${}^3T_{1g}$.

Die früher von den Verfassern entwickelte Methode zur Berechnung der Intensität von elektronischen d^n-Übergängen in anorganischen Komplexen wird dahingehend erweitert, dass auch solche Elektronensysteme umfasst werden, die eine konfigurationelle Wechselwirkung zeigen. Die Oszillatorstärken von spin-erlaubten und spin-verbotenen Spektralübergängen in Komplexsalzen von zweiwertigem Nickel und von dreiwertigem Vanadium werden abgeschätzt und mit dem Experiment verglichen. Die Übereinstimmung ist ziemlich gut. Es werden einige kritische Kommentare über den relativen Wert solcher Berechnungen mitgeteilt. Die Enveloppe der roten Bande in Ni(II) wird mit Hilfe der Spin–Bahn-Feinstruktur des elektronischen ${}^3T_{1g}$-Zustandes aufgeklärt.

REFERENCES

[1] VAN VLECK, J. H., 1937, *J. phys. Chem.*, **41,** 67.
[2] BROER, L. J. F., GORTER, C. J., and HOOGSCHAGEN, J., 1945, *Physica*, **11,** 231.
[3] ILSE, F. E., and HARTMANN, H., 1951, *Z. phys. Chem.*, **197,** 239.
[4] ILSE, F. E., and HARTMANN, H., 1951, *Z. Naturf.*, **6a,** 751.
[5] TANABE, Y., and SUGANO, S., 1954, *J. phys. Soc. Japan*, **9,** 776.
[6] SATTEN, R. A., 1957, *J. chem. Phys.*, **27,** 286.
[7] SATTEN, R. A., 1958, *J. chem. Phys.*, **29,** 658; 1959, *Ibid.*, **30,** 590 (Errata).
[8] BALLHAUSEN, C. J., and MOFFITT, W. E., 1956, *J. inorg. Nucl. Chem.*, **3,** 178.
[9] LIEHR, A. D., and BALLHAUSEN, C. J., 1957, *Phys. Rev.*, **106,** 1161.
[10] BALLHAUSEN, C. J., and LIEHR, A. D., 1958, *J. mol. Spectrosc.*, **2,** 342.
[11] KOIDE, S., and PRYCE, M. H. L., 1958, *Phil. Mag.*, **3,** 607.
[12] MOFFITT, W. E., and BALLHAUSEN, C. J., 1956, *Annu. Rev. phys. Chem.*, **7,** 107.
[13] HERZBERG, G., and TELLER, E., 1933, *Z. phys. Chem.* B, **21,** 410.
[14] LIEHR, A. D., 1957, *Ann. Phys., N.Y.*, **1,** 221.
[15] LIEHR, A. D., 1958, *Z. Naturf.*, **13a,** 311; 1958, *Ibid.*, **13a,** 596 (Errata).
[16] LIEHR, A. D., and BALLHAUSEN, C. J., 1959, *Ann. Phys., N.Y.*, **6,** 134.
[17] CONDON, E. U., and SHORTLEY, G. H., 1935, *The Theory of Atomic Spectra* (London and New York: Cambridge University Press).
[18] MULLIKEN, R. S., 1932, *Phys. Rev.*, **43,** 279.
[19] BETHE, H. A., 1929, *Ann. Phys., Lpz.*, **3,** 133.
[20] LIEHR, A. D., and BALLHAUSEN, C. J., 1958, *Ann. Phys., N.Y.*, **3,** 304.
[21] JØRGENSEN, C. K., 1955, *Acta chem. scand.*, **9,** 1362.
[22] HOLMES, O. G., and MCCLURE, D. S., 1957, *J. chem. Phys.*, **26,** 1686.
[23] BALLHAUSEN, C. J., and ANCMON, E. M., 1958, *K. danske vidensk., Selsk.*, **31,** 9.
[24] HARTMANN, H., and FURLANI, C., 1956, *Z. phys. Chem.*, **9,** 162.
[25] LOW, W., 1957, *Z. phys. Chem.* **13,** 107.
[26] BALLHAUSEN, C. J., 1958, *Z. phys. Chem.* **17,** 246.
[27] VAN VLECK, J. H., 1939, *J. chem. Phys.*, **7,** 61.
[28] VAN VLECK, J. H., 1939, *J. chem. Phys.*, **7,** 72.
[29] ÖPIK, U., and PRYCE, M. H. L., 1957, *Proc. roy. Soc.* A, **238,** 425.
[30] MOFFITT, W. E., and LIEHR, A. D., 1957, *Phys. Rev.*, **106,** 1195.
[31] MOFFITT, W. E., and THORSON, W. R., 1957, *Phys. Rev.*, **108,** 1251.
[32] LONGUET-HIGGINS, H. C., ÖPIK, U., PRYCE, M. H. L., and SACK, R. A., 1958, *Proc. roy. Soc.* A, **244,** 1.
[33] LIEHR, A. D., 1957, *Canad. J. Phys.*, **35,** 1123; 1958, *Ibid.*, **36,** 1588 (Errata).
[34] CRAIG, D. P., 1950, *J. chem. Soc.*, 59.
[35] MURRELL, J. N., and POPLE, J. A., 1956, *Proc. phys. Soc. Lond.* A, **69,** 245.
[36] POPLE, J. A., and SIDMAN, J. W., 1957, *J. chem. Phys.*, **27,** 1270.

Theory of anisotropic hyperfine interactions in π-electron radicals[†]

by HARDEN M. McCONNELL[‡]
Gates and Crellin Laboratories of Chemistry[§],
California Institute of Technology, Pasadena, California

JOHN STRATHDEE[||]
Shell Development Company, Emeryville, California

(*Received* 20 *October* 1958)

Anisotropic proton hyperfine interactions in π-electron radicals are approximated by a magnetic dipole interaction between each proton and an electron spin magnetization that is distributed in 2s and 2p Slater atomic orbitals centred on carbon atoms.

1. Introduction

A 'π-electron radical' is a paramagnetic molecule containing a number of co-planar atoms, usually carbon and hydrogen, such that the spin paramagnetism is largely distributed in atomic orbitals having a node in the molecular plane. This distribution of spin in a π-electron radical can be conveniently discussed in terms of a density matrix formalism introduced previously [1]. Thus, if $\hbar\mathbf{S}\,\rho(x, y, z)$ is the vector density of electron spin angular momentum at a point x, y, z in a paramagnetic molecule, then the density function $\rho(x, y, z)$ can be expressed in terms of a density matrix [1] $\rho_{\lambda\mu}$:

$$\rho(x, y, z) = \sum_{\lambda\mu} \rho_{\lambda\mu} \phi_\mu{}^* \phi_\lambda. \tag{1}$$

In (1), ϕ_λ and ϕ_μ are one-electron atomic orbitals from which the exact many electron molecular wave function Ψ can be constructed. In π-electron radicals the atomic orbitals ϕ_λ fall naturally into two classes: the π-orbitals ϕ_π are antisymmetric to the molecular plane, and the σ-orbitals ϕ_σ are symmetric to the molecular plane. Since the spin density function $\rho(x, y, z)$ must be symmetric to reflection in the molecular plane, it follows that the total spin density is a separable sum of σ- and π-contributions, since the sum of the non-diagonal elements $\rho_{\sigma\pi}$ connecting σ and π orbitals must be zero.

$$\rho(x, y, z) = \rho^\pi(x, y, z) + \rho^\sigma(x, y, z), \tag{2}$$

$$\rho^\pi(x, y, z) = \sum_{\pi\pi'} \rho_{\pi\pi'} \phi_{\pi'}{}^* \phi_\pi, \tag{3}$$

$$\rho^\sigma(x, y, z) = \sum_{\sigma\sigma'} \rho_{\sigma\sigma'} \phi_{\sigma'}{}^* \phi_\sigma. \tag{4}$$

In previous work [1, 2] we have developed a theory of isotropic σ-proton hyperfine splittings in π-electron radicals, and have shown how the isotropic splittings may be related to the elements of the π-electron spin density matrix, $\rho_{\pi\pi'}$. The present work is concerned with the anisotropic part of the σ-proton hyperfine interaction. However, the reader will note that many of the formulae we develop can be applied to hydrocarbon radicals with protons other than those of the σ-type, and to molecules other than hydrocarbon radicals. We take the anisotropic part of the hyperfine coupling to be entirely (nuclear-spin)–(electron-spin) dipole interaction. We assume that there is no molecular axis about which electron orbital angular momentum is conserved. This assumption, together with the small spin-orbit interactions [2, 3] in hydrocarbon radicals, signifies that we may neglect orbital contributions to the hyperfine interaction. Since the vector spin magnetic moment density $\mathbf{m}$ is simply

---

[†] Sponsored in part by the Office of Ordnance Research, U.S. Army, and by the United States Public Health Service.

[‡] Alfred P. Sloan Fellow.

[§] Contribution No. 2408.

[||] Present address: Cambridge University, England.

$$\mathbf{m} = -g|\beta|\mathbf{S}\rho(x, y, z) \tag{5}$$

the spin Hamiltonian for the anisotropic hyperfine interaction is

$$\mathscr{H}_d = \int \mathbf{m} . \mathbf{T} . (\gamma\hbar\mathbf{I})\, dv \tag{6}$$

where

$$\mathbf{T} = \frac{1}{(r')^3}\left\{\mathbf{U} - \frac{3\mathbf{r}'\mathbf{r}'}{(r')^2}\right\}, \tag{7}$$

$\mathbf{U}$ is the unit dyadic and $\mathbf{r}'$ is the vector from the proton in question to the position of the electron. The dipolar spin Hamiltonian $\mathscr{H}_d$ in (6) is evidently

$$\mathscr{H}_d = -g|\beta|\gamma\hbar\mathbf{S} . \textstyle\sum_{\lambda\mu}\rho_{\lambda\mu}(\phi_\mu{}^*|\mathbf{T}|\phi_\lambda) . \mathbf{I}$$

or

$$\mathscr{H}_d = -g|\beta|\gamma\hbar\mathbf{S} . \mathrm{Trace}\,(\rho\mathbf{T}) . \mathbf{I} \tag{8}$$

where

$$\mathbf{T}_{\lambda\mu} = (\phi_\lambda{}^*|\mathbf{T}|\phi_\mu). \tag{9}$$

Experimentally observed anisotropies of the hyperfine interaction can then lead to information about the spin density matrix when the matrix elements (9) are known. The principal task of the present work has been the evaluation of these matrix elements. Before proceeding with these calculations we list the approximations and assumptions that are involved in the present work; the most important of these involves the choice of an incomplete set ϕ_λ, and the neglect of certain terms in (8).

2. Basic approximations

Approximation (1). For the purpose of calculating dipolar hyperfine interactions, it is assumed that the spin distribution function $\rho(x, y, z)$ in (1) is adequately represented by 2s- and 2p-atomic orbitals centred on carbon, and 1s atomic orbitals centred on the protons.

Approximation (2). Slater 2s and 2p carbon atomic orbitals are used with an effective nuclear charge $Z = 3{\cdot}18$.

Approximation (3). In calculating the hyperfine splitting due to proton N, all matrix elements $(\phi_\lambda{}^*|\mathbf{T}|\phi_\mu)$ are neglected except those for which ϕ_λ and ϕ_μ are both centred on carbon atom N.

Approximation (4). The calculations are somewhat simplified when one only considers electron and nuclear spin states that are diagonal in S_h and I_h, where $\mathbf{h}$ is a unit vector in the direction of a strong externally applied field. For x-band paramagnetic resonance at *ca.* 9000 M/c and 3000 gauss, the paramagnetic field at the nucleus is sometimes of the same order as the externally applied field, and I_h is not a good quantum number. For brevity most of the following *discussion* is given assuming the validity of Approximation (4). However, general formulae are also given for cases where this approximation breaks down.

3. π-ELECTRON CONTRIBUTION

We employ the coordinate representation given in the figure. The σ-proton is located at the origin N, and the carbon nucleus at origin C. The 2p carbon atomic orbital ϕ_π is then centred at the origin C, and has its symmetry axis parallel with the X-axis in the figure.

$$\phi_\pi = \left(\frac{\mathrm{K}^3}{32\pi}\right)^{1/2} \rho\, \mathrm{e}^{-\rho/2} \sin\vartheta \cos\varphi. \tag{10}$$

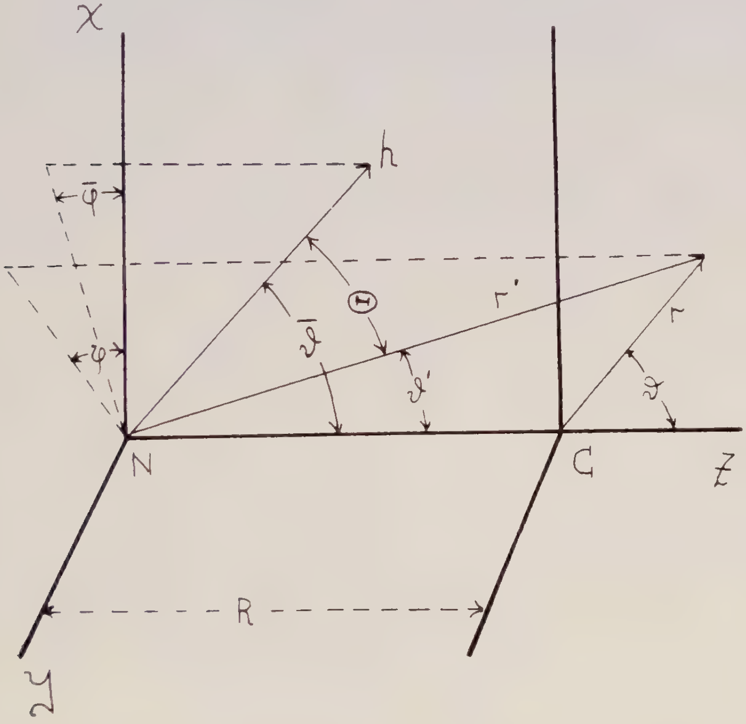

In (10), $\mathrm{K} = Z/a_0$, where $Z = 3{\cdot}18$, and a_0 is the 'radius' of atomic hydrogen, 0·529 Å. Also, $\rho = \mathrm{K}r$. Under approximations (1)–(4) the dipolar spin Hamiltonian for proton N is therefore

$$\mathscr{H}_d = -g|\beta|\gamma\hbar\rho_{\pi\pi} S_h I_h \left(\phi_\pi \left| \frac{1}{(r')^3}[1-3\cos^2\Theta] \right| \phi_\pi\right). \tag{11}$$

In (11), Θ is the angle between $\mathbf{r}'$ and the direction of the externally applied magnetic field, $\mathbf{h}$. We use the abbreviation,

$$(\phi_\pi|\mathbf{h}\,.\,\mathbf{T}\,.\,\mathbf{h}|\phi_\pi) = \left(\phi_\pi \left| \frac{1}{(r')^3}[1-3\cos^2\Theta] \right| \phi_\pi\right) \tag{12}$$

$$= \frac{1}{32\pi}\int\!\!\int\!\!\int \left\{\frac{1}{(r')^3}[1-3\cos^2\Theta]\right\} \mathrm{e}^{-\rho}\rho^4 \sin^3\vartheta \cos^2\varphi \, d\vartheta\, d\varphi\, d\rho.$$

Evaluation of the matrix element in (12) is facilitated by use of the addition theorem for Legendre polynomials:

$$\begin{aligned}1-3\cos^2\Theta = {} & (1-3\cos^2\vartheta')P_2^0(\cos\bar{\vartheta}) \\ & -2\sin\vartheta'\cos\vartheta'\cos\varphi\cos\bar{\varphi}P_2^1(\cos\bar{\vartheta}) \\ & -2\sin\vartheta'\cos\vartheta'\sin\varphi\sin\bar{\varphi}P_2^1(\cos\bar{\vartheta}) \\ & -\tfrac{1}{2}\sin^2\vartheta'\cos 2\varphi\cos 2\bar{\varphi}P_2^2(\cos\bar{\vartheta}) \\ & -\tfrac{1}{2}\sin^2\vartheta'\sin 2\varphi\sin 2\bar{\varphi}P_2^2(\cos\bar{\vartheta}). \qquad (13)\end{aligned}$$

In (13) the Legendre polynomials are defined through the equations,

$$P_2^0(x)=\tfrac{1}{2}(3x^2-1),\ P_2^1(x)=3x(1-x^2)^{1/2},\ P_2^2(x)=3(1-x^2).$$

The angles $\bar{\vartheta}$ and $\bar{\varphi}$ measure the orientation of the externally applied magnetic field relative to the molecular axes x, y, z. The integration indicated in (12) is most conveniently carried out in terms of the polar coordinates ϑ, φ, r (or ρ) centred on C, and the operator in (12) (and (13)) may be transformed to these coordinates through the equations

$$r'\sin\vartheta' = r\sin\vartheta, \qquad (14)$$

$$r'\cos\vartheta' = r\cos\vartheta + R. \qquad (15)$$

With the foregoing transformations one may now write

$$\begin{aligned}\frac{(1-3\cos^2\Theta)}{(r')^3} = \frac{-1}{2\mathrm{K}^2}\Big\{ & (A+C+F)P_2^0(\cos\bar{\vartheta}) \\ & +(B+D)\cos\bar{\varphi}P_2^1(\cos\bar{\vartheta}) \\ & +(B'+D')\sin\bar{\varphi}P_2^1(\cos\bar{\vartheta}) \\ & +E\cos 2\bar{\varphi}P_2^2(\cos\bar{\vartheta}) \\ & +E'\sin 2\bar{\varphi}P_2^2(\cos\bar{\vartheta})\Big\}. \qquad (16)\end{aligned}$$

In (16),

$$\left.\begin{aligned} A &= 4(r')^{-5}(\rho^2+4a^2), \\ B &= 8(r')^{-5}\rho a\sin\vartheta\cos\varphi, \\ B' &= 8(r')^{-5}\rho a\sin\vartheta\sin\varphi, \\ C &= 16(r')^{-5}\rho a\cos\vartheta, \\ D &= 4(r')^{-5}\rho^2\sin\vartheta\cos\vartheta\cos\varphi, \\ D' &= 4(r')^{-5}\rho^2\sin\vartheta\cos\vartheta\sin\varphi, \\ E &= (r')^{-5}\rho^2\sin^2\vartheta\cos 2\varphi, \\ E' &= (r')^{-5}\rho^2\sin^2\vartheta\sin 2\varphi, \\ F &= -6(r')^{-5}\rho^2\sin^2\vartheta, \end{aligned}\right\} \qquad (17)$$

where $a=\mathrm{K}R/2$.

In evaluating (12) using (17), the straightforward integration over φ is carried out first, and yields the following factors for each of the terms in (17). $A(\pi)$; $B(0)$; $B'(0)$; $C(\pi)$; $D(0)$; $D'(0)$; $E(\frac{1}{2}\pi)$; $E'(0)$; $F(\pi)$. The substitution,

$$1/(r')^5 = \mathrm{K}^5 G \qquad (18)$$

where

$$G = |(\rho^2+4a^2+4a\rho\cos\vartheta)^{-5/2}| \qquad (19)$$

enables the integration on ϑ to be carried out. In using (12) together with (16), (17), (18) and (19) a number of integrals involving $\sin\vartheta$, $\cos\vartheta$ and G appear.

These integrals, along with a few others, are given in Appendix I. In evaluating such integrals one must be careful to insure that G is always taken as a positive root; this leads to two expressions for the integrands, corresponding to the two cases where $\rho < 2a$ and $\rho > 2a$.

By using (16), (17), (18) and (19) and the integrals in Appendix I, the integral (12) can be reduced to an integral on ρ, as follows.

$$(\phi_\pi|\mathbf{h}\,.\,\mathbf{T}\,.\,\mathbf{h}|\phi_\pi)$$

$$= \frac{-\mathrm{K}^3}{64}\left\{P_2^{\,0}(\cos\bar{\vartheta})\int_0^\infty [(4\rho^2+16a^2)J_e+16\rho aJ_f-6\rho^2J_h]\,\mathrm{e}^{-\rho}\rho^4\,d\rho + \cos 2\bar{\varphi}P_2^{\,2}(\cos\bar{\vartheta})\int_0^\infty [\tfrac{1}{2}\rho^2J_h]\rho^4\,d\rho\right\} \tag{20}$$

$$= \frac{-\mathrm{K}^3}{64}\left\{P_2^{\,0}(\cos\bar{\vartheta})\left[\int_0^{2a}\left(\frac{2}{3a^3}\rho^4\,\mathrm{e}^{-\rho}\,d\rho - \frac{1}{5a^5}\rho^6\,\mathrm{e}^{-\rho}\,d\rho\right) + \int_{2a}^\infty \frac{-16}{15}\rho\,\mathrm{e}^{-\rho}\,d\rho\right] + \cos 2\bar{\varphi}P_2^{\,2}(\cos\bar{\vartheta})\left[\int_0^{2a}\frac{1}{60a^5}\rho^6\,\mathrm{e}^{-\rho}\,d\rho + \int_{2a}^\infty \frac{8}{15}\rho\,\mathrm{e}^{-\rho}\,d\rho\right]\right\}. \tag{21}$$

These integrals on ρ are easily evaluated, with the result

$$(\phi_\pi|\mathbf{h}\,.\,\mathbf{T}\,.\,\mathbf{h}|\phi_\pi)$$

$$= \frac{1}{R^3}\left[1-\frac{9}{a^2}+\left(a^3+4a^2+10a+17+\frac{18}{a}+\frac{9}{a^2}\right)\mathrm{e}^{-2a}\right](1-3\cos^2\bar{\vartheta}) + \frac{1}{R^3}\left[\frac{9}{2a^2}-\left(a^3+3a^2+6a+9+\frac{9}{a}+\frac{9}{2a^2}\right)\mathrm{e}^{-2a}\right](\cos^2\bar{\vartheta}-1)\cos 2\bar{\varphi}. \tag{22}$$

It may be noted that as $Z \to \infty$, $a \to \infty$, and (22) yields the expected point dipole–dipole interaction formula. Also, (22) is valid in the limit $R \to 0$, $a \to 0$.

Modifications of the foregoing calculations are required in the event that we no longer make approximation (4), but merely assume that the external field is sufficiently strong that S_h is a good quantum number (but not I_h). In this case we must evaluate the vector matrix element

$$(\phi_\pi|\mathbf{h}\,.\,\mathbf{T}|\phi_\pi) \tag{23}$$

that is required for the more general spin Hamiltonian,

$$\mathscr{H}_d = -g|\beta|\gamma\hbar\rho_{\pi\pi}S_h(\phi_\pi|\mathbf{h}\,.\,\mathbf{T}|\phi_\pi)\,.\,\mathbf{I}. \tag{24}$$

The matrix element (23) is easily evaluated if $\mathbf{T}$ is first expressed in terms of the unit vectors $\mathbf{i}$, $\mathbf{j}$, $\mathbf{k}$ fixed in the molecule. Then

$$\begin{aligned}\mathbf{h}\,.\,\mathbf{T} = \frac{1}{(r')^3}\{&\mathbf{i}\xi(1-3\sin^2\vartheta'\cos^2\varphi)\\ &+\mathbf{j}\eta(1-3\sin^2\vartheta'\sin^2\varphi)\\ &+\mathbf{k}\zeta(1-3\cos^2\vartheta')\\ &+[\mathbf{i}\eta+\mathbf{j}\xi]\sin^2\vartheta'\sin\varphi\cos\varphi\\ &+[\mathbf{i}\zeta+\mathbf{k}\xi]\sin\vartheta'\cos\vartheta'\cos\varphi\\ &+[\mathbf{j}\zeta+\mathbf{k}\eta]\sin\vartheta'\cos\vartheta'\sin\varphi\}.\end{aligned} \tag{25}$$

In (25), ξ, η and ζ are simply the direction cosines of the magnetic field in the reference frame **i**, **j**, **k**. This calculation of (23) is easily carried out using the results leading to (22), and the result is

$$
\begin{aligned}
(\phi_\pi|\mathbf{h}\,.\,\mathbf{T}|\phi_\pi) &\\
= \mathbf{i}\xi R^{-3}&\left\{1-\frac{27}{2a^2}+\left(2a^3+7a^2+16a+26+\frac{27}{a}+\frac{27}{2a^2}\right)\mathrm{e}^{-2a}\right\}\\
&+\mathbf{j}\eta R^{-3}\left\{1-\frac{9}{2a^2}+\left(a^2+4a+8+\frac{9}{a}+\frac{9}{2a^2}\right)\mathrm{e}^{-2a}\right\}\\
&+\mathbf{k}\zeta R^{-3}\left\{-2+\frac{18}{a^2}-\left(2a^3+8a^2+20a+34+\frac{36}{a}+\frac{18}{a^2}\right)\mathrm{e}^{-2a}\right\}. \qquad (26)
\end{aligned}
$$

In diagonalizing the nuclear spin functions one must then use the spin Hamiltonian (24) with (26) and include the Zeeman coupling of the nuclear spin to the external field.

4. σ-ELECTRON CONTRIBUTION

Again we employ approximations (1)–(4). We consider only the $2p_z$, $2p_y$ and 2s atomic orbitals centred on the carbon atom adjacent to the proton in question. To simplify the calculations we further assume that there is a plane of symmetry formed by the x and z axes. In π-electron radicals such as CH_3 or $C_6H_6^-$ this is true; in other radicals such as $C_{10}H_8^-$ it is only an approximation. Under these assumptions only the following terms in the σ-density function about a particular carbon atom can be different from zero.

$$
\begin{aligned}
\rho^\sigma(x,y,z)=\rho_{zz}|\phi_z|^2+\rho_{ss}|\phi_s|^2+\rho_{yy}|\phi_y|^2&\\
+\rho_{sz}\phi_z{}^*\phi_s+\rho_{zs}\phi_s{}^*\phi_z.& \qquad (27)
\end{aligned}
$$

Thus, we are concerned with integrals of the type (12) or, more generally, (23), for $|\phi_y|^2, |\phi_z|^2, |\phi_s|^2$ and one of mixed type, $\phi_z\phi_s$. Now ϕ_y is precisely the same as ϕ_π(i.e. ϕ_x) except for orientation of the 2p-orbital axis. Thus, $(\phi_y|\mathbf{T}_{hh}|\phi_y)$ is the same as $(\phi_\pi|\mathbf{T}_{hh}|\phi_\pi)$ in (22) except that $\cos 2\varphi$ has to be replaced by $-\cos 2\varphi$. (Note that if $\rho_{\pi\pi}$ were exactly equal to ρ_{yy} we would have complete cylindrical symmetry in the spin density, and terms in $\cos 2\varphi$ would then disappear. Of course, this is not a possibility in π-electron radicals.) Similarly $(\phi_y|\mathbf{h}\,.\,\mathbf{T}|\phi_y)$ can be obtained from $(\phi_\pi|\mathbf{h}\,.\,\mathbf{T}|\phi_\pi)$ by interchanging **i** and **j** and ξ and η in (26). The remaining cylindrically symmetric spin distributions can be calculated using methods similar to those used in the preceding section, together with integrals given in Appendix I. The results are:

$$
\begin{aligned}
(\phi_s|\mathbf{h}\,.\,\mathbf{T}\,.\,\mathbf{h}|\phi_s)&\\
=\frac{1}{R^3}&\left[1-\left(\frac{2}{3}a^4+\frac{4}{3}a^3+2a^2+2a+1\right)\mathrm{e}^{-2a}\right](1-3\cos^2\bar{\vartheta}) \qquad (28)
\end{aligned}
$$

where $\phi_s=\dfrac{1}{4\sqrt{(6\pi)}}\mathrm{K}^{3/2}\rho\,\mathrm{e}^{-\rho/2}$

$$
\begin{aligned}
(\phi_z|\mathbf{h}\,.\,\mathbf{T}\,.\,\mathbf{h}|\phi_z)&\\
=\frac{1}{R^3}&\left[1+\frac{18}{a^2}-\left(2a^4+6a^3+14a^2+26a+37+\frac{36}{a}+\frac{18}{a^2}\right)\mathrm{e}^{-2a}\right](1-3\cos^2\bar{\vartheta}) \qquad (29)
\end{aligned}
$$

$$
\begin{aligned}
(\phi_z|\mathbf{h}\,.\,\mathbf{T}\,.\,\mathbf{h}|\phi_s)&\\
=\frac{-1}{2\sqrt{3}R^3}&\left[\frac{15}{a}-\left(4a^4+10a^3+20a^2+30a+30+\frac{15}{a}\right)\mathrm{e}^{-2a}\right]. \qquad (30)
\end{aligned}
$$

The vector matrix elements $(\phi|\mathbf{h}.\mathbf{T}|\phi)$ corresponding to the scalar matrix elements (28)–(30) can be obtained from the right-hand members of these equations by replacing $(1-3\cos^2\vartheta)$ by $[\mathbf{i}\xi+\mathbf{j}\eta-2\mathbf{k}\zeta]$.

5. NUMERICAL VALUES

Consider a CH fragment in its valence state that is abstracted from a π-electron radical. For direct application to experimentally observed spectra it is convenient to write the dipolar Hamiltonian in the form

$$\mathscr{H}_d=\mu_{eh}\gamma\hbar\,\mathrm{Trace}\,(\rho\mathbf{h}.\mathbf{T}.\mathbf{h})I_h \tag{31}$$

where μ_{eh} is the component of the electronic spin moment in the field direction, and $\rho_{\lambda\mu}$ and $\mathbf{h}.\mathbf{T}.\mathbf{h}$ refer to the 2s and 2p valence orbitals of the fragment. The isotropic hyperfine contribution to the spin Hamiltonian is

$$\mathscr{H}_i=\rho_{\pi\pi}|Q|\mu_{eh}I_h. \tag{32}$$

The sign of the right-hand member of (32) involves the assumption that the contact interaction has an anomalous sign, due to negative spin density at the proton, as has been suggested by previous theoretical work [2].

The total spin Hamiltonian is then

$$\mathscr{H}=\mu_{eh}(\rho_{\pi\pi}|Q|+\gamma\hbar\,\mathrm{Trace}\,(\rho\mathbf{h}.\mathbf{T}.\mathbf{h}))I_h. \tag{33}$$

This corresponds to a magnetic field acting on the electron spin equal to

$$B_e=-(\rho_{\pi\pi}|Q|+\gamma\hbar\,\mathrm{Trace}\,(\rho\mathbf{h}.\mathbf{T}.\mathbf{h}))I_h. \tag{34}$$

Equation (34) has been evaluated, using the following numerical values for the various parameters:

$$\left.\begin{aligned}Q&=-23\text{ gauss},\\ Z&=3{\cdot}18,\\ \mathrm{K}&=6{\cdot}01\times10^{8}\text{ cm}^{-1},\\ a&=3{\cdot}275,\\ R&=1{\cdot}088\times10^{-8}\text{ cm}.\end{aligned}\right\} \tag{35}$$

The result is:

$$\begin{aligned}B_e=&-23\rho_{\pi\pi}I_h\\ &-\{7{\cdot}69\rho_{\pi\pi}+7{\cdot}69\rho_{yy}+17{\cdot}0\rho_{ss}+35{\cdot}6\rho_{zz}-18{\cdot}3\rho_{sz}\}\times(1-3\cos^2\bar{\varphi})I_h\\ &-\{5{\cdot}95\rho_{\pi\pi}-5{\cdot}95\rho_{yy}\}\cos2\bar{\varphi}(\cos^2\vartheta-1)I_h.\end{aligned} \tag{36}$$

For purposes of a semi-quantitative discussion it is convenient to simplify (36) as follows. Use a localized bond orbital to describe the bonding of a carbon atom to the rest of the molecular frame. For simplicity the orbitals are here taken to be sp^3 hybrid orbitals (h_1, h_2, h_3) on the carbon atom (and 1s on the hydrogen atoms). As long as the bonding is localized—either the electron pair bonds of valence bond theory, or localized molecular orbitals—then the σ-spin density matrix is diagonal in the hybrid orbitals h_1, h_2, h_3:

$$\rho^{\sigma}(x,y,z)=\rho_{11}|h_1|^2+\rho_{22}|h_2|^2+\rho_{33}|h_3|^2. \tag{37}$$

That is, non-diagonal elements (e.g. $\rho_{13}h_1h_3$) are zero. The result (37) is obtained by a straightforward extension of our previous calculations of σ–π interaction to the case of three bonds. These calculations moreover indicated that the ρ_{ii} have the same sign as does $\rho_{\pi\pi}$ on the same atom (Hund's rule). For simplicity further assume that the hybrids h_1, h_2 and h_3 are equivalent by symmetry, and that

$\rho_{11}=\rho_{22}=\rho_{33}\equiv\rho_{\sigma\sigma}$. Under these approximations it can be shown that $\rho_{yy}=\rho_{ss}=\rho_{zz}$; $\rho_{sz}=0$. Therefore, (36) becomes

$$\begin{aligned}B_e=&-23\rho_{\pi\pi}I_h\\&-\{7{\cdot}69\rho_{\pi\pi}+60{\cdot}3\rho_{\sigma\sigma}\}(1-3\cos^2\bar{\vartheta})I_h\\&-5{\cdot}95\{\rho_{\pi\pi}-\rho_{\sigma\sigma}\}\cos 2\bar{\varphi}\,(\cos^2\bar{\vartheta}-1)I_h.\end{aligned}\tag{38}$$

Previous work has indicated that $\rho_{\sigma\sigma}$ is probably between 1 per cent and 10 per cent as large as $\rho_{\pi\pi}$. Therefore we conclude that the σ-spin distribution probably makes a significant contribution to the anisotropic proton hyperfine interaction that is proportional to $P_2^0(\cos\bar{\vartheta})$; the σ-contribution to the $P_2^2(\cos\bar{\vartheta})$ term is estimated to be negligible, however.

6. EXPERIMENTAL CONSIDERATIONS

Very little experimental work has yet been done on measurements of anisotropic proton hyperfine interactions in organic radicals. The experimentalist who wishes to be guided by the foregoing calculations may wish to consider the following comments.

(*a*) Although theoretical calculations suggest that the isotropic (σ-proton)–(π-electron) hyperfine coupling constant is negative, it is possible that this is not so. In that event the leading term in (38) (and in the corresponding previous equations) should be $+23\ \rho_{\pi\pi}I_h$. The two possible signs of the isotropic interaction lead to different overall splittings.

(*b*) The dipolar integrals depend rather strongly on the effective nuclear charge, Z. Thus, in the range $Z=3{\cdot}0$–$3{\cdot}4$, the coefficients of $\rho_{\pi\pi}$ and $\rho_{\sigma\sigma}$ in the $(1-3\cos^2\bar{\vartheta})$ term in (38) vary by as much as ~20 per cent and ~40 per cent respectively, and the coefficient of the $(\rho_{\pi\pi}-\rho_{\sigma\sigma})\cos 2\bar{\varphi}(\cos^2\bar{\vartheta}-1)$ term varies by as much as 30 per cent for this range of Z values. It is possible that the best Z-value to use in calculations of this sort would match the outer regions of the Slater orbitals to the outer regions of Hartree orbitals.

(*c*) It is possible that our estimate of the σ-contribution to the anisotropic term that is proportional to $P_2^0(\cos\bar{\vartheta})$ is in error because of neglect of the two-centre carbon atom hydrogen atom spin distribution. The sign of this contribution is even uncertain because of the likelihood that the σ-spin density changes sign between the carbon and hydrogen atoms.

(*d*) The mathematical calculation of the resonance line shape expected from (38) for a polycrystalline sample is quite involved, and will be given in a later paper. The net result of this calculation is that the polycrystalline resonance spectrum corresponding to (38) spans a range of 39 gauss, and has a rather broad doublet structure with peak-to-peak separation of 28 gauss.

APPENDIX I

AUXILIARY INTEGRALS

In the following integrals, the first result given applies to the case $\rho<2a$, and the second result is for the case $\rho>2a$.

$$J_a=\int_0^\pi G\sin\vartheta\,d\vartheta=\frac{1}{3a}\frac{12a^2+\rho^2}{(4a^2-\rho^2)^3};\ \frac{2}{3\rho}\frac{3\rho^2+4a^2}{(\rho^2-4a^2)^3},$$

$$J_b = \int_0^\pi G \cos\vartheta \sin\vartheta \, d\vartheta = \frac{-\rho}{6a^2}\frac{20a^2-\rho^2}{(4a^2-\rho^2)^3}\,; \quad -\frac{4}{3}\frac{a}{\rho^2}\frac{5\rho^2-4a^2}{(\rho^2-4a^2)^3},$$

$$J_c = \int_0^\pi G \cos^2\vartheta \sin\vartheta \, d\vartheta$$

$$= -\frac{1}{6a^3}\frac{8a^4+10a^2\rho^2-\rho^4}{(4a^2-\rho^2)^3}\,; \quad \frac{2}{3\rho^2}\frac{\rho^4+20a^2\rho^2-32a^4}{(\rho^2-4a^2)^3},$$

$$J_d = \int_0^\pi G \cos^3\vartheta \sin\vartheta \, d\vartheta$$

$$= -\frac{\rho}{12a^4}\frac{24a^4+6a^2\rho^2-\rho^4}{(4a^2-\rho^2)^3}\,; \quad -\frac{4}{3}\frac{a}{\rho^4}\frac{3\rho^4+12a^2\rho^2-32a^4}{(\rho^2-12a^2)^3},$$

$$J_e = \int_0^\pi G \sin^3\vartheta \, d\vartheta$$

$$= \frac{1}{6a^3}\frac{1}{4a^2-\rho^2}\,; \quad \frac{4}{3\rho^3}\frac{1}{\rho^2-4a^2},$$

$$J_f = \int_0^\pi G \sin^3\vartheta \cos\vartheta \, d\vartheta$$

$$= -\frac{\rho}{12a^4}\frac{1}{4a^2-\rho^2}\,; \quad -\frac{8}{3}\frac{a}{\rho^4}\frac{1}{(\rho^2-4a^2)}$$

$$J_g = \int_0^\pi G \sin^3\vartheta \cos^2\vartheta \, d\vartheta$$

$$= \frac{1}{30a^5}\frac{a^2+\rho^2}{4a^2-\rho^2}\,; \quad \frac{4}{15\rho^5}\frac{\rho^2+16a^2}{\rho^2-4a^2},$$

$$J_h = \int_0^\pi G \sin^5\vartheta \, d\vartheta$$

$$= \frac{1}{30a^5}\,; \quad \frac{16}{15}\frac{1}{\rho^5}.$$

On calcule de façon approchée les interactions hyperfines anisotropiques des protons dans les radicaux à électrons π au moyen d'une interaction dipolaire magnétique entre chaque proton et une magnétisation de spin électronique qui est répartie dans des orbitales atomiques de Slater, 2s et 2p, centrées sur les atomes de carbone.

Anisotrope Hyperfein-Wechselwirkungen in π-Elektronenradikalen werden angenähert beschrieben durch eine magnetische Dipol-Wechselwirkung zwischen jedem Proton, sowie eine Elektron-Spin-Magnetisierung die über 2s- und 2p-Atomzustände nach Slater verteilt ist, welche um die Kohlenstoffatome konzentriert sind.

Note added in proof.—From (38) one can derive the complete hyperfine spin Hamiltonian

$$\mathscr{H} = AS_zI_z + BS_xI_x + CS_yI_y,$$
$$A = h^{-1}g|\beta|[-7{\cdot}69\rho_{\pi\pi} + 120\rho_{\sigma\sigma}],$$
$$B = h^{-1}g|\beta|[-24{\cdot}7\rho_{\pi\pi} - 66\rho_{\sigma\sigma}],$$
$$C = h^{-1}g|\beta|[-36{\cdot}7\rho_{\pi\pi} - 54\rho_{\sigma\sigma}].$$

When $\rho_{\pi\pi}=1$, $\rho_{\sigma\sigma}\approx 0$, $A=-21$ M/c, $B=-69$ M/c, $C=-103$ M/c. Recent resonance work on the oriented $CH(COOH)_2$ radical shows that (*a*) the α CH group is an excellent approximation to the CH fragment with $\rho_{\pi\pi}=1$, and (*b*) the constants A, B, C have the magnitudes 30, 61·5, 92·5 M/c, respectively, *and are all of the same sign.* (COLE, T., HELLER, C., and MCCONNELL, H. M., *Proc. nat. Acad. Sci., Wash.* (in the press).)

These results show that the isotropic interaction is negative (cf. § 6 (*a*)) and that the π-electron distribution alone gives an excellent approximation to the anisotropic coupling. The apparently negligible σ-spin contribution to the anisotropic coupling is not surprising in view of the fact that the σ-spin density must change sign between the carbon and hydrogen atoms (cf. § 6 (*c*)).

REFERENCES

[1] MCCONNELL, H. M., 1958, *J. chem. Phys.*, **28**, 1188.
[2] MCCONNELL, H. M., and CHESNUT, D. B., 1958, *J. chem. Phys.*, **28**, 107; MCCONNELL, H. M., and ROBERTSON, R. E., 1958, *J. chem. Phys.*, **28**, 991.
[3] MCCONNELL, H. M., and ROBERTSON, R. E., 1957, *J. phys. Chem.*, **61**, 1018.

The electronic structure of hydrogen fluoride

by R. A. BALLINGER
National Physical Laboratory, Teddington, Middlesex

(*Received* 10 *September* 1958)

Self-consistent field (SCF) calculations have been carried out for hydrogen fluoride at the experimental internuclear distance using a single determinantal wave function composed of molecular orbitals (MO's) expressed as linear combinations of atomic orbitals (LCAO's). The AO's used are of Slater-type in which the parameters have been varied within the framework of the variational method. The improvement in the energy and other physical quantities brought about by the variation of the Slater parameters has been discussed in relation to the results of other methods of obtaining improved wave functions for this molecule.

1. Introduction

It is well known that for a molecule having a closed-shell ground state the MO method is particularly convenient, it being generally accepted that in this case the total wave function can be represented by a single determinant composed of MO's; for a comprehensive review of MO theory the reader is referred to Roothaan [1]. For this single determinant the variational method provides a straightforward way in which to choose the MO's; these are varied to obtain minimum energy in the same way as Hartree–Fock AO's are varied in the case of atoms but with the added complexity now of having more than one centre. Calculations along these lines are therefore almost prohibitive at the present time even with the availability of high-speed computers.

If the MO's however are restricted to be of analytical form (containing parameters with respect to which the energy expression can be minimized) then the problem is rendered more tractable, for now the integrals involved in the calculations contain analytical as distinct from numerical functions. The customary way of ensuring the analytical nature of the MO's is to write them as LCAO's in which the AO's are analytical and centred on the various atoms in the molecule; their coefficients are then regarded as the variable parameters in the application of the variational method. Regarding the choice of the analytical AO's, those given by Slater [2] are most often used, and LCAO calculations using these have been made for a number of molecules. From a mathematical standpoint only a few of these calculations have been carried out rigorously within the LCAO MO framework. In the majority of cases further approximations have been made in order to permit the mathematical solution of the various problems; in particular, inner–outer shell mixing has often been neglected, and in the evaluation of certain molecular integrals it has been found necessary to make mathematical or empirical approximations, especially for systems containing more than two atoms. Whilst calculations in which such approximations are made are often instructive they do little to test the validity of the MO theory, and in this connection the results can only be regarded with caution.

Until the Hartree–Fock type of MO's (i.e. one-electron functions which are not restricted to be LCAO MO's but which are allowed to vary quite freely in the application of the variational method) become available for molecules it is impossible to predict how successful the single determinant approximation to the total wave function can be in principle. It is therefore important to investigate the effect of improving the restricted type of MO's in any conceivable way which is practical and which can be executed without the need to make additional approximations in the mathematical solution of the problem. The rigorous SCF LCAO MO calculations using Slater-type AO's whilst being moderately successful have shown themselves to have serious shortcomings (see for example Scherr [3] and Sahni [4]) and the most obvious way in which LCAO MO's of this type can be improved is to allow the exponents in the Slater AO's to vary in addition to the LCAO coefficients; this involves carrying out many SCF LCAO MO calculations for various sets of the Slater parameters until the latter have adjusted themselves to give minimum energy.

In order to establish precisely how sensitive various physical quantities are to the choice of the Slater parameters, and to investigate the sort of improvement one might reasonably expect to be brought about by allowing the parameters to take on minimum values, calculations have been carried through for the hydrogen fluoride molecule. The advantage of choosing a 'light' diatomic molecule to be the subject of investigation is that in this case it is relatively easy to perform the calculations completely rigorously from a mathematical point of view; hydrogen fluoride was chosen owing to the fact that much attention has recently been devoted to obtaining improved wave functions for this molecule by various workers and it is of interest to compare the present findings with the results of these calculations. Much of this work just referred to has been carried out by Slater's group at M.I.T. during the period of the present project. Of the extensive calculations carried out there, the LCAO MO computations using numerical Hartree–Fock AO's as distinct from the more easily handled Slater-type AO's, which have just been reported (Karo [5]), are particularly interesting, for when compared with the present work one would expect that amongst other things the problem of the choice of AO's will be clarified.

2. Details of the calculation of the SCF LCAO MO's

Unless otherwise stated Hartree atomic units are used throughout the calculation (i.e. $e=m=\hbar=1$, the unit of length is the Bohr radius a_0 and the unit of energy is e^2/a_0).

2.1. *Choice of AO's*

In constructing the MO's the basic AO's are restricted to the 1s, 2s, $2p_x$, $2p_y$, $2p_z$ centred on the fluorine atom and to the 1s hydrogen function; the z axis of the AO's centred on F is taken as the symmetry axis of the molecule, the positive axis being in the direction of H (see figure 1). The AO's are taken to be of Slater-type:

$$\left.\begin{array}{rcl}
(1s)_F = (\alpha^3/\pi)^{1/2} \exp(-\alpha r_f) & = & \chi_1, \\
(2s)_F = (\beta^5/3\pi)^{1/2}\, r_f \exp(-\beta r_f) & = & \chi_2, \\
\left.\begin{array}{l}(2p_x)_F \\ (2p_y)_F \\ (2p_z)_F\end{array}\right\} = (\gamma^5/\pi)^{1/2} \left\{\begin{array}{c} x_f \\ y_f \\ z_f \end{array}\right\} \exp(-\gamma r_f) & = & \left\{\begin{array}{l}\chi_5, \\ \chi_6, \\ \chi_3,\end{array}\right. \\
(1s)_H = (\delta^3/\pi)^{1/2} \exp(-\delta r_h) & = & \chi_4,
\end{array}\right\} \tag{1}$$

in which α, β, γ, δ are regarded as variable parameters; the internuclear distance ρ is also a parameter which can be varied. It is worth while to point out that it is often convenient if the AO's belonging to a particular atom are orthogonal to each other. For this purpose the 2s orbital must be expressed as a linear combination of the Slater-type 1s and 2s orbitals. The usual procedure is to use χ_1 and χ_2, in terms of which the new 2s orbital becomes

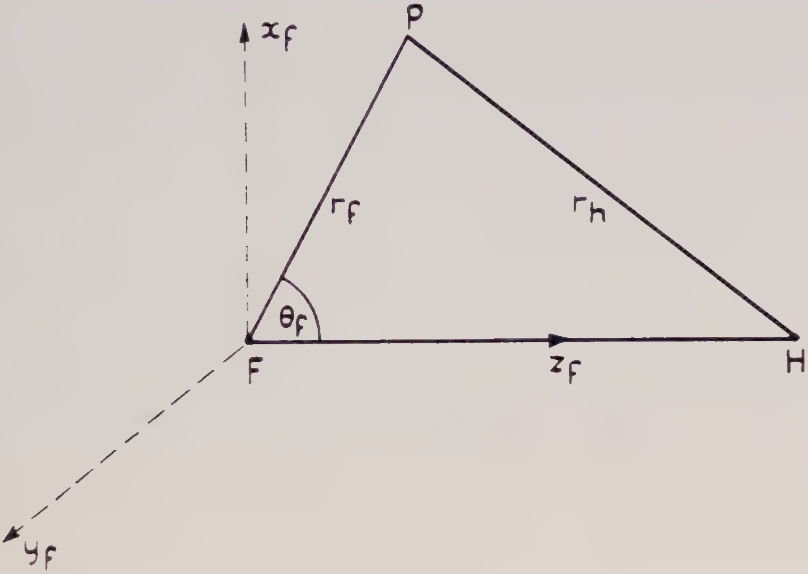

Figure 1.

$$2s^* = (1-S^2)^{-1/2}(\chi_2 - S\chi_1)$$

where

$$S = \int \bar{\chi}_1 \chi_2 \, dv.$$

If complete mixing of the AO's is not allowed in constructing LCAO MO's, as for example in neglecting inner–outer shell interaction, then the final results will depend upon the set of AO's used, and in this case the modified 2s orbital ought to be employed. In the present calculation, however, complete mixing of the AO's is permitted and clearly therefore nothing is to be gained by preferring 2s* to 2s. Nevertheless, it must be pointed out that although customary, it is not essential to use χ_1 in forming 2s*, for it is possible to use a 1s-type wave function with a screening constant different from that of χ_1 in forming the orthogonalized 2s wave function. There seems little point however in introducing a further variational parameter into the MO's in this way.

2.2. *Construction of the MO's*

The HF molecule belongs to the symmetry group $C_{\infty v}$ and the MO's which are formed from the above six AO's are chosen so that they belong to irreducible representations of this symmetry group. For this purpose the numbering of the χ's on the right-hand side of (1) is particularly convenient, for then the

LCAO MO's take the form

$$\begin{aligned}(n\sigma)&=\phi_m=\chi_1c_{1m}+\chi_2c_{2m}+\chi_3c_{3m}+\chi_4c_{4m}, \quad m=1,2,3,4,\\ 1\pi^+&=\phi_5=\chi_5,\\ 1\pi^-&=\phi_6=\chi_6.\end{aligned}$$

The MO's and AO's are thus related through the matrix equation

$$(\phi_1, \phi_2, \ldots, \phi_6)=(\chi_1, \chi_2, \ldots, \chi_6)\begin{bmatrix} c_{11} & c_{12} & c_{13} & c_{14} & 0 & 0\\ c_{21} & c_{22} & c_{23} & c_{24} & 0 & 0\\ c_{31} & c_{32} & c_{33} & c_{34} & 0 & 0\\ c_{41} & c_{42} & c_{43} & c_{44} & 0 & 0\\ 0 & 0 & 0 & 0 & 1 & 0\\ 0 & 0 & 0 & 0 & 0 & 1\end{bmatrix}$$

i.e. $\boldsymbol{\varphi}=\boldsymbol{\chi}\mathbf{C}$.

2.3. *Roothaan's equations to determine* **C**

For molecules having a closed-shell ground state the total wave function Φ is taken to be the normalized Slater determinant composed of all the ϕ's which are doubly filled, and the electronic energy of the state is then given through the relation

$$E=\int \bar{\Phi}\mathscr{H}\Phi\, d\tau$$

where $\mathscr{H}$ is the Hamiltonian of the system. For a given set of the parameters α, β, γ, δ and ρ, the best MO's are found by allowing the c's to vary so as to make E a minimum subject to the constraint that the ϕ's be kept orthonormal to each other. Applying the variational method in this way leads to the matrix equation

$$\mathbf{FC}=\mathbf{SC}\boldsymbol{\epsilon} \tag{2}$$

where **F** is the sum of the two symmetric matrices **H** and **G** with elements

$$\begin{aligned}H_{pq}&=\int \bar{\chi}_p\left(-\frac{1}{2}\nabla^2-\frac{9}{r_f}-\frac{1}{r_h}\right)\chi_q\, dv,\\ G_{pq}&=\sum_i{}'\sum_{r,t}\bar{c}_{ri}\{2(pq:rt)-(pt:rq)\}c_{ti}\end{aligned}$$

respectively; the prime indicates summation over filled MO's only and

$$(pq:rt)=\int \frac{\bar{\chi}_p{}^{\mu}\chi_q{}^{\mu}\bar{\chi}_r{}^{\nu}\chi_t{}^{\nu}}{r^{\mu\nu}}\, dv^{\mu\nu}.$$

The symmetric overlap matrix **S** has the elements

$$S_{pq}=\int \bar{\chi}_p\chi_q\, dv$$

and $\boldsymbol{\epsilon}$ without loss of generality can be assumed to be a diagonal matrix, the diagonal elements $\epsilon_1, \epsilon_2, \ldots, \epsilon_6$ of which represent the orbital energies of ϕ_1, $\phi_2, \ldots, \phi_6$ respectively.

The c's required to give minimum energy are determined by an iterative procedure. A trial of c's consistent with the orthonormality condition

$$\mathbf{C'SC}=\mathbf{I}$$

where **I** is the unit matrix, is first of all chosen. The corresponding **F** matrix is then evaluated in terms of these c's and equation (2) is solved for the matrix **C**.

The set of c's calculated in this way will in general be different from the initial c's and so the procedure is repeated, each time using the previously determined set of c's, until self-consistency is obtained. Because self-consistency is introduced in this way the method is often referred to as the SCF LCAO MO method.

2.4. *Modification of Roothaan's equations to facilitate the determination of* $\mathbf{C}$

If equation (2) is premultiplied by $\mathbf{S}^{-1}$ then it is clear that at each stage of the iteration one is faced with the task of finding the latent roots and vectors of the matrix $\mathbf{S}^{-1}\mathbf{F}$ which is an unsymmetric matrix despite the fact that both $\mathbf{S}$ and $\mathbf{F}$ are symmetric. In view of the fact that it is much easier to find latent roots and vectors of matrices which are symmetric rather than unsymmetric, it is desirable to transform (2) in the following manner.

There exists a triangular matrix $\mathbf{L}$ such that $\mathbf{S}=\mathbf{L}\mathbf{L}'$. In terms of $\mathbf{L}$, equation (2) becomes $\mathbf{F}\mathbf{C}=\mathbf{L}\mathbf{L}'\mathbf{C}\boldsymbol{\epsilon}$. Putting now

$$\mathbf{X}=\mathbf{L}'\mathbf{C} \quad \text{or} \quad \mathbf{C}=(\mathbf{L}^{-1})'\mathbf{X} \tag{3}$$

it can easily be shown that

$$(\mathbf{L}^{-1})\mathbf{F}(\mathbf{L}^{-1})'\mathbf{X}=\mathbf{X}\boldsymbol{\epsilon}. \tag{4}$$

Since $(\mathbf{L}^{-1})\mathbf{F}(\mathbf{L}^{-1})'$ is now a symmetric matrix whose latent vectors are simply related to the c's through (3) it is clear that from a computational point of view (4) is to be preferred to (2). Also it is worth while to point out that the matrix $(\mathbf{L}^{-1})'$ serves as an initial guess for the matrix $\mathbf{C}$ since $(\mathbf{L}^{-1})\mathbf{S}(\mathbf{L}^{-1})'=\mathbf{I}$.

For a detailed discussion of the computational techniques adopted in the evaluation of the matrix elements and the solution of the iterative process the reader is referred to Appendix 1.

3. VARIATION OF THE SLATER PARAMETERS AT THE EXPERIMENTAL INTERNUCLEAR DISTANCE

The experimental value for ρ is $0{\cdot}9171\times10^{-8}$ cm (Herzberg [6]), that is 1·7331 atomic units (A.U.) using the value for a_0 given by Cohen [7]. However, for the purposes of these calculations, the experimental vaue of ρ is taken to be 1·7328 A.U., which will clearly lead to negligible error and has the advantage that direct comparison can be made between the present findings and the results of the work carried out at M.I.T. for this molecule.

Initially the values of α, β, γ and δ are taken to be Slater's values for the isolated atoms, i.e. 8·6, 2·6, 2·6 and 1·0 respectively. The iterative procedure employed is to vary α, β, γ and δ independently and in strict rotation. As each parameter is varied to give a 'better' value in the sense of the variational method, then this modified value is adopted in the variation of the next parameter, the procedure being repeated until each of the parameters has been varied. This so-called cycle of the iteration to get the best values for the parameters is repeated and the results of two cycles are given in table 1, where E_{total} is the total energy of the molecule defined as $E_{\text{total}}=E+9/\rho$.

In all the calculations it is found that E (which is of the order of -105 A.U.) has converged to one in the sixth decimal place after at most six iterations, although the ϵ's and c's by this time have not settled down to anything like the same accuracy. The ϵ's, which lie in the range -27 to $+1$ A.U., have converged only to one in the fourth decimal at this stage whilst the c's, which roughly speaking vary from

	α	$\Delta\alpha$	β	$\Delta\beta$	γ	$\Delta\gamma$	δ	$\Delta\delta$	E_{total}	ΔE_{total}
Initial	8·700	—	2·600	—	2·600	—	1·000	—	−99·4786	—
End of 1st cycle	8·647	−0·053	2·536	−0·064	2·536	−0·064	1·321	+0·321	−99·5307	−0·0521
End of 2nd cycle	8·655	+0·008	2·556	+0·020	2·533	−0·003	1·322	+0·001	−99·5312	−0·0005

Table 1. Variation of parameters for E_{total}.

	α	$\Delta\alpha$	β	$\Delta\beta$	γ	$\Delta\gamma$	δ	$\Delta\delta$	$E_{\text{F+H}}$	$\Delta E_{\text{F+H}}$
Initial	8·700	—	2·600	—	2·600	—	1·000	—	−99·4317	—
End of 1st cycle	8·644	−0·056	2·550	−0·050	2·552	−0·048	1·000	0·000	−99·4419	−0·0102
End of 2nd cycle	8·651	+0·007	2·563	+0·013	2·550	−0·002	1·000	0·000	−99·4421	−0·0002
End of 3rd cycle	8·650	−0·001	2·564	+0·001	2·550	0·000	1·000	0·000	−99·4421	0·0000

Table 2. Variation of parameters for $E_{\text{F+H}}$.

-1 to $+1$, are correct only to two in the fourth decimal. In the event of the MO's being required to greater accuracy for the calculation of other physical quantities, however, it is found that the c's are correct to one in the sixth decimal by the tenth iteration.

In order to find the binding energy of the molecule it is necessary to evaluate and minimize the energy of the two isolated atoms given by

$$E_{\mathrm{F+H}} = \sum_{i}^{\alpha+\beta} \int \bar{\chi}_i \left(-\frac{1}{2}\nabla^2 - \frac{9}{r_f} \right) \chi_i \, dv + \frac{1}{2} \sum_{i}^{\alpha+\beta} \sum_{j}^{\alpha+\beta} (ii:jj)$$
$$- \frac{1}{2} \left\{ \sum_{i}^{\alpha} \sum_{j}^{\alpha} + \sum_{i}^{\beta} \sum_{j}^{\beta} \right\} (ij:ij) + \int \bar{\chi}_4 \left(-\frac{1}{2}\nabla^2 - \frac{1}{r_h} \right) \chi_4 \, dv,$$

where $\sum^{\alpha}$, $\sum^{\beta}$, $\sum^{\alpha+\beta}$ denote summations over α spins, β spins and both α and β spins respectively for the F atom in which χ_1, χ_2, χ_5 and χ_6 are doubly filled and χ_3 singly filled (i.e. $(1s)_F{}^2(2s)_F{}^2(2p_x)_F{}^2(2p_y)_F{}^2(2p_z)_F{}^1$). In calculating $E_{\mathrm{F-H}}$, the modified 2s orbital $(1-S^2)^{-1/2}(\chi_2 - S\chi_1)$ in which $S = \int \bar{\chi}_1 \chi_2 \, dv$, is used in preference to χ_2, for in this case there is no such thing as complete mixing of the AO's as in the evaluation of the energy of HF. Variation of the parameters α, β and γ in $E_{\mathrm{F+H}}$ is effected in exactly the same way as for the parameters in E, there being no need to vary δ in this case since its optimum value is obviously unity. Three cycles are carried out and the results are displayed in table 2. It can be seen that at the end of the third cycle the best parameters are determined to three decimal places and the energy to four.

Although not shown in the table, $E_{\mathrm{F-H}}$ is changed by only one in the sixth decimal by the third cycle and it is evident that the third cycle is rather unnecessary, for to stop at the end of the second cycle would give the parameters to an accuracy of one in the third decimal place besides giving more than the required four decimal place accuracy in the energy. Because of this, and also the striking similarity in the way in which parameters and energy converge in tables 1 and 2, it is felt that nothing is to be gained by performing a third cycle in the case of HF and the final values for the parameters and energy given in table 1 are estimated to be correct to one in the final decimal place given.

The LCAO coefficients and orbital energies corresponding to initial and final values of the Slater parameters (i.e. those given in the first and last lines respectively of table 1) are given in table 3. $c_{1i}{}^*$ and $c_{2i}{}^*$ are the modified values of c_{1i} and c_{2i} respectively when the MO's are written in terms of 2s* in preference to 2s. Their evaluation in terms of c_{1i}, c_{2i} and S is of course completely trivial, and is necessary for the purposes of carrying out an electron population analysis (see § 4) where orthogonal AO's are implicit in the theory; furthermore their tabulation is useful for the purposes of comparison with other work on HF where it is customary to give LCAO coefficients referred to orthogonal AO's.

In table 4 the present values for the total energy and binding energy are compared with the results of other methods of obtaining improved wave functions for HF. It will be noticed that there are slight discrepancies between the values for the initial SCF LCAO MO calculation and those of Allen and Karo [8]; more will be said about this question in Appendix 2, where the reader will find a discussion concerning the accuracy of the present calculations. In the calculation (*a*) of table 4 the minimum parameters found for $E_{\mathrm{F+H}}$ are used in the evaluation of $E_{\mathrm{F-H}}$, whereas in (*b*) the minimum parameters found for E_{total} are used throughout. The experimental values quoted for $E_{\mathrm{F+H}}$ and the binding

	ϕ	c_{1i}^*	c_{2i}^*	c_{1i}	c_{2i}	c_{3i}	c_{4i}	ϵ_i
Initial	1σ	1·0002	0·0159	0·9963	0·0163	0·0024	−0·0046	−26·1396
Final		1·0001	0·0125	0·9971	0·0129	0·0021	−0·0034	−26·2601
Initial	2σ	−0·0219	0·9055	−0·2435	0·9322	0·0907	0·1605	−1·4766
Final		−0·0179	0·9153	−0·2375	0·9412	0·0905	0·1511	−1·4849
Initial	3σ	−0·0282	−0·4581	0·0839	−0·4716	0·6869	0·5762	−0·5657
Final		−0·0217	−0·4008	0·0745	−0·4122	0·7165	0·4953	−0·5940
Initial	4σ	−0·0531	−0·5439	0·0800	−0·5599	−0·8065	1·0502	0·4769
Final		−0·0499	−0·5349	0·0784	−0·5500	−0·8186	1·1007	0·6717
Initial	$1\pi^+, 1\pi^-$	—	—	—	—	—	—	−0·4646
Final								−0·4697

Table 3. LCAO coefficients and orbital energies.

Author	Type of calculation	$-E_{\text{total}}$	$-E_{\text{F+H}}$	Binding energy
Ballinger	SCF LCAO MO; initial Slater AO's	99·479	99·432	0·047
Allen and Karo [8]		99·484	99·433	0·051
Karo [5]	SCF LCAO MO+CI; initial Slater AO's	99·511	99·433	0·078
Kastler [13]	Valence bond+CI	99·526	99·454	0·072
Ballinger	SCF LCAO MO; final Slater AO's	99·531	(*a*) 99·442	0·089
		99·531	(*b*) 99·390	0·141
Karo [5]	SCF LCAO MO; Hartree–Fock AO's	(*c*) 99·963	99·906	0·057
Karo [5]	SCF LCAO MO+CI; Hartree–Fock AO's	(*d*) 99·984	99·906	0·078
Experimental		100·528	100·304	0·224

Table 4. Experimental and various theoretical results for the molecular and atomic energies. Configuration interaction is written as CI for brevity.

energy of the molecule, and hence E_{total}, are those which are derived in great detail by Allen [9, 10]. It is worth while to point out that extensive calculations have been carried out at M.I.T. using one-centre approximations to molecular Hartree–Fock functions. Since there are a great number they are not included in the table; it is sufficient here to say that after various refinements regarding the number and choice of basis functions an E_{total} almost as good as (*c*) is found. When an estimate for the inclusion of an f function is made then E_{total} is improved to a value between (*c*) and (*d*).

4. CALCULATION OF THE DIPOLE MOMENT AND ELECTRON DENSITY

Having now obtained the best set of Slater parameters at the experimental bond length it is of interest to calculate how the changes in the parameters affect other physical quantities. Using the LCAO coefficients given in table 3 it is possible to calculate dipole moments and electron densities and also carry out an electron population analysis.

For the dipole moment it is necessary to find the centres of charge of each occupied MO. The distance of the centre of charge of ϕ_i from F in the direction of H is given by $\bar{z}_i = \int \bar{\phi}_i z_f \phi_i \, dv$. $\bar{z}_5$ and $\bar{z}_6$ are of course zero, and by taking moments about F it is easy to see therefore that the dipole moment in the direction H⁻F⁻ is given by the simple relation $\mu = \rho - 2(\bar{z}_1 + \bar{z}_2 + \bar{z}_3)$. To find $\bar{z}_1$, $\bar{z}_2$ and $\bar{z}_3$ it is convenient to construct the matrix $\bar{\mathbf{Z}}$, the *pq*th element of which is

$$\bar{z}_{pq} = \int \bar{\chi}_p z_f \chi_q \, dv,$$

and with the known matrix $\mathbf{C}$ form the product $\mathbf{C}'\bar{\mathbf{Z}}\mathbf{C}$ since the diagonal elements of the latter matrix are simply the centres of charge of $\phi_1, \phi_2, \ldots, \phi_6$. The fourth diagonal element is not required since it corresponds to the unfilled MO and as previously mentioned the last two diagonal elements are zero.

The change in the value of the dipole moment brought about by the variation in the Slater parameters is quite considerable. For the initial parameters $\mu = 0{\cdot}345$ A.U. and for the final parameters $\mu = 0{\cdot}584$ A.U.; when these are converted into Debye units using Cohen's values for *e* and a_0 they become 0·88D and 1·49D respectively and are to be compared with the experimental value of 1·74D†.

For the purposes of calculating the electron density, since ϕ_4 is unoccupied, $\mathbf{C}$ was modified to $\mathbf{C}_{\text{mod}}$ by making the fourth column completely zero; in this case the density is simply given as $2(\boldsymbol{\chi}\mathbf{C}_{\text{mod}}\mathbf{C}'_{\text{mod}}\boldsymbol{\chi}')$. Because of the axial symmetry it is only necessary to find the density in one half of any plane containing the line HF, and contours of equal density in such a region are given in figure 2. It will be seen that most of the change in the distribution of charge occurs in the neighbourhood of the H nucleus; this is also demonstrated in figure 3 where the density distribution along the line of the HF axis is shown. At $z_f = -1{\cdot}5$ A.U. the initial density is less than the final density. For larger values of z_f the reverse is true, the curves crossing at $z_f = -0{\cdot}78$. For $z_f = 0$ the initial and final densities are 443·93 and 435·92 respectively. There is another crossing point at $z_f = 0{\cdot}2$

---

† Until recently the accepted value of μ has been 1·91D found by Hannay and Smyth [11]. However, a new absolute value of 1·74D by Dr. G. A. Kuipers has become available (see *Quart. Progr. Rep. Solid-State Molec. Theory* Gp. M.I.T., 15 January 1958, p. 42).

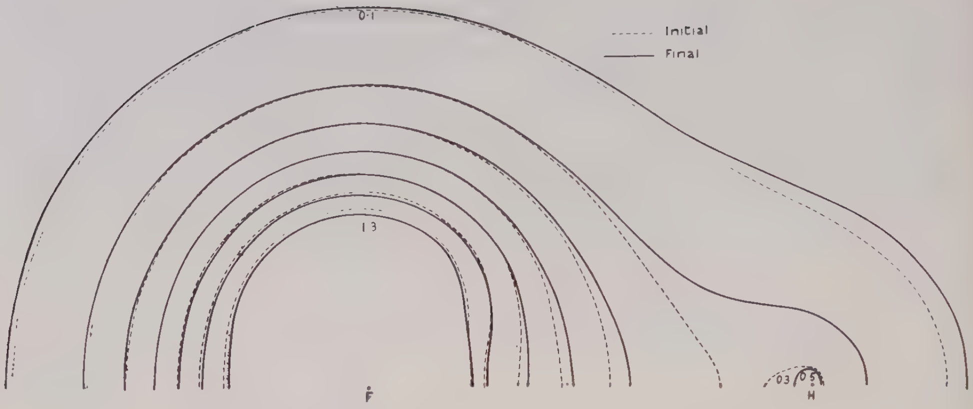

Figure 2. Electron density contours for a half-plane containing the HF axis. Interval is 0·2 electrons/cubic A.U.

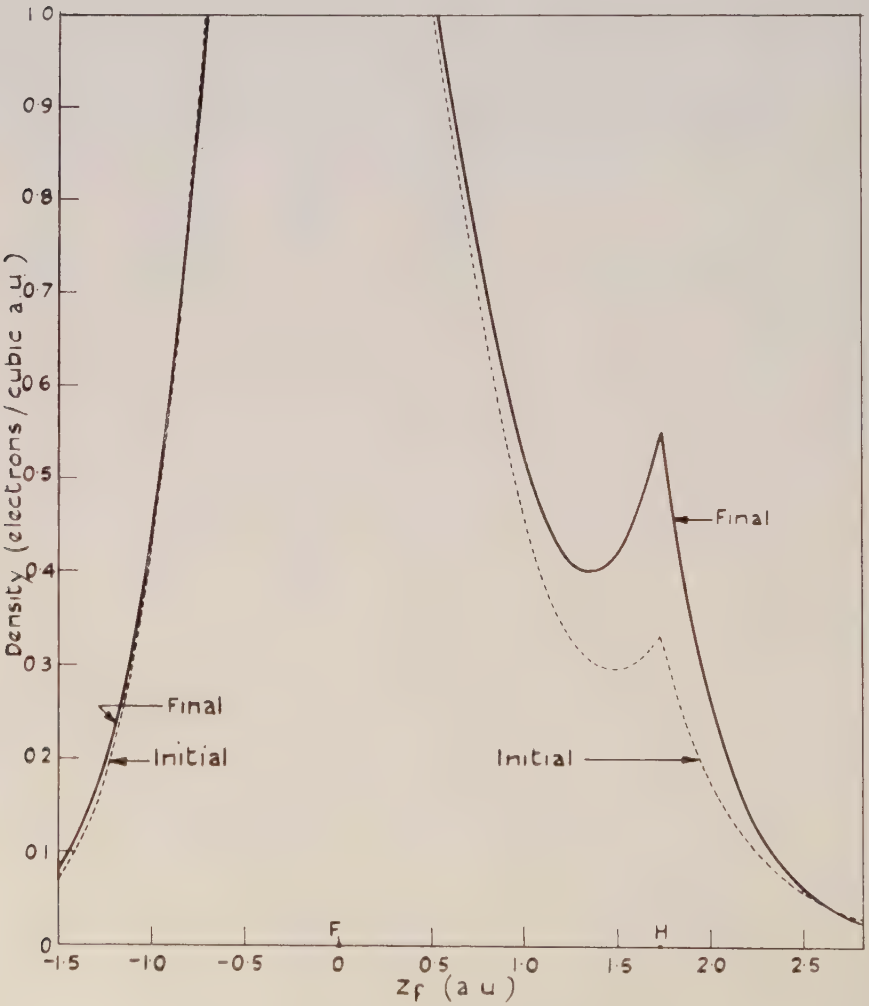

Figure 3. Electron densities along the HF axis.

and in the neighbourhood of the H nucleus the final density is considerably larger than the initial one.

In order to obtain further qualitative information about the distribution of electrons as well as an insight into the characteristics of the individual MO's, an electron population analysis has been carried out using the theory of Mulliken [12]. The analysis is based on the following definitions for a diatomic molecule with centres k and l;

$$\left.\begin{aligned} n(i;\, r_k, s_l) &= 2N(i)\, c_{r_k i} c_{s_l i} S_{r_k s_l}, \\ n(i) &= \sum_{r_k s_l} n(i;\, r_k, s_l), \\ n(r_k, s_l) &= \sum_i n(i;\, r_k, s_l), \\ n &= \sum_i n(i), \end{aligned}\right\} \text{overlap populations}$$

$$\left.\begin{aligned} N(i;\, r_k) &= N(i) c_{r_k i}{}^2 + N(i) \sum_{l \neq k} c_{r_k i} c_{s_l i} S_{r_k s_l}, \\ N(i) &= \sum_{r_k} N(i;\, r_k), \\ N(r_k) &= \sum_i N(i;\, r_k), \end{aligned}\right\} \text{atomic populations}$$

where the MO ϕ_i contains $N(i)$ electrons, r_k and s_l are AO's based on the centres k and l respectively and $S_{r_k s_l} = \int \bar{r}_k s_l \, dv$. $n(i;\, r_k, s_l)$ and $n(r_k, s_l)$ are partial and subtotal overlap populations respectively, the sign and magnitude of $n(i)$ indicates the bonding or antibonding nature of ϕ_i and n, the total overlap population, is a measure of the total covalent strength. $N(i;\, r_k)$ is the partial and $N(r_k)$ the total gross atomic population in AO r_k; the difference $Q(r_k)$ between $N(r_k)$ and $N_0(r_k)$, the number of electrons in the AO r_k in the ground state of the free neutral atom k, can be expressed in terms of amounts of promotion.

For the purposes of this analysis the AO's belonging to a single atom must be mutually orthogonal and therefore 2s* and the corresponding c's are used. The results are presented in table 5.

5. Discussion of the results

On the whole the results are somewhat disappointing, primarily due to the fact that the variation of the four parameters in the usual Slater-type LCAO MO's has only a slight effect on the total energy. It is perhaps surprising that the improvement brought about by the variation of these parameters is so small compared with that due to using Hartree–Fock AO's in preference to the Slater AO's.

5.1. *Total energy of the molecule*

From table 4 it will be seen that the calculations of E_{total} divide themselves into two quite substantially separated groups, those using Slater AO's with energies of $-99{\cdot}5$ A.U. and those using Hartree–Fock AO's or one-centre approximation to molecular Hartree–Fock functions with energies of $-100{\cdot}0$ A.U.; these values are to be compared with the experimental value of $-100{\cdot}5$ A.U. The improvement brought about by variation of the Slater parameters in the LCAO MO's is $0{\cdot}05$ A.U., thus representing only a tenth of the difference separating the two groups of calculations. Nevertheless, it is gratifying to find that

		Overlap populations					AO populations				
		$n(i;\, 1s_F,\, 1s_H)$	$n(i;\, 2s_F{}^*,\, 1s_H)$	$n(i;\, 2p_{zF},\, 1s_H)$	$n(i)$		$N(i;\, 1s_F)$	$N(i;\, 2s_F{}^*)$	$N(i;\, 2p_{zF})$	$N(i;\, 1s_H)$	$N(i)$
Initial	1σ	−0·0010	−0·0001	0·0000	−0·0011	1σ	2·0001	0·0004	0·0000	−0·0005	2·0000
Final		−0·0007	−0·0001	0·0000	−0·0008		2·0001	0·0003	0·0000	−0·0004	2·0000
Initial	2σ	−0·0008	0·2746	0·0174	0·2912	2σ	0·0006	1·7771	0·0252	0·1972	2·0001
Final		−0·0005	0·2427	0·0197	0·2619		0·0004	1·7968	0·0262	0·1766	2·0000
Initial	3σ	−0·0036	−0·4986	0·4733	−0·0289	3σ	−0·0002	0·1703	1·1802	0·6497	2·0000
Final		−0·0021	−0·3483	0·5108	0·1604		−0·0001	0·1471	1·2821	0·5709	2·0000
Initial	$n(r_k, s_l)$	−0·0054	−0·2241	0·4907	—	$N(r_k)$	2·0005	1·9478	1·2054	0·8464	—
Final		−0·0033	−0·1057	0·5305	—		2·0004	1·9442	1·3083	0·7471	—
Initial	n	—	—	—	0·2612	$Q(r_k)$	0·0005	−0·0522	0·2054	−0·1536	—
Final		—	—	—	0·4215		0·0004	−0·0558	0·3083	−0·2529	—

Table 5. Population analysis.

the improvement is such as to give a slightly better energy than either the calculation using the initial Slater LCAO MO's but including CI or the valence-bond calculation also including CI. It must be borne in mind that the latter calculation by Kastler [13] is carried out at $\rho=1{\cdot}7332$ A.U., but it is found by performing SCF LCAO MO calculations for both the initial and final parameters at this value of ρ that the energy value is only changed slightly in the fifth decimal place by the change in ρ, and therefore it is perfectly in order to compare Kastler's calculation with the ones carried out at at $\rho=1{\cdot}7328$ A.U.

It will be noticed that the introduction of CI into the calculations using both initial Slater AO's and Hartree–Fock AO's has a rather small effect, being about half that due to varying the Slater parameters for the single configuration. It would appear therefore that efforts to improve the present calculations by introducing CI would be rather futile. It is fairly clear that variation of Slater parameters together with the inclusion of a limited amount of CI would never approach the true energy as well as by simply using Hartree–Fock AO's for the single ground state configuration.

The calculations using Slater AO's in the first group without exception restrict the number of AO's employed to the ones used in the present calculation and whilst this is the case it would seem impossible to improve the value of E_{total} very much by using either CI or full variation of parameters. However it is conceivable that if more AO's corresponding to excited levels in the isolated atoms are included then the improvement might be encouraging.

5.2. *Binding energy of the molecule*

It is the custom in LCAO MO calculations to use the same AO's in the evaluation of both molecular and atomic energies for the purposes of calculating binding energies of molecules. However, when the parameters of the AO's are being varied in the molecular calculation it would seem reasonable to calculate the energy of the isolated atoms also by allowing the AO parameters to take on minimum values which are different from those in the molecular calculation. As will be seen in table 4, the binding energy calculated in this way is 0·089 A.U., whereas when the calculation is made in the usual way a value of 0·141 A.U. is obtained. Although the latter value is by far the better it is felt that little significance can be attached to it, simply because the value of δ used (1·322) is such as to give a very poor description of the H atom in the calculation of $E_{\mathrm{F+H}}$; this means that whilst the variation of the parameters in the molecular case obviously gives a better E_{total}, these parameters give a much worse $E_{\mathrm{F+H}}$ and hence a better binding energy.

The binding energy found by independently varying the parameters in both the molecular and atomic calculations is appreciably improved, but when values of E_{total} and $E_{\mathrm{F+H}}$ in any type of calculation are in error, it is impossible to attach much significance to results for the binding energy, and in fact a very good value must be necessarily fortuitous.

5.3. *Ionization and excitation energies*

It is well known [1] that ϵ_i is a good approximation to the ionization potential corresponding to the removal of an electron from the ith MO. In the case of HF^+, it is only recently that experimental information has become available (see Coope *et al.*, [14]). Two states have been found, the ground state $^2\Pi_i$ and the first excited state $A^2\sum^+$, corresponding to ionization potentials of 15·8 and 17·0 ev respectively; these are to be compared with $\begin{Bmatrix}\epsilon_5\\\epsilon_6\end{Bmatrix}$ and ϵ_3. The former is only changed slightly by the variation in parameters from 12·6 to 12·8 ev, whereas the latter is changed rather more from 15·4 to 16·2 ev. These values are in quite good agreement with the experimental values and it will be noticed that in both cases the change brought about by the variation of the parameters is in the right direction. It is perhaps surprising that the one corresponding to the first excited state of HF^+ is so good; it is so very much better than the one corresponding to the ground state of HF^+ that the possibility of the result being fortuitous cannot be discounted.

No reference has yet been made to the excited states of HF and the corresponding excitation energies, the main reason being the unfortunate lack of definite experimental results. Nevertheless one or two observations are worth making at this stage. Duncan [15] suggests that since excitation of an electron from $\begin{Bmatrix}\phi_5\\\phi_6\end{Bmatrix}$ to ϕ_4 can occur only at very high energies, the lower energy electronic transition occurs when an electron from $\begin{Bmatrix}\phi_5\\\phi_6\end{Bmatrix}$ is excited to a *n*s or *n*d atom-like orbital. Whilst this may be the case, it is of interest to evaluate the high energy necessary to excite an electron from $\begin{Bmatrix}\phi_5\\\phi_6\end{Bmatrix}$ to ϕ_4 predicted by the present results, mainly with a view to finding how sensitive this excitation energy is to the change in Slater parameters. Using the formula given by Roothaan [1] it is found that for the singlet excited state the excitation energy changes from 9·7 ev for the initial case to 15·0 ev for the final case and for the triplet the change is found to be from 8·0 to 13·3 ev. These changes, which are surprisingly large, are due principally to the substantial alteration in the value of ϵ_4 and clearly demonstrate that excitation energies are critically dependent on the choice of AO's.

5.4. *Electron distribution*

As will be seen from figures 2 and 3 the distribution of charge appears to be changed most in the neighbourhood of the H nucleus. Although it would seem from these curves that things do not alter very much around the F nucleus it must be borne in mind that the value of the density is reduced by 8·01 electrons/cubic A.U. by the change in the parameters, and whilst this change is less than 2 per cent of the absolute value at F it is much larger than the change in the value of the density at H. It is clear that there is a transference of charge from the region around F to the region around H which intuitively one feels ought to lead to a lower value for the dipole moment instead of a greater value as in fact is the case. The reason for this apparent inconsistency is found on a closer examination of this transference of charge. Taking the HF axis for example, it will be seen that the density is lowered for $-0{\cdot}78 < z_f < 0{\cdot}20$ (by 8·01 at $z_f = 0$) and raised for $0{\cdot}20 < z_f < 2{\cdot}65$ (by 0·22 at $z_f = \rho$). Hence it is clear that charge is lost rather severely from a relatively small volume surrounding F and distributed more gently over a much greater volume surrounding H. Bearing these observations in mind when taking moments about F it is easy to understand why it is possible for μ to be increased by the change in parameters instead of decreased and it is clear therefore that it is extremely dangerous to make loose correlations of charge transfer with changes in the values of μ.

Turning now to tables 3 and 5 it will be seen that for either set of parameters the 1σ and 2σ MO's are formed almost completely from the $(1s)_F$ and $(2s^*)_F$ AO's respectively and are therefore concentrated around F. The $n(i)$ for 2σ is large and positive and therefore the MO is considered to be bonding. However, for 3σ, although in either case the electron population is distributed around F and H, the $n(i)$ changes appreciably both in magnitude and sign. For the initial parameters the MO is slightly antibonding whereas in the final case it is significantly bonding in character.

It is of interest here to look at the results of the population analysis for the calculations using Hartree–Fock AO's carried out by Karo [16]. Karo's values for $n(i)$ are $-0{\cdot}0002$, $0{\cdot}2346$ and $0{\cdot}1767$ for 1σ, 2σ and 3σ respectively and are in remarkable agreement with the present findings for the final parameters. It is particularly gratifying to find in the case of 3σ the variation of parameters has changed the value of $n(i)$ considerably to a value which is substantially in agreement with that corresponding to a calculation in which better AO's have been employed (better in the sense that they lead to a much superior value for the energy). It will also be noticed that whilst the changes in the values of $n(i)$ for 1σ and 2σ are not significant, the trends nevertheless are in the direction of Karo's results. Primarily because of this change in the value of $n(i)$ for 3σ, the total overlap population is seen to change from $0{\cdot}2612$ to $0{\cdot}4215$, thus indicating a greater covalent strength, and as might be expected the latter value is in good agreement with Karo's value for n of $0{\cdot}4111$.

From the values of $\underset{\sim}{Q}(1s_H)$ it will be seen that in either case there is a charge transfer from H to F. It is not possible however to be sure into which of the AO's $(1s)_F$, $(2s^*)_F$ and $(2p_z)_F$ the charge is transferred because of the reorganization of charge which also occurs amongst these AO's. Nevertheless it is almost certain that it is transferred to the $(2p_z)_F$ AO. It is worth while to point out that whilst one expects there to be a net charge transfer from H to F to provide the polarity of the molecule as H^+F , the amount of transfer is greater for the final parameters in contradiction with the results for the absolute charge distribution displayed in figures 2 and 3. This clearly raises doubts as to the validity of assigning transference of charge from one atom to another simply by evaluating the difference in the total gross AO population for the molecule and atoms.

6. CONCLUSIONS

The variation of Slater parameters in the Slater-type LCAO MO's is found to have a rather disappointing effect on the energy of the molecule and for HF at least it would appear that it is highly preferable to use Hartree–Fock AO's in the construction of LCAO MO's. It is believed that efforts to improve the energy by introducing CI in the present scheme would be rather futile and that a more hopeful line of attack would be to include further Slater-type AO's corresponding to the lower excited states of the isolated atoms in the LCAO MO's for the single configuration without necessarily finding the minimum Slater parameters.

The changes brought about in other physical quantities is on the whole rather more marked and the variations which occur always have the correct experimental trend. The final values for the dipole moment, ionization energies and overlap population of the 3σ MO are particularly gratifying but the improvement in the energy, which was the main reason underlying the present investigation and which has been found to be rather poor, leaves much to be desired.

It is a pleasure to acknowledge the award of a Government Research Fellowship during the tenure of which this work has been carried out. The author also wishes to express his thanks to members of the Mathematics Division at the National Physical Laboratory who have been most helpful in rendering help and advice on the computational aspects of the problem, to Drs. N. H. March and H. H. Robertson for helpful comments regarding the MS., and to the Director of the Laboratory for permission to publish this work.

APPENDIX 1

Computational techniques

Implicit in the determination of the matrix elements is the calculation of many molecular integrals. Of these, the one-electron integrals involved only in the construction of the $\mathbf{H}$ and $\mathbf{S}$ matrices can be expressed in analytical form (Coulson [17]) and their computation therefore presents little difficulty. On the other hand the two-electron integrals occurring exclusively in the matrix $\mathbf{G}$ are extremely tedious to evaluate. With the exception of the exchange integrals these two-electron integrals were calculated using the ζ function method of Barnett and Coulson [18]. The Gaussian method of integration was employed in three ranges, one from the origin to the point where the standard Bessel functions I and K interchange in the definition of the ζ function, and two beyond this point extending to 'infinity'. It is only very recently (Barnett [19]) that the ζ function method has been extended to deal with the exchange integrals and in this case therefore it was necessary to employ the method of Rüdenberg [20]. The method involves double integration and so the integrals were evaluated by the Simpson method of integration.

Once the necessary integrals have been evaluated it is then a fairly simple matter to construct the matrix elements using the definitions. Since the $\mathbf{H}$ and $\mathbf{S}$ (and therefore $\mathbf{L}$ and $\mathbf{L}^{-1}$) matrices are independent of the c's, they clearly remain unchanged during the iterative procedure of a SCF calculation carried out for prescribed values of α, β, γ, δ and ρ. These matrices were therefore evaluated once and for all using the one-electron integrals at the commencement of each SCF calculation. The $\mathbf{G}$ matrix on the other hand depends on the c's, and in this case it is convenient to express each matrix element G_{pq} as the scalar product $\mathbf{d}\,.\,\mathbf{D}_{pq}$, where the elements of the row vector $\mathbf{d}$ are made up entirely of the c's and those of the column vector $\mathbf{D}_{pq}$ are simple combinations of the two-electron integrals. The $\mathbf{D}_{pq}$'s can be written down alongside each other to form a matrix $\mathbf{D}$, taking account of the fact that $\mathbf{G}$ is a symmetric matrix, and it is evident that at each stage of the iterative process every element of $\mathbf{G}$ (and therefore $\mathbf{F}$, since $\mathbf{H}$ is known) can readily be generated by performing the product $\mathbf{d}\,.\,\mathbf{D}$. All the elements of $\mathbf{D}$ are independent of the iterative procedure; it was thus only necessary to calculate this matrix once at the beginning of each SCF calculation. Such a procedure for calculating the matrices required for the iterative solution of equation (4) in terms of matrix and vector operations is particularly convenient for high-speed computers. The techniques are also quite general and in principle can be applied to any molecule.

In order to simplify the calculations, one of course takes proper account of the symmetry of the molecule so as to factorize (4) into a set of matrix equations of lower order by means of group theoretical arguments. In the case of HF, because of the way in which the MO's have been constructed, equation (4) reduces to a 4 × 4 matrix equation to determine ϕ_1, ϕ_2, ϕ_3 and ϕ_4 and their orbital energies and two identical 1 × 1 matrix equations corresponding to the known orbitals ϕ_5 and ϕ_6 to determine their orbital energy; the latter equation is of course completely trivial. The way in which the various orbitals are filled with electrons is reflected only in the construction of **d**. In the case of HF in its ground state, ϕ_1, ϕ_2, ϕ_3, ϕ_5 and ϕ_6 are doubly filled and ϕ_4 is unoccupied.

At the beginning of each SCF calculation $\mathbf{L}^{-1}$, **H** and **D** were calculated and stored; in representing **S** as $\mathbf{LL}'$, the matrix **L** was taken to be the lower triangular in preference to the upper triangular, for then $(\mathbf{L}^{-1})'$ is clearly the more reasonable first approximation to **C** (in this case ϕ_1 is approximated by χ_1, i.e. $(1s)_F$ is taken to be the MO with the lowest energy). At each stage of the iteration, in order to prepare the matrix $(\mathbf{L}^{-1})\mathbf{F}(\mathbf{L}^{-1})'$ whose latent roots and vectors are required, it is simply a matter of evaluating the vector **d** in terms of the c's and then computing $(\mathbf{L}^{-1})\mathbf{F}(\mathbf{L}^{-1})'$ from the known matrices by the method described above. The latent roots and vectors of the 4 × 4 matrices were found by the method of Givens [21] and each new set of c's was obtained from the vectors through (3). At each stage of the iteration the electronic energy of the molecule was evaluated by summing all the diagonal elements of the matrix $\mathbf{C}'(2\mathbf{H}+\mathbf{G})\,\mathbf{C}$ corresponding to the filled MO's, i.e. $E=\sum_i{}'\{\mathbf{C}'(2\mathbf{H}+\mathbf{G})\mathbf{C}\}_{ii}$, in which the **G** matrix is calculated with the c's of **C**.

APPENDIX 2

Discussion of computational errors

Every conceivable test was made during the construction of the programme designed for the automatic computation of the necessary molecular integrals. The one-electron integrals are of course given exactly, but in the case of the two-electron integrals, extensive variation of the orders of the Gaussians, the intervals of the Simpsons and the cut-off points taken to represent infinity left little doubt that the latter integrals are certainly given correct to four decimal places by the present programme. Furthermore, judging by the agreement found between Kastler's integrals [13] and those given by the present programme for his parameters, it is safe to say that four-decimal place accuracy is very much an understatement, for in many cases agreement was found to all the six decimal places given by Kastler. However, it was decided as an additional check on the correctness of this part of the SCF programme to compute with it some of the molecular integrals listed in the scientific literature by various workers. In this connection the reader is advised to regard such tables with caution, for on several occasions discrepancies between tabulated values and those calculated by means of the present programme were discovered; on careful scrutiny such disagreement was invariably found to exist on account of errors in the tabulated values. In the particular case of HF for example the integrals given by Duncan [15] contain numerous errors (see Allen and Karo [8] for a corrected version of Duncan's work).

In view of the slight discrepancies between the present results and those of Allen and Karo [8] (see table 4), it was thought worth while to investigate how sensitive the energy is to the accuracy of the two-electron integrals. This was effected by truncating the values of these integrals to a fixed number of binary places thereby introducing arbitrary errors ranging from zero to a maximum value which is clearly dependent on the point of truncation. It was found that it was possible to vary the energy over a range of 0·0020 A.U. by this method, allowing errors up to and including 0·00003 in the two-electron integrals. This is quite appreciable when compared with the discrepancy of 0·0050 A.U. in the two energy values $-99{\cdot}4836$ A.U. and $-99{\cdot}4786$ A.U. found respectively by Allen and Karo and the author for the initial set of parameters, and suggests that unless all the molecular integrals can be calculated to a high accuracy, care should be exercised in stating just how many figures of the energy are significant.

In a computation of this magnitude clearly the chance that an error has been made is quite considerable. Apart from errors in the evaluation of molecular integrals the other most likely source of error is in the solution of the latent root process and evaluation of the corresponding latent vectors. It must be pointed out that it is possible to obtain numerically latent vectors which are incorrect in so far as they do not correspond exactly to the latent roots from which they are obtained if an injudicious process is used such as the iterative method (see Wilkinson [22]). Since each set of latent vectors is used in the subsequent stage of the iteration it is therefore conceivable that a bad process of determining the vectors would lead to erroneous results.

Before concluding the discussion on the accuracy of the present calculations, particularly in connection with the work of Allen and Karo, it is perhaps pertinent to point out that there is also a discrepancy in the values for E_{F+H} (the author's value of $-99{\cdot}4317$ A.U. is to be compared with $-99{\cdot}4333$ A.U.). Here it has been possible to establish that the error almost certainly lies in the latter value, for in carrying out the variation of α in the first cycle, it was found that for Kastler's parameters, $\alpha=8{\cdot}67$, $\beta=\gamma=2{\cdot}60$, the values of E_{F+H} agreed to six decimal places. It is worth mentioning also that this error in E_{F+H} could not be due to the two possible causes previously mentioned, since neither awkward two-electron two-centre integrals nor a latent root and vector process are required in the evaluation of E_{F+H}. Despite these comments it will be seen that the two calculations of both E_{total} and E_{F+H} agree to two decimal places, and this is almost adequate for the purpose of comparison with other methods of obtaining improved wave functions as will be seen from table 4. With regard to the binding energy, although again two decimal places are almost sufficient for the purposes of comparison it would be more positive to have three decimal place accuracy. However, in view of the discussion of the accuracy of the present calculations, the third decimal figure given for all energy values by the author is believed to be correct.

On a effectué des calculs par la méthode du champ self-consistent sur le fluorure d'hydrogène, pour la distance internucléaire expérimentale, en utilisant une fonction d'onde en forme de déterminant unique, composée d'orbitales moléculaires (OM) écrites en combinaison linéaire d'orbitales atomiques (LCAO). Les orbitales atomiques employées sont du type orbitales de Slater pour lesquelles on a obtenu les paramètres selon la méthode de variation. On discute, en relation avec les résultats d'autres méthodes d'obtention de fonctions d'onde améliorées pour cette molécule, l'amélioration, due à la variation des paramètres de Slater, de la valeur de l'énergie et d'autres quantités physiques.

Self-consistent-field-Berechnungen wurden für Fluorwasserstoff beim experimentellen Kernabstand ausgeführt. Hierzu wurde eine einzige Determinanten-Wellenfunktion benutzt, die aus molecular orbitals aufgebaut ist, welche ihrerseits als Linearkombinationen von atomic orbitals ausgedrückt sind. Die benutzten atomic orbitals sind vom Slater'schen Typ, dabei werden die Parameter nach der Variationsmethode variiert. Die durch Variation der Slater'schen Parameter erzielte Verbesserung für die Energie und andere physikalische Grössen wird für diese Molekel im Hinblick auf die Ergebnisse anderer Verfahren zur Berechnung verbesserter Wellenfunktion diskutiert.

REFERENCES

[1] ROOTHAAN, C. C. J., 1951, *Rev. mod. Phys.*, **23,** 69.
[2] SLATER, J. C., 1930, *Phys. Rev.*, **36,** 57.
[3] SCHERR, C. W., 1955, *J. chem. Phys.*, **23,** 569.
[4] SAHNI, R. C., 1956, *J. chem. Phys.*, **25,** 332.
[5] KARO, A. M., 1957, *Quart. Progr. Rep. Solid-State Molec. Theory Gp.* M.I.T. (15 October).
[6] HERZBERG, G., 1950, *Spectra of diatomic molecules* (New York: Van Nostrand), p. 536.
[7] COHEN, E. R., 1957, *Il Nuovo Cim. Suppl.* **6,** 43.
[8] ALLEN, L. C., and KARO, A. M., 1957, *Quart. Progr. Rep. Solid-State Molec. Theory* Gp. M.I.T. (15 April).
[9] ALLEN, L. C., 1956, *Quart. Progr. Rep. Solid-State Molec. Theory Gp.* M.I.T. (15 October).
[10] ALLEN, L. C., 1957, *Quart. Progr. Rep. Solid-State Molec. Theory Gp.* M.I.T. (15 January).
[11] HANNAY, N., and SMYTH, C., 1946, *J. Amer. chem. Soc.*, **68,** 171.
[12] MULLIKEN, R. S., 1955, *J. chem. Phys.*, **23,** 1833.
[13] KASTLER, D., 1953, *J. Chim. phys.*, **50,** 556.
[14] COOPE, J. A. R., FROST, D. C., and MCDOWELL, C. A., 1957, *Nature, Lond.*, **179,** 1186.
[15] DUNCAN, A. B. F., 1955, *J. Amer. chem. Soc.*, **77,** 2107.
[16] KARO, A. M., 1958, *Quart. Progr. Rep. Solid-State Molec. Theory Gp.* M.I.T. (15 January).
[17] COULSON, C. A., 1942, *Proc. Camb. phil. Soc.*, **38,** 210.
[18] BARNETT, M. P., and COULSON, C. A., 1951, *Phil. Trans.* A, **243,** 221.
[19] BARNETT, M. P., 1958, *The evaluation of multi-centre and exchange molecular integrals by use of the zeta function method.* WIS ONR 29 (University of Wisconsin: Naval Research Laboratory).
[20] RÜDENBERG, K., 1951, *J. chem. Phys.*, **19,** 1459.
[21] GIVENS, W., 1954, *Numerical computation of the characteristic values of a real symmetric matrix.* ORNL 1574 (Oak Ridge: United States Atomic Energy Commission).
[22] WILKINSON, J. H., *The algebraic eigenvalue problem* (in the press).

Molecular-orbital treatment of a new type of heteroaromatic compound

by R. D. BROWN and B. A. W. COLLER
Chemical Laboratories, University of Melbourne, Carlton N.3, Victoria, Australia

(*Received* 7 *August* 1958)

The π-electron systems in four electron-rich heterocyclic nitrogen compounds of a new type were studied by the simple molecular-orbital method. Resonance energies, π-electron densities and energies of excited states were studied as a function of the nitrogen electronegativity parameter. Although only one of the compounds has yet been synthesized, the present results suggest that all would be stable once formed. Definite predictions of the positions of highest chemical reactivity towards electrophils can be made in the case of the two tricyclic compounds (I) and (II).

1. Introduction

The heteroaromatic compounds (I)–(IV) represent a type of system not previously investigated by the molecular-orbital method; in all previous cases the heteroatoms have been on the periphery of the aromatic system. They are of particular interest in that they contain more π-electrons than conjugated atoms. Qualitatively therefore they would be expected to be particularly reactive towards electrophils. All previously studied examples of such electron-rich cyclic systems have involved five-membered rings (we exclude systems such as aniline and phenol as not entirely cyclic) whereas compounds (I), (III) and (IV) contain only six-membered rings. The nitrogen atoms are in unusual environments in these compounds and might be expected to have different electronic properties, e.g. electronegativity, from a pyridine-type nitrogen or a pyrrole-type nitrogen. As part of a programme [1, 2, 3, 4, 5] to study the molecular-orbital theory of chemical reactivity of heterocyclic systems it was of interest to study compounds having nitrogen in this new environment.

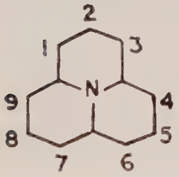

(I)

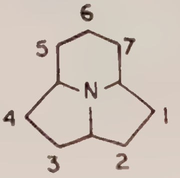

(II)

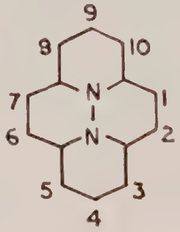

(III)

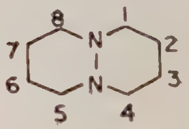

(IV)

While the present calculations were in progress the synthesis of (II) was announced [6] and the names cyclazine(3,3,3) and cyclazine(3,2,2) were proposed for (I) and (II) respectively.

2. Method of treatment

We used the same procedure as in previous studies. The overlap integral was neglected, all resonance integrals were taken to have the standard value β and the coulomb integrals of all carbon atoms were assigned the standard value α. Taking the coulomb integral of nitrogen to be $\alpha + h\beta$, we carried through the calculations for various values of h. Calculations were also done using a value for β_{CN} slightly different from the standard value to determine the sensitivity of the results to the value of this resonance integral.

3. Results and discussion

Since all compounds are π-electron rich they are expected to be very reactive towards electrophils, unreactive towards nucleophils. The orientation of electrophilic substitution, particularly in the case of strong electrophils such as NO_2^+ and Br^+, is expected to be determined by the π-electron distribution rather than by electrophilic atom-localization energies [7].

The π-electron densities of cyclazine(3,3,3) are shown as a function of h in figure 1. For all values of h the 1-position has a greater charge than the 2-position and electrophilic substitution is therefore expected primarily at the former position. The results assuming $\beta_{CN} = 1{\cdot}2\beta$ (figure 2) show that this prediction is not affected for moderate changes in the value of this resonance integral.

For any value of h the charge at the 1-position is considerably greater than unity so that the reactivity of cyclazine(3,3,3) can be predicted to be considerably greater than that of benzenoid compounds towards electrophils.

The π-electron densities for cyclazine(3,2,2) are shown in figure 3 for $\beta_{CN} = \beta$ and figure 4 for $\beta_{CN} = 1{\cdot}1\beta$, the qualitative order of electron densities being seen to be virtually unaffected by such variations in the resonance integral. For all values of h the 1-position is expected to be most reactive to electrophils but the position next in order of reactivity depends upon h, being the 2-position for $h > -0{\cdot}6$ (for $\beta_{CN} = \beta$) and the 6-position for $h < -0{\cdot}6$. Thus some indication of the appropriate value of h for such electron-rich compounds might be obtained for example by studying the position of electrophilic substitution in 1,4-dimethylcyclazine(3,2,2). The fact that charge densities appreciably exceeding unity occur at all values of h means that a high reactivity towards electrophils may be predicted even if we are not certain of the appropriate value of h for nitrogen in this environment.

The π-electron densities for diazapyrene (III) are shown in figures 5 and 6 for two different values of β_{CN}, the standard value β being assumed for β_{NN} in both cases. The results are seen to be qualitatively independent of β_{CN}, the 1-position bearing the greatest π-electron density for $h > 1{\cdot}5$, the 3-position for $h < 1{\cdot}5$. One interesting feature is the singular behaviour at $h = 1{\cdot}5$. This arises from a change in the relative energies of two molecular orbitals such that their occupation numbers for the ground state of diazapyrene change at $h = 1{\cdot}5$. There is thus no value of h for which the reactivities of the 1 and 3-positions are expected to be similar, other than the physically unlikely value of $h = -3{\cdot}2$ (for $\beta_{CN} = \beta$).

As with the cyclazines, there is always one group of carbon atoms with a π-electron density above unity for all values of h, pointing to a high reactivity towards electrophils.

The π-electron densities of diazalene (figures 7 and 8), insensitive to the value chosen for β_{CN}, show a similar abrupt change, in this case at $h = 1$. For h greater than this, the 2-position has a greater electron density than has the 1-position whereas the reverse applies for $h < 1$. Again a high reactivity towards electrophils is predicted for all values of h. If diazapyrene and diazalene could be synthesized

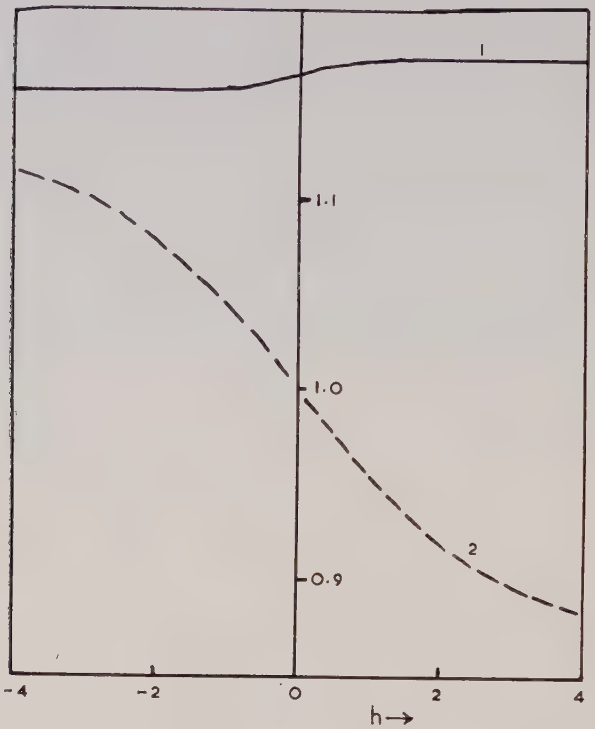

Figure 1. π-electron densities of cyclazine(3,3,3); $\beta_{CN}=\beta$.

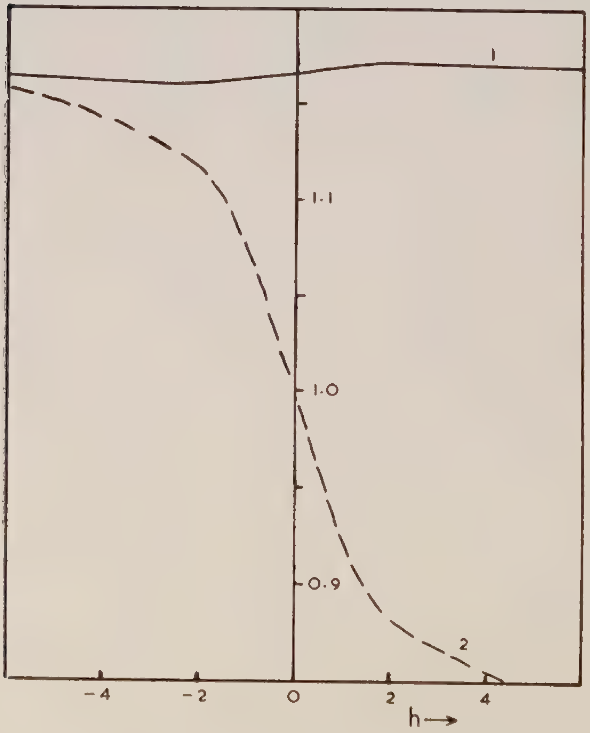

Figure 2. π-electron densities of cyclazine(3,3,3); $\beta_{CN}=1{\cdot}2\beta$.

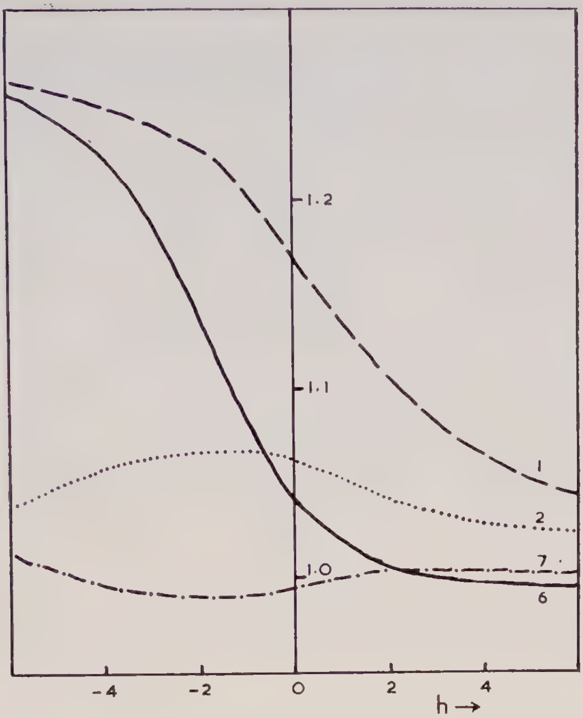

Figure 3. π-electron densities of cyclazine(3,2,2); $\beta_{CN} = \beta$.

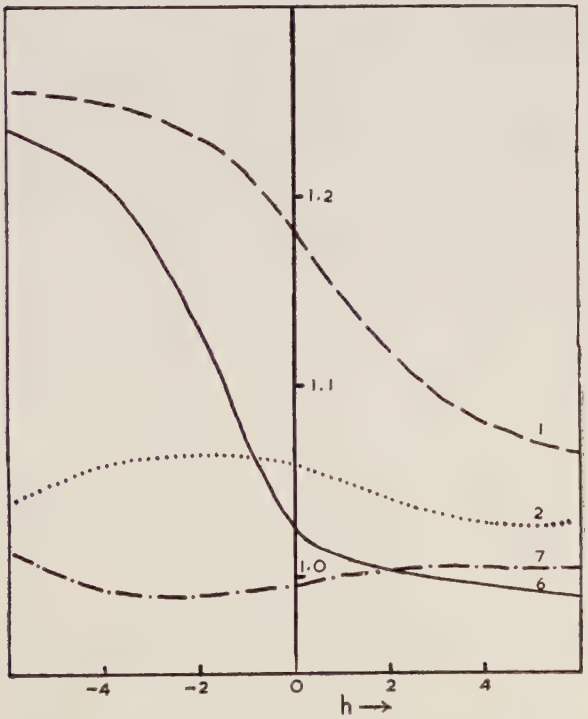

Figure 4. π-electron densities of cyclazine(3,2,2); $\beta_{CN} = 1{\cdot}1\beta$.

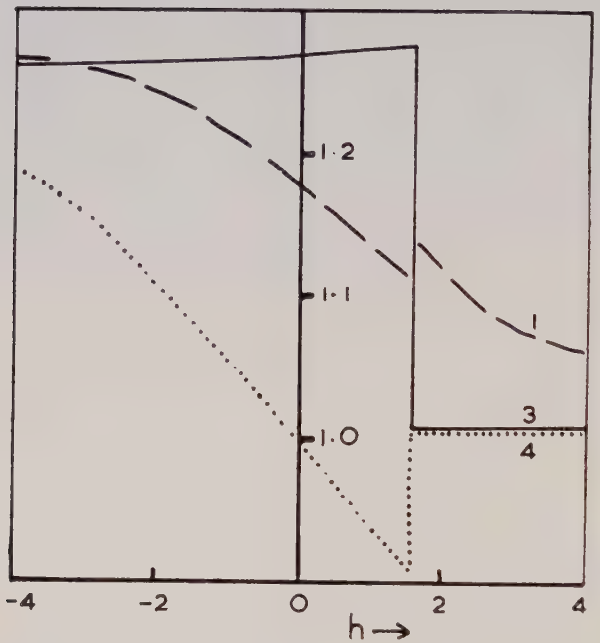

Figure 5. π-electron densities of diazapyrene; $\beta_{CN}=\beta$.

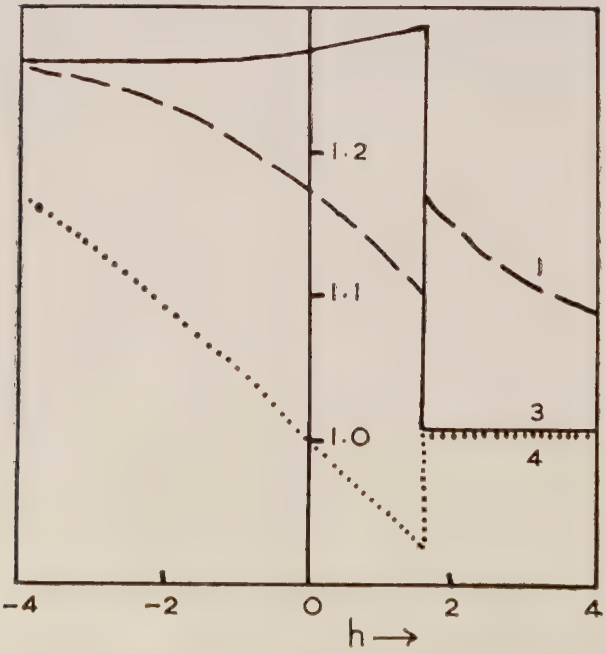

Figure 6. π-electron densities of diazapyrene; $\beta_{CN}=1{\cdot}2\beta$.

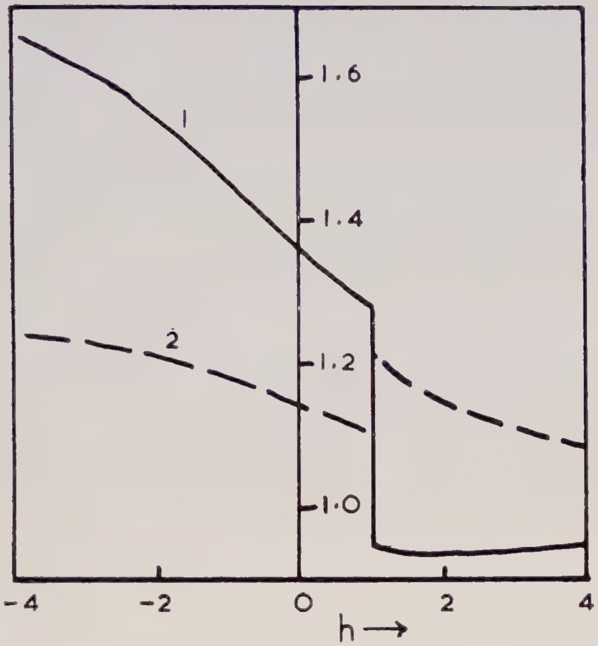

Figure 7. π-electron densities of diazalene; $\beta_{CN} = \beta$.

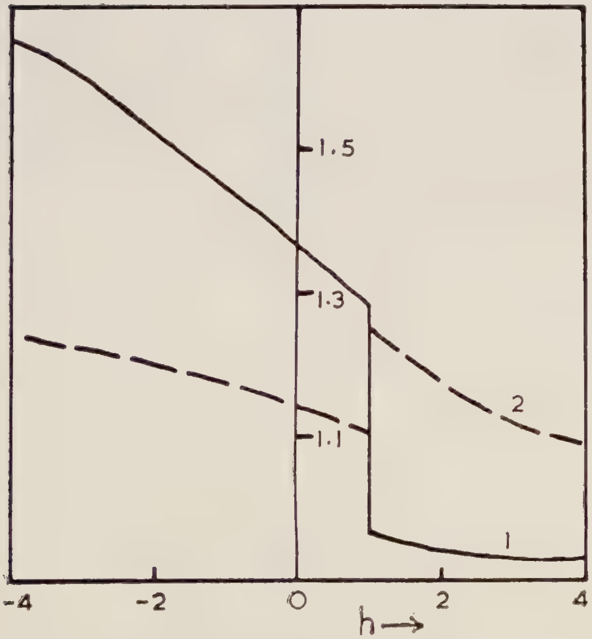

Figure 8. π-electron densities of diazalene; $\beta_{CN} = 1{\cdot}1\beta$.

and the orientations of electrophilic substitutions in these heterocycles determined valuable light would be thrown on the most suitable value of h for nitrogen in this unusual environment.

As some indication of the probable stabilities of these heterocycles the resonance energies of the four compounds are shown as a function of h in figures 9 and 10. The resonance energies of related aromatic hydrocarbons are also indicated for comparison. All four curves show a bifurcation at $h = -1$. The upper branches give the resonance energies if in the non-conjugated reference structures two π-electrons are assigned to the central nitrogen in the cyclazines or four to the N, N in diazapyrene and diazalene. The lower branches give the resonance energy if π-electrons are assigned to the lowest available orbitals in the non-conjugated fragments. In addition the curves for diazalene and diazapyrene have discontinuous slopes at $h = 1$ or $1{\cdot}5$ because at this point a change in the occupation numbers of two orbitals occurs (see above).

If the appropriate value of h for nitrogen in these compounds is similar to that appropriate for nitrogen in pyridine, i.e. 0 to 0·5 [5, 8, 9], then the present molecular-orbital data indicate considerable stability for these compounds, comparable to that of related aromatic hydrocarbons. In the case of cyclazine

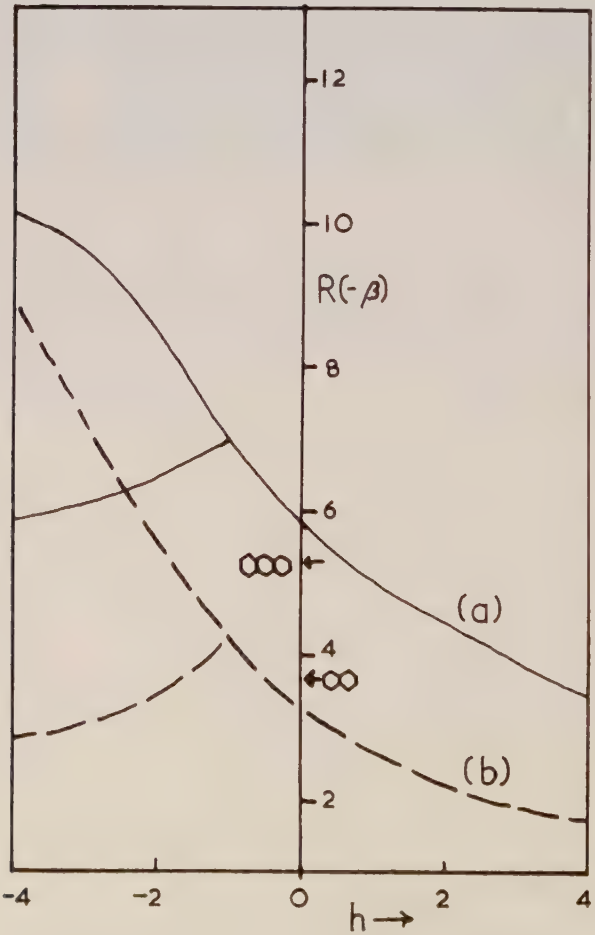

Figure 9. Resonance energies of (*a*) cyclazine(3,3,3), (*b*) cyclazine(3,2,2).

(3,2,2) the stability might be somewhat lower owing to σ-electron strain energy not included in the present study but preliminary reports [6] nevertheless indicate considerable stability.

The positions of some of the lower excited configurations of these heterocycles, obtained by the simple product-of-molecular-orbitals picture, are shown in figures 11 to 14, as functions of h. Excited configurations for which spectroscopic combination with the ground state is symmetry forbidden are shown by dotted lines. The symmetry designations are those given for example by Sponer and Teller [10]. The major symmetry axis was always taken as the z axis, and when this lies in the molecular plane, as in the case of cyclazine(3,2,2), diazapyrene and diazalene, the x axis was chosen to lie in the molecular plane also. For diazapyrene and diazalene the z axis was chosen to lie along the N–N bond.

The resultant energies cannot be taken to indicate more than the qualitative order of configurations because the simple molecular-orbital approximation is known to be unreliable in predicting spectroscopic intervals. In addition the present results will be altered if other values were used for β_{CN} and β_{NN}. However, they might prove useful in the qualitative appraisal of ultraviolet absorption

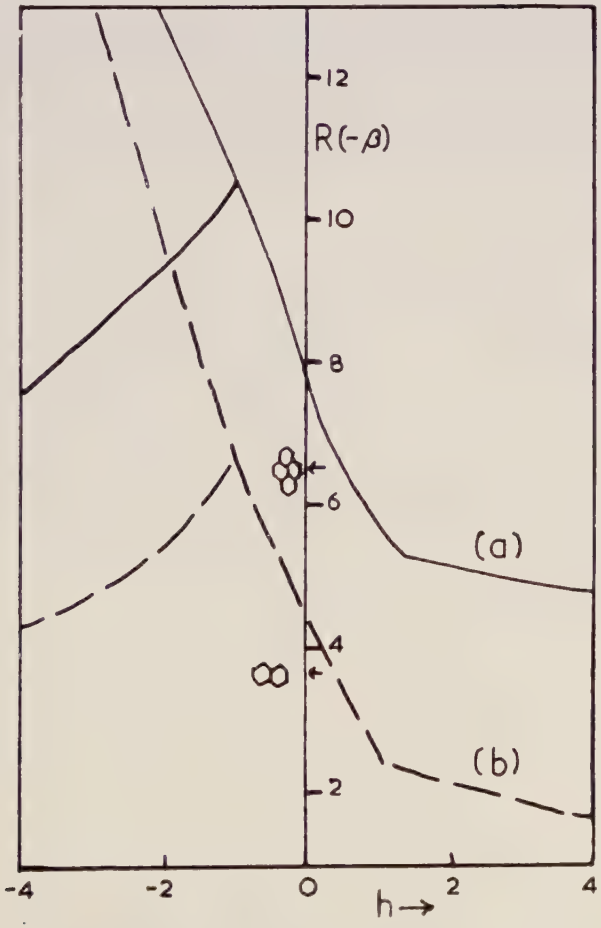

Figure 10. Resonance energies of (*a*) diazapyrene, (*b*) diazalene.

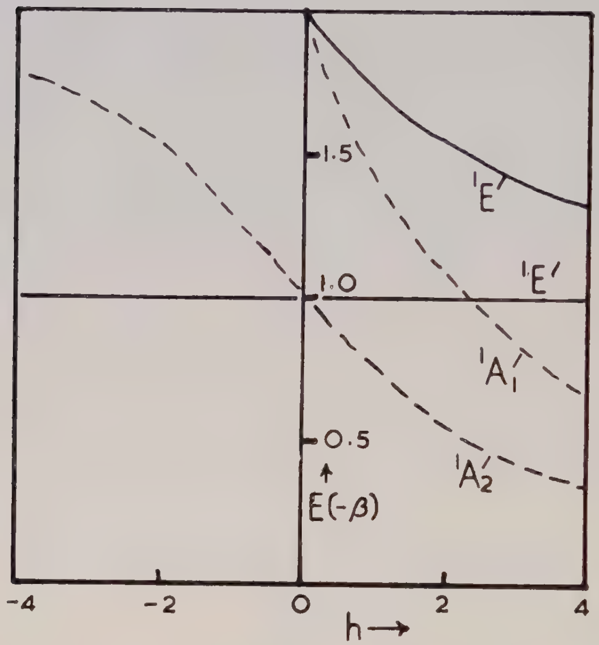

Figure 11. Excited states of cyclazine(3,3,3).

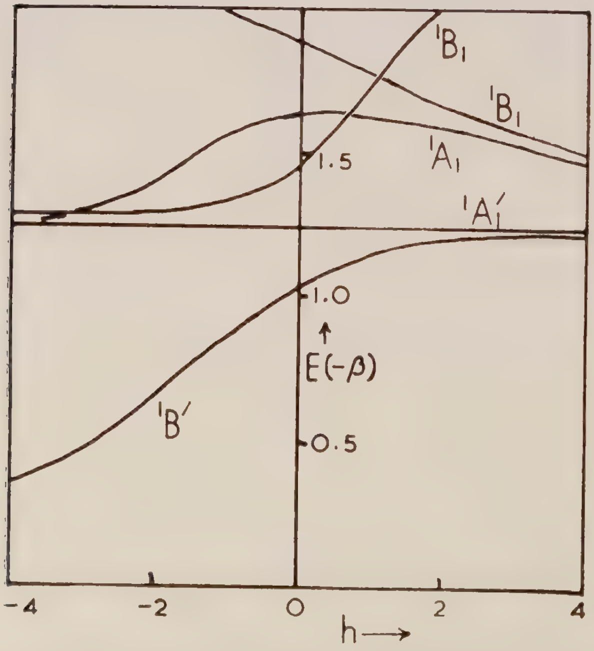

Figure 12. Excited states of cyclazine(3,2,2).

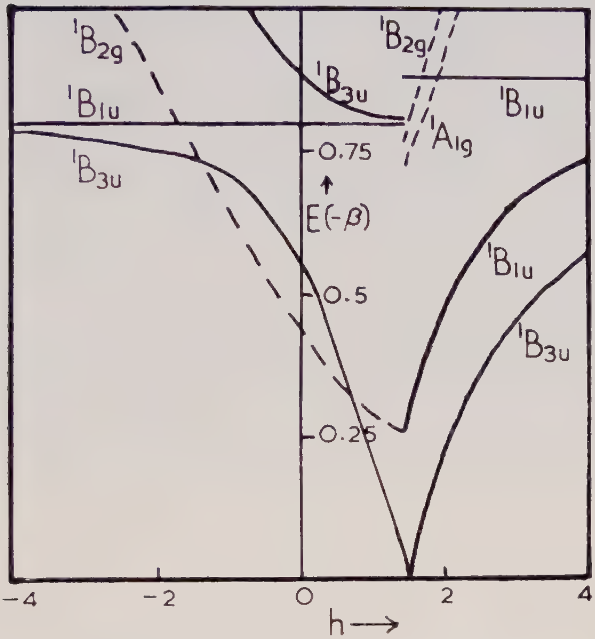

Figure 13. Excited states of diazapyrene.

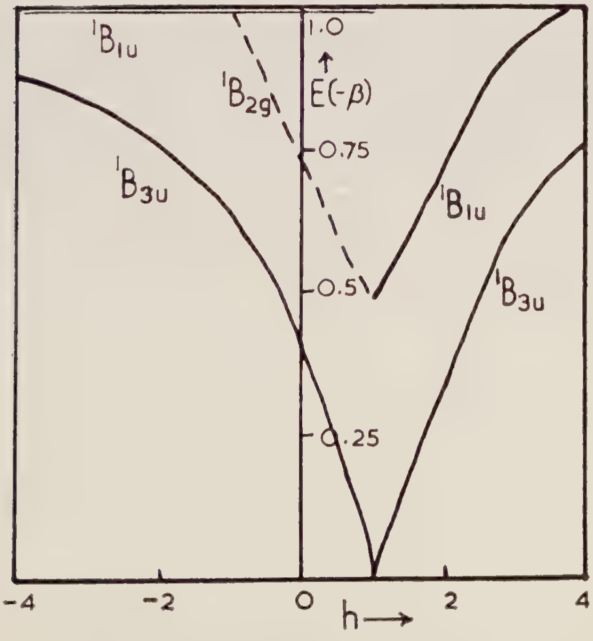

Figure 14. Excited states of diazalene.

spectra of the present compounds and as a starting point for more elaborate calculations. The results suggest that all compounds will be coloured, several low-energy transitions being present for cyclazine(3,3,3), diazapyrene and diazalene for small positive values of *h*.

The authors are grateful to Mr. A. Jones of the Mathematics Department whose programmes for obtaining eigenvalues and eigenvectors were used on the electronic computer CSIRAC to obtain the results reported above, and to the staff of the Computation Laboratory for facilitating the calculations. One of us (B.A.W.C.) gratefully acknowledges the award of a Dunlop Research Scholarship.

On a étudié les systèmes d'électrons π dans quatre composés hétérocycliques azotés d'un type nouveau, riches en électrons, par la méthode des orbitales moléculaires simple. Les énergies de résonance, les densités d'électrons π, et les énergies d'états excités ont été étudiées en fonction du paramètre d'électronégativité de l'azote. Bien qu'il n'y ait, jusqu'à maintenant, qu'un seul des composés dont on ait fait la synthèse, les résultats obtenus suggèrent que tous seraient stables une fois formés. On peut prévoir de façon précise les positions de plus forte réactivité chimique envers les réactifs électrophiles dans le cas des deux composés tricycliques (I) et (II).

Die π-Elektronensysteme in vier elektronenreichen N-Heterozyklen eines neuen Typs wurden mittels einer einfachen MO-Methode untersucht. Die Resonanzenergien, die π-Elektronendichten und die Energien der angeregten Zustände wurden als Funktion des Elektronegativitätsparameters von Stickstoff studiert. Obgleich bisher nur eine der Verbindungen synthetisch dargestellt wurde, sprechen die gegenwärtigen Ergebnisse dafür, dass alle Verbindungen stabil sind. Für die beiden trizyklischen Verbindungen (I) und (II) lassen sich die Stellen höchster chemischer Reaktionsbereitschaft gegenüber elektrophilen Agenzien mit Bestimmtheit voraussagen.

[1] Bassett, I. M., and Brown, R. D., 1954, *J. chem. Soc.*, 2701.
[2] Brown, R. D., 1955, *Aust. J. Chem.*, **8,** 100.
[3] Bassett, I. M., Brown, R. D., and Penfold, A., 1956, *Chem. & Ind.* (*Rev.*), 892.
[4] Brown, R. D., and Heffernan, M. L., 1956, *J. chem. Soc.*, 4288.
[5] Brown, R. D., and Heffernan, M. L., 1957, *Aust. J. Chem.*, **10,** 211.
[6] Boekelheide, V., and Windgassen, R. J., 1958, *J. Amer. chem. Soc.*, **80,** 2020.
[7] Brown, R. D., 1958, *Current Trends in Heterocyclic Chemistry* (London: Butterworths), p. 13.
[8] Brown, R. D., 1956, *J. chem. Soc.*, 272.
[9] Hameka, H. F., and Liquori, A. M., 1958, *Mol. Phys.*, **1,** 9.
[10] Sponer, H., and Teller, E., 1941, *Rev. mod. Phys.*, **13,** 75.

Statistical mechanics of solid and liquid mixtures of ortho- and para-hydrogen

by A. BELLEMANS and AGNESSA BABLOYANTZ
Faculty of Sciences, Université Libre de Bruxelles, Belgium

(*Received* 16 *June* 1958)

It is known from experimental measurements that the configurational free energy of solid and liquid mixtures of p-H_2 and o-H_2 is approximately of the form

$$F_{\mathrm{conf}} = A - Bx_{o\text{-}H_2} - Cx^2_{o\text{-}H_2}$$

where $x_{o\text{-}H_2}$ is the mole fraction of o-H_2. Assuming that this dependence of F_{conf} on $x_{o\text{-}H_2}$ is due solely to orientational forces a quantum-mechanical calculation of F_{conf} is developed which is valid for moderately low temperatures. A simplified statistical model is used consisting of a rigid lattice. The theoretical free energy obtained is however much smaller than the experimental one probably on account of the crudeness of the model. Various refinements are discussed.

1. Introduction

The present paper is devoted to a theoretical study of the thermodynamic properties of solid and liquid mixtures of para- and ortho-hydrogen. Owing to the extremely small rate of transformation of one of these forms into the other they can be considered as two different chemical compounds and their mixtures can be treated as ordinary solutions.

There are strong indications that in condensed phases the average interaction between hydrogen molecules depends on whether they are rotating or not. The vapour pressure of mixtures of p-H_2 and o-H_2 is actually a decreasing function of the mole fraction of o-H_2 at constant temperature [1]. This shows that the *configurational free energy* of such mixtures decreases as the mole fraction of o-H_2 increases. Our final purpose is to obtain a theoretical expression for this free energy. We start from the hypothesis that the intermolecular potential energy between two molecules depends on their distance and relative orientation at a given moment, but not on their rotational states. Under this assumption all dependence of the *configurational free energy* on the mole fraction of o-H_2 is traced to the existence of orientational forces between the molecules.

Throughout this paper we use a rigid lattice model which has already been used for a discussion of the anomalous specific heat of solid mixtures of p-H_2 and o-H_2 [2] by Nakamura [3]. However, the calculations are conducted here in an entirely different way, our goal being the free energy.

All the calculations which follow are valid for H_2, D_2 and T_2. As a rule we avoid using the terms ‘ para- ’ and ‘ ortho- ’ during the calculations. The reason is that some confusion can arise from the fact that for H_2 and T_2 ortho- and para-molecules are respectively in odd and even rotational states while the reverse is true for D_2. As we confine ourselves to systems at moderately low temperatures ($T \leqslant 20^\circ$K) the proportion of molecules in states other than $l=0$ and $l=1$ is completely negligible. Hence we shall speak of molecules ‘ 0 ’ and molecules ‘ 1 ’.

2. THE STATISTICAL MODEL

Consider an assembly of N diatomic homonuclear molecules. Each molecule may rotate in space but its centre of mass is fixed on a site of a regular lattice. These sites are numbered $1, 2, \ldots, i, \ldots, N$.

The existence of the lattice is ensured by central forces between the molecules. This lattice may be conveniently chosen as a cubic face-centred one or an hexagonal close-packed one; hydrogen crystallizes in this last structure.

We further assume that the intermolecular potential between a pair of molecules is independent of their rotational energies. Then if the interactions between neighbouring molecules were independent of their relative orientations they would behave as free rotators and the *configurational free energy* would be independent of the rotational motions of the various molecules. Actually, orientational forces are small. Thus we start with an assembly of free rotating molecules and introduce orientational forces as a perturbation, in order to get the configurational free energy. Moreover, on account of the smallness of the moment of inertia I of hydrogen molecules it is legitimate (up to a temperature of the order of 20°K) to take as unperturbed state an assembly of molecules whose rotational states are either $l=0$ or $l=1$. The present model thus postulates two different energy scales:

(*a*) the energy gap $\sim \hbar^2/2I$ between levels of free-rotating molecules is large compared to kT;

(*b*) the orientational (perturbation) energy between two neighbouring molecules is small compared to kT.

Thus the present model is not valid near the λ-point which occurs in the solid state at $\simeq 1{\cdot}5$°K.

One may argue that the rigid lattice model used here is a poor approximation for a liquid and even for a solid. It may, however, be refined in a straightforward way by allowing lattice vibrations.

We now briefly sketch the lines of the rest of the paper. A general expression for the orientational interactions is given in § 3. The fundamental formulae for the perturbation calculations are given in § 4; the problem is then reduced to the evaluation of a series of matrix elements (§§ 5 and 6). The theoretical expression of the free energy is given in § 7 and compared with the available experimental data in § 8.

3. MOLECULAR INTERACTIONS ON THE LATTICE

A systematic expansion of the potential energy of two axially symmetric molecules i and j in terms of surface harmonics has been given by Pople [4]. In the present case the molecules are

(*a*) homonuclear,

(*b*) identical.

Their interaction energy is given by

$$\epsilon(ij) = \sum_{l_i=0}^{\infty} \sum_{l_j=0}^{\infty} \sum_{m} \zeta^{l_i l_j : m}(r_{ij})\, S_{l_i m}(\bar{\theta}_i, \bar{\phi}_i)\, S_{l_j m}(\bar{\theta}_j, \bar{\phi}_j) \tag{3.1}$$

where

$$S_{lm} = \left\{ (2l+1) \frac{(l-|m|)!}{(l+|m|)!} \right\}^{1/2} P_l^{|m|}(\cos\bar{\theta}) \exp(im\bar{\phi}) \tag{3.2}$$

($P_l^{|m|}$ is the associated Legendre polynomial). Summations are carried out over even values of l_i, l_j and on $|m| \leqslant \min(l_i, l_j)$; r_{ij} is the distance between the centres of the molecules and $\bar{\theta}_i$, $\bar{\phi}_i$, $\bar{\theta}_j$, $\bar{\phi}_j$ are their angular coordinates shown in the figure. This microscopic coordinate system is specific to the pair of molecules i and j and will be called the i–j coordinate system in the rest of this paper.

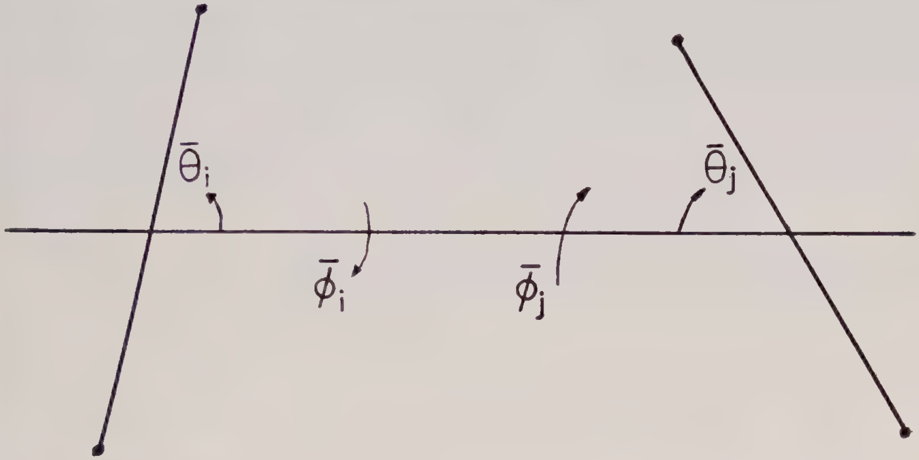

Angular coordinates of interacting molecules i and j; (i–j) coordinate system.

Since $\epsilon(ij)$ is real and an even function of $(\bar{\phi}_i + \bar{\phi}_j)$,

$$\zeta^{ll'\,:\,m} = \zeta^{ll'\,:\,-m}.$$

Further, as i and j are identical,

$$\zeta^{ll'\,:\,m} = \zeta^{l'l\,:\,m}.$$

The coefficients $\zeta^{ll'\,:\,m}$ will be explained later in § 8.

Let a be the distance between neighbouring lattice sites and U the potential energy of the N interacting molecules:

$$U = \sum_{i<j}\sum \epsilon(ij) \tag{3.3}$$

(we limit this summation to nearest neighbour interactions). We now split U into a central part U_0 and an angular part V. From (3.1) we get

$$U_0 = (\tfrac{1}{2})Nz\zeta^{00\,:\,0}(a) \tag{3.4}$$

(z = coordination number of the lattice). All other terms of (3.1) contribute to V but we keep only the $\zeta^{l_il_j\,:\,m}$ where l_i and $l_j \leqslant 2$†.

Further, the terms $\zeta^{20\,:\,0}$ and $\zeta^{02\,:\,0}$ give no contribution to V on account of the symmetry of the lattice; this is proved in Appendix A. V is thus a function of the coefficients $\zeta^{22\,:\,m}$ alone. Defining

$$\eta(ij) = \sum_{m=-2}^{2} \zeta^{22\,:\,m}(a) S_{2m}(\bar{\theta}_i, \bar{\phi}_i) S_{2m}(\bar{\theta}_j, \bar{\phi}_j) \tag{3.5}$$

we have

$$V = \sum_{i<j}\sum \eta(ij). \tag{3.6}$$

V is the perturbational part of the Hamiltonian of the system.

---

† An accurate evaluation of the coefficients $\zeta^{l_il_j\,:\,m}$ from the theory of intermolecular forces seems hopeless for l_i and $l_j > 2$. Moreover, these coefficients would give very small contributions to the partition function for low rotational levels on account of the orthogonality properties of surface harmonics.

4. FORMAL EXPRESSION FOR THE PERTURBATIONAL FREE ENERGY

The Hamiltonian H_N of the system of N interacting molecules can be decomposed into the sum

$$H_N = \sum_{i=1}^{N} H_i^0 + U_0 + V \, ; \tag{4.1}$$

H_i^0 is the Hamiltonian of the free rotating molecule i whose eigenfunctions and eigenvalues are respectively

$$\left.\begin{aligned} Y_{l_i m_i} &= \left\{ \frac{(2l_i+1)}{4\pi} \frac{(l_i-|m_i|)!}{(l_i+|m_i|)!} \right\}^{1/2} P_{l_i}^{|m_i|}(\cos\theta_i) \exp(i m_i \phi_i) \\ \epsilon_{l_i m_i} &= (\hbar^2/2I) l_i (l_i+1) \, ; \end{aligned}\right\} \tag{4.2}$$

θ_i and ϕ_i specify the orientation of the molecule i in a macroscopic coordinate system M; they should not be confused with $\bar{\theta}_i$ and $\bar{\phi}_i$ introduced in § 3.

The unperturbed eigenfunctions of the whole system are

$$Y_{\mathbf{lm}} = \prod_{1}^{N} Y_{l_i m_i}(\theta_i, \phi_i) \tag{4.3}$$

where **l** and **m** are abbreviations to represent the quantum numbers $l_1, \ldots, l_N$ and $m_1, \ldots, m_N$ of the N molecules.

Let E_q be the energy of the unperturbed level q of the whole assembly. The many possible wavefunctions associated with E_q will be numbered $1, \ldots, \rho, \ldots$:

(1) among the N molecules, N_α are in the state l_α, N_β in the state $l_\beta, \ldots$; this can be realized in various ways provided that

$$\sum_\alpha N_\alpha = N \text{ and } E_q = U_0 + (\hbar^2/2I) \sum_\alpha N_\alpha l_\alpha (l_\alpha + 1). \tag{4.4}$$

(2) The number of distinct arrangements of the molecules in states $l_\alpha, l_\beta, \ldots$ on the lattice is

$$N! / \prod_\alpha N_\alpha! \tag{4.5}$$

(3) Each molecule in the state l_α is capable of $2l_\alpha+1$ different wavefunctions. Hence the degeneracy number G_q of E_q is:

$$G_q = \sum_\rho 1 = \sum_{\{N_\alpha\}} \sum_{P(\mathbf{l})} \sum_{\mathbf{m}} 1 = N! \sum_{\{N_\alpha\}} \prod_\alpha \frac{(2l_\alpha+1)^{N_\alpha}}{N_\alpha!} \tag{4.6}$$

where $\sum_{\mathbf{m}}$ is taken over all possible values of $m_1, \ldots, m_N$, $\sum_{P(\mathbf{l})}$ is a summation over all distinct distributions of the states $l_\alpha, l_\beta, \ldots$ between the molecules and $\sum_{\{N_\alpha\}}$ is taken over sets of numbers N_α compatible with (4.4).

A general expression for the quantum mechanical partition function of a perturbed system has been given by Chester [5]. When limited to second order terms in V it reduces to

$$\begin{aligned} Z_N = \sum_q G_q \exp(-\beta E_q) \Big\{ 1 - \beta G_q^{-1} \sum_q V_{q\rho,\, q\rho} \\ + \tfrac{1}{2}\beta^2 G_q^{-1} \sum_\rho \sum_{\rho'} |V_{q\rho, q\rho'}|^2 + \beta G_q^{-1} \sum_{q'}{}' \frac{\sum_\rho \sum_{\rho'} |V_{q\rho,\, q'\rho'}|^2}{E_{q'} - E_q} \Big\} \end{aligned} \tag{4.7}$$

where $\beta = 1/kT$ and $V_{q\rho, q'\rho'}$ is the matrix element of V between the ρth wave function of E_q and the ρ'th wavefunction of E_q'.

Here the unperturbed system is an assembly of N molecules of which N_0 are in the state 0 and N_1 in the state 1 (the contribution of excited states to the partition function being negligible) . Hence we retain only the first term of (4.7); this gives the following perturbational free energy:

$$F_{\text{pert}} = G_0^{-1}\left\{\sum_{\rho} V_{0\rho,0\rho} - \tfrac{1}{2}\beta\sum_{\rho}\sum_{\rho'}|V_{0\rho,0\rho'}|^2 - {\sum_{q'}}' \frac{\sum\limits_{\rho}\sum\limits_{\rho'}|V_{0\rho,\,q'\rho'}|^2}{E_{q'}-E_q} + \tfrac{1}{2}\beta\Big(\sum_{\rho} V_{0\rho,\,0\rho}\Big)^2\right\}. \tag{4.8}$$

The subscript 0 stands for the lowest level and q' for all excited levels of the unperturbed system. G_0 is given by

$$G_0 = \sum_{P(\mathbf{l})}\sum_{\mathbf{m}} 1 = 3^{N_1}\frac{N!}{N_0!N_1!}\,; \tag{4.9}$$

F_{pert} contains four terms; the first one is linear in V and will be proved later to be equal to zero. The same occurs for the fourth one. The second one is related to the splitting of the G_0 times degenerate lowest level into separate ones; the third term involves virtual excitations. The problem is now reduced to an evaluation of the matrix elements of V.

5. MATRIX ELEMENTS OF $\eta(ij)$

We shall employ the following notation

$$V_{q'\rho',q\rho} = \int Y^*_{\mathbf{l}'\mathbf{m}'} V\, Y_{\mathbf{lm}}\, d\Omega^N = \langle \mathbf{l}'\mathbf{m}'|V|\mathbf{lm}\rangle. \tag{5.1}$$

Integration is carried out over all orientations of the N molecules; $Y_{\mathbf{lm}}$ and $Y_{\mathbf{l}'\mathbf{m}'}$ are the eigenfunctions of the unperturbed states $q\rho$ and $q'\rho'$ respectively. In terms of the $\eta(ij)$ we obtain by means of (3.6):

$$V_{q'\rho',q\rho} = \sum_{i<j}\sum \langle l_i'm_i';\, l_j'm_j'|\eta(ij)|l_im_i;\, l_jm_j\rangle \prod_{\substack{h\neq i\\ \neq j}} \delta(l_hm_h;\, l_h'm_h'). \tag{5.2}$$

The matrix elements of $\eta(ij)$ are thus ultimately required. We notice that $\eta(ij)$ depends on $\bar{\theta}_i$ and $\bar{\phi}_i$ while $Y_{l_im_i}$ is expressed in terms of the angles θ_i and ϕ_i in the macroscopic coordinate system M. $Y_{l_im_i}(\theta_i\phi_i)$ is, however, easily expressed in terms of the corresponding functions $\bar{Y}_{l_im_i}(\bar{\theta}_i\bar{\phi}_i)$ by a unitary transformation [6]:

$$\left.\begin{aligned} &Y_{l_im_i} = \sum_{m'_i} a_{m_im_i'}\bar{Y}_{l_im_i'}, \qquad \bar{Y}_{l_im_i'} = \sum_{m_i} a^*_{m_im_i'} Y_{l_im_i}\\ &\qquad\sum_{m_i} a^*_{m_im_i'} a_{m_im_i''} = \delta_{m_i'm_i''}. \end{aligned}\right\} \tag{5.3}$$

The coefficients $a_{m_im_i'}$ depend on the relative orientations of the coordinate systems M and $(i\text{–}j)$ but their explicit values will not be needed further.

We now give three useful properties of the matrix elements of $\eta(ij)$:

(I) $$\langle 0_i0_i;\, l_j'm_j'|\eta(ij)|0_i0_i;\, l_jm_j\rangle = 0 \tag{5.4}$$

whatever the values of l_jm_j, $l_j'm_j'$ are.

(II) $$\sum_{m_i} \langle l_im_i;\, l_j'm_j'|\eta(ij)|l_im_i;\, l_jm_j\rangle = 0 \tag{5.5}$$

whatever the values of l_i, l_jm_j, $l_j'm_j'$ are.

(III) The sum

$$K_{l_il_j,l_i'l_j'} = \sum_{\substack{m_i\\ m_i'}} \sum_{\substack{m_j\\ m_j'}} \frac{\langle l_im_i;\, l_jm_j|\eta(ij)|l_i'm_i';\, l_j'm_j'\rangle^2}{(2l_i+1)(2l_j+1)} \tag{5.6}$$

is independent of the particular coordinate system in which the eigenfunctions for i and j are expressed.

The proof of (I) is trivial; we have

$$Y_{0_i0_i}(\theta_i, \phi_i) = \bar{Y}_{0_i0_i}(\bar{\theta}_i, \bar{\phi}_i) = (4\pi)^{-1/2}$$

and the integration of $\eta(ij)$ over θ_i and ϕ_i yields zero. The proof of (II) follows from (I): as $\eta(ij)$ commutes with the wavefunctions we can transform (5.5) into (5.4) by means of the relation

$$\sum_{m_i} Y^*_{l_im_i} Y_{l_im_i} = (2l_i+1) Y^*_{0_i0_i} Y_{0_i0_i}.$$

Finally (III) is easily proved by the aid of (5.3). The sums $K_{l_i'l_j;l_i'l_j'}$ will be needed later on and their property of invariance (III) considerably simplifies their calculation, by allowing us to choose the simplest coordinate system, i.e. the $(i$–$j)$ one. All sums $K_{l_il_j,l_i'l_j'}$ for l_i and l_j equal to zero or 1 have been studied. The non-vanishing ones are listed below (the result is of course independent of i and j, all pairs of neighbouring molecules being equivalent):

$$\left.\begin{aligned} &K_{00,22} = \zeta_{22}(a); && K_{01,21} = K_{10,12} = \tfrac{2}{5}\zeta_{22}(a),\\ &K_{01,23} = K_{10,32} = \tfrac{3}{5}\zeta_{22}(a); && K_{11,11} = \tfrac{4}{25}\zeta_{22}(a),\\ &K_{11,13} = K_{11,31} = \tfrac{6}{25}\zeta_{22}(a); && K_{11,33} = \tfrac{9}{25}\zeta_{22}(a). \end{aligned}\right\} \tag{5.7}$$

$\zeta_{22}(a)$ is a compact notation for the sum

$$\sum_{m=-2}^{2} [\zeta^{22:m}(a)]^2. \tag{5.8}$$

6. MATRIX ELEMENTS OF V

We now proceed to express the following sums required for F_{pert} in terms of the matrix elements of η:

$$\left.\begin{aligned} &(\text{A}) \qquad \sum_{\rho} V_{0\rho,\,0\rho}\,,\\ &(\text{B}) \qquad \sum_{\rho}\sum_{\rho'} |V_{0\rho,\,0\rho'}|^2,\\ &(\text{C}) \qquad \sum_{\rho}\sum_{\rho'} |V_{0\rho,\,q'\rho'}|^2. \end{aligned}\right\} \tag{6.1}$$

The summation over all degeneracies of the unperturbed system (N_0 molecules 0 and N_1 molecules 1) will be carried out in two steps (cf. § 4):

$$\sum_{\rho} = \sum_{P(1)} \sum_{\mathbf{m}}. \tag{6.2}$$

(*a*) *Sum (A):*

On account of (5.2) and (6.1) we get

$$\sum_{\rho} V_{0\rho,\,0\rho} = \sum_{i<j} \sum_{P(1)} \sum_{\mathbf{m}} \langle l_im_i;\, l_jm_j|\eta(ij)|l_im_i;\, l_jm_j\rangle. \tag{6.3}$$

This expression vanishes because it decomposes itself into a sum of terms of the type (5.5).

(*b*) *Sum* (*B*):

On account of (5.2) and (6.1) we have

$$\sum_{\rho}\sum_{\rho'}|V_{0\rho,0\rho'}|^2=\sum\sum_{i<j}\ \sum\sum_{k<n}\ \sum_{P(\mathbf{l})}\ \sum_{P(\mathbf{l}')}\ \sum\sum_{\mathbf{m}\,\mathbf{m}'}$$
$$\langle l_im_i;l_jm_j|\eta(ij)|l_i'm_i';l_j'm_j'\rangle\langle l_k'm_k';l_n'm_n'|\eta(kn)|l_km_k;l_nm_n\rangle$$
$$\prod_{\substack{h\neq i\\ \neq j}}\delta(l_hm_h;l_h'm_h')\prod_{\substack{h\neq k\\ \neq n}}\delta(l_hm_h;l_h'm_h'). \tag{6.4}$$

Only terms with $i=k$ and $j=n$ have to be kept. If $i\neq k$ we must have $l_im_i\equiv l_i'm_i'$ and $l_km_k\equiv l_k'm_k'$; then there appear partial sums of the type (5.5) which vanish. Further reductions of (6.4) arise from the Kronecker's δ; we finally get by using the definition (5.6):

$$\sum_{\rho}\sum_{\rho'}|V_{0\rho,0\rho'}|^2=\sum\sum_{i<j}3^{N_1}\sum_{P(\mathbf{l})}\sum_{l_i',l_j'}K_{l_il_j,l_i'l_j'} \tag{6.5}$$

where the allowed values of l_i' and l_j' must satisfy the equation

$$l_i'(l_i'+1)+l_j'(l_j'+1)-l_i(l_i+1)-l_j(l_j+1)=0. \tag{6.6}$$

All pairs of neighbouring molecules being equivalent we replace the sum $\sum\sum_{i<j}$ by $\frac{1}{2}Nz$ and the subscripts i,j by 1,2. We then sum over all permutations of the numbers l which is equivalent to summing over all configurations of N_0 molecules 0 and N_1 molecules 1 on the lattice. The number of configurations corresponding to the occupation of the pair of sites 1,2 by two molecules 0, two molecules 1, one molecule 0 and one molecule 1 are, respectively

$$\frac{N!}{N_0!N_1!}x_0^2,\quad \frac{N!}{N_0!N_1!}x_1^2,\quad 2\frac{N!}{N_0!N_1!}x_0x_1, \tag{6.7}$$

where x_0 and x_1 are the mole fractions of components 0 and 1. We finally have by taking account of equation (6.6):

$$\sum_{\rho}\sum_{\rho'}|V_{0\rho,0\rho'}|^2=G_0\tfrac{1}{2}Nz$$
$$\times[x_0^2K_{00,00}+2x_0x_1(K_{01,01}+K_{01,10})+x_1^2K_{11,11}]. \tag{6.8}$$

(*c*) *Sum* (*C*):

In a similar way we obtain

$$\sum_{\rho}\sum_{\rho'}|V_{0\rho,q'\rho'}|^2=G_0\tfrac{1}{2}Nz\Big[x_0^2\sum_{l_1'l_2'}K_{00,l_1'l_2'}$$
$$+2x_0x_1\sum_{l_1'l_2'}K_{01,l_1'l_2'}+x_1^2\sum_{l_1'l_2'}K_{11,l_1'l_2'}\Big] \tag{6.9}$$

where for each sum on $K_{l_1l_2,l_1'l_2'}$ l_1' and l_2' must satisfy the equation

$$l_1'(l_1'+1)+l_2'(l_2'+1)-l_1(l_1+1)-l_2(l_2+1)=E_q-E_0. \tag{6.10}$$

7. PERTURBATIONAL FREE ENERGY

The results of the preceding section combined with the explicit values of the sums $K_{l_1l_2,l_1'l_2'}$ given in § 5 enable us to derive the value of F_{pert}. We have:

$$\tfrac{1}{2}G_0^{-1}\sum_{\rho}\sum_{\rho'}|V_{0\rho,0\rho'}|^2=N\frac{z}{25}\zeta_{22}(a)x_1^2. \tag{7.1}$$

Similarly by collecting terms for which $K_{l_1l_2,l_1'l_2'}$ is different from zero we find:

$$G_0^{-1}\sum_{q'}\frac{\sum_{\rho}\sum_{\rho'}|V_{0\rho,q'\rho'}|^2}{E_{q'}-E_0}=N\frac{z}{24}\frac{\zeta_{22}(a)}{(\hbar^2/2I)}\left[1+\tfrac{1}{2}x_1-\frac{177}{250}x_1^2\right]. \tag{7.2}$$

Hence the perturbational free energy

$$\frac{F_{\text{pert}}}{N} = -\frac{z}{25}\frac{\zeta_{22}(a)}{kT}x_1{}^2 - \frac{z}{24}\frac{\zeta_{22}(a)}{(\hbar^2/2I)}\left(1+\tfrac{1}{2}x_1 - \frac{177}{250}x_1{}^2\right). \qquad (7.3)$$

For the pure components 0 and 1 we have respectively

$$F^0{}_{\text{pert}}/N = -\frac{z}{24}\frac{\zeta_{22}(a)}{(\hbar^2/2I)}. \qquad (7.5)$$

$$F^1{}_{\text{pert}}/N = -\frac{z}{25}\frac{\zeta_{22}(a)}{kT} - \frac{z}{24}\frac{\zeta_{22}(a)}{(\hbar^2/2I)}\frac{99}{125}. \qquad (7.6)$$

In both cases orientational forces increase the stability of the system. However, for the non-rotating molecules 0 the increment of free energy is obtained entirely by virtual transitions from the state $l=0$ to the states $l=2$. For the rotating molecules 1 there exists, besides a term of this kind, an exchange term related to virtual transitions between degenerate states $l=1$; we may perhaps say that some correlations have appeared between the quantum numbers m of two neighbouring molecules 1. This exchange term is the more important one; it is, moreover, inversely proportional to T, thus increasing as the temperature is lowered†.

It is convenient to introduce a quantity ΔF:

$$\Delta F = F_{\text{pert}} - F^0{}_{\text{pert}}$$

for it is this quantity which is obtained experimentally from measurements of the vapour pressure of a liquid or a solid mixture of molecules 0 and 1. Taking $z=12$ and defining

$$k\theta_{\text{rot}} = \hbar^2/2I$$

we have

$$\Delta F/N = -\frac{\zeta_{22}(a)}{k\theta_{\text{rot}}}\left[0\cdot25x_1 + 0\cdot48\left(\frac{\theta_{\text{rot}}}{T} - 0\cdot7375\right)x_1{}^2\right]. \qquad (7.7)$$

8. Comparison with experimental data and conclusions

To make a quantitative estimate of ΔF we need the function $\zeta^{22:m}$. We have listed below the values of the $\zeta^{ll':m}$ for two interacting hydrogen molecules; they have been taken from Nakamura's paper [3].

$$\zeta^{00:0}(r) = \left(83\cdot5\times10^{-1\cdot5330r} - \frac{1\cdot04}{r^6}\right)10^{-11}\,\text{erg},$$

$$\zeta^{20:0}(r) = \left(18\cdot3\times10^{-1\cdot5330r} - \frac{0\cdot055}{r^6}\right)10^{-11}\,\text{erg},$$

$$\zeta^{22:0}(r) = \left(4\cdot0\times10^{-1\cdot5330r} + \frac{0\cdot0336}{r^5} - \frac{0\cdot0086}{r^6}\right)10^{-11}\,\text{erg},$$

$$\zeta^{22:1}(r) = \left(\frac{0\cdot0224}{r^5} - \frac{0\cdot0057}{r^6}\right)10^{-11}\,\text{erg},$$

$$\zeta^{22:2}(r) = \left(\frac{0\cdot0056}{r^5} - \frac{0\cdot0029}{r^6}\right)10^{-11}\,\text{erg},$$

(r is expressed in angstroms in these formulae).

---

† If one is interested in the specific heat C_V this last term alone is needed; hence Nakamura neglected all virtual transitions with excited states [3]. His formula for F_{pert} would reduce to the first term of (7.3).

This total interaction is taken as the sum of three kinds of terms:

(*a*) exchange repulsive forces (exponential term);

(*b*) dispersion forces ($\sim r^{-6}$)†;

(*c*) quadrupole-quadrupole interactions ($\sim r^{-5}$).

This quadrupole term is probably the most accurate one and fortunately gives the dominant contribution to the $\zeta^{22:m}$'s.

Let us first consider mixtures of p-H_2 and o-H_2 ($\theta_{\text{rot}} = 85{\cdot}4\,^\circ\text{K}$). At 20·3 °K the average distance a between neighbouring molecules in liquid hydrogen is nearly equal to 4·05 Å. This gives

$$\zeta_{22}(a) = 17{\cdot}7 \times 10^{-32}\ \text{erg}^2.$$

Hence from (7.7) we get:

$$\Delta G \simeq \Delta F = -0{\cdot}05 x_1 - 0{\cdot}36 x_1^2\ \text{cal mole}^{-1} \tag{8.1}$$

where x_1 is the mole fraction of o-H_2. The corresponding enthalpy and entropy are obtained by differentiating ΔG with respect to T at *constant pressure*. We have thus‡

$$\Delta S = -\left(\frac{\partial \Delta F}{\partial T}\right)_a - \left(\frac{\partial \Delta F}{\partial a}\right)_T \frac{da}{dT}. \tag{8.2}$$

As our model is too crude to provide us with an equation of state we have deduced da/dT from the experimental coefficient of thermal expansion:

$$dv/dT = 0{\cdot}44\ \text{cm}^3\ \text{mole}^{-1}\ \text{deg}^{-1} \text{ at } 20\,^\circ\text{K},$$

$$v\sqrt{2} = Na^3 \text{ (cubic face-centred lattice).}$$

This gives

$$\left.\begin{aligned} T\Delta S &= -0{\cdot}07 x_1 - 0{\cdot}89 x_1^2\ \text{cal mole}^{-1},\\ \Delta H &= -0{\cdot}12 x_1 - 1{\cdot}25 x_1^2\quad ,, \quad . \end{aligned}\right\} \tag{8.3}$$

From the vapour pressure data of Woolley *et al.* [1], Friedman [7] has obtained the following values for ΔG, ΔH and ΔS at 20 °K:

$$\left.\begin{aligned} \Delta G &= -0{\cdot}89 x_1 - 1{\cdot}13 x_1^2\ \text{cal mole}^{-1},\\ \Delta H &= -0{\cdot}9 x_1 - 3{\cdot}1 x_1^2\ \text{cal mole}^{-1},\\ T\Delta S &= -0{\cdot}0 x_1 - 2{\cdot}0 x_1^2\ \text{cal mole}^{-1}. \end{aligned}\right\} \tag{8.4}$$

ΔS and ΔH are much less accurate than ΔG because they have been obtained by a differentiating process. From an analysis of latent heats of vaporization by Woolley, Scott and Brickwedde [1] it is found that

$$\Delta H \simeq -1{\cdot}4 x_1 - 2{\cdot}8 x_1^2\ \text{cal mole}^{-1} \tag{8.4$'$}$$

which combined with Friedman's value of ΔG gives

$$T\Delta S \simeq -0{\cdot}5 x_1 - 1{\cdot}7 x_1^2\ \text{cal mole}^{-1}. \tag{8.4$''$}$$

The quantitative agreement between the calculated and the experimental thermodynamic functions is very poor. The theoretical terms proportional to x_1^2 are too small by a factor of 2 or 3 while the discrepancy is still larger for terms proportional to x_1.

---

† Higher terms in r^{-8}, r^{-10}, . . . have not been included as they may reasonably be expected to be smaller than the r^{-6} term. The latter is already small compared to the dominant quadrupolar contribution.

‡ We assume here that the lattice distance a may vary with temperature (and pressure).

The same disagreement is obtained for solid hydrogen at 13·8°K. Here $a=3{\cdot}80$ Å and

$$\zeta_{22}(a)=35{\cdot}4\times 10^{\ 32}\,\mathrm{erg}^2.$$

This leads to the theoretical free energy

$$\Delta G=-0{\cdot}1x_1-1{\cdot}1x_1{}^2\,\mathrm{cal\,mole}^{-1},$$

whereas a very rough estimation from vapour pressure data gives

$$\Delta G\simeq -0{\cdot}7x_1-2{\cdot}6x_1{}^2\,\mathrm{cal\,mole}^{-1}.$$

The lack of experimental data does not permit us to discuss the case of o-D_2 and p-D_2 mixtures. The vapour pressure has been measured but at a single composition : 33 per cent p-D_2. It indicates that $|\Delta G|$ is larger for D_2 than for H_2 at the same temperature. This is in qualitative agreement with our model; we have in effect for liquid D_2 at 20°K:

$$a=3{\cdot}80\,\text{Å},$$

$$\zeta_{22}(a)=35{\cdot}4\times 10^{-32}\,\mathrm{erg}^2.$$

The characteristic temperature of rotation of D_2 is

$$\theta_{\mathrm{rot}}=42{\cdot}7°.$$

This leads to

$$\Delta G=-0{\cdot}22x_1-0{\cdot}57x_1{}^2\,\mathrm{cal\,mole}^{-1}$$

which is larger than (8.1).

As there is poor agreement between experimental and theoretical values of ΔG, ΔH and ΔS we must now look for some refinements of the statistical model.

The smallness of the theoretical quadratic terms of ΔG, ΔH and ΔS may be due to:

(*a*) an inaccurate knowledge of the functions $\zeta^{22:m}$;

(*b*) the rigidity of the lattice; preliminary calculations have shown that a vibrating lattice model leads to a higher value of $|\Delta G|$.

The theoretical terms proportional to x_1 are so small compared to the experimental ones that we may think that some effect has been 'forgotten'. Two possibilities may be suggested:

(*a*) the function $\zeta^{20:0}$ gives no contribution because of the rigidity of the lattice; for a more realistic model where the centre of mass of the molecules can move $\zeta^{20:0}$ gives rise to a term proportional to x_1 in ΔG;

(*b*) the intermolecular field between pairs of molecules could be somewhat different for rotating and non-rotating ones. In fact, the polarizability is somewhat changed by the rotational motion; this would modify to some extent the dispersion forces† [8, 9].

The present model can quite easily be modified in order to take account of the refinements discussed above. Further calculations are in hand which give rise to the hope that agreement with experiment will be largely improved.

We would like to express our gratitude to Professor I. Prigogine, who suggested this work, for constant interest and advice.

The research reported in this publication has been made possible through the support of The General Electric Research Laboratory, Schenectady, N.Y., through its European Office.

---

† We are indebted to Mr. Harry Friedman for suggesting this effect.

APPENDIX

On a regular lattice consider a central molecule (called 0) and its z first neighbours numbered $1, \ldots, i, \ldots, z$. The interaction energy of the type $\zeta^{20:0}$ between the molecule 0 and its neighbours is (cf. § 3.):

$$\zeta^{20:0}(a) \sum_{i=1}^{z} S_{20}(\bar{\theta}_0^{(i)}, \bar{\phi}_0^{(i)}) \; ; \tag{A 1}$$

$\bar{\theta}_0^{(i)}$ and $\bar{\phi}_0^{(i)}$ determine the orientation of the molecule 0 in the coordinate system $(0\text{–}i)$; see figure 1. Let us choose a new macroscopic coordinate system M centred on the lattice site 0. In M let θ_0, ϕ_0 be the angular coordinates of the molecule 0 and $\alpha_1, \beta_1, \ldots, \alpha_i, \beta_i, \ldots$ the angular coordinates of the lattice sites $1, \ldots, i, \ldots$. The relation

$$\cos \bar{\theta}_0^{(i)} = \cos \theta_0 \cos \alpha_i + \sin \theta_0 \sin \alpha_i \cos (\phi_0 - \beta_i) \tag{A 2}$$

permits us to transform (A1) into

$$\zeta^{20:0}(a) \sum_{m=-2}^{2} S_{2m}(\theta_0, \phi_0) \left[\frac{1}{\sqrt{5}} \sum_{i=1}^{z} S_{2m}(\alpha_i, \beta_i) \right] \tag{A 3}$$

by the aid of the Addition Theorem of Legendre polynomials. The sum in brackets depends on the lattice structure only and may be put equal to some constant A_m; a closed form for (A 1) is then:

$$\zeta^{20:0}(a) \sum_{m=-2}^{2} A_m S_{2m}(\theta_0, \phi_0). \tag{A 4}$$

Now this expression depends on the orientation of the molecule 0 in the field of its neighbours and should present at least the same symmetry as the lattice itself. For cubic and hexagonal close-packed lattices this is not the case. Hence all the coefficients A_m must be identically zero (as it may be verified numerically). This shows that the coefficient $\zeta^{20:0}$ does not contribute to V.

On sait, à partir de mesures expérimentales, que l'énergie libre configurationnelle des mélanges, solides ou liquides, de p-H_2 et de o-H_2 est approximativement de la forme

$$F_{\mathrm{conf}} = A - Bx_{o\text{-}H_2} - Cx^2_{o\text{-}H_2}$$

où $x_{o\text{-}H_2}$ est la fraction molaire de o-H_2. On a développé par la mécanique quantique, et en supposant que F_{conf} dépend de $x_{o\text{-}H_2}$ par la seule présence de forces d'orientation, un calcul, valable pour des températures modérément basses, de F_{conf}. Un modèle statistique simple, celui d'un réseau rigide, est utilisé. Cependant l'énergie libre théorique obtenue est beaucoup plus petite que l'énergie expérimentale, probablement du fait de la grande simplicité du modèle. On discute diverses améliorations.

Aus Messdaten ist bekannt, dass die konfigurationelle freie Energie von festen und flüssigen Mischungen von p-H_2 und o-H_2 annähernd der Beziehung

$$F_{\mathrm{conf}} = A - Bx_{o\text{-}H_2} - Cx^2_{o\text{-}H_2}$$

genügt, wobei $x_{o\text{-}H_2}$ der Molenbruch des o-H_2 ist. Unter der Annahme, dass diese Abhängigkeit zwischen F_{conf} und $x_{o\text{-}H_2}$ ausschliesslich auf Richtkräfte zurückgeht, wird eine quantenmechanische Rechnung entwickelt, die für einigermassen niedrige Temperaturen gültig ist. Ein vereinfachtes statistisches Modell wird benutzt, das von einem starren Gitter ausgeht. Die errechnete freie Energie ist jedoch erheblich kleiner als die gefundene, wahrscheinlich infolge der groben Vereinfachungen des Modelles. Verschiedene Verfeinerungen werden erörtert.

REFERENCES

[1] WOOLLEY, H. W., SCOTT, R. B., and BRICKWEDDE, F. G., 1948, *J. Res. nat. Bur. Stand.*, **41,** 379.

[2] HILL, R. W., and RICKETSON, W. A., 1954, *Phil. Mag.*, **45,** 277.

[3] NAKAMURA, T., 1955, *Progr. theor. Phys., Osaka*, **14,** 135.

[4] POPLE, J. A., 1953, *Disc. Faraday Soc.*, **15,** 35.

[5] CHESTER, G. V., 1954, *Phys. Rev.*, **93,** 606.

[6] HIRSCHFELDER, J. O., CURTISS, C. F., and BIRD, R. B., 1954, *The Molecular Theory of Gases and Liquids* (New York: Wiley & Sons), p. 909.

[7] FRIEDMAN, HAROLD L., 1957, *J. chem. Phys.*, **27,** 220.

[8] ISHIGURO, E., ARAI, T., KOTANI, M., and MIZUSHIMA, M., 1952, *Proc. phys. Soc. Lond.* A, **65,** 178.

[9] MARGENAU, H., 1943, *Phys. Rev.*, **63,** 385; *Ibid.*, **64,** 131.

On the motion of a particle coupled to lattice vibrations

by THOR A. BAK†, M. GOCHE and F. HENIN‡
Faculté des Sciences, Université Libre de Bruxelles, Belgium

(*Received* 14 *October* 1958)

The approach to equilibrium of a particle interacting with the vibrations of an equilibrium lattice is studied using the methods developed by Prigogine and co-workers. For a low energy particle it is found that the approach to equilibrium is characterized by a relaxation time which is proportional to the square of the mass of the particle, and that the autocorrelation function is a simple exponential function. For a high energy particle no ordinary relaxation time exists, and the apparent relaxation time increases proportionally to the three halves power of the energy of the particle, and is inversely proportional to the square root of its mass. The fact that it depends on the energy is understood when one considers the number of phonons with frequencies high enough to make interaction possible.

1. Introduction

In a recent paper Brout and Prigogine [1] have proposed a general theory for irreversible processes in weakly coupled systems. Applications of the method have been published by Prigogine and Balescu [2], who studied the Brownian motion of a normal mode in a lattice, and by Prigogine and Philippot [3], who discussed thermal conductivity of crystals. In this paper we shall study the motion of a particle in a lattice of weakly coupled harmonic oscillators. Only the two limiting cases will be treated here, namely the case where the energy of the particle is small compared to the height of the potential barrier between two equilibrium positions in the lattice, and the case where the energy of the particle is large compared to this energy. In the first case the particle executes a Brownian motion, and the present work makes a connection with the abovementioned paper of Prigogine and Balescu. In both cases we study only the approach to equilibrium of a homogeneous system. We hope later to be able to deal with the general problem of a potential barrier of finite height.

Let us first briefly summarize the method. The Hamiltonian is written in action-angle variables in the following way:

$$\begin{aligned}\mathscr{H} &= H_L + H_P + \lambda V \\ &= \sum \omega_i J_i + \omega J + \lambda \sum_{\{n\},\,\nu} V_{\{n\},\,\nu}(J_1 \ldots J_N) \exp\left(i \textstyle\sum_k n_k \alpha_k + \nu\alpha\right) \qquad (1)\end{aligned}$$

where ω_i and J_i $(i = 1 \ldots N)$ are the frequencies and the action variables for the lattice, ω and J are the frequency and the action variable for the particle, and the last term is the Fourier expansion in the angle variables α_i and α of the interaction between the particle and the lattice.

---

† On leave of absence from Institute for Physical Chemistry, University of Copenhagen, Copenhagen, Denmark.

‡ Aspirant du Fonds national de la Recherche scientifique Belge.

Liouville's equation is

$$i\frac{\partial}{\partial t}\rho=L\rho$$

where L is the Liouville operator in action-angle variables:

$$L=i\sum_k\left(\frac{\partial\mathscr{H}}{\partial\alpha_k}\frac{\partial}{\partial J_k}-\frac{\partial\mathscr{H}}{\partial J_k}\frac{\partial}{\partial\alpha_k}\right)+i\left(\frac{\partial\mathscr{H}}{\partial\alpha}\frac{\partial}{\partial J}-\frac{\partial\mathscr{H}}{\partial J}\frac{\partial}{\partial\alpha}\right). \tag{2}$$

We now split the Liouville operator into two parts corresponding to the unperturbed Hamiltonian and the perturbation. For the unperturbed operator we have simply:

$$L_0=-i\sum_k\omega_k\frac{\partial}{\partial\alpha_k}-i\omega\frac{\partial}{\partial\alpha}$$

so that the solution of the non-perturbed Liouville equation is

$$\sum_{\{n\},\nu}\rho_{\{n\},\nu}(J_1\ldots J_N,J)\exp\left[i\textstyle\sum_k n_k(\alpha_k-\omega_k t)+i\nu(\alpha-\omega t)\right]. \tag{3}$$

To solve the perturbed Liouville equation we use a time-dependent perturbation technique; letting the $\rho_{\{n\},\nu}$ be functions of t we obtain

$$\frac{\partial\rho_{\{n\},\nu}}{\partial t}=\lambda\sum_{\{n'\},\nu'}\exp\left[i\textstyle\sum_k(n_k\omega_k-n_k'\omega_k)t+i(\nu\omega-\nu'\omega)t\right]\langle\{n\},\nu|\delta L|\{n'\},\nu'\rangle\rho_{\{n'\},\nu'}. \tag{4}$$

Here the matrix element $\langle\{n\},\nu|\delta L|\{n'\},\nu'\rangle$ is a differential operator acting on the action variables (see [1], equation (2.11)).

These equations are solved [1] by an iteration method for the special case of an initially homogeneous system, i.e. a system where the density is angle-independent. It is then shown that this solution satisfies an equation of the Fokker–Planck type

$$\frac{\partial\rho_{\{0\},0}}{\partial t}=\lambda^2\sum_{\{n\},\nu}{}'\langle\{0\},0|\delta L|\{n\},\nu\rangle\langle\{n\},\nu|\delta L|\{0\},0\rangle\rho_{\{0\},0}. \tag{5}$$

The summation on the right-hand side extends only over transitions which conserve the sum of frequencies.

This equation contains no longer explicitly the time on the right-hand side, and the evolution described by this equation is therefore a systematic one, which after a time of order $\lambda^2 t$ brings the system to equilibrium.

Since a system which is initially homogeneous remains homogeneous, we have only one density function $\rho_{\{0\},0}$, and we shall therefore in general drop the index $\{0\},0$.

2. Low energy particle

We consider the motion of a particle whose energy is small compared to the maximum interaction energy. We therefore can consider the unperturbed motion of the particle as a motion in a harmonic potential with spring constant γ. The distance from its equilibrium position is r, and its total energy (neglecting interaction with the lattice) is therefore:

$$H_P=\frac{1}{2m}p^2+\tfrac{1}{2}\gamma r^2.$$

Introducing the action-angle variables

$$J = \frac{1}{2\pi}\oint p\,dr \quad \text{and} \quad \alpha = \frac{\partial W}{\partial J}$$

where

$$W = \sqrt{(m\gamma)}\int dr\sqrt{\left(\frac{2H}{\gamma} - r^2\right)}$$

is Hamilton's characteristic function, we obtain

$$r = \left(\frac{2H}{\gamma}\right)^{1/2}\sin\alpha = r_0\sin\alpha,$$

$$J = H\left(\frac{m}{\gamma}\right)^{1/2}.$$

The total energy of lattice plus particle is

$$\mathscr{H} = \sum \omega_i J_i + H_P + \lambda V$$

where J_i and ω_i are the action variable and the frequency of the ith normal mode of the lattice, and V is the interaction energy between particle and lattice. λ is a dimensionless parameter which measures the strength of the interaction.

For V we take, as is usually done in the theory of the solid state [4],

$$V(r) = \sum W(r - \alpha_n)u_n$$

where u_n is the displacement of the nth particle, $r - a_n$ the distance between the particle and the nth lattice point and $W(r - a_n)$ is the force exerted on the particle by an infinitesimal displacement of the nth particle. Expressing u_n in normal coordinates q_f we obtain ([4], p. 125):

$$V = \sum_f V_f q_f \exp(ifr)$$

with

$$V_f = \sum_n W(r - a_n)\exp[-f(r - a_n)].$$

As an approximation we take V_f to be independent of r for all values of f.

We have then

$$V = \sum_f V_f q_f \exp(ifr) = \sum_m \sum_f [V_{mf}{}^{+}\exp i(\alpha_f + m\alpha) + V_{mf}{}^{-}\exp i(-\alpha_f + m\alpha)] \qquad (6)$$

with

$$V_{mf}{}^{+} = V_f q_{f+}{}^{0} J_m(fr_0),$$
$$V_{mf}{}^{-} = V_f q_{f-}{}^{0} J_m(fr_0).$$

The last expression for V is obtained from the first by using

$$q_f = q_{f+}{}^{0}\exp(i\alpha_f) + q_{f-}{}^{0}\exp(-i\alpha_f)$$

and Fourier expanding $\exp(ifr)$ to get $\exp(ifr) = \sum_m J_m(fr_0)\exp(im\alpha)$ where $J_m(fr_0)$ is the mth Bessel function. Since V is real we have $q_{f+}{}^{0} = (q_{f-}{}^{0})^*$ and $V_{-f} = V_f{}^*$.

To the perturbation λV in the total energy corresponds a perturbation $\lambda\delta L$ in the Liouville operator (2), written in angle-action variables, which is

$$\begin{aligned}\delta L = {} & i\sum_m\sum_f \frac{\partial V_{mf}{}^{-}}{\partial J_f}\exp i(\alpha_f + m\alpha)\frac{\partial}{\partial\alpha_f} + \sum_m\sum_f V_{mf}{}^{+}\exp i(\alpha_f + m\alpha)\frac{\partial}{\partial J_f} \\ & + i\sum_m\sum_f \frac{\partial V_{mf}{}^{-}}{\partial J_f}\exp i(-\alpha_f + m\alpha)\frac{\partial}{\partial\alpha_f} - \sum_m\sum_f V_{mf}{}^{-}\exp i(-\alpha_f + m\alpha)\frac{\partial}{\partial J_f} \\ & + i\sum_m\sum_f \frac{\partial V_{mf}{}^{+}}{\partial J}\exp i(\alpha_f + m\alpha)\frac{\partial}{\partial\alpha} + \sum_m\sum_f mV_{mf}{}^{+}\exp i(\alpha_f + m\alpha)\frac{\partial}{\partial J} \\ & + i\sum_m\sum_f \frac{\partial V_{mf}{}^{-}}{\partial J}\exp i(-\alpha_f + m\alpha)\frac{\partial}{\partial\alpha} + \sum_m\sum_f mV_{mf}\exp i(-\alpha_f + m\alpha)\frac{\partial}{\partial J}. \qquad (7)\end{aligned}$$

The only two interaction processes between the lattice and the particle which give non-vanishing matrix elements are the processes where the particle changes its momentum by creating or absorbing a phonon. The Feynman diagrams corresponding to these are (time running from right to left):

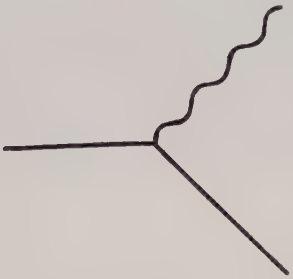

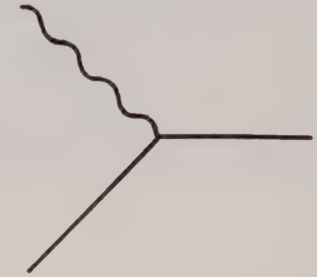

To the creation of a phonon with wave vector f corresponds for instance the matrix element

$$\langle\{n_i=0\},\ n_f=0;\ m=0|\delta L|\{n_i=0\},\ n_f=1;\ m=\nu\rangle=-\left(\frac{\partial}{\partial J_f}+\nu\frac{\partial}{\partial J}\right)V_{-\nu,-f}^{-} \quad (8\,\mathrm{a})$$

$\{n_i=0\}$ means all n except n_f equal to zero.

The other three matrix elements which are of interest are

$$\langle\{n_i=0\},\ n_f=0;\ m=0|\delta L|\{n_i=0\},\ n_f=-1;\ m=\nu\rangle=\left(\frac{\partial}{\partial J_f}-\nu\frac{\partial}{\partial J}\right)V_{-\nu,-f}^{-}, \quad (8\,\mathrm{b})$$

$$\langle\{n_i=0\},\ n_f=1;\ m=\nu|\delta L|\{n_i=0\},\ n_f=0;\ m=0\rangle=V_{\nu,f}^{+}\left(\frac{\partial}{\partial J_f}+\nu\frac{\partial}{\partial J}\right), \quad (8\,\mathrm{c})$$

$$\langle\{n_i=0\},\ n_f=-1;\ m=\nu|\delta L|\{n_i=0\},\ n_f=0;\ m=0\rangle=-V_{\nu,f}^{+}\left(\frac{\partial}{\partial J_f}-\nu\frac{\partial}{\partial J}\right). \quad (8\,\mathrm{d})$$

From these we can construct the matrix elements corresponding to the diagrams:

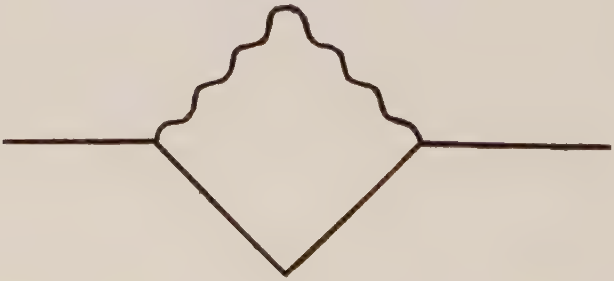

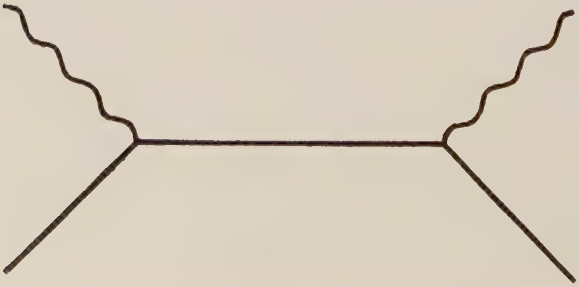

They are

$$\left(\frac{\partial}{\partial J_f}+\nu\frac{\partial}{\partial J}\right)|V_{\nu,f}|^2\left(\frac{\partial}{\partial J_f}+\nu\frac{\partial}{\partial J}\right) \tag{9 a}$$

and

$$\left(\frac{\partial}{\partial J_f}-\nu\frac{\partial}{\partial J}\right)|V_{\nu,f}|^2\left(\frac{\partial}{\partial J_f}-\nu\frac{\partial}{\partial J}\right). \tag{9 b}$$

These are the only processes which correspond to the evolution as long as only powers of $\lambda^2 t$ are retained.

We now add these two processes and sum over all transitions which conserve the sum of frequencies. In this way we get the final equation for ρ, the density in action space:

$$\frac{\partial\rho}{\partial t}=\pi\lambda^2\left(\frac{L}{2\pi}\right)\sum_\nu\int d\omega_f\,\frac{\partial f}{\partial\omega_f}\left\{\left(\frac{\partial}{\partial J_f}+\nu\frac{\partial}{\partial J}\right)|V_{\nu,f}|^2\,\delta(\nu\omega+\omega_f)\left(\frac{\partial}{\partial J_f}+\nu\frac{\partial}{\partial J}\right)\right.$$
$$\left.+\left(\frac{\partial}{\partial J_f}-\nu\frac{\partial}{\partial J}\right)|V_{\nu,f}|^2\,\delta(\nu\omega-\omega_f)\left(\frac{\partial}{\partial J_f}-\nu\frac{\partial}{\partial J}\right)\right\}\rho$$

where we have replaced the summation over f by an integration, thereby getting the density factor in f-space $L/2\pi$ and subsequently changed the variable of integration from f to ω_f.

We now use the fact that

$$|V_{\nu,f}|^2=|V_f|^2\,|q_f|^2 J_\nu^{\,2}(fr_0) \tag{10}$$

and

$$|q_f|^2=\frac{J_f}{M^{(N)}\omega_f} \tag{11}$$

where $M^{(N)}$ is the total mass of the lattice. Also we have

$$\sum_{\nu=-\infty}^{+\infty}\nu^2 J_\nu^{\,2}(\nu z)=\frac{z^2(4+z^2)}{8(1-z^2)^{1/2}} \tag{12}$$

a result due to Schott ([7] p. 573). Since in our case $|z|$ has the value $\omega r_0/c\ll 1$, we shall replace the expression on the right-hand side by $\frac{1}{2}z^2$.

Following Peierls ([4], p. 130) we shall finally assume that $|V_f|^2/\omega_f^{\,2}$ is a constant. It is convenient to introduce the abbreviations

$$\kappa=\lambda^2\frac{|V_f|^2}{\omega_f^{\,2}}\qquad\text{and}\qquad\mu=\frac{M^{(N)}}{L}.$$

κ and μ are then constants independent of N, the number of particles in the lattice.

We now simplify the equations by assuming that the lattice is in equilibrium so that we can set

$$\rho=\phi(J,t)\exp\left(-\frac{1}{kT}\sum\omega_f J_f\right).$$

Using a Debye spectrum, that is, setting $\partial\omega_f/\partial f=c$, the velocity of sound, we obtain by integrating over ω_f and summing over ν, and setting $\omega_f J_f=kT$,

$$\frac{\partial\phi}{\partial t}=\frac{\kappa\,kT}{\mu c^3 m}\frac{\partial}{\partial J}\omega J\left(\frac{\omega}{kT}+\frac{\partial}{\partial J}\right)\phi. \tag{13}$$

This equation can be simplified by introducing the dimensionless energy $x=\omega J/kT$ and the dimensionless time $\tau=t/\tau_c$, with

$$\tau_c=\frac{\mu c^3 m^2}{\kappa\gamma} \tag{14}$$

where m is the mass of the particle. We then have

$$\frac{\partial\phi}{\partial\tau}=\frac{\partial}{\partial x}x\left(1+\frac{\partial}{\partial x}\right)\phi. \tag{15}$$

The equation for ϕ is solved using the Laguerre polynomials. We get

$$\phi = \exp(-x) \sum c_n \exp(-n\tau) L_n(x).$$

It is seen that when $\tau \to \infty$, ϕ approaches the equilibrium distribution $\exp(-x)$.

In particular the solution which reduces to $\delta(x-x_0)$ at $\tau=0$ is

$$\phi = \exp(-x) \sum \exp(-n\tau) L_n(x) L_n(x_0). \tag{16}$$

This is seen using the completeness relation for the Laguerre functions. Using well-known formulae ([5], p. 189) we find for this solution

$$\int_0^\infty \phi x^n \, dx = n! \, [1-\exp(-\tau)]^n \, L_n\left(-\frac{x_0 \exp(-\tau)}{1-\exp(-\tau)}\right) \tag{17}$$

from which all moments of the distribution can be calculated. In particular we have

$$\bar{x} = 1 - \exp(-\tau) + x_0 \exp(-\tau),$$

$$\overline{x^2} = (1-\exp(-\tau))^2 \left[2 + 4\frac{x_0 \exp(-\tau)}{1-\exp(-\tau)} + \frac{x_0{}^2 \exp(-2\tau)}{(1-\exp(-\tau))^2} \right].$$

The autocorrelation function at equilibrium is

$$C(\tau) = \overline{x(t+\tau)x(t)}^{\text{eq}} - (\bar{x}^{\text{eq}})^2,$$

and since $\bar{x}^{\text{eq}} = \lim\limits_{t\to\infty} \bar{x} = 1$ and $\overline{x^2}^{\text{eq}} = \lim\limits_{t\to\infty} \overline{x^2} = 2$ we get $C(\tau) = \exp(-\tau)$.

We have therefore here, as in the work by Prigogine and Balescu, a Markoffian process which has an exponential autocorrelation function. This is an unexpectedly simple result, since the stochastic process which we consider is not Gaussian, and it is known, that a sufficient condition for an exponential autocorrelation function is that the Markoffian process is Gaussian [6].

3. HIGH ENERGY PARTICLE

We now consider the motion of a particle whose energy is high compared to the maximum interaction energy so that we can neglect the periodic variations of the latter. The energy of the particle is then simply:

$$H_P = \frac{1}{2m} p^2.$$

As action-angle variables for the particle we choose $\mathbf{p}$ and $\mathbf{r}$, and we have:

$$\mathscr{H} = \tfrac{1}{2}\mathbf{pv} + \sum \omega_f J_f + \lambda V$$

where $\mathbf{v} = \dot{\mathbf{r}}$ is the velocity of the particle.

For the lattice we have

$$q_f = \left(\frac{J_f}{M^{(N)} \omega_f} \right)^{1/2} \exp(i\alpha_f)$$

where $\mathbf{f}$ is the wave vector.

The normalized eigenfunctions of the unperturbed Liouville operator are:

$$\frac{1}{L^{3/2}} \exp\{i\mathbf{fr} + i \sum n_k \alpha_k\}$$

and the Fourier expansion of the perturbing potential is

$$V = \frac{1}{L^3} \sum V_f q_f \exp(i\mathbf{fr}).$$

In these expressions L^3 is the volume of the system.

Using the same matrix elements as above we obtain:

$$\frac{\partial\rho}{\partial t}=\pi\lambda^2\frac{1}{(2\pi)^3L^3}\int d\mathbf{f}\left\{\left(\frac{\partial}{\partial J_f}+\mathbf{f}\frac{\partial}{\partial\mathbf{p}}\right)|V_f|^2\frac{J_f}{M^{(N)}\omega_f}\delta(\omega_f+\mathbf{fv})\left(\frac{\partial}{\partial J_f}+\mathbf{f}\frac{\partial}{\partial\mathbf{p}}\right)\right.$$
$$\left.+\left(\frac{\partial}{\partial J_f}-\mathbf{f}\frac{\partial}{\partial\mathbf{p}}\right)|V_f|^2\frac{J_f}{M^{(N)}\omega_f}\delta(\omega_f-\mathbf{fv})\left(\frac{\partial}{\partial J_f}-\mathbf{f}\frac{\partial}{\partial\mathbf{p}}\right)\right\}\rho. \tag{19}$$

When we set

$$\rho=\phi(\mathbf{p},t)\exp\left(-\frac{1}{kT}\sum\omega_fJ_f\right) \tag{20}$$

we get:

$$\frac{\partial\phi}{\partial t}=\frac{2\pi\lambda^2|V_f|^2kT}{M^{(N)}\omega_f{}^2(2\pi)^3L^3}\int d\mathbf{f}\,\mathbf{f}\frac{\partial}{\partial\mathbf{p}}\delta\left(\omega_f+\frac{1}{m}\mathbf{fp}\right)\left(-\frac{\omega_f}{kT}+\mathbf{f}\frac{\partial}{\partial\mathbf{p}}\right)\phi.$$

The integral is evaluated using polar coordinates in **f**-space. With a Debye spectrum we obtain

$$\frac{\partial\phi}{\partial t}=\frac{\lambda^2}{8\pi}\frac{|V_f|^2}{\omega_f{}^2}\frac{kT\omega_{\mathrm{D}}{}^4m^3}{M^{(N)}c^2L^3}\frac{1}{p}\mathbf{p}\frac{\partial}{\partial\mathbf{p}}\frac{1}{p^2}\left[\frac{1}{mkT}+\frac{1}{p^2}\mathbf{p}\frac{\partial}{\partial\mathbf{p}}\right]\phi. \tag{21}$$

From this it is seen that $\partial\phi/\partial t=0$ for the equilibrium distribution

$$\phi=\exp\left[-(p^2/2mkT)\right].$$

To bring out clearly the interesting features of this equation we consider the solutions which depend only on p and t. Setting $\phi=\exp(-p^2/2mkT)\psi(p,t)$ and introducing the dimensionless momentum $y=p/\sqrt{(mkT)}$ and the dimensionless time

$$s=\frac{\lambda^2}{8\pi}\frac{|V_f|^2}{\omega_f{}^2}\frac{\omega_{\mathrm{D}}{}^4(kT)^{3/2}}{M^{(N)}L^3c^2m^{1/2}}t=t/t_0, \tag{22}$$

we obtain

$$\frac{\partial}{\partial s}\psi=y^{-3}\frac{\partial}{\partial y^2}\psi-(y^{-2}+3y^{-4})\frac{\partial}{\partial y}\psi. \tag{23}$$

This equation is meaningful only in the limit $y\to\infty$, since it was assumed in the derivation that the energy of the particle is very high. We have not yet been able to solve this equation, but even without the complete solution one can use it to find the rate at which the particle loses energy to the lattice. To get an estimate of $\overline{d(p^2)/ds}$ we shall assume ϕ to be $\delta(y-y_0)$ where y_0 is a function of t. We then have

$$\begin{aligned}\frac{\overline{d(y^2)}}{ds}&=\int_0^\infty y^2\frac{\partial}{\partial s}\phi\,dy\\&=\int_0^\infty y^2\exp(-y^2/2)\left\{y^{-3}\frac{\partial^2}{\partial s^2}-(y^{-2}+3y^{-1})\frac{\partial}{\partial s}\right\}\exp(y^2/2)\delta(y-y_0)\,dy\\&=-\frac{2}{y_0}+\mathrm{O}(y_0{}^{-3}).\end{aligned} \tag{24}$$

The last term is neglected and we have the apparent relaxation time

$$\begin{aligned}-\left[\frac{1}{y^2}\frac{\overline{d(y^2)}}{dt}\right]^{-1}&=\frac{t_0}{2}y^3\\&=\frac{8\pi\sqrt{2}}{\lambda^2}\frac{\omega_f{}^2}{|V_f|^2}\frac{M^{(N)}L^3c^2}{\omega_{\mathrm{D}}{}^4}\frac{1}{m^{1/2}}\left(\frac{1}{2m}p^2\right)^{3/2}.\end{aligned} \tag{25}$$

It should be pointed out that this is not a real relaxation time, since it depends on the energy of the particle.

4. CONCLUSION

The most striking difference between the two cases discussed above is the fact that the apparent relaxation time for the high energy particle depends on its energy. Although this kind of relaxation hardly can be observed experimentally since collisions with lattice vibrations only contribute very little to the stopping of a high energy particle, it is nevertheless interesting to compare (14) with (25). It is intuitively clear that the rate with which a high energy particle loses energy to the lattice vibrations must depend on the energy of the particle, since the higher the energy of the particle, the fewer phonons there are with a frequency sufficiently high to make an interaction possible. The relaxation time must therefore increase with the energy of the particle.

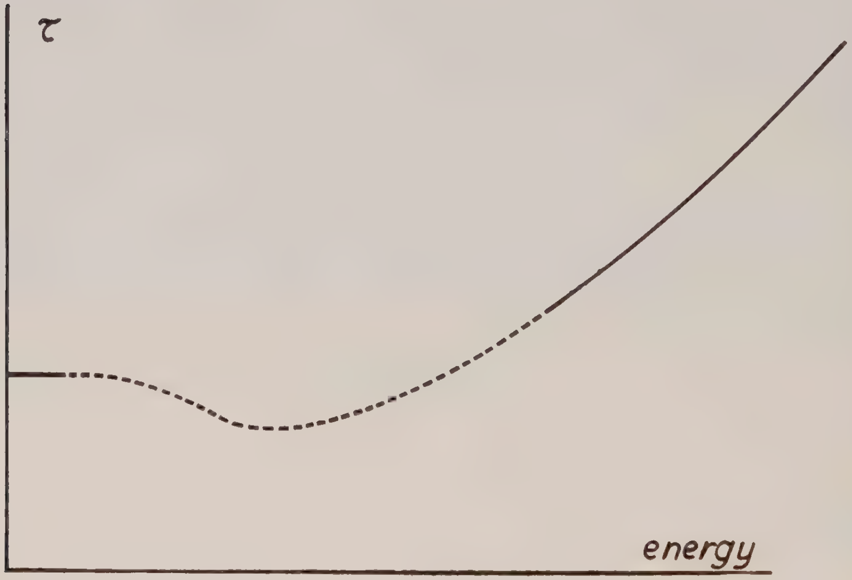

Figure 1. Apparent relaxation time τ as a function of the energy of the particle.

Figure 1 indicates how the relaxation time depends on the energy. In the region between high and low energy we have not yet determined how the relaxation time depends on the energy, but preliminary investigation indicates that it may go through a minimum.

Both for the high and low energy particles the relaxation times are—in this approximation—independent of temperature. The dependence on the mass of the particle is, however, quite different in the two cases. For the low energy particle the relaxation time is proportional to the square of the mass, whereas for the high energy particle it is inversely proportional to the square root of the mass. That is, for a given energy, a low energy particle will come to equilibrium faster the lighter it is, whereas for a high energy particle the converse holds true, the particle loses energy faster the heavier it is.

The authors are indebted to Professor I. Prigogine for his constant advice, and to Dr. R. Brout for many discussions. The research was made possible by the support and sponsorship of the Air Research and Development Command, United States Air Force, through its European Office. Thanks are also due to Teknisk Videnskabelig Forskningsraad, Denmark, for granting a fellowship to T. A. B.

On étudie, en utilisant les méthodes développées par Prigogine et ses associés, l'approche vers l'équilibre d'une particule en interaction avec les vibrations d'un réseau en équilibre thermique. Pour une particule de faible énergie on trouve que l'approche vers l'équilibre est caractérisée par un temps de relaxation proportionnel au carré de la masse de la particule et que la fonction d'autocorrélation est une simple fonction exponentielle. Pour une particule d'énergie élevée il n'existe pas de temps de relaxation au sens ordinaire; le temps apparent de relaxation augmente proportionnellement à la puissance trois demis de l'énergie de la particule et est inversement proportionnel à la racine carrée de sa masse. Le fait que ce temps dépende de l'énergie se comprend quand l'on considère le nombre de phonons à fréquence suffisamment grande pour rendre l'interaction possible.

Mit Hilfe der Verfahren von Prigogine und Mitarbeitern wird für ein Teilchen, das mit den Schwingungen eines Gleichgewichtsgitters in Wechselwirkung steht, die Annäherung an den Gleichgewichtszustand untersucht. Für ein Teilchen kleiner Energie wird gefunden, dass diese Annäherung an den Gleichgewichtszustand durch eine Relaxationszeit gekennzeichnet ist, die dem Quadrat der Teilchenmasse proportional ist; die Autokorrelationsfunktion ist dann eine einfache Exponentialfunktion. Für ein Teilchen hoher Energie existiert keine gewöhnliche Relaxationszeit; die scheinbare Relaxationszeit nimmt mit der Potenz 3/2 der Teilchenenergie zu und ist der Quadratwurzel aus der Teilchenmasse umgekehrt proportional. Die Tatsache, dass die scheinbare Relaxationszeit von der Energie abhängt, wird verständlich, wenn man die Zahl derjenigen Phononen berücksichtigt, deren Frequenz für eine Wechselwirkung ausreicht.

REFERENCES

[1] BROUT, R., and PRIGOGINE, I., 1956, *Physica*, **22**, 621.
[2] PRIGOGINE, I., and BALESCU, R., 1957, *Physica*, **23**, 555.
[3] PRIGOGINE, I., and PHILIPPOT, J., 1957, *Physica*, **23**, 569.
[4] PEIERLS, R. E., 1955, *Quantum Theory of Solids* (Oxford: Clarendon Press).
[5] Bateman Manuscript Project, 1953, *Higher Transcendental Functions*, **2** (New York: McGraw-Hill).
[6] DOOB, J. L., 1942, *Ann. Math.*, **43**, 351.
[7] WATSON, G. N., 1941, *Theory of Bessel Functions* (Cambridge: University Press).

The singularities of the integrals in Mayer's ionic solution theory

by HAROLD L. FRIEDMAN[†]
Faculté des Sciences, Université Libre de Bruxelles

(*Received* 8 *October* 1958)

The terms of the expression previously obtained by Friedman for the cluster integral sum in Mayer's theory are examined as to order in total ion concentration, c, at the limit, $c=0$. The order of the singularity at $c=0$ is calculated for several of those terms of the irreducible cluster integrals that correspond to graphs of low connectivity but with an arbitrary number of vertices. On the basis of these calculations and two postulates concerning the relation of the singularities of these integrals to others, it is concluded that the terms of the cluster integral sum, when arranged in order of increasing index, are also in increasing order of concentration, and that the first term, $\kappa^3/12\pi$, has a lower order than any other. The order in concentration of the higher terms depends on whether the third moment of the concentration of charge types, $\Sigma c_s z_s^3$, vanishes, as it does in solutions of electrolytes of symmetrical charge type.

---

1. INTRODUCTION

A recent extension [1] of Mayer's ionic solution theory [2] leads to the following expression for the cluster integral sum,

$$\mathbf{S}=\kappa^3/12\pi+\sum_{u\geqslant 2}\mathbf{S}_u, \tag{1.1}$$

where the Debye parameter, κ, is given by

$$\kappa^2=\lambda\sum c_s z_s^2, \tag{1.2}$$

$$\lambda=4\pi\epsilon^2/DkT \tag{1.3}$$

and D is the dielectric constant of the solvent, ϵ is the electronic charge, the charge on a molecule[‡] of species s is $-z_s\epsilon$, and the concentration of this species in molecules per unit volume is c_s. The function $\mathbf{S}$ has simple thermodynamic properties and its calculation from the potentials of average force of sets of ions in the pure solvent is regarded as the objective of the theory [1].

The partial cluster integral sum is

$$\mathbf{S}_u=[u!]^{-1}[\sum c_s]^u\times I^{(u)} \tag{1.4}$$

where the $\times$ product is a sum of irreducible cluster integrals on clusters of u molecules. The integrand of $I^{(u)}$ is a sum of terms, each of which corresponds to a graph on a skeleton of u vertices. Each vertex of the skeleton corresponds to a molecule of a definite species and this correspondence is made, following the multinomial expansion of $[\sum c_s]^u$, by multiplying each term of this expansion by an integral, $I^{(u)}$, which corresponds to graphs on a skeleton of the same composition as the term itself. This operation is associated with the $\times$ sign in this paper. Thus for $u=4$ the term, $c_a^2c_bc_c4!/2!$, is multiplied by an integral,

---

[†] On leave from the Department of Chemistry, University of Southern California, Los Angeles 7, California.

[‡] The term 'molecule' is used for neutral molecules as well as for ions.

$I^{(4)}$, which corresponds to graphs on a skeleton of two vertices occupied by species a, one vertex by species b, and one vertex by species c. The instructions for forming the integrand of $I^{(u)}$ which are reviewed in the following paragraph ensure that it makes no difference which vertex of the skeleton is assigned to a given species—the overall composition of the skeleton alone is sufficient to define the integrals.

In the graphs with which we are concerned, the vertices of the skeleton are connected by bonds corresponding to the following functions:

$$q_{ab} = -\lambda z_a z_b \exp(-\kappa R_{ab})/4\pi R_{ab}, \tag{1.5}$$

$$\Phi_{ab} = \exp(q_{ab} - w_{ab}^*/kT), \tag{1.6}$$

$$\Phi_{ab}'' = \Phi_{ab} - 1 - q_{ab}, \tag{1.7}$$

$$\Phi_{ab}''' = \Phi_{ab} - 1 - q_{ab} - q_{ab}^2/2, \tag{1.8}$$

$$\gamma_{abc\ldots}^{(n)} = \exp(-w_{abc\ldots}^{(n)}/kT) - 1, \qquad n \geqslant 3. \tag{1.9}$$

The pairwise function, q_{ab}, is a function of the charges of the species, a and b, at two vertices and of the distances between these vertices. The Φ functions are also pairwise, but they depend in addition upon w_{ab}^* which is a measure of the short-range interaction of molecules of the two species in the pure solvent [1]. The $w^{(n)}$ are the higher components of the potentials of average force of sets of molecules in the pure solvent, and $\gamma^{(n)}$, like $w^{(n)}$, is a function of the coordinates of n vertices and of the species at each of these vertices. We are concerned with systems such that the interactions measured by w^* and $w^{(n)}$ are short range compared to the screened Coulomb interaction measured by q. These conditions appear in more explicit form below in equations (2.1) to (2.4).

For $u = 2$ we have

$$I^{(2)} = 4\pi \int_0^\infty \Phi''' R^2 \, dR, \tag{1.10}$$

and for $u \geqslant 3$ the terms of the integrand of $I^{(u)}$ may be formulated by the following process:

(1) Form every possible graph of $\gamma^{(n)}$ bonds on a skeleton of u vertices, beginning with the skeleton itself as the first such graph. Only those graphs are possible in the present sense such that there are no two $\gamma^{(n)}$ bonds that connect exactly the same n vertices.

(2) In each graph formed in (1), every pair of vertices that is at least doubly connected by edges of $\gamma^{(n)}$ bonds must also be connected by a Φ bond.

(3) In each graph formed by (1), (2), each pair of vertices which remains not directly connected by a bond may either be left in this condition, or connected by a q bond, or connected by a Φ'' bond.

Every graph which can be formed by this sequence which is an at least doubly connected graph on the skeleton of u vertices and which has no q-bond nodes is called an element of a protograph. A protograph consists of a group of such elements that are topologically distinguishable from each other if and only if the vertices of the skeleton are labelled, for example, if they are numbered from 1 to u. Finally, there is a one-to-one correspondence between the terms of the integrand of $I^{(u)}$ and all of the elements of protographs on a skeleton of u vertices.

It is because $I^{(u)}$ is a function of κ that equation (1.1) is not a simple power series in the concentrations, c_a, c_b, ... Furthermore, if all of the solute species are ions then every $I^{(u)}$ diverges in the limit, $\kappa=0$. We express this divergence as

$$I^{(u)} < O(\kappa^0), \qquad \kappa^0=1. \tag{1.11}$$

This notation is used here in the sense that if $g(x)$ is of order $f(x)$,

$$g(x)=O(f(x)),$$

then as $x\to 0$, both $g(x)/f(x)$ and its reciprocal are of bounded variation. But if

$$g(x)\gtrless O(f(x)),$$

then as $x\to 0, |g(x)/f(x)|$ approaches 0 for the upper sign and ∞ for the lower†. Then as a result of equation (1.11) we have

$$\mathbf{S}_u < O(c^u), \tag{1.12}$$

where $c=\sum c_s$.

The objective of this investigation is to see whether

$$\mathbf{S}_u \leqslant O(\mathbf{S}_{u'}), \qquad u<u' \tag{1.13}$$

and

$$\mathbf{S}_u > O(\kappa^3)=O(c^{3/2}), \qquad u\geqslant 2. \tag{1.14}$$

We expect equation (1.13) to be satisfied for any physically reasonable grouping of the terms of the cluster expansion of the grand partition function. Unless equation (1.14) is satisfied, the theory is not consistent with experiment, for the $\kappa^3/12\pi$ term of equation (1.1) is the Debye–Hückel limiting law for $\mathbf{S}$.

The determination of the singularities that result from those terms of the integrals which correspond to highly connected graphs of q and Φ'' bonds proves to be difficult, but while we have not succeeded in obtaining a "rigorous and complete proof" [3] of the validity of equations (1.13) and (1.14), the following analysis does appear to make it "transparent and obvious" [4] that the theory passes these tests. The present contribution is therefore offered only as satisfying the second and less stringent of these criteria.

The part of the analysis which is common to all of the integrals is given in § 2. The exact analysis of several terms of one class of singular integrals is given in § 3 and the generality of these results is discussed in § 4. The application of the same methods to the other class of singular integrals is briefly outlined in § 5. The results are collected and discussed in § 6.

2. GENERAL ANALYSIS

We choose a length, L, that is great enough so that to a satisfactory approximation we have

$$\gamma_{abc\ldots}{}^{(n)}(R_{ab}, R_{bc}, \ldots L, \ldots)=0, \tag{2.1}$$

$$\Phi_{ab}(L)=1, \tag{2.2}$$

$$\Phi_{ab}''(L)=q^2(L)/2!+q^3(L)/3!+\ldots, \tag{2.3}$$

$$\Phi_{ab}'''(L)=q^3(L)/3!+q^4(L)/4!+\ldots. \tag{2.4}$$

Then we divide the configuration space of the integration in $I^{(u)}$ into three parts as follows:

A: All intermolecular distances less than L.

B: Some intermolecular distances less than L and some greater.

C: All intermolecular distances greater than L.

---

† Thus the comparison of orders has the opposite sense to the comparison of magnitudes.

Dividing the integral into terms corresponding to integration over the three parts of configuration space,

$$I^{(u)} = I_A^{(u)} + I_B^{(u)} + I_C^{(u)}, \tag{2.5}$$

we have at once

$$I_A^{(u)} = O(\kappa^0), \tag{2.6}$$

because this is the integral of a bounded function over a finite part of the configuration space, even when $\kappa = 0$.

On the other hand, as will be shown below, $I_C^{(u)}$ is singular at $\kappa = 0$ because of the long range of the q bonds. It is expected that

$$I_C^{(u)} \leqslant O(I_B^{(u)}) \tag{2.7}$$

because the part of the configuration space that leads to the divergence of $I_B^{(u)}$ is equivalent to a part of the range of integration of $I_C^{(u)}$, namely that part in which some of the intermolecular distances are held fixed near L. On the basis of equation (2.7) we need only to analyse $I_C^{(u)}$ to find the strongest singularity of $I^{(u)}$. However, we will see that in some circumstances the contribution to $\mathbf{S}$ of the most singular terms in $I_C^{(u)}$ vanishes because of a sort of generalized electroneutrality condition and then we must turn to $I_B^{(u)}$ to find the most singular term remaining.

We will first consider the $I_C^{(u)}$ integrals in detail and will return to the $I_B^{(u)}$ integrals in § 5.

The only protographs with non-vanishing contributions to $I_C^{(u)}$ are those with no $\gamma^{(u)}$ bonds (equation (2.1)). We now work with expansions of such protographs, based upon equations (2.3) and (2.4). The lowest term of such an expansion will be that in which each Φ'' bond is replaced by a $q^2/2!$ bond, i.e. a double q bond. In the following terms all of the Φ'' bonds are replaced by either double q bonds, triple q bonds, etc., or by any combination of these. Because of the fact that $q(L) \ll 1$, the terms of the expansion of a protograph with the fewest q bonds make the largest contribution to the integral of that protograph over C. However, as will be shown, the contributions of such terms to $\mathbf{S}$ may vanish for solutions of certain compositions, and then we may wish to consider terms with more q bonds which make a non-vanishing contribution to $\mathbf{S}$.

The terms from the expansion of the protographs have the essential properties of the protographs themselves [1] and they will be designated as $\boldsymbol{\tau}'$, $\boldsymbol{\tau}''$, etc. Thus, the expansion of a protograph may be represented by the equation

$$\boldsymbol{\tau} = \boldsymbol{\tau}' + \boldsymbol{\tau}'' + \dots.$$

The contribution to $\mathbf{S}_u$ of all of the terms in $I_C^{(u)}$ which correspond to the elements of a single protograph, $\boldsymbol{\tau}'$, is

$$\mathbf{S}_u(\boldsymbol{\tau}', C) = [u!]^{-1}[\textstyle\sum c_s]^u \times \sum_{\tau_i'} \displaystyle\int_C \Pi\,[q_{jj'}{}^{\nu_{jj'}}/\nu_{jj'}!]\, d\{u\}, \tag{2.8}$$

where the summation over τ_i' is over the elements of the term of the protograph [1] and where $\nu_{jj'}$ is the number of q bonds connecting the vertices, j and j', of the skeleton, and the product is over all pairs of vertices of the skeleton. The symbol, $\{u\}$, represents the set of coordinates of all of the vertices but one. The bonds, $q_{jj'}$, are not defined until the multinomial expansion of $[\sum c_s]^u$ is made and each term of the expansion is associated with a sum, $\sum_{\tau_i'}$, of integrals on a skeleton of the same composition as the term. However, the bonds depend upon the composition of the vertices only by multiplicative factors and therefore equation (2.8) can be written in another way in which the operation expressed by the × sign in equation (2.8) has already been performed.

We define $J_u(\tau_i')$ as the integral of equation (2.8), less the coordinate-independent coefficients:

$$J_u(\tau_i') = \int_C \Pi[\exp(-\kappa R_{jj'})/4\pi R_{jj'}]^{\nu_{jj'}}\, d\{u\}. \tag{2.9}$$

This is the same for all of the elements of a term of a protograph and therefore the designation, i, of the elements may be eliminated and equation (2.8) becomes

$$\mathbf{S}_u(\boldsymbol{\tau}', C) = [u!\,\Pi[\nu_{jj'}!]]^{-1}[-\lambda]^t J_u(\boldsymbol{\tau}')[\textstyle\sum c_s]^u \times \sum_{\tau_{i'}} \Pi[z_j z_{j'}]^{\nu_{jj'}}. \tag{2.10}$$

Here t is the total number of q bonds in the term, $\boldsymbol{\tau}'$, of the protograph. The × product in this equation yields terms of the form,

$$c_a{}^{u_a} . c_b{}^{u_b} \ldots z_a{}^{3h_{3a}+4h_{4a}+\cdots} z_b{}^{3h_{3b}+4h_{4b}+\cdots} \ldots, \tag{2.11}$$

where u_s is the number of molecules of species s in the cluster (i.e. in the term of the multinomial expansion) and h_{ws} is the number of molecules of species s which are at vertices of the wth degree in the graph corresponding to this term of the × product. The degree of a vertex is the number of q bonds which it intersects. The restrictions on the topology of the protographs limits us to $w \geqslant 3$. It is advantageous here to introduce the set notation of the previous paper [1]:

$$\mathbf{c} = c_1, c_2, \ldots c_s, \ldots,$$

$$\mathbf{u} = u_1, u_2, \ldots u_s, \ldots,$$

$$\langle h \rangle = \begin{vmatrix} h_{3,1} & h_{3,2} & \cdots \\ h_{4,1} & h_{4,2} & \cdots \\ . & . & \cdots \\ . & . & \cdots \end{vmatrix},$$

$$h_s = h_{3s} + h_{4s} + \ldots,$$

$$h_w = h_{w1} + h_{w2} + \ldots,$$

$$\mathbf{h} = h_{w=3}, h_{w=4}, \ldots,$$

$$\mathbf{c}^{\mathbf{u}} = c_1{}^{u_1} c_2{}^{u_2} \ldots,$$

$$\mathbf{h}! = h_{w=3}!\, h_{w=4}! \ldots,$$

$$\langle h \rangle ! = \Pi_s \Pi_w h_{sw}!.$$

We now calculate the numerical coefficient of the general term, (2.11), of the × product. First, there is a factor, $u!/\mathbf{u}!$, that is associated with $\mathbf{c}^{\mathbf{u}}$ from the multinomial expansion. Then there is the number of elements of the term of the protograph which corresponds to the same array, $\langle h \rangle$. If T is the total number of elements of the term of the protograph then this second factor is T multiplied by

$$\frac{\mathbf{u}!\,\mathbf{h}!/\langle h \rangle!}{u!},$$

the ratio of the number of permutations of the labels, $1, 2, \ldots j, \ldots u$, of the vertices which correspond to the same s and w for each j, to the total number of permutations of the labels of the vertices, $u!$. This ratio corrects for the fact that in general not all of the T elements of the term of the protograph correspond to the same $\langle h \rangle$. If either all of the molecules are of the same species or all of the vertices of the same degree, it reduces to unity. The general term from the × product in equation (2.9), including the numerical coefficient, is then

$$[T\mathbf{h}!/\langle h \rangle!]\mathbf{c}^{\mathbf{u}} \Pi_s [z_s{}^{3h_{3s}+4h_{4s}+\cdots}]. \tag{2.12}$$

There may be many terms with different $\langle h \rangle$ but the same $\mathbf{c}^{\mathbf{u}}$ and the same $\sum_w [wh_{sw}]$ for every s, and these terms may be added together for some purposes, but it is important to note that we have not done so here. It is also noted that $u_s = h_s$ for every s.

It is convenient to generate the terms of the form (2.12) in a more concise way. We define the moments of the concentration of charge types as follows:

$$\mu_w = \sum c_s z_s^w, \qquad w = 0, 1, 2, \ldots, \tag{2.13}$$

and note that

$$\mu_0 = c, \qquad \mu_1 = 0, \qquad \mu_2 = \kappa^2/\lambda.$$

The general term from the product of moments, $\boldsymbol{\mu}^{\mathbf{h}}$, is readily calculated to be

$$[\mathbf{h}!/\langle h \rangle !]\mathbf{c}^{\mathbf{u}} \Pi_s [z_s^{3h_{3s}+4h_{4s}+\cdots}]. \tag{2.14}$$

Upon comparing (2.12) and (2.14) we see that equation (2.10) may be written as

$$\mathbf{S}_u(\boldsymbol{\tau}', C) = [u! \, \Pi[\nu_{jj'}!]]^{-1}[-\lambda]^l T(\boldsymbol{\tau}')\boldsymbol{\mu}^{\mathbf{h}} J_u(\boldsymbol{\tau}'), \tag{2.15}$$

where the set, $\mathbf{h}$, is specified by the protograph, $\boldsymbol{\tau}'$, and of course, $h = u$.

In this paper we are not concerned with factors which are independent of composition and concentration of the solute and it is often convenient to omit these factors. The proportionality sign will be used to indicate that this has been done. Thus equation (2.15) becomes

$$\mathbf{S}_u(\boldsymbol{\tau}', C) \propto \boldsymbol{\mu}^{\mathbf{h}} J_u(\boldsymbol{\tau}'). \tag{2.16}$$

As has already been pointed out, one may expect the most singular $J_u(\boldsymbol{\tau}')$ to be derived from the $\boldsymbol{\tau}'$ with the fewest possible bonds. This implies that in such a graph all, or all but one, of the vertices will be of the lowest possible degree, namely $w = 3$. But it is clear from equation (2.16) that the contribution to $\mathbf{S}_u$ from such a term vanishes if $\mu_3 = 0$, as it does in solutions of electrolytes of symmetrical charge type. In this case the most singular integral which makes a non-vanishing contribution to $\mathbf{S}_u$ must correspond to a term of the protograph in which $w \geqslant 4$ for every vertex.

We now proceed with the calculation of the singularities of various $J_u(\boldsymbol{\tau}')$, seeking for each u both the most singular integral and the most singular integral whose contribution to $\mathbf{S}_u$ does not vanish when $\mu_3 = 0$.

3. CALCULATION OF SINGULARITIES

The procedures used in this section for $u = 2$ have already been used by Mayer [2] and for $u = 3$ and 4 by Haga [5]. However, it seems worth while to repeat them here to show the application of equation (2.16) and as an introduction to the treatment of the J integrals in the general problem.

The notation of the Bateman manuscripts [6, 7] is employed for the higher transcendental functions. This source may also be referred to for most of the integrals in this paper.

3.1. $u = 2$

The only protograph is a Φ''' bond connecting the two vertices. The lowest term in this protograph, with a triple bond, is designated $\boldsymbol{\alpha}$. Then

$$J_2(\boldsymbol{\alpha}) = [[4\pi]^2 3!]^{-1} \int_L^{\infty} [\exp(-3R\kappa)/R^3] R^2 \, dR \propto E_1(3\kappa L) = O(\log \kappa) \tag{3.1}$$

and

$$\mathbf{S}_2(\boldsymbol{\alpha}, C) \propto \mu_3{}^2 E_1(3\kappa L) = O(c^2 \log c). \tag{3.2}$$

If $\mu_3=0$, the contribution from $\boldsymbol{\alpha}$ vanishes and then we consider the next term of the protograph, $\boldsymbol{\beta}$, in which there is a quadruple bond

$$J_2(\boldsymbol{\beta})=[4^3\pi^3 4!]^{-1}\int_L^\infty [\exp(-4\kappa R)/R^2]\,dR=O(\kappa^0). \tag{3.3}$$

That is, this integral is convergent even if $\kappa=0$. Then we have

$$\mathsf{S}_2(\boldsymbol{\beta},C)\propto\mu_4{}^2=O(c^2). \tag{3.4}$$

This illustrates the general observation that the contributions of the most singular integrals vanish if $\mu_3=0$.

3.2. $u=3$

The protographs which contribute to $I_C{}^{(3)}$ are shown in figure 1 (*a*), (*b*). The corresponding integrals are most readily analysed by a convolution method, but for this purpose it is best to re-define the bonds so that the integrals extend over the entire configuration space.

We define $f(L,R)$ to be 0 if $L>R$ and to be $\exp(-\kappa R)/4\pi R$ if $R>L$. The integral corresponding to the lowest term of the protograph of figure 1 (*b*) is then

$$J_3(\boldsymbol{\alpha})=\int f_{1,2}[f_{2,3,}{}^2/2][f_{1,3}{}^2/2]\,d\{1,2,3\}, \tag{3.5}$$

where the integration is over the finite range of coordinates of two of the vertices, the third being chosen as the origin.

The Fourier transform of a single bond is [5,8],

$$\begin{aligned} F_1(t)&=4\pi\int_0^\infty f(L,R)[R/t]\sin(Rt)\,dR\\ &=[\kappa^2+t^2]^{-1}-[1-\cos(Lt)]/t^2+\kappa t^{-3}[\sin(Lt)-Lt\cos(Lt)]+\dots\\ &\cong[\kappa^2+t^2]^{-1}, \end{aligned} \tag{3.6}$$

where the omitted terms are found to be without effect in determining the singularities of integrals. (An example of an analysis that leads to conclusions like this is given in the Appendix.) The Fourier transform of a double bond is

$$\begin{aligned} F_2(t)&=4\pi\int_0^\infty [f^2/2!][R/t]\sin(Rt)\,dR\\ &\cong[8\pi t]^{-1}[\tan^{-1}(t/2\kappa)-\mathrm{Si}(Lt)], \end{aligned} \tag{3.7}$$

where again we have omitted terms which are without effect in the present calculations. Indeed, $\mathrm{Si}(Lt)$ can also be omitted in most cases.

The convolution theorem is now applied to equation (3.5) to obtain

$$\begin{aligned} J_3(\boldsymbol{\alpha})&=[2\pi^2]^{-1}\int_0^\infty F_1F_2{}^2t^2\,dt\\ &\propto\int_0^\infty[\tan^{-1}(t/2\kappa)-\mathrm{Si}(Lt)]^2[t^2+\kappa^2]^{-1}\,dt. \end{aligned} \tag{3.8}$$

This integral converges even at $L=0$ if $\kappa>0$, and therefore the $\mathrm{Si}(Lt)$ term is without effect on the singularity at $\kappa=0$. Omitting this term and making the substitution, $x=t/\kappa$, we have

$$J_3(\boldsymbol{\alpha})\propto\kappa^{-1}\int_0^\infty[\tan^{-1}(x/2)]^2[1+x^2]^{-1}\,dx\propto\kappa^{-1}, \tag{3.9}$$

because the remaining integral is convergent and independent of κ. The contribution to $\mathbf{S}_3$ is

$$\mathbf{S}_3(\boldsymbol{\alpha}, C) \propto \mu_3{}^2\mu_4\kappa^{-1} = O(c^{5/2}), \tag{3.10}$$

which is the result obtained by Haga [5]. If $\mu_3 = 0$ this contribution vanishes and we turn to the lowest term of the protograph of figure 1 (*a*). This gives

$$J_3(\boldsymbol{\beta}) = \int [f_{1,2}{}^2/2][f_{1,3}{}^2/2][f_{2,3}{}^2/2]\, d\{1,2,3\} = [2\pi^2]^{\ 1} \int_0^\infty F_2{}^3 t^2\, dt$$

$$\propto \int_0^\infty [\tan^{-1}(t/2\kappa) - \mathrm{Si}(Lt)]^3 t^{-1}\, dt. \tag{3.11}$$

This integral diverges at $L = 0$ even for $\kappa > 0$ and therefore $\mathrm{Si}(Lt)$ must be retained. Although it is easy to see that this integral is also singular at $\kappa = 0$, $L > 0$, the order of this singularity is difficult to determine by straightforward analysis. However we note that if, and only if,

$$g(x) = O(\log x),$$

then

$$x[d(g(x))/dx] = O(x^0).$$

We apply this procedure to $J_3(\boldsymbol{\beta})$ to see whether it is $0(\log \kappa)$:

$$\kappa\, dJ_3(\boldsymbol{\beta})/d\kappa \propto \int_0^\infty [\tan^{-1}(t/2\kappa) - \mathrm{Si}(Lt)]^2[1 + t^2/4\kappa^2]^{-1}\kappa^{-1}\, dt. \tag{3.12}$$

This integral converges even as $L \to 0$ for $\kappa > 0$, so the $\mathrm{Si}(Lt)$ term may be omitted. Then substituting $x = t/\kappa$ makes it clear that the remaining integral is independent of κ. Therefore

$$J_3(\boldsymbol{\beta}) = O(\log \kappa) \tag{3.13}$$

and the contribution of this to $\mathbf{S}_3$ is

$$\mathbf{S}_3(\boldsymbol{\beta}, C) \propto \mu_4{}^3 O(\log \kappa) = O(c^3 \log c). \tag{3.14}$$

3.3. $u > 3$, cycles

We first consider the terms of J_u which correspond to cycle graphs, in which each vertex is connected by bonds to exactly two other vertices. Examples of such graphs are the terms of figure 1 (*c*) and (*g*) and the terms of the protographs that are related to these by substituting some of the Φ'' bonds by q bonds. The cycle graph term of J_u with the fewest possible bonds, $J_u(\boldsymbol{\alpha})$, must have $\frac{1}{2}(u-\delta)$ single bonds and $\frac{1}{2}(u+\delta)$ double bonds where $\delta = 0$ if u is even, $\delta = 1$ if u is odd. Applying the convolution method to this integral we have

$$J_u(\boldsymbol{\alpha}) = (2\pi^2)^{-1} \int_0^\infty F_1{}^{\frac{1}{2}(u-\delta)} F_2{}^{\frac{1}{2}(u+\delta)} t^2\, dt, \tag{3.15}$$

and after substituting equations (3.6) and (3.7) noting that the $\mathrm{Si}(Lt)$ term may be omitted, and then substituting $x = t/\kappa$, we obtain

$$J_u(\boldsymbol{\alpha}) \propto \kappa^{(3+\frac{1}{2}(\delta-3u))} \int_0^\infty [\tan^{-1}(x/2)]^{\frac{1}{2}(u+\delta)}[1+x^2]^{\frac{1}{2}(\delta-u)} x^{\frac{1}{2}(4-u-\delta)}\, dx. \tag{3.16}$$

The integral is convergent and is not a function of κ so it may be omitted. Then we have

$$\mathbf{S}_u(\boldsymbol{\alpha}, C) \propto \mu_3{}^{u-\delta}\mu_4{}^{\delta}\kappa^{\frac{1}{2}(6+\delta-3u)} = O(c^{\frac{1}{4}(6+u+\delta)}), \tag{3.17}$$

which vanishes if $\mu_3 = 0$. In this case we consider $J_u(\boldsymbol{\beta})$, the integral corresponding to the cycle with all double bonds, and $J_u(\boldsymbol{\gamma})$, the integral corresponding to the cycle with alternating single and triple bonds if u is even, and with one extra triple bond if u is odd. The usual method yields for $J_u(\boldsymbol{\beta})$

$$J_u(\boldsymbol{\beta}) = [2\pi^2]^{-1} \int_0^\infty F_2{}^u t^2 \, dt \propto \kappa^{(3-u)}. \tag{3.18}$$

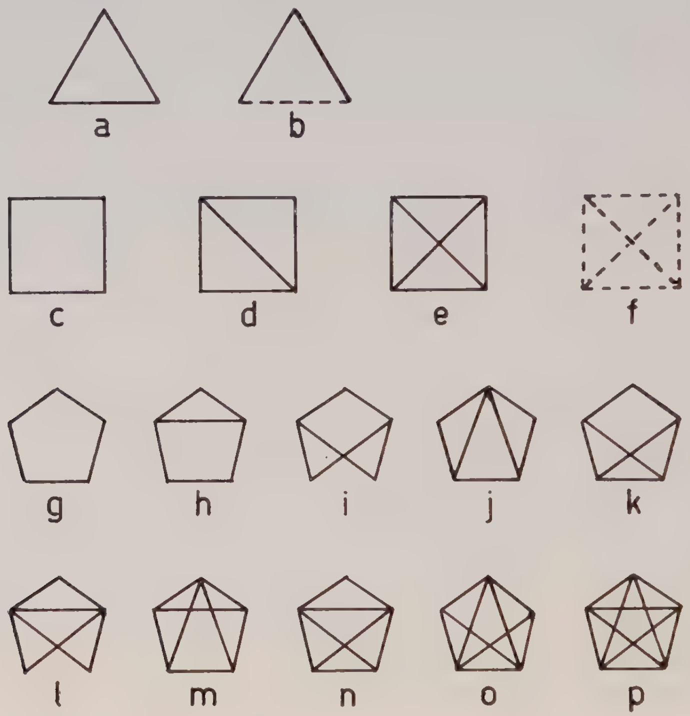

Figure 1. Representations of some protographs which contribute to $I_C{}^{(u)}$ for $u=3$, 4, and 5. Except for (b) and (f), only protographs with only Φ'' bonds (solid lines) are shown. The remaining protographs for $u=4$ and 5 can be constructed from these by substituting Φ'' bonds by q bonds (broken lines in this figure), subject to the restriction that there be no q-bond nodes. This is illustrated by the relation of (b) to (a) and (f) to (e).

For the other integral we need the transform of a triple bond:

$$F_3(t) = 4\pi \int_0^\infty [f^3/3\,!][R/t] \sin(Rt) \, dR. \tag{3.19}$$

The evaluation of F_3 and the calculation of the singularities of integrals in which F_3 appears are discussed in the Appendix. The result of interest here is

$$J_u(\boldsymbol{\gamma}) = [2\pi^2]^{-1} \int_0^\infty F_3{}^{\frac{1}{2}(u+\delta)} F_1{}^{\frac{1}{2}(u-\delta)} t^2 \, dt = O(\kappa^{3-u+\delta} [\log \kappa]^{\frac{1}{2}(u+\delta)}). \tag{3.20}$$

If u is even, then $\boldsymbol{\beta}$ and $\boldsymbol{\gamma}$ have the same number of bonds and $J_u(\boldsymbol{\gamma})$ is more singular than $J_u(\boldsymbol{\beta})$. But if u is odd, then $\boldsymbol{\beta}$ has one less bond than $\boldsymbol{\gamma}$ and then we find that $J_u(\boldsymbol{\beta})$ is the more singular. As a result we have for the most singular contribution to $\mathbf{S}_u$ from cycle integrals when $\mu_3 = 0$:

$$\mathbf{S}_u(\boldsymbol{\gamma}) \propto \mu_4{}^u O(\kappa^{3-u} [\log \kappa]^{\frac{1}{2}u}) = O(c^{\frac{1}{2}(u-3)} [\log c]^{\frac{1}{2}u}), \qquad u \text{ even}, \tag{3.21}$$

$$\mathbf{S}_u(\boldsymbol{\beta}) \propto \mu_4{}^u O(\kappa^{3-u}) = O(c^{\frac{1}{2}(u-3)}), \qquad u \text{ odd}. \tag{3.21$'$}$$

3.4. $u > 4$, bicycles

There are many more complex graphs than cycles among the terms of J_u which have a low enough connectivity to be treated readily by convolution methods. Some other examples are illustrated in figure 2. We discuss here the general case, $u > 4$, for one class of such graphs, namely those that may be obtained by rearranging the bonds in a cycle of type $\boldsymbol{\alpha}$ to form a bicycle in which the two cycles have in common two vertices connected by a single bond and in which h_3 and h_4 are the same as in the cycle, $\boldsymbol{\alpha}$. An example is the rearrangement figure 2 (A)→figure 2 (B).

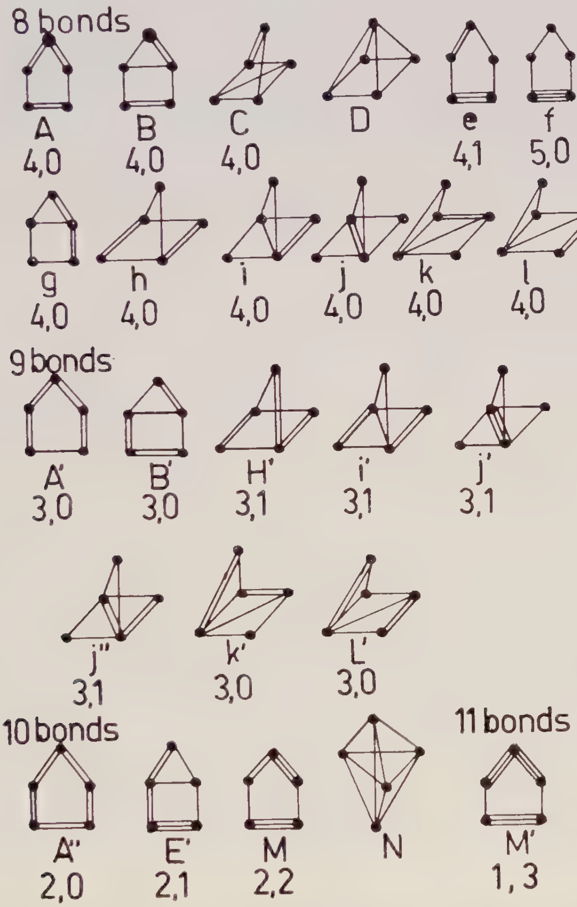

Figure 2. Graphs related to J_5. The graphs designated by capital letters are among the terms of J_5 while the others are included for comparison. The numbers indicate the singularity of the integral on the graph according to the following code : $O(\kappa^{-p}\,[\log\kappa]^q) = p, q$. The graphs designated by primed letters may be formed by adding one or two bonds to the graphs designated by the corresponding unprimed letters. Note that the singularity is never found to increase when bonds are added. The calculation of the singularity of the integral on (C) is based on Haga's calculation for the graph of figure 1 (*f*) [5] and the fact that $\tilde{f}_1$ has the same R dependence as $f(L, R)$.

The integral on a general bicycle of this kind is

$$J_u(\Delta) = \int_L^\infty f(L,R)\tilde{f}_a(L,R)\tilde{f}_b(L,R)4\pi R^2\,dR, \tag{3.22}$$

where $\tilde{f}_a$ and $\tilde{f}_b$ are effective bond functions for the two chains of the bicycle, obtained by integrating over the coordinates of the intermediate vertices in each chain. The numbers of interior vertices in the chains are a and b, respectively, and we have

$$u = a + b + 2. \tag{3.23}$$

The simplest possible such chain has one vertex of the third degree, and its effective bond function is,

$$\begin{aligned}\tilde{f}_1(L, R) &= [2\pi^2]^{-1} \int_0^\infty F_1 F_2[t/R] \sin(Rt)\, dt \\ &= [\exp(-\kappa R)/\kappa R 2^5 \pi^2][\tfrac{1}{2}\log(3) - E_1(\kappa R) + \exp(2\kappa R) E_1(3\kappa R) + \ldots].\end{aligned} \tag{3.24}$$

For our application it is sufficient to note that the second factor is $O(\kappa^0)$ and has no effect upon the singularity of any of the following integrals. The transform of the first factor is

$$\tilde{F}_1(t) \propto 1/\kappa[t^2 + \kappa^2]. \tag{3.25}$$

A chain with an odd number, $2n - 1 > 1$, of interior vertices, all third degree, has the effective bond function

$$\tilde{f}_{2n-1} = [2\pi^2]^{-1} \int_0^\infty \tilde{F}_1^{\,n}[t/R] \sin(Rt)\, dt \propto \exp(-\kappa R) \kappa^{3-3n}. \tag{3.26†}$$

A chain with an even number, $2n$, of third degree interior vertices has the effective bond function

$$\tilde{f}_{2n} = [2\pi^2]^{-1} \int_0^\infty \tilde{F}_1^{\,n} F_1[t/R] \sin(Rt)\, dt \propto \exp(-\kappa R) \kappa^{1-3n}. \tag{3.27†}$$

If u is even, all of the vertices in Δ are third degree and therefore both a and b are even. In this case

$$J_u(\Delta) \propto \kappa^{-3(a+b)/2} = \kappa^{3-3u/2}, \qquad u \text{ even}. \tag{3.28}$$

If u is odd, there must be one fourth degree vertex in Δ and therefore either a or b must be odd. Then we have

$$J_u(\Delta) \propto \kappa^{2-3(a+1+b)/2} = \kappa^{\frac{1}{2}(7-3u)}, \qquad u \text{ odd}. \tag{3.29}$$

These are exactly the same orders as for the $J_u(\boldsymbol{\alpha})$, and therefore the rearrangement of bonds, $\boldsymbol{\alpha} \to \Delta$, has no effect upon the singularity of the integral.

4. GENERAL GRAPHS IN J_u, $u > 3$

A complete solution to this problem has not yet been found, but a partial analysis of the general problem together with a survey of the order of the singularity for a variety of integrals on graphs related to J_5 provides a basis for the tentative conclusion that there are no terms in J_u which are more singular than the terms corresponding to cycle graphs.

We approach the general problem by considering first the numbers of bonds in graphs of various types and then the relation of this number to the singularity of the integral on the graph. It is convenient to separate J_u into two parts,

$$J_u = J_u(\neq) + J_u(=), \tag{4.1}$$

---

† Terms of higher order have been neglected.

corresponding, respectively, to the group of graphs which contributes to $\mathbf{S}_u$ only when $\mu_3 \neq 0$ and the group of graphs which contribute to $\mathbf{S}_u$ even when $\mu_3 = 0$.

The number of bonds, N, in a graph of any topology is related to the degrees, w, of the vertices of the graph by the equation

$$N = \tfrac{1}{2}\sum wh_w. \tag{4.2}$$

The minimum N is obtained when as many vertices as possible have the minimum degree, namely 3. In the case that u is odd, at least one vertex must be of even degree, the fourth degree for N minimum. Assuming that it is possible to make a graph satisfying these conditions, the number of bonds in it is

$$N_{\min} = \tfrac{1}{2}[3u + \delta], \tag{4.3}$$

and this graph is counted in $J(\neq)$. We note that the graphs, $\boldsymbol{\alpha}$, meet all of these conditions and thus have the minimum number of bonds possible for any graph in J_u. In a similar way we find that the cycle graphs, $\boldsymbol{\beta}$, have the minimum number of bonds, $2u$, that is possible for any graph which is counted in $J_u(=)$.

We represent the integral on a given graph, $\boldsymbol{\tau}'$, with N bonds on u vertices as

$$J_u(\boldsymbol{\tau}') = \int_C \Pi_i[\exp(-\kappa R_i)/R_i]\Pi_j[dx_j] \tag{4.4}$$

where the bonds of the graph are numbered, $1, \ldots i, \ldots N$ and where $\mathbf{x}$ is a set of Cartesian coordinates which determines all of the intervertex distances of the graph. These coordinates are numbered $1, \ldots j, \ldots U$, where $U = 3(u-1)$. Now we change variables to $y_i = \kappa R_i$, and note that this corresponds to a change from x_j to κx_j. In this way we obtain

$$J_u(\boldsymbol{\tau}') = \kappa^{N-U}\int_{C\kappa} \Pi_i[\exp(-y_i)/y_i]\Pi_j[d(\kappa x_j)], \tag{4.5}$$

where $C\kappa$ is the part of the κx_j space such that for every i, $y_i > \kappa L$.

If the integral in equation (4.5) is convergent as $L \to 0$, then $J_u(\boldsymbol{\tau}')$ is $O(\kappa^{N-U})$. But this is not necessarily the case, and it appears that adding bonds to a given graph tends to raise the order of the integral by the effect on the κ^{N-U} factor, but also tends to make the integral singular or more singular at $L = 0$, with the opposite effect on the order. It does not seem possible to discuss the singularity at $L = 0$ without taking into account the detailed topology of the graph and no way of doing this has been found, so we turn to the examination of some particular cases.

Upon comparing the order of $J_u(\boldsymbol{\alpha})$ and $J_u(\boldsymbol{\beta})$ with the result of equation (4.5) it is apparent that these integrals are not singular at $L = 0$. The same conclusion is easily reached by examining the convolution integrals. However, $J_u(\boldsymbol{\gamma})$ is singular at $L = 0$, as shown either by a comparison of the calculated order with equation (4.5) or directly from the convolution integrals. The comparison of $J_u(\boldsymbol{\beta})$ with $J_u(\boldsymbol{\gamma})$ offers a clue as to the feature of topology that is associated with singularity at $L = 0$, namely the concentration of bonds between a few pairs of vertices. This is also illustrated in figure 2 (*e*), (*f*), (*j*′), (*E*′), (*M*), and (*M*′).

There is a certain subtlety in this effect as shown by figure 2 (H′), (*i*′), and (*j*″), which are singular at $L = 0$ but have only single and double bonds. But we note that the effective bond function for a chain consisting of one single and one double bond, $\tilde{f}_1$, has the same dependence on R as a single bond (see equation (3.24), this comparison refers only to the principle terms in f and $\tilde{f}_1$). Then these three graphs each have an *effective* triple bond between one pair of vertices in relation to the behaviour of the integrals at $L=0$, and this corresponds exactly to the $\log \kappa$ factor from the convolution analysis. Furthermore, figure 2 (f) suggests that a quadruple bond produces an extra factor, κ^{-1}, in the order of the integral due to divergence at $L=0$, and it is readily shown that the graph made by connecting another single bond–double bond chain to the two unique vertices of figure 2 (H′) also has an extra factor, κ^{-1}, in the order when compared to the $\boldsymbol{\beta}$ graph with the same number of vertices and bonds. Thus, in this respect, four such chains are equivalent to a quadruple bond.

Returning now to the general problem, we note that rearranging the bonds of a graph of type $\boldsymbol{\alpha}$, $\boldsymbol{\beta}$, or $\boldsymbol{\gamma}$, to produce a more highly connected graph is distributing the given number of bonds among more pairs of vertices and therefore tends to lower the singularity at $L=0$. This is offered as the basis of our first assumption, namely that the cycle graphs in $J_u(\neq)$ and $J_u(=)$ are at least as singular as any other graphs in their respective groups.

5. THE INTEGRALS $I_B^{(u)}$

Some of the terms of $I_B^{(u)}$ correspond to protographs that are cycles of Φ'' bonds and q bonds. On the basis of considerations similar to those of §4 it seems likely that among these terms are some that are at least as singular as any other integrals in $I_B^{(u)}$, and the second assumption of this paper is that this is indeed the case.

We will call bonds with a maximum length of L, short bonds, and bonds with a minimum length of L, long bonds. Now we expand (eqn. 2.3) the long Φ'' bonds of the cycles consisting of Φ'' bonds and q bonds, and then, using the methods of §3 we may easily show that those terms of protographs that we designate, $\boldsymbol{\alpha}'$, are at least as singular as any other terms derived from cycles in $I_B^{(u)}$. The $\boldsymbol{\alpha}'$ terms of $I_B^{(u)}$ are those in which there is one short Φ'' bond whose ends are connected by a chain of alternating long single and double q bonds, and in which at least one of the terminal bonds of this chain is a single bond. The integral of such a term is designated, $K_u(\boldsymbol{\alpha}')$. We have

$$K_u(\boldsymbol{\alpha}') \propto \int_0^L \Phi''_{ik}(R)\tilde{f}_{u-2}(R)\, R^2\, dR \tag{5.1}$$

where i and k are the vertices at the ends of the short bond and Φ''_{ik} depends on the species occupying these vertices, and where $\tilde{f}$ is the effective bond function of a chain of alternate single and double q bonds (equations 3.26 and 3.27). The approximations previously obtained for $\tilde{f}$ lead to the equations

$$K_3(\boldsymbol{\alpha}') \propto \kappa^{-1}\int_0^L \Phi''_{ik}(R) \exp(-\kappa R)\, R\, dR \tag{5.2}$$

$$K_u(\boldsymbol{\alpha}') \propto \kappa^{4+(8-3u)/2}\int_0^L \Phi''_{ik}(R) \exp(-\kappa R) R^2\, dR,\ u=4, 5, 6, \ldots. \tag{5.3}$$

The remaining integral in each case is evidently not singular at $\kappa=0$. On the other hand, since these integrals do depend upon the short-range interactions of the ions at i and k, it is not possible to have a cancellation of the $K_u(\boldsymbol{\alpha}')$ integrals like that found for the $J_u(\boldsymbol{\alpha})$ integrals for the case, $\mu_3=0$.

Finally we note that $K_u(\boldsymbol{\alpha}')$ is less singular than $J_u(\boldsymbol{\alpha})$ except for $u=3$, and it is always more singular than $J_u(\boldsymbol{\beta})$ and $J_u(\boldsymbol{\delta})$, so that if $\mu_3=0$ the most singular contributions to $\mathbf{S}_u$ come from $K_u(\boldsymbol{\alpha}')$.

6. Discussion

The results that we derive from these calculations and the two assumptions are summarized in the table for the first few $\mathbf{S}_u$. On the basis of these results we conclude that the Mayer theory satisfactorily meets the conditions, (1.13) and (1.14). The duplication of orders in successive terms reflects the irregular dependence on u of the number of q bonds in an $\boldsymbol{\alpha}$ or $\boldsymbol{\alpha}'$ graph.

Order of $\mathbf{S}_u$ near $c=0$.

u	2	3	4	5	6	7
Order if $\mu_3 \neq 0$	$c^2 \log c$	$c^{5/2}$	$c^{5/2}$	c^3	c^3	$c^{7/2}$
Order if $\mu_3 = 0$	c^2	$c^{5/2}$	c^3	$c^{7/2}$	$c^{7/2}$	c^4

The difference in orders for $\mu_3=0$ and $\mu_3 \neq 0$ illustrates that the effect of the long range Coulomb forces which cause the singularities of the integrals is a function not only of κ^2/λ, the second moment of the concentration of charge types, but of the higher moments as well (equation (2.16)).

In order to compare the Mayer theory with experimental data it is in general necessary to make a detailed calculation from a model in order to include the effects of the w^* and $w^{(n)}$ potentials because these may be large compared to the effects of the long range forces in the experimental concentration range. However there are limiting laws for the concentration dependence of various thermodynamic properties at low κ which arise from the singularities of the cluster integrals and are therefore independent of the short range forces. Of course the Debye-Hückel limiting law is the most important of these but it seems that in certain circumstances one may hope to observe additional limiting laws arising from the $c^2 \log c$ and $c^{5/2}$ terms of the table. Detailed studies of these applications are in progress.

It is a pleasure to record here my obligation to Professors I. Prigogine and S. Ono for the benefit of many discussions during the course of this research. I also wish to thank the John Simon Guggenheim Memorial Foundation for the fellowship which made this work possible.

Appendix

Integrals on graphs with triple bonds

First we calculate the transform of a triple bond, equation (3.19)

$$F_3(t, \kappa, L) = [A/t] \int_L^\infty [\exp(-3\kappa R)/R^2] \sin(Rt)\, dR, \tag{A 1}$$

$$A = 1/96\pi^2.$$

Note first the limiting behaviour of F_3, which is readily calculated:

$$F_3(0, \kappa, L) = AE_1(3\kappa L), \tag{A 2}$$

$$F_3(t, 0, L) = A[\sin(Lt)/Lt - \mathrm{Ci}(Lt)] \xrightarrow[t\to\infty]{} A \cos(Lt)/[Lt]^2. \tag{A 3}$$

The behaviour at large t follows from the asymptotic expansion of the cosine integral [6]. Integrating by parts in (A 1) gives

$$F_3/A=\exp(-3\kappa L)\sin(Lt)/Lt-[3\kappa/t][\tan^{-1}(t/3\kappa)-\mathrm{Si}(Lt)+\dots]+I_a,$$

$$I_a=\int_L^\infty \cos(Rt)[\exp(-3\kappa R)/R]\,dR,$$

$$=E_1(3\kappa L)-\int_0^\infty [1-\cos(RT)][\exp(-3\kappa R)/R]\,dR$$

$$+\int_0^L [1-\cos(Rt)][\exp(-3\kappa R)/R]\,dR.$$

The second term is found in tables after noting, $1-\cos x=\sin^2(x/2)$. In the third term we make the approximation,

$$\exp(-3\kappa R)=1, \qquad 0\leqslant R\leqslant L,$$

and then this integral is [6],

$$\gamma+\log(Lt)-\mathrm{Ci}(Lt).$$

The final result is

$$F_3/A=E_1(3\kappa L)-\tfrac{1}{2}\log(1+t^2/9\kappa^2)+\gamma+\log(Lt)-\mathrm{Ci}(Lt)+\exp(-3\kappa L)\sin(Lt)/Lt$$
$$-[3\kappa/t][\tan^{-1}(t/3\kappa)-\mathrm{Si}(Lt)]+\dots. \qquad \text{(A 4)}$$

This correctly reduces to (A 2) and (A 3) and the neglected terms have no effect in the following calculations. Under the conditions

$$Lt\ll 1 \quad \text{and} \quad L\kappa\ll 1,$$

F_3 becomes

$$F_3/A=-\gamma-\log(L)-\tfrac{1}{2}\log(9\kappa^2+t^2)+1-[3\kappa/t][\tan^{-1}(t/3\kappa)]. \qquad \text{(A 5)}$$

It appears that F_3 contributes a factor of $\log\kappa$ to the singularity of an integral in which F_3 appears in the integrand if and only if the integrand is $\leqslant O(t^{-p})$, where p is larger than zero. Only the sufficiency condition is employed here and this is illustrated by considering the integral of interest.

We divide the integral of equation (3.20) into three terms corresponding to the three ranges of integration:

$$I_B \text{ in } B<t<\infty, \quad I_{AB} \text{ in } A<t<B, \quad \text{and} \quad I_A \text{ in } 0<t<A,$$

where A is a very small number and B is very large. In I_B we examine the behaviour of the (A 3) form of F_3 and obtain

$$I_B=\int_B^\infty [\cos(Lt)/[Lt]^2]^a[t^2+\kappa^2]^{-b}\,t^2\,dt=O(\kappa^0), \qquad \text{(A 6)}$$

where the order follows from the fact that this integral converges when $\kappa=0$. The same result must be obtained if the accurate form of F_3 is employed, because (A 3) applies to $\kappa=0$. Therefore this range of integration does not contribute to the singularity of $J_n(\Delta)$. The integral I_{AB} is also $O(\kappa^0)$ because it is an integral of a bounded function over a finite range of the variable.

For the third integral the approximation (A 5) is appropriate. This will appear to the ath power, and we consider the integral on each of the terms obtained by the multinomial expansion of $F_3{}^a$. The term of the expansion which gives the most singular integral is

$$\begin{aligned}\int_0^A [\tfrac{1}{2}\log(9\kappa^2+t^2)]^a[t^2+\kappa^2]^{-b}t^2\,dt\\ &=\kappa^{3-2b}\int_0^{A/\kappa}[\tfrac{1}{2}\log(9+x^2)-\log(\kappa)]^a[1+x^2]^{-b}x^2\,dx\\ &=\kappa^{3-2b}\int_0^{A/\kappa}\{[\tfrac{1}{2}\log(9+x^2)]^a+\ldots+[-\log\kappa]^a\}[1+x^2]^{-b}x^2\,dx\\ &=O(\kappa^{3-2b}[\log\kappa]^a).\end{aligned} \qquad \text{(A 7)}$$

This is the most singular term in

$$I_A+I_{AB}+I_B$$

and with

$$a=\tfrac{1}{2}(u+\delta), \qquad b=\tfrac{1}{2}(u-\delta)$$

it has the same order as $J_u(\Delta)$.

On examine, quant à l'ordre en la concentration ionique totale c, à la limite $c=0$, les termes de l'expression obtenue au préalable par Friedman pour la somme d'intégrales d'essaim dans la théorie de Mayer. On calcule l'ordre de la singularité au point $c=0$ pour plusieurs d'entre les termes des intégrales d'essaim irréductibles qui correspondent à des diagrammes ayant peu de traits connectifs mais possédant un nombre arbitraire de sommets. Sur la base de ces calculs et de deux postulats concernant la relation entre les singularités de ces intégrales et d'autres, on conclut que les termes de la somme d'intégrales d'essaim, lorsqu'ils sont rangés en ordre croissant de l'indice, sont aussi en ordre croissant des puissances de la concentration, et que le premier terme $\kappa^3/12\pi$ a un ordre inférieur à celui de tous les autres. Pour les termes plus élevés l'ordre en la concentration dépend de la disparition possible du troisième moment de la concentration des charges ioniques $\Sigma c_s z_s{}^3$ telle qu'elle se produit pour les solutions d'électrolytes à type de charge symmétrique.

Die Glieder des Ausdruckes, den Friedman seinerzeit für die Cluster-Integralsumme der im Titel genannten Theorie erhalten hatte, werden auf ihre Ordnung bezüglich der totalen Ionenkonzentration c für den Grenzfall $c=0$ untersucht. Die Ordnung der Singularität bei $c=0$ wird für einige von denjenigen Gliedern des unreduzierbaren Clusterintegrals berechnet, welche Diagrammen mit geringem Zusammenhang aber mit willkürlicher Scheitelzahl entsprechen. Diese Berechnungen führen bei Benutzung von zwei Postulaten, die sich auf die Relation der Singularitäten dieser Integrale zu anderen Integralen beziehen, zu folgendem Schluss: Wenn die Terme der Cluster-Integralsumme nach wachsendem Index geordnet werden, so nimmt auch ihre Ordnung hinsichtlich der Konzentration zu; die Ordnung des ersten Gliedes $\kappa^3/12\pi$ ist dann niedriger als die irgendeines anderen Gliedes. Die Ordnung der höheren Glieder bezüglich der Konzentration hängt davon ab, ob das dritte Moment der Konzentration von Ladungstypen $\Sigma c_s z_s{}^3$ verschwindet, wie das bei Elektrolytlösungen von symmetrischem Ladungstyp der Fall ist.

REFERENCES

[1] FRIEDMAN, H. L., 1959, *Mol. Phys.*, **2,** 23.

[2] MAYER, J. E., 1950, *J. chem. Phys.*, **18,** 1426.

[3] MEERON, E., 1957, *J. chem. Phys.*, **26,** 804.

[4] KIRKWOOD, J. G., and POIRIER, J. C., 1954, *J. phys. Chem.*, **58,** 591.

[5] HAGA, E., 1953, *J. phys. Soc. Japan*, **8,** 714.

[6] ERDÉLYI, MAGNUS, OBERHETTINGER and TRICOMI, 1953, *Higher Transcendental Functions* (New York: McGraw-Hill Book Co.).

[7] ERDÉLYI, MAGNUS, OBERHETTINGER and TRICOMI, 1954, *Tables of Integral Transforms* (New York: McGraw-Hill Book Co.).

[8] MONTROLL, E., and MAYER, J., 1941, *J. chem. Phys.*, **9,** 626.

Calculation of vibrational relaxation times in gaseous cyanogen

by P. G. DICKENS
Inorganic Chemistry Laboratory, Oxford

(*Received* 8 *January* 1959)

A calculation of vibrational relaxation times in gaseous cyanogen at 300°K is presented. It is suggested that two well separated dispersion regions should be found in sound velocity measurements at ultrasonic frequencies, the higher frequency region being associated with the relaxation of the combined vibrational specific heat contributions of the two lowest modes and the lower frequency region being associated with the relaxation of the corresponding contribution of the next highest mode.

---

1. Introduction

Several calculations of vibrational relaxation times in gases have been made recently [1, 2, 3, 4]. These have been based on the general quantum-mechanical method of calculation developed by Schwartz *et al.* [1], Schwartz and Herzfeld [2] and Tanczos [3]. Agreement between calculated and experimental relaxation times for simple molecules has been found to order of magnitude; some results are compared in two recent review articles [5, 6].

For a pure gas consisting of polyatomic molecules a single experimental relaxation time is commonly found, despite the presence of several different vibrational modes, each of which could, in principle, have its own characteristic relaxation time. For two molecules at least, CH_2Cl_2 and SO_2, two distinct relaxation times have been found [7, 8], which give rise to two well separated dispersion regions in sound velocity measurements at ultrasonic frequencies.

Theoretical relaxation times have been calculated for CH_2Cl_2 by Tanczos [3] and for SO_2 by Dickens and Linnett [4]. In both cases semi-quantitative agreement with experiment was obtained. The reasons underlying the similar relaxation behaviour of these two molecules have been discussed by Dickens and Linnett [4]. Basically the double dispersion appears to arise in both cases because of a rather uncommon pattern of fundamental vibration frequencies of the lower modes. In each molecule there is a large gap in frequencies between the lowest mode and the next highest one (SO_2, $\nu_1 = 519\,\mathrm{cm}^{-1}$, $\nu_2 = 1151\,\mathrm{cm}^{-1}$, CH_2Cl_2, $\nu_1 = 283\,\mathrm{cm}^{-1}$, $\nu_2 = 704\,\mathrm{cm}^{-1}$). This leads to a low probability of energy transfer to the higher mode irrespective of whether the excitation of this mode takes place by a 'simple' (translation vibration) or a 'complex' (vibration - vibration) transfer mechanism. Calculation shows [3, 4] that in general a complex type mechanism leads to higher transfer probability than does a corresponding simple or 'parallel' mechanism. For both SO_2 and CH_2Cl_2 the calculated rate of internal transfer of energy from the first to the second mode, which appears to take place principally by the loss or gain of two quanta by the first mode and the simultaneous gain or loss of one quantum by the second, is considerably slower than the rate of energy transfer between the lowest mode and translation. There are consequently two separate relaxation times, one (the longer) associated with the internal transfer between the first and second modes, the other associated with the direct vibration–translation exchange of the lowest mode.

Dickens and Linnett [4] have suggested, on the basis of fundamental frequency patterns, further molecules which might be expected to show multiple dispersion phenomena. One of these is C_2N_2. Calculations are presented here which suggest that two well separated dispersion regions should be found in ultrasonic experiments.

2. METHOD

The method of calculation is the same as that used for SO_2[4]. This in turn is an application of the general method described in detail by Tanczos [3]. Only an outline of the method is presented here.

The calculation can be divided into four stages:

(i) The calculation of individual transition probabilities, $P_{k-l}^{i-j}(a, b)$, for all plausible types of vibrational transfers, both complex and simple. $P_{k-l}^{i-j}(a, b)$ is the probability that *on collision* mode a changes its vibrational state from i to j and simultaneously mode b changes its state from k to l, any energy difference being supplied by means of a change in the relative translational energy of the colliding molecules.

(ii) The conversion of the calculated transition probabilities into transition rate constants $k_{k-l}^{i-j}(a, b)$, as defined by Tanczos [3], and their incorporation as appropriate sums k_{aa}, k_{ab}, into temperature relaxation equations applicable to a pure polyatomic gas [3],

$$\frac{d}{dt}(\Delta T_a) = k_{aa}(\Delta T - \Delta T_a) - \sum_{b \neq a}^{n} k_{ab}(\Delta T - \Delta T_b). \tag{2.1}$$

ΔT, ΔT_a, etc. are the temperature increments of the translational and vibrational temperature respectively. There is one such equation for each vibrational mode of interest, (n in all).

(iii) Effective relaxation times, τ_i, and associated constants, D_i, are defined in terms of the variation of complex sound velocity, u, with angular frequency, ω, by

$$\left(\frac{u}{u_0}\right)^2 = 1 + \sum_{i}^{n} \frac{D_i i\omega\tau_i}{1 + i\omega\tau_i}. \tag{2.2}$$

The subscript 0 refers to zero frequency. τ_i and D_i are evaluated in terms of k_{aa}, k_{ab}, C_a, C_{v0} and C_{p0} by means of the temperature relaxation equations (2.1) and an equation relating $(u/u_0)^2$ to ΔT, ΔT_a, etc.

$$\left(\frac{u}{u_0}\right)^2 = \frac{1 + \sum_{a}^{n} \frac{C_a}{C_{p0}} \frac{(\Delta T_a - \Delta T)}{\Delta T}}{1 + \sum_{a}^{n} \frac{C_a}{C_{v0}} \frac{(\Delta T_a - \Delta T)}{\Delta T}}. \tag{2.3}$$

C_a is the static specific heat contribution of the ath mode and C_{v0} and C_{p0} are the total specific heats at constant volume and pressure respectively.

(iv) The presentation of the results in the form of the variation of the effective specific heat, $C_{v\,\mathrm{eff}}$, with the experimental variable, f/p ($f = \omega/2\pi$).

3. CALCULATION

Figure 1 is a vibrational energy diagram for cyanogen illustrating some of the more probable transitions.

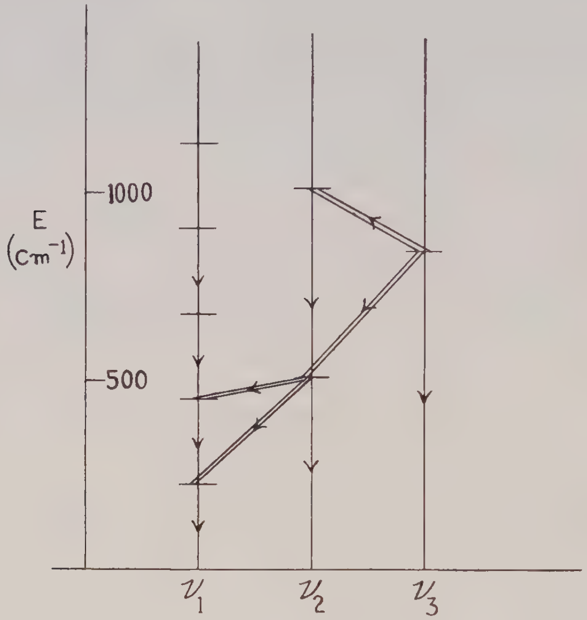

Figure 1. Vibrational energy diagram illustrating some possible transitions.

The fundamental vibration frequencies of the three lowest modes are [9]: $^*\nu_1(\pi_u) = 226\ \mathrm{cm}^{-1}$, $^*\nu_2(\pi_g) = 506\ \mathrm{cm}^{-1}$, $\nu_3(\sigma_g^+) = 842\ \mathrm{cm}^{-1}$ (* = doubly degenerate). Their corresponding specific heat contributions at 300° K are, $C_1 = 3{\cdot}606$, $C_2 = 2{\cdot}486$, $C_3 = 0{\cdot}575$ cals/mol° C respectively. The remaining modes, (σ_u^+, σ_g^+) have fundamental frequencies above 2000 cm^{-1} and hence make a negligible contribution to the vibrational specific heat at 300° K.

Transition probabilities at 300° K for both simple( )and complex( ) type transfers were calculated according to the prescription of Tanczos [3]. The necessary intermolecular force constants were obtained by matching an expression $V = V_0 \exp(-\alpha r) - \epsilon$ to the Lennard-Jones potential function, $V = 4\epsilon\{(r_0/r)^{12} - (r_0/r)^6\}$ and are shown in table 1. The vibrational amplitude coefficients, $\overline{A_a^2}$, etc. [4] are also shown.

ϵ/k† (°K)	r_0† (Å)	α*‡ (10^8 cm^{-1})	$\overline{A_1^2}$	$\overline{A_2^2}$	$\overline{A_3^2}$
339	4·38	5·43	$\frac{0{\cdot}233}{m_C}$	$\frac{0{\cdot}246}{m_C}$	$\frac{0{\cdot}310}{m_C}$

Table 1.

† Data from Hirschfelder *et al.* [10].
‡ Calculated for simple deactivation of the lowest mode.
m_C = atomic mass of carbon.

The steric factors used, $P_0(a)$, etc., were 1/3 for simple transitions involving the non-degnerate mode ν_3 and 2/3 for the transitions involving the doubly degenerate modes ν_1 and ν_2. Values for $P^{i-j}_{k-l}(a, b)$ for small values of $\Delta\nu$ ($< 100\,\text{cm}^{-1}$) were obtained by graphical interpolation making use of the formula at exact resonance ($\Delta\nu = 0$) given by Tanczos [3].

Transition rate constants, $k^{i-j}_{k-l}(a, b)$, were calculated for the eight most facile transitions and are shown, together with the appropriate sums k_{aa} and k_{ab}, in table 2.

i	j	k	l	a	b	$k^{i-j}_{k-l}(a, b)$	$k^{j-i}_{l-k}(a, b)$	$k'^{i-j}_{k-l}(a, b)$	$k'^{j-i}_{l-k}(a, b)$
1	0	0	0	1	–	846·30	—	—	—
1	0	0	1	1	2	2·924	22·117	6·547	9·878
2	0	0	1	1	2	28·966	321·64	95·162	97·904
1	0	0	0	2	–	3·637	—	—	—
1	0	0	1	2	3	0·0685	0·8797	0·1152	0·5228
2	0	0	1	2	3	0·0405	0·5645	0·0739	0·3096
1	0	0	2	3	1	0·0732	0·00164	0·0133	0·00901
1	0	0	1	3	1	0·00691	0·00007	0·00184	0·000267

a	b	k_{aa}	k_{ba}	k_{ab}
1	–	878·19	—	—
2	–	347·51	—	—
3	–	1·524	—	—
1	2	—	107·78	101·71
1	3	—	0·01513	0·00928
2	3	—	0·83245	0·18914

Table 2. Calculated values of transition rate constants (10^6 sec^{-1}).

It can be said at this stage that the reciprocals of k_{11}, k_{22}, and k_{33} will roughly correspond to the three effective relaxation times of the system.

The effective relaxation times, τ_i, as defined by equation (2.2), were found as the roots of a cubic equation, in $1/i\omega$, set up by elimination of ΔT, ΔT_a, etc, from equations (2.1) and (2.3) for the special condition $(u/u_0)^2 = \infty$ when $1/i\omega = -\tau_i$ [3]. Relaxation constants, D_i, were found as described elsewhere [4]. The results are shown in table 3.

i	D_i	τ_i (10^{-8} sec)
1	0·1472	0·06844
2	0·0410	0·2227
3	0·0076	62·370

Table 3. Calculated values of effective relaxation times, τ_i and associated constants, D_i.

The real part of equation (2.2) can be written as

$$\left(\frac{a}{a_0}\right)^2 = 1 + \sum_{i=1}^{3} \frac{D_i(\omega\tau_i)^2}{1 + (\omega\tau_i)^2}$$

whence $(a/a_0)^2(\omega)$ can be calculated. A plot of

$$C_{v\,\mathrm{eff}}=\left(\frac{C_{p0}}{C_{v0}}\right)\frac{R}{(a/a_0)^2-1}$$

versus $\log_{10} f/p$ is shown in figure 2.

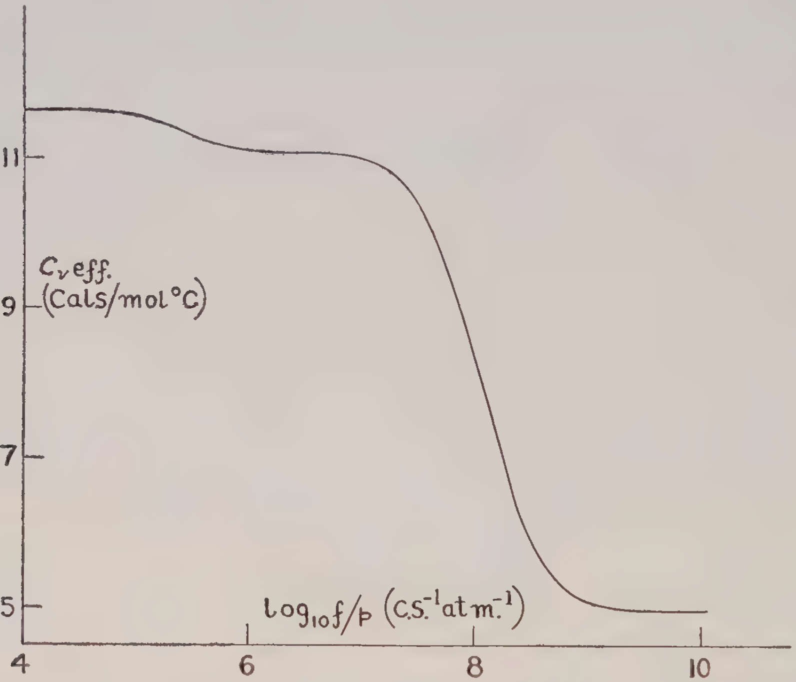

Figure 2. Plot of $C_{v\,\mathrm{eff}}$ versus $\log f/p$.

4. DISCUSSION

Inspection of the rate constants, $k^{i-j}_{k-l}(a, b)$, of table 2 indicates that the main routes of deactivation of the three lowest modes are by means of the processes whose rate constants are $k_{1-0}(1)$ (mode 1), $k^{1-0}_{0-2}(2, 1)$ and $k^{1-0}_{0-1}(2, 1)$ (mode 2), and, $k^{1-0}_{0-1}(3, 2)$ and $k^{1-0}_{0-2}(3, 2)$ (mode 3).

The rate constants k_{11}, k_{22} and k_{33} are rough guides to the overall rates of deactivation of these three modes, and on this basis it can be seen that the rate of exchange of vibrational energy for mode 3 is considerably less than that for modes 1 and 2. The detailed calculation shows that τ_1 and τ_2 are of the same order but that $\tau_3 \sim 300\tau_2$. Two main ultrasonic dispersion regions result in figure 2. The high-frequency region is actually the composite of two overlapping dispersion regions, but the corresponding relaxation times τ_1 and τ_2 are close together and a single inflection in the plot of $C_{v\,\mathrm{eff}}$ versus $\log f/p$ results (see ref. [4]).

The values of the calculated relaxation times τ_1 and τ_2 are probably too small, since the perturbation method involved in the calculation of vibrational transition probabilities [1] is not strictly valid for such high transition probabilities.

The relaxing specific heat, $C_{3\,\mathrm{rel}}$, associated with τ_3 is given by the relation,

$$D_3=\frac{R}{C_{p0}}\frac{C_{3\,\mathrm{rel}}}{(C_{v0}-C_{3\,\mathrm{rel}})}$$

whence $C_{3\,\mathrm{rel}} \sim 0{\cdot}575$ cals/mol °C—the Einstein contribution of mode 3 at 300° K. Similarly $(D_1 + D_2)$ corresponds to the remaining vibrational specific heat contribution $(C_1 + C_2)$.

Thus it can be predicted, on the basis of this calculation, that the variation of the effective specific heat with frequency at 300° K could be represented by two well separated dispersion regions, the low frequency region ($\sim 10^5$–10^6 c sec^{-1} atm^{-1}) corresponding to the relaxation of the specific heat contribution of mode 3 ($\sim 0{\cdot}6$ cals/mol° C) and the high-frequency region ($\sim 10^8$ c sec^{-1} atm^{-1}) corresponding to the relaxation of the combined specific heat contributions of modes 1 and 2 (~ 6 cals/mol° C).

At higher temperatures the relative contribution of mode 3 to the total vibrational specific heat is greater, consequently the first 'step' in figure 2 would be more marked and easier to detect experimentally. The high-frequency dispersion region is probably outside the range of present acoustic techniques.

No experimental relaxation data could be found for this molecule and it is hoped that some work may be done on this problem in the near future, thus providing a test for the theory on which this analysis is based.

Thanks are due to the Harmsworth Trust and the Department of Scientific and Industrial Research for providing grants.

On présente un calcul des temps de relaxation vibrationnelle dans le cyanogène gazeux à 300°K. Il est suggéré que l'on doit trouver, dans les mesures de vitesse du son aux fréquences ultrasonores, deux régions de dispersion bien séparées, la région de haute fréquence étant associée à la relaxation de la combinaison des contributions à la chaleur spécifique vibrationnelle des deux modes les plus bas, et la région de basse fréquence à la relaxation de la contribution correspondante du prochain mode au dessus.

Die Schwingungs-Relaxationszeiten werden für gasförmiges Dicyan bei 300 K berechnet. Es ergibt sich, dass in Messungen der Schallgeschwindigkeiten bei ultrasonoren Frequenzen zwei deutlich voneinander getrennte Dispersionsgebiete zu erwarten sind. Dabei entspräche das Gebiet höherer Frequenzen dann einer Relaxation der aus den beiden niedrigsten Eigenschwingungen kombinierten Beiträge zur spezifischen Wärme, während andererseits das Gebiet niederer Frequenzen der Relaxation das entsprechenden Beitrages der nächst höheren Eigenschwingung zuzuordnen wäre.

REFERENCES

[1] Schwartz, R. N., Slawsky, Z., and Herzfeld, K. F., 1952, *J. chem. Phys.*, **20**, 1951.
[2] Schwartz, R. N., and Herzfeld, K. F., 1954, *J. chem. Phys.*, **22**, 767.
[3] Tanczos, F. I., 1956, *J. chem. Phys.*, **25**, 439.
[4] Dickens, P. G., and Linnett, J. W., 1957, *Proc. roy. Soc.* A, **243**, 84.
[5] Herzfeld, K. F., 1955, *Thermodynamics and Physics of Matter* (Princeton).
[6] Dickens, P. G., and Linnett, J. W., 1957, *Annu. Rev. phys. Chem.*, **8**, 155.
[7] Busala, A., Sette, D., and Hubbard, J. C., 1955, *J. chem. Phys.*, **23**, 787.
[8] Lambert, J. D., and Salter, R., 1957, *Proc. roy. Soc.* A, **243**, 78.
[9] Herzberg, G., 1954, *Infra-red and Raman Spectra of Polyatomic Molecules* (New York: Van Nostrand).
[10] Hirschfelder, J. O., Curtiss, C. F., and Bird, R. B., 1954, *Molecular Theory of Gases and Liquids* (New York: Wiley).

Thermodynamic properties of clathrates: I. The heat capacity and entropy of argon in the argon quinol clathrates

by N. G. PARSONAGE and L. A. K. STAVELEY
Inorganic Chemistry Laboratory, Oxford

(*Received* 1 *December* 1958)

Measurements have been made of the heat capacity C_p from ~13°K to ~273°K of five clathrates of argon and β-quinol. The argon content ranged from ~20 per cent to ~80 per cent of the maximum possible amount. Over much of the temperature range studied, C_p proved to be a linear function of the argon content, but from 13°K to 20°K, and from 50°K to 100°K the relation between C_p and argon content is obscure, and may, in fact, be non-linear. Estimates have been made of the contribution to C_p made by a mole of argon in the temperature region where C_p is a linear function of composition, and these experimental values have been compared with those calculated according to the theory of J. H. van der Waals, which is based on the cell model of Lennard-Jones and Devonshire. The agreement between theory and experiment is satisfactory.

1. Introduction

The existence of the β-quinol clathrates depends on the occurrence in pure β-quinol of regularly spaced cavities. These cavities are approximately spherical and of about 8 Å diameter, which permits them to accommodate a variety of small molecules, though it appears that not more than one molecule can be contained in any one hole. For the smaller molecules there is virtually no distortion of the cavity [1].

An examination of the thermodynamic properties of clathrates therefore gives information about the contribution to the thermodynamic properties of the system made by small molecules each constrained to move in a cell of fixed size. Such information would seem to be of value since a clathrate provides an idealized case of the cell model, which has been widely applied both to pure liquids and solutions. We have therefore studied the argon quinol clathrates and we hope to extend these experiments to clathrates containing molecules with more degrees of freedom. Shortly after we had begun this work J. H. van der Waals [2] published a treatment of quinol clathrates based on the theory of Lennard-Jones and Devonshire. Our results make it possible to carry out a further test of his theory, in addition to those which he himself applied, since his theory gives an expression for the energy of formation of the clathrate and hence, by differentiation, of the contribution made to the heat capacity by the molecules in the holes.

2. Experimental

Experiments were carried out on five samples of different compositions designated A1, A2, A3, A4, A5, the argon content ranging from ~20 per cent to ~80 per cent of the maximum possible amount. It was thought unwise to attempt experiments on the pure β-quinol because of the risk of change into the same stable α-form during the two or three weeks needed to complete a calorimetric study. Evans and Richards [3] showed that the rate of change from the β- to the α-form is much decreased by filling even a small fraction of the holes.

2.1. *Preparation of the argon clathrates*

The clathrates were prepared by slow crystallization of quinol by gradually cooling a hot (~90°C) solution in *n*-propanol under an argon atmosphere. For the sample richest in argon the pressure was maintained at ~105 atm and crystallization was carried out over a period of 48 hours, while for that with the smallest argon content crystallization was effected over a period of ~10 hours under a pressure of ~14 atm. Before the preparation the quinol had been purified by recrystallization from *n*-propanol (A4, A5) or successively from water and *n*-propanol (A1, A2, A3); the *n*-propanol had been freed from water by refluxing with ignited calcium oxide, followed by distillation. In the case of the clathrate with the lowest argon content (A2), where there is considerable danger of contamination with α-quinol, the substance was examined both under a polarizing microscope and by flotation to ensure that none of the α-form was present.

2.2. *Analysis*

The clathrates were analysed by measuring the amount of gas liberated when they were decomposed by fusion. Two analysis apparatuses were constructed, one handling up to 1200 ml at one atmosphere and the other up to 10 ml at one atmosphere. Before each experiment the compositions of at least two small samples (~0·25 g) of each clathrate were determined. When the heat capacity measurements had been completed, the whole of the substance used in the measurements was taken from the calorimeter (as far as was possible) and analysed in a single experiment in the larger apparatus. This was thought desirable because of the possibility of inhomogeneity of the substance, but in fact these final analyses were always consistent with those done on the small-scale apparatus.

2.3. *The calorimetric apparatus*

The calorimeter was of the conventional adiabatic type. It had previously been used for experiments on salt hydrates and will be described elsewhere. Calibration experiments on very pure benzoic acid had shown that an accuracy of ~0·2 per cent could readily be achieved in the heat capacity measurements except at the lowest temperatures, where the accuracy was ~1 per cent.

2.4. *Instability of the clathrates*

As is usual in low-temperature calorimetry, after the calorimeter had been filled the air was pumped away and helium admitted to a pressure of a few mm Hg before the calorimeter was sealed. During several of the experiments some argon escaped from the clathrates. This formed a condensate on the crystals at very low temperatures which volatilized as the argon boiling-point was approached and so caused a large apparent increase in the heat capacity. By experiments in which samples of argon clathrate were sealed into an all-glass system and subjected to different thermal treatments, it was found that this escape of argon was due to alternate cooling to liquid oxygen temperatures and subsequent re-warming, and that the crystals were particularly susceptible to it if they still contained traces of solvent. No comparable build-up of pressure occurred when a solvent-free sample was subjected to the same treatment of cooling and re-warming, or when the imperfectly dried sample was allowed to stand at room temperature or at liquid oxygen temperatures. It is suggested that the decomposition is caused by the distillation of the traces of residual solvent from point to point as the solid is cooled or warmed, some argon being released from each crystal on which the solvent condenses.

To reduce the amount of the decomposition during the measurements, the period during which the solid was dried in a vacuum desiccator over phosphorus pentoxide was increased from three days to several weeks. Further, in the runs in which a significant escape of argon occurred, corrections could readily be applied to the values of the heat capacity and composition to take account of the decomposition. The amount of argon which had escaped from the crystals could be calculated from the known dead-space in the calorimeter and from the anomalous contribution to the heat capacity associated with the heating period in which the last of the argon volatilized into the dead-space. Knowing the amount of argon, corrections to the apparently anomalous points at lower temperatures could be evaluated from the known heat of sublimation of argon. Very much smaller corrections were applied at higher temperatures for the contribution to the heat capacity from the gaseous argon. In the worst case, the amount of argon liberated resulted only in a change of composition from $3C_6H_4(OH)_2 . 0{\cdot}359\,A$ to $3C_6H_4(OH)_2 . 0{\cdot}335\,A$.

3. Discussion

This experimental work was begun on the basis that it was reasonable to expect that the partial molar heat capacity of the argon at a given temperature would be independent of composition, so that the molar heat capacity of the clathrate $3C_6H_4(OH)_2 . xA$ would be a linear function of x. Extrapolation would then give the heat capacity of pure β-quinol ($C_p{}^Q$) and the contribution to C_p of one mole of argon (C_A). That such a linear relation between C_p and x was probable, at least at higher temperatures, was suggested by the facts that small molecules produce no significant change in the lattice parameters, and that the heat of formation at 25°C for several clathrates is a linear function of x. It may also be noted that in van der Waals' statistical treatment [2], it is assumed that the presence of molecules in the holes does not affect the partition function of the lattice.

The results in table 1 for each clathrate were plotted on a large scale, and from the smoothed curves values of C_p were obtained at regular intervals. When these smoothed values were plotted against x it proved that C_p is indeed, within experimental error, a linear function of x over the following ranges of temperature: 20°K to 40°K and 110°K to 273°K. But this is not so from 13°K to 20°K and

A1. $3C_6H_4(OH)_2 . 0{\cdot}785$ A (0·05308 moles in the calorimeter)

T (°K)	C_p (cal. deg^{-1}/mole)	T (°K)	C_p (cal. deg^{-1}/mole)	T (°K)	C_p (cal. deg^{-1}/mole)
12·88	2·82	85·60	36·34	175·14	61·55
15·12	4·30	85·83	36·22	179·62	62·92
17·91	6·25	89·62	37·26	184·05	64·31
21·60	9·09	89·84	37·27	188·63	65·49
26·97	12·75	95·97	38·74	193·57	67·28
30·82	15·08	102·00	40·66	198·44	68·92
34·25	17·07	108·27	42·15	203·95	70·51
38·42	19·07	112·27	43·22	211·83	73·36
43·33	21·35	117·81	44·65	220·32	75·94
48·26	23·87	123·57	46·54	228·66	78·83
52·28	25·39	128·87	47·93	235·85	80·93
57·17	27·71	134·04	49·46	243·86	83·61
61·38	29·25	141·41	51·81	251·64	86·14
68·36	31·31	146·34	53·07	257·01	88·11
73·08	32·67	151·12	54·00	264·52	90·51
77·28	34·20	155·92	55·72	271·76	93·12
77·50	34·19	160·60	57·09	278·75	95·07
81·49	35·40	166·21	58·95	285·34	97·59
81·72	35·19	170·81	60·25	291·77	99·85

A2. $3C_6H_4(OH)_2 . 0{\cdot}219$ A
$^*3C_6H_4(OH)_2 . 0{\cdot}202$ A } (0·03765 moles in the calorimeter)

T (°K)	C_p (cal. deg^{-1}/mole)	T (°K)	C_p (cal. deg^{-1}/mole)	T (°K)	C_p (cal. deg^{-1}/mole)
*13·80	2·18	87·70	34·27	162·34	55·06
*16·49	3·71	*90·48	34·74	167·04	56·54
*19·35	5·69	91·64	35·15	172·18	58·14
*21·83	7·61	95·23	36·21	177·24	59·61
*23·92	8·70	*95·32	35·94	182·23	61·22
*41·17	17·61	*99·78	37·17	187·15	62·69
*41·89	17·88	101·14	37·64	193·46	64·62
*45·68	19·47	*104·47	38·23	201·11	66·82
*46·95	20·27	105·40	38·79	209·47	69·85
*50·02	22·18	*109·36	39·72	215·94	71·91
*54·40	24·11	109·88	40·02	223·08	74·29
*60·07	26·29	115·10	41·22	230·77	76·88
*65·50	27·99	119·64	42·24	238·65	79·47
70·11	29·19	124·40	44·19	246·37	82·12
74·86	30·42	129·35	45·47	254·41	84·70
*75·90	30·68	134·20	46·89	262·26	87·35
79·34	31·75	139·75	48·33	269·42	89·84
*81·08	32·47	145·57	49·99	276·37	91·74
83·61	32·99	151·26	51·94	—	—
*85·67	33·63	156·84	53·60	—	—

A3. $3C_6H_4(OH)_2 . 0{\cdot}488$ A (0·04745 moles in the calorimeter)

T (°K)	C_p (cal. deg^{-1}/mole)	T (°K)	C_p (cal. deg^{-1}/mole)	T (°K)	C_p (cal. deg^{-1}/mole)
13·61	2·63	74·30	31·25	156·47	54·35
13·82	2·62	75·62	31·52	161·45	55·91
16·15	4·65	79·14	32·63	166·83	57·50
16·26	4·62	80·40	33·01	172·51	59·31
16·82	5·11	84·10	34·06	178·09	61·03
19·08	6·36	85·31	34·45	183·59	62·65
22·96	9·05	89·18	35·52	188·99	64·45
27·59	12·03	89·67	35·64	195·49	66·68
32·33	14·39	93·80	36·59	203·11	69·01
37·05	17·03	98·51	37·76	211·08	71·35
38·02	17·49	106·38	39·89	218·96	73·97
42·30	19·79	111·50	41·42	226·63	76·62
48·90	22·35	116·48	42·89	234·58	79·44
54·41	24·80	121·19	44·26	242·80	81·87
59·11	26·62	126·22	45·48	249·81	84·36
60·68	27·04	131·22	46·88	258·20	87·01
64·11	28·33	136·10	48·36	266·31	89·75
65·58	28·71	141·14	49·81	274·15	92·46
69·15	29·73	146·00	51·56	281·89	94·93
70·54	30·02	151·19	52·94	—	—

A4. $3C_6H_4(OH)_2\,.\,0{\cdot}579$ A (0·04349 moles in the calorimeter)

T (°K)	C_p (cal. deg^{-1}/mole)	T (°K)	C_p (cal. deg^{-1}/mole)	T (°K)	C_p (cal. deg^{-1}/mole)
13·87	3·43	98·46	38·66	167·98	58·58
16·77	5·35	98·61	38·43	172·57	59·94
20·27	7·72	103·31	39·75	177·49	61·42
23·63	9·60	107·88	41·08	182·82	62·94
28·30	12·74	112·51	42·31	188·55	64·79
33·16	15·60	112·64	42·50	194·22	66·67
37·94	17·60	117·88	43·98	201·62	69·13
43·20	20·34	124·71	45·80	209·58	71·70
48·77	23·07	129·51	47·18	217·41	74·09
54·50	25·58	134·09	48·39	225·10	76·64
60·53	27·96	138·07	49·58	232·68	79·08
65·71	29·27	142·95	50·80	240·61	81·65
70·37	30·63	142·97	50·79	248·48	84·41
75·17	32·04	147·81	52·28	256·71	87·09
80·12	33·45	147·85	52·28	265·16	89·92
84·82	34·91	152·70	53·93	273·36	92·76
89·31	36·11	157·78	55·54	—	—
93·75	37·26	162·92	57·04	—	—

A5. $3C_6H_4(OH)_2\,.\,0{\cdot}359$ A, *$3C_6H_4(OH)_2\,.\,0{\cdot}335$ A (0·04533 moles in the calorimeter)

	T (°K)	C_p (cal. deg^{-1}/mole)		T (°K)	C_p (cal. deg^{-1}/mole)	T (°K)	C_p (cal. deg^{-1}/mole)
	*17·84	5·40	Second series	*59·95	26·97	173·95	59·44
	*20·16	7·08		*65·40	28·76	176·91	60·36
	*23·84	9·44		*70·84	30·35	180·19	61·41
	*28·37	11·90		*75·86	31·80	183·08	62·28
	*33·02	14·67		*80·60	32·93	186·36	63·30
	*37·75	16·99		*85·20	33·96	189·57	64·29
	*43·05	19·76		*89·65	35·14	192·33	65·21
	*48·61	22·10		*95·31	36·65	196·72	66·71
	*54·27	24·51		*100·43	38·02	204·78	68·98
First series	60·43	27·84		*105·70	39·40	212·81	71·59
	62·01	28·57		110·80	40·85	221·11	74·29
	65·80	29·48		115·77	42·34	229·39	76·97
	68·41	30·20		120·89	43·76	237·90	79·75
	71·23	30·59		126·15	45·26	246·61	82·56
	73·69	30·63		131·65	46·83	255·07	85·37
	76·33	31·45		137·13	48·32	263·30	88·11
	78·67	32·18		159·19	55·07	271·48	90·85
	81·16	32·86		164·82	56·74	280·27	93·93
	85·76	34·28		170·72	58·51	288·81	96·85
	90·16	35·49		—	—	—	—

Table 1. Experimental values of the heat capacities of the samples of argon clathrate

from 50°K to 100°K, as is illustrated in figure 1. In each of these regions, for at least one of the samples studied the heat capacity versus temperature plot was obviously anomalous when compared with those for the other samples. This is apparent in figure 2. A further complication was that for the sample A5, which at first showed a marked heat capacity anomaly in the region 60 to 75°K, the heat capacity was found to change in this region as its investigation in the calorimeter proceeded, and this anomaly became much less marked though it never completely vanished (figure 3). (There is no reason to suppose that these anomalies were due to the escape of argon previously mentioned. In the regions concerned the uncertainty in the corrections applied was altogether too small to explain the non-linearity.)

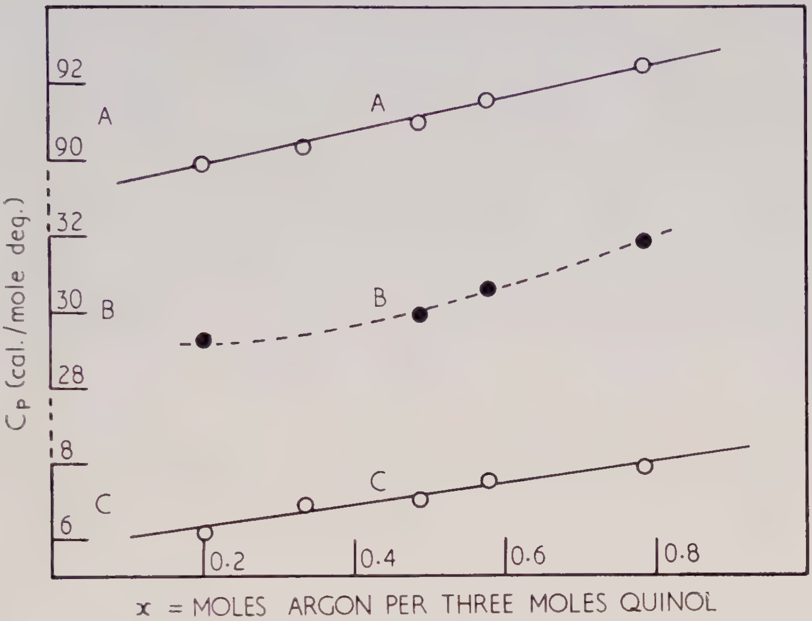

Figure 1. Plots of C_p of $3C_6H_4(OH)_2 . xA$ against x, showing a linear relation at 20°K (A) and 270°K (C) and an apparently non-linear relation at 70°K (B). The point for the clathrate with 35·9 per cent argon has been omitted from curve B because C_p for this sample changed irreversibly in the neighbourhood of 70°K and it was not certain that reproducible values had been reached.

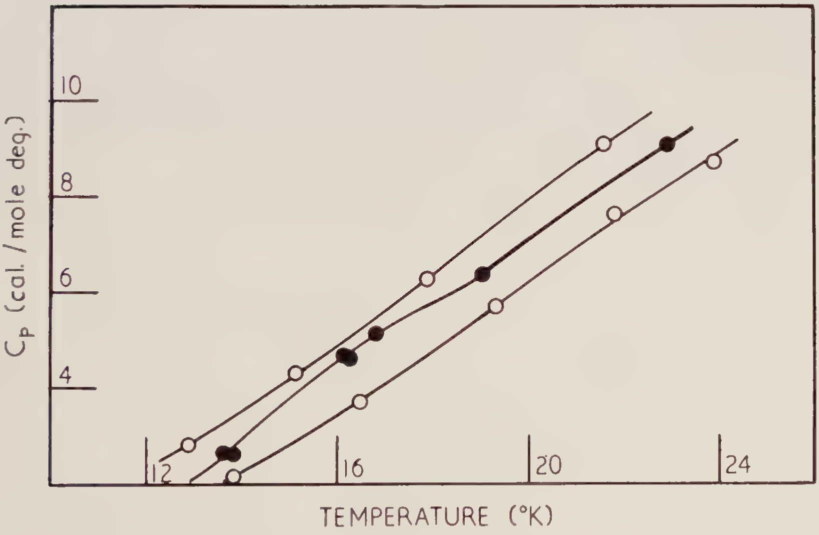

Figure 2. Plots of C_p of $3C_6H_4(OH)_2 . xA$ against temperature between 12 and 24°K for $x=0{\cdot}785$ (upper curve), $x=0{\cdot}488$ (middle curve, full circles), $x=0{\cdot}202$ (lower curve). The middle curve shows a clear anomaly.

Although these anomalies appear to be quite marked the entropy contributions associated with them are very small, so that if they are connected with structural changes in the lattice these changes must be very slight. We have considered the possibility that the non-linearity between 12°K and 20°K might arise from the interactions between argon atoms in neighbouring cages. An estimate of the energy of two argon atoms at 8 Å (the distance between the centres of two neighbouring cages) shows that this energy is so small that it could not possibly produce macroscopic thermal effects at temperatures as high as 12°K. It is possible that at low temperatures the β-quinol lattice undergoes some minor modification which may be affected by the degree of filling of the holes. Alternatively, the anomalies may be connected with the relief of strain: irreversibility is implied by the observations on A5 between 60 and 75°K (figure 3).

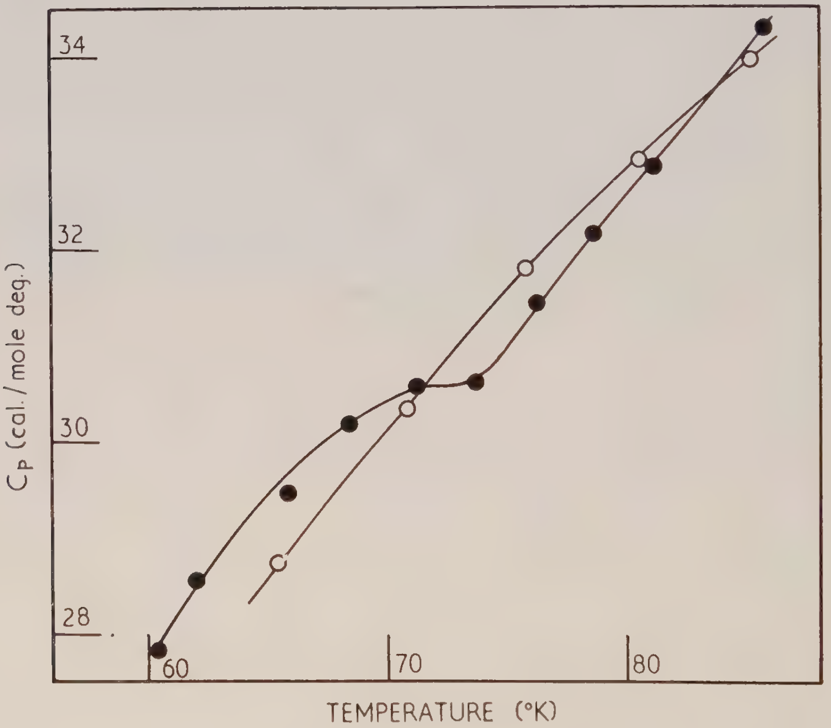

Figure 3. Plot of C_p against temperature for the clathrate with 35·9 per cent argon showing the almost complete disappearance of an anomaly after repeated cooling and warming. Full circles, first values obtained; open circles, values obtained after repeated cooling and warming.

For the temperatures at which C_p is clearly a linear function of x we have evaluated C_A and C_p^Q, which are respectively the molar heat capacity of argon in the clathrate and the heat capacity of three gram-molecules of β-quinol. These are given in table 2.

T (°K)	C_A theor	C_A exp	$C_p{}^Q$
	(cal. deg^{-1}/mole A)		(cal. deg^{-1}/3 moles β-quinol)
15	5·735		
20		2·61	5·85
25	5·626		
30		4·45	11·22
40		4·85	16·15
45	5·462		
70	5·293		
C_p versus x non-linear in this region			
110		4·70	38·89
120	5·123	4·65	41·75
130		4·57	44·61
140		4·58	47·49
150		4·60	50·39
160		4·25	53·55
170		4·40	56·55
180		4·50	59·45
190		4·50	62·60
200	4·938	4·24	66·06
210		4·40	69·14
220		4·50	72·35
230		4·53	75·60
240		4·47	78·90
250		4·43	82·20
260		4·50	85·49
270		4·66	88·81
273·16		4·67	89·84
300	4·794		

Table 2. Experimental and theoretical values of the argon contribution to C_p and the heat capacity of three moles of β-quinol at regular temperature intervals.

Van der Waals' theoretical treatment of clathrates leads to the following expression for ΔU_m, the heat of formation per mole of gas at constant total volume:

$$\frac{\Delta U_m}{RT} = \frac{\Lambda^*}{kT}\left\{-2\left(\frac{V^*}{V_0}\right)^2\left(1+\frac{g_m}{g}\right)+\left(\frac{V^*}{V_0}\right)^4\left(1+\frac{g_l}{g}\right)\right\}$$

where

$$g=\int_0^{1/4} y^{1/2}\exp\left\{-\frac{\Lambda^*}{kT}\left(\frac{V^*}{V_0}\right)^4 l(y)+2\frac{\Lambda^*}{kT}\left(\frac{V^*}{V_0}\right)^2 m(y)\right\}dy,$$

$$g_l=\int_0^{1/4} y^{1/2}l(y)\exp\left\{-\frac{\Lambda^*}{kT}\left(\frac{V^*}{V_0}\right)^4 l(y)+2\frac{\Lambda^*}{kT}\left(\frac{V^*}{V_0}\right)^2 m(y)\right\}dy,$$

$$g_m=\int_0^{1/4} y^{1/2}m(y)\exp\left\{-\frac{\Lambda^*}{kT}\left(\frac{V^*}{V_0}\right) l(y)+2\frac{\Lambda^*}{kT}\left(\frac{V^*}{V_0}\right)^2 m(y)\right\}dy,$$

$l(y)=(1+12y+25{\cdot}2y^2+12y^3+1)(1-y)^{-10}-1,$

$m(y)=(1+y)(1-y)^{-4}-1,$

$\Lambda^*=z(\epsilon_A\bar{\epsilon})^{1/2},$

$z=$ the number of elements forming the wall of one cage,

$\epsilon_A=$ the depth of the minimum in the potential energy versus distance plot for two argon atoms.

$\bar{\epsilon}$, $\bar{\sigma}=$ constants characteristic of the quinol lattice,

$V^*=(\sigma^*)^3,$

$$\sigma^*=\frac{\sigma_A+\bar{\sigma}}{2},$$

σ_A = distance apart at which the potential energy of two argon atoms is zero,

$V_0 = \dfrac{1}{\sqrt{2}} a^3$,

a = average distance of the elements of the wall from the centre of the cage.

The corresponding value for the heat capacity C_A can be readily obtained by differentiation of the expression for ΔU_m, which gives:

$$C_A = \frac{3}{2} R + \frac{R(\Lambda^*/kT)^2 (V^*/V_0)^4}{g^2} \left[\left(\frac{V^*}{V_0}\right)^4 g g_{ll} + 4 g g_{mm} - \left(\frac{V^*}{V_0}\right)^4 g_l^2 - 4 g_m{}^2 - 4 \left(\frac{V^*}{V_0}\right)^2 g g_{lm} + 4 \left(\frac{V^*}{V_0}\right)^2 g_l g_m \right]$$

where

$$g_{ll} = \int_0^{1/4} y^{1/2} \{l(y)\}^2 \exp\left\{ - \frac{\Lambda^*}{kT} \left(\frac{V^*}{V_0}\right)^4 l(y) + 2 \frac{\Lambda^*}{kT} \left(\frac{V^*}{V_0}\right)^2 m(y) \right\} dy,$$

$$g_{mm} = \int_0^{1/4} y^{1/2} \{m(y)\}^2 \exp\left\{ - \frac{\Lambda^*}{kT} \left(\frac{V^*}{V_0}\right)^4 l(y) + 2 \frac{\Lambda^*}{kT} \left(\frac{V^*}{V_0}\right)^2 m(y) \right\} dy,$$

$$g_{lm} = \int_0^{1/4} y^{1/2} l(y) m(y) \exp\left\{ - \frac{\Lambda^*}{kT} \left(\frac{V^*}{V_0}\right)^4 l(y) + 2 \frac{\Lambda^*}{kT} \left(\frac{V^*}{V_0}\right)^2 m(y) \right\} dy.$$

For comparison with experiment we have chosen the same values of $z\sqrt{(\bar{\epsilon}/k)}$, $\bar{\sigma}$, ϵ_A/k and σ_A as those proposed by van der Waals, namely $z\sqrt{(\bar{\epsilon}/k)} = 283$, $\bar{\sigma} = 3{\cdot}30$ Å, $\epsilon_A/k = 119{\cdot}8°$ and $\sigma_A = 3{\cdot}405$ Å, and we have evaluated C_A at 15, 25, 40, 70, 120, 200 and 300°K. The integrals g, g_l, g_m, g_{ll}, g_{mm} and g_{lm} were evaluated on an electronic computer at the National Physical Laboratory. The calculated values of C_A are given in table 2 and are plotted, with the experimental values, in figure 4. Van der Waals' treatment is based on classical statistics, and in the region in which these can be expected to hold, the agreement between experiment and theory is satisfactory. The difference does not exceed 0·5 cals and part of this could be attributed to experimental error. The agreement should give confidence in employing the theory in analysing the heat capacities of clathrates with potential rotational degrees of freedom which we hope to do.

Finally, using our experimental C_A values we have evaluated the contribution to the entropy of the clathrate at 298·16°K given by the integral

$$\int_0^{298\cdot16} \frac{C_A}{T} \, dT.$$

Because of the uncertainty in the values of C_A in some of the temperature regions, this was done by evaluating

$$\int_0^{298\cdot16} \frac{C_p}{T} \, dT$$

for each sample and plotting these against the composition (x). The figure obtained is 12·80 cal. deg $^{-1}$/mole argon, in fair agreement with the value of 14·61 for the entropy per mole of argon (exclusive of the configurational contribution) calculated by differentiating van der Waals' expression for F.

One of us (N. G. P.) thanks the British Oxygen Company for a Fellowship, and we are also indebted to this Company for constructing the high-pressure crystallization apparatus for us and for defraying the cost of the evaluation of the

integrals. We are also grateful to Imperial Chemical Industries Ltd. for financial assistance, and to Mr. M. G. B. Wright for help with the preliminary experiments.

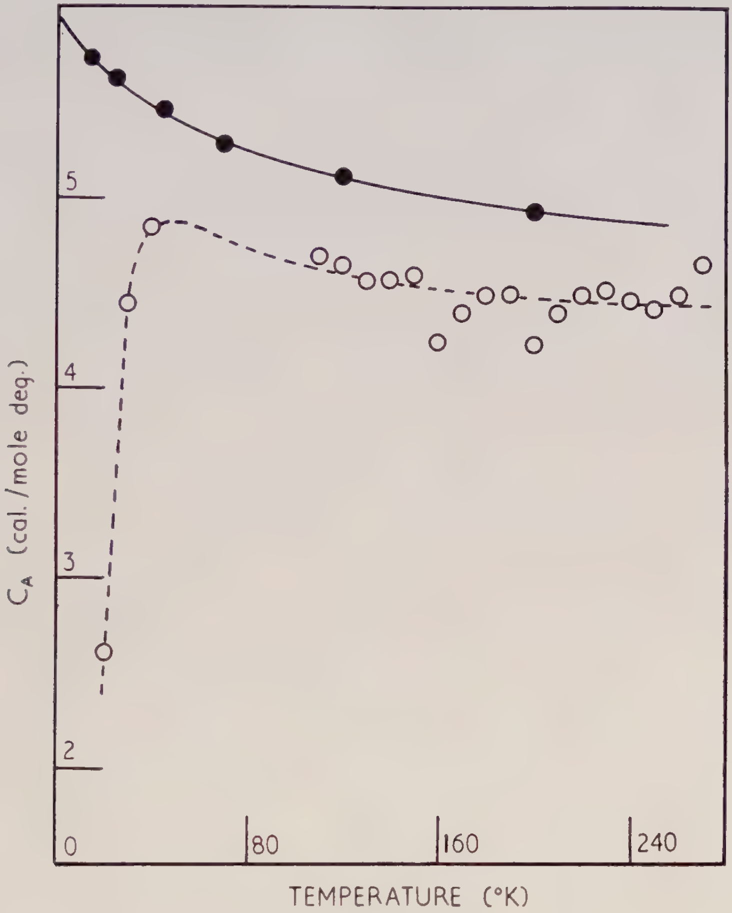

Figure 4. Comparison of C_A, the molar heat capacity of argon in the clathrate, as calculated from van der Waals' theory (full circles) and as estimated experimentally (open circles).

On a mesuré, de 13°K à 273°K, la capacité calorifique C_p de 5 composés 'clathratés' d'argon et de β-quinol. On a fait varier le contenu en argon de 20 pour cent à 80 pour cent de la quantité maximum possible. Sur la plus grande partie de l'intervalle de température étudié C_p se trouve être une fonction linéaire du contenu en argon, mais entre 13°K et 20°K et entre 50°K et 100°K il y a des déviations importantes à partir de la linéarité. On a fait une estimation de la contribution d'une mole d'argon à C_p dans la région de témperature où C_p est une fonction linéaire de la composition, et ces valeurs expérimentales ont été comparées à celles calculées d'après la théorie de J. H. van der Waals qui est basée sur le modèle cellulaire de Lennard-Jones et Devonshire. La théorie et les résultats expérimentaux sont en accord satisfaisant.

Für fünf Klathrate von Argon und β-Chinol wurde die Molwärme C_p im Bereich zwischen ~13°K und ~273°K gemessen. Der Gehalt an Argon lag zwischen ~20 Prozent und ~80 Prozent des höchstmöglichen. Im grössten Teil des untersuchten Temperaturbereiches erwies sich C_p als lineare Funktion des Argongehaltes; lediglich zwischen 13°K

und 20°K, sowie zwischen 50°K und 100°K ist die Beziehung zwischen C_p und dem Argongehalt unklar und möglicherweise nicht-linear. In dem Temperaturgebiet, wo C_p linear von der Zusammensetzung abhängt, wurde der Beitrag eines Mols Argon zu C_p abgeschätzt; diese experimentellen Werte wurden dann mit den berechneten Werten verglichen, die man mit Hilfe der Theorie von J. H. van der Waals erhält, die auf dem Zellenmodell von Lennard-Jones und Devonshire basiert. Die Übereinstimmung zwischen Theorie und Experiment ist befriedigend.

REFERENCES

[1] PALIN, D. E., and POWELL, H. M., 1947, *J. chem. Soc.*, 208; 1948, *Ibid.*, 815.
[2] WAALS, J. H. VAN DER, 1956, *Trans. Faraday Soc.*, **52,** 184.
[3] EVANS, D. F., and RICHARDS, R. E., 1952, *J. chem. Soc.*, 3932.

RESEARCH NOTES

The signs of the valence bond wave functions in an alternant hydrocarbon

by A. D. McLACHLAN
Department of Theoretical Chemistry, University Chemical Laboratory,
Lensfield Road, Cambridge, England

(*Received* 17 *February* 1959)

McConnell [1] has pointed out some interesting general results which would hold if the valence bond wave function of every alternant hydrocarbon in its ground state Ψ_0 were a linear combination of 'alternant' canonical structures Φ_A with positive coefficients:

$$\Psi_0 = \sum_A \lambda_A \Phi_A, \quad \lambda_A \geqslant 0. \tag{1}$$

In this note we prove his conjecture, under the conditions that

(*a*) Polar structures are not considered.

(*b*) Exchange integrals J_{pq} vanish when atoms p and q are both starred or both unstarred.

(*c*) All other exchange integrals are negative.

The 'alternant' canonical structures are ones in which all bonds run from a starred to an unstarred atom. To obtain them one arranges the n starred and n unstarred atoms alternately round a circle and joins them in every possible way by n bonds that do not cross. To prove that the coefficients in (1) are all positive one needs a theorem by Frobenius [2]. He proves that if M is a matrix with all its off-diagonal elements $m_{ij} \leqslant 0$ the lowest eigenvalue corresponds to an eigenvector in which all the coefficients are positive. M need not be symmetric, and he also showed that if $m_{ij} < 0$ the lowest level is not degenerate. We therefore wish to show that (1) is the lowest eigenvector of a matrix M with negative off-diagonal elements.

If one writes down the matrix $\| H_{AB} - \epsilon S_{AB} \|$ for the structures of an alternant hydrocarbon the H_{AB} are all negative, but the off-diagonal S_{AB} prevent us from using Frobenius' theorem. It is impossible to choose orthogonal combinations of the Φ_A so that the H_{AB} are still all negative. Instead we consider the equations

$$\mathscr{H}\Psi_0 = \epsilon_0 \Psi_0, \quad \Psi_0 = \sum_A \lambda_A \Phi_A \tag{2}$$

satisfied by the ground state. The operator $\mathscr{H}$ transforms each Φ_A into a linear combination of the Φ's,

$$\mathscr{H}\Phi_A = \sum_B \mathscr{H}_{AB} \Phi_B, \quad \mathscr{H}_{AB} \neq \mathscr{H}_{BA}, \tag{3}$$

and since the Φ's are linearly independent we can equate the coefficients of each Φ separately in (2);

$$\sum_A \lambda_A \mathscr{H}_{AB} = \epsilon_0 \lambda_B. \tag{4}$$

Our theorem holds if the off-diagonal elements of $\mathscr{H}$ are all negative.

To find these elements we decompose the Φ's into their component Slater determinants.

$$\phi_i = \begin{pmatrix} a^* \ldots c^* & d \ldots f \\ \alpha \ldots \alpha & \beta \ldots \alpha \end{pmatrix} \qquad (S_z = 0) \tag{5}$$

Here $a^* \ldots c^*$ are the atomic orbitals of starred atoms and $d \ldots f$ those of unstarred atoms. The ϕ_i are orthonormal, and in an alternant hydrocarbon they can be replaced by signed $\bar{\phi}_i$ classified according to the total resolved spin $S_z{}^*$ and $S_z{}^0$ on the starred and unstarred atoms

$$\bar{\phi}_i = (-)^{r+1} \phi_i \quad \text{where} \quad r = \tfrac{1}{2}(S_z{}^* - S_z{}^0). \tag{6}$$

The bond eigenfunction $\Phi_{ad:\,be:\,cf}$ is simply the sum of all the $\bar{\phi}_i$ in which the pairs of atoms a^*d, b^*e, c^*f have opposed spins.

$$\Phi_{ad:\,be:\,cf} = \textstyle\sum_{ad:\,be:\,cf} \bar{\phi}_i. \tag{7}$$

The Hamiltonian of the molecule may be written in the form

$$H = \sum_{ad} J_{ad} \sigma_{ad}; \quad \sigma_{ad} = -\tfrac{1}{2}(1 + \sigma_a \cdot \sigma_d). \tag{8}$$

The non-vanishing matrix elements of σ_{ad} between the $\bar{\phi}_i$ are:

$\langle \bar{\phi}_i | \sigma_{ad} | \bar{\phi}_i \rangle = -1$ if spins of a and d are parallel

$\langle \bar{\phi}_i | \sigma_{ad} | \bar{\phi}_j \rangle = +1$ if $\bar{\phi}_i$ differs from $\bar{\phi}_j$ only by the interchange of spins

$$ad(\alpha\beta \longleftrightarrow \beta\alpha). \tag{9}$$

The off-diagonal elements are therefore 0 or +1.

From this and the definition (7) it follows that

$$\sigma_{ad} \Phi_A = \Phi_A \tag{10}$$

when the orbitals a, d are bonded in Φ_A, and that when they are not bonded, but a is bonded to x, d to y

$$(1 + \sigma_{ad}) \Phi_A = \Phi_A{}' \tag{11}$$

where $\Phi_A{}'$ is related to Φ_A by switching the bonds $(a^*x)(dy^*)$ to $(a^*d)(xy^*)$

$$\Phi_A = \begin{array}{c} {}^*a\text{—}x \\ \\ d\text{—}y^* \end{array} \qquad \Phi_A{}' = \begin{array}{cc} {}^*a & x \\ | & | \\ b & y^* \end{array} \tag{12}$$

and is a member of the same canonical set. Thus

$$\sigma_{ad} \Phi_A = \sum C_{AB}{}^{(ad)} \Phi_B, \tag{13}$$

where the matrix $C_{AB}{}^{(ad)}$ has off-diagonal elements +1 or 0. Hence

$$H\Phi_A = \sum J_{ad} \sigma_{ad} \Phi_A = \sum J_{ad} C_{AB}{}^{(ad)} \Phi_B \equiv \mathscr{H}_{AB} \Phi_B \tag{14}$$

and $\mathscr{H}_{AB}$ has negative off-diagonal elements because $J_{ad} \leqslant 0$.

The theorem has three important immediate consequences:

(i) The signs of the contact part of the electron-coupled π-electron nuclear spin-spin coupling should alternate with the number of bonds between the nuclei.

(ii) The spin densities on the atoms of neutral alternant radicals are alternately positive and negative.

(iii) The bond orders $P_{ab} = -\tfrac{1}{2}(1 + \langle \sigma_a \cdot \sigma_b \rangle)$ are $<$ or $> -\tfrac{1}{2}$ for atoms ab of different or the same sets.

REFERENCES

[1] McConnell, H. M., 1959, *J. chem. Phys.*, **30**, 126.
[2] Frobenius, S. B., 1909, *Preuss. Akad. Wiss.*, p. 514.

A self-consistent field for the H_2 molecule

by G. BERTHIER
Laboratoire de Chimie Théorique de la Faculté des Sciences,
34 rue d'Ulm, Paris (V^e)

(*Received* 29 *November* 1958)

Recently [1] the author has proposed to solve the Hartree–Fock equations for diatomic molecules in elliptical coordinates, by assuming that the wave function contains an 'angular' part, which is a solution of the corresponding one-electron problem, i.e. in the case of homopolar molecules the angular wave function of the H_2^+ molecule. The present note gives some results which this approximation yields for the H_2 molecule.

For the ground state of the hydrogen molecule, the 'angular' function $S(\nu, \phi)$ can be expressed by an expansion in Legendre polynomials:

$$S(\nu, \phi) = (1/\sqrt{2})N(\nu) = (1/\sqrt{2}) \sum_{s} a_{2s} P_{2s}(\nu)$$

which satisfies the spheroidal wave equation:

$$\frac{d}{d\nu}(1-\nu^2)\frac{dN}{d\nu} + (q^2\nu^2 - A)N = 0. \tag{1}$$

The 'radial' function $M(\mu)$ is a solution of the differential equation:

$$\frac{d}{d\mu}(\mu^2-1)\frac{dM}{d\mu} + (A' + 2R\mu - p^2\mu^2 - V)M = 0 \tag{2}$$

where R is the internuclear distance and V the self-consistent potential, to which each electron of the molecule is subjected. The constant A' is related to the separation constant A of the selected spheroidal function N by

$$A' = A - c_0(p^2 - q^2)$$

where c_0 is the first coefficient of the series $\nu^2 N(\nu)$, and p^2 the eigenvalue of the differential equation (2). The value of p^2 gives the energy ϵ of the occupied orbital in the ground state:

$$p^2 = -(1/2)R^2 e.$$

In principle, the parameter q must be determined by a variational process, but it was found that the total energy is not very sensitive to the precise value of q. By analogy with the H_2^+ molecule, it seemed to us more interesting to retain finally the case $q = p$.

q	0·70	0·7602	0·80
p	0·7597	0·7602	0·7605
ϵ	−0·5889	−0·5897	−0·5901
E	−1·8368	−1·8378	−1·8385

SCF energies (in A.U.) for the equilibrium internuclear distance of H_2.

The orbital energy ϵ is in rough agreement with the ionization potential of the hydrogen molecule (0·57 A.U.), which shows that the Koopmans theorem applies well here. On the other hand, the total electronic energy corresponds to a weak dissociation energy (3·36 ev). In fact, such a result is not very different from those which can be obtained from analytical wave functions of the same form [2, 3], but the present method should be able to be generalized more straightforwardly to other diatomic molecules. Concerning the virial theorem, it can be added that the ratio $-2T/U$ has the value 0·742.

A full account of this work, with numerical tables, will be given later.

The author wishes to thank the Institut Européen de Calcul Scientifique for a grant of time on its IBM 704 electronic computer.

REFERENCES

[1] Berthier, G., 1957, Colloque sur le Calcul des Fonctions d'Onde Moléculaires, Paris.
[2] Coulson, C. A., 1938, *Proc. Camb. phil. Soc.*, **34**, 204.
[3] Murai, T., 1955, *Prog. Rep. Tokyo*, **5**, 6.

Proton acceptor properties of lycopene

by ALBERT WASSERMANN
William Ramsay and Ralph Forster Laboratories, University College, London

(*Received* 4 *December* 1959)

The conjugated polyene, lycopene [1] reacts with trichloroacetic acid (A), like β-carotene [2] to form a protonated mesomeric cation. The electronic spectrum of lycopene (m.p. 173°) in benzene solution, before and after protonation, is shown in the figure. The equilibrium coefficient, relating to the proton transfer from (A) to lycopene (B), defined and determined as in the earlier work [2, 3] is 0·5 ± 0·1 l/mole in benzene solution at 20°. The equilibrium measurements make it probable that one proton only is taken up by (B). Tests with dioxan [2, 3] show that the proton transfer is reversible. The negative logarithms of the molar electrical conductivity, Λ, of protonated (B) in benzene solution, 25·0°, are listed below. The concentrations c of the protonated species were obtained from stoichiometric concentrations, using the results of equilibrium measurements. In calculating the specific conductance a correction, taking care of the specific conductance of trichloroacetic acid alone, was applied [2, 3]

$-\log_{10}\Lambda$ (Λ in l./mole ohm cm)	5·63	4·78	4·31	3·82
$-\log_{10}c$ (c in mole/l.)	2·65	3·65	4·54	5·54

The A . . . B complex decomposes gradually, like the acid adducts of β-carotene [2], and therefore, the electronic spectrum and the electrical conductance were determined with the help of the back extrapolation technique previously employed [2, 3].

In transferring a proton to lycopene, it is assumed that π-electrons are withdrawn from the system of eleven conjugated double bonds, with formation of a new methylenic grouping, like in the protonation of aromatic hydrocarbons [4]. In this manner eleven different mesomeric cations can be formed. An attempt is now made to decide between two extreme cases, namely protonation of the terminal and the central carbon atom, the resulting carbonium ions being designated by (I) and (II). An upper limit of the long wavelength peak λ_1 of the electronic spectrum of protonated lycopene can be calculated from [5]

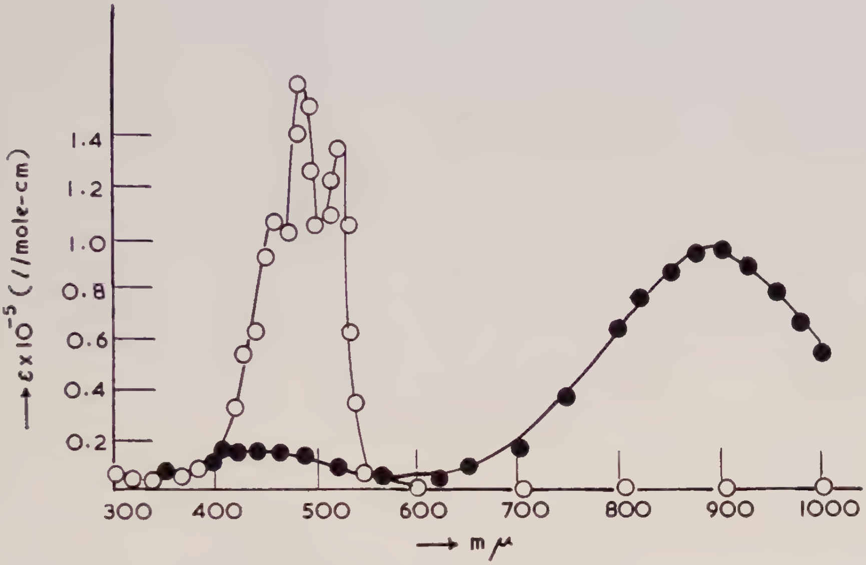

Light absorption of lycopene in benzene solution, at 20°. Concentration of lycopene $4{\cdot}09 \times 10^{-5}$ M. O = No acid; ● = 2·00 M with respect to trichloroacetic acid.

$$\lambda_1 = \frac{8mv}{h}\frac{L^2}{N+1}$$

where m is the mass of the electron, v the velocity of light, h is Planck's constant, L the length of the chromophore and N the number of π-electrons. The species (I) and (II) are like asymmetric cyanine dyes [6, 7], in that the limiting resonance structures are not identical. In such systems the correct value of λ_1, not merely an upper limit, can be obtained by a treatment [5, 7] in which the π-electrons are considered to be placed in a one-dimensional potential, having a sine curve periodicity, but in general the numerical value of the potential is not known.

The chromophore lengths L of the carbonium ions (I) and (II), as obtained by proton transfer to lycopene, are respectively 30·4 and 16·6 Å [8], while the N values are 20 and 10. It follows, therefore, from (1), that the calculated upper limits of λ_1 are respectively 14 500 and 8300 Å for (I) and (II). The first value is larger than the experimentally observed light absorption maximum, 9000 Å, so that end-on protonation is not inconsistent with the results of these calculations. If, on the other hand, the protonation of the central carbon atom is assumed, the calculated upper limit of λ_1 turns out to be too small. Moreover, the species (II) contains five 'ordinary' conjugated double bonds, apart from those which form the mesomeric portion of the carbonium ion, so that a second light absorption peak at about 3300 Å (like, for instance, in vitamin A) should be present. No such peak has been observed.

REFERENCES

[1] ZECHMEISTER, L., 1934, *Carotinoide* (Springer).
[2] WASSERMANN, A., 1954, *J. chem. Soc.*, 4329.
[3] WASSERMANN, A., 1955, *J. chem. Soc.*, 585; 1958, *Ibid.*, 1014.
[4] DALLINGA, G., MACKOR, E. L., and VERRIJN STUART, A. A., 1958, *Mol. Phys.*, **1**, 123.
[5] KUHN, H., 1949, *J. chem. Phys.*, **17**, 1198.
[6] BROOKER, L. C. S., 1942, *Rev. mod. Phys.*, **14**, 275.
PAULING, L., 1939, *Proc. nat. Acad. Sci., Wash.*, **25**, 577.
[7] KUHN, H., 1948, *Helv. chim. acta*, **31**, 1441; 1949, *Ibid.*, **32**, 2247; 1955, *Chimia*, **9**, 237.
[8] LENNARD-JONES, J. E., 1937, *Proc. roy. Soc.* A, **158**, 280.

Long-range interaction of two 1s-hydrogen atoms expressed in terms of natural spin-orbitals†

by J. O. HIRSCHFELDER
Theoretical Chemistry Laboratory, Chemistry Department, University of Wisconsin, Madison, Wisconsin

and P. O. LÖWDIN
Quantum Chemistry Group, University of Uppsala, Uppsala, Sweden

(*Received* 6 *December* 1958)

The interaction between two hydrogen atoms in their ground state at large separation is treated by means of a variational form of the perturbation theory, which essentially involves the calculation of the reciprocal of the unperturbed matrix by means of successive inversion. A basic set which avoids the continuum is used. The energy of the system of two hydrogen atoms at large separations is found to be

$$E=[-1-6\cdot499026/R^6-144\cdot8497/R^8-\ldots]e^2/a_0$$

where the separation R is measured in units of a_0. The coefficient of R^{-6} agrees with the calculations of Pauling and Beach but the coefficient of R^{-8} is quite different from theirs. The wave function is greatly simplified by introducing natural orbitals. If the wave function is approximated by using only one or two sets of natural orbitals, very little error results in the calculated dispersion energy. Also, it is shown that such an approximation leads to very little error in the mean square deviation of the approximate wave function from the exact function. This illustrates the theorem that an approximate wave function composed of n natural orbitals has a smaller mean square deviation from the true function than an approximate wave function made up from n other sorts of orbitals. An application of long-range intermolecular force calculations to collision theory is also given.

1. INTRODUCTION

The long-range interaction of two 1*s* hydrogen atoms provides an excellent molecular example where the use of natural orbitals greatly simplifies the description of the wave function. In § 2 through § 5, the terms in the dispersion energy which vary as the inverse sixth and inverse eighth powers of the separation are calculated by means of a variational form of the perturbation theory. The corresponding wave function is expressed as a linear combination of products of *p* and *d* orbitals as well as the initial unperturbed product of 1*s* orbitals. This wave function contains a great many terms and is difficult to interpret. In § 6, this wave function is rearranged into a rapidly converging series of products of natural orbitals. Very little error is made either in the wave function or in the dispersion energy if this series is truncated so as to obtain an approximate wave function composed of only one or two sets of natural orbitals. This illustrates the inherent advantage of natural orbitals. They lead to simple wave functions which have simple physical interpretations. In §7, the results of the dispersion energy calculations are applied to the determination of collisional transition probabilities.

---

† Most of this work was carried out at Uppsala University and was supported by the Aeronautical Research Laboratory, Wright Air Development Center of the Air Research and Development Command through its European Office under a contract with Uppsala University. A small part of this work was supported by the United States Air Force under Contract AF33(616)–3414 with the University of Wisconsin, monitored by Aeronautical Research Laboratory, Wright Development Center.

The interaction of two 1*s* hydrogen atoms is a simple two-electron problem. The Hamiltonian for the interaction of the hydrogen atoms *a* and *b* with electrons '1' and '2' may be written in the form [1]

$$\mathscr{H}(1,2)=\mathscr{H}_a(1)+\mathscr{H}_b(2)+\varphi_e \tag{1}$$

where

$$\mathscr{H}_a(1)=-\tfrac{1}{2}\Delta_1-\frac{1}{r_{a1}}, \qquad \mathscr{H}_b(2)=-\tfrac{1}{2}\Delta_2-\frac{1}{r_{b2}}, \tag{2}$$

$$\varphi_e=\frac{1}{R}+\frac{1}{r_{12}}-\frac{1}{r_{a2}}-\frac{1}{r_{b1}}. \tag{3}$$

In making the calculations, it is convenient to use the coordinates as shown in figure 1. Here θ_{a1} and θ_{b2} are interior angles and ϕ_{a1} and ϕ_{b2} are measured in opposite directions. This choice of coordinates makes the problem symmetrical with respect to atoms *a* and *b*. Throughout this paper distance is measured in units of Bohr radii, a_0, and energy is expressed in atomic units, e^2/a_0.

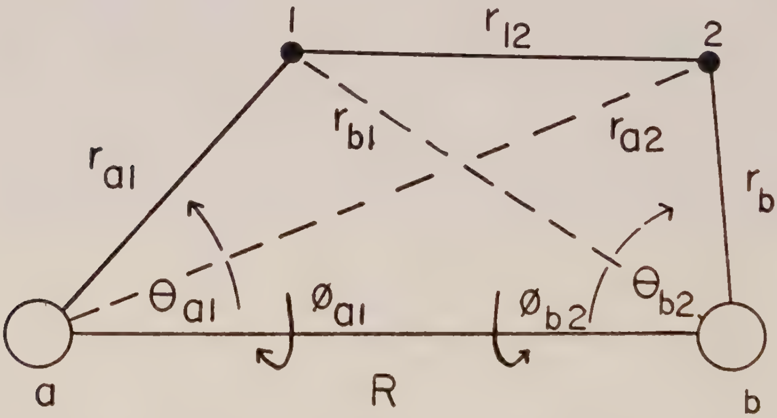

Figure 1. Distances and angles used in the calculations. Note that the angles θ_{a1} and θ_{b2} are interior and the angles ϕ_{a1} and ϕ_{b2} are measured in opposite directions. This definition of the angles makes the formulae symmetrical with respect to the two atoms.

At the very large separations where the dispersion energy predominates, the overlapping of the atomic charge distributions may be neglected. Under such circumstances, the interaction potential φ_e may be expanded [2] in an infinite series

$$\varphi_e=\sum_{k=1}^{\infty}\sum_{l=1}^{\infty}\varphi_{k,l} \tag{4}$$

where

$$\varphi_{k,l}=\frac{(k+l)!\,r_{a1}{}^k r_{b2}{}^l}{R^{k+l+1}}\sum_{m=-<}^{<}\frac{P_k{}^{|m|}(\cos\theta_{a1})P_l{}^{|m|}(\cos\theta_{b2})\exp\left[im(\phi_{a1}+\phi_{b2})\right]}{(k+|m|)!\,(l+|m|)!}. \tag{5}$$

Here the symbol $<$ corresponds to the lesser of k and l. It is convenient to introduce the normalized spherical harmonics

$$Y_l^m(\theta,\phi) = i^{|m|-m}\sqrt{\left(\frac{(2l+1)}{4\pi}\frac{(l-|m|)!}{(l+|m|)!}\right)}\,P_l^{|m|}(\cos\theta)\exp(im\phi) \tag{6}$$

and the set of ortho-normal angular functions

$$\Theta_{k,l} = \frac{(k+l)!}{N_{k,l}\sqrt{[(2k+1)(2l+1)]}}\sum_{m=-<}^{<}\frac{Y_k^m(\theta_{a1},\phi_{a1})Y_l^m(\theta_{b2},\phi_{b2})}{\sqrt{[(k+m)!\,(k-m)!\,(l+m)!\,(l-m)!]}} \tag{7}$$

where

$$N_{k,l} = \frac{(k+l)!}{\sqrt{[(2k+1)(2l+1)]}}\left[\sum_{m=-<}^{<}\{(k+m)!\,(k-m)!\,(l+m)!\,(l-m)!\}^{-1}\right]^{1/2}. \tag{8}$$

The $\Theta_{k,l}$ are ortho-normal in the sense that

$$\int_0^{\pi}\int_0^{\pi}\int_0^{2\pi}\int_0^{2\pi}\Theta^*_{k',l'}\Theta_{k,l}\sin\theta_{a1}\sin\theta_{b2}\,d\theta_{a1}\,d\theta_{b2}\,d\phi_{a1}\,d\phi_{b2} = \delta_{k'k}\delta_{l'l}. \tag{9}$$

In terms of these ortho-normal functions,

$$\varphi_{k,l} = \frac{4\pi N_{k,l}r_{a1}{}^k r_{b2}{}^l}{R^{k+l+1}}\Theta_{k,l}. \tag{10}$$

The term $\varphi_{1,1}$ is the dipole–dipole interaction operator, $\varphi_{1,2}+\varphi_{2,1}$ is the dipole–quadrupole interaction operator, $\varphi_{2,2}$ is the quadrupole–quadrupole interaction operator, etc.

The long-range energy of interaction of two 1*s*-hydrogen atoms can be expressed in the form of a power series in $1/R$,

$$\Phi = -\frac{B_6}{R^6}-\frac{B_8}{R^8}-\frac{B_9}{R^9}-\frac{B_{10}}{R^{10}}-\dots. \tag{11}$$

The term $-B_6/R^6$ is the usual London dispersion energy which results from the second-order perturbation considering $\varphi_{1,1}$ as the perturbation potential. The term $-B_8/R^8$ corresponds to the second-order perturbation considering $[\varphi_{1,2}+\varphi_{2,1}]$ as the perturbation potential. The term $-B_9/R^9$ corresponds to the third-order perturbation considering $\varphi_{1,1}$ as the perturbation potential. The term $-B_{10}/R^{10}$ results from the second-order perturbation considering $[\varphi_{2,2}+\varphi_{1,3}+\varphi_{3,1}]$ as the perturbation potential. The higher terms in the series originate from a variety of terms in the interaction potential and a variety of orders in the perturbation. In order to keep the present treatment simple, we shall restrict our calculations to B_6 and B_8.

2. THE BASIC ORBITALS AND THEIR PROPERTIES

Now let the complete set of basic atomic orbitals be [3]†

$$\psi_{nlm} = \bar{R}_{nl}(r)Y_l^m(\theta,\phi) \tag{12}$$

where

$$\bar{R}_{nl}(r) = \frac{2^{3/2}}{(n+l+1)!}\sqrt{\left(\frac{(n-l-1)!}{(n+l+1)!}\right)}(2r)^l L^{2l+2}_{n+l+1}(2r)\exp(-r). \tag{13}$$

---

† Note that the associated Laguerre polynomials here are defined in the same manner as in L. Pauling and B. Wilson, *Introduction to Quantum Mechanics* (McGraw-Hill, 1935),

$$L_n(x) = \exp(x)\frac{d^n}{dx^n}(x^n\exp(-x)) \quad\text{and}\quad L_n^k(x) = \frac{d^k}{dx^k}L_n.$$

Throughout this paper we use the bar over the R or over the term symbol to indicate these special orbitals as contrasted to the usual hydrogen orbitals. These radial functions form an ortho-normal set:

$$\int_0^\infty \bar{R}_{nl}(r)\bar{R}_{n'l}(r)r^2\,dr=\delta_{nn'}. \tag{14}$$

Because the $\bar{R}_{nl}$ form a complete set, they are for computational purposes superior to the hydrogenic orbitals, which are not complete until the wave functions for the continuum are taken into full account. It will be noted that our $\psi(1s)$ is the same as the hydrogen $1s$ orbital, but the two sets of orbitals differ for all other states. Since

$$\bar{R}_{10}=2\exp(-r) \tag{15}$$

and $L^{2l+2}_{2l+2}(2r)=(2l+2)\,!$, it follows that

$$r^l\bar{R}_{10}=\frac{1}{2^l}\sqrt{\left(\frac{(2l+2)\,!}{2}\right)}\,\bar{R}_{l+1,l}. \tag{16}$$

If $\mathscr{H}_{\mathrm{H}}=-\frac{1}{2}\Delta-1/r$ is the Hamiltonian for an isolated hydrogen atom, then

$$\mathscr{H}_{\mathrm{H}}\psi_{nlm}=Y_l^m(\theta,\phi)[K_l-1/r]\bar{R}_{nl} \tag{17}$$

where K_l is the kinetic energy operator

$$K_l=\frac{1}{2r^2}\left[l(l+1)-\frac{d}{dr}\left(r^2\frac{d}{dr}\right)\right]. \tag{18}$$

Using these non-hydrogenic orbitals, the matrix components between two states of the same atom are then

$$(n'l'm'|\mathscr{H}_{\mathrm{H}}|nlm)=\delta_{l'l}\delta_{m'm}\left[\int_0^\infty \bar{R}_{n'l}K_l\bar{R}_{nl}r^2\,dr\;-\;\int_0^\infty \bar{R}_{n'l}\bar{R}_{nl}r\,dr\right]. \tag{19}$$

The kinetic energy integral can be transformed by integration by parts to the more convenient form [4]

$$\int_0^\infty \bar{R}_{n'l}K_l\bar{R}_{nl}r^2\,dr=\frac{1}{2}\int_0^\infty \frac{d}{dr}\left(\frac{\bar{R}_{n'l}}{r^l}\right)\frac{d}{dr}\left(\frac{\bar{R}_{nl}}{r^l}\right)r^{2l+2}\,dr. \tag{20}$$

Making use of equations (A 13) and (A 14) in Appendix I, the diagonal elements of the matrix for the energy of an isolated hydrogen atom are

$$(nlm|\mathscr{H}_{\mathrm{H}}|nlm)=\frac{4n-2l-1}{2(2l+3)}-\frac{1}{l+1}. \tag{21}$$

The non-diagonal matrix elements with $n>n'$ are

$$(n'l'm'|\mathscr{H}_{\mathrm{H}}|nlm)=\delta_{l'l}\delta_{m'm}\left(\frac{\epsilon_{n'l}}{\epsilon_{nl}}\right)\left[\frac{2n'+1}{2l+3}-\frac{1}{l+1}\right]. \tag{22}$$

Here

$$\epsilon_{nl}=\sqrt{\left(\frac{(n+l+1)\,!}{(n-l-1)\,!}\right)}. \tag{23}$$

3. THE MATRIX COMPONENTS FOR THE ENERGY OF TWO INTERACTING HYDROGEN ATOMS

The spatial part of the wave function for two interacting hydrogen atoms can be written in the form

$$\Phi=N2^{-1/2}\sum_{\substack{nlm\\ n'l'm'}} C_{nlm;\,n'l'm'}[\psi_{nlm}(a1)\psi_{n'l'm'}(b2)\;\pm\;\psi_{nlm}(a2)\psi_{n'l'm'}(b1)]. \tag{24}$$

Here the plus sign would refer to a singlet state whereas the minus sign would be appropriate for a triplet state. The notation $\psi_{nlm}(a1)$ corresponds to electron 1 in the *nlm*th orbital, defined by equation (12), having proton *a* as its coordinate origin. Similarly $\psi_{nlm}(b2)$ corresponds to electron 2 in an atomic orbital centred on proton *b*. Here N is the normalization constant. Because the set of orbitals completely spans one electron space, we can be sure that equation (24) is the most general form for a two-electron wave function.

At very large separations, the exchange energy becomes negligible as compared to the dispersion energy and the energies of the singlet and triplet states become equal. In the limit of large separations, no error in the energy of interaction results from replacing the wave function of equation (24) by the function

$$\Psi(a1, b2) = N \sum_{\substack{nlm \\ n'l'm'}} C_{nlm\,;\,n'l'm'}\psi_{nlm}(a1)\psi_{n'l'm'}(b2). \tag{25}$$

Thus, in the calculations of the dispersion energy we can use either form for the wave function. The resulting values of the coefficients, $C_{nlm\,;\,n'l'm'}$, are unaffected by the form which we assume.

In the limit of large separations of the hydrogen atoms, it can be shown that each of the coefficients of equation (24) may be expressed in a power series in $1/R$. Thus

$$C_{nlm\,;\,n'l'm'} = \sum_{k=0}^{\infty} \frac{1}{R^k} C^{(k)}_{nlm\,;\,n'l'm'}. \tag{26}$$

If the two hydrogen atoms are in the 1*s* state when they are infinitely separated, this corresponds to

$$C^{(0)}_{100\,;\,100} = 1, \tag{27}$$

$$C^{(0)}_{nlm\,;\,n'l'm'} = 0, \qquad n \text{ or } n' > 1. \tag{28}$$

Since the interaction potential, φ_e, can be expanded in a power series in $1/R$ beginning with a term in $1/R^3$, it follows that all of the quantities $C^{(1)}$ and $C^{(2)}$ are zero.

The wave function corresponding to the two 1*s*-hydrogen atoms at infinite separation is

$$\psi_{100}(a1)\psi_{100}(b2) = (1/4\pi)\bar{R}_{10}(r_{a1})\bar{R}_{10}(r_{b2}). \tag{29}$$

It follows from equations (10) and (16) that

$$\varphi_{k,l}\psi_{100}(a1)\psi_{100}(b2) = \frac{A_{k,l}\bar{R}_{k+1,k}(a1)\bar{R}_{l+1,l}(b2)\,\Theta_{k,}}{R^{k+l+1}} \tag{30}$$

where

$$A_{k,l} = \sqrt{\left(\frac{(2k+2)!\,(2l+2)!}{2^{k+l+1}}\right)} N_{k,l}. \tag{31}$$

Values of $N_{1,1}$, $N_{1,2}$, $A_{1,1}$ and $A_{1,2}$ are given in Table 1. The form of equation (30) makes it very easy to calculate the B_6 and B_8 of equation (11).

$N_{1,1} = (2/3)^{1/2}$ $N_{1,2} = 1$	$A_{1,1} = (6)^{1/2}$ $A_{1,2} = (3/2)(30)^{1/2}$

Table 1.

4. CALCULATION OF THE INVERSE SIXTH POWER DISPERSION ENERGY, $-B_6/R^6$

In the calculation of B_6 it is only necessary to consider $\varphi_{1,1}$ as the perturbation operator and furthermore, it is permissible to neglect those matrix components which would lead to energy of interaction terms of the order of $1/R^9$ or higher powers in $1/R$. From equation (30), and the angular orthogonality relation equation (9), it follows that the initial $(1s)^2$ wave function $\psi_{100}(a1)\psi_{100}(b2)$ interacts dipole–dipole-wise only with the $(\overline{2p})^2$ wave function [5],

$$\Omega_{21;\,21} = \bar{R}_{21}(r_{a1})\bar{R}_{21}(r_{b2})\Theta_{1,1}. \tag{32}$$

Here, from equation (7) and table 1,

$$\Theta_{1,1} = \frac{2}{\sqrt{6}}\, Y_1^0(a1)Y_1^0(b2) + \frac{1}{\sqrt{6}}\, Y_1^1(a1)Y_1^1(b2) + \frac{1}{\sqrt{6}}\, Y_1^{-1}(a1)Y_1^{-1}(b2). \tag{33}$$

Thus, making use of equation (30), we obtain

$$\int \Omega^*_{21;\,21}\mathscr{H}\Psi_{100;\,100}\,d\tau = \sqrt{6}/R^3. \tag{34}$$

The energy of the two hydrogen atoms in interaction is now easily found by the special form of perturbation theory sketched in Appendix II. According to equation (A 22), we obtain

$$E = (1s^2|\mathscr{H}^{(0)}|1s^2) - (6/R^6)(\overline{2p}^2|\,(\mathbf{H}_{22}^{(0)} - E\,\mathbf{1})^{-1}|\overline{2p}^2). \tag{35}$$

Noting that $(1s^2|\mathscr{H}^{(0)}|1s^2) = -1$, one gets the first approximation $E = -1$ and

$$B_6 = 6(\overline{2p}^2|\mathbf{T}|\overline{2p}^2). \tag{36}$$

Here

$$\mathbf{T} = [\mathbf{H}_{22}^{(0)} + \mathbf{1}]^{-1}. \tag{37}$$

Thus our problem is solved by taking a special element of the reciprocal of the unperturbed matrix. In forming the latter, we observe that, by virtue of equation (22), $\Omega_{21;\,21}$ has unperturbed matrix components with all the $(\overline{2p}, \overline{np})$ states having the wave functions

$$\Omega_{21;\,n1} = 2^{-1/2}[\bar{R}_{21}(r_{a1})\bar{R}_{n1}(r_{b2}) + \bar{R}_{n1}(r_{a1})\bar{R}_{21}(r_{b2})]\Theta_{1,1}. \tag{38}$$

The $\Omega_{21;\,n1}$ wave functions also have independent energy matrix components with the $(\overline{np}, \overline{np})$ states whose wave functions are

$$\Omega_{n1;\,n1} = \bar{R}_{n1}(r_{a1})\bar{R}_{n1}(r_{b2})\Theta_{1,1} \tag{39}$$

and with the $(\overline{n'p}, \overline{np})$ states with n' different from n. The wave functions for the $(\overline{n'p}, \overline{np})$ states are

$$\Omega_{n'1;\,n1} = 2^{-1/2}[\bar{R}_{n'1}(r_{a1})\bar{R}_{n1}(r_{b2}) + \bar{R}_{n1}(r_{a1})\bar{R}_{n'1}(r_{b2})]\Theta_{1,1}. \tag{40}$$

Thus, making use of equations (21) and (22), we get

$$\int \Omega^*_{n1;\,n1}\mathscr{H}\,\Omega_{n1;\,n1}\,d\tau = \tfrac{4}{5}(n-2), \tag{41}$$

$$\begin{aligned}\int \Omega^*_{n1;\,n1}\mathscr{H}\,\Omega_{n1;\,n'1}\,d\tau &= \left(\frac{4n'-3}{10}\right)\frac{\epsilon_{n'}}{\epsilon_n}\sqrt{2}, \quad n' < n \\ &= \left(\frac{4n-3}{10}\right)\frac{\epsilon_n}{\epsilon_{n'}}\sqrt{2}, \quad n' > n,\end{aligned} \tag{42}$$

$$\int \Omega^*_{n1;\,n'1}\mathscr{H}\,\Omega_{n1;\,n'1}\,d\tau = \frac{2}{5}(n + n' - 4) \tag{43}$$

	$1s^2$	$\overline{2p}^2$	$\overline{2p}\,\overline{3p}$	$\overline{3p}^2$	$\overline{2p}\,\overline{4p}$	$\overline{3p}\,\overline{4p}$	$\overline{4p}^2$	$\overline{2p}\,\overline{5p}$	$\overline{3p}\,\overline{5p}$	$\overline{4p}\,\overline{5p}$	$\overline{5p}^2$
$1s^2$	-1	$\sqrt{6}/R^3$	0	0	0	0	0	0	0	0	0
$\overline{2p}^2$	$\sqrt{6}/R^3$	0	0·316228	0	0·182574	0	0	0·119523	0	0	0
$\overline{2p}\,\overline{3p}$	0	0·316228	0·400000	0·316228	0·519615	0·129099	0	0·340168	0·084515	0	0
$\overline{3p}^2$	0	0	0·316228	0·800000	0	0·734847	0	0	0·481070	0	0
$\overline{2p}\,\overline{4p}$	0	0·182574	0·519615	0	0·800000	0·223607	0·182574	0·851050	0	0·084515	0
$\overline{3p}\,\overline{4p}$	0	0	0·129099	0·734847	0·223607	1·200000	0·734847	0	0·851050	0·340168	0
$\overline{4p}^2$	0	0	0	0	0·182574	0·734847	1·600000	0	0	1·203566	0
$\overline{2p}\,\overline{5p}$	0	0·119523	0·340168	0	0·851050	0	0	1·200000	0·223607	0·129099	0·119523
$\overline{3p}\,\overline{5p}$	0	0	0·084515	0·481070	0	0·851050	0	0·223607	1·600000	0·519615	0·481070
$\overline{4p}\,\overline{5p}$	0	0	0	0	0·084515	0·340168	1·203566	0·129099	0·519615	2·000000	1·203566
$\overline{5p}^2$	0	0	0	0	0	0	0	0·119523	0·481070	1·203566	2·400000

Table 2. The relevant part of the energy matrix **H** of order eleven in calculating B_6.

and for n, n', and n'' all having different values,

$$\int \Omega^*_{n1;\,n'1} \mathscr{H} \Omega_{n1;\,n''1}\, d\tau = \left(\frac{4n'-3}{10}\right)\frac{\epsilon_{n'}}{\epsilon_{n''}}, \quad n' < n''. \tag{44}$$

Each of these $(\overline{np}, \overline{n'p})$ states has matrix components with various $(\overline{np}, \overline{n''s})$ and $(\overline{np}, \overline{n''d})$ states, etc. which vary as $1/R^3$ or higher powers of $1/R$. However, such interactions have no effect on the value of B_6, which is given quite rigorously by equation (36).

In treating the unperturbed matrix $[\mathbf{H}_{22}{}^{(0)} + \mathbf{1}]^{-1}$, it is convenient to arrange the configurations in the following ‘lexicographic’ order:

$$(\overline{2p})^2 \; (\overline{3p}, \overline{2p}) \; (\overline{3p})^2 \; (\overline{4p}, \overline{2p}) \; (\overline{4p}, \overline{3p}) \; (\overline{4p})^2 \ldots$$

and to calculate the reciprocal matrix by means of the method of successive inversion, described in Appendix III. The relevant part of the energy matrix of the eleventh order is shown in table 2. In table 3, the values of B_6

Last configuration included	B_6
$(\overline{2p})^2$	6·0000000
$(\overline{3p})^2$	6·4821428
$(\overline{4p})^2$	6·4984439
$(\overline{5p})^2$	6·4990025
$(\overline{6p}, \overline{2p})$	6·4990230
$(\overline{6p}, \overline{3p})$	6·4990252

Table 3. Successive approximations of B_6 obtained by means of equation (36).

are given corresponding to the inclusion of a successively larger number of states in the secular equation. After the configuration $(\overline{6p}, \overline{3p})$ we interrupted our lexicographic series. Addition of the extra configuration $(\overline{7p}, \overline{2p})$ leads to the result

$$B_6 = 6{\cdot}4990260,$$

and further addition of the configuration $(\overline{8p}, \overline{2p})$ did not change this result, which is in close agreement with the value obtained by Pauling and Beach [6] by solving a secular equation. It is interesting to note that, if we had carried out the corresponding calculation by means of hydrogen-like orbitals, an appreciable fraction of B_6 would have originated from the continuum energy states [7].

The wave function for two $1s$-hydrogen atoms in long-range interaction may be obtained by using formula (A 20) in Appendix II which, to the order of $1/R^3$, gives

$$\Psi = (1s)^2 - \frac{\sqrt{6}}{R^3} \sum_{n \leqslant n'} \Omega_{n1;\,n'1} (\overline{np}, \overline{n'p} | \mathbf{T} | \overline{2p}^2). \tag{45}$$

Here the coefficients of $\Omega_{n1;\,n'1}$ are the first column of the inverse matrix $\mathbf{T} = (\mathbf{H}_{22}{}^{(0)} + \mathbf{1})^{-1}$. The coefficients of this matrix are given in table 4. The numerical calculation of these coefficients was carried out using the procedure explained in Appendix III.

	$\overline{2p}^2$	$\overline{2p}\,\overline{3p}$	$\overline{3p}^2$	$\overline{2p}\,\overline{4p}$	$\overline{3p}\,\overline{4p}$	$\overline{4p}^2$	$\overline{2p}\,\overline{5p}$	$\overline{3p}\,\overline{5p}$	$\overline{4p}\,\overline{5p}$	$\overline{5p}^2$
$\overline{2p}^2$	+1·083167	−0·238117	+0·040301	−0·038417	+0·004125	+0·001344	−0·007144	−0·000569	+0·000406	+0·000188
$\overline{2p}\,\overline{3p}$	−0·238117	+0·894613	−0·165888	−0·218676	+0·023477	+0·007651	−0·040661	−0·003234	+0·002310	+0·001069
$\overline{3p}^2$	+0·040301	−0·165888	+0·691393	+0·064737	−0·228273	+0·055978	+0·002830	−0·050520	+0·008628	+0·003994
$\overline{2p}\,\overline{4p}$	−0·038417	−0·218676	+0·064737	+0·762054	−0·096212	−0·027692	−0·264072	+0·048487	+0·002966	+0·001373
$\overline{3p}\,\overline{4p}$	+0·004125	+0·023477	−0·228273	−0·096212	+0·675273	−0·198556	+0·050344	−0·192808	+0·031229	+0·014456
$\overline{4p}^2$	+0·001344	+0·007651	+0·055978	−0·027692	−0·198556	+0·556265	+0·010812	+0·088819	−0·245375	+0·073913
$\overline{2p}\,\overline{5p}$	−0·007144	−0·040661	+0·002830	−0·264072	+0·050344	+0·010812	+0·570726	−0·060757	−0·014037	−0·006498
$\overline{3p}\,\overline{5p}$	−0·000569	−0·003234	−0·050520	+0·048487	−0·192808	+0·088819	−0·060757	+0·485675	−0·081506	−0·037731
$\overline{4p}\,\overline{5p}$	+0·000406	+0·002310	+0·008628	+0·002966	+0·031229	−0·245375	−0·014037	−0·081506	+0·510554	−0·168705
$\overline{5p}^2$	+0·000188	+0·001069	+0·003994	+0·001373	+0·014456	+0·073913	−0·006498	−0·037731	−0·168705	+0·359405

Table 4. The matrix $\mathbf{T}=(\mathbf{H}_{22}^{(0)}+\mathbf{1})^{-1}$ of order ten found by successive inversion.

From the definitions of the $\Omega_{n1;\,n'1}$, as given by equations (39) and (40) together with equation (33), it follows that

$$\Omega_{n1,\,n1}=6^{-1/2}[2\psi_{n10}(a1)\psi_{n10}(b2)+\psi_{n11}(a1)\psi_{n11}(b2)+\psi_{n1-1}(a1)\psi_{n1-1}(b2)] \tag{46}$$

and, when n' is not equal to n,

$$\Omega_{n1;\,n'1}=\frac{1}{\sqrt{12}}\begin{bmatrix} 2\psi_{n10}(a1)\psi_{n'10}(b2) & +2\psi_{n'10}(a1)\psi_{n10}(b2) \\ +\psi_{n11}(a1)\psi_{n'11}(b2) & +\psi_{n'11}(a1)\psi_{n11}(b2) \\ +\psi_{n1-1}(a1)\psi_{n'1-1}(b2) & +\psi_{n'1-1}(a1)\psi_{n1-1}(b2) \end{bmatrix}. \tag{47}$$

Thus, comparing equation (45) with equation (25) and making use of equation (26) we find

$$C^{(3)}_{n10;\,n10}=-2(\overline{np},\overline{np}|\mathbf{T}|\overline{2p}^2), \tag{48}$$

$$C^{(3)}_{n11;\,n11}=C^{(3)}_{n1-1,\,n1-1}=-(\overline{np},\overline{np}|\mathbf{T}|\overline{2p}^2), \tag{49}$$

and, when n' is not equal to n,

$$C^{(3)}_{n10;\,n'10}=-\sqrt{2}(\overline{np},\overline{n'p}|\mathbf{T}|\overline{2p}^2), \tag{50}$$

$$C^{(3)}_{n11;\,n'11}=C^{(3)}_{n1-1;\,n'1-1}=-2^{-1/2}(\overline{np},\overline{n'p}|\mathbf{T}|\overline{2p}^2). \tag{51}$$

The matrix of coefficients $C^{(3)}_{n11;\,n'11}$ is given in table 5. Here the states are designated by numbers as follows:

Number	1	2	3	4
State	$\overline{2p}$	$\overline{3p}$	$\overline{4p}$	$\overline{5p}$

$j \backslash i$		1	2	3	4
		$\overline{2p}$	$\overline{3p}$	$\overline{4p}$	$\overline{5p}$
1	$\overline{2p}$	−1·083167	+0·168374	+0·027165	+0·005052
2	$\overline{3p}$	+0·168374	−0·040301	−0·002917	+0·000402
3	$\overline{4p}$	+0·027165	−0·002917	−0·001344	−0·000287
4	$\overline{5p}$	+0·005052	+0·000402	−0·000287	−0·000188

Table 5. The matrix of coefficients $C^{(3)}_{n11;n'11}=C^{(3)}_{n1-1;n'1-1}=(\frac{1}{2})C^{(3)}_{n10;n'10}$.

5. CALCULATION OF THE INVERSE EIGHTH POWER DISPERSION ENERGY, $-B_8/R^8$

The calculation of B_8 is very similar to the determination of B_6. There is no interference between these two orders of the dispersion energy or their corresponding wave functions. Thus the inverse eighth power dispersion energy is obtained by using $[\varphi_{1,2}+\varphi_{2,1}]$ as the perturbation operator. Now in addition to the $(1s)^2$ state we must consider the whole family of $(\overline{np},\overline{n'd})$ states whose wave functions are

$$\Omega_{n1;\,n'2}=2^{-1/2}[\bar{R}_{n1}(r_{a1})\bar{R}_{n'2}(r_{b2})\Theta_{1,2}+\bar{R}_{n'2}(r_{a1})\bar{R}_{n1}(r_{b2})\Theta_{2,1}]. \tag{52}$$

Here

$$\Theta_{1,2}=5^{-1/2}[\sqrt{3}Y_1^0(a1)Y_2^0(b2)+Y_1^1(a1)Y_2^1(b2)+Y_1^{-1}(a1)Y_2^{-1}(b2)], \tag{53}$$

$$\Theta_{2,1}=5^{-1/2}[\sqrt{3}Y_2^0(a1)Y_1^0(b2)+Y_2^1(a1)Y_1^1(b2)+Y_2^{-1}(a1)Y_1^{-1}(b2)]. \tag{54}$$

Thus

$$\Omega_{n1;\,n'2}=\frac{1}{\sqrt{10}}\left[\begin{array}{l} 3[\psi_{n10}(a1)\psi_{n'20}(b2) \;+\; \psi_{n'20}(a1)\psi_{n10}(b2)] \\ +[\psi_{n11}(a1)\psi_{n'21}(b2) \;+\; \psi_{n'21}(a1)\psi_{n11}(b2)] \\ +[\psi_{n1-1}(a1)\psi_{n'2-1}(b2)+\psi_{n'2-1}(a1)\psi_{n1-1}(b2)] \end{array}\right]. \tag{55}$$

The initial $(1s)^2$ state interacts only with the $(\overline{2p}, \overline{3d})$ state to give the perturbation matrix element

$$\int \Omega^*{}_{21;\,32}\mathscr{H}\Psi_{100;\,100}\,d\tau=\frac{3\sqrt{15}}{R^4} \tag{56}$$

and, by using equation (A 22), we then conclude that B_8 is given by the expression

$$B_8=135(\overline{2p}, \overline{3d}|\mathbf{T}|\overline{2p}, \overline{3d}). \tag{57}$$

Here, as before, $\mathbf{T}=(\mathbf{H}_{22}{}^{(0)}+\mathbf{1})^{-1}$ and our problem is solved by taking a special element of the reciprocal of the unperturbed matrix. In handling the unperturbed matrix $\mathbf{T}$, we arrange the configurations $(\overline{np}, \overline{n'd})$ in the following order:

$$(\overline{2p}, \overline{3d}),\ (\overline{3p}, \overline{3d}),\ (\overline{2p}, \overline{4d}),\ (\overline{3p}, \overline{4d}),\ (\overline{4p}, \overline{4d}),\ (\overline{2p}, \overline{5d}),\ (\overline{3p}, \overline{5d}),\ (\overline{4p}, \overline{5d}),$$
$$(\overline{5p}, \overline{5d}),\ (\overline{4p}, \overline{3d}),\ (\overline{5p}, \overline{3d}),\ (\overline{5p}, \overline{4d}),\ \ldots. \tag{58}$$

The matrix elements are easily calculated from equations (21) and (22) since

$$\int \Omega^*{}_{n1;\,n'2}\mathscr{H}\,\Omega_{n''1;\,n'''2}\,d\tau=\delta_{nn''}(n'20|\mathscr{H}_{\mathrm{H}}|n'''20)+\delta_{n'n'''}(n10|\mathscr{H}_{\mathrm{H}}|n''10). \tag{59}$$

If $n=n''$ and $n'=n'''$,

$$\int \Omega^*{}_{n1;\,n'2}\mathscr{H}\,\Omega_{n1;\,n'2}\,d\tau=\tfrac{2}{5}(n-2)+\tfrac{2}{7}(n'-3). \tag{60}$$

If $n=n''$ but $n'\neq n'''$,

$$\begin{aligned}\int \Omega^*{}_{n1;\,n'2}\mathscr{H}\,\Omega_{n1;\,n'''2}\,d\tau&=\left(\frac{\epsilon_{n'2}}{\epsilon_{n'''2}}\right)\left(\frac{4n'-5}{14}\right), \quad n'''>n', \\ &=\left(\frac{\epsilon_{n'''2}}{\epsilon_{n'2}}\right)\left(\frac{4n'''-5}{14}\right), \quad n'''<n'.\end{aligned} \tag{61}$$

If $n\neq n''$ but $n'=n'''$,

$$\begin{aligned}\int \Omega^*{}_{n1;\,n'2}\mathscr{H}\,\Omega_{n''1;\,n'2}\,d\tau&=\left(\frac{\epsilon_{n1}}{\epsilon_{n''1}}\right)\left(\frac{4n-3}{10}\right), \quad n''>n, \\ &=\left(\frac{\epsilon_{n''1}}{\epsilon_{n1}}\right)\left(\frac{4n''-3}{10}\right), \quad n''<n.\end{aligned} \tag{62}$$

The relevant part of the energy matrix of the twelfth order is shown in table 6. The matrix $\mathbf{T}$ of order 12 is given in table 7. The values of B_8 considering various numbers of configurations are listed in table 8.

From table 8 it appears that the calculations including twelve configurations give the result

$$B_8=144{\cdot}8497.$$

This agrees with a rough calculation of Lynn and Dalgarno [8] who obtained $B_8=146$. Unfortunately, it does not agree with the value of $B_8=124{\cdot}399$ obtained by Pauling and Beach [6]. We do not know the reason for this discrepancy.

	$\overline{2p}\,\overline{3d}$	$\overline{3p}\,\overline{3d}$	$\overline{2p}\,\overline{4d}$	$\overline{3p}\,\overline{4d}$	$\overline{4p}\,\overline{4d}$	$\overline{2p}\,\overline{5d}$	$\overline{3p}\,\overline{5d}$	$\overline{4p}\,\overline{5d}$	$\overline{5p}\,\overline{5d}$	$\overline{4p}\,\overline{3d}$	$\overline{5p}\,\overline{3d}$	$\overline{5p}\,\overline{4d}$
$\overline{2p}\,\overline{3d}$	0	0·223607	0·188982	0	0	0·094491	0	0	0	0·129099	0·084515	0
$\overline{3p}\,\overline{3d}$	0·223607	0·400000	0	0·188982	0	0	0·094491	0	0	0·519615	0·340168	0
$\overline{2p}\,\overline{4d}$	0·188982	0	0·285714	0·223607	0·129099	0·392857	0	0	0	0	0	0·084515
$\overline{3p}\,\overline{4d}$	0	0·188982	0·223607	0·685714	0·519615	0	0·392857	0	0	0	0	0·340168
$\overline{4p}\,\overline{4d}$	0	0	0·129099	0·519615	1·085714	0	0	0·392857	0	0·188982	0	0·851050
$\overline{2p}\,\overline{5d}$	0·094491	0	0·392857	0	0	0·571429	0·223607	0·129099	0·084515	0	0	0
$\overline{3p}\,\overline{5d}$	0	0·094491	0	0·392857	0	0·223607	0·971429	0·519615	0·340168	0	0	0
$\overline{4p}\,\overline{5d}$	0	0	0	0	0·392857	0·129099	0·519615	1·371429	0·851050	0·094491	0	0
$\overline{5p}\,\overline{5d}$	0	0	0	0	0	0·084515	0·340168	0·851050	1·771429	0	0·094491	0·392857
$\overline{4p}\,\overline{3d}$	0·129099	0·519615	0	0	0·188982	0	0	0·094491	0	0·800000	0·851050	0
$\overline{5p}\,\overline{3d}$	0·084515	0·340168	0	0	0	0	0	0	0·094491	0·851050	1·200000	0·188982
$\overline{5p}\,\overline{4d}$	0	0	0·084515	0·340168	0·851050	0	0	0	0·392857	0	0·188982	1·485714

Table 6. The relevant part of the energy matrix **H** of order twelve used in calculating B_8.

	$\overline{2p}\,\overline{3d}$	$\overline{3p}\,\overline{3d}$	$\overline{2p}\,\overline{4d}$	$\overline{3p}\,\overline{4d}$	$\overline{4p}\,\overline{4d}$	$\overline{2p}\,\overline{5d}$	$\overline{3p}\,\overline{5d}$	$\overline{4p}\,\overline{5d}$	$\overline{5p}\,\overline{5d}$	$\overline{4p}\,\overline{3d}$	$\overline{5p}\,\overline{3d}$	$\overline{5p}\,\overline{4d}$
$\overline{2p}\,\overline{3d}$	1·072961	−0·165367	−0·156627	0·037909	0·002628	−0·025898	0·002915	0·001320	0·000258	0·027138	−0·005127	−0·000414
$\overline{3p}\,\overline{3d}$	−0·165367	0·847720	0·037908	−0·108708	0·042841	0·002916	−0·021054	0·005348	0·001992	0·218523	−0·040419	0·001678
$\overline{2p}\,\overline{4d}$	−0·156627	0·037908	0·892765	−0·125375	0·023151	−0·220883	0·046763	0·005483	0·000070	0·002628	−0·000413	−0·005250
$\overline{3p}\,\overline{4d}$	0·037909	−0·108708	−0·125375	0·719333	−0·171107	0·046763	−0·159450	0·056952	0·005793	0·042842	0·001677	−0·036637
$\overline{4p}\,\overline{4d}$	0·002628	0·042841	0·023151	−0·171107	0·643662	0·005482	0·056953	−0·138464	0·063548	−0·094124	0·044964	0·209634
$\overline{2p}\,\overline{5d}$	0·025898	0·002916	−0·220883	0·046763	0·005482	0·706912	−0·083651	−0·019170	−0·005423	0·001325	0·000259	0·000071
$\overline{3p}\,\overline{5d}$	0·002915	−0·021054	0·046763	−0·159450	0·056953	0·083651	0·587353	−0·121956	−0·032979	0·005349	0·001993	0·005792
$\overline{4p}\,\overline{5d}$	0·001320	0·005348	0·005483	0·056952	−0·138464	−0·019170	−0·121956	0·529185	−0·156211	−0·018428	0·007501	0·063545
$\overline{5p}\,\overline{5d}$	0·000258	0·001992	0·000070	0·005793	0·063548	0·005423	−0·032979	0·156211	0·426074	0·007502	−0·013889	−0·088836
$\overline{4p}\,\overline{3d}$	−0·027138	0·218523	0·002628	0·042842	−0·094124	0·001325	0·005349	−0·018428	0·007502	0·755041	−0·261434	0·044964
$\overline{5p}\,\overline{3d}$	−0·005127	−0·040419	−0·000413	0·001677	0·044964	0·000259	0·001993	0·007501	−0·013889	0·261434	0·567581	−0·056567
$\overline{5p}\,\overline{4d}$	0·000414	0·001678	−0·005250	−0·036637	−0·209634	0·000071	0·005792	0·063545	−0·088836	0·044964	−0·056567	0·497606

Table 7. The matrix $\mathbf{T}=(\mathbf{H}_{22}^{(0)}+\mathbf{1})^{-1}$ of order twelve used in calculating B_8. This matrix was found by successive inversions.

The wave function corresponding to two hydrogen atoms separated by a very large distance and having the perturbation potential $\varphi_{1,2}+\varphi_{2,1}$ is given by

$$\Psi=(1s)^2-\frac{3\sqrt{15}}{R^4}\sum_{n,n'}\Omega_{n1;\,n'2}(\overline{np},\overline{n'd}|\mathbf{T}|\overline{2p},\overline{3d}). \tag{63}$$

Comparing equation (63) with equation (25), with the help of equations (26) and (47), it follows that

$$C^{(4)}_{n10;\,n'20}=-\tfrac{9}{2}\sqrt{2}(\overline{np},\overline{n'd}|\mathbf{T}|\overline{2p},\overline{3d}), \tag{64}$$

$$C^{(4)}_{n11;\,n'21}=C^{(4)}_{n1-1;\,n'2-1}=-\tfrac{3}{2}\sqrt{6}(\overline{np},\overline{n'd}|\mathbf{T}|\overline{2p},\overline{3d}). \tag{65}$$

Furthermore,

$$C^{(4)}_{n'2m;\,nlm}=C^{(4)}_{nlm;\,n'2m}. \tag{66}$$

Number of configurations considered	Last configuration in the sequence equation (58) considered	Value of B_8 obtained
1	$\overline{2p}\ \overline{3d}$	135·0000
2	$\overline{3p}\ \overline{3d}$	140·0000
3	$\overline{2p}\ \overline{4d}$	144·1525
4	$\overline{3p}\ \overline{4d}$	144·5309
5	$\overline{4p}\ \overline{4d}$	144·5309
6	$\overline{2p}\ \overline{5d}$	144·6552
7	$\overline{3p}\ \overline{5d}$	144·6582
8	$\overline{4p}\ \overline{5d}$	144·6583
9	$\overline{5p}\ \overline{5d}$	144·6583
10	$\overline{4p}\ \overline{3d}$	144·8433
11	$\overline{5p}\ \overline{3d}$	144·8497
12	$\overline{5p}\ \overline{4d}$	144·8497

Table 8.

In order to express the wave function in concise form, let us number the states in the following manner:

Number	1	2	3	4	5	6	7
State	$\overline{2p}$	$\overline{3p}$	$\overline{4p}$	$\overline{5p}$	$\overline{3d}$	$\overline{4d}$	$\overline{5d}$

(67)

Thus the coefficient $C^{(4)}_{32m;\,21m}$ would be designated $C^{(4)}_{5m;\,1m}$. This notation has the advantage that it makes it possible to express the coefficients in the form of a symmetrical matrix. The matrix for the $C^{(4)}_{i1;\,j1}$ is given in table 9.

6. ANALYSIS OF THE WAVE FUNCTIONS IN TERMS OF NATURAL ORBITALS

In the previous sections we have obtained the unsymmetrized wave function up to terms of the order of $1/R^5$ for the long-range interaction of two $1s$ hydrogen atoms. This function is expressed in terms of a doubly infinite series involving $\overline{np}$ and $\overline{n'd}$ orbitals. Our only approximation consists in truncating this series

j \ i		1	2	3	4	5	6	7
		$\overline{2p}$	$\overline{3p}$	$\overline{4p}$	$\overline{5p}$	$\overline{3d}$	$\overline{4d}$	$\overline{5d}$
1	$\overline{2p}$	0	0	0	0	−3·942310	+0·575484	+0·095155
2	$\overline{3p}$	0	0	0	0	+0·607597	−0·139287	−0·010710
3	$\overline{4p}$	0	0	0	0	+0·099711	−0·009656	−0·004850
4	$\overline{5p}$	0	0	0	0	+0·018838	+0·001521	−0·000948
5	$\overline{3d}$	−3·942310	+0·607597	+0·099711	+0·018838	0	0	0
6	$\overline{4d}$	+0·575484	−0·139287	−0·009656	+0·001521	0	0	0
7	$\overline{5d}$	+0·095155	−0·010710	−0·004850	−0·000948	0	0	0

Table 9. Matrix of coefficients $C^{(4)}_{i1;\,j1}$. Here $C^{(4)}_{i1;\,j1} = C^{(4)}_{i-1;\,j-1} = 3^{-1/2} C^{(4)}_{i0;\,j0}$. The notation is explained in the text.

by omitting all of the terms involving either n or n' greater than 5. This unsymmetrized wave function has the form

$$\Psi(a1, b2) = N\left[\psi_{100}(a1)\psi_{100}(b2) + \sum_{m=-1}^{1}\sum_{i,j=1}^{7} C_{ij}(m)\psi_{im}(a1)\psi_{jm}(b2)\right]. \quad (68)$$

Here the i and j correspond to the various $\overline{np}$ and $\overline{n'd}$ states as indicated in equation (67). The $C_{ij}(m)$ are

$$C_{ij}(m) = \frac{1}{R^3} C^{(3)}_{im;\,jm} \qquad i \leqslant 4 \quad \text{and} \quad j \leqslant 4, \quad (69)$$

$$= \frac{1}{R^4} C^{(4)}_{im;\,jm} \qquad i > 4 \quad \text{or} \quad j > 4, \quad (70)$$

$$= 0 \qquad i > 4 \quad \text{and} \quad j < 4. \quad (71)$$

The coefficients $C^{(3)}_{im;\,jm}$ are given in table 5 and the $C^{(4)}_{im;\,jm}$ are given in table 9. Depending upon the coupling of the electron spins, the 1s hydrogen atoms can interact to form either a ${}^1\Sigma_g{}^+$ or a ${}^3\Sigma_u{}^+$ state of the H_2 molecule. The corresponding wave functions are

$$\Phi({}^1\Sigma_g{}^+) = \frac{1}{\sqrt{2}}(\Psi(a1, b2) + \Psi(a2, b1)), \quad (72)$$

$$\Phi({}^3\Sigma_u{}^+) = \frac{1}{\sqrt{2}}(\Psi(a1, b2) - \Psi(a2, b1)). \quad (73)$$

It is easy to express our wave functions in terms of natural orbitals. This form is most significant since, as Löwdin [9] has shown, the occupation numbers of the successive natural orbitals decrease more rapidly than the occupation numbers for any other ortho-normal set of orbitals. The natural orbitals for two-electron systems have been studied extensively by Löwdin and Shull [10]. However, natural orbitals have not previously been determined for molecules.

The first step in determining the natural orbitals is the diagonalization of equation (68) to obtain the unsymmetrized wave function in the form

$$\left.\begin{aligned}
&\Psi(a1, b2) = N \sum_{m=-1}^{1}\sum_{k=0}^{7} \lambda_{km}\omega_{km}(a1)\omega_{km}(b2),\\
&\omega_{00} = \psi_{100}, \qquad \omega_{01} = \omega_{0-1} = 0,\\
&\lambda_{00} = 1, \qquad \lambda_{k1} = \lambda_{k-1},\\
&\omega_{km} = \sum_{i=1}^{7} \alpha_{ik}(m)\psi_{im},
\end{aligned}\right\} \quad (74)$$

where the coefficients $\alpha_{ik}(m)$ form a unitary matrix. The ω_{km} might be called atomic-natural orbitals. The functions ω_{k0} are real, but the ω_{k1} and ω_{k-1} are complex. In place of these complex orbitals it is possible to use the real atomic-natural orbitals ω_{kx} and ω_{ky} defined as

$$\left.\begin{aligned}
\omega_{kx} &= \frac{1}{\sqrt{2}}(\omega_{k1} + \omega_{k-1}),\\
\omega_{ky} &= \frac{1}{i\sqrt{2}}(\omega_{k1} - \omega_{k-1}).
\end{aligned}\right\} \quad (75)$$

In terms of these real atomic-natural orbitals, equation (74) becomes

$$\Psi(a1,b2)=N\left[\begin{array}{l}\sum\limits_{k=0}^{7}\lambda_{k0}\omega_{k0}(a1)\omega_{k0}(b2)\\ +\sum\limits_{k=1}^{7}\lambda_{k1}[\omega_{kx}(a1)\omega_{kx}(b2)-\omega_{ky}(a1)\omega_{ky}(b2)]\end{array}\right]. \tag{76}$$

The negative sign for the coefficient of the $\omega_{ky}(a1)\omega_{ky}(b2)$ is due to our using right-hand coordinate systems for both a and b with the Z-axes pointed internally. Thus, $x_a=x_b$ but $y_a=-y_b$.

The true natural orbitals are molecular orbitals. From each pair of real atomic-natural orbitals can be formed two true natural orbitals

$$\begin{array}{ll}\chi_{k0}{}^{g}(1)=\dfrac{1}{\sqrt{2}}[\omega_{k0}(a1)+\omega_{k0}(b1)], & \chi_{k0}{}^{u}(1)=\dfrac{1}{\sqrt{2}}[\omega_{k0}(a1)-\omega_{k0}(b1)],\\ \chi_{kx}{}^{g}(1)=\dfrac{1}{\sqrt{2}}[\omega_{kx}(a1)-\omega_{kx}(b1)], & \chi_{kx}{}^{u}(1)=\dfrac{1}{\sqrt{2}}[\omega_{kx}(a1)+\omega_{kx}(b1)],\\ \chi_{ky}{}^{g}(1)=\dfrac{1}{\sqrt{2}}[\omega_{ky}(a1)+\omega_{ky}(b1)], & \chi_{ky}{}^{u}(1)=\dfrac{1}{\sqrt{2}}[\omega_{ky}(a1)-\omega_{ky}(b1)].\end{array} \tag{77}$$

The orbitals with the superscript g have the gerade symmetry and those with the superscript u are ungerade. Substituting equation (76) into equation (72) and making use of equation (77), the wave function for the ${}^{1}\Sigma_{g}{}^{+}$ state can be expressed in terms of the natural orbitals,

$$\Phi({}^{1}\Sigma_{g}{}^{+})=N\left[\begin{array}{l}\sum\limits_{k=0}^{7}\dfrac{\lambda_{k0}}{\sqrt{2}}[\chi_{k0}{}^{g}(1)\chi_{k0}{}^{g}(2)-\chi_{k0}{}^{u}(1)\chi_{k0}{}^{u}(2)]\\ -\sum\limits_{k=1}^{7}\dfrac{\lambda_{k1}}{\sqrt{2}}\left[\begin{array}{l}\chi_{kx}{}^{g}(1)\chi_{kx}{}^{g}(2)-\chi_{kx}{}^{u}(1)\chi_{kx}{}^{u}(2)\\ +\chi_{ky}{}^{g}(1)\chi_{ky}{}^{g}(2)-\chi_{ky}{}^{u}(1)\chi_{ky}{}^{u}(2)\end{array}\right]\end{array}\right]. \tag{78}$$

In a similar manner, the wave function for the ${}^{3}\Sigma_{u}{}^{+}$ state, equation (73), can be expressed in the form

$$\Phi({}^{3}\Sigma_{u}{}^{-})=N\left[\begin{array}{l}\sum\limits_{k=0}^{7}\dfrac{\lambda_{k0}}{\sqrt{2}}[\chi_{k0}{}^{u}(1)\chi_{k0}{}^{g}(2)-\chi_{k0}{}^{g}(1)\chi_{k0}{}^{u}(2)\\ -\sum\limits_{k=1}^{7}\dfrac{\lambda_{k1}}{\sqrt{2}}\left[\begin{array}{l}\chi_{kx}{}^{u}(1)\chi_{kx}{}^{g}(2)-\chi_{kx}{}^{g}(1)\chi_{kx}{}^{u}(2)\\ +\chi_{ky}{}^{u}(1)\chi_{ky}{}^{g}(2)-\chi_{ky}{}^{g}(1)\chi_{ky}{}^{u}(2)\end{array}\right]\end{array}\right]. \tag{79}$$

Alternatively, we can follow Löwdin and Shull in defining the complex natural orbitals

$$\chi'(1)=\frac{1}{\sqrt{2}}[\chi^{u}(1)+i\chi^{g}(1)]. \tag{80}$$

In terms of these orbitals,

$$\Phi({}^{1}\Sigma_{g}{}^{+})=N\left[\begin{array}{l}\sum\limits_{k=0}^{7}\dfrac{\lambda_{k0}}{\sqrt{2}}[\chi_{k0}{}'^{*}(1)\chi_{k0}{}'(2)+\chi_{k0}{}'(1)\chi_{k0}{}'^{*}(2)]\\ -\sum\limits_{k=1}^{7}\dfrac{\lambda_{k1}}{\sqrt{2}}\left[\begin{array}{l}\chi_{kx}{}'^{*}(1)\chi_{kx}{}'(2)+\chi_{kx}{}'(1)\chi_{kx}{}'^{*}(2)\\ +\chi_{ky}{}'^{*}(1)\chi_{ky}{}'(2)+\chi_{ky}{}'(1)\chi_{ky}{}'^{*}(2)\end{array}\right]\end{array}\right], \tag{81}$$

$$\Phi({}^{3}\Sigma_{u}{}^{+})=iN\left[\begin{array}{l}\sum\limits_{k=0}^{7}\dfrac{\lambda_{k0}}{\sqrt{2}}[\chi_{k0}{}'^{*}(1)\chi_{k0}{}'(2)-\chi_{k0}{}'(1)\chi_{k0}{}'^{*}(2)]\\ -\sum\limits_{k=1}^{7}\dfrac{\lambda_{k1}}{\sqrt{2}}\left[\begin{array}{l}\chi_{kx}{}'^{*}(1)\chi_{kx}{}'(2)-\chi_{kx}{}'(1)\chi_{kx}{}'^{*}(2)\\ +\chi_{ky}{}'^{*}(1)\chi_{ky}{}'(2)-\chi_{ky}{}'(1)\chi_{ky}{}'^{*}(2)\end{array}\right]\end{array}\right]. \tag{82}$$

The problem of determining the natural orbitals then becomes the problem of diagonalizing equation (68). As the first step, let us ignore the $\overline{n'd}$ states (5, 6, and 7) and achieve a diagonalization of the $\overline{np}$ by solving the set of equations

$$\sum_{j=1}^{4} [C_{ij}^{(3)}(m) - \gamma_{lm}\delta_{ij}]\alpha_{jl}^{0}(m) = 0, \qquad (83)$$
$$i = 1, 2, 3, 4; \quad l = 1, 2, 3, 4; \quad m = -1, 0, +1$$

subject to the ortho-normalization conditions

$$\sum_{j=1}^{4} \alpha_{jk}^{0}(m)\alpha_{jl}^{0}(m) = \delta_{kl}. \qquad (84)$$

Equations (83) and (84) determine the four sets of roots γ_{lm} and the corresponding eigenvectors

$$\omega_{lm}^{0} = \sum_{i=1}^{4} \alpha_{il}^{0}\psi_{im}. \qquad (85)$$

Since the $C_{ij}^{(3)}(m)$ are the coefficients of hermitian matrices, it follows that the roots are real and the $\alpha_{jk}^{0}(m)$ correspond to a unitary transformation. Because the transformation is unitary,

$$\psi_{jm} = \sum_{k=1}^{4} \alpha_{jk}^{0}\omega_{km}^{0}, \qquad j = 1, 2, 3, 4. \qquad (86)$$

After this partial diagonalization, the wave function equation (68) can be written in the form

$$\Psi(a1, b2) = N\left[\begin{array}{l} \psi_{100}(a1)\psi_{100}(b2) + \dfrac{1}{R^3}\displaystyle\sum_{m=-1}^{1}\sum_{i=1}^{4}\gamma_{im}\omega_{im}^{0}(a1)\omega_{im}^{0}(b2) \\ + \dfrac{1}{R^4}\displaystyle\sum_{m=-1}^{1}\sum_{i=1}^{4}\sum_{j=5}^{7}F_{ij}(m)\omega_{im}^{0}(a1)\psi_{jm}(b2) \\ + \dfrac{1}{R^4}\displaystyle\sum_{m=-1}^{1}\sum_{i=5}^{7}\sum_{j=1}^{4}F_{ij}(m)\psi_{im}(a1)\omega_{jm}^{0}(b2) \end{array}\right]. \qquad (87)$$

Here

$$F_{ij}(m) = \sum_{k=1}^{4} C_{jk}^{(4)}(m)\alpha_{ki}^{0}(m) = F_{ji}(m), \qquad i = 1, 2, 3, 4; \; j = 5, 6, 7. \qquad (88)$$

Now we can complete the diagonalization by introducing the new unitary transformation

$$\left.\begin{array}{ll} \psi_{jm} = \displaystyle\sum_{k=1}^{7} \alpha_{jk}(m)\omega_{km}, & j = 5, 6, 7, \\ \omega_{jm}^{0} = \displaystyle\sum_{k=1}^{7} \beta_{jk}(m)\omega_{km}, & j = 1, 2, 3, 4. \end{array}\right\} \qquad (89)$$

Since the transformation is unitary

$$\sum_{j=1}^{4} \beta_{jk}\beta_{jl} + \sum_{j=5}^{7} \alpha_{jk}\alpha_{jl} = \delta_{kl}. \qquad (90)$$

Because of this unitary property, we can obtain the inverse transformation in the form

$$\omega_{lm} = \sum_{j=1}^{4} \beta_{jl}(m)\omega_{jm}^{0} + \sum_{j=5}^{7} \alpha_{jl}(m)\psi_{jm}. \qquad (91)$$

Substituting equation (91) into equation (74) and comparing with equation (87), it follows that

$$\sum_{l=1}^{7} \lambda_{lm}\beta_{jl}(m)\beta_{kl}(m)=\frac{1}{R^3}\gamma_{jm}\delta_{jk}, \qquad j=1,2,3,4, \quad k=1,2,3,4, \tag{92}$$

$$\sum_{l=1}^{7} \lambda_{lm}\beta_{jl}(m)\alpha_{kl}(m)=\frac{1}{R^4}F_{jk}(m), \qquad j=1,2,3,4, \quad k=5,6,7, \tag{93}$$

$$\sum_{l=1}^{7} \lambda_{lm}\alpha_{jl}(m)\beta_{kl}(m)=\frac{1}{R^4}F_{jk}(m), \qquad j=5,6,7, \quad k=1,2,3,4, \tag{94}$$

$$\sum_{l=1}^{7} \lambda_{lm}\alpha_{jl}(m)\alpha_{kl}(m)=0, \qquad j=5,6,7, \quad k=5,6,7. \tag{95}$$

Now, multiply equation (92) by $\beta_{kn}(m)$ and sum over k from one to four; then, multiply equation (93) by $\alpha_{kn}(m)$ and sum over k from five to seven; finally, add together the two sums to obtain

$$\sum_{l=1}^{7} \lambda_{lm}\beta_{jl}(m)\left[\sum_{k=1}^{4}\beta_{kl}(m)\beta_{kn}(m)+\sum_{k=5}^{7}\alpha_{kl}(m)\alpha_{kn}(m)\right]$$
$$=\frac{1}{R^3}\gamma_{jm}\beta_{jn}(m)+\frac{1}{R^4}\sum_{k=5}^{7}F_{jk}(m)\alpha_{kn}(m). \tag{96}$$

Making use of equation (90), we obtain

$$\left[\lambda_{nm}-\frac{\gamma_{jm}}{R^3}\right]\beta_{jn}(m)=\frac{1}{R^4}\sum_{k=5}^{7}F_{jk}(m)\alpha_{kn}(m), \quad j=1,2,3,4, \; n=1,2,3,4,5,6,7. \tag{97}$$

In a similar manner, from equations (94) and (95),

$$\lambda_{nm}\alpha_{jn}(m)=\frac{1}{R^4}\sum_{k=1}^{7}F_{jk}(m)\beta_{kn}(m), \qquad j=5,6,7, \quad m=1,2,3,4,5,6,7. \tag{98}$$

Using equation (98) to eliminate the α_{jn} from equation (97) (and dropping the indications of m for simplicity of notation),

$$0=\left[\frac{\gamma_1}{R^3}-\lambda_n+\frac{G_{11}}{R^8\lambda_n}\right]\beta_{1n}+\frac{G_{12}}{R^8\lambda_n}\beta_{2n}+\frac{G_{13}}{R^8\lambda_n}\beta_{3n}+\frac{G_{14}}{R^8\lambda_n}\beta_{4n}, \tag{99}$$

$$0=\frac{G_{12}}{R^8\lambda_n}\beta_{1n}+\left[\frac{\gamma_2}{R^3}-\lambda_n+\frac{G_{22}}{R^8\lambda_n}\right]\beta_{2n}+\frac{G_{23}}{R^8\lambda_n}\beta_{3n}+\frac{G_{24}}{R^8\lambda_n}\beta_{4n}, \tag{100}$$

$$0=\frac{G_{13}}{R^8\lambda_n}\beta_{1n}+\frac{G_{23}}{R^8\lambda_n}\beta_{2n}+\left[\frac{\gamma_3}{R^3}-\lambda_n+\frac{G_{33}}{R^8\lambda_n}\right]\beta_{3n}+\frac{G_{34}}{R^8\lambda_n}\beta_{4n}, \tag{101}$$

$$0=\frac{G_{14}}{R^8\lambda_n}\beta_{1n}+\frac{G_{24}}{R^8\lambda_n}\beta_{2n}+\frac{G_{34}}{R^8\lambda_n}\beta_{3n}+\left[\frac{\gamma_4}{R^3}-\lambda_n+\frac{G_{44}}{R^8\lambda_n}\right]\beta_{4n}. \tag{102}$$

Here

$$G_{ij}=\sum_{k=5}^{7}F_{ik}F_{jk}. \tag{103}$$

In order to determine the roots, λ_n, we set the determinant of the coefficients of the β_{in} in equations (99) through (102) equal to zero. The roots are expressed as series in powers of $1/R$. The determinant is then expanded and regrouped into a sum of coefficients times various powers of $1/R$. Since the determinant must vanish for all values of R, it follows that each coefficient must be equal to zero. Thus we find that four of the seven roots are

$$\lambda_n=\frac{\gamma_n}{R^3}+\frac{G_{nn}}{R^5\gamma_n}+\ldots, \qquad n=1,2,3,4. \tag{104}$$

The terms omitted vary as $1/R^7$ or a higher power of $1/R$ and do not affect either the inverse sixth or inverse eighth power dispersion energies. Substituting these roots into equations (97) and (98), we find that

$$\alpha_{jn} = \frac{F_{jn}}{R\gamma_n} + \ldots, \qquad n = 1, 2, 3, 4, \tag{105}$$

$$\beta_{jn} = \delta_{jn}\left[1 - \frac{1}{2}\frac{G_{nn}}{R^2\gamma_n{}^2}\right] + \ldots, \qquad n = 1, 2, 3, 4. \tag{106}$$

The terms omitted in equation (105) vary as $1/R^3$ or higher; the terms omitted in equation (106) vary as $1/R^4$ or higher. It is easy to see that

$$\alpha_{5n}{}^2 + \alpha_{6n}{}^2 + \alpha_{7n}{}^2 = \frac{G_{nn}}{R^2\gamma_n{}^2} + \ldots, \qquad n = 1, 2, 3, 4. \tag{107}$$

The terms omitted in equation (107) are of the order of $1/R^4$ or higher.

The other three roots can also be obtained from equations (99) to (102). However, it is somewhat easier to determine them from the set of three simultaneous equations which result from the use of equation (97) to eliminate the β_{jn} from equation (98). Expanding the determinant of the coefficients of α_{in} in these equations in powers of $1/R$, as before, we find that

$$\lambda_n = \frac{A_n}{R^5} + \ldots, \qquad n = 5, 6, 7, \tag{108}$$

where the terms omitted in equation (108) are of the order of $1/R^7$ or higher. Furthermore, the corresponding β_{jn} vary as $1/R$. Since the λ_n vary as $1/R^5$ and the β_{jn} vary as $1/R$, we can ascertain that the roots 5, 6, and 7 cannot contribute to either the inverse sixth or the inverse eighth power dispersion energies. Thus we can ignore these roots and their eigenvectors and concentrate our attention on the first four roots.

The constants for the first four natural orbitals for $m = 1$ are given in table 10.

Root	1	2	3	4
γ_{n1}	$-$ 1·110371	$-$ 0·014029	$-$ 0·000541	$-$ 0·000059
$\alpha_{1n}{}^0(1)$	$+$ 0·987527	$+$ 0·151308	$+$ 0·0414	$+$ 0·014
$\alpha_{2n}{}^0(1)$	$-$ 0·155451	$+$ 0·979596	$+$ 0·1034	$+$ 0·074
$\alpha_{3n}{}^0(1)$	$-$ 0·024599	$-$ 0·100704	$+$ 0·9893	$-$ 0·103
$\alpha_{4n}{}^0(1)$	$-$ 0·004444	$-$ 0·085769	$+$ 0·0944	$+$ 0·991
$R\alpha_{5n}(1)$	$+$ 3·593507	$+$ 0·923834	$-$ 0·067089	$+$ 31·0
$R\alpha_{6n}(1)$	$-$ 0·531524	$+$ 3·45910	$-$ 0·025256	$-$ 4·26
$R\alpha_{7n}(1)$	$-$ 0·086238	$-$ 0·319051	$+$ 3·79962	$-$ 1·69
$G_{nn}(1)/\gamma_{n1}{}^2$	+13·2032	+12·9206	+14·4423	+985·0

Table 10. Constants for natural orbitals having $m = 1$. All the constants are the same for $m = -1$.

To get the constants for $m = 0$, there are the following relations:

$\gamma_{n0} = 2\gamma_{n1}$; $\alpha_{jk}{}^0(0) = \alpha_{jk}{}^0(1)$ for $j = 1, 2, 3, 4$; $\alpha_{jk}(0) = (3^{1/2}/2)\alpha_{jk}(1)$ for $j = 5, 6, 7$; $G_{ij}(0) = 3G_{ij}(1)$

All of these constants are the same for $m = -1$. Since $C^{(3)}_{n10\,;\,n'10} = 2C^{(3)}_{n11\,;\,n'11}$ and $C^{(4)}_{n20\,;\,n'20} = (3)^{1/2}C^{(4)}_{n21\,;\,n'21}$, it follows that

$$\gamma_{n0} = 2\gamma_{n1}, \tag{109}$$

$$\alpha_{jk}{}^0(0) = \alpha_{jk}{}^0(1), \qquad j = 1, 2, 3, 4, \tag{110}$$

$$\alpha_{jk}(0)=\frac{\sqrt{3}}{2}\alpha_{jk}(1), \qquad j=5,6,7, \tag{111}$$

$$F_{ij}(0)=\sqrt{3}F_{ij}(1), \tag{112}$$

$$G_{ij}(0)=3G_{ij}(1). \tag{113}$$

Since γ_{31} and γ_{41} are exceedingly small, very little error is made in the wave function and in the corresponding physical properties of the system by neglecting the terms corresponding to the third and fourth roots. To this approximation,

$$\Psi_2(a1, b2)=N\left[\begin{array}{l} \psi_{100}(a1)\psi_{100}(b2) \\ -\dfrac{1\cdot110371}{R^3}\left[\begin{array}{l}\left(1+\dfrac{13\cdot2032}{R^2}\right)[\omega_{11}(a1)\omega_{11}(b2)+\omega_{1\,-1}(a1)\omega_{1-1}(b2)] \\ +2\left(1+\dfrac{9\cdot9024}{R^2}\right)\omega_{10}(a1)\omega_{10}(b2)\end{array}\right] \\ -\dfrac{0\cdot014029}{R^3}\left[\begin{array}{l}\left(1+\dfrac{12\cdot9206}{R^2}\right)[\omega_{21}(a1)\omega_{21}(b2)+\omega_{2-1}(a1)\omega_{2-1}(b2)] \\ +2\left(1+\dfrac{9\cdot6905}{R^2}\right)\omega_{20}(a1)\omega_{20}(b2)\end{array}\right]\end{array}\right]. \tag{114}$$

Here

$$N=1-\frac{3\cdot699363}{R^6}-\frac{81\cdot4055}{R^8}, \tag{115}$$

$$\begin{aligned}\omega_{1\pm1}=&\left(1-\frac{6\cdot6016}{R^2}\right)\left(\begin{array}{l}+0\cdot987527\psi_{21\pm1}-0\cdot155451\psi_{31\pm1}\\-0\cdot024599\psi_{41\pm1}-0\cdot004444\psi_{51\pm1}\end{array}\right)\\&+\frac{3\cdot593507}{R}\psi_{32\pm1}-\frac{0\cdot531524}{R}\psi_{42\pm1}-\frac{0\cdot086238}{R}\psi_{52\pm1},\end{aligned} \tag{116}$$

$$\begin{aligned}\omega_{10}=&\left(1-\frac{4\cdot9512}{R^2}\right)\left(\begin{array}{l}+0\cdot987527\psi_{210}-0\cdot155451\psi_{310}\\-0\cdot024599\psi_{410}-0\cdot004444\psi_{510}\end{array}\right)\\&+\frac{3\cdot112068}{R}\psi_{320}-\frac{0\cdot460313}{R}\psi_{420}-\frac{0\cdot074684}{R}\psi_{520},\end{aligned} \tag{117}$$

$$\begin{aligned}\omega_{2\pm1}=&\left(1-\frac{6\cdot4603}{R^2}\right)\left(\begin{array}{l}+0\cdot151308\psi_{21\pm1}+0\cdot979596\psi_{31\pm1}\\-0\cdot100704\psi_{41\pm1}-0\cdot085769\psi_{51\pm1}\end{array}\right)\\&+\frac{0\cdot923834}{R}\psi_{31\pm2}+\frac{3\cdot45910}{R}\psi_{42\pm1}-\frac{0\cdot319051}{R}\psi_{52\pm1},\end{aligned} \tag{118}$$

$$\begin{aligned}\omega_{20}=&\left(1-\frac{4\cdot8453}{R^2}\right)\left(\begin{array}{l}+0\cdot151308\psi_{210}+0\cdot979596\psi_{310}\\-0\cdot1007044\psi_{410}-0\cdot085769\psi_{510}\end{array}\right)\\&+\frac{0\cdot800064}{R}\psi_{320}+\frac{2\cdot99567}{R}\psi_{420}-\frac{0\cdot276306}{R}\psi_{520}.\end{aligned} \tag{119}$$

It will be remembered that the energy of the system of two hydrogen atoms calculated using our best values of B_6 and B_8 is

$$E=-1-6\cdot499026/R^6-144\cdot8497/R^8-\ldots. \tag{120}$$

Here the energy is measured in units of e^2/a_0 and the separation is expressed in units of a_0. Actually, the very best value of B_6 obtained from combinations of $\overline{2p}$, $\overline{3p}$, $\overline{4p}$, and $\overline{5p}$ configurations was 6·499003. The value of 6·499026 was obtained by including $\overline{6p}$ and $\overline{7p}$ configurations. Let us compare this optimum energy of the system with the energy calculated with the wave function of equation (114) using only two sets of natural orbitals,

$$E \text{ (two natural orbitals)} = -1 - 6{\cdot}498988/R^6 - 144{\cdot}8499/R^8. \qquad (121)$$

It is seen that the energy calculated in the two ways agrees very well, with most of the discrepancy due to rounding errors. Indeed, high accuracy is obtained even if we considered only one set of natural orbits for the wave function

$$\Psi_1(a1,b2) = \left[1 - \frac{3{\cdot}698772}{R^6} - \frac{81{\cdot}3927}{R^8}\right]\psi_{100}(a1)\psi_{100}(b2)$$
$$-\frac{1{\cdot}110371}{R^3}\left[\begin{array}{l}\left(1+\dfrac{13{\cdot}2032}{R^2}\right)[\omega_{11}(a1)\omega_{11}(b2)+\omega_{1-1}(a1)\omega_{1-1}(b2)] \\ +2\left(1+\dfrac{9{\cdot}9024}{R^2}\right)\omega_{10}(a1)\omega_{10}(b2)\end{array}\right]. \qquad (122)$$

In this case the energy is

$$E \text{ (one natural orbital)} = -1 - 6{\cdot}497066/R^6 - 144{\cdot}8084/R^8. \qquad (123)$$

The energies given by equations (121) and (123) are obtained by a direct evaluation of the energy integral,

$$\int \Psi \mathscr{H} \Psi \, d\tau_1 \, d\tau_2,$$

making use of equations (34) and (56) as well as tables 2 and 6.

Except for truncation errors which arise from not considering additional $\overline{np}$ and $\overline{n'd}$ states, the wave function given by equation (68) is exact for a system composed of two 1*s* hydrogen atoms separated at sufficiently large separation so that only the dipole–dipole and dipole–quadrupole types of interaction potential terms are appreciable. However, the wave function of equation (68) contains a very large number of terms. With the use of natural orbitals we obtain a much more concise and meaningful expression.

It is interesting to note that the occupation numbers of the functions with $m=0$ change with separation as compared with the occupation numbers for the functions with $m=1$ or -1. Thus, both the occupation numbers and the natural orbitals themselves change with separation.

In order to study the natural orbitals in greater detail, we have plotted the radial parts of $\omega_{1m}{}^0$ and $\omega_{2m}{}^0$ in figure 2 together with the hydrogen 1*s* and 2*p* orbitals. We note that, whereas the hydrogen-orbitals with increasing quantum numbers n get more and more extended over the space, the natural orbitals $\omega_{1m}{}^0$ and $\omega_{2m}{}^0$ still remain localized within the same region around the nucleus as the 1*s* orbital. This means that the polarization caused by the long-range interaction is associated mainly with an angular deformation of the electron cloud which otherwise stays within the original region.

This result may be obvious, but it explains also why it sometimes may be much more difficult to calculate the influence of a perturbation by means of the conventional perturbation theory than by the variational formulation which is applied here and which is based on a more appropriate complete set and a final transformation to natural orbitals. In their conventional treatment, Eisenschitz and London [11] needed a large number of hydrogen-like orbitals 2*p*, 3*p*, 4*p*, ... and part of the continuum in order to obtain the energy constant $B_6 = 6{\cdot}47$, and the reason is simply that in order to describe a change of the electronic cloud within the region of the original 1*s* orbital a very large number of the more and more extended hydrogen orbitals would be necessary; see the graph of $2p$ in figure 2. On the other hand, by using a single set of additional

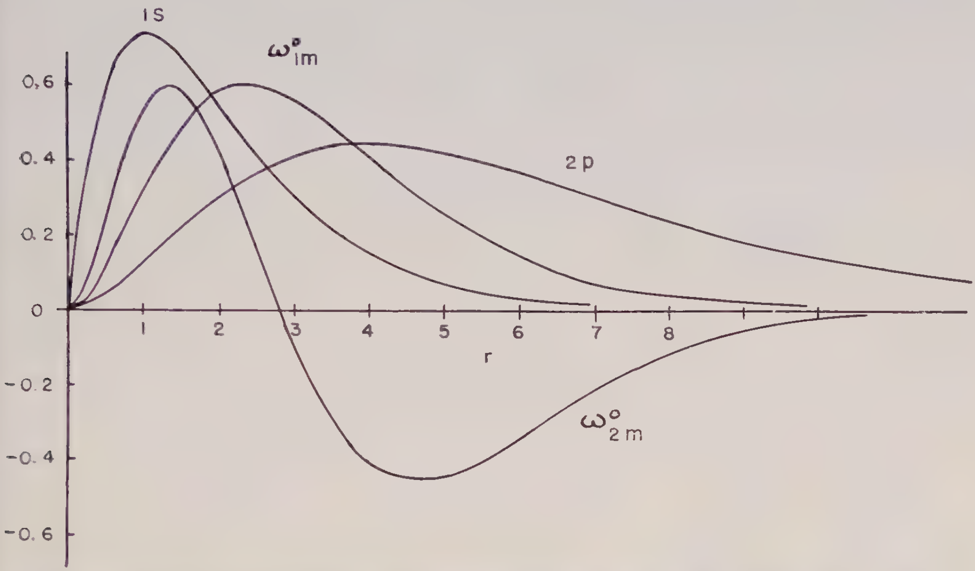

Figure 2. Radial part of natural atomic orbitals as compared with hydrogen $1s$ and $2p$ orbitals. Here r is in units of a_0.

orbitals $\omega_{1m}{}^0$, we have here been able to obtain the considerably better energy constant $B_6 = 6{\cdot}497066$. The comparison shows the inherent weakness of the conventional approach: in treating a certain perturbation the basic set formed by the unperturbed functions may be far from appropriate, and we should try instead to use a complete set which is at least an approximation to the natural set characterized by leading to most rapid convergence.

In conclusion, we give in table 11 the radial part of the natural orbitals $\omega_{nm}{}^0$ expressed as polynomials times the exponential factor $\exp(-r)$:

	$\omega_{1m}{}^0$	$\omega_{2m}{}^0$	$\omega_{3m}{}^0$	$\omega_{4m}{}^0$
$r\exp(-r)$	$+0{\cdot}598557$	$+1{\cdot}66774_6$	$+5{\cdot}384_2$	$+6{\cdot}51_6$
$r^2\exp(-r)$	$+0{\cdot}284987$	$+0{\cdot}05166_3$	$-4{\cdot}420_2$	$-7{\cdot}83_2$
$r^3\exp(-r)$	$-0{\cdot}026811$	$-0{\cdot}29441_4$	$+0{\cdot}847_9$	$+2{\cdot}64_7$
$r^4\exp(-r)$	$+0{\cdot}001157$	$+0{\cdot}02232_1$	$-0{\cdot}024_6$	$-0{\cdot}25_8$

Table 11.

Since the eigenvalues γ_3 and γ_4 are almost zero, the coefficients in $\omega_{3m}{}^0$ and $\omega_{4m}{}^0$ are correspondingly undetermined.

7. THEORY OF ATOMIC COLLISIONS IN TERMS OF LONG-RANGE INTERMOLECULAR FORCES

In this section we evaluate the probability of an atom being excited to a particular quantum state as the result of a collision. This is an application of long-range intermolecular force calculations which is useful in the study of stellar and planetary atmospheres.

Let us suppose that before a two atom collision, each of the two participants is in its ground state. Then the state of the system at any subsequent time may be determined by time dependent perturbation theory. The wave function at a time t is given by

$$\Psi = \sum_j a_j(t) \exp(iE_j^{(0)}t/\hbar)\Psi_j. \tag{124}$$

Here the subscript j refers to an actual quantum state of the system of two atoms and Ψ_j is a time dependent wave function for the system of two atoms. Thus

$$(\mathscr{H}_a + \mathscr{H}_b)\Psi_j = E_j^{(0)}\Psi_j. \tag{125}$$

The total wave function must satisfy the Schrödinger time dependence equation

$$\frac{\hbar}{i}\frac{\partial\Psi}{\partial t} = \mathscr{H}\Psi \tag{126}$$

where

$$\mathscr{H} = \mathscr{H}_a + \mathscr{H}_b + \mathscr{V}(R). \tag{127}$$

Substituting equation (124) into equation (126), it follows that

$$\sum_k \frac{da_k}{dt}\Psi_k \exp(iE_k^{(0)}t/\hbar) = \frac{i}{\hbar}\sum_j a_j \mathscr{V}\Psi_j \exp(iE_j^{(0)}t/\hbar). \tag{128}$$

Initially, at time $t = -\infty$, $a_0(-\infty) = 1$ and $a_n(-\infty) = 0$ where $n \neq 0$. Also, we should limit ourselves to a discussion of those glancing collisions where even after the collision is over, at time $t = +\infty$, all of the $a_n(\infty)$, where $n \neq 0$, are small compared to unity, and $a_0(\infty)$ remains close to unity. Under such conditions we can neglect all of the terms on the right-hand side of equation (128) except the one with $j = 0$. Thus, setting $a_0 = 1$:

$$\sum_k \frac{da_k}{dt}\Psi_k \exp(iE_k^{(0)}t/\hbar) = \frac{i}{\hbar}\exp(iE_0^{(0)}t/\hbar)\mathscr{V}\Psi_0. \tag{129}$$

Now multiplying both sides of the equation by Ψ_n^* and integrating over two-electron space, we obtain

$$\frac{da_n}{dt} = \frac{i}{\hbar}\exp[-i(E_n^{(0)} - E_0^{(0)})t/\hbar]\ (n|\mathscr{V}|0) \tag{130}$$

and integrating gives

$$a_n(t) = \frac{i}{\hbar}\int_{-\infty}^{t} (n|\mathscr{V}|0)\exp\left[-\frac{i}{\hbar}(E_n^{(0)} - E_0^{(0)})t\right]dt. \tag{131}$$

After the collision is over, at time $t = \infty$, the probability of the system being left in the state n is given by

$$P_{0\to n} = |a_n(\infty)|^2 = \frac{1}{\hbar^2}\left\{\left[\int_{-\infty}^{\infty}(n|\mathscr{V}|0)\cos\left(\frac{E_n^{(0)} - E_0^{(0)}}{\hbar}t\right)dt\right]^2 + \left[\int_{-\infty}^{\infty}(n|\mathscr{V}|0)\sin\left(\frac{E_n^{(0)} - E_0^{(0)}}{\hbar}t\right)dt\right]^2\right\}. \tag{132}$$

For most collision processes, the angular frequency $(E_n^{(0)} - E_0^{(0)})/\hbar$ is so large that in the time of one period there is very little change in the matrix component $(n|\mathscr{V}|0)$. Under these conditions, the exponential factor in equation (131) can be replaced by unity without sensibly affecting the value of the integral and the transition probability becomes

$$P_{0\to n} = |a_n(\infty)|^2 = \frac{1}{\hbar^2}\left(\int_{-\infty}^{+\infty}(n|\mathscr{V}|0)\,dt\right)^2. \tag{133}$$

In collision processes, the matrix components, such as $(n|\hat{\mathcal{V}}|0)$, are functions of the internuclear separation R, which itself is a function of time. In glancing collisions, it is customary [12] to approximate the relative trajectory of the collision by a straight line and assume that the relative velocity, v, remains constant. Let β be the impact parameter or the closest distance of the straight line from the second molecule, as shown in figure 3. Then,

$$R=(\beta^2+v^2t^2)^{1/2}. \tag{134}$$

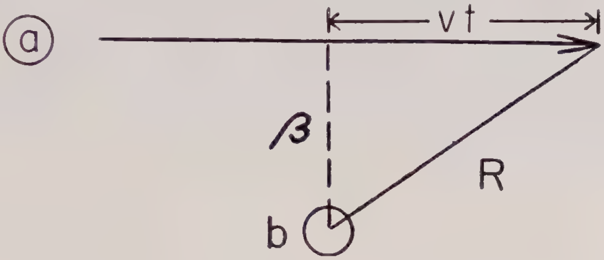

Figure 3. Approximate trajectory corresponding to a glancing collision of two hydrogen atoms.

Now we can consider the transitions which are induced by collisions between two hydrogen atoms in 1s states. It should be stressed that the states to which these atoms are excited are the *true hydrogen* atomic states and not the fictitious states (indicated by a bar) which we have previously considered. If both atoms are excited to the state with quantum numbers n and l, the wave function becomes

$$\chi_{nl,\,nl}=R_{nl}(r_{a1})R_{nl}(r_{b2})\Theta_{l,\,l}. \tag{135}$$

If the two atoms are excited to different quantum states, the wave function becomes

$$\chi_{nl,\,n'l'}=\frac{1}{\sqrt{2}}\{R_{nl}(r_{a1})R_{n'l'}(r_{b2})\Theta_{l,\,l'}+R_{n'l'}(r_{a1})R_{nl}(r_{b2})\Theta_{l',\,l}\}. \tag{136}$$

The distinction between the χ's and the Ω's (as generalized from equations (32) and (38)) is that the χ's contain the true hydrogen normalized radial wave functions

$$R_{nl}=-\frac{1}{2}\left(\frac{2}{n}\right)^{l+2}\frac{[(n-l-1)!]^{1/2}}{[(n+l)!]^{3/2}}\,r^l\,L_{n+l}^{2l+1}\left(\frac{2r}{n}\right)\exp(-r/n). \tag{137}$$

Then, as a result of equations (4) and (30) together with the orthonormality of the Θ's, it follows that if both atoms are excited to the same state,

$$(nl,\,nl|\varphi_e|1s,\,1s)=\frac{A_{l,\,l}}{R^{2l+1}}\left\{\int_0^\infty R_{nl}(r)\bar{R}_{l+1,\,l}(r)r^2\,dr\right\}^2. \tag{138}$$

Or, if the two atoms are excited to different states,

$$(nl,\,n'l'|\varphi_e|1s,\,1s)=$$

$$\frac{A_{l,\,l'}\sqrt{2}}{R^{l+l'+1}}\left\{\int_0^\infty R_{nl}(r)\bar{R}_{l+1,\,l}(r)r^2\,dr\right\}\left\{\int_0^\infty R_{n'l'}(r)\bar{R}_{l'+1,\,l'}(r)r^2\,dr\right\}. \tag{139}$$

The values of the A's are obtained from equation (31) and the $\bar{R}$'s and R's are defined by equations (13) and (137) respectively. The evaluation of the integrals is easy. For example,

$$(2p,\,2p|\varphi_e|1s,\,1s)=A/R^3 \tag{140}$$

where $A=2(128/243)^2(6)^{1/2}=1{\cdot}3593a_0^3(e^2/a_0)=8{\cdot}7803\times10^{-36}\,\mathrm{erg\,cm}^3$;

$$(2p,3d|\varphi_e|1s,1s)=B/R^4 \tag{141}$$

where $B=(10)^{1/2}=3{\cdot}1623a_0^4(e^2/a_0)=1{\cdot}0809\times10^{-43}\,\mathrm{erg\,cm}^4$.

Substituting equations (140) and (141) into equation (133) and making use of equation (134),

$$P_{(1s)^2\to(2p)^2}=\frac{1}{\hbar^2}\left\{\int_{-\infty}^{\infty}\frac{A\,dt}{(\beta^2+v^2t^2)^{3/2}}\right\}^2=\frac{4A^2}{v^2\beta^4\hbar^2}, \tag{142}$$

$$P_{(1s)^2\to(2p,3d)}=\frac{1}{\hbar^2}\left\{\int_{-\infty}^{\infty}\frac{B\,dt}{(\beta^2+v^2t^2)^2}\right\}^2=\frac{\pi^2B^2}{4v^2\beta^6\hbar^2}. \tag{143}$$

The relative kinetic energy of the two atoms is $\epsilon=m_{\mathrm{H}}v^2/4$ where m_{H} is the mass of a hydrogen atom. If ϵ is expressed in electron volts and β is expressed in angstroms, then equations (142) and (143) become simply

$$P_{(1s)^2\to(2p)^2}=\frac{724{\cdot}2}{\epsilon\beta^4}, \tag{144}$$

$$P_{(1s)^2\to(2p,3d)}=\frac{6770{\cdot}6}{\epsilon\beta^6}. \tag{145}$$

Tables 12 and 13 give the values of β (Å) corresponding to preassigned values of the relative kinetic energy and the transition probabilities. It will be noted that, except for very high energies, the probability of a transition to the $(2p)^2$ state is greater than the probability of a transition to the $(2p,3d)$ state. However, when the product of the transition probability and ϵ (ev) exceeds 8·3, transitions to the $(2p,3d)$ state become the more probable.

ϵ (ev) $P_{(1s)^2\to(2p)^2}$	0·001	0·010	0·1	1·0	10·0	100·0
0·5	34·7	19·5	11·0	6·2	3·5	2·0
0·1	51·9	29·2	16·4	9·2	5·2	2·9
0·01	92·2	51·9	29·2	16·4	9·2	5·2
10^{-4}	291·7	164·0	92·2	51·9	29·2	16·4
10^{-8}	2917·0	1640·0	922·0	519·0	292·0	164·0

Table 12. Values of β(Å) for which $P_{(1s)^2\to(2p)^2}$ has assigned values.

ϵ (ev) $P_{1s)^2\to(2p,3d)}$	0·001	0·01	0·1	1·0	10·0	100·0
0·5	15·4	10·5	7·2	4·9	3·3	2·3
0·1	20·2	13·8	9·4	6·4	4·3	3·0
0·01	29·6	20·2	13·8	9·4	6·4	4·3
10^{-4}	63·8	43·5	29·6	20·2	13·8	9·4
10^{-8}	296·0	202·0	138·0	94·0	64·0	43·0

Table 13. Values of β(Å) for which $P_{(1s)^2\to(2p,3d)}$ has assigned values.

One of us (J. O. H.) would like to thank the U.S. National Science Foundation for a Senior Post-Doctoral Fellowship and the Wisconsin Alumni Foundation for financial support which made it possible for this work to be carried out at the University of Uppsala.

The authors would further like to express their sincere gratitude to King Gustaf VI Adolf's 70-years Fund for Swedish Culture, to Knut and Alice Wallenberg's Foundation, and to the Swedish Natural Science Research Council for most generous support.

We would like to thank Elizabeth S. Hirschfelder for most valuable help in carrying out some of the algebraic derivations, and Klaus Appel for his most capable assistance in carrying out many of the numerical computations. Also, they want to thank James Blair for some additional computations.

APPENDIX I

Integrals involving associated Laguerre polynomials

In many atomic quantum mechanical problems, integrals of the following type arise

$$I^{m,\alpha,\beta}_{q,s}=\int_0^\infty \exp(-x)x^m L^\alpha_q(x)L^\beta_s(x)\,dx. \tag{A 1}$$

Here the functions $L_q(x)$ are the associated Laguerre functions as defined in reference [3]. The $I_{q,s}$ may be evaluated by making use of the generator functions for the associated Laguerre polynomials,

$$\sum_{q=\alpha}^{\infty}\frac{u^q}{q!}L^\alpha_q(x)=(-1)^\alpha\frac{u^\alpha\exp\left[-\left(\frac{ux}{1-u}\right)\right]}{(1-u)^{\alpha+1}}. \tag{A 2}$$

Thus it follows directly that

$$\begin{aligned}\sum_{q=\alpha}^{\infty}\sum_{s=\beta}^{\infty}\frac{u^q v^s}{q!\,s!}&\int_0^\infty \exp(-x)x^m L^\alpha_q(x)L^\beta_s(x)\,dx\\ &=\frac{(-1)^{\alpha+\beta}u^\alpha v^\beta}{(1-u)^{\alpha+1}(1-v)^{\beta+1}}\int_0^\infty x^m\exp\left[-x\left(\frac{u}{1-u}+\frac{v}{1-v}+1\right)\right]dx\\ &=(-1)^{\alpha+\beta}m!\,u^\alpha v^\beta(1-u)^{m-\alpha}(1-v)^{m-\beta}(1-uv)^{-m-1}.\end{aligned} \tag{A 3}$$

The integral defined in equation (A 1) is then

$I^{m,\alpha,\beta,}_{q,s}=$ coefficient of $u^q v^s$ in the expansion of

$$(-1)^{\alpha+\beta}q!\,s!\,m!\,u^\alpha v^\beta(1-u)^{m-\alpha}(1-v)^{m-\beta}(1-uv)^{-m-1}. \tag{A 4}$$

In this manner, we find:

(1) $$I^{\alpha,\alpha,\alpha}_{q,s}=\delta_{qs}\frac{(s!)^3}{(s-\alpha)!}, \tag{A 5}$$

(2) $$I^{(\alpha-1),\alpha,\alpha}_{q,s}=\frac{q!\,(s!)^2}{\alpha(s-\alpha)!},\qquad s\leqslant q, \tag{A 6}$$

(3) $$\begin{aligned}I^{\alpha,\alpha,(\alpha+1)}_{q,s}&=-\frac{s!\,(q!)^2}{(q-\alpha)!},\qquad q<s,\\ &=0,\qquad q\geqslant s\end{aligned} \tag{A 7}$$

(4) $$I^{(\alpha-1),\alpha,(\alpha+1)}_{q,s}=-\frac{q!\,(s!)^2}{\alpha(\alpha+1)(s-\alpha-1)!},\qquad q\geqslant s, \tag{A 8}$$

and, in general:

$$I_{q,s}^{m,\alpha,\beta}=(-1)^{m+\alpha+\beta}q!\,s!\sum_{k=0}^{q-\alpha}\sum_{j=0}^{s-\beta}(-1)^{m+j+k}\frac{(j+k+m)!}{j!\,k!}\binom{q}{\alpha+k}\binom{s}{\beta+j}. \tag{A 9}$$

The kinetic energy integrals of equation (20) can now be written in the form

$$\int_0^\infty \bar{R}_{n'l}K_l\bar{R}_{nl}r^2\,dr=\frac{1}{2}\left(\sqrt{\left[\frac{(n'-l-1)!\,(n-l-1)!}{[(n'+l+1)!\,(n+l+1)!]^3}\right]}\right)$$
$$\times\left[I_{(n'+l+1),(n+l+1)}^{(2l+2),(2l+2),(2l+2)}-2I_{(n'+l+1),(n+l+1)}^{(2l+2),(2l+3),(2l+2)}\right.$$
$$\left.-2I_{(n'+l+1),(n+l+1)}^{(2l+2),(2l+2),(2l+3)}+4I_{(n'+l+1),(n+l+1)}^{(2l+2),(2l+3),(2l+3)}\right]. \tag{A 10}$$

The corresponding potential energy integrals can be expressed as

$$-\int_0^\infty \bar{R}_{n'l}\,\bar{R}_{nl}r\,dr=-2\left(\sqrt{\left[\frac{(n'-l-1)!\,(n-l-1)!}{[(n'+l+1)!\,(n+l+1)!]^3}\cdot\right]}\right)I_{(n'+l+1),(n+l+1)}^{(2l+1),(2l+2),(2l+3)}. \tag{A 11}$$

If we make use of equations (A 5), (A 6) and (A 7) and define the constants

$$\epsilon_{kl}=\sqrt{\left[\frac{(k+l+1)!}{(k-l-1)!}\right]} \tag{A 12}$$

then the kinetic energy integrals become for $n\geqslant n'$,

$$\int_0^\infty \bar{R}_{n'l}K_l\bar{R}_{nl}r^2\,dr=\tfrac{1}{2}\delta_{nn'}+\left(\frac{\epsilon_{n'l}}{\epsilon_{nl}}\right)\left[(1-\delta_{n'n})+\frac{2(n'-l-1)}{2l+3}\right] \tag{A 13}$$

and the corresponding potential energy integrals become

$$-\int_0^\infty \bar{R}_{n'l}\bar{R}_{nl}r\,dr\quad=\quad-\quad\frac{1}{(l+1)}\left(\frac{\epsilon_{n'l}}{\epsilon_{nl}}\right)\quad\text{where } n\geqslant n'. \tag{A 14}$$

Appendix II

Variational formulation of perturbation method

In order to solve the Schrödinger equation $\mathscr{H}\Psi=E\Psi$ for the perturbed Hamiltonian, equation (1), we will use a special form of perturbation theory [13] which is based on a partitioning of the energy matrix in the secular equation in the conventional variation method. Let us introduce a complete orthonormal system of functions Ψ_k forming a basic set in the configuration space under consideration, so that

$$\Psi=\sum_k\Psi_kC_k. \tag{A 15}$$

The variational principle leads to a system of linear equations

$$\sum_l(\mathscr{H}_{kl}-E\delta_{kl})C_l=0,$$

where

$$\mathscr{H}_{kl}=\int\Psi_k^*\mathscr{H}\Psi_l\,d\tau.$$

This system may be condensed in the matrix form

$$\mathbf{HC}=E\mathbf{C} \tag{A 16}$$

where $\mathbf{C}$ is a column vector formed by the coefficients C_k. Dividing this vector into two parts, $\mathbf{C}_1$ and $\mathbf{C}_2$, we get the following partitioning

$$\mathbf{C}=\begin{pmatrix}\mathbf{C}_1\\ \mathbf{C}_2\end{pmatrix};\qquad \mathbf{H}=\begin{pmatrix}\mathbf{H}_{11}\mathbf{H}_{12}\\ \mathbf{H}_{21}\mathbf{H}_{22}\end{pmatrix}. \tag{A 17}$$

Equation (A 16) then gives

$$\mathbf{H}_{11}\mathbf{C}_1 + \mathbf{H}_{12}\mathbf{C}_2 = E\mathbf{C}_1, \qquad \text{(A 18)}$$

$$\mathbf{H}_{21}\mathbf{C}_1 + \mathbf{H}_{22}\mathbf{C}_2 = E\mathbf{C}_2. \qquad \text{(A 19)}$$

Solving equation (A 19) for $\mathbf{C}_2$,

$$\mathbf{C}_2 = (E\mathbf{1} - \mathbf{H}_{22})^{-1}\mathbf{H}_{21}\mathbf{C}_1. \qquad \text{(A 20)}$$

Here **1** is the unit matrix. Substituting equation (A 20) into equation (A 18),

$$[\mathbf{H}_{11} + \mathbf{H}_{12}(E\mathbf{1} - \mathbf{H}_{22})^{-1}\mathbf{H}_{21}]\mathbf{C}_1 = E\mathbf{C}_1. \qquad \text{(A 21)}$$

In the case of a non-degenerate level, we may choose the component 1 to have only one dimension. In this case, both $\mathbf{C}_1$ and $\mathbf{H}_{11}$ are scalar quantities so that equation (A 21) reduces to our basic equation,

$$E = H_{11} + \mathbf{H}_{12}(E\mathbf{1} - \mathbf{H}_{22})^{-1}\mathbf{H}_{21}. \qquad \text{(A 22)}$$

A power series expansion of $(E\mathbf{1} - \mathbf{H}_{22})^{-1}$ would lead to the conventional perturbation theory. However, in the present treatment we apply equation (A 22) directly.

APPENDIX III

Successive inversion of a matrix

In the applications of the basic perturbation formula, equation (A 22), the evaluation of the reciprocal matrix is the most laborious point, but this problem may be conveniently solved by means of the method of 'successive inversion' [14]. If $\mathbf{A}$ is an arbitrary matrix in a partitioned form

$$\mathbf{A} = \begin{pmatrix} \mathbf{A}_{11}\mathbf{A}_{12} \\ \mathbf{A}_{21}\mathbf{A}_{22} \end{pmatrix} \qquad \text{(A 23)}$$

the successive solution of the equation system $\mathbf{Ax} = \mathbf{B}$ in partitioned form leads immediately to the formula

$$\mathbf{A}^{-1} = \begin{pmatrix} \mathbf{A}_{11}^{-1} + \mathbf{N}_{12}\mathbf{D}_{22}^{-1}\mathbf{N}_{21} & -\mathbf{N}_{12}\mathbf{D}_{22}^{-1} \\ -\mathbf{D}_{22}^{-1}\mathbf{N}_{21} & \mathbf{D}_{22}^{-1} \end{pmatrix} \qquad \text{(A 24)}$$

where

$$\mathbf{N}_{12} = \mathbf{A}_{11}{}^{-1}\mathbf{A}_{12}, \qquad \text{(A 25)}$$

$$\mathbf{N}_{21} = \mathbf{A}_{21}\mathbf{A}_{11}{}^{-1}, \qquad \text{(A 26)}$$

$$\mathbf{D}_{22} = \mathbf{A}_{22} - \mathbf{A}_{21}\mathbf{N}_{12}. \qquad \text{(A 27)}$$

If the matrix $\mathbf{A}_{22}$ is chosen to consist of a single element, the matrices $\mathbf{A}_{12}$ and $\mathbf{A}_{21}$ become column and row vectors, respectively, and $\mathbf{D}_{22}$ will have a single element and simply be a number. One can now successively find the reciprocal of a given matrix by starting out from the upper left corner element if, in each step, one adds a row and a column to the previously handled matrix and then uses equation (A 23) and equation (A 24). Even physically the process is of importance, since one can directly follow the convergence obtained by adding successively one new element after another to the basis under consideration.

On traite l'interaction de deux atomes d'hydrogène dans leur état fondamental, et à grande distance, au moyen de la forme variationnelle de la théorie des perturbations, qui met en jeu essentiellement le calcul de la réciproque de la matrice non perturbée au moyen d'inversions successives. On emploie un ensemble de base qui évite la region du continuum. L'énergie du système de deux atomes d'hydrogène à grande distance se trouve être:

$$E = [-1 - 6{\cdot}499026/R^6 - 144{\cdot}8497/R^8 - \ldots]e^2/a_0$$

ou la distance R est mesurée en unités a_0. Le coefficient de R^{-6} est en accord avec les calculs de Pauling et Beach mais le coefficient de R^{-8} est sensiblement différent du leur. La fonction d'onde est grandement simplifiée par l'introduction d'orbitales naturelles. Si on construit une fonction d'onde approchée en employant un ou deux ensembles, seulement, d'orbitales naturelles, il en resulte une erreur minime pour l'énergie de dispersion calculée. Aussi, l'on montre qu'une telle approximation mène à une erreur minime sur l'écart quadratique moyen entre la fonction d'onde approchée et la fonction exacte. Ceci est un exemple du théorème selon lequel l'écart quadratique moyen entre la fonction vraie et une fonction d'onde approchée composée de n orbitales naturelles est plus petit qu'entre la fonction vraie et une fonction d'onde approchée bâtie à partir de n autres types d'orbitales. On donne aussi une application des calculs de forces intermoléculaires à grande distance à la théorie des collisions.

Die Wechselwirkung zwischen zwei Wasserstoffatomen in ihrem Grundzustand bei grossem Abstand wird mit Hilfe der Störungstheorie in einer Variationsform untersucht. Eine wesentliche Rolle spielt hierbei die Berechnung des Reziproken der ungestörten Matrix mittels sukzessiver Inversion. Ein Grundschema wird benutzt, das das Kontinuum vermeidet. Für die Energie des Systems der beiden Wasserstoffatome bei grossem Abstand wird gefunden:

$$E=[-1-6\cdot499026/R^6-144\cdot8497/R^8-\ldots]e^2/a_0$$

wobei der Abstand R in Einheiten von a_0 ausgedrückt wird. Der Zahlenfaktor von R^{-6} stimmt mit den Berechnungen von Pauling und Beach überein; dagegen ist der Faktor von R^{-8} deutlich verschieden von dem Wert dieser Autoren. Die Wellenfunktion wird durch Einführung 'natürlicher Bahnfunktionen' stark vereinfacht. Wenn man näherungsweise zur Berechnung der Wellenfunktion nur eine oder zwei Gruppen natürlicher Bahnfunktionen benutzt, so ist der Fehler in der berechneten Dispersionsenergie nur sehr klein. Ausserdem wird gezeigt, dass eine solche Näherungsrechnung nur zu einem sehr kleinen Fehler hinsichtlich des mittleren Fehlerquadrates führt, das den Unterschied zwischen angenäherter und exakter Wellenfunktion angibt. Hierdurch wird das Theorem verdeutlicht, wonach eine angenäherte Wellenfunktion, die aus n natürlichen Bahnfunktionen zusammengesetzt ist, von der wirklichen Wellenfunktion um ein kleineres mittleres Fehlerquadrat abweicht als jede andere angenäherte Wellenfunktion, die aus n anderen Funktionen aufgebaut ist. Eine Anwendung von Berechnungen der zwischenmolekularen Fernwirkungen auf die Theorie der Zusammenstösse wird ebenfalls gezeigt.

REFERENCES

[1] HIRSCHFELDER, J. O., CURTISS, C. F., and BIRD, R. B., 1954, *Molecular Theory of Gases and Liquids* (John Wiley and Co.), p. 922.

[2] DAHLER, J. S., and HIRSCHFELDER, J. O., 1956, *J. chem. Phys.*, **25**, 986. See especially pp. 992 and 993. Note that they use a different coordinate system.

[3] LÖWDIN, P. O., and SHULL, H., 1956, *Phys. Rev.*, **101**, 1730.

[4] FREEMAN, A. J., and LÖWDIN, P. O., 1958, *Phys. Rev.*, **111**, 1212.

[5] HYLLERAAS, E. A., 1949, *Avh. norske VidenskAkad.* (Oslo), *I. Mat. Naturv. Klasse*, No. 5. Our use of the functions $\Theta_{k\ l}$ to reduce the complexity of the wave functions is closely associated with the technique of this author.

[6] PAULING, L., and BEACH, J. Y., 1935, *Phys. Rev.*, **47**, 686.

[7] SHULL, H., and LÖWDIN, P. O., 1955, *J. chem. Phys.*, **23**, 1362.

[8] DALGARNO, A., 1958, April, private communication. Dalgarno has found a discrepancy of a factor of approximately 3 in Pauling and Beach's value for B_{10}

[9] LÖWDIN, P. O., 1955, *Phys. Rev.*, **97**, 1474; 1957, June, LÖWDIN, P. O., and YOSHIZUMI, H., Quantum Chemistry Group Uppsala University Tech. Note, No. 1.

[10] LÖWDIN, P. O., and SHULL, H., 1956, *Phys. Rev.*, **101**, 1730.

[11] EISENSCHITZ, R., and LONDON, F., 1930, *Z. Phys.*, **60**, 491.

[12] See reference [1], p. 1024.

[13] LÖWDIN, P. O., 1951, *J. chem. Phys.*, **19**, 1396; and in a forthcoming publication.

[14] HOUSEHOLDER, A. S., 1953, *Principles of Numerical Analysis* (New York: McGraw-Hill), p. 78.

Efficiencies of third bodies in the reaction $H+O_2+M=HO_2+M$

by P. G. DICKENS and J. W. LINNETT
Inorganic Chemistry Laboratory, Oxford

(*Received* 6 *February* 1959)

Vibrational transition probabilities have been calculated by the Schwartz, Slawsky and Herzfeld method [3] for the deactivation of HO_2^* in collision with H_2, O_2 and CO_2. The relative efficiencies of H_2, O_2 and CO_2 are compared with their third-body efficiencies found experimentally and it is concluded that the transfer of large vibrational quanta from HO_2^* is unlikely to play an important part in determining the position of the second explosion limit of the H_2/O_2 reaction. This conclusion is at variance with the explanation put forward by Walsh [1] of the ' anomalous ' third-body efficiencies of H_2O and CO_2 in this reaction.

1. INTRODUCTION

An interesting theory has been proposed by Walsh [1] to account for the 'anomalous' efficiencies of CO_2 and H_2O as third bodies in the reaction $H+O_2+M=HO_2+M$. This reaction (which may be thought of as taking place in two stages

$$H+O_2 \rightleftharpoons HO_2^* \tag{1.1}$$
$$HO_2^*+M=HO_2+M) \tag{1.2}$$

together with the chain branching step

$$HO_2^*=O+OH, \tag{1.3}$$

are generally agreed to be the competing reactions which determine the position of the second explosion limit in the H_2/O_2 reaction. Third-body efficiencies of M in reaction (1.2) are determined by studying the effect of varying $p(H_2+O_2)\ pM$ ratio on the position of this limit, at constant temperature [2].

If efficiencies are compared on a 'collision for collision' basis, it is found that the relative efficiencies of H_2, O_2, CO_2 and H_2O fall in the approximate ratios,

$$H_2:O_2:CO_2:H_2O=1:1:2:10.$$

Walsh concludes that such third-body efficiencies are a measure of the efficiency of M in removing excess vibrational energy from HO_2^*. He seeks to explain the anomalous efficiencies of CO_2 and H_2O on the basis of a near coincidence of one of their fundamental vibration frequencies with one of the two he postulates for the radical HO_2. In the language of the Schwartz, Slawsky and Herzfeld theory for the calculation of vibrational relaxation times [3], vibrational transition probabilities, $P_{0\,1}^{1\,0}(HO_2^*\ M)$, for 'complex' (vibration-vibration) transfers, are high for the collision pairs HO_2^*-CO_2 and HO_2^*–H_2O, but are low for pairs such as HO_2^*–H_2 and HO_2^* O_2, since H_2 and O_2 do not possess fundamental frequencies close to those of HO_2 whereas CO_2 and H_2O do. Presumably 'simple' (direct vibration–translation) type transfers are thought to be of lower transition probability than the complex transfers entered into by CO_2 and H_2O. At first sight this viewpoint seems reasonable.

A major assumption is that the fundamental frequencies of HO_2 are involved, i.e. large vibrational quanta are to be transferred. Walsh justifies this by pointing out that the energy of formation of HO_2^* can be distributed over several vibrational modes and hence the energy in any one mode may not be high enough to cause the vibrational energy spacings to be so very different from the fundamental separation (*unlike* the case of the association of two atoms to form a diatomic molecule).

The fundamental vibration frequencies of HO_2 are not known. Walsh makes reasonable estimates of two of these, viz. $\sim 3700\ \mathrm{cm}^{-1}$ (controlled by O–H stretching) and $\sim 1230\ \mathrm{cm}^{-1}$ (controlled by O–O stretching). The high efficiencies of CO_2 and H_2O are then explained in terms of the near-coincidence of one of their fundamentals (ν_1, $H_2O = 3652\ \mathrm{cm}^{-1}$, ν_2, $CO_2 \sim 1285\ \mathrm{cm}^{-1}$) with those of HO_2.

Crude calculations of vibrational transition probabilities are presented here which demonstrate a serious limitation of Walsh's theory.

2. Calculations

Vibrational transition probabilities were calculated by application of the formulae given by Tanczos [4] and used by us in a previous paper [5].

The calculations are inevitably very crude since no experimental data are available of either the shape, fundamental vibration frequencies or intermolecular force constants for the HO_2 radical. Values of Lennard-Jones coefficients for HO_2 were somewhat arbitrarily taken as $\epsilon/k = 100$°K and $r_0 = 3{\cdot}85$ Å (values for O_2 are $\epsilon/k = 88$°K, $r_0 = 3{\cdot}54$ Å). Fortunately the exact values used make little difference to the calculated relative transition probabilities. The L.-J. force constants used for H_2, O_2 and CO_2 are shown in table 1; the values taken for the various collision pairs were obtained by application of the empirical combining laws, $\epsilon_{AB} = (\epsilon_{AA}\epsilon_{BB})^{1/2}$; $(r_0)_{AB} = \frac{1}{2}[(r_0)_{AA} + (r_0)_{BB}]$.

Molecule	ϵ/k (°K)	r_0 (Å)
H_2	38·05	2·91
O_2	88·0	3·54
CO_2	213·0	3·90

Table 1. Intermolecular force constants. Data from Hirschfelder, Curtiss and Bird [6].

The additional intermolecular force constant, α^*, required for the evaluation of transition probabilities was approximated to by $17{\cdot}5/r_0$ [3]. Use was made of Walsh's estimates of the fundamental vibration frequencies of HO_2. These are quantities which have a dominating influence on the magnitude of the calculated vibrational transition probabilities. A linear configuration of HO_2 was assumed for the sake of simplicity, but the more realistic assumption of a bent structure [7] would affect the final answer by very little.

The following collision pairs were considered, HO_2^*–H_2, HO_2^*–O_2 and HO_2^*–CO_2. Probabilities of direct vibration translation exchange for the $1230\ \mathrm{cm}^{-1}$ frequency of HO_2^* were calculated in all three cases ($P^{1-0}(1230)$) and in addition the probability of the complex vibration–vibration exchange was also calculated for the last pair. In the last case, the probability, $P^{1-0}_{0-1}(1230\text{–}1340)$, refers to a process in which the excited HO_2 radical, on collision, loses one quantum of vibrational energy, $h\nu_1$ ($\nu_1 = 1230\ \mathrm{cm}^{-1}$) and the CO_2 molecule simultaneously gains one quantum, $h\nu_2$ ($\nu_2 = 1340\ \mathrm{cm}^{-1}$, the mean of the two frequencies in Fermi resonance) the small energy difference ($\Delta\nu \sim 100\ \mathrm{cm}^{-1}$) being supplied by an appropriate change in the initial and final relative translational energies of the colliding pair.

Calculated transition probabilities are shown in table 2. The value of $P^{1-0}_{0-1}(1230\text{–}1340)$ was obtained graphically following Tanczos [4].

Collision pair	P^{1-0}	P^{1-0}_{0-1}
HO_2–H_2	$3{\cdot}6 \times 10^{-3}$	—
HO_2–O_2	$0{\cdot}9 \times 10^{-5}$	—
HO_2–CO_2	$2{\cdot}7 \times 10^{-6}$	$4{\cdot}0 \times 10^{-4}$

Table 2. Vibrational transition probabilities at 800°K ($\Delta\nu(HO_2^*) = 1230\ \mathrm{cm}^{-1}$).

The calculated relative efficiencies fall in the approximate ratios,

$$H_2 : CO_2(^{1-0}_{0-1}) : O_2 : CO_2(^{1-0}_{0-0}) = 100 : 11 : 0{\cdot}25 : 0{\cdot}075.$$

Next, transition probabilities were calculated for the same collision pairs on the assumption of the removal from HO_2^* of a quantum only half as large as that postulated previously ($\Delta\nu = 615\ \mathrm{cm}^{-1}$). Only probabilities for direct vibrational–translational exchange were calculated. The results are shown in table 3.

Collision pair	P^{1-0}
HO_2–H_2	$1{\cdot}1 \times 10^{-2}$
HO_2–O_2	$1{\cdot}7 \times 10^{-3}$
HO_2–CO_2	$1{\cdot}2 \times 10^{-3}$

Table 3. Vibrational transition probabilities at 800°K ($\Delta\nu(HO_2^*) = 615\ \mathrm{cm}^{-1}$).

The calculated relative efficiencies now fall in the approximate ratios,

$$H_2 : O_2 : CO_2 = 100 : 15{\cdot}3 : 10{\cdot}5.$$

3. DISCUSSION

The results in table 2 show that the complex type of deactivation of HO_2^* by CO_2 (vibration–vibration exchange) is much more efficient than the corresponding simple deactivation (vibration–translation exchange), as was suggested by Walsh. A small adjustment of the value of the unknown vibration frequency of HO_2 could lead to a calculated probability for the HO_2^*–CO_2 exchange of about twice that for the HO_2^*–O_2 exchange, in agreement with experiment. A similar result could be expected for HO_2–H_2O collisions. However, the effect of mass on transition probabilities for direct vibration–translation transfers, involving large vibrational quanta, is such that the calculated efficiency of H_2 in deactivating HO_2^* is several hundred times greater than that of O_2, in complete disagreement with experiment.

This sort of result is perfectly general. There are extensive experimental data [8] to show that very light atoms or molecules, in non-reacting systems, are much more efficient than heavier molecules in effecting vibrational energy transfer, so long as large vibrational quanta are involved (as for example in ultrasonic experiments with simple molecules). Thus H_2 is found [3] to be some thousand times more efficient than O_2 in the vibrational deactivation of O_2 at room temperature ($\Delta\nu = 1580\ \mathrm{cm}^{-1}$). However, McCoubrey, Parke and Ubbelohde [9] have found that H_2 is only ten times as efficient as N_2 in deactivating the $815\ \mathrm{cm}^{-1}$ vibration of ethylene; here a smaller vibrational quantum is involved than in the case of O_2. A decrease in the relative efficiencies of lighter molecules in vibrational deactivation, with decreasing size of vibrational quanta, is predicted theoretically as is shown in table 3. For $\Delta\nu = 615\ \mathrm{cm}^{-1}$, H_2 is found to be only six times as efficient as O_2, whereas for $\Delta\nu = 1230\ \mathrm{cm}^{-1}$ H_2 was found to be several hundred times as efficient (table 2).

A marked dependence on mass is rarely found in experimental studies of the changeover from first to second order of unimolecular reactions [10], where small vibrational quanta are nearly certainly involved.

Hence both on experimental and theoretical grounds it seems unlikely that the exchange of large quanta is involved in the deactivation of HO_2^*. But if such quanta are not involved, the near coincidence of fundamentals of CO_2 and H_2O with *fundamentals* of HO_2 is irrelevant to the mechanism of energy transfer.

If large vibrational quanta are involved in deactivation processes of this type, H_2 and other light molecules should show a high efficiency. Such a situation is thought to occur in the oxidation of n-hexane. Small and Ubbelohde [11] explain the high efficiency of H_2 in inhibiting this reaction in terms of an efficient vibrational deactivation of the radical RO_2^* by H_2. Since there are many more vibrational modes amongst which the energy of collision can be partitioned than in the case of HO_2^*, it is more probable that the removal of large vibrational quanta will be involved. Hence the experimental results and their interpretation are in accord with our previous remarks. However, it should be stressed that there may be plausible explanations of H_2's inhibiting effect in this rather complicated reaction in terms other than that of simple physical deactivation.

On these grounds then, it seems to us best to consider HO_2^* as a complex closely akin to the type formed by the recombination of two atoms; one in which the energy in one or more modes is very close to that needed to cause dissociation. The vibrational energy level spacings will probably be very small and the factors which lead to efficiency of vibrational energy transfer in ultrasonic experiments, such as small reduced mass and coincidence of fundamental vibration frequencies will be unimportant.

Other explanations must then be found for the high efficiencies of H_2O and CO_2. Empirically, H_2O is almost invariably found to be efficient in vibrational energy transfer [8], irrespective of the magnitudes of the vibrational quanta involved. Its 'anomalous' behaviour with HO_2^* is therefore not altogether surprising. The almost identical behaviour of D_2O [12] follows naturally. CO_2 would not be expected to be more efficient than other more complicated molecules, with many vibrational degrees of freedom, but there seems to be little or no experimental evidence available to verify this. Alternatively, if HO_2^* were electronically excited, and there is no experimental evidence on this point, quite different factors would be involved than have been discussed hitherto, but such factors would be expected to be specific in character.

Until experimental determinations of the detailed structure of HO_2 have been undertaken, little progress towards a quantitative theoretical understanding of third-body efficiencies in the H_2/O_2 reaction can be made.

On a calculé par la méthode de Schwartz, Slawsky et Herzfeld [3] les probabilités de transition vibrationnelle dans la désactivation de $HO_2{}^*$ en collision avec H_2, O_2, et CO_2. On compare les efficacités relatives de H_2, O_2, et CO_2 avec leur efficacité en tant que catalyseurs et on trouve qu'il est peu probable que le transfert de nombreux quanta de vibration a partir de $HO_2{}^*$ joue un rôle important dans la détermination de la seconde limite d'explosion de la réaction H_2/O_2. Cette conclusion est en désaccord avec l'explication fournie par Walsh [1] de l'efficacité catalytique ' anormale ' de HO_2 et de CO_2 dans cette réaction.

Die vibrationellen Übergangswahrscheinlichkeiten werden nach den Methoden von Schwartz, Slawsky und Herzfeld [3] für die Desaktivierung von $HO_2{}^*$ bei Zusammenstössen mit H_2, O_2, und CO_2 berechnet. Die relativen Wirkungsgrade für H_2, O_2 und CO_2 werden mit ihren experimentell gefundenen Wirkungsgraden gegenüber dritten Körpern verglichen. Es wird geschlossen, dass der Übergang grosser Schwingungsquanten vom $HO_2{}^*$ wahrscheinlich keine ausschlaggebende Rolle für die Lagebestimmung der zweiten Explosionsgrenze der Knallgasreaktion spielt. Diese Schlussfolgerung weicht von der Erklärung ab, die Walsh [1] für die ' anomalen ' Wirkungsgrade von H_2O und CO_2 gegenüber dritten Körpern in dieser Reaktion gab.

REFERENCES

[1] WALSH, A. D., 1954, *Fuel*, **23**, 247.
[2] WILLBOURN, A. H., and HINSHELWOOD, C. N., 1946, *Proc. roy. Soc.* A, **185**, 353.
[3] SCHWARTZ, R. N., SLAWSKY, Z., and HERZFELD, K. F., 1952, *J. chem. Phys.*, **20**, 1952.
[4] TANCZOS, F. I., 1956, *J. chem. Phys.*, **25**, 439.
[5] DICKENS, P. G., and LINNETT, J. W., 1957, *Proc. roy. Soc.* A, **243**, 84.
[6] HIRSCHFELDER, J. O., CURTISS, C. F., and BIRD, R. B., 1954, *Molecular Theory of Gases and Liquids* (New York: Wiley).
[7] WALSH, A. D., 1953, *J. chem. Soc.*, 2290.
[8] HERZFELD, K. F., 1955, *Thermodynamics and Physics of Matter* (Princeton: University Press).
[9] MCCOUBREY, J. C., PARKE, J. B., and UBBELOHDE, A. R., 1954, *Proc. roy. Soc.* A, **223**, 155.
[10] TROTMAN-DICKENSON, A. F., 1955, *Gas Kinetics* (London: Butterworths).
[11] SMALL, N. J. H., and UBBELOHDE, A. R., 1952, *J. chem. Soc.*, 4619.
[12] DANBY, C. J., and HINSHELWOOD, C. N., 1940, *J. chem. Soc.*, 464.

Diffusion coefficients of gases from the rate of approach to the steady state in thermal diffusion†

by S. C. SAXENA and E. A. MASON
Institute for Molecular Physics, University of Maryland, College Park

(*Received* 11 *December* 1958)

The rate of approach to the steady state in a convection-free two-bulb thermal diffusion experiment is treated in a more rigorous manner than previously available, in order that reliable ordinary diffusion coefficients may be derived from thermal diffusion measurements. The final results are of the same form as in the original simplified Jones and Furry treatment, but the parameters are now interpreted somewhat differently and a new correction term appears. Application to Nettley's measurements on H_2–N_2 mixtures removes an apparent discrepancy with the kinetic theory prediction of the composition dependence of the diffusion coefficient for this system.

1. INTRODUCTION

Measurements of gaseous diffusion coefficients are of interest for several reasons. Historically, the variation of the diffusion coefficient D with composition has served as a test of kinetic theory [1, 2], and some difficulties still remain in this connection. More recently, interest has centred on the use of measurements of D as a function of temperature to obtain information on forces between unlike molecules [3–6], since D depends directly on the unlike molecular interactions in a gas mixture, and only in a minor way on the like molecular interactions [7].

A simplified theoretical treatment by Jones and Furry [8, 9] of the rate of approach to the steady state in gaseous thermal diffusion has shown that the approach to the steady state is exponential, with a relaxation time that is inversely proportional to D. The use of thermal diffusion measurements to determine D presents several advantages over conventional methods of measuring D by gas-mixing experiments. First, the change in composition during a thermal diffusion experiment can be kept small, so that difficulties over the composition dependence of D are essentially avoided. This is not done in conventional diffusion measurements unless special tracer techniques are used. Secondly, a greater temperature range can be covered without encountering the experimental difficulties involved in the operation of taps or stopcocks at extreme temperatures. Finally, the value of the thermal diffusion factor α_T is obtained in the same experiment, and α_T also depends directly and sensitively on the unlike molecular interactions [10].

Nettley [11] has used this procedure to investigate the composition dependence of D in the system H_2–N_2. Because of the simplifying assumptions in the theory of Jones and Furry, Nettley did not attempt to calculate absolute values of D, but only relative values. Even so, the observed apparent variation of D with composition was only in qualitative agreement with kinetic theory, the observed variation being larger than could be accounted for theoretically. Lonsdale and

---

† This research was supported in part by the U.S. Atomic Energy Commission.

Mason [12] attempted to obtain the temperature dependence and the absolute value of D for H_2–CO_2 and He–CO_2, using $^{14}CO_2$ tracer. They succeeded in removing several of the simplifying assumptions of Jones and Furry, and their preliminary results were promising, although their accuracy could not be reliably assessed because of non-ideal apparatus geometry.

Recent work in this laboratory with apparatus of improved geometry, as well as Nettley's lack of quantitative agreement with kinetic theory, has indicated the necessity of even further refinement of the theoretical treatment of the rate of approach to the steady state in thermal diffusion. The purpose of the present paper is to present such a more rigorous treatment, which we believe eliminates all but one basic approximation, the so-called quasi-stationary state assumption. As a test, Nettley's measurements are analyzed on the basis of this treatment, with results that are in agreement with the predictions of kinetic theory for a reasonable molecular force law.

2. Derivation

Consider a binary mixture undergoing one-dimensional diffusion through a narrow tube which connects two large bulbs held at different temperatures. The fundamental equation of diffusion for one of the components in the connecting tube is [8–10],

$$J = -nD\left[\frac{\partial x}{\partial z} + x(1-x)\alpha_T \frac{\partial \ln T}{\partial z}\right], \tag{1}$$

where J is the flux density of the component, x its mole fraction, n the total number of both kinds of molecules per unit volume, z the space coordinate, and T the absolute temperature. Integration of equation (1) along the entire effective length of the connecting tube at some fixed time, t, yields

$$\int_0^L \frac{J}{nD}\,dz = -\int_0^L \frac{\partial x}{\partial z}\,dz - \int_0^L x(1-x)\alpha_T \frac{\partial \ln T}{\partial z}\,dz, \tag{2}$$

where L is the effective length of the tube. The basic assumption of the quasi-stationary state must now be made, which states that the flux density J is constant along the length of the tube, and is therefore a function only of the variable t, and not of z. Physically, this condition should be fulfilled if the connecting tube is fairly long and narrow and the volumes of the two bulbs are each much larger than the volume of the tube. How closely these conditions must be met for a reasonable accuracy in the final result is not known, and may have to be investigated experimentally. In any event, J is brought outside the integral on the left side of (2), and the integration variables on the right side are changed to yield

$$J\int_0^L \frac{dz}{nD} = -\int_{x_1(t)}^{x_2(t)} dx - \int_{T_1}^{T_2} x(1-x)\alpha_T \, d\ln T, \tag{3}$$

where the subscripts 1 and 2 refer to the two bulbs.

The equation of continuity for the component of interest is [8, 9]

$$\frac{dx_1(t)}{dt} - \frac{dx_2(t)}{dt} = -JA\left(\frac{1}{N_1} + \frac{1}{N_2}\right), \tag{4}$$

where A is the cross-sectional area of the connecting tube, and N_1 and N_2 are the total numbers of molecules of both kinds in the two bulbs. It should be noted that the quasi-stationary state assumption has again been made in (4) by giving J the same value at each bulb. Elimination of J between (3) and (4), and use of the relations $n=p/kT$, $N_1=pV_1/kT_1$, $N_2=pV_2/kT_2$ yields the following differential equation for the approach to the steady state:

$$\frac{dS(t)}{dt}+\frac{1}{\tau}S(t)=\frac{1}{\tau}\int_{T_1}^{T_2}x(1-x)\alpha_T\,d\ln T, \tag{5}$$

where

$$S(t)=x_1(t)-x_2(t), \tag{6}$$

$$\tau=\frac{L}{A}\left(\frac{T_1}{V_1}+\frac{T_2}{V_2}\right)^{-1}\left[\frac{T}{D}\right]_{\text{av}}, \tag{7}$$

$$\left[\frac{T}{D}\right]_{\text{av}}=\frac{1}{L}\int_0^L\frac{T}{D}\,dz. \tag{8}$$

Several points should be made about equations (5)–(8). First, the relaxation time τ is independent of t only if the composition change during the experiment is small so that D remains essentially constant. Secondly, the diffusion coefficient obtained from τ is a peculiar kind of average coefficient, but it has previously been shown how this average value can be identified with a particular value of D at some average temperature between T_1 and T_2 [12]. Thirdly, the quasi-stationary state assumption has been shown to be a sufficient condition, but not a necessary condition. It is entirely possible that the form of equations (5)–(8) is correct even though the quasi-stationary state assumption itself is only approximately correct. For instance, if (3) is generalized slightly by using an average flux density defined as

$$\bar{J}=\int_0^L\frac{J}{nD}\,dz\bigg/\int_0^L\frac{dz}{nD}, \tag{9}$$

and (4) is similarly generalized by defining

$$\bar{J}'=(N_1J_2+N_2J_1)/(N_1+N_2), \tag{10}$$

the only result is to change the expression (7) for τ by multiplication by the ratio $\bar{J}/\bar{J}'$. It may happen that it is a good approximation to take this ratio of average fluxes to be a constant, even though it is not such a good approximation to take the ratio as unity, the value demanded by the quasi-stationary state assumption. More light can be thrown on this point by accurate experimental measurements of τ in apparatus of carefully chosen geometry.

Equation (5) is easily solved formally by multiplication by $\exp(t/\tau)$ and integration,

$$S(t)=\frac{1}{\tau}\exp(-t/\tau)\int_0^t\exp(t/\tau)\,dt\int_{T_1}^{T_2}x(1-x)\alpha_T\,d\ln T. \tag{11}$$

Equation (11) can be solved approximately by a sort of iteration scheme, in which a first approximation is obtained by assuming that $x(1-x)\alpha_T$ is independent of time. The result is

$$S(t)=S_0[1-\exp(-t/\tau)], \tag{12}$$

where

$$S_0=\int_{T_1}^{T_2}x(1-x)\alpha_T\,d\ln T. \tag{13}$$

This is of the same form as the Jones and Furry result, but the present expression for τ is more general. It is clear from (6) and (12) that the mole fraction x must be a function of t, and so S_0 is not really a constant and (12) is not really the correct solution of (11). For a second approximation the composition dependence of α_T is neglected, and the time dependence of x is assumed to be the same everywhere along the connecting tube. The time dependence of x in the connecting tube can then be taken to be of the same exponential form as the first approximation in (12),

$$x(t)=x(\infty)+[x(0)-x(\infty)]\exp(-t/\tau), \tag{14}$$

where $x(\infty)$ is the steady-state distribution along the connecting tube, and $x(0)$ is the initial distribution, which is presumed to be uniform. Both $x(t)$ and $x(\infty)$ are also functions of z (and hence of T), but $x(0)$ is simply a constant. Equation (11) thus becomes, on changing the order of integration,

$$S(t)=\frac{1}{\tau}\exp(-t/\tau)\int_{T_1}^{T_2}\alpha_T d\ln T\int_0^t x(t)[1-x(t)]\exp(t/\tau)\,dt, \tag{15}$$

with $x(t)$ given by (14). Carrying out the integration and keeping only first-order correction terms, we obtain

$$S(t)=S(\infty)\{1-[1-(t\delta/\tau)]\exp(-t/\tau)\},$$

or

$$S(t)\approx S(\infty)\{1-\exp[-t(1+\delta)/\tau]\}, \tag{16}$$

where $S(\infty)$ is a true constant defined as

$$S(\infty)\equiv\int_{T_1}^{T_2}x(\infty)[1-x(\infty)]\alpha_T\,d\ln T=x_1(\infty)-x_2(\infty), \tag{17}$$

and δ is a small correction given by

$$\delta=\frac{1}{S(\infty)}\int_{T_1}^{T_2}[x(0)-x(\infty)][1-2x(\infty)]\alpha_T\,d\ln T. \tag{18}$$

It turns out that δ is a significant correction, but small enough in relation to experimental errors that still higher approximations are probably unnecessary. Comparison of (12) and (16) shows that the rate of approach to the steady state is exponential in both approximations, but that the relaxation time must be interpreted differently.

The expression (18) for δ must next be evaluated in terms of measurable quantities in the two bulbs. This can be readily done in several ways, depending on the particular experimental arrangement under consideration. Since the only comparison with experiment possible at present is with Nettley's results, it is convenient to take as the known quantities only α_T, $x_1(\infty)$ and the volumes and temperatures of the bulbs. The steady-state composition along the connecting tube will vary approximately as [13]

$$\ln\left\{\frac{x(\infty)[1-x_1(\infty)]}{x_1(\infty)[1-x(\infty)]}\right\}=-\alpha_T\ln(T/T_1), \tag{19}$$

and the equation of material balance will be [13]

$$x_1(\infty)-x_2(\infty)=[x_1(\infty)-x(0)](1+f),\quad \text{where}\quad f=V_1T_2/V_2T_1. \tag{20}$$

Substitution of (19) and (20) into (18) leads after some manipulation to the following result:

$$\delta = \frac{1}{S(\infty)}\{x(0)\ln q - 2S(\infty) - [1-2x(0)]\ln[1-(1-q^{-1})x_1(\infty)]\}, \tag{21}$$

where

$$\ln q = \alpha_T \ln(T_2/T_1), \tag{22}$$

$$S(\infty) = x_1(\infty)[1-x_1(\infty)]\left[\frac{q-1}{q-(q-1)x_1(\infty)}\right], \tag{23}$$

$$x(0) = x_1(\infty) - (1+f)^{-1}S(\infty). \tag{24}$$

3. APPLICATION AND DISCUSSION

To correct Nettley's reported values of τ, it is only necessary to multiply by $(1+\delta)$, as shown by (12) and (16). Sufficiently accurate values of α_T for the correction were obtained from the summary of Hirota and Sasaki [14]. The results are given in the table. The correction to τ is 2 per cent at 0 per cent H_2 and 6 per cent in the opposite sense at 100 per cent H_2, for a net reduction of 8 per cent in the overall composition dependence of τ. This is sufficient to bring the experimental results into satisfactory agreement with the composition dependence predicted theoretically [15], as shown in the figure, where comparison is made with the theoretical prediction for molecules interacting according to Lennard-Jones (12 – 6) potentials. The maximum theoretical variation occurs for rigid elastic sphere interactions, and is also shown in the figure. For both potentials, τ was calculated according to Kihara's second approximation formula [15]. The parameters used for the Lennard-Jones (12 – 6) potential were: $\epsilon_{11}/k = 91{\cdot}5\,^\circ\mathrm{K}$, $\epsilon_{22}/k = 33{\cdot}3\,^\circ\mathrm{K}$, $\epsilon_{12}/k = 55{\cdot}2\,^\circ\mathrm{K}$, $\sigma_{11} = 3{\cdot}681$ A, $\sigma_{22} = 2{\cdot}968$ A, and $\sigma_{12} = 3{\cdot}325$ A. The rigid sphere parameters used were $\sigma_{11}/\sigma_{22} = 1{\cdot}38$. The two theoretical curves have been adjusted so as to pass through the mean of the experimental points, since Nettley's results are only relative values. The present treatment would permit the calculation of absolute values of D if the temperature variation along the length of the connecting tube were known [12].

Percentage H_2	τ, minutes	
	Nettley	Corrected
6·4	7·30	7·42
13·7	7·53	7·72
18·3	7·52	7·65
26·3	7·66	7·78
30·5	7·63	7·71
39·8	7·76	7·82
54·5	7·72	7·70
60·3	8·23	8·16
73·2	8·18	8·01
82·7	8·13	7·87

Corrected and uncorrected variation of relaxation time with composition for H_2–N_2.

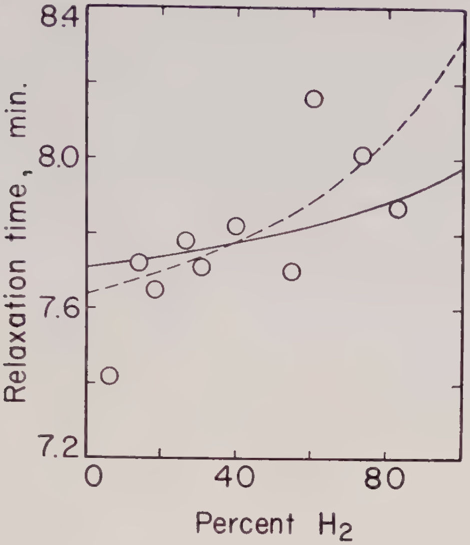

Composition dependence of the relaxation time for H_2–N_2. The circles are Nettley's corrected experimental points. The solid line is predicted from the Lennard-Jones (12 − 6) potential, and the dashed line from a rigid sphere potential.

The magnitude of the correction term δ depends on the gas pair, the apparatus geometry, and the temperatures employed. It seems probable, however, that the approximate form given by (21) is sufficiently accurate for any case likely to be encountered in practice. The physical meaning of the correction term is that it takes into account the time variation of the thermal diffusion ratio, $k_T = x(1-x)\alpha_T$, before the steady state is reached. Except for approximately equimolar mixtures, for which $\delta \approx 0$, this correction should always be taken into account in the interpretation of experimental results.

On traite de façon plus rigoureuse que cela ne l'a été fait jusqu'à présent la vitesse d'approche vers l'état stationnaire dans une expérience de diffusion thermale à deux lampes, et libre de phénomènes de convection, afin d'obtenir à partir de mesures de diffusion thermale des coefficients de diffusion ordinaires qui soient sûrs. Les résultats definitifs prennent la même forme que dans le traitement simple original de Jones et Furry, mais les paramètres sont maintenant interprêtés de façon sensiblement différente et un nouveau terme correctif apparait. L'application de ces résultats aux mesures de Nettley sur les mélanges H_2–N_2 supprime un apparent désaccord avec les prévisions de la théorie cinétique relatives à la variation du coefficient de diffusion de ce système en fonction de la composition.

Die Geschwindigkeit, mit der bei einer konvektionsfreien Messung der Wärmediffusion zwischen zwei Kugeln der stationäre Zustand erreicht wird, wird einer strengeren Behandlung unterworfen, als dies bisher geschehen ist. Das hierbei angestrebte Ziel ist die zuverlässige Berechnung der gewöhnlichen Diffusionskoeffizienten aus Messungen der Wärmediffusion. Die Endergebnisse sind von der gleichen Form wie in der ursprünglichen vereinfachten Behandlung nach Jones und Furry; doch die Parameter werden nun in etwas anderer Weise gedeutet, ausserdem tritt ein neues Korrekturglied auf. Eine Anwendung auf die Messwerte von Nettley an H_2–N_2-Mischungen beseitigt einen scheinbaren Widerspruch zu den Voraussagen der kinetischen Theorie hinsichtlich der Abhängigkeit des Diffusionskoeffizienten dieses Systems von der Zusammensetzung.

REFERENCES

[1] KENNARD, E. H., 1938, *Kinetic Theory of Gases* (New York: McGraw-Hill), pp. 196–197.

[2] LONIUS, A., 1909, *Ann. Physik*, **29**, 664.

[3] AMDUR, I., ROSS, J., and MASON, E. A., 1952, *J. chem. Phys.*, **20**, 1620.

[4] STREHLOW, R. A., 1953, *J. chem. Phys.*, **21**, 2101.

[5] AMDUR, I., and SCHATZKI, T. F., 1957, *J. chem. Phys.*, **27**, 1049.

[6] WALKER, R. E., and WESTENBERG, A. A., 1958, *J. chem. Phys.*, **29**, 1139, 1147.

[7] HIRSCHFELDER, J. O., CURTISS, C. F., and BIRD, R. B., 1954, *Molecular Theory of Gases and Liquids* (New York: John Wiley), p. 539.

[8] JONES, R. C., and FURRY, W. H., 1946, *Rev. mod. Phys.*, **18**, 151.

[9] GREW, K. E., and IBBS, T. L., 1952, *Thermal Diffusion in Gases* (Cambridge: University Press), pp. 123–125.

[10] See ref. [9], Chap. 2.

[11] NETTLEY, P. T., 1954, *Proc. phys. Soc. Lond.*, B, **67**, 753.

[12] LONSDALE, H. K., and MASON, E. A., 1957, *J. phys. Chem.*, **61**, 1544.

[13] See ref. [9], pp. 37–38.

[14] HIROTA, K., and SASAKI, K., 1954, *Bull. chem. Soc. Japan*, **27**, 27.

[15] MASON, E. A., 1957, *J. chem. Phys.*, **27**, 75.

The pairing of electronic states in alternant hydrocarbons

by A. D. McLACHLAN
Department of Theoretical Chemistry, University Chemical Laboratory,
Lensfield Road, Cambridge, England

(*Received* 3 *March* 1959)

The pairing of Hückel molecular orbitals in an alternant hydrocarbon holds in a more general sense for wave functions which make complete allowance for the correlation of π electrons within the atomic orbital scheme. The new pairing property holds exactly in the scope of Pariser, Parr, and Pople's approximations, and leads to an exact correspondence between every detail of the excited states, the electronic spectra and electron resonance spectra of positive and negative hydrocarbon ions. Neutral molecules have a half-filled electron shell in which electrons and holes are on an equal footing. This causes the electron distribution to be uniform in every electronic state, and leads to two kinds of excited state—' even ' and ' odd '—as Pariser first suggested. Transitions between states of the same parity are forbidden. In neutral radicals the spin density vanishes in all the bonds, and in both radicals and molecules the bond orders vanish between atoms of the same set (starred or unstarred).

1. INTRODUCTION

The electron resonance spectra of the positive and negative ions of an alternant hydrocarbon are often remarkably similar in hyperfine structure. Examples are anthracene, tetracene, and perylene [1, 2], which form negative ions in solutions containing free sodium or potassium and positive ions in strong sulphuric acid. The spectra of corresponding ions match in every detail and, as Carrington's experimental data in table 1 illustrate, the splitting constants from corresponding hydrogen atoms are almost equal. On the other hand there is no such spectral resemblance in the positive and negative ions of non-alternant hydrocarbons like acepleiadylene [1]. Hoijtink and Weijland [3] have found another interesting similarity between positive and negative ions of alternant hydrocarbons in the electronic spectra of perylene ions. The two spectra are almost indistinguishable, not only in the energies of the transitions, but also in their intensities, down to the smallest detail.

The similarity of these ions arises from a close correspondence between their electronic structures, which is peculiar to alternant hydrocarbons and is lost if the molecule contains odd-membered rings or if the aromatic system includes other atoms such as nitrogen.

In the molecular orbital theory of alternant hydrocarbons these peculiar electronic relationships arise from a pairing property between the energies and wave functions of the bonding and antibonding π orbitals. This accounts for all the observed similarities between corresponding positive and negative ions, and leads to many other interesting general properties of neutral molecules and radicals. However, the molecular orbital method has a serious limitation. No wave function constructed from a single configuration of orbitals can allow fully for the effect of the Coulomb forces between the electrons. Yet one has to use a wave function containing several configurations to interpret the electronic spectra in detail, or to account for the negative spin densities [4] which play an important part in the electron resonance spectra of many radicals.

Molecule	Ion	Splitting constants (gauss)		
		α	β	γ
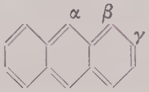	+	6·65	3·11	1·40
	−	5·56	2·74	1·57
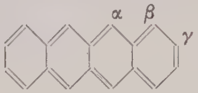	+	5·17	1·74	1·17
	−	4·25	1·49	1·03
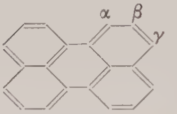	+	3·09	0·46	4·11
	−	3·09	0·46	5·53

Table 1. Hyperfine splitting constants in corresponding positive and negative ions.

The special result of the molecular orbital theory is by itself too crude to account for the closeness of the resemblance between positive and negative ions. We therefore suggest that the pairing property of the states in an alternant hydrocarbon holds in a more general sense, even when the wave functions include every possible configuration. In this paper we shall show that the wave function for each electronic state of a positive alternant ion is paired in this extended sense with a corresponding state of the negative ion. In the scope of the L.C.A.O. and π-electron approximations and the semi-empirical theory of Pople [5, 6] the new pairing theorem holds exactly. This is true even when the ground configuration is allowed to mix with every excited configuration, so that the effects of electron correlation are treated as exactly as possible. The new theorem confirms and extends many predictions of the simple molecular orbital theory, including those about the spectra of hydrocarbon ions.

Pairing relations arise in their simplest form in the Hückel molecular orbital theory [7, 8]. In an alternant hydrocarbon the aromatic system contains only even-membered rings of atoms, and alternate carbon atoms round the ring then divide into two groups called the starred and unstarred.

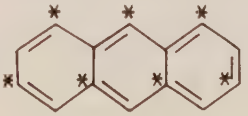

Each molecular orbital

$$\psi_i = \sum_{1}^{n} C_{ri}\phi_r \qquad (1.1)$$

now has an image orbital ψ_i' with the opposite energy and with coefficients C'_{ri}.

$$\left.\begin{aligned} C'_{ri} &= C_{ri} \text{ on starred atoms,} \\ C'_{ri} &= -C_{ri} \text{ on unstarred atoms,} \\ \epsilon_i' &= -\epsilon_i. \end{aligned}\right\} \qquad (1.2)$$

For this pairing relation to hold three conditions are necessary:
(*a*) the atomic orbitals $\phi_1 \ldots \phi_n$ are orthogonal;
(*b*) the 'Coulomb integrals' α_r are all equal;
(*c*) the 'resonance integral' β_{rs} vanishes if the two atoms do not form a bond.
Figure 1 (*a*), (*b*) and (*c*) shows the relations between the electronic structures of the neutral molecule, the monopositive ion, and the mononegative ion. The neutral molecule has two electrons in each of the bonding orbitals $\psi_1 \ldots \psi_m$, while the ions have a vacancy in ψ_m or an extra electron in ψ'_m. The excited states of the positive and negative ions are also related in pairs. The promotion of an electron from ψ_i to ψ'_j is matched by one from ψ_j to ψ'_i, and the excitation energies are both equal to $(\epsilon_j+\epsilon_i)$. Thus it is better to regard the pairing property in ions as a relation between the occupied orbitals of one ion and the empty ones of the other (figure 1 (*b*), (*c*)).

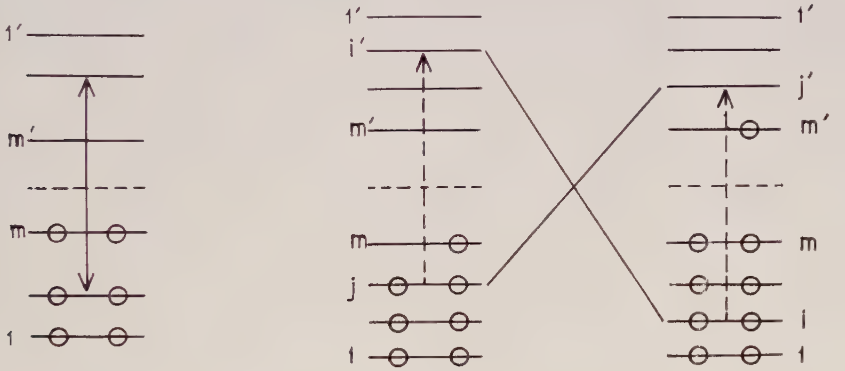

(*a*) (*b*) (*c*)

Figure 1. Electronic structure of alternant hydrocarbons according to Hückel theory.

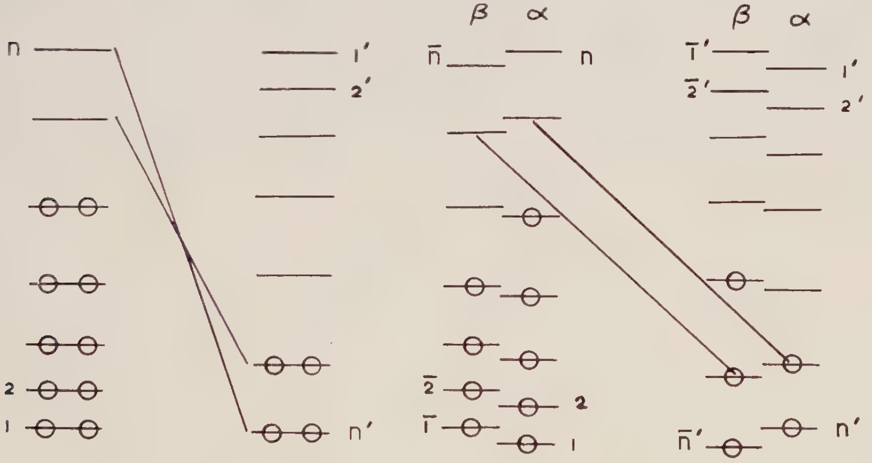

(*a*) (*b*)

Figure 2. Pairing of self-consistent orbitals in (*a*) closed shell ions; (*b*) radical ions.

Pople [6] found that the self-consistent orbitals calculated according to the Pariser and Parr method are paired in neutral molecules, and Hush and Pople [9] were able to deduce a relation

$$I+A=\text{const.} \tag{1.3}$$

between their ionization potentials and electron affinities. Pople and Brickstock [10] went further, showing that the occupied self-consistent orbitals of a positive closed shell ion are the images of the vacant orbitals in the negative ion (figure 2 (*a*)). Two approaches have been adopted in the self-consistent molecular orbital theory of radicals. In Pople and Longuet-Higgins' method [11] the $(2m+1)$ electrons occupy m orbitals in pairs and one other, to give a single determinant of the form

$$\psi = \| \psi_1^{\alpha} \psi_1^{\beta} \ldots \psi_m^{\alpha} \psi_m^{\beta} \psi_0^{\alpha} \|. \tag{1.4}$$

Lefèbvre [12] showed that the bonding and antibonding orbitals in (1.4) are paired so that $\psi_{n-r+1} = \psi'_r$, $\psi_0 = \psi'_0$. In Pople and Nesbet's theory [13] the electrons of α and β spin occupy two parallel but slightly different sets of self-consistent orbitals $\psi_1 \ldots \psi_n$ and $\bar{\psi}_1 \ldots \bar{\psi}_n (\psi_r \simeq \bar{\psi}_r)$, and the wave function is

$$\psi = \| \psi_1^{\alpha} \bar{\psi}_1^{\beta} \ldots \psi_m^{\alpha} \bar{\psi}_m^{\beta} \psi_0^{\alpha} \|. \tag{1.5}$$

In radical ions ψ_r for the negative ion is the image of $\bar{\psi}_{n-r}$ from the positive ion [10], as shown in figure 2 (*b*).

2. THE PAIRING OF CONFIGURATIONS

The pairing convention which we shall adopt for the general method is a simple extension of that illustrated in figure 2 (*a*). In an alternant hydrocarbon with n carbon atoms we begin by forming a basic set of n orthonormal molecular orbitals $\psi_1 \ldots \psi_n$ which are linear combinations of the n atomic orbitals $\phi_1 \ldots \phi_n$. (Since we are going to include every possible configuration it does not matter how we choose the set $\psi_1 \ldots \psi_n$.) There need not be any pairing relations between the coefficients of the ψ's, but we note that $\psi'_1 \ldots \psi'_n$, the set of images of ψ, is another equally good orthonormal basic set of molecular orbitals. The molecular orbitals give rise to a basic set of $2n$ orthonormal spin-orbitals $\psi_1^{\alpha} \psi_1^{\beta} \ldots \psi_n^{\alpha} \psi_n^{\beta}$ which we denote by $\bar{\psi}_1 \ldots \bar{\psi}_{2n}$. Similarly the images ψ' give spin orbitals $\psi'^{\beta}_1 \psi'^{\alpha}_1 \ldots \psi'^{\beta}_n \psi'^{\alpha}_n$, which we write $\bar{\psi}'_1 \ldots \bar{\psi}'_{2n}$. Each $\bar{\psi}$ has the opposite spin to its image.

Suppose now that we have a positive ion with $(n-r)$ electrons, and the corresponding negative ion with $(n+r)$. The wave function Φ of any electronic state of the positive ion will be built up as a sum of Slater determinants χ_{λ}, each of $(n-r)$ spin-orbitals

$$\Phi = \sum_{\lambda} a_{\lambda} \chi_{\lambda}, \tag{2.1}$$

where

$$\chi_{\lambda} = \langle abc \ldots d| = \|abc \ldots d\|. \tag{2.2}$$

In the configuration represented by χ_{λ} an electron occupies each of the spin-orbitals $a, b, c, \ldots, d$ and $\|abc \ldots d\|$ is a normalized Slater determinant. The remaining $(n+r)$ spin-orbitals $e, f, \ldots, g$ are all vacant, and we could use them to form a corresponding configuration of the negative ion. Such a configuration would have a very different energy; so instead we take their images $e', f', \ldots, g'$ and form

$$\chi'_{\lambda} = |e'f' \ldots g'\rangle = \pm \|e'f' \ldots g'\|. \tag{2.3}$$

The corresponding complete wave function is

$$\Phi' = \sum_{\lambda} a_{\lambda} \chi'_{\lambda}. \tag{2.4}$$

This definition is perfectly general. If $\psi_1, \ldots, \psi_n$ are Hückel orbitals it agrees with the usual interpretation of figure 1, and it includes all the pairing relations between different types of self-consistent orbitals. The wave function (1.5) with different orbitals for different spins also pairs according to (2.4) if it is expanded in terms of configurations from a single set of orbitals $\psi_1, \ldots, \psi_n$.

Suppose that Φ_x is the correct wave function for the positive ion in a particular electronic state. We now wish to show that the negative ion has a corresponding electronic state Φ'_x, and further, that the excitation energies of the two states from their respective ground states are equal.

$$\left.\begin{aligned} &\Phi_x \to \Phi'_x;\ E_x \to E_{x'}, \\ &E_x - E_0 = E'_x - E'_0. \end{aligned}\right\} \tag{2.5}$$

This can only be true if the matrix elements of the energy satisfy the equations

$$\begin{aligned} \langle \chi_\lambda | H | \chi_\mu \rangle &= \langle \chi'_\lambda | H | \chi'_\mu \rangle, \qquad \lambda \neq \mu, \\ \langle \chi_\lambda | H | \chi_\lambda \rangle &= \langle \chi'_\lambda | H | \chi'_\lambda \rangle + \text{const.} \end{aligned} \tag{2.6}$$

for all corresponding pairs of configurations. In establishing (2.6) there are two points to consider. First are the approximations we make in the Hamiltonian so that corresponding matrix elements are equal in magnitude. This is discussed in the next section. Second are the signs of the matrix elements. We must be sure that it is possible to choose the sign of χ'_λ in (2.3) so that (2.6) is internally consistent. Suppose that *ab* . . . *c* or $\alpha\beta \ldots \gamma$ are the spin-orbitals which

$$\left.\begin{aligned} &\chi_\lambda = \langle ab.p..q..c| \\ \text{and} \qquad &\chi_\mu = \langle \alpha\beta..r..s.\gamma| \end{aligned}\right\} \tag{2.7}$$

have in common, though not necessarily in the same order, and those which are not common occur in the order $p\ldots q$ and $r\ldots s$ respectively. Then we can derive χ_μ from χ_λ in two stages. First apply a permutation P^+ to the orbitals of χ_λ which puts the common orbitals $ab\ldots c$ into the order $\alpha\beta\ldots\gamma$, p in the position of $r,\ldots$, and q in the position of s.

$$P^+\chi_\lambda = \langle \alpha\beta..p..q.\gamma|. \tag{2.8}$$

Then perform a substitution $T(p\ldots q \to r\ldots s)$ which replaces spin-orbital p of χ_λ by the spin-orbital r of χ_μ, q by s, and so on. We write

$$\chi_\mu = TP^+\chi_\lambda. \tag{2.9}$$

In the corresponding negative ion

$$\left.\begin{aligned} \chi'_\lambda &= |d'e'.r'..s'..f'\rangle, \\ \chi'_\mu &= |\delta'\epsilon'..p'..q'.\zeta'\rangle, \end{aligned}\right\} \tag{2.10}$$

and we have a permutation P^- which rearranges the common orbitals of χ'_λ:

$$P^-\chi'_\lambda = |\delta'\epsilon'..r'..s'.\zeta'\rangle. \tag{2.11}$$

The substitution corresponding to T is $T^{-1} = T(r'\ldots s' \to p'\ldots q')$, so that

$$\chi'_\mu = T^{-1}P^-\chi'_\lambda. \tag{2.12}$$

We now define the symbol $(p\ldots q|H|r\ldots s)$ to stand for the energy matrix element between two determinants like χ_μ and $P^+\chi_\lambda$ whose common orbitals are matched in the correct order and which differ by the substitution $T(p\ldots q \to r\ldots s)$. The corresponding matrix element for the states of the negative ion is

$$(r'\ldots s'|H|p'\ldots q').$$

It is here that the difficulty of sign arises, because the approximations we make later on show that

$$(p\ldots q|H|r\ldots s) = (-)^t(r'\ldots s'|H|p'\ldots q') \tag{2.13}$$

where t is the number of orbitals which differ in χ_λ and χ_μ. To reconcile equations (2.13) and (2.6) we have to show that if the signs of one corresponding pair of states are chosen arbitrarily so that $\langle ab\ldots c| = \|ab\ldots c\|$ corresponds to $|d'e'\ldots f'\rangle = +\|d'e'\ldots f'\|$, then $\langle\alpha\beta\ldots\gamma| = \|\alpha\beta\ldots\gamma\|$ must correspond to $|\delta'\epsilon'\ldots\zeta'\rangle = (-)^P\|\delta'\epsilon'\ldots\zeta'\|$ where $(-)^P$ is the sign of the permutation

$$\langle\alpha\beta\ldots\gamma|\delta\epsilon\ldots\zeta\rangle = P\langle ab\ldots c|de\ldots f\rangle. \tag{2.14}$$

To see this we note that P is the product of the three permutations P^+, P^-, and the transpositions $t=(pr)\ldots.(qs)$:

$$P = tP^+P^-. \tag{2.15}$$

$$\begin{aligned}
\text{Then } \langle ab\ldots c|H|\alpha\beta\ldots\gamma\rangle &= \|ab\ldots c|H|\alpha\beta\ldots\gamma\| \text{ by (2.2)}\\
&= (-)^{P^+}(p\ldots q|H|r\ldots s),\\
&= (-)^{P^-}(-)^t(-)^P(p\ldots q|H|r\ldots s) \text{ by (2.15)}\\
&= (-)^P(-)^{P^-}(r'\ldots s'|H|p'\ldots q') \text{ from (2.13)}\\
&= (-)^P\|d'e'\ldots f'|H|\delta'\epsilon'\ldots\zeta'\|\\
&= \langle d'e'\ldots f'|H|\delta'\epsilon'\ldots\zeta'\rangle \text{ by hypothesis,}
\end{aligned} \tag{2.16}$$

so that our conclusion is indeed self-consistent.

3. MATRIX ELEMENTS OF THE ENERGY

We shall base our treatment on the Pariser and Parr theory of π electron molecules. In this theory it is assumed that the main features of the electronic spectra of hydrocarbons depend solely on the π electrons. Their energy is described by a Hamiltonian of the type

$$H = \sum_\mu U(\mathbf{r}_\mu) + \sum_{\mu\nu}\frac{e^2}{r_{\mu\nu}}, \tag{3.1}$$

in which the first term is the energy of the electron in the averaged field of a core of nuclei and σ electrons, while the last is the mutual Coulomb repulsion of the π electrons. The wave function for the π electrons is always assumed to be formed from combinations of n $2pz$ atomic orbitals $\phi_1\ldots\phi_n$, one from each carbon atom, so that the expectation value of H is expressed in terms of integrals over atomic orbitals. These may be core integrals

$$\left.\begin{aligned}
\beta_{rs} &= \int\phi_r U\phi_s d\tau \quad (r\neq s),\\
E_r &= \int\phi_r U_r\phi_r d\tau,\\
g_{rt} &= -\int\phi_r U_t\phi_r d\tau \quad (r\neq t),\\
\alpha_r &= E_r - \sum_t g_{rt}
\end{aligned}\right\} \tag{3.2}$$

(in which U_t stands for the potential energy of an electron in the field of atom t), or electron repulsion integrals

$$\left.\begin{aligned}
\langle rs|tu\rangle &= \int\phi_r\phi_t(1)\frac{e^2}{r_{12}}\phi_s\phi_u(2)d\tau_1\,d\tau_2,\\
\langle rs|rs\rangle &\equiv \gamma_{rs}.
\end{aligned}\right\} \tag{3.3}$$

Up to this point the theory is perfectly general except for the assumption of only one atomic orbital per atom. But several further approximations are usually made to simplify the method, and these are all necessary for proving the pairing theorem. The assumptions are:

(1) The orbitals $\phi_1 \ldots \phi_n$ are exactly orthogonal.

(2) We neglect electron repulsion integrals which arise from the overlap of two orbitals;

$$\langle rs|tu\rangle = \delta_{rt}\delta_{su}\gamma_{rt}. \tag{3.4}$$

This is the assumption of 'zero differential overlap'.

(3) An electron is perfectly shielded from the nuclear charges of other atoms when the other atom bears a π electron;

$$g_{rt} = \gamma_{rt} \text{ when } r \neq t. \tag{3.5}$$

(4) The effective potential energy of a π electron is the same on each carbon atom;

$$E_r + \tfrac{1}{2}\gamma_{rr} = \text{const.} = K \text{ for all atoms.} \tag{3.6}$$

(5) An alternant hydrocarbon is characterized by the division of its atoms into the starred and unstarred sets. $\beta_{rs}=0$ when atoms r, s belong to the same set (in which case they cannot be neighbours).

Let $\psi_1 \ldots \psi_n$ be a complete set of real orthogonal molecular orbitals of the form $\psi_i = \sum C_{ri}\phi_r$. Their coefficients then have the property

$$\sum_{i=1}^{n} C_{ri}C_{si} = \delta_{rs}. \tag{3.7}$$

We form pairs of configurations χ_λ, χ'_λ, and define bond orders and electron densities for electrons of α and β spins in any configuration of a positive ion, and the corresponding configuration of the negative ion by summation over the occupied orbitals in each system.

$$\left.\begin{aligned} q_r^{+\alpha} &= \sum_i {}^{\alpha}C_{ri}^2, & q_r^{+\beta} &= \sum_i {}^{\beta}C_{ri}^2, \\ p_{rs}^{+\alpha} &= \sum_i {}^{\alpha}C_{ri}C_{si}, & p_{rs}^{+\beta} &= \sum_i {}^{\beta}C_{ri}C_{si}. \end{aligned}\right\} \tag{3.8}$$

We may also use the total bond orders and electron densities p_{rs} and q_r. The orthogonality relations (3.7) and the definitions (1.2) and (2.3) of the pairing property show that

$$\left.\begin{aligned} &q_r^{+\alpha} + q_r^{-\beta} = 1, \\ &\quad p_{rs}^{+\alpha} = p_{rs}^{-\beta} \text{ if } r, s \text{ are in different sets} \\ &\qquad\quad = -p_{rs}^{-\beta} \text{ if } r,\ s \text{ are in the same sets.} \end{aligned}\right\} \tag{3.9}$$

The matrix elements of the energy for corresponding pairs of configurations are now expressed in terms of integrals over molecular orbitals. The diagonal elements ϵ_λ and ϵ'_λ for χ_λ and χ'_λ are

$$\left.\begin{aligned} \epsilon_\lambda &= \sum_i (A_{ii}+B_{ii}) + \sum_{ij} \{\langle ij|ij\rangle - \sigma_{ij}\langle ij|ji\rangle\} \\ \epsilon'_\lambda &= \sum_i{}' (A'_{ii}+B'_{ii}) + \sum_{ij}{}' \{\langle i'j'|i'j'\rangle - \sigma_{ij}\langle i'j'|j'i'\rangle\}, \end{aligned}\right\} \tag{3.10}$$

where

$$\left.\begin{aligned} A_{ii} &= \sum_r C_{ri}^2\alpha_r = \sum_r C_{ri}'^2\alpha_r = A'_{ii}, \\ B_{ii} &= \sum_{rs} C_{ri}C_{si}\beta_{rs} = -\sum_{rs} C'_{ri}C'_{si}\beta_{rs} = -B'_{ii}, \end{aligned}\right\} \tag{3.11}$$

$$\langle ij|ij\rangle = \langle i'j'|i'j'\rangle = \sum_{rs} C_{ri}^2 C_{sj}^2 \gamma_{rs}, \tag{3.12}$$

$$\langle ij|ji\rangle = \langle i'j'|j'i'\rangle = \sum_{rs} (C_{ri}C_{si})(C_{rj}C_{sj})\gamma_{rs}, \tag{3.13}$$

and $\sigma_{ij} = 1$ or 0 when the spin orbitals $\bar{\psi}_i$, $\bar{\psi}_j$ have the same or opposite spins.

When these substitutions and summations are made the total π-electron energy of χ is

$$\epsilon = U + G, \tag{3.14}$$

with

$$U = \sum_r q_r(E_r - \sum_t{}' g_{rt}) + 2 \sum_{r<s} p_{rs}\beta_{rs}, \tag{3.15}$$

$$G = \sum_{r<s} [(q_r q_s - (p^\alpha_{rs})^2 - (p^\beta_{rs})^2)]\gamma_{rs} + \sum_r q^\alpha_r q^\beta_r \gamma_{rr}. \tag{3.16}$$

The term G may be rearranged into the form

$$\begin{aligned} G = \sum_{r<s} [(q_r - 1)(q_s - 1) - 1 - (p^\alpha_{rs})^2 - (p^\beta_{rs})^2]\,\gamma_{rs} \\ + \sum_r q_r(\tfrac{1}{2}\gamma_{rr} + \sum_t{}' \gamma_{rt}) + \sum_r [(q^\alpha_r - \tfrac{1}{2})(q^\beta_r - \tfrac{1}{2}) - \tfrac{1}{4}]\gamma_{rr}. \end{aligned} \tag{3.17}$$

It is now evident from (3.9), and the fact that β_{rs} vanishes for atoms of the same set, that many of the terms in (3.15) and (3.17) are unchanged when we pass from the positive to the negative ion. The difference between the energies of the two molecules is

$$\epsilon^+ - \epsilon^- = \sum_r 2(q^+_r - 1)[E_r + \tfrac{1}{2}\gamma_{rr} + \sum_t (\gamma_{rt} - g_{rt})]. \tag{3.18}$$

This is equal to $\sum_r 2(q^+_r - 1)K$ by the assumptions (3) and (4), so that

$$\epsilon^+ - \epsilon^- = -2rK = \text{const.} \tag{3.19}$$

for all electronic states of an ion with $(n-r)$ electrons, and we have proved the second result of (2.6).

The off-diagonal elements of H are between states which differ by the excitation of either one or two electrons. For one-electron excitations we wish to show that, in the notation of (2.10)

$$(p|H|q) = -(q'|H|p'). \tag{3.20}$$

Now

$$\left.\begin{aligned} (p|H|q) &= U_{pq} + \sum_x \{\langle px|qx\rangle - \sigma_{px}\langle px|xq\rangle\} \\ (q'|H|p') &= U_{p'q'} + \sum_{x'}{}' \{\langle p'x'|q'x'\rangle - \sigma_{p'x'}\langle p'x'|x'q'\rangle\} \end{aligned}\right\} \tag{3.21}$$

where $\sum$, $\sum'$ stand for summation over all the other occupied spin orbitals x, x' of their respective ions. It is easy to show from the pairing relations that

$$\langle px|qx\rangle = \langle p'x'|q'x'\rangle; \quad \langle px|xq\rangle = \langle p'x'|x'q'\rangle \tag{3.22}$$

and the coefficients of β_{rs} in $(U_{pq} + U_{p'q'})$ vanish. Thus

$$\begin{aligned} (p|H|q) + (q'|H|p') = \sum_r 2C_{rp}C_{rq}(E_r - \sum_t{}' g_{rt}) \\ + \sum_1^{2n} \{\langle px|qx\rangle - \tfrac{1}{2}\langle px|xq\rangle\}. \end{aligned} \tag{3.23}$$

The electrostatic integrals may now be written

$$\sum_{x=1}^{2n} \sum_{rs} \{C_{rp}C_{rq}C^2_{xs} - \tfrac{1}{2}C_{rp}C_{sq}C_{xr}C_{xs}\}\gamma_{rs} \tag{3.24}$$

which the orthogonality relations reduce to

$$\sum_r C_{rp}C_{rq}(2 \sum_{r \neq s} \gamma_{rs} + \gamma_{rr}). \tag{3.25}$$

Hence finally

$$\begin{aligned}(p|H|q)+(q'|H|p') &= 2\sum_{r} C_{rp}C_{rq}[E_r+\tfrac{1}{2}\gamma_{rr}+\sum_{t}(\gamma_{rt}-g_{rt})]\\ &= 2\sum_{r} C_{rp}C_{rq}K\\ &= 0, \text{ by } (3.7). \end{aligned} \tag{3.26}$$

The matrix elements $(pq|H|rs)$ for a double excitation depend only on electron repulsion integrals like $\langle pq|rs\rangle$ between molecular orbitals. Since

$$\langle p'q'|r's'\rangle = \langle pq|rs\rangle,$$

because of (2.3), it follows that

$$(pq|H|rs) = (r's'|H|p'q') \tag{3.27}$$

and the result anticipated in the previous section is proved. There is therefore an exact parallel between every detail of the electronic energy levels and excited states of corresponding alternant hydrocarbon positive and negative ions. This theorem holds under assumptions which are physically reasonable and have proved useful for understanding the electronic spectra of these molecules. They also appear to be the most general ones within which the desired result is true. Assumptions (3) and (4) together are essential to (3.19) and (3.26)—the pairing property does not hold if the ring contains nitrogen atoms. Assumption (1) is necessary for the orthogonality relations (3.7), and (2) is responsible for the special form of the Coulomb energy in (3.16). If we allow overlap, and form new orthogonal orbitals from the original set, they will have resonance integrals β_{rs} between atoms of the same set, and the hydrocarbon will no longer be truly 'alternant'. Any extension of this pairing theorem would require special and purely coincidental relations between the values of overlap integrals, Coulomb integrals $\langle rs|tu\rangle$, and resonance integrals β_{rs}.

4. ELECTRONS AND HOLES

One can regard the motion of $(n+r)$ electrons over n atomic orbitals as the motion of $(n-r)$ positive holes in a closed shell of 2n electrons. On going from a positive to a negative ion electrons are replaced by holes, and the holes have their own wave functions and effective Hamiltonian. In this view the special properties of alternant hydrocarbons arise because the neutral molecule has a half-filled shell of electrons, and there is a special symmetry between the Hamiltonians of holes and electrons in the ions. The results of the previous section can be interpreted in this way. Corresponding to the configuration

$$\chi = \|ab\ldots c\| \tag{4.1}$$

for the electrons, (2.2) we define

$$\bar{\chi} = (-)^{P}\|\ de\,..f\| \tag{4.2}$$

for the holes. The bond orders $\bar{p}^{\alpha}_{rs}$, $\bar{q}^{\alpha}_{r}$ for the holes are then

$$\bar{p}^{\alpha}_{rs} = -p^{\alpha}_{rs},\ \bar{q}^{\alpha}_{r} = 1-q^{\alpha}_{r}\,; \tag{4.3}$$

and the energy of χ can be written in terms of quantities derived from $\bar{\chi}$ by substituting (4.3) into (3.17). The result is that

$$\begin{aligned} E &= 2\sum_{r}\,[E_r+\tfrac{1}{2}\gamma_{rr}+\sum_{r\neq t}(\gamma_{rt}-g_{rt})]+\langle\bar{\chi}|\bar{H}|\bar{\chi}\rangle\\ &= 2nK+\langle\bar{\chi}|\bar{H}|\bar{\chi}\rangle, \end{aligned} \tag{4.4}$$

where $\bar{H}$ is now an effective Hamiltonian for the holes, of the form

$$\bar{H} = \sum_{\mu} \bar{U}(\mathbf{r}_{\mu}) + \sum_{\mu\nu} \frac{e^2}{r_{\mu\nu}}, \tag{4.5}$$

representing the sum of a core energy $\bar{U}$ and the mutual Coulomb repulsions of the holes. The expectation value of the Coulomb repulsions is to be calulated with the same integrals γ_{rs} as before. The core energy is determined by the new integrals

$$\left.\begin{aligned} \bar{\alpha}_r &= -[E_r + \gamma_{rr} + \sum_t{}' (2\gamma_{rt} - g_{rt})], \\ \bar{\beta}_{rs} &= -\beta_{rs}, \end{aligned}\right\} \tag{4.6}$$

which are closely related to those for electrons since

$$\left.\begin{aligned} \bar{\alpha}_r &= -K - (\tfrac{1}{2}\gamma_{rr} + \sum_t{}' \gamma_{rt}), \\ \alpha_r &= K - (\tfrac{1}{2}\gamma_{rr} + \sum_t{}' \gamma_{rt}). \end{aligned}\right\} \tag{4.7}$$

Hence, apart from a constant,

$$\left.\begin{aligned} \alpha_r &= +\bar{\alpha}_r, \\ \beta_{rs} &= -\bar{\beta}_{rs}. \end{aligned}\right\} \tag{4.8}$$

To establish a complete parallel between electrons and holes we need to consider the off-diagonal matrix elements of $\bar{H}$. Adapting the notation of § 3 we find that

$$\left.\begin{aligned} (p|H|q) + (q|\bar{H}|p) &= 0, \\ (pq|H|rs) &= (rs|\bar{H}|pq), \end{aligned}\right\} \tag{4.9}$$

so that the correspondence between the wave functions of electrons and holes is defined similarly to that between paired configurations of positive and negative ions. If, for example, the spin orbitals are *abcdef* and $\chi = \|abc\|$ corresponds to $\bar{\chi} = \|def\|$, then $\|\alpha\beta\gamma\|$ corresponds to $(-)^P \|\delta\epsilon\zeta\|$, where P is the permutation

$$P = \begin{pmatrix} a & b & c & d & e & f \\ \alpha & \beta & \gamma & \delta & \epsilon & \zeta \end{pmatrix}. \tag{4.10}$$

(4.10) shows that it is possible to speak consistently of the holes in any closed shell system whatsoever having a definite wave function and Hamiltonian. The special feature of alternant hydrocarbons is the connection (4.8) between the Hamiltonians of the electrons and the effective Hamiltonian of the holes. This leads to the result that the wave function Φ' of the $(n+r)$ electrons in a negative ion is identical with $\bar{\Phi}$ for the $(n+r)$ holes in the corresponding state Φ of the positive ion, provided that each spin orbital $\bar{\psi}$ is replaced by its image $\bar{\psi}'$. Thus for

$$\left.\begin{array}{lll} \text{electrons in the positive ion,} & \chi = \langle ab\ldots c| & ; \\ \text{for holes in the positive ion,} & \bar{\chi} = & |de\ldots f\rangle; \\ \text{for electrons in the negative ion,} & \chi' = & |d'e'\ldots f'\rangle. \end{array}\right\} \tag{4.11}$$

5. THE ELECTRONIC SPECTRA OF IONS

The intensities of corresponding transitions

$$\Phi_x \to \Phi_y \; : \; \Phi'_x \to \Phi'_y \tag{5.1}$$

are determined by the dipole moments $\mathbf{M}_{xy}$ and $\mathbf{M}'_{xy}$:

$$\mathbf{M}_{xy} = \langle \Phi_x | \mathbf{M} | \Phi_y \rangle, \; \mathbf{M} = \sum_i -e(\mathbf{r}_i). \tag{5.2}$$

These can be expressed in terms of integrals over single configurations by substituting

$$\Phi_x = \sum a_{\lambda x}\chi_\lambda, \ \Phi_y = \sum a_{\mu y}\chi_\mu, \tag{5.3}$$

and finally reduced to integrals over the atomic orbitals $\phi_1 \ldots \phi_n$;

$$\langle \chi_\lambda | \mathbf{M} | \chi_\mu \rangle = \mathbf{M}_{\lambda\mu} = \sum_r (q_r)^{\lambda\mu}\mathbf{M}_r + 2\sum_{r<s}(p_{rs})^{\lambda\mu}\mathbf{M}_{rs}, \tag{5.4}$$

where

$$\left.\begin{aligned} \mathbf{M}_r &= \int \phi_r \mathbf{M} \phi_r \, d\tau, \\ \mathbf{M}_{rs} &= \int \phi_r \mathbf{M} \phi_s \, d\tau. \end{aligned}\right\} \tag{5.5}$$

Here $(q_r)^{\lambda\mu}$ and $(p_{rs})^{\lambda\mu}$ are generalized electron densities and bond orders, which have the usual meaning when $\lambda = \mu$, and when $\lambda \neq \mu$ are defined as the coefficients of α_r and β_{rs} in $H_{\lambda\mu}$. Similarly we can define $(q_r)^{xy}$ and $(p_{rs})^{xy}$ to be the coefficients of α_r and β_{rs} in $\langle \Phi_x | H | \Phi_y \rangle$ so that

$$(q_r)^{xy} \equiv \frac{\partial H_{xy}}{\partial \alpha_r} \quad \text{and} \quad (p_{rs})^{xy} \equiv \frac{\partial H_{xy}}{\partial \beta_{rs}}. \tag{5.6}$$

Their values are found from (5.3) to be

$$\left.\begin{aligned} (q_r)^{xy} &= \sum a_{\lambda x} a_{\mu y} (q_r)^{\lambda\mu}, \\ (p_{rs})^{xy} &= \sum a_{\lambda x} a_{\mu y} (p_{rs})^{\lambda\mu}. \end{aligned}\right\} \tag{5.7}$$

The pairing theorem leads to special relations between the bond orders of corresponding transitions.

and

$$\left.\begin{aligned} (q_r^\alpha)^x + (q_r'^\beta)^x = 1, \ (q_r^\alpha)^{xy} + (q_r'^\beta)^{xy} = 0, \\ (p_{rs}^\alpha)^x = \pm (p_{rs}'^\beta)^x, \ (p_{rs}^\alpha)^{xy} = \pm (p_{rs}'^\beta)^{xy}, \end{aligned}\right\} \tag{5.8}$$

for bonds between atoms of different or the same sets respectively. The dipole moments of the transitions reduce to

$$\mathbf{M}_{xy} = \sum_r (q_r)^{xy}\mathbf{M}_r + 2\sum_{r<s}(p_{rs})^{xy}\mathbf{M}_{rs} \tag{5.9}$$

and

$$\mathbf{M}'_{xy} = -\sum_r (q_r)^{xy}\mathbf{M}_r + 2\sum_{r<s}(p_{rs})^{xy}\mathbf{M}_{rs}, \tag{5.10}$$

since all the bonds are between atoms of different sets. We have already neglected the effects of overlap, so in the same spirit we neglect the contributions to $\mathbf{M}$ from bonds. Then

$$\mathbf{M} \simeq -\mathbf{M}'; \ |\mathbf{M}|^2 = |\mathbf{M}'|^2 \tag{5.11}$$

and the equality of transition moments and transition energies leads to identical electronic spectra for the two hydrocarbon ions. Some further consequences of the relations (5.8) are of interest.

(1) The charge densities at each atom of the two ions are complementary in every state; $q_r + q_r' = 2$.

(2) The bond orders are equal between bonded atoms, and opposite in magnitude between atoms of the same sets; $p_{rs} = \pm p_{rs}'$.

(3) The spin densities $\rho_r = (q_r^\alpha - q_r^\beta)$ are the same on each atom in a radical or triplet molecule; $\rho_r = \rho_r'$. In the bonds $\rho_{rs} = (p_{rs}^\alpha - p_{rs}^\beta)$ is equal but opposite to ρ_{rs}'. This explains the resemblance of the electron resonance spectra of the two species.

(4) The result of (3.19) that $\epsilon - \epsilon' = -2rK$, applied to both ions in their ground states, leads to the relation

$$I + A = -2K = (E^{+} - E^{-})$$

between the first ionization potential and electron affinity of a neutral hydrocarbon. In theory the second ionization potential and electron affinity should be similarly related by

$$I_2 + A_2 = -4K,$$

but in this case the validity of the approximation is more doubtful.

6. The electronic states of neutral molecules and radicals

If the pair of a negative ion is the positive one, the pair of a neutral molecule is itself, and for this reason its electronic structure is especially simple. If Φ_x and Φ'_x represent one electronic state and its pair, they are both states of the same molecule, and both have the same energy, according to (3.19). Thus

$$\Phi_x = \pm \Phi'_x \tag{6.1}$$

except when there is an accidental degeneracy. The pairing operation commutes with the energy operator in all neutral alternant hydrocarbons and every state is either 'even' or 'odd' to this operation. The ground configuration χ_0 of a neutral molecule, which is shown in figure 1 (*a*), is its own pair

$$\chi_0 = \chi'_0 \tag{6.2}$$

but all other configurations give rise to even and odd combinations

$$(\chi_i + \chi'_i), \quad (\chi_i - \chi'_i); \tag{6.3}$$

and the two kinds of electronic state are of characteristic form

$$\begin{aligned} \Phi_e &= 2a_0\chi_0 + \sum a_i(\chi_i + \chi'_i), \quad \text{even;} \\ \Phi_o &= \phantom{2a_0\chi_0 +{}} \sum b_i(\chi_i - \chi'_i), \quad \text{odd.} \end{aligned} \tag{6.4}$$

One may easily show from the results of § 3 that, as anticipated, the energy has no matrix elements between even and odd terms, so that this classification of states is indeed legitimate. Pariser's [14] classification of the singly-excited states into plus and minus types is a special example of the more general theorem. His minus states are even. Pariser's discovery that transitions are only allowed between states of opposite type is also confirmed; for example, between two even states the transition moment is

$$\begin{aligned} &\langle \Phi_x + \Phi'_x | \mathbf{M} | \Phi_y + \Phi'_y \rangle \\ &= (\mathbf{M}_{xy} + \mathbf{M}_{x'y'}) + (\mathbf{M}_{x'y} + \mathbf{M}_{xy'}) = 0, \end{aligned} \tag{6.5}$$

and vanishes according to (5.11). Pariser's third result that the singly-excited even singlets and triplets ${}^1\Omega_{ij}$ and ${}^3\Omega_{ij}$ have the same energy does not hold in general, because only the singlets can mix with the ground term.

In a neutral molecule with $2m$ carbon atoms the ground state configuration is

$$\chi_0 = \| \psi_1^2 \ldots\ldots \psi_m^2 \|. \tag{6.6}$$

The corresponding configuration for a radical is

$$\chi_0 = \| \psi_1^2 \ldots\ldots \psi_m^2 \psi_0^{\alpha} \| \tag{6.7}$$

and in the singly excited configurations $\chi(i\to j')$ the spin-orbital $\bar{\psi}_i$ of χ_0 is replaced by $\bar{\psi}_j$. According to our sign convention in (2.15)

$$\chi'(i\to j') = -\chi(j\to i'), \tag{6.8}$$

so that we classify the excited states of molecules according to the scheme of table 2. The parity is the same for triplets as for singlets.

	Even	Odd
Molecule	χ_0 $\chi(i\to j')-\chi(j\to i')$	$\chi(i\to i')$ $\chi(i\to j')+\chi(j\to i')$
Radical	χ_0 $\chi(0\to i')-\chi(i\to 0)$ $\chi(i\to j')-\chi(j\to i')$	$\chi(i\to i')$ $\chi(0\to i')+\chi(i\to 0)$ $\chi(i\to j')-\chi(j\to i')$

Table 2. Even and odd states of alternant hydrocarbons.

Many of the special results derived by Coulson and Longuet-Higgins [15] from the Hückel molecular orbital theory still hold, and follow from (6.4) taken with the bond order relations (5.8).

(1) The charge density on each atom is 1 in every electronic state, whether even or odd; so that one is justified in using the same self-consistent field molecular orbitals to describe the ground and excited states.

(2) Bond orders vanish between pairs of atoms in the same set (starred or unstarred).

(3) The law of alternating polarity does not hold rigorously, but should do if the long range Coulomb repulsion integrals are not too large. (This is true in self-consistent molecular orbital theory.)

(4) In a neutral radical the spin densities should vanish in all the real bonds. This confirms McConnell's [16] calculation of the spin density matrix of allyl.

Two other general theorems may be true. One is the alternation of bond-bond polarizabilities deduced by Coulson and Longuet-Higgins. The other is that the spin densities in a neutral radical alternate in sign, being always positive on the starred atoms and negative on the unstarred ones. I have proved that this is true for a valence-bond wave function without any polar structures, but cannot extend the result.

7. Conclusions

The most important consequence of these theorems is that they thoroughly confirm the previous predictions of the Hückel molecular orbital theory, and show that their validity does not depend on any special approximate treatment of the electron correlation problem. The success of the Hückel theory depends more on the special geometrical structure of alternant molecules than on the reasonableness of its physical assumptions. In this paper the most unreasonable assumptions we made were the neglect of overlap between atomic orbitals at the ends of a bond, and a concealed assumption that the same set of atomic orbitals is used by the electrons in both positive and negative ions. However the theoretical framework used here is probably the most general one within which a pairing theorem holds exactly, and one must justify the method by its excellent agreement with the experimental facts.

I would like to thank Professor H. C. Longuet-Higgins, F.R.S. for discussions and suggestions throughout this problem; Mr. J. S. Griffith for first raising the discussion of the signs of configurations in § 3; and the Department of Scientific and Industrial Research for a maintenance grant.

L'apparîment des orbitales moléculaires de Hückel dans un hydrocarbure alternant est valable dans un sens plus général pour des fonctions d'onde qui tiennent compte de façon complète de la corrélation des électrons π dans la molécule. La nouvelle propriété d'apparîment est parfaitement valable dans la limite des approximations de Pariser, Parr, et Pople, et conduit à une correspondance exacte entre chaque détail des états excités, des spectres électroniques, et des spectres de résonance électronique des ions hydrocarbonés positifs et négatifs. Les molécules neutres ont une couche électronique à demi-saturée dans laquelle les électrons et les trous sont sur un pied d'égalité. Ceci entraîne une distribution électronique uniforme dans chaque état électronique et conduit à deux types d'état excité—pair ou impair—comme l'avait d'abord suggéré Pariser. Les transitions entre états de parité semblable sont défendues. Dans les radicaux neutres, la densité de spin est nulle dans touts les liaisons, et dans les radicaux aussi bien que les molécules l'indice de liaison est nul pour les atomes d'un même ensemble (atomes à astérisque ou atomes sans astérisque).

Die paarweise Zuordnung Hückelscher *molecular orbitals* in einem alternierenden Kohlenwasserstoff bleibt in einem allgemeineren Sinne auch für solche Wellenfunktionen gültig, die die Korrelation der Elektronen in der Molekel vollständig berücksichtigen. Die neue Form der paarweisen Zuordnung gilt genau innerhalb der Näherungen von Pariser, Parr und Pople und führt zu einer exakten Korrespondenz zwischen jeder Einzelheit in den angeregten Zuständen, den Elektronenspektren und den Elektronenresonanzspektren von positiven und negativen Kohlenwasserstoffionen. Neutrale Molekeln haben eine halbgefüllte Elektronenschale, in der Elektronen und Löcher gleichberechtigt sind. Hieraus folgt eine gleichförmige Elektronenverteilung für jeden Elektronenzustand; ausserdem müssen zwei Arten angeregter Zustände existieren, nämlich gerade und ungerade, wie Pariser erstmalig vorschlug. Übergänge zwischen Zuständen gleicher Parität sind verboten. In neutralen Radikalen verschwindet die Spindichte in allen Bindungen, und in Radikalen, sowie Molekeln verschwinden die Bindungsordnungen zwischen Atomen der gleichen Klasse (mit bzw. ohne Stern).

REFERENCES

[1] DE BOER, E., and WEISSMAN, S. I., 1958, *J. Amer. chem. Soc.*, **80,** 4549; 1957, *J. chem. Phys.*, **26,** 963.
[2] CARRINGTON, A., 1959, *J. chem. Soc.*, 947.
[3] HOIJTINK, G. J., and WEIJLAND, W. P., 1957, *Rec. Trav. chim. Pays-Bas*, **76,** 836.
[4] MCCONNELL, H. M., and CHESNUT, D. B., 1957, *J. chem. Phys.*, **27,** 984.
[5] PARISER, R., and PARR, R. G., 1953, *J. chem. Phys.*, **21,** 466, 767.
[6] POPLE, J. A., 1953, *Trans. Faraday Soc.*, **49,** 1375.
[7] HÜCKEL, E., 1932, *Z. Phys.*, **76,** 628.
[8] COULSON, C. A., and RUSHBROOKE, G. S., 1940, *Proc. camb. Phil. Soc.*, **36,** 193.
[9] HUSH, N. S., and POPLE, J. A., 1955, *Trans. Faraday Soc.*, **51,** 600.
[10] POPLE, J. A., and BRICKSTOCK, A., 1954, *Trans. Faraday Soc.*, **50,** 901.
[11] POPLE, J. A., and LONGUET-HIGGINS, H. C., 1955, *Proc. phys. Soc. Lond.*, A, **68,** 591.
[12] LEFÈBVRE, R., 1957, *J. Chim. phys.*, **54,** 168.
[13] POPLE, J. A., and NESBET, R. K., 1954, *J. chem. Phys.*, **22,** 571.
[14] PARISER, R., 1956, *J. chem. Phys.*, **24,** 250.
[15] COULSON, C. A., and LONGUET-HIGGINS, H. C., 1947, *Proc. roy. Soc.* A, **191,** 39; 1947, *Ibid.*, **192,** 16.
[16] MCCONNELL, H. M., 1958, *J. chem. Phys.*, **28,** 1188.

The electron spin resonance spectrum of a γ-irradiated single crystal of glycine

by D. K. GHOSH and D. H. WHIFFEN
Chemistry Department, University of Birmingham

(*Received* 22 *January* 1959)

It is shown that γ rays act on glycine to give the free radical $NH_3^+—\dot{C}H—CO_2^-$ which remains trapped in the solid. Electron spin resonance spectra from an irradiated single glycine crystal show marked anisotropy and it is deduced that the radicals are precisely oriented in the crystal lattice. The symmetry shown by the spectra is consistent with that of the crystal lattice. Despite overlapping of lines, the spectra due to the $NH_3^+—CH—CO_2^-$ radical have been interpreted in terms of electron–nucleus coupling tensors for the N, the $H_{(C)}$ and the three $H_{(N)}$ nuclei, the latter being equivalent by virtue of a rotation or tunnelling of the $—NH_3^+$ grouping. A qualitative interpretation of these tensors in terms of the electronic structure of the radical is given. This is consistent with the negative spin density on the $H_{(C)}$ atoms and a positive spin density on the $H_{(N)}$ atoms, as predicted by theoretical treatments. The radicals appear to be oriented in the lattice in approximately the same way as their parent molecules.

1. Introduction

Interpretation of the hyperfine structure of electron resonance spectra is regularly made in terms of a coupling between the unpaired electron and any magnetic nuclei in its vicinity. In measurements on metallic ions and their complexes [1, 2], where there are partly filled d or f orbitals, this coupling is commonly expressed as a tensor. Many of the measurements on organic radicals have been made on solutions, and for this state it can be shown that the rotational motion averages the anisotropy and only an isotropic coupling remains, so that the observations are fully expressed by means of a scalar coupling constant for each nucleus; its numerical value is the average value of the tensor, that is one-third of its trace. For amorphous and polycrystalline solids, in which the radicals are oriented at random with respect to the magnetic field, the anisotropic contribution to the coupling leads to a considerable increase of line width, and so to overlapping lines and a blurring of the spectrum. Moreover, different lines are broadened to a different extent and their relative intensities thereby falsified; the broadest lines may not be observed at all.

It is clearly of importance to obtain oriented radicals in which the full coupling tensor may be determined, especially because such three-dimensional second order tensors contain six different elements and inherently contain six times as much information as a scalar. This information is the magnitudes and directions of the three principal axes of the tensor.

The smaller organic radicals are too reactive for it to be possible to incorporate preformed radicals in a crystal lattice, but fortunately it is possible, by high energy irradiation, to form the radical inside a single crystal and for it to be trapped in a specific orientation. This was shown by Uebersfeld and Erb [3] who used glycine. The present work has developed from a repetition and confirmation of their findings using a recording spectrometer [4]. The present spectra are more fully resolved and many features of the spectra are, consequently, more readily interpreted.

Glycine is a suitable material for study for a variety of reasons. (i) The radicals formed are stable and spectra obtained a year after irradiation are identical with those obtained initially. (ii) The crystal structure and positions of the host molecules are known [5] and there are only two magnetically distinguishable classes of sites so that only two orientations of chemically identical radicals are to be distinguished. More than two such overlapping spectra would be difficult to disentangle. (iii) Large crystals (250 mg) are easily grown from water solutions. (iv) There are several magnetic nuclei in the radical and their coupling tensors can be oriented with respect to each other. The chief disadvantage to glycine lies in the complexity of its spectrum with overlapping lines and the production of two chemically distinct radicals on irradiation [5].

2. EXPERIMENTAL

2.1. *Instrument—Materials*

The crystals of glycine were grown from water solution which was left standing in the laboratory and they were either self-seeded or grew on a small crystal hung in the bulk liquid on a nylon thread. The irradiations were carried out at room temperature with a ^{60}Co γ-ray source, under which treatment the crystals turned a light brown colour. The electron resonance spectrometer at 9200 Mc/s has already been described [4]. The crystal was mounted with lanoline grease on a Perspex pillar at the centre of a H_{012} rectangular cavity. It could be rotated from outside the cavity about an axis perpendicular to the magnetic field and such angles of rotation read to 2° on a scale. For rotations about other axes the crystal was remounted and set in the desired new orientation by eye. Spectra relating to the same field orientation on different occasions showed that, with care, the settings could be reproduced to $\pm 3°$. Several hundred spectra have been obtained in the course of a year's work and there is no indication of a change of spectra with time at room temperature or between different crystals. The hyperfine splittings were measured from the fractional change of current in the electromagnet. The spectra were close to the free spin g value but no accurate measurements were attempted.

2.2. *Spin Hamiltonian*

For interpretation of the spectra there are three important types of term in the Hamiltonian, namely, the interaction of the electron with the magnet field $\mathbf{H}_0$; of the electron with each magnetic nucleus, and of the nuclei with the magnetic field. Consequently the Hamiltonian can be written

$$\mathscr{H} = -\beta \mathbf{S}.g.\mathbf{H}_0 + \sum_j \mathbf{S}.T^j.\mathbf{I}^j - \sum_j (\mu^j/I^j)\mathbf{I}^j.\mathbf{H}_0$$

where the superscript j differentiates the magnetic nuclei. The nitrogen quadrupole interaction and the nucleus–nucleus couplings are small and have been omitted. Given numerical values, it is straightforward to predict the transition frequencies and intensities from such a Hamiltonian, but to infer the constants from the observed spectrum is more difficult and certain further approximations, justified in part by the results themselves, have been made. These are: (i) That the electron-field term (~9200 Mc/s) is overwhelmingly larger than the electron-nuclei interactions (~250 Mc/s) and that the latter can be neglected in determining the direction of $\mathbf{S}$. (ii) That orbital angular moments are effectively quenched so that the g tensor is isotropic with elements equal to the free spin value. The spectra are not symmetrical to their own centres, indicating that the different radicals have different g values. Displacements of the centres do not exceed 50 Mc/s so that the $g = -2{\cdot}00$ with an error of less than $\pm 0{\cdot}01$ and the approximation of isotropic g is sufficiently valid. It may then be assumed that the effective direction of $\mathbf{S}$ is exactly along the magnetic field direction (say the Z direction) so that $\mathbf{S}$ may be replaced by $M_S\mathbf{Z}$ where $\mathbf{Z} = \mathbf{H}_0 \, |H_0|$. $M_S = -\frac{1}{2}$ for the lower and $+\frac{1}{2}$ for the upper state of the transition. (iii) That to a first approximation the nuclei are also aligned along the $\mathbf{Z}$ direction. This last assumption drastically reduces the labour of computing the energy levels from the Hamiltonian. Without this restriction the calculation of the 2304 transitions in a general case for the $NH_3{}^+—\dot{C}HCO_2{}^-$ radical would require the solution of two different secular equations each involving 48 eigenstates and eigenvalues. This approximation requires that if the states with the nuclei aligned along $\mathbf{Z}$ are taken as the basis of the representation, then all off diagonal terms are negligible. The diagonal elements are readily calculated and the eigenstates are such that the selection rule $\Delta M_I = 0$ holds for each nucleus and only 48 transitions have non-zero intensity and these have equal intensity. In contrast with a parallel investigation on glycollic acid [6] no weak transitions were observed in the glycine spectrum and this justifies the assumption. However, the degree of overlapping is such that weak lines would not easily be observed. With these approximations

$$\mathscr{H} = -\beta g M_S H_0 + M_S \sum_j . \mathbf{Z} . T^j . \mathbf{Z} M_I{}^j - \sum_j (\mu^j / I^j) M_I{}^j H_0.$$

For the transition $M_S \ \tfrac{1}{2} \longleftrightarrow -\tfrac{1}{2}$ the transition frequency is given by

$$-\beta g H_0 h^{-1} + h^{-1} \sum_j \mathbf{Z} . T^j . \mathbf{Z} M_I{}^j ;$$

$-\beta g H_0 h^{-1}$ may be dropped if the frequency is referred to the centre of the pattern and h^{-1} may be omitted if T^j is expressed in frequency units. Each individual radical gives a transition at $\sum_j \mathbf{Z}^j . T . \mathbf{Z} M_I{}^j$ and for a large assembly of radicals there will be a series of transitions according to the permitted values of $M_I{}^j$. $M_I{}^j$ may be $\pm\frac{1}{2}$ for each hydrogen and 0, ± 1 for a nitrogen.

2.3. *Choice of axes*

If the orientation of the radicals were known *a priori* it would be natural to refer the coupling tensors to radical axes, but in the absence of such knowledge the axes must be chosen with respect to those of the crystal. The crystal is monoclinic [7] and grows somewhat elongated along the a axis. The a axis can be identified precisely from the intersection of the faces (011) ($0\bar{1}1$) and the c axis from the intersection of (210) ($2\bar{1}0$) faces which develop at the ends of the crystal. The b axis is perpendicular to the ac plane. It is most convenient to express the tensors in rectangular coordinates and right-handed coordinates x, y, z were chosen with $x \equiv a$ and $y \equiv b$. The direction cosines of the c axis are then $-0{\cdot}368$, 0, $+0{\cdot}930$ since $\beta = 111^\circ 38'$.

2.4. *Nature of radical orientation*

Before interpreting the spectra it is necessary to be satisfied that the radicals are precisely aligned and to discuss the number of distinguishable orientations. Figures 1 (*a*) and 1(*b*) show two spectra observed with a single crystal and refer to orientations of the magnetic field differing by only 10°. From the sharpness of these lines and the marked change produced by such a small rotation it seems that the radicals are as well aligned in the crystal as are the host molecules. These spectra are very different from those from polycrystalline material [8, 9].

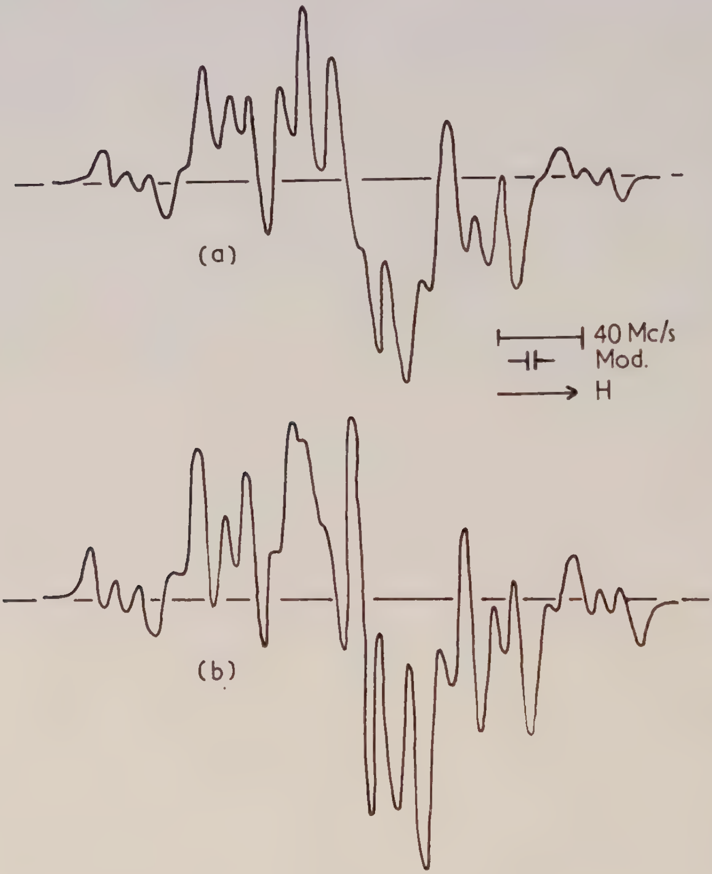

Figure 1. Derivative spectra for the magnetic field in the directions (*a*) +0·87, 0, +0·50, (*b*) +0·94, 0, +0·34 which differ by 10°.

Further, certain different directions for the magnetic field lead to the same spectra. Firstly the spectra with **Z** having direction cosines *l*, *m*, *n* and $-l$, $-m$, $-n$ are always identical. This is to be expected since the two positions differ only in the sense of the magnetic field and this can have no effect on the spectrum. In all cases the microwave magnetic field was perpendicular to **Z** and the spectra were unaffected by a change of its direction relative to the crystal axes. Further the spectra with $\mathbf{Z} \equiv l, m, n$ and $l, -m, n$ are identical. This identity stems from the symmetry of the glycine crystal. The space group [5] is $P2_1/n$. On irradiation a few molecules are transformed into radicals with the formation of defects capable of trapping such radicals. For the dosages used only a small number of unit cells contain such trapped radicals. In any individual unit cell, which contains originally four molecules, the same shape of defect can be formed in four equivalent ways, which are related to each other by the crystal symmetry. Ignoring translation, which is irrelevant to electron resonance, a specified direction l, m, n in one site is equivalent to the directions $-l, -m, -n$; $-l, m, -n$; and $l, -m, n$; in the alternative sites. The first two and the last two sites are indistinguishable by electron resonance, but the two pairs of sites can be distinguished from each other by virtue of the reversal of the sign of the direction cosine with the y axis, that is the b axis of the crystal. This means that for any given chemical species of radical in a specific shape of trapping site the coupling tensors of half the radicals, hereafter referred to as *a* radicals, will differ from those of the remainder, referred to as *b* radicals, in the sign of their xy and yz elements. It follows that the spectrum of *a* radicals for $\mathbf{Z}=l, m, n$ and of *b* radicals for $\mathbf{Z}=l, -m, n$ will be the same. In the crystal *a* and *b* radicals are present together in equal amounts and the spectra for these two directions will be identical, in agreement with experiment. This symmetry property provides a useful check on crystal alignment. For the special case when $\mathbf{Z}$, the magnetic field direction, lies in the xz plane $m=0$ and the spectra of *a* and *b* radicals are identical. The spectra are interpreted in terms of two such related sites for *a* and *b* radicals respectively, and there is no evidence of radicals being trapped in different sites which are not crystallographically related.

2.5. *Identification of the radicals*

Figure 2 shows the spectrum for $\mathbf{Z}=1, 0, 0$. The outermost features are clearly three lines of equal intensity and these can arise in only one way, namely from radicals for which the nitrogen spin has values $+1$, 0 and -1 along the $\mathbf{Z}$ direction. The next outermost feature is another group of three lines with the same spacing and three times the intensity. This suggests three identical hydrogen atoms whose coupling equals the separation between the groups of three and suggests that the —NH_3^+ group remains in the radical. The mutual equivalence of the three hydrogens persists for other $\mathbf{Z}$ directions and is not a unique occurrence in the $\mathbf{Z}=1, 0, 0$ spectrum. This requires that the —NH_3^+ is rotating or tunnelling at a rate faster than the difference between the hydrogen couplings—say 10 Mc/s. Some confirmation of this was obtained by cooling the crystal to liquid air temperatures when a change of spectrum occurred. The low temperature spectrum has not been analysed, but it is suggested that the frequency of rotation or tunnelling is less than 10 Mc/s at this temperature. This change was reversible, and the original spectrum subsequently reappeared at room temperature.

If this pattern is correct there should be another set of three lines of the stronger intensity and another of the weaker at equal spacings. As can be seen from figure 2 these would be obscured. The $\text{H}_{(\text{N})}$ and N couplings are insufficient to account for the total spacing between the outermost lines and another hydrogen must remain in the radical. It is found that one such hydrogen is both necessary and sufficient and this is presumed to be attached to the central carbon atom. In the absence of ^{13}C substitution it cannot be proved that the —CO_2^- group remains in the molecule, but the most rational explanation of the outermost parts of the spectrum is that they arise from the radical $\text{NH}_3^+\text{—}\dot{\text{C}}\text{H—CO}_2^-$

derived from glycine by loss of one H atom. This radical will not account for the whole of the central portion of the spectrum and it is suggested [3] that a second chemical species is present. Its chemical nature is still uncertain. Glycollic acid has been shown [10] to give the corresponding radical, HO—$\dot{\mathrm{C}}$H—COOH on irradiation with γ rays.

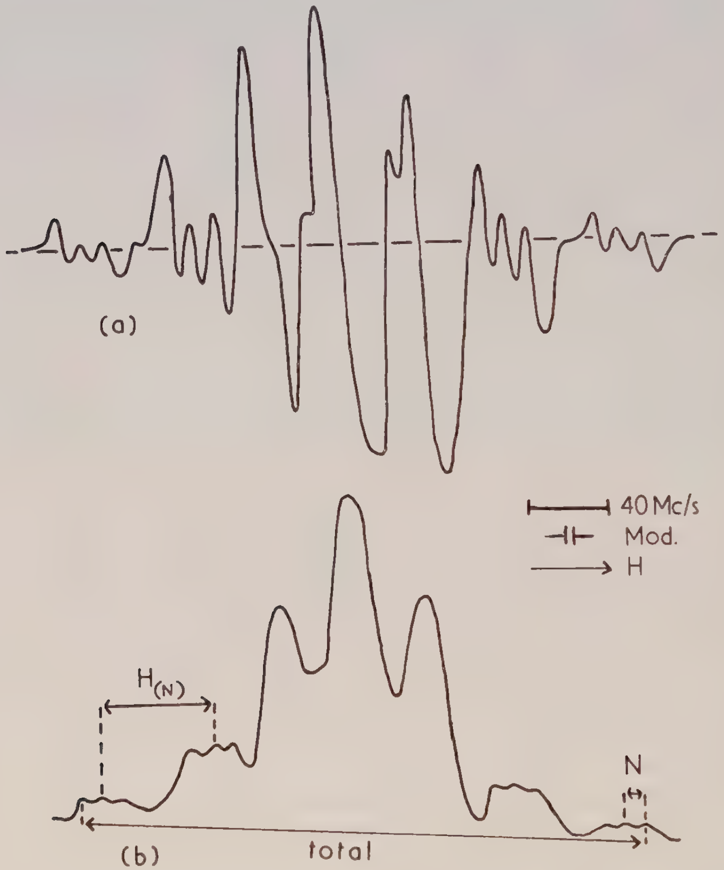

Figure 2. (*a*) Derivative and (*b*) absorption spectrum for magnetic field along 1, 0, 0. Sloping base line of integrated curve is due to experimental inaccuracies.

2.5.1. *The nitrogen coupling tensor*

The coupling tensors of the H_3N^+—$\dot{\mathrm{C}}$H—COO$^-$ radical have been deduced from the measurement. For magnetic fields in the *xz* plane the outermost features of the spectra consist of three lines due to differing nitrogen spin directions and the splitting gives the value of $\mathbf{Z} . T^{\mathrm{N}} . \mathbf{Z}$ for the corresponding field direction. The low and high field lines have the same splitting and show no evidence of further structure even under conditions (as figure 3) in which most of the spectrum would be off the recorder scale. The splitting does not vary greatly with rotation of the magnetic field in the *xz* plane, though as the splitting is of the same order of magnitude as the width of the individual lines the resolution varies markedly. Comparison derivative curves were constructed by numerical synthesis for three, equal intensity, equally spaced, Gaussian lines and examples are shown in

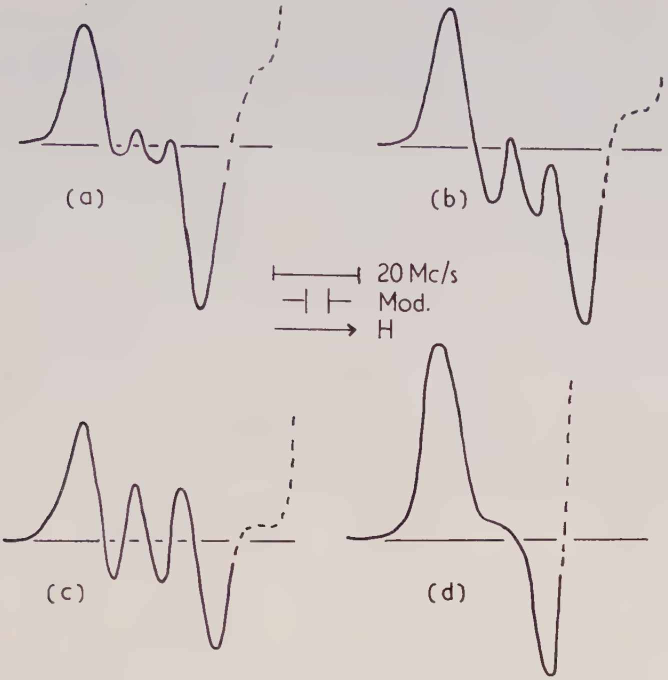

Figure 3. Low field section of derivative spectra for magnetic field along (*a*) 0, 0, 1, (*b*) $+2^{-1/2}$, 0, $-2^{-1/2}$, (*c*) 1, 0, 0, (*d*) 0, 1, 0. Dotted sections include a contribution from neighbouring lines.

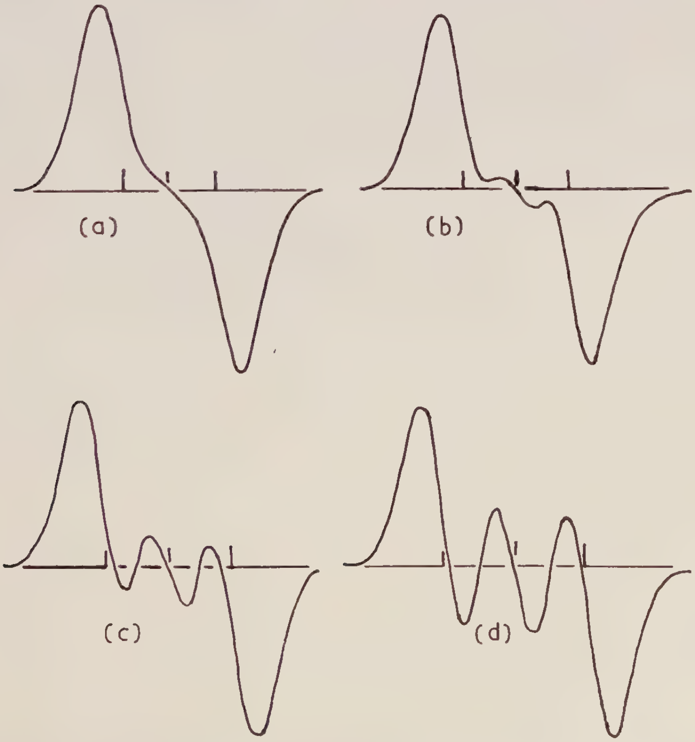

Figure 4. Synthetic spectra for three equal Gaussian lines with separation (*a*) $0{\cdot}85\Delta H_{\mathrm{m.s.}}$, (*b*) $1{\cdot}00\Delta H_{\mathrm{m.s.}}$, (*c*) $1{\cdot}15\Delta H_{\mathrm{m.s.}}$, (*d*) $1{\cdot}30\Delta H_{\mathrm{m.s.}}$ where $\Delta H_{\mathrm{m.s.}}$ is the maximum slope width.

figure 4. Synthetic curves based on Lorentzian line shape were less satisfactory. There is a strong resemblance in shape between the derivatives of figures 3 and 4. It can be seen from figure 4, in which the centres of the individual lines are

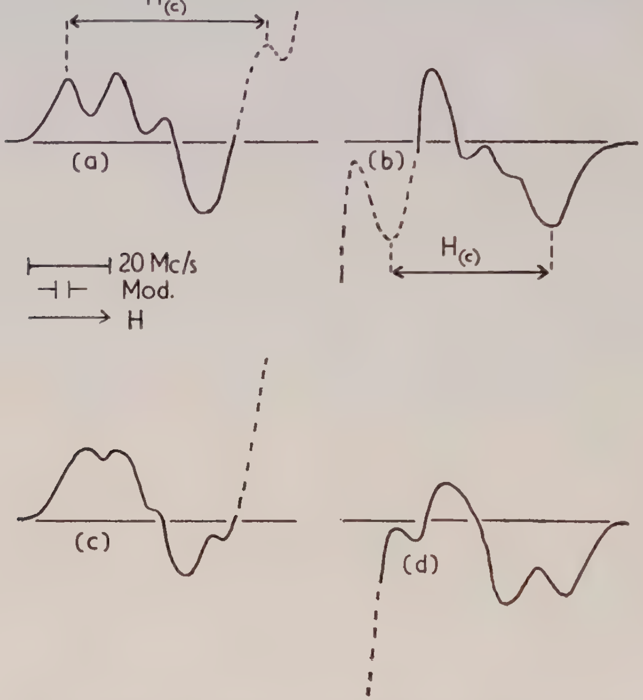

Figure 5. Derivative spectra for magnetic field along (*a*) 0, $2^{-1/2}$, $2^{-1/2}$ low field, (*b*) 0, $2^{-1/2}$, $2^{-1/2}$ high field, (*c*) $2^{-1/2}$, $2^{-1/2}$, 0 low field, (*d*) $2^{-1/2}$, $2^{-1/2}$, 0 high field. Dotted sections include a contribution from neighbouring lines.

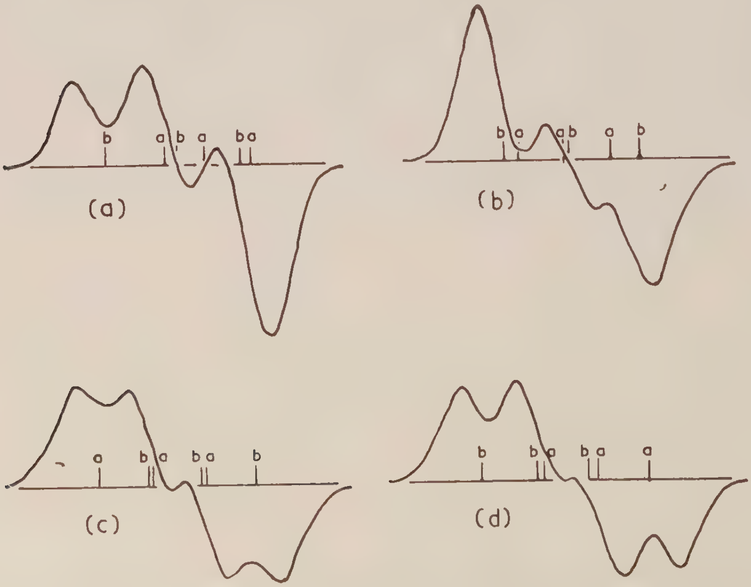

Figure 6. Synthetic spectra for six equal intensity Gaussian lines at the positions indicated.

indicated, that these centres do not correspond accurately to the zeros of the derivative curve. Consequently accurate splittings are not too easily obtained from the curves of figure 3. By a comparison of shapes, values of the nitrogen splitting to 1 Mc/s could be obtained. For $\mathbf{Z}$ in the xz plane the maximum was 11·5 Mc/s at $\mathbf{Z} = 1, 0, 0$ (figure 3 (c)) and the minimum 9·5 Mc/s at $\mathbf{Z} = 0, 0, 1$ (figure 3 (a)) with an individual line width, $\Delta H_{\text{m.s.}}$, between points of maximum slope of 9 Mc/s. For $\mathbf{Z} = 0, 1, 0$ the a and b radicals again give the same spectra and the coupling is 8·5 Mc/s (figure 3 (d)).

Nucleus	Tensor in relation to $x\ y\ z$ axes	Isotropic component	Anisotropic component	
			Principal values	Direction cosines
N	(−) $\begin{vmatrix} +11\cdot5 & 0\cdot0 & 0\cdot0 \\ 0\cdot0 & +8\cdot5 & \mp3\cdot0 \\ 0\cdot0 & \mp3\cdot0 & +9\cdot5 \end{vmatrix}$	(−) 9·8	(−) 2·3 (−) 1·7 (+) 3·9	0·00, ∓0·65, +0·76 1·00, 0·00, 0·00 0·00, ±0·76, +0·65
$H_{(N)}$	(+) $\begin{vmatrix} +52 & \pm2 & -5 \\ \pm2 & +52 & \mp8 \\ -5 & \mp8 & +55 \end{vmatrix}$	(+) 53	(+) 11 (−) 3 (−) 8	−0·40, ∓0·56, +0·73 +0·87 ∓0·47 +0·12 +0·28 ±0·68 +0·68
$H_{(C)}$	(−) $\begin{vmatrix} +92 & \pm6 & -25 \\ \pm6 & +63 & \pm22 \\ -25 & \pm22 & +70 \end{vmatrix}$	(−) 75	(−) 34 (−) 5 (+) 39	+0·78 ±0·18 −0·60 +0·50 ±0·75 +0·43 +0·37 ∓0·63 +0·68

Table 1. Coupling tensors. Upper signs throughout refer to a radicals. Absolute signs for each nucleus are not experimentally determined. All values in Mc/s.

For other directions the outermost regions of the spectra consist of three lines from the a and b radicals which may have different spacings and different centres. By virtue of a slight anistropy of the g factor tensor, the centres of the a and b patterns may not coincide so that the spectrum would not be symmetrical about its own centre even if the second chemical species of radical were disregarded. Consequently the high and low field sections of the spectra must be analysed separately even though the nitrogen splittings must be the same in both wings.

Figure 5 shows the relevant sections for the directions $0, 2^{-1/2}, 2^{-1/2}$ and $2^{-1/2}, 2^{-1/2}, 0$ and figure 6 the corresponding synthetic curves for six Gaussian lines. The vertical intensity scale is arbitrary and the splittings can be obtained from the ratio of the horizontal scales. Similar curves were constructed to match those observed in four other directions. The whole set was consistent with the N coupling tensor of table 1 within experimental error. There was some evidence for a small change of line width with orientation but this cannot be satisfactorily studied with the present signal to noise ratio.

2.5.2. *—NH_3^+ group coupling tensor*

Evidence was presented in § 2.5 to suggest that the $-NH_3^+$ group is tunnelling and that all its hydrogens should have identical coupling coefficients. The lines discussed in the preceding section must arise from those radicals for which all these hydrogen spins are parallel.

Two sets of lines with the same nitrogen hyperfine structure and with three times the intensity are to be expected and these will be located towards the centre of the pattern and separated by the hydrogen coupling from the outer set. Such sets are clearly visible in figures 1 and 2. Again the *a* and *b* radicals overlap exactly when the magnetic field is in the *xz* plane or in the *y* direction, and the coupling is readily measured for these crystal orientations. For magnetic fields in the *xy* plane these inner peaks are not seriously overlapped by the rest of the spectra and the pattern is similar to that for the outer set which suggests that the coupling to the $—NH_3^+$ group of the *a* and *b* radicals is similar, though there is indication of a small off diagonal contribution in this plane. It is of such a sign that the difference between the *a* and *b* radicals is reduced compared to the outermost peaks. Analysis of the spectra for $\mathbf{Z}$ in the *yz* plane proves difficult since there is overlapping from other lines. It seems that the difference between the centres of the *a* and *b* patterns are reduced and for some orientations just reversed in sign. The observations on the $H_{(N)}$ coupling are collated in the tensors of table 1.

2.5.3. *C–H coupling tensor*

For almost all crystal orientations the overlapping of lines is such that there is no interval directly observed, which corresponds to the coupling of the hydrogen attached to the carbon and the required quantity must be derived indirectly. With the assumptions made in § 2.2 the total frequency difference between the outermost lines for each radical transforms like a tensor. Its value is the sum of the magnitudes of all the individual coupling tensors, and if all but one of these are known the last can be derived. The total splitting tensor is easily obtained

$$\begin{vmatrix} +271 & \pm 12 & -40 \\ \pm 12 & +236 & \mp 8 \\ -40 & \mp 8 & +254 \end{vmatrix}$$

Table 2. Total coupling tensor in relation to *xyz* axes. Upper sign *a* radicals. In Mc/s.

from the experimental curves, since its value for any crystal orientation is the difference between the first maxima and the last minima of the *derivative* curve minus $\Delta H_{\text{m.s.}}$ for one individual line, i.e. 9 Mc/s. The tensor is given in table 2. Although measurements with the magnetic field in the *xy*, *yz* and *zx* planes are sufficient to obtain all the numerical values the *xy* and *yz* elements are ambiguous in relative sign since the value for *a* radicals is equal to minus that for *b* radicals.

The relative signs of the *xy* and *yz* elements for each radical can be obtained from a measurement in a skew direction. The total coupling for $\mathbf{Z} = +3^{-1/2}$, $+3^{-1/2}$, $-3^{-1/2}$ for the radical with the greatest coupling in this direction was found to be 294 Mc/s. The distinction between the *a* and *b* radicals is such that this may be said to belong to the *a* radical by definition. With the relative signs as in table 2 the computed coupling in this direction is 294 Mc/s and with reversed signs 283 Mc/s. The total splitting for the *b* radicals in this direction from the spectrum is *c.* 264 Mc/s and the computed value is 267 Mc/s (278 Mc/s signs reversed). These values, and especially the difference between *a* and *b* splittings, (observed 30 Mc/s, computed 27 Mc/s, signs reversed 5 Mc/s) settle the relative signs beyond doubt. The spectrum with the magnetic field along $3^{1/2}$, $3^{1/2}$, $3^{1/2}$

fully confirms this choice of signs. The signs in the other tensors can be related to the *a* and *b* radicals since each N and $H_{(N)}$ coupling can be identified with a particular total splitting.

It remains to subtract from the total splitting the contribution from the nitrogen, which is twice its coupling tensor since $I=1$, and three times the tensor of individual hydrogens of the $—NH_3^+$ group. The resulting C—H coupling tensor is given in table 1.

For field directions close to 0, $+2^{-1/2}$, $+2^{-1/2}$ the $H_{(C)}$ coupling of *b* radicals is less than the $H_{(N)}$ coupling and may be directly measured from the spectrum. The values for $\mathbf{Z}=0, +2^{-1/2}, +2^{-1/2}$ are 47 and *c*. 41 Mc/s from the observations of figure 5 (*a*) and (*b*) respectively which are to be compared with the 45 Mc/s computed from the $H_{(C)}$ tensor of table 1.

2.5.4. *The reliability of the experimental couplings*

The coupling tensors may be rotated to new axes in which they are in diagonal form. The isotropic contributions and the principal values of the traceless anisotropic tensors and their directions in the crystal coordinates are given in table 1. In each tensor this isotropic contribution exceeds the anisotropic contribution for all directions which indicates that the contact or Fermi interaction always exceeds any dipole–dipole coupling of the opposite sign. It is this result which enables assumption (iii) in § 2.2 to be justified. If the net coupling were to approach the value for the nucleus–magnetic field interaction (14 Mc/s for H, 1 Mc/s for N in 3300 gauss fields) and especially if it were to become zero for any direction, then extra lines would be observed [6, 11] resulting from the breakdown of the $\Delta M_I=0$ selection rule. It seems unlikely that such lines of appreciable intensity would have been missed in the analysis of the spectra but there remains a slight possibility that the relative sign of one or more principal values should be reversed.

The details of the analysis are such that the numerical magnitude and directions of the principal values would scarcely be affected by such a reversal, though the tensors would have different numerical elements in *xyz* coordinates. The absolute signs of the tensors are not determined by the experiments and neither are the relative signs for different nuclei. The absolute signs given to the tensors in table 1 are derived from the discussion below and refer to a Hamiltonian term $+\mathbf{S}.T.\mathbf{I}$. The principal elements of the nitrogen tensor are believed to be accurate to ± 1 Mc/s, those of the $-NH_3^+$ coupling to ± 3 Mc/s and the C—H coupling to ± 8 Mc/s. The uncertainty in the directions is probably ± 15° of which ± 3° arises from crystal alignment and ± 12° from the coupling values. Two principal values of the nitrogen tensor are the same within the errors and their directions are therefore essentially indeterminate and are only quoted for completeness: the perpendicular direction remains well defined.

3. DISCUSSION

The coupling between the electrons and nuclear spins is usually divided into two parts, the isotropic contact or Fermi [12] term and the traceless classical dipole–dipole coupling. It is the former term which alone remains in solution spectra since the other is averaged to zero by the tumbling motion. It may be written

$$(\mu_0/S)(\mu^j/I^j)(8\pi/3)\sum_k \delta(r_{jk})\mathbf{S}^k.\mathbf{I}^j$$

where the summation extends over all the electrons. This term has been discussed, especially for aromatic hydrocarbon radicals and radical ions, by McConnell [13, 14], Jarrett [15] and co-workers. For such radicals it is concluded that for a C—H group in such a molecule the coupling may be represented by $Q\rho\mathbf{S}\,.\,\mathbf{I}^j$ where ρ is the probability of the unpaired electron being in a p orbital on the carbon atom in the planar aromatic radicals. Q is only slightly dependent on the chemical nature of the radical and is normally in the range -65 ± 10 Mc/s. This value is to be compared with ± 75 Mc/s, for $H_{(C)}$ coupling in the present case. This suggests that $\rho \sim 1$, that is that the unpaired electron is located mainly in the central carbon atom in a p orbital and scarcely on the $—CO_2^-$ groups. It also suggests an absolute sign for the $H_{(C)}$ tensor such that its mean value is negative. This argument has the implied assumption that the N—CH—C section of the radical is planar, as in the methyl radical [16]. The crystal lattice is likely to cause small distortions from planarity but it is improbable that these will invalidate the qualitative conclusions.

The second or dipole–dipole term in the Hamiltonian may be written

$$\sum_k [\boldsymbol{\mu}^k\,.\,\boldsymbol{\mu}^j\, r_{jk}^{-3} - 3(\boldsymbol{\mu}^k\,.\,\mathbf{r}_{jk})(\boldsymbol{\mu}^j\,.\,\mathbf{r}_{jk})r_{jk}^{-5}]$$

in which $\mathbf{r}_{jk}$ is the vector joining the jth nucleus to the kth electron. In an approximation in which the wave function may be expressed as a simple product of one-electron wave functions, the summation over pairs of electrons in the same space orbital gives zero contribution and only the unpaired electron, u, need be considered. If r_{ju} is its distance from the jth nucleus and θ the angle between this radius vector and a principal axis of the coupling tensor, then the corresponding principal value is

$$(\mu_0/S)(\mu^j/I^j)\langle(1-3\cos^2\theta)r_{ju}^{-3}\rangle_{\text{average}}.$$

A numerical evaluation of this average is complicated by the fact that the electron wave function is not centred on the jth nucleus.

In the absence of accurate values, the relative sizes and signs of the three principal values for $H_{(C)}$ may be judged from figure 7. There is a local symmetry to the problem which requires that the three principal axes lie approximately parallel to the C—H bond, parallel to the p orbital occupied by the unpaired electron, and perpendicular to the C—H bond in the plane of the radical. In each case space may be divided into two parts by a conical surface of half angle $\cos^{-1}3^{-1/2} = 55°$: in one part $(1-3\cos^2\theta)$ is positive and in the other negative. The contribution to the coupling tensor will be of the opposite sign since the electron magnetic moment is negative. Figure 7 (*a*) shows that for the principal axis along the C—H bond the orbital lies predominantly in that part of the space whence the positive contributions to the coupling tensor arise and the most positive principal value is expected, therefore, to occur in a direction parallel to the C—H bond. Likewise figure 7 (*b*) shows that for the principal axis in the plane of the radical and perpendicular to the C—H bond the electron density lies almost exclusively in the negative region. For the axis parallel to the p orbital, figure 7 (*c*), the nodal surface, for which $\theta = 55°$, intersects the regions of high electron density and a numerically small coupling contribution is to be expected. Comparison of these expectations with table 1, indicates that the C—H link is parallel to the axis of the tensor with the value (+) 39 Mc/s and that the perpendicular to the plane of the radical is parallel to that axis with the value (−) 5 Mc/s.

For the arrangement of figure 7 (*b*) $\theta \sim 90^\circ$ for all parts of space with a high unpaired electron density, and so

$$\langle(1-3\cos^2\theta)r_{ju}^{-3}\rangle_{\text{average}} \sim \langle r_{ju}^{-3}\rangle_{\text{average}}.$$

The dipole contribution for this direction is (−)34 Mc/s whence

$$\langle r_{ju}^{-3}\rangle_{\text{average}} = 0\cdot43\times10^{24} \quad \text{and} \quad [\langle r_{ju}^{-3}\rangle_{\text{average}}]^{-1/3} = 1\cdot3\ \text{Å}.$$

This is slightly greater than a typical C—H bond length and is therefore of the correct order of magnitude.

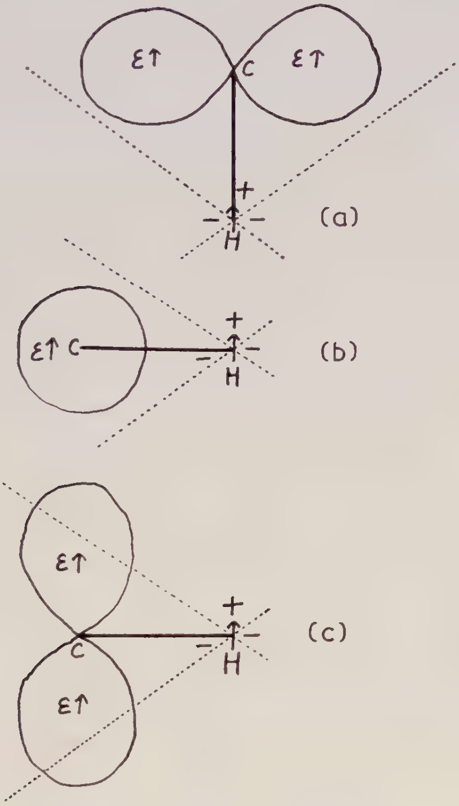

Figure 7. Guide to principal values of $H_{(C)}$ dipole–dipole coupling. Principal axis (*a*) parallel to C—H bond, (*b*) perpendicular to C—H bond in the plane of radical, (*c*) perpendicular to the plane of the radical. Spin density inside cone of half-angle 55° gives positive coupling as indicated.

A similar theory applies to the N coupling and it is to be expected that one of the principal axes would lie parallel to the p orbital. The nearest is that associated with a coupling (+) 3·9 Mc/s which is at 31° to the (−) 5 Mc/s axis of the $H_{(C)}$ tensor. This angle, though not small, is not outside the combined uncertainties arising from experimental error and from distortions of the radical from strict planarity. It is probable that the isotropic contribution is again negative for the same reasons that were applied to $H_{(C)}$, and with this assumption the contribution of the anisotropic interaction in the direction perpendicular to the plane of the radical is +3·9 Mc/s. The contribution from the unpaired electron distribution in the carbon orbital is likely to be small and negative (say ~ -2 Mc/s) and the result indicates considerable unpaired electron character in the p orbital of the nitrogen perpendicular to the plane of the radical. This may arise from hyperconjugation between the carbon and the $—NH_3^+$ group of orbitals. The spin density would need to be positive. This distribution requires 2s and 2p orbitals to contain a net preponderance of electrons with mutually opposed spins. Hund's rule of maximum multiplicity, which would require parallel spins in such an instance, is inapplicable since the net electron spin in each of these orbitals is correlated with that in the carbon 2p orbital.

Theory [17, 18] strongly suggests that the isotropic coupling of the $H_{(N)}$ atoms is positive. The anisotropic coupling is small. The contribution $(-)$ 8 Mc/s arises in a direction essentially perpendicular to the radical plane being at 19° to the principal direction of the $H_{(C)}$ tensor and 16° to that of the N tensor already chosen as being approximately perpendicular to the radical plane. A contribution of $(-)$ 3 Mc/s arises in a direction believed to be approximately parallel to the C—N bond (see below) and of $(+)$11 Mc/s in the perpendicular direction. This may arise in part from the distribution in the nitrogen 2p orbital. The major part may come from the spin distribution on the other hydrogens of the $—NH_3^+$ group. The inter-hydrogen distance in the $—NH_3^+$ group is likely to be *c.* 0·7 Å so that the coupling is considerable especially when the two hydrogens are situated on the same side of the plane of the radical.

The one electron orbital to be considered is the composite hydrogen orbital $(\psi_a+\psi_b-2\psi_c)$ as in discussions of hyperconjugation [19] and a qualitative inspection of the integrals involved suggests that the maximum positive value of the coupling lies in the radical plane and perpendicular to the C—N bond, when the averaging effect of tunnelling is considered, i.e. it is between hydrogen *a* and the electron distribution in ψ_b and the $\psi_a\psi_b$ overlap region.

It is possible to place numerical values to the integrated spin densities, by assuming the coupling parameters for one electron in the orbital specified. The results are given in table 3. The assumptions have been made that the coupling for 1s hydrogen orbital $= 1420$ Mc/s as in the free atom, that $\psi^2(0)$ for a 2s nitrogen orbital $= 34 \times 10^{24}$ cm^{-3} and that $\langle r^{-3}\rangle_{\text{average}}$ for a 2p nitrogen $= 22{\cdot}5 \times 10^{24}$ cm^{-3} [20].

C 2s	?
C 2p	$\sim +1$
$H_{(C)}$ 1s	$-0{\cdot}053$
N 2s	$-0{\cdot}006$
N 2p	$\sim +0{\cdot}015$
$H_{(N)}$ 1s	$+0{\cdot}037$ each
$—CO_2^-$	~ 0

Table 3. Integrated spin densities.

Since the radicals are similar in size and atomic arrangement to the molecules it is reasonable to expect that they occupy the site previously occupied by the parent molecule and that their orientation in the site is similar. The molecules are approximately planar and from the x-ray investigation [5] it is known that the directions of the C_I-C_{II} and $C_{II}-N$ links of the molecules are $-0{\cdot}34$, $\mp 0{\cdot}12$, $+0{\cdot}93$ and $+0{\cdot}91$, $\mp 0{\cdot}39$, $-0{\cdot}13$ respectively. The upper signs refer to molecules C and D and the lower to A and B in the diagrams of Albrecht and Corey [5]. The perpendicular to the $C_IC_{II}N$ plane makes angles of 14°, 28°

and 33° with the directions of the principal axes of the anisotropic tensors $H_{(C)}$ at (−) 5 Mc/s, N at (+) 3·9 Mc/s, and $H_{(N)}$ at (−) 8 Mc/s respectively. The bisector of the $C_I C_{II} N$ angle is approximately the expected position of the C—H bond in the radical and lies at 13° to the $H_{(C)}$ principal axis of (+) 39 Mc/s. The C_{II}—N bond lies at 17° to the $H_{(N)}$ principal axis of (−) 3 Mc/s. These angles are computed assuming the radicals called *a* in this work replace molecules C and D of the x-ray structure [5] and the *b* replace A and B. If this assignment were reversed the angles corresponding to those quoted above are all greater than 45° and the orientation of the radical would bear no simple relation to the parent molecule.

The chain of argument in the whole discussion is such that each conclusion is largely invalid if any of the other conclusions is incorrect and under this circumstance a claim that any conclusion was proved is hardly justified. Nevertheless, the suggested interpretation is self-consistent and requires that the radical is approximately planar apart from the three $H_{(N)}$ atoms, that the orientation of the heavy atoms in the *a* radicals is close to that in the C and D molecules from which they are derived. It requires that the isotropic coupling constants of $H_{(C)}$ and N are negative and of $H_{(N)}$ positive and it requires that the major unpaired electron density resides in the 2p carbon orbital perpendicular to the radical plane, but that this orbital mixes with a 2p nitrogen orbital and a related composite hydrogen orbital of the tunnelling $—NH_3^+$ group to provide a delocalization of the unpaired spin and that these provide the major contribution to the anisotropic coupling of the N and $H_{(N)}$ atoms.

We wish to thank the Royal Society for a grant for the purchase of the magnet and the University Appeals Fund for a Fellowship for D.K.G. We also thank Mr. B. P. Goddard for this technical assistance in maintaining the spectrometer and growing the crystals.

On montre que les rayons γ agissent sur la glycine pour donner le radical libre $NH_3^+—\dot{C}H—CO_2^-$ qui reste attrapé à l'intérieur du solide. Les spectres de résonance de spin électronique d'un crystal unique de glycine irradié montrent une anisotropie marquée et on en déduit que les radicaux sont orientés de manière bien définie dans le réseau crystallin. La symétrie des spectres est consistante avec celle du réseau crystallin. En dépit du chevauchement des lignes, on a pu interpréter les spectres dûs au radical $NH_3^+—\dot{C}H—CO_2^-$ en fonction de tenseurs de couplage nucléo-électronique pour les noyaux N, $H_{(C)}$, et les trois $H_{(N)}$, ces derniers étant équivalents par rotation ou inversion du groupement $—NH_3^+$. On donne une interprétation qualitative de ces tenseurs en fonction de la structure électronique du radical. Cette interprétation est en accord avec une densité de spin négative sur les atomes $H_{(C)}$ et une densité de spin positive sur les atomes $H_{(N)}$, telles qu'elles sont prédites par les traitements théoriques. Les radicaux paraissent être orientés approximativement de la même façon, dans le réseau, que leurs molécules-mères.

Es wird gezeigt, dass bei der Einwirkung von γ-Strahlen auf Glykokoll das freie Radikal $NH_3^+—\dot{C}H—CO_2^-$ gebildet wird, das im Festkörper eingeschlossen bleibt. Elektronenspin-Resonanzspektren eines bestrahlten Glykokoll-Einkristalls zeigen eine deutliche Anisotropie; hieraus wird gefolgert, dass die Radikale im Kristallgitter genau ausgerichtet sind. Die von den Spektren gezeigte Symmetrie ist mit der des Kristallgitters vereinbar. Trotz einer Überlappung der Linien gelang es, die Spektren des $NH_3^+—\dot{C}H—CO_2^-$ Radikals zu deuten unter Benutzung der Elektron-Kern-Koppelungstensoren für die N-, die $H_{(C)}$- und die drei $H_{(N)}$-Kerne. Die letzteren sind dank einer Rotation oder eines Durchschwingens der $—NH_3^+$ Gruppe äquivalent. Diese Tensoren werden in Hinblick auf die

Elektronenstruktur des Radikales qualitativ interpretiert. Die Deutung ist mit einer negativen Spindichte an den $H_{(C)}$-Atomen, sowie mit einer positiven Spindichte an den $H_{(N)}$-Atomen vereinbar, wie sie sich aus theoretischen Behandlungen ergeben. Die Radikale sind in dem Gitter offensichtlich in der gleichen Weise orientiert wie die dazugehörigen Molekeln.

REFERENCES

[1] BLEANEY, B., and STEVENS, K. W. H., 1953, *Rep. Prog. Phys.*, **16,** 108.
[2] BOWERS, K. D., and OWEN, J., 1955, *Rep. Prog. Phys.*, **18,** 304.
[3] UEBERSFELD, J., and ERB, E., 1956, *Compt. Rend.*, **242,** 478.
[4] ABRAHAM, R. J., OVENALL, D. W., and WHIFFEN, D. H., 1958, *Trans. Faraday Soc.*, **54,** 1128.
[5] ALBRECHT, G., and COREY, R. B., 1939, *J. Amer. chem. Soc.*, **61,** 1087.
[6] ATHERTON, N. M., and WHIFFEN, D. H. (to be published).
[7] GROTH, P., 1910, *Chemische Krystallographie* (Leipzig), Vol. III, 98.
[8] GORDY, W., ARD, W. B., and SHIELDS, H., 1955, *Proc. Nat. Acad. Sci.*, **41,** 983.
[9] EHRENBERG, A., EHRENBERG, L., and ZIMMER, K. G., 1957, *Acta Chimica Scand.*, **11,** 199.
[10] GRANT, P. M., WARD, R. B., and WHIFFEN, D. H., 1958, *J. chem. Soc.*, 4635.
[11] TRAMMELL, G. I., ZELDES, H., and LIVINGSTON, R., 1958, *Phys. Rev.*, **110,** 630.
[12] FERMI, E., 1930, *Z. Phys.*, **60,** 320.
[13] MCCONNELL, H. M., and DEARMON, H. H., 1958, *J. chem. Phys.*, **28,** 51.
[14] MCCONNELL, H. M., and CHESNUT, D. B., 1958, *J. chem. Phys.*, **28,** 107.
[15] JARRETT, H. S., 1956, *J. chem. Phys.*, **25,** 1289.
[16] COLE, T., PRITCHARD, H. O., DAVIDSON, N. R., and MCCONNELL, H. M., 1958, *Mol. Phys.*, **1,** 406.
[17] MCLACHLAN, A. D., 1958, *Mol. Phys.*, **1,** 233.
[18] CHESNUT, D. B., 1958, *J. chem. Phys.*, **29**, 43.
[19] COULSON, C. A., 1952, *Valence* (Oxford), 310.
[20] DOUSMANIS, G. C., 1953, *Phys. Rev.*, **97,** 967.

Thallium nuclear resonance spectra, Part II

by R. FREEMAN, R. P. H. GASSER, and R. E. RICHARDS
Physical Chemistry Laboratory, South Parks Road, Oxford

(*Received* 4 *February* 1959)

Chemical shifts are recorded for the thallium resonance of ^{203}Tl and ^{205}Tl in a number of thallium compounds in the solid state and in aqueous solutions. Different chemical shifts are found for Tl^+, $TlCl_4'$ and $TlCl_6'''$. Solid Tl_2Cl_3 shows two thallium resonances with intensities in the ratio 3 : 1, consistent with the formula $Tl_3(TlCl_6)$. Hydrated thallic chloride in the solid state shows three thallium resonances which may be due to the presence of $Tl(H_2O)_x^{+++}$, $TlCl_4'$ and $TlCl_6'''$. The chemical shifts of the thallium resonance in aqueous thallic chloride and bromide solutions in the presence of added halides are consistent with the stepwise formation of complex ions. The second moments of the resonances of the two thallium isotopes in solid compounds shows that there is spin–spin coupling between the thallium isotopes, and a weak coupling in some cases between thallium nuclei and the nuclei of anions.

1. Introduction

Chemical shifts of thallium nuclear resonance spectra have been studied by Gutowsky and McGarvey [1] for aqueous solutions of thallous acetate and nitrate and thallic nitrate. Extensive measurements of chemical shifts of thallous salts in various media have been made by Freeman *et al.* [2] and interpreted in terms of molecular association in solution. Rowland and Bromberg [3] describe chemical shift measurements on some thallous and thallic salts in the liquid state and in the solid at the melting point. Bloembergen and Rowland [4] have studied second moments of thallium resonances in thallium metal and in thallium sesquioxide and interpreted them in terms of spin–spin coupling between thallium isotopes. Saito [5] has described measurements of the line width of nuclear resonances in solid thallous fluoride and thallous bromide.

Further measurements of chemical shifts and of second moments of thallium resonances are described below in an attempt to obtain more information about the ways in which thallium atoms interact with their surroundings. Chemical shifts and second moments of the resonances of both isotopes of thallium have been studied for some solid thallous and thallic compounds, and chemical shifts have been measured for certain solutions of thallic salts.

2. Experimental

The compounds thallous chloride, nitrate, sulphate, carbonate, bromide, iodide and formate were obtained from Messrs. B. D. H. and used without further purification. Thallous fluoride and thallous perchlorate were prepared by the reaction of thallous carbonate with the appropriate acid and recrystallized from water.

Thallium sesquichloride and thallic chloride were prepared by the methods of Cushman [6]. Potassium and ammonium thallichlorides were prepared by Rammelsberg's method [7] and zinc and barium thallichlorides by the method of Gewecke [8]. The solutions of thallic chloride and bromide were prepared by oxidizing a suspension of thallous chloride or thallous bromide in water with chlorine or bromine until all the solid had dissolved. Excess halogen was removed by bubbling nitrogen through the solution.

Thallium sesquichloride was analysed and gave the following results:

	Tl (per cent)	Cl (per cent)
Estimated	$79{\cdot}2_3$	$20{\cdot}4_8$
Calculated for Tl_2Cl_3	$79{\cdot}3_5$	$20{\cdot}6_5$

The measurements were made with a recording nuclear resonance spectrometer [9]. The magnetic field of 4370·9 gauss was provided by an electromagnet of gap 11 in. × 2 in. with a nuclear resonance feed-back loop to regulate the field. An oscillating detector [10] was used to detect the resonances, using magnetic field modulation at 325 c/s and conventional methods of phase-sensitive detection and recording.

Chemical shifts are expressed as

$$\delta = \frac{\nu_{\text{ref}} - \nu_{\text{compound}}}{\nu_{\text{ref}}} \times 10^4$$

so that positive values of δ imply that the sample is *more* shielded than the reference, which is taken for this work to be a 0·3 M aqueous solution of thallous nitrate†.

3. RESULTS

3.1. *Solids*

The line widths vary considerably among the compounds studied, and so the precision with which the chemical shifts can be measured is often low. Nevertheless the chemical shifts are large enough to allow multiple lines to be observed.

Compound	^{205}Tl Second moment	^{203}Tl Second moment	δ ^{205}Tl
Thallous perchlorate	1 gauss^2	1	+3·7
nitrate	2	7	−2·8
chloride	2	4	−6·1
sulphate	3	9	−0·9
formate	6	10	−11·1
carbonate	8	—	−11·2
fluoride	12	—	−7·9
bromide	13	31	−10·8
iodide	18	28	−23·3
$K_3(TlCl_6)$	1	—	−22·3
$(NH_4)_3(TlCl_6)$	2	—	−22·3
$Zn(TlCl_4)_2$	4	—	−29·7

---

† Note that the sign convention used in this paper for chemical shifts is opposite to that used in Part I.

3.1.1. *The chemical shifts*

Figure 1 summarizes the chemical shifts of the ^{205}Tl resonance in some halides and complex halides. Other chemical shifts are given in the table. The spectra of thallium sesquichloride and of hydrated thallic chloride were complex with overlapping lines, and have been separated graphically into their components. This process is illustrated in figures 2 and 3, and the reliability of the result is clearly limited by the overlap of the lines. In thallium sesquichloride the areas of the two components are in the ratio of 3 : 1, while for the hydrated thallic chloride the three lines overlap so much that areas cannot be estimated reliably.

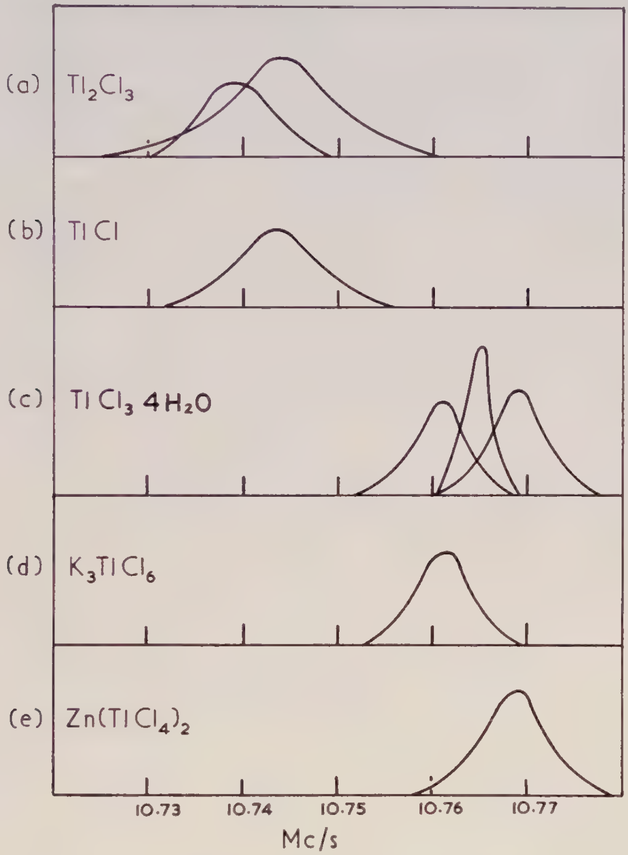

Figure 1. ^{205}Tl resonances in solid compounds of thallium and chlorine. (*a*) Tl_2Cl_3, (*b*) TlCl, (*c*) $TlCl_3 4H_2O$, (*d*) $K_3TlCl_6xH_2O$ and $(NH_4)_3TlCl_6xH_2O$, (*e*) $Zn(TlCl_4)_2xH_2O$.

3.1.2. *The line widths*

The line widths are best expressed in terms of the second moments of the absorption curves. These values are given for both isotopes of thallium in the table; in some cases the ^{203}Tl resonance was too weak to obtain a meaningful value.

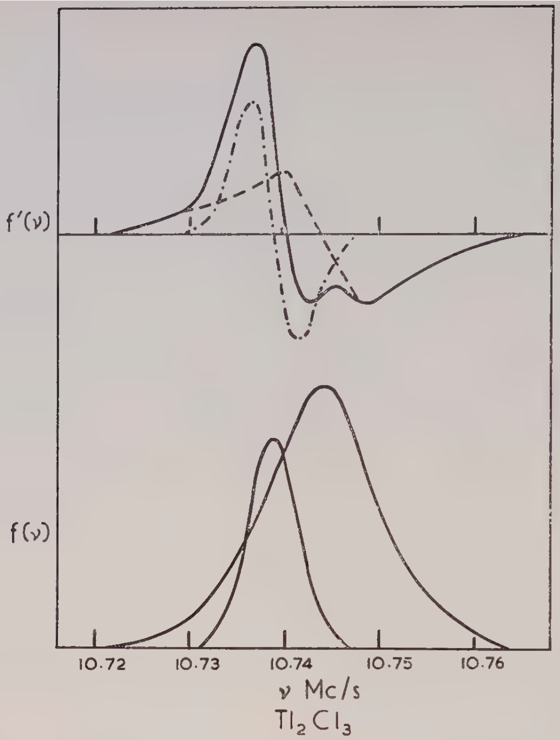

Figure 2. ^{205}Tl resonance in solid Tl_2Cl_3.

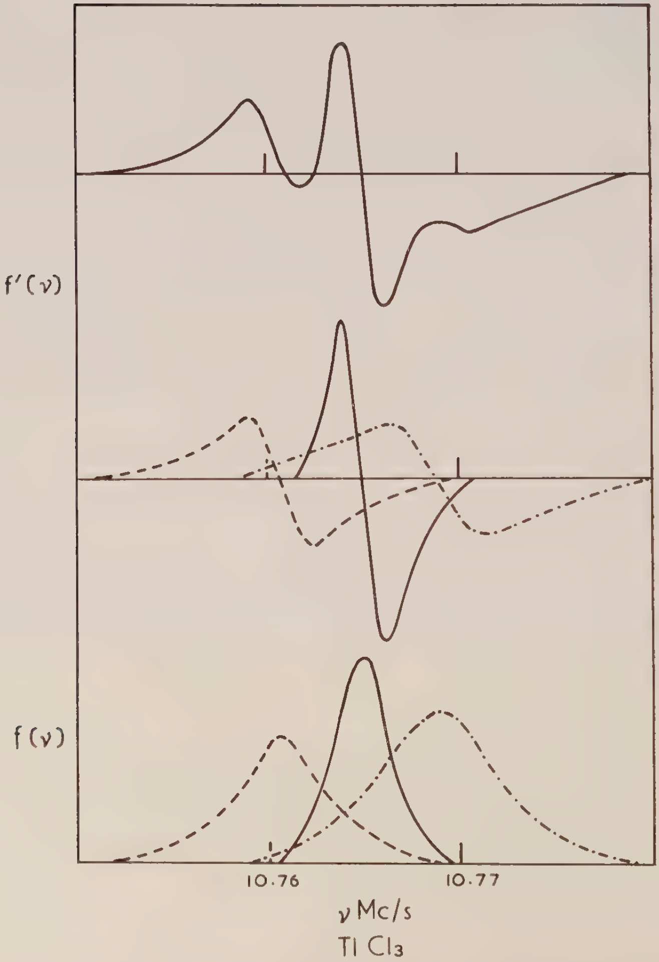

Figure 3. ^{205}Tl resonance in solid $TlCl_34H_2O$.

3.2. *Solutions*

The chemical shifts of the ^{205}Tl resonance of thallic chloride in aqueous solutions of hydrochloric acid and of potassium chloride are shown in figure 4. Chemical shifts for thallic bromide in aqueous solutions of hydrobromic acid are also shown. In each experiment the thallium concentration was maintained at 0·3 molar.

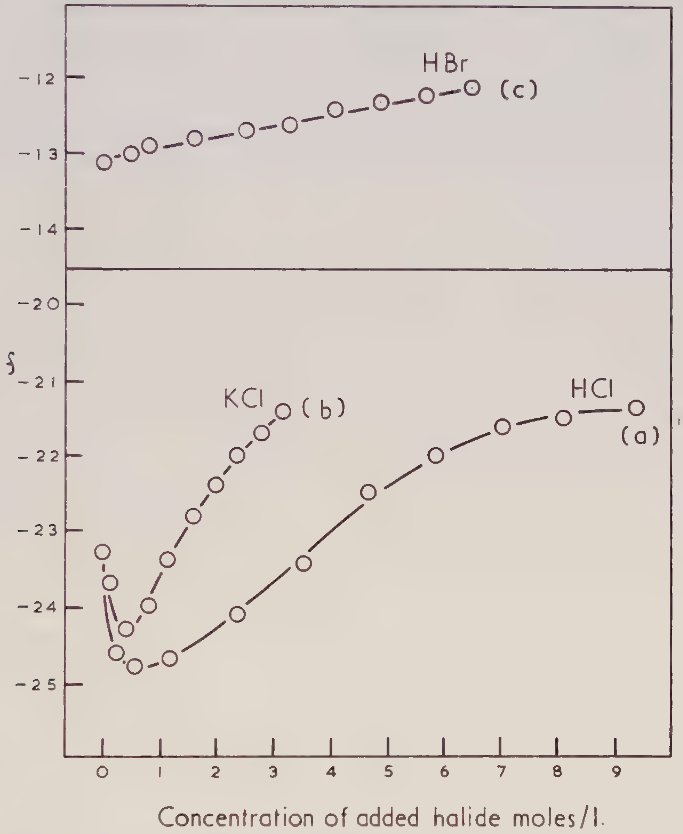

Figure 4. Shifts of ^{205}Tl resonance in solutions of 0·3 M $TlCl_3$ and of 0·3 M $TlBr_3$. (*a*) $TlCl_3$ + added HCl, (*b*) $TlCl_3$ + added KCl, (*c*) $TlBr_3$ + added HBr.

4. DISCUSSION

4.1. *The chemical shifts*

4.1.1. *The chlorides*

In the crystals, the chemical shift of the ^{205}Tl resonance lies at values of δ of about -6, -22 and -30 for Tl^+, $TlCl_6'''$ and $TlCl_4'$ respectively (figure 1 (*b*), (*d*), (*e*)), the thallous ion being more shielded than the thallichloride ion. This order of chemical shifts is in step with the decreasing number of electrons surrounding the thallium nucleus. The hydrated thallous ion, with a shift on this scale of 0, is still more shielded than in solid thallous chloride, presumably by the extra electrons contributed by the hydration atmosphere. The differences in the chemical shifts between thallous chloride and $Zn(TlCl_4)_2\,xH_2O$ is 0·24 per cent and this is in close agreement with that found by Rowland and Bromberg [3] for the shift between Tl^+ and $TlCl_4^-$ in molten Tl_2Cl_4.

Thallium sesquichloride shows two resonances for each thallium isotope, which must be assigned to thallous and thallic atoms. The ratio of the intensities of the two lines is consistent with the formula, $Tl_3^{I}(Tl^{III}Cl_6)$ for the sesquichloride. The chemical shifts of the lines are, however, not the same as those observed for the same ions in different solids (figure 1(b)) and so there must be significant effects from intermolecular interactions in the crystals.

Hydrated thallic chloride shows three resolvable lines in the solid, indicating the presence of three types of thallium atom, which may be $Tl^{III}Cl_4'$, $Tl^{III}(H_2O)_x$ and $Tl^{III}Cl_6'''$. There appears to be no other evidence about the structure of hydrated thallic chloride, although X-ray measurements on anhydrous thallic chloride show it to be a monoclinic crystal with a distorted sodium chloride lattice.

The chemical shifts of aqueous solutions of thallic chloride are summarized in figure 4. The resonance line shifts with the addition of chlorides from values of δ of about -23 for a 0·3 molar thallic chloride solution with no added chloride, to lower fields (at about $\delta = -24$ to -25 with about 0·5 molar added chloride ion) and then to higher fields again as the amount of added chloride is increased still further. Peschanski and Valladas-Dubois [11] have shown conclusively that there is stepwise addition of chlorine atoms to thallic ions in aqueous solutions from $Tl\,aq$ to $TlCl_6'''$. The shape of the chemical shift curve is consistent with this because the resonance line of $TlCl_4'$ lies at low applied fields (figure 1) relative to $TlCl_6'''$; the minimum in the chemical shift curve is presumably due to the increase of the concentration of $TlCl_4'$ as the chloride ions are added, followed by its replacement by $TlCl_6'''$ which has a chemical shift at higher applied fields. This sudden change in the magnetic shielding of the thallium nucleus may be interpreted as the interaction of two shielding factors which come into effect as ligands are added around the central ion. The increase in the number of ligands and their associated negative charges produces an increase in the shielding but this is opposed by a decrease in shielding arising from an induced temperature independent paramagnetism. From the work of Peschanski and Valladas-Dubois [11] it may be seen that at the lowest concentration studied in this work the thallium is present predominantly as $TlCl_2^+$ and $TlCl_3$. When the ratio of chloride ion to thallic ion is about 5, which is the case near the minima of the curves of the chemical shifts, the predominant species are $TlCl_3$ and $TlCl_4'$. For a concentration of hydrochloric acid of 1·5 M, the resonance fields are increasing quite rapidly with increasing chloride concentration; the ratio of chloride ion to thallic ion is now 8 and in the solution the thallium atoms are present mainly as $TlCl_4'$ and $TlCl_5''$ with some $TlCl_6'''$ and $TlCl_3$. This suggests that the magnetic shielding in $TlCl_4'$ is smaller than for any of the other thallium chlorine complexes. The difference in the effects of added hydrochloric acid and of potassium chloride suggests that the cation also has some effect on the chemical shifts, as the activity coefficients of the chloride ion in the two solutions would be expected to produce the reverse effect from that observed.

The dissociation constants obtained by Peschanski and Valladas-Dubois [12] for the thallic bromide complexes are all larger than the corresponding ones for thallic chloride, and the equilibrium moves even more rapidly towards the formation of $TlBr_6'''$ than it did towards $TlCl_6'''$. The addition of about 0·4 M hydrobromic acid causes most of the thallium to change to $TlBr_4'$ and with further addition of bromide ions this is quickly replaced by the higher complex bromides. The change of δ for the bromides is much smaller than for the chlorides and this may explain why no minimum has been observed due to $TlBr_4'$.

The intermediate bromide Tl_2Br_4 was prepared, but its thallium resonance in the solid was very broad and no fine structure could be detected.

4.2. *Line widths*

In solution, the dipolar broadening of the thallium resonance is virtually removed by the rapid molecular motion. Furthermore, any spin–spin coupling between the thallium nucleus and a halogen atom is likely to be removed because of the strong electric quadrupole moments of the halogen nuclei. The homogeneity over the sample of the electromagnet used for this work was not better than 0·4 gauss, and so the line widths of the solution measurements were all determined by the magnet used.

The dipolar broadening of the thallium resonance in the solids is usually small; in the halides the second moment due to dipole–dipole interaction should be less than 1 gauss^2. For thallous fluoride, the second moment expected for dipolar broadening is greater because of the strong magnetic moment of the fluorine atom and would be about 2·5 gauss^2 [5]. The observed second moments (see table) are however very much larger than this in most cases and must arise from some other mechanism. Since for thallium, $I = \frac{1}{2}$, for metallic thallium and for thallium sesquioxide this mechanism can only be the one found by Bloembergen and Rowland [4]. In these substances the second moment of the thallium resonance is much greater than expected for dipolar broadening alone, and this is attributed to spin–spin coupling between unlike thallium isotopes. In the compounds described in the table there is the possibility of spin–spin coupling between the unlike thallium isotopes, and also between each thallium isotope and the nuclei of the anion.

If the broadening arises primarily from coupling between the thallium atom and the anion, then the second moments of the resonances from both isotopes of the thallium should be the same. This is not the case, except for thallous perchlorate, where the second moment is only slightly greater than expected for dipolar broadening alone, and in which spin–spin coupling must therefore be nearly absent. The second moments of the resonances for ^{203}Tl and ^{205}Tl are usually very different, and so the spin–spin coupling must be largely between the different thallium isotopic nuclei.

If the broadening arises *only* from spin–spin coupling between unlike thallium isotopes, then the ratio of the second moments of the ^{205}Tl and ^{203}Tl resonances would be a constant depending only on the relative abundances of the two isotopes. On the other hand, if some coupling also occurs between thallium nuclei and anions, then this ratio would become more nearly unity. In the case of the nitrate and sulphate, the ratio of the second moments of the resonances of the two isotopes is about 3, but this ratio becomes smaller with the bromide, chloride, iodide and formate. In these latter compounds there must be an increasing contribution of spin–spin coupling between thallium nuclei and anions, and this implies increasing electronic interaction between cations and anions.

This conclusion is in accord with the results obtained for solid thallous bromide by Saito [5], whose results also suggest that in thallous bromide there is some spin–spin coupling between the thallium isotopes. The values of second moments recorded by Saito are not in close agreement with those reported in this work, but the difference does not affect these conclusions. The signal to noise ratio obtained by Saito was about 3; in this work the signal to noise ratio in a typical case was about 12.

We are grateful to the Department of Scientific and Industrial Research for a Maintenance Grant to R.F. and to R.P.H.G. We also thank the Hydrocarbon Research Group of the Institute of Petroleum and the Coal Board for Grants in aid of apparatus.

On donne les déplacements chimiques dans la résonance thallique de ^{203}Tl et ^{205}Tl, pour un certain nombre de composés du thallium à l'état solide et en solution aqueuse. On trouve des déplacements chimiques différents pour Tl^+, $TlCl_4'$, et $TlCl_6'''$. Tl_2Cl_3, à l'état solide, donne deux résonances thalliques dont les intensités sont dans le rapport 3 : 1, ce qui est conséquent avec la formule $Tl_3(TlCl_6)$. Le chlorure thallique hydraté donne à l'état solide trois résonances thalliques qui sont peut-être dues à la présence de $Tl(H_2O)_x^{+++}$, $TlCl_4'$, et $TlCl_6'''$. Les déplacements chimiques de la résonance thallique pour des solutions de chlorure et bromure thalliques sont en accord avec la formation d'ions complexes par étapes. Les seconds moments trouvés dans la résonance des deux isotopes du thallium pour des composés solides montrent qu'il y a couplage spin–spin entre les isotopes, et parfois un faible couplage entre les noyaux de thallium et les noyaux des anions.

In einer Reihe von Thalliumverbindungen im festen Zustand, sowie in wässriger Lösung wurden für die Thallium-Resonanz von ^{203}Tl und ^{205}Tl die chemischen Verschiebungen bestimmt. Für Tl^+, $TlCl_4'$ und $TlCl_6'''$ wurden unterschiedliche Verschiebungen gefunden. Festes Tl_2Cl_3 zeigt zwei Thalliumresonanzen mit Intensitäten im Verhältnis 3 : 1 in Übereinstimmung mit der Formel $Tl_3(TlCl_6)$. Wasserhaltiges Thallichlorid zeigt im festen Zustand drei Thalliumresonanzen, die auf die Anwesenheit von $Tl(H_2O)_x^{+++}$, $TlCl_4'$, sowie $TlCl_6'''$ zurückzuführen sein dürften. Die chemische Verschiebung der Thalliumresonanz in wässrigem Thallichlorid- sowie -bromidlösungen bei Anwesenheit zugefügter Halogenide sind mit einer schrittweisen Bildung komplexer Ionen vereinbar. Die zweiten Momente der Resonanz beider Thalliumisotope in festen Verbindungen zeigen, dass zwischen den Thalliumisotopen eine Spin–Spin-Kopplung auftritt, sowie zuweilen eine schwache Kopplung zwischen den Kernen des Thalliums und denen der Anionen.

REFERENCES

[1] GUTOWSKY, H. S., and MCGARVEY, B. R., 1953, *Phys. Rev.*, **91**, 81.
[2] FREEMAN, R., GASSER, R. P. H., RICHARDS, R. E., and WHEELER, D. H., 1959, *Mol. Phys.*, **2**, 75.
[3] ROWLAND, T. J., and BROMBERG, J. P., 1958, *J. chem. Physics*, **29**, 626.
[4] BLOEMBERGEN, N., and ROWLAND, T. J., 1955, *Phys. Rev.*, **97**, 1679.
[5] SAITO, Y., 1958, *J. phys. Soc. Japan*, **13**, 72.
[6] CUSHMAN, A. S., 1900, *Amer. chem. J.*, **24**, 222.
[7] RAMMELSBERG, C. F., 1870, *Ber.*, **3**, 360.
[8] GEWECKE, J., 1909, *Liebigs. Ann.*, **366**, 217.
[9] FREEMAN, R., MURRAY, G. R., and RICHARDS, R. E., 1957, *Proc. roy. Soc.* A, **242**, 455.
[10] POUND, R. V., 1952, *Progr. nucl. Phys.*, **2**, 21.
[11] PESCHANSKI, D., and VALLADAS-DUBOIS, S., 1956, *Bull. Soc. chim. France*, 1170.
[12] PESCHANSKI, D., and VALLADAS-DUBOIS, S., 1955, *Compt. rend.*, **241**, 1046.

Electron transfer spectra of hexahalide complexes

by CHR. KLIXBÜLL JØRGENSEN

Chemistry Department A, Technical University of Denmark, Copenhagen

(*Received* 30 *December* 1958)

The electron transfer spectra of the chloro, bromo, and iodo complexes of Ru(III), Ru(IV), Rh(III), Pd(IV), Sn(IV), Sb(V), W(VI), Re(IV), Os(III), Os(IV), Ir(III), Ir(IV), Pt(IV), and Pb(IV) are studied and interpreted by group-theoretical methods as transitions of π (and at higher wave-numbers, σ) electrons, mainly localized in the ligands, to the available orbitals of even parity γ_5, γ_3 and γ_1, representing mainly d, d, and s electrons of the central ion. The half-widths and intensities of the bands support the identification. The remarkable similarity between the spectra of d^4 and d^5 systems with the same set of ligands is explained by the presence of only one effective excited state of the central ion. The structure expected of the group of π transfer bands as function of increasing Landé parameter ζ_{np} of the halogen is calculated. The use of pure molecular orbital (M.O.) configurations as a convenient classification (but not a very good approximation to the wave-function) is compared to the analogous case of atomic spectroscopy. It is recommended to estimate the M.O. energies from absorption spectra rather than to try to calculate them from unreliable approximations.

The ligand field theory has interpreted the weak (Laporte-forbidden) absorption bands of transition group complexes, caused by internal transitions in the partly filled shell, which approximately is composed of d electrons [1–4]. Especially, in octahedral complexes, the energy levels can be described by the energy difference Δ (also called $10\,Dq$ or $(E_1 - E_2)$) between the two equivalent γ_3 and three equivalent γ_5 orbitals. Δ is found by comparison with an Orgel diagram [5] with Δ as variable, or with a Tanabe–Sugano diagram [1] as function of Δ divided by an expression for the interelectronic repulsion parameters. The variation of Δ with central ion and with the ligands is the spectrochemical series, while the variation of $(1 - \beta)$ with central ion and ligands (the ions or molecules directly attached to the central ion) is the nephelauxetic series [6, 7]. β is the ratio between the values of the interelectronic repulsion parameters in the complex and the values in the corresponding gaseous ion.

It might now be hoped that the strong electron transfer bands can be explained by a similar theory. We shall here discuss the bands connected with a single central ion only; in many solid compounds and in solutions of polynuclear complexes with mixed oxidation states, there occur strong colours caused by the cooperative effects of more metal ions (cf. the Pt–Pt interactions [8]). However, the octahedral hexahalide complexes exhibit strong bands, which obey Beer's law on dilution in solvents, which do not dissociate the complexes measurably. The wave-numbers of these bands behave qualitatively as expected for an electron transfer from the halide to the central ion: they decrease with increasing oxidizing character of the central ion and with reducing character of the halide ion. (Reviews have been given by Rabinowitch [50], Mulliken and Rieke [51] and Orgel [52], but they have mainly treated molecules not containing transition group elements.)

For a closer study, we must use group theory, expressing the conditions for energy levels to be invariant to operations such as rotations of the coordinate system in a way which does not change the physical situation. Atomic spectroscopy [9] describes the energy levels of gaseous atoms and ions where one has spherical symmetry, so that any direction of the coordinate axes corresponds to the same physical situation. The presence of more than one nucleus in molecules degrades the symmetry from spherical to a lower one. A relatively very high symmetry, which retains several of the properties of the spherical, is the cubic–octahedral symmetry O_h, represented by a regular octahedral complex ML_6. Bethe [10] described the group-theoretical quantum numbers Γ_n in this and many other, lower symmetries. The analogy with the concepts of atomic spectroscopy can be seen from the following table:

	Spherical symmetry	O_h symmetry
Spin quantum number of a system:	S	S
Orbital angular momentum quantum number of a system:	$L=0, 1, 2, 3, 4, \ldots$ (called S, P, D, F, G, . . .)	$\Gamma_n=\Gamma_1, \Gamma_2, \Gamma_3, \Gamma_4, \Gamma_5$ (called A_1, A_2, E, T_1, T_2 by Mulliken)
Total (spin + orbital) angular momentum quantum number of a system:		
Odd number of electrons:	$J=1/2, 3/2, 5/2, \ldots$	$\Gamma_J=\Gamma_6, \Gamma_7, \Gamma_8$ (called E′, E″, U′ by Griffith [25])
Even number of electrons:	$J=0, 1, 2, \ldots$	$\Gamma_J=\Gamma_1, \Gamma_2, \ldots, \Gamma_5$
Orbital angular momentum quantum number of an electron:	$l=0, 1, 2, 3, \ldots$	$\gamma_1, \gamma_2, \gamma_3, \gamma_4, \gamma_5$
Spin + orbital angular momentum quantum number of an electron:	$j=l\pm\frac{1}{2}$	$\gamma_6, \gamma_7, \gamma_8$

The quantum numbers L, J, Γ_n, Γ_J, and γ_n are either combined with odd or even parity. It must be realized that only the capital letters indicate strict quantum numbers of the system; the electron configurations with an integral number of electrons in each shell (characterized by a file number n, and l or γ_n in the two symmetries) may or may not be a good approximation; but they have no group-theoretical approbation. The Russell–Saunders approximation assumes that not only J (or Γ_J), but also L (or Γ_n) and S are good quantum numbers. The multiplet terms (L, S) or (Γ_n, S) can then be assembled to empirical configurations, where the energy differences can be expressed by interelectronic repulsion parameters and the splitting of multiplet terms by Landé parameters such as ζ_{nl}. This concept of empirical electron configuration does not imply that the wave-function to a very high accuracy can be described as an antisymmetrized Slater determinant [9]. Rather, it is convenient for enumerating the number of energy levels.

Group theory must to some extent be applied *cum grano salis*. On the one hand, gaseous ions are not surrounded by perfect spherical symmetry for a very long distance in a terrestrial experiment, and octahedral complexes are surrounded by other atoms in crystals and solutions, producing a much lower macro-symmetry. However, experience shows that at least the bands described by ligand field theory are very insensitive towards influences outside the ligands in the first coordination sphere, and we may therefore try to use the higher micro-symmetry for our arguments. On the other hand, group theory does only indicate which matrix elements shall be zero and rarely the possible size of a given matrix element, which may deviate from zero. Thus, the absence of a centre of inversion in complexes such as MA_5B and the creation of levels of opposite parity in dinuclear complexes A_5MBMA_5 with a centre of inversion should both destroy Laporte's rule, according to which transitions between levels with the same parity are forbidden as electric dipole radiation. Nevertheless, these deviations do not generally produce higher intensities among the ligand field bands than found in MA_6.

Bethe [10] indicated the values of γ_n, corresponding to the values of l for spherical symmetry. Thus, *s* electrons have even γ_1, *p* electrons odd γ_4, *d* electrons even γ_3 and even γ_5, etc. The molecular orbital (M.O.) theory describes covalent bonding as an intermixing of orbitals from the central ion and the ligands, having the same γ_n and parity. While M in an octahedral complex ML_6 is surrounded by a ligand field of symmetry O_h, the ligand field acting on L has the symmetry C_{4v}, which can be approximated rather well as linear symmetry [11] without a centre of inversion, i.e. $C_{\infty v}$. In the latter symmetry, L is substituted by $\Lambda = 0, 1, 2, \ldots$ (called $\Sigma, \Pi, \Delta, \ldots$), J by Ω, l by λ ($= 0, 1, 2, \ldots$ and at most l in the corresponding spherical case) and j is substituted by $\omega = \lambda \pm \frac{1}{2}$. Thus, a p shell of, e.g. a halide ion is divided in the Russell–Saunders case into two σ electrons with $\lambda = 0$ and four π electrons with $\lambda = 1$. Due to the absence of a centre of inversion of the ligand field, p electrons with σ character can be mixed with s and d electrons of the halide and π electrons with d electrons, etc. On the other hand, δ electrons cannot be produced with lower values of l than 2. Van Vleck [12], Kimball [13] and Flodmark [14] calculated the γ_n values in O_h of respectively 12σ, 24π, and 24δ electrons from the six ligands:

σ even γ_1 and γ_3, odd γ_4,
π even γ_4 and γ_5, odd γ_4 and γ_5,
δ even γ_2, γ_3, and γ_5, odd γ_2, γ_3, and γ_5.

Owen [15] indicated the expected interaction between the corresponding linear combinations of the ligands' σ electrons with s, d and p electrons from the central ion, and the π electrons with d (even γ_5) and p (odd γ_4), respectively.

If we can use M.O. configurations as a classification, we may expect four types of electron transfer bands to occur in transition group hexahalide complexes: $\pi \rightarrow \gamma_5$, $\pi \rightarrow \gamma_3$, $\sigma \rightarrow \gamma_5$ and $\sigma \rightarrow \gamma_3$. We know the energy difference Δ between γ_5 and γ_3 electrons in the partly filled shell from the ligand field spectra [2, 3, 15] to be 20–30 kK (1 kilokayser = 1000 cm^{-1}) in hexachloro and hexabromo complexes of $4d^n$ and $5d^n$ ions. We may guess that the energy difference between π and σ electrons has the same order of magnitude.

Actually, figures 1–5 demonstrate that d^4 and d^5 systems with the same six halide ligands have the same number and distribution of electron transfer bands with a shift on the wave-number scale (6–9 kK between corresponding $4d^n$ and $5d^n$ in the same oxidation state and 15 kK between isoelectronic trivalent and tetravalent central ions). Similar regularities are found among the d^6 systems with the same six halides. The wave-number as a function of the number of electrons in the partly filled shell is more difficult to compare, but a general trend in a series with the same oxidation state is $d^3 > d^4 > d^5 \ll d^6$. This can be rationalized if it is assumed that the electron transfer bands with lowest wave-number in each complex are caused by the transfer of the same electrons from the halides (and evidence will be presented that these electrons are mainly π rather than σ) to the partly filled γ_5 subshell in d^3, d^4, d^5 and to the empty γ_3 subshell in d^6 systems.

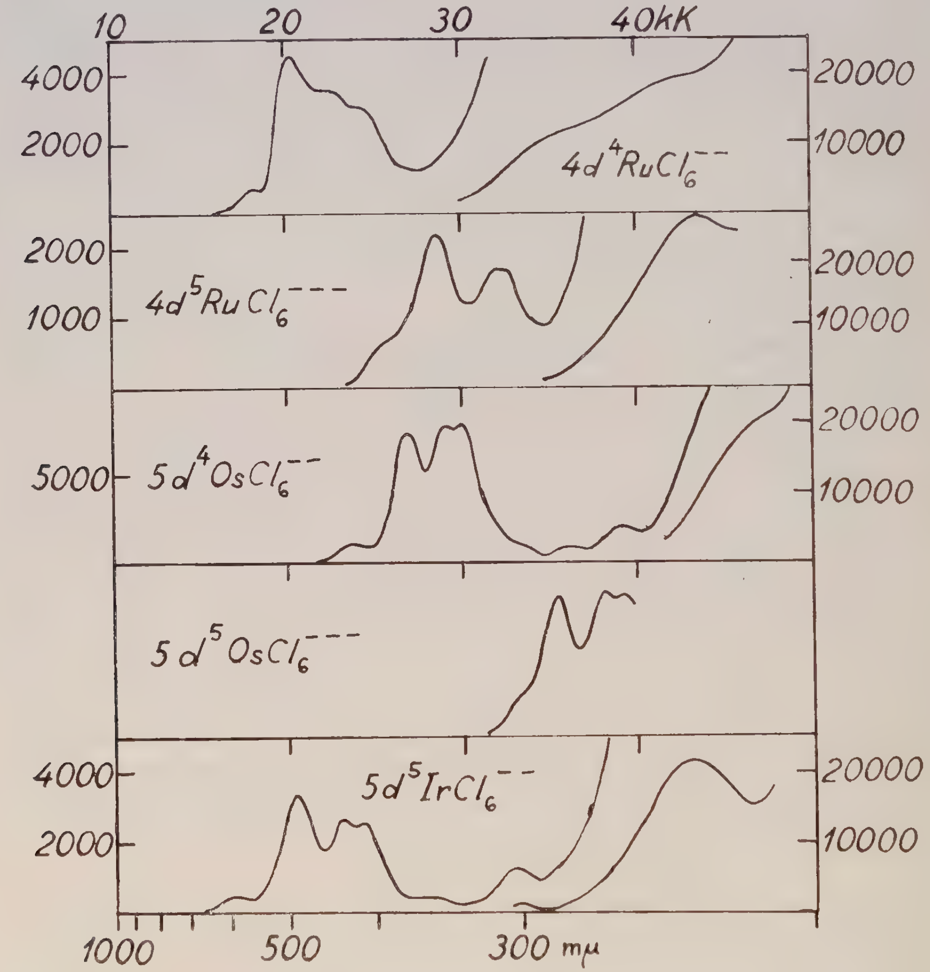

Figure 1. Absorption spectra of d^4 and d^5 hexachloro complexes.

If we assume that the orbital energy of the γ_5 electrons varies linearly with their number q, we can write it $W - qE$, while the orbital energy of γ_3 electrons then is $W-qE+\Delta$. The interelectronic repulsion energy gives a contribution approximately

$$q(q-1)A/2-DS(S+1), \tag{1}$$

where D represents the spin-pairing energy [3]. If the energy of the π electrons is assumed to be constant (or its variation being linear in q and thus it can be incorporated in E), the variation of the wave-number with q in a series of $4d^q$ or $5d^q$ complexes with the same ligands will be:

$$\left.\begin{array}{llll} d^0 & V-3/4D & d^5 & V+3/4D+5A-5E \\ d^1 & V-5/4D+\ \ A-\ \ E & d^6 & V-3/4D+6A-6E+\Delta \\ d^2 & V-7/4D+2A-2E & d^7 & V-5/4D+7A-7E+\Delta \\ d^3 & V+7/4D+3A-3E & d^8 & V+5/4D+8A-8E+\Delta \\ d^4 & V+5/4D+4A-4E & d^9 & V+3/4D+9A-9E+\Delta \end{array}\right\} \tag{2}$$

assuming pure low-spin subshell configurations in O_h. The trend in the series $ReCl_6^{--}$, $OsCl_6^{--}$, $IrCl_6^{--}$, $PtCl_6^{--}$ can be accounted for by the set of parameters $D=3$ kK and $(E-A)=6$ kK, while Δ is known from the ligand field bands to be some 29 kK.

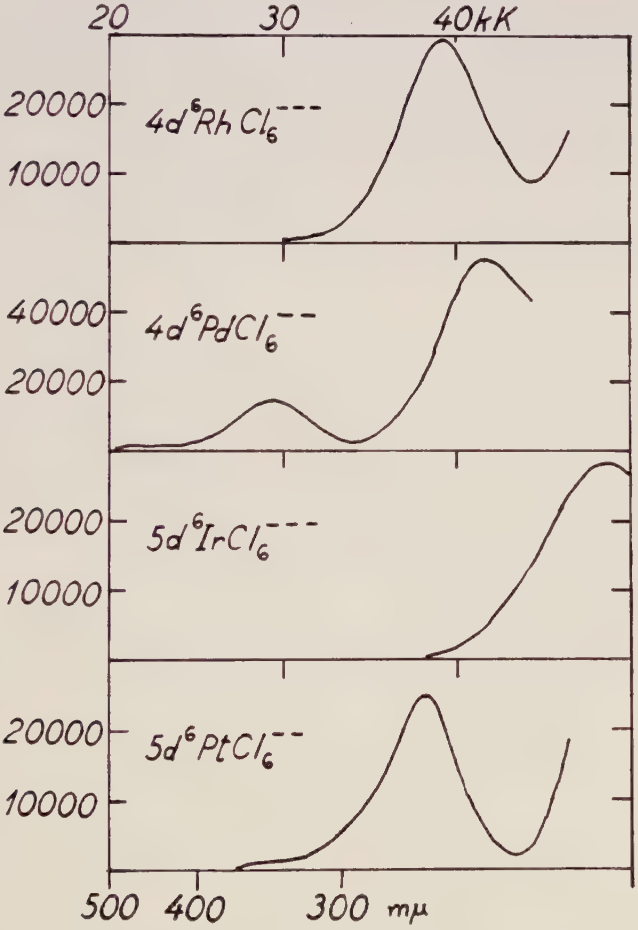

Figure 2. Absorption spectra of d^6 hexachloro complexes.

The approximation (1) (with the somewhat dubious assumption that A does not vary with q) gives for the ionization $d^q \to d^{q-1}$ of gaseous ions with high-spin behaviour (the maximum value of S in the ground state) if the orbital energy is approximated by a linear function $-I - Z_0 Q - qE$ of the ionic charge $Z_0 - 1$ and of q, that the ionization energy is:

$$\left.\begin{array}{ll} q<5 & I+(Z_0-q+1)Q+(2q-1)E-(q-1)A+(2q+1)D/4 \\ q>5 & I+(Z_0-q+1)Q+(2q-1)E-(q-1)A+(2q-23)D/4 \end{array}\right\} \quad (3)$$

representing two straight lines with the same slope in a graph versus q, but with the hump $6D$ at the half-filled shell d^5. It has previously been shown [16] that the ionization potential $M^{+2} \to M^{+3}$ among the gaseous $3d^n$ ions has the slope 2·2 ev and a d^5 hump 4·8 ev, corresponding to $D = 6{\cdot}4$ kK. The standard oxidation potentials for the M(II) : M(III) hexaaquo ions of the first transition group, when corrected for ligand field stabilizations [16], has the slope 1·5 v and the d^5 hump is 4 v ($D = 5{\cdot}3$ kK). (Contrary to the case of equation (3) the Franck–Condon principle is assumed to prevent the orbital energy from dropping from $W - qE$ to $W - (q+1)E$ in equation (2).)

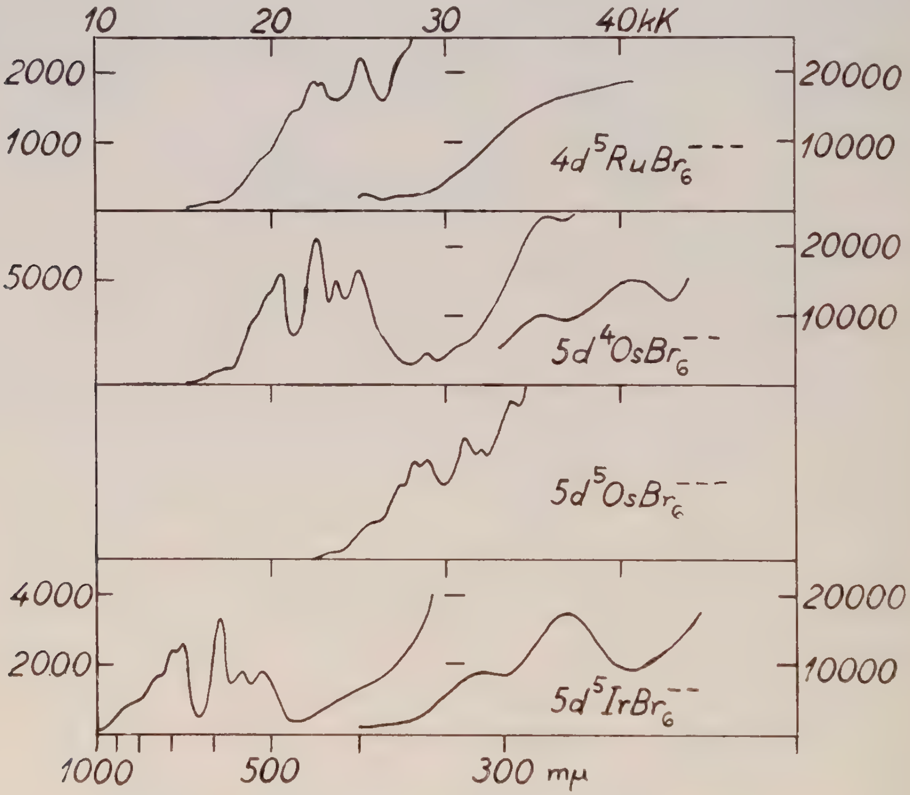

Figure 3. Absorption spectra of d^4 and d^5 hexabromo complexes.

Orgel [17] applied the Franck–Condon principle to ligand field transitions, where the band-width is proportional to the slope of the potential curve of the excited state as function of internuclear distances at the equilibrium point of the ground state. We expect the half-widths of electron transfer bands to be a measure of the antibonding character of the excited state. It is surprising that the half-widths $\delta(-)$ of the narrow bands of d^4 and d^5 chloro complexes between 1 and 1·5 kK have the same magnitude as the ligand field bands [15] and are much smaller, 0·5–0·8 kK in bromo and 0·3–0·5 kK in iodo complexes, approaching the values for bands caused by transitions within the same subshell configuration. We could hardly assume that $\sigma \rightarrow \gamma_5$ transitions would not produce increased internuclear equilibrium distances, while $\pi \rightarrow \gamma_5$ does not necessarily change the electron density in the complex very much. The development as function of the halogen mass m might be interpreted as the decreasing amplitude

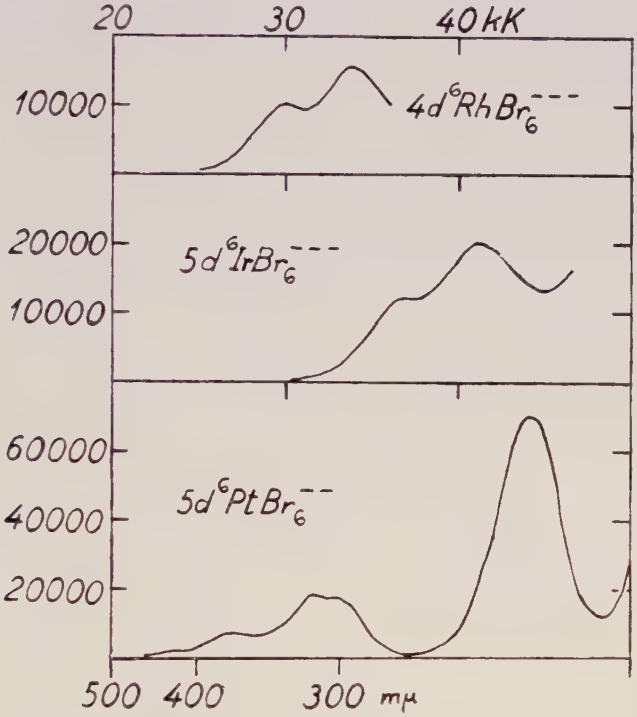

Figure 4. Absorption spectra of d^6 hexabromo complexes.

(proportional to $m^{-1/4}$) of the vibrational ground state [18]. However, this argument is only valid in the not too probable case that $\frac{1}{2}h\nu_0$ is large compared to kT at room temperature [19]. Rather, the smaller δ of iodo than of chloro complexes is caused by an intrinsic change of the π electron and γ_5 delocalization.

The much larger half-widths (2–3 kK) of the first band of d^6 systems can be explained by a $\pi \rightarrow \gamma_3$ transition, since we may assume the half-width to be the sum of the half-widths of $\gamma_5 \rightarrow \gamma_3$ ligand field and $\pi \rightarrow \gamma_5$ electron transfer transitions. There is one important difference between the $\pi \rightarrow \gamma_5$ and the $\pi \rightarrow \gamma_3$ bands: the molar extinction coefficients ϵ of the maxima are 3–6 times and the oscillator strengths P 5–20 times larger of the latter, compared to the former bands. The d^4 and d^5 systems exhibit similar, large, broad bands at high wave-numbers which might be $\sigma \rightarrow \gamma_5$ or $\pi \rightarrow \gamma_3$ transitions. The latter possibility is the most probable, when the regular decrease of the wave-numbers in the pairs $RuCl_6^{-3}$ (43·6 kK), $RhCl_6^{-3}$ (39·2), or $OsCl_6^{--}$ ($\sim$48), $IrCl_6^{--}$ (43·1), $PtCl_6^{--}$ (38·2), or OsI_6^{--} (26·8, 30·5, 37), PtI_6^{--} (20·2, 22·7, 29·1) is considered. The energy of the σ orbitals is a rather intricate problem, they might be nearly degenerate with the π orbitals or have much lower energy. The very large oscillator strength $P \sim 1{\cdot}5$ of the last band of $PdCl_6^{--}$, OsI_6^{--}, $PtBr_6^{--}$ and PtI_6^{-} suggest a $\sigma \rightarrow \gamma_3$ transition (which could hardly produce all the high d^6 bands, and therefore, the bands with $P \sim 0{\cdot}3$ at lower wave-numbers are mainly caused by $\pi \rightarrow \gamma_3$). While the groups of $\pi \rightarrow \gamma_5$ bands of d^4 and d^5 systems have only a total spreading of some 7 kK, the distances 12–20 kK among the high d^6 bands represent probably the energy differences between π and σ. Similar estimates can be arrived at for Cu(II) chloro and bromo complexes which have much higher, broader bands at 12 kK higher wave-number than the narrow, first band (which is double in the bromo complex [20]). $PbCl_6^{--}$ has transitions, probably to the empty 6*s* shell, at 32·6 and 48·1 kK with $\epsilon = 9700$ and 24000 [21]. The values of Δ, derived from the wave-number differences between the $\pi \rightarrow \gamma_3$ and $\pi \rightarrow \gamma_5$ transitions are smaller (by an amount 12 kK in d^3, 9 kK in d^4, and 6 kK in d^5) than those estimated directly from $\gamma_5 \rightarrow \gamma_3$ ligand field transitions. Surprisingly enough, this can be explained by the different maximum value of S in γ_5^{n+1} and $\gamma_5^{n}\gamma_3$, producing a relative stabilization of the latter configuration by $4D$, $3D$, and $2D$, according to equation (2).

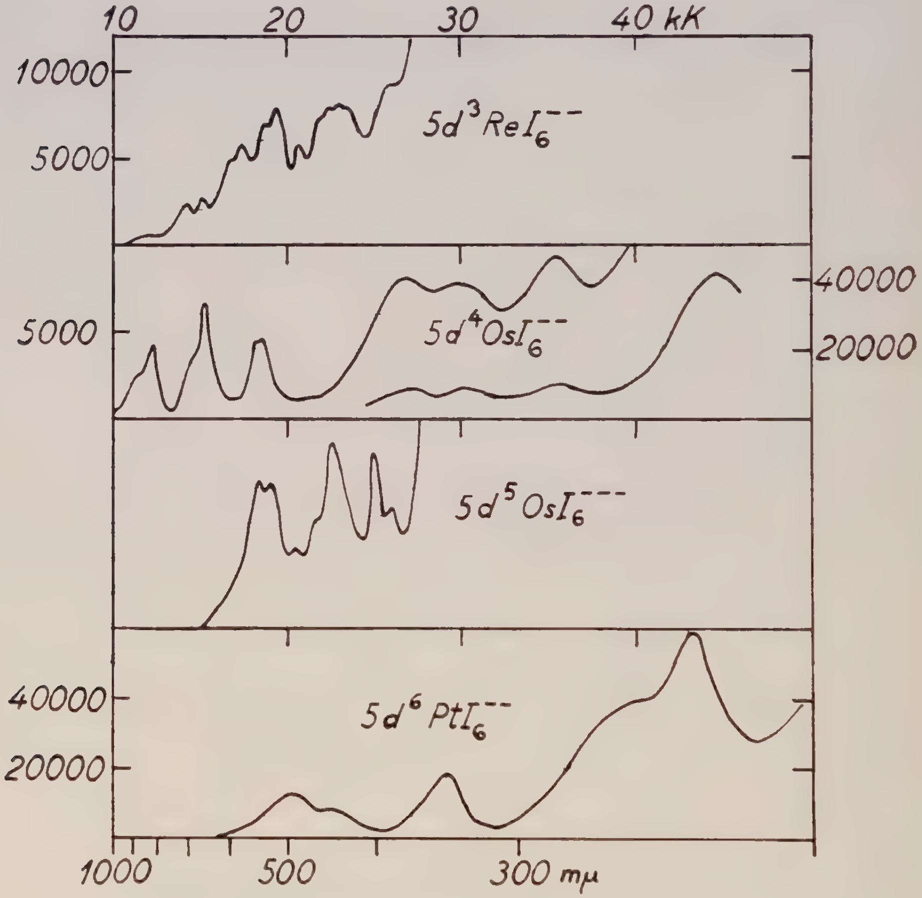

Figure 5. Absorption spectra of hexaiodo complexes.

We may wonder why $\sigma \rightarrow \gamma_5$ transitions are not observed at slightly smaller wave-numbers than $\pi \rightarrow \gamma_3$ in the d^4 and d^5 systems. One possible explanation may be relatively small oscillator strengths P of the former transitions. To a first, rough approximation, P may be related to the one-electron transition dipole moments $\langle e\bar{\mathbf{r}} \rangle$, since P is $(\sigma/R)\langle e\bar{\mathbf{r}} \rangle^2$, σ being the wave-number and R the Rydberg constant 109·7 kK, and the quantities in the average dipole moment measured in atomic units. Figure 6 shows that the one-electron values of $\langle e\bar{\mathbf{r}} \rangle$ are expected to be very small for $\pi \rightarrow \gamma_3$ and $\sigma \rightarrow \gamma_5$, considerably greater for $\pi \rightarrow \gamma_5$ and very large for the strongly overlapping orbitals in $\sigma \rightarrow \gamma_3$. With reasonable values of the overlap integrals, we would expect $P = 0{\cdot}1$ and 1 for the two latter types of transitions. This agrees with the observed values, while the intensities of the $\pi \rightarrow \gamma_3$ bands cannot be explained by one-electron transfer from an orbital with pure $\lambda = 1$.

The energy differences between $\pi \rightarrow \gamma_5$ and $\pi \rightarrow \gamma_3$ are some 5 to 12 kK smaller than Δ of the central ion, found from $\gamma_5 \rightarrow \gamma_3$ ligand field bands. This was interpreted above as the effect of decreased interelectronic repulsion in the central ion for increased spin values. However, the attraction between the hole and the electron in a configuration as $\sigma^{-1}\gamma_3$ will be larger, due to small separation in space, than in $\sigma^{-1}\gamma_5$. Therefore, larger distances are expected between $\pi \rightarrow \gamma_5$ and $\sigma \rightarrow \gamma_5$ than between $\pi \rightarrow \gamma_3$ and $\sigma \rightarrow \gamma_3$. This effect may very well increase the former distance to 30 kK, making the $\sigma \rightarrow \gamma_5$ bands practically unobservable.

The structure of the $\pi \rightarrow \gamma_5$ band groups is very interesting. As previously discussed [20], the behaviour of low-spin d^5 systems is particularly illuminating,

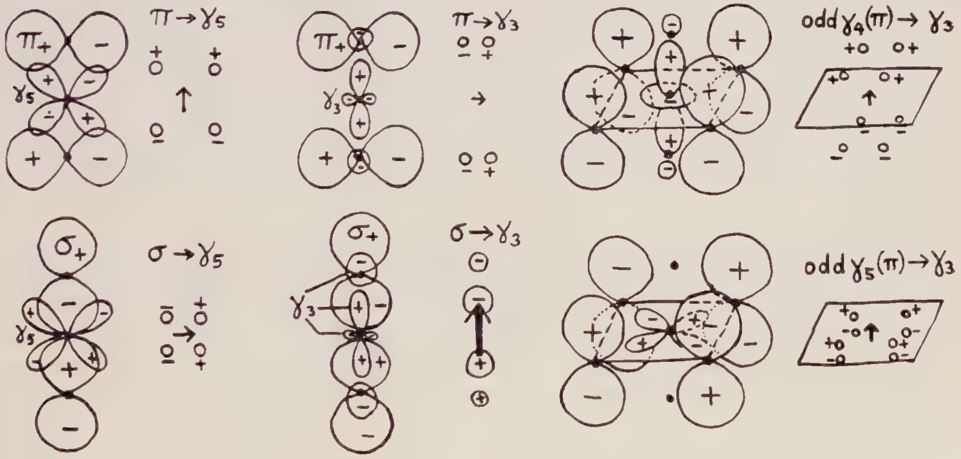

Figure 6. Dipole moments of six possible one-electron transfer transitions in octahedral complexes. The signs + and − indicate the signs of the wave-functions. Linear combinations of odd parity are chosen for the σ and π orbitals. The anti-bonding γ_3 orbital has a supplementary maximum in the ligands which does not occur for pure d electrons [18]. Actually, the left-hand side of the figure applies to a complex of the same symmetry as *trans*-$\mathrm{M(NH_3)_4Cl_2}$, but the right-hand side demonstrates that no important differences occur in regularly octahedral complexes. The transitions shown go to the $z^2 - \frac{1}{2}(x^2 + y^2)$ from the odd γ_4 shown and to the $x^2 - y^2$ component of γ_3 from the odd γ_5. It can be proved from group theory (the values of γ_n in tetragonal symmetry) that the opposite choice would give no resulting dipole moment. The strong $\pi \rightarrow \gamma_3$ bands observed in hexahalides are probably caused by intermixing of σ and π properties among the odd γ_4 orbitals.

because only one state of the central ion + one electron has low energy, the filled subshell γ_5^6 known from the diamagnetic d^6 complexes. Thus, the ligand orbitals γ_k are expected to form a set of excited configurations $\gamma_5^6\gamma_k^{-1}$, each consisting of only one doublet term $^2\Gamma_k$. The observed transitions from the ground state $^2\Gamma_5$ of γ_5^5 to these doublets would give an image of all the γ_k orbital energies. No transitions would be spin-forbidden, and the configurations would not show splittings dependent on ζ_{nd} or on exchange integrals $K(\gamma_5, \gamma_k)$. Actually, the hexachloro complexes of d^5 systems exhibit a weak band, followed by two strong bands. The latter of these two is often double. If we do not adopt the rather improbable opinion that one of these bands is caused by $\sigma \rightarrow \gamma_5$, the first, weak band must be Laporte-forbidden, since we can only procure two Laporte-allowed bands without use of intermediate coupling with large values of ζ_{np} (of the halogen), the transitions from the two odd π orbitals γ_4 and γ_5. The splitting of the 12 degenerate π orbitals to four sets of three equivalent orbitals is caused by two reasons: the halide–halide interactions, destroying the validity of $\lambda = 1$; and halide–central ion interactions as described above. We would expect these interactions to increase in the order

$$\begin{array}{lclclcll} \text{even } \gamma_4 & < & \text{odd } \gamma_5 & < & \text{even } \gamma_5 & \sim & \text{odd } \gamma_4, & \text{perturbed by} \\ \geqslant g & & f & & d & & p \text{ and } f & \text{electrons,} \end{array} \tag{4}$$

since p and d orbitals presumably interact more strongly with the low-energy π orbitals than do the highly excited orbitals with higher l. The doublet structure of the second, strong $\pi \rightarrow \gamma_5$ band may be caused by the near degeneracy of even γ_5 and odd γ_4, since it seems too large to be explained by intermediate coupling in the chloro complexes (except those caused by p orbital contributions of the central ion).

The development observed in the bromo and iodo complexes can be connected with the increasing ζ_{np}, which is in the gaseous atoms and ions:

$$\begin{array}{llllllll} \text{F} & 0{\cdot}269 & \text{Cl} & 0{\cdot}587 & \text{Br} & 2{\cdot}457 & \text{I} & 5{\cdot}069 \text{ kK} \\ \text{Ne}^+ & 0{\cdot}521 & \text{A}^+ & 0{\cdot}955 & \text{Kr}^+ & 3{\cdot}581 & \text{Xe}^+ & 7{\cdot}025 \end{array} \tag{5}$$

By analogy with the positive effective charge of central ions, which is decreased by covalent bonding, we might expect the effective charge of the halides to be less negative than -1, producing increased values of ζ_{np}. The hexabromo d^4 and d^5 complexes have seven bands, of which three are particularly strong. Qualitatively similar features prevail in the hexaiodo complexes. The two intervals between the three band groups is remarkably identical in all cases, 2·5 to 3 kK.

Figure 7 shows the splitting of $^2\Gamma_4$ and $^2\Gamma_5$ from π $^1\gamma_5^6$ as function of increasing ζ_{np}. The left-hand side illustrates the case expected from (4) that the odd $^2\Gamma_5$ has the lower energy; but we also give the opposite case (the right-hand side) for comparison and for treatment of the even levels according to (4). The splitting is introduced via the splitting of each π orbital [22] into states with $\omega = 3/2$ (with the L, S coupling energy $+1/2\zeta_{np}$) and $\omega = 1/2(-1/2\zeta_{np})$. By consideration of the Γ_J values of the σ electrons, which also have $\omega = 1/2$, we learn that both the odd and even Γ_6 levels belong to the pure states $\omega = 1/2$ (having increasing energy among the transitions figure 7) while correspondingly, the Γ_7 levels have one hole $\omega = 3/2$. The two sets of Γ_8 levels are mixed and form a hyperbola in the diagram with the diagonal elements $\pm 1/4\zeta_{np}$ and the non-diagonal element $\surd 3/4\zeta_{np}$, as can be found from the rule of constant sum of the squares of all elements of two equivalent secular determinants.

While none of the Laporte-allowed transitions $\gamma_4 \rightarrow \gamma_5$ and $\gamma_5 \rightarrow \gamma_5$ is symmetry-forbidden, one of the four $\pi \rightarrow \gamma_5$ transitions expected in intermediate coupling of low-spin d^5 complexes with large ζ_{np} is forbidden. Γ_7 of $^2\Gamma_5$ has lower energy $(-\zeta_{nd})$ than Γ_8 $(+1/2\zeta_{nd})$, and thus, the d^5 systems are stable against Jahn–Teller distortions for large ζ_{nd} (as are also d^4, where the component Γ_1 has lowest energy of $^3\Gamma_4$, while d^3 with Γ_8 of $^4\Gamma_2$ is unstable). The transition even $\Gamma_7 \leftrightarrow$ odd Γ_6 has no electric dipole moment, and we can only expect three Laporte-allowed transitions, to Γ_7 and the two Γ_8, in figure 7.

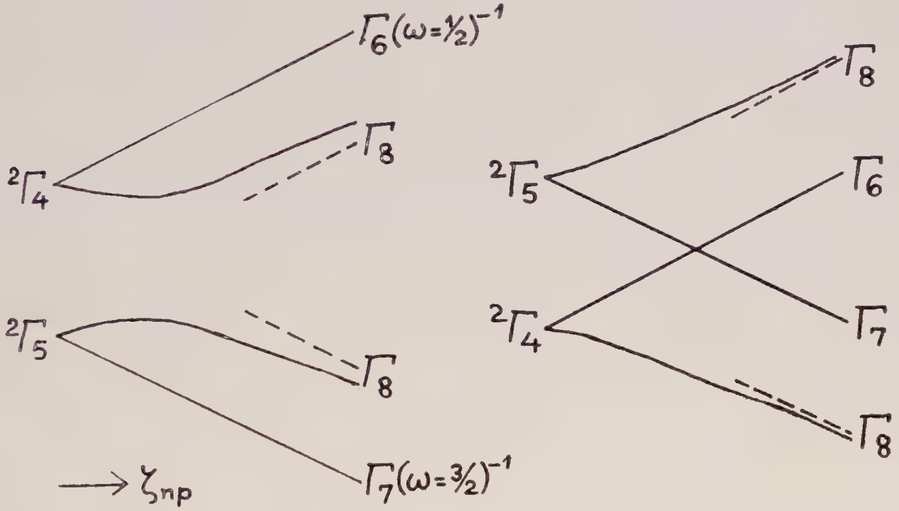

Figure 7. Energy levels of a π hole in an octahedral complex with a non-degenerate excited state $^1\Gamma_1$ of the central ion. The variable is ζ_{np} of the halogen, expressing the extent of intermediate coupling.

Actually, the mutual distances of the three strong band groups of bromo and iodo complexes do not agree perfectly with any of the two cases in figure 7. One of the reasons can be the interaction between the $\omega = 1/2$ components of the σ and π orbitals having [22] the non-diagonal element $\surd 2/2\zeta_{np}$. If the energy difference between σ and π is small, compared to ζ_{np}, we get an asymptotic re-establishment of the quantum number J $(=3/2$ or $1/2)$ for large ζ_{np}, as shown in figure 8. The depression of the upper Γ_8 level in the case (4) produces a fair agreement with the observed three band groups. Of course, we could not expect that our model would agree within 1 kK. Another possible effect is the admixture of the empty $6p$ orbital in the π orbitals of symmetry odd γ_4. ζ_{6p} is not known in Ir(IV), but has probably the order of magnitude 5 kK. If the wave-function contains some 20 per cent of this contribution, $^2\Gamma_4$ would be split some 1·5 kK with Γ_8 at lowest energy (the same direction as in figure 7), which might explain the doublet structure at 23·1 and 24·4 kK of $IrCl_6^{--}$.

The conspicuous doublet structure, especially of the iodo bands, may be related to splitting into two Kramers doublets of the Γ_8 levels by influences lacking octahedral symmetry, e.g. from the solvent water molecules. Since the ground state is Jahn–Teller stable, we would not expect an excessive excitation of non-totally symmetric vibrations. The structure can hardly be caused by ordinary vibrational structure as found [23, 24] in MnO_4^- or OsO_4, since the vibrational quanta must be at most 0·3 kK in the hexaiodo complexes. It is difficult to disprove the presence of several species in the iodide solutions (e.g. of Os(IV)), but the spectra seem remarkably constant as function of iodide and hydrogen ion concentration (when both are above 0·5 M).

It is rather unexpected that d^4 systems such as Os(IV) present nearly the same distribution of electron transfer bands as the d^5 systems such as Ir (IV). The former have two accessible excited states of central ion + one electron, Γ_7 and

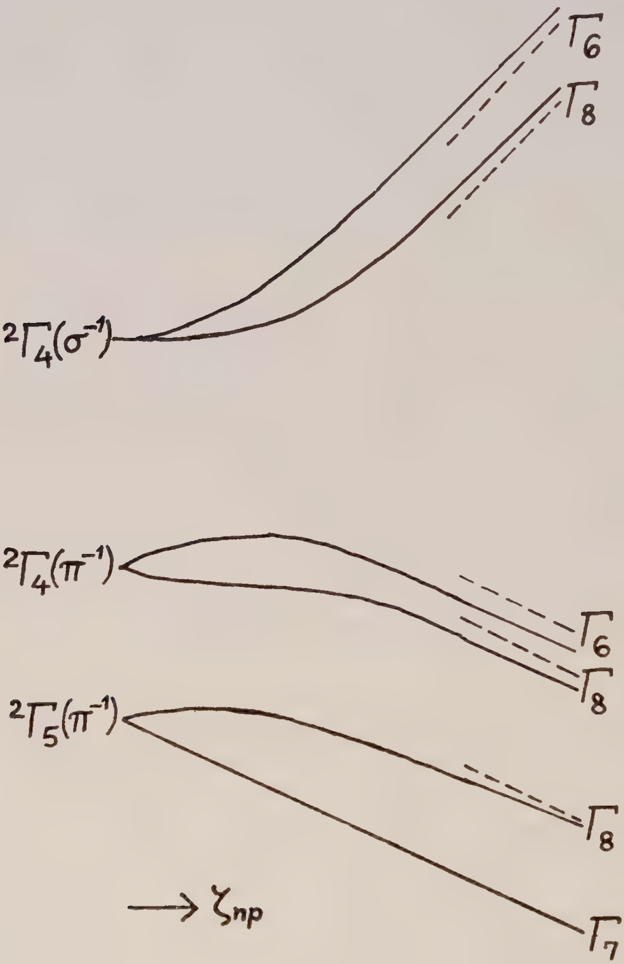

Figure 8. Energy levels of interacting states, formed by the presence of a σ or a π hole with the same conditions as figure 7. The asymptotic behaviour for $\zeta_{np} \to \infty$ corresponds to the dashed lines: states with $J = \frac{1}{2}$ have the energy

$$\Gamma_6 \quad \zeta_{np} + \tfrac{1}{3}\sigma_4 + \tfrac{2}{3}\pi_4$$
$$\Gamma_8 \quad \zeta_{np} + \tfrac{1}{3}\sigma_4 + \tfrac{1}{6}\pi_4 + \tfrac{1}{2}\pi_5$$

and with $J = \frac{3}{2}$ the energy $-\frac{1}{2}\zeta_{np}$ plus

$$\Gamma_6 \quad \tfrac{2}{3}\sigma_4 + \tfrac{1}{3}\pi_4$$
$$\Gamma_7 \quad \pi_5$$
$$\Gamma_8 \quad \tfrac{3}{4}\pi_4 + \tfrac{1}{4}\pi_5$$
$$\Gamma_8 \quad \tfrac{2}{3}\sigma_4 + \tfrac{1}{12}\pi_4 + \tfrac{1}{4}\pi_5$$

where σ_4, π_4, and π_5 denote the energies of $^2\Gamma_4(\sigma^{-1})$, $^2\Gamma_4(\pi^{-1})$, and $^2\Gamma_5(\pi^{-1})$ for $\zeta_{np} = 0$.

Γ_8 of γ_5^5, separated by $3/2\zeta_{5d}$ which is at least 4 kK in $OsCl_6^{--}$, as can be implied from ligand field transitions within γ_5^4. However, we do not observe two sets of electron transfer bands, because Γ_1 of γ_5^4 has a nearly pure γ_j configuration γ_8^4, allowing the uptake of a γ_7 electron as a one-electron process, but not the formation of Γ_8 from $\gamma_8^3\gamma_7^2$. As pointed out by Griffith [25], the L, S coupling matrices of γ_5^n have the same form for d electrons as p^{6-n} in spherical symmetry. Thus [9], by analogy with p^2, the two Γ_1 (of $^3\Gamma_4$ and $^1\Gamma_1$) have the diagonal elements (as γ_8^4 and $\gamma_8^2\gamma_7^2$) $5\,K/3-2\zeta_{nd}$ and $10\,K/3+\zeta_{nd}$ with the non-diagonal element $5\sqrt{2}/3\,K$. Since the most probable values for $OsCl_6^{--}$ are the exchange integral [7] $K=2{\cdot}5$ kK and $\zeta_{5d}=2{\cdot}8$ kK, the ground state has a purity in the squares of the wave-function about 85 per cent. Since the relative intensity between the transitions to Γ_7 and Γ_8 might very well vary accidentally over a factor 3, it is not incompatible with the theory that the transitions to Γ_8 at higher wave-numbers (where the background in the spectrum is rather high) are not observed. Actually, the spectrum of $RuCl_6^{--}$ with a much smaller ζ_{4d} deviates rather much from that of $OsCl_6^{--}$.

On the other hand, d^3 systems with four Γ_J components of $^3\Gamma_4$ of γ_5^4 as possible excited states are expected to exhibit a much more complicated structure. Unfortunately, ReI_6^{--} decomposes very quickly in acidic iodide solutions, but it seems to have a large number of very narrow bands in the visible (figure 5). The first, low band at 11·7 kK is followed by two stronger bands at 14·35 and 15·1 kK. Similar bands are observed of $ReBr_6^{--}$ at 20·4, 22·9 and 23·8 kK.

Even when we have convinced ourselves that d^4 systems have only one effective excited state of the central ion, we may still be surprised by the close analogy to the d^5 systems. Group theory tells us that each of the $^2\Gamma_4$ or $^2\Gamma_5$ states of the π holes will be the parent term (multiplied by Γ_7 of the central ion) of five Γ_J levels of the complex. Even though electric dipole transitions are allowed only to Γ_4 from the ground state Γ_1, we would expect considerable vibrationally created intensity of the symmetry-forbidden transitions. The explanation may simply be that the interaction between γ_5 and π electrons, especially in terms of $K(\gamma_5, \pi)$, is very weak and the complicated configurations are nearly degenerate.

The d^6 systems may perhaps indicate the magnitude of K integrals occurring in electron transfer problems. Each of the configurations $\gamma_4^{-1}\gamma_3$ and $\gamma_5^{-1}\gamma_3$ corresponds to four multiplet terms in Russell-Saunders coupling, $^3\Gamma_4$, $^3\Gamma_5$, $^1\Gamma_4$, and $^1\Gamma_5$. From the ground state $^1\Gamma_1$, the only symmetry-allowed transition goes to odd $^1\Gamma_4$. Among the hexahalides, the evolution in the series Cl, Br, I indicates an increasing intensity of some levels at lower wave-number than the first strong maximum, perhaps caused by triplet singlet intermixing (each of the triplets contain a Γ_4 component). Another explanation may be a distribution of σ character between the two odd γ_4 orbitals. For small values of ζ_{np}, this would only affect the two terms $^2\Gamma_4$ in figure 8, while in bromo (and iodo) complexes, the lowest Γ_8 will be a mixture of $^2\Gamma_4$ and $^2\Gamma_5$ and thus borrowing intensity from the next Γ_8. In the systems $Co(NH_3)_5Cl^{++}$, $Co(NH_3)_5Br^{++}$, $Co(NH_3)_5I^{++}$ (ref. [26]), $Rh(NH_3)_5Br^{++}$ and $Rh(NH_3)_5I^{++}$ (ref. [22]), two bands occur in the ultra-violet with the nearly constant energy difference 8 kK. The first band has a small intensity, proportional with ζ_{np}^2 in the halogen, while the second has $\epsilon \sim 20\,000$ and $P \sim 0{\cdot}5$. This may be interpreted in two different ways: Orgel [27] and Yamatera [28] assume the weak band to be caused by the transfer of a π, and the strong band a σ electron, to the same acceptor orbital (the $2z^2-x^2-y^2$ orbital of the cubic γ_3 type, which points towards the halogen, and is highly attracted by a hole in the halogen electron cloud. x^2-y^2 as acceptor orbital [49] seems rather improbable to the present author). In the notations of linear symmetry, as found in diatomic molecules [11], the π transfer corresponds to the excited terms $^3\Pi$ and $^1\Pi$, while the σ transfer corresponds to $^3\Sigma$ and $^1\Sigma$. If the pure π transfer has a very small intensity (cf. figure 6), the main part of the intensity of the first band might be caused by intermediate coupling with the σ transfer states. Quite another type of explanation is that both bands are caused by π transfer, and that the first, weak band has $^3\Pi_1$ as excited state, of which the S value is mixed with $^1\Pi_1$ of the strong band. In this case, the exchange integral $K(\pi, \gamma_{t1})$ must be 4 kK, i.e. nearly half the distance observed between the two bands. It is nearly impossible to calculate the value of such K integrals *a priori* with our present, very restricted knowledge of the wave-functions, and it is even not certain that a correct value would correspond to the actual energies, due to breakdown of the configurations. In the gaseous atoms of the first transition group, $K(3s, 4d)$ is remarkably constant 1·2 to 1·3 kK, while in neutral† Hg, $K(6s, 6p)$ is 6·08 kK, but $K(6s, 6d)$ only some 0·03 kK. However, the very low values of K integrals often encountered in atomic spectroscopy can be explained by the very small 'squared overlap' $(=\int \Psi_1{}^2\Psi_2{}^2)$ of the orbitals of the ground state with the extended, excited orbitals. In a complex, the average radii of the orbitals cannot exceed some 3 Å, and all the electrostatic parameters have a chance of being at least some per cent of 2 Rydberg/6 Bohr (=37 kK). Many arguments can be given for each of the two possibilities. Ammonia has only one lone pair, which must have mainly σ symmetry, and actually, $Co(NH_3)_6{}^{+++}$ has a broad band [26] at 50 kK with P above 0·6. It can hardly be anything but a $\sigma \rightarrow \gamma_3$ band (excluding tunnelling electron uptake from the solvent), and therefore, the strong band of $Co(NH_3)_5X^{++}$ has a reasonable wave-number and intensity for being due to σ transfer. On the other hand, d^6 hexahalide complexes have two sets of bands with $P=0·3$–$0·8$ at lower and $P=1·5$ at higher wave-numbers. Since a given set of σ orbitals does only contain one odd orbital set γ_4, the former bands with considerable intensity must be ascribed to $\pi \rightarrow \gamma_3$, since $K(\sigma, \gamma_3)$ cannot be sufficiently large to explain a splitting of the configuration $\sigma^{-1}\gamma_3$ over 15 kK. (Especially, the terms of the configuration $\gamma_4(\sigma)^{-1}\gamma_3$ are expected to have the order of energy $^3\Gamma_4 < {}^1\Gamma_4 < {}^3\Gamma_5 \sim {}^1\Gamma_5$, since $J(2,1) > J(2,3)$ and $K(2,1) > K(2,3)$ in the notation of ref. [7]. These terms are not affected to first order by L, S coupling, neither from ζ_{np} of the halogen nor ζ_{nd}.)

It is not easy to compare the monohalide–pentammine and the hexahalide–d^6 complexes since the bands are strongly shifted towards lower wave-numbers in the latter case. This can be ascribed to decreased values of Δ, the energy difference between γ_5 and γ_3, which is 14 kK smaller in $RhCl_6{}^{-3}$ than in $Rh(NH_3)_6{}^{3+}$. In d^5 systems, the transitions $\pi \rightarrow \gamma_5$ have wave-numbers remarkably independent of the number of halogen ligands bound to a given central ion. Thus, $Ru(NH_3)_5Cl^{++}$, *cis*- and *trans*-$Ru(NH_3)_4Cl_2{}^+$ [29] and $Ru(H_2O)_5Cl^{++}$

---

† In the chloro complexes of Tl(I), Pb(II), and Bi(III), two bands can be observed which can be interpreted as transitions between the states which in atomic spectroscopy would be $6s^2\,{}^1S_0$, $6s6p\,{}^3P_1$, and $6s6p\,{}^1P_1$. As will be discussed elsewhere, $K(6s, 6p)$ turn out to be 3 kK and ζ_{6p} 5 kK in these complexes. These values and the orbital energy difference $6s-6p$ are all decreased, compared to the gaseous ions, and have a tendency to decrease with increasing oxidation state and with the series of ligands

$$H_2O > OH^- \sim enta^{-4} > Cl^- > Br^- > I^-$$

for a given central ion.

and $Ru(H_2O)_4Cl_2^{+}$ [30] all have their bands at nearly the same place, 30 kK, as $RuCl_6^{\ 3}$. This situation is contrary to all predictions from primitive, electrostatic models, where electron transfer to a positive central ion is greatly facilitated by the accumulation of several, negatively charged ligands.

It is well known [31] that the position of ligand field bands is very little influenced by formation of solid compounds. Thus, at the present studies, the band groups at 10·8–11·7 kK of $OsCl_6^{--}$ and $OsBr_6^{--}$, and at 17·3 kK of $OsCl_6^{-}$, representing internal transitions in γ_5^4 (as will be discussed in another paper) are found at nearly the same positions in solution and in solids. A similar invariance can at least sometimes be observed of the electron transfer bands. Figure 9 shows the reflection spectrum of $[N(C_2H_5)_4]_2OsI_6$. It is seen that the wave-numbers of the maxima are some 3 per cent smaller than of the solution, but the close correspondence indicates that the spectrum is caused by the same chemical entity. The high background in the solid sample is peculiar and might be related to weak bands (the intensity of reflection bands increases only very slowly with the molar extinction coefficient in solution [31]), for instance of the green hydrolysis products, which evolve in aqueous solution, if the iodide concentration is below 0·1 M. However, the purplish brown crystalline powder has a very uniform appearance.

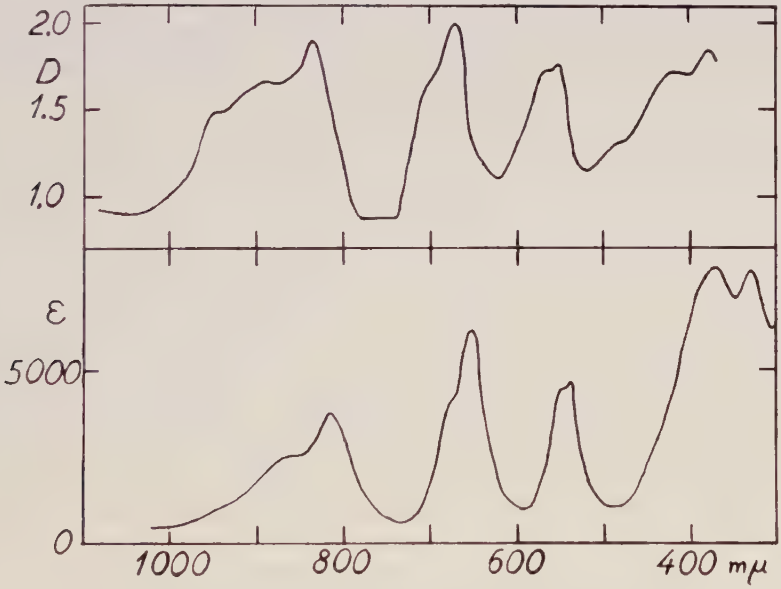

Figure 9. The reflection spectrum of tetra(ethyl)ammonium hexaiodo-osmiate (IV) and the absorption sqectrum of OsI_6^{--} in solution. Since the features are most interesting in the red, a wavelength scale 1100–300 mμ has been used rather than a wave-number scale (here 9·1 to 33·3 kK) as in figures 1–5.

The wave-number in kK of the first, strong band in each of the groups, which were identified above as transitions to γ_5 (absent in d^6) and γ_3 can be interpolated with an average accuracy of some 2 kK from the formula

$$\left\{\begin{array}{lll} 4d^q & 51 & -7q \\ 5d^q & 58 & -7q \end{array}\right\} + \left\{\begin{array}{lr} \mathrm{Cl} & 0 \\ \mathrm{Br} & -6 \\ \mathrm{I} & -16 \end{array}\right\} + \left\{\begin{array}{lr} \text{trivalent } (\rightarrow\gamma_5) & +15 \\ \text{tetravalent } (\rightarrow\gamma_5) & 0 \\ \text{trivalent } (\rightarrow\gamma_3) & +30 \\ \text{tetravalent } (\rightarrow\gamma_3) & +20 \end{array}\right\} \qquad (6)$$

giving the impression of numerous regularities in the orbital energy differences between the highest, filled shell and the partly filled shell of a hexahalide complex as function of the electron configuration of the gaseous ion, of the oxidation number and of the halogen. The order of halogens is that expected from general knowledge of the reducing character of the halides. However, the spreading from F to I is much larger (some 44 kK) than the spreading of the electron affinities of the gaseous halogen atoms, amounting to only 4 kK. The value of +28 for F of the second term in (6) can be implied from WF_6, which has the first strong band [32] at 57 kK, while strong bands of WCl_6 at 26·4 and 29·9 kK have been observed here. H_2O seems to have the second term of (6) equal to +15 kK, as can be implied from the relatively weak band [30] of $Ru(H_2O)_6^{+3}$ at 44·5 kK, if it is identified as a $\pi \rightarrow \gamma_5$ transition.

Katzin [33] considers all electron transfer spectra of halide complexes as bands shifted from the position at 44·2 and 52 kK of I^- in aqueous solution, and at 54 kK of Br^- and 62 kK of Cl^-. These bands were assigned by Franck and Scheibe [34] to electron transfer to one effective state of the solvent, leaving, e.g. the iodine atoms in one of the two states $^2P_{3/2}$ or $^2P_{1/2}$, separated by $3/2\zeta_{5p}$. This approximation to the complexes is only valid in so far as ζ_{np} is larger than the splitting into π and σ orbitals introduced by the central ion [22]. However, as seen above, we may very well consider the electron transfer spectra as determined by the number of effectively excited acceptor states of the central ion, multiplied by the number of excited states of the resonance structure of five halide ions and one halogen atom. Actually, the spectrum of I^- in alkali halides shows a fine structure (thus [35–37], CsI has at least four bands, the most prominent at 46·4 and 48·3 kK). Overhauser [38] applied group theory to find the large number of excited levels of a halogen atom in a NaCl or CsI lattice. Moreover, the solid alkali halides exhibit several more bands in the range up to 100 kK, demonstrating the presence of several acceptor orbitals (cf. also gaseous CsI and Rabinowitch's review [50]). Petersen [39] made an analogy with the excited configurations of inert gases, e.g. $5p^5 6s$ of Xe, where the $6s$ orbital plays the rôle of an accessible orbital of opposite parity somewhat below the ionization potential.

The doublet structure of the first transition to γ_3 of hexabromo complexes with the distance 3·8–5·5 kK between a weaker and a stronger component is rather remarkable. In addition to ζ_{4p} (cf. equation (5)) of the bromine atom, this distance is probably partly caused by differences in the interelectronic repulsion.

When the corresponding gaseous ion has a filled shell d^{10}, the absorption bands all have high wave-numbers and are very strong. They might to some approximation have d^9p as excited states, but in this case, Laporte-forbidden transitions to d^9s were expected at lower wave-numbers. Even though narrow lines of solid Cu(I) halides often have been reported 24 27 kK, the present author has not been able to observe any weak bands of solutions of CuCl and CuBr in concentrated HCl and saturated NaBr, respectively. Rather, the bands observed in Hg(II) and Pb(IV) complexes are caused by odd $\gamma_4(\pi) \rightarrow \gamma_1$ (and perhaps $\sigma \rightarrow \gamma_1$ at higher wave-number) where γ_1 represents the mainly $6s$ orbital, which is doubly occupied in the Pb(II) complexes. The $6s \rightarrow 6p$ (or more accurately, $\gamma_1 \rightarrow$ odd γ_4) transitions in the latter type of complexes have so large wave-numbers that $\gamma_3(5d) \rightarrow \gamma_4(6p)$ is not likely to be observed in Pb(IV).

A distinction between ligand field and electron transfer transitions is only possible, in so far as the M.O. configurations are well defined. We know that this is only an approximation, but we have seen above that the classification of the energy levels of transition group complexes is possible, assuming a consistent order of σ, π and partly filled γ_5 and γ_3 orbitals. Group theory cannot be used as the only source of information about the distribution of the energy levels of a given complex. Generally, a very large number would be possible, and the orbital energies cannot be calculated with any reasonable certainty except by comparison within series of chemically related complexes. (The Helmholz–Wolfsberg method [23] has recently been applied by several authors [48, 49] assuming hydrogenic radial functions and neglecting the interelectronic repulsion. However, the diagonal elements of energy assumed produce a crowding of many orbitals of which no trace is observed in the spectra.) Actually, the range of wave-numbers, 8–50 kK, available for spectrophotometric investigations of aqueous solutions, is relatively small, compared to the spreading of exceedingly numerous energy levels, which in principle continue up in the x-ray region and which are responsible for most of the oscillator strength P, equalling the number of electrons. The partly filled shell (γ_5 and γ_3) has still $l=2$ to a rather good approximation and is rather isolated in energy from other orbitals, except in cases such as OsI_6^{--} or $IrBr_6^{--}$, where the loosest bound electrons of the ligands have energies only slightly below the γ_5 orbitals.

It is believed that atomic spectroscopy and M.O. treatment of complexes present nearly the same type of difficulties for a strict quantum-mechanical theory. In both cases, the orbital energies can be estimated from observed spectra, and the splitting of each configuration to a number of energy levels can be interpreted by a semi-empirical theory, using interelectronic repulsion parameters and Landé factors ζ_{nl}. In neither of the two cases do the wave-functions correspond to pure configurations (i.e. anti-symmetrized Slater determinants) and even very refined Hartree-Fock calculations on atoms in spherical symmetry do not give very satisfactory results for the orbital energies, while these hardly can be obtained with any success in complexes. However, the use of M.O. configurations as a classification, which was shown by Mulliken, Hund, and many others [53, 54] to be fruitful for the gaseous diatomic molecules [11] has in the last eight years been shown to be applicable to the partly filled shells of transition group complexes in solution and in salts; and the present paper attempts to show that the M.O. classification is equally useful for the transitions in the latter complexes, where an electron is excited from a filled M.O. to the partly filled shell. Perhaps, it is not always advantageous to separate out ligand field theory as a special case, nearly in contrast to M.O. theory. The latter point of view is supported by the fact that pure d^n and f^n configurations are so well known in the theory of systems in spherical symmetry, and that they may be incorporated in complexes in a way that many effects can be qualitatively explained by first-order 'electrostatic' perturbations on the angular functions (hydrogenic for well-defined l) and by expanded radial functions. However, from another point of view, the 'ligand field' and 'electron transfer' transitions occur both between M.O. configurations which do not have many other conspicuous differences than that the latter transitions generally involve excited states of odd parity, while the ground state and the excited states of the 'ligand field' bands all have even parity. It can be concluded from the half-width that $\pi \rightarrow \gamma_5$ transitions in halide complexes have less antibonding character, i.e. produce less increased internuclear equilibrium distances, than the $\gamma_5 \rightarrow \gamma_3$ transitions.

The quantum-mechanical treatment of such transitions is necessarily semi-empirical. One of the simplest molecules, where a given configuration produces several energy levels, is O_2, where the triplet (ground state) and two singlet levels have the same internuclear equilibrium distance and according to simple M.O. theory belong to the same configuration, separated only by K integrals between the π electrons. Moffitt [40] remarked that the excited states also correspond to a simple M.O. classification, and tried to support the concept of 'atoms in molecules' by theoretical arguments. It has not yet been proved that such a treatment is feasible even though it is extremely appealing to chemical intuition. The *a priori* calculations have only been performed for one- and two-electron systems (He and H_2) and can hardly yet be extended to more than some four electrons. A tremendous amount of work done on the oxygen molecule [41] has not yet succeeded to the same extent as in the simpler systems. On the other hand, it must be emphasized that the energy levels of transition group complexes can be described with a very high accuracy by parameters, which can easily be interpolated in a series of complexes. The absorption spectra are especially compatible with a M.O. description, while the usual valence-bonds methods often mentioned in classical literature seem to have very little connection with the distribution of energy levels. This can be explained by the high degree of freedom of localization of the M.O., e.g. in the L.C.A.O. approximation, it can be distributed in any way between the central ion and the ligands. The states of hybridizations, on the other hand, are very artificial special cases of the M.O. theory [7], and the difficulties cannot easily be removed by intermixing of ionic structures and of different states of hybridization. An important difference between atomic spectroscopy and chemistry is that the orbital energies in the gaseous atoms increase with increasing average distance from the nucleus, and that increasing ionic charge always corresponds to strongly increasing energy. In the complexes, the ligands stabilize several orbitals at a larger distance and a lower energy than the loosest bound orbitals of the central ion; and most metals form the stablest complexes with the oxidation number +3 or +4. Therefore, the absorption bands correspond in some cases to a larger average distance of the electron ($\gamma_5 \rightarrow \gamma_3$; $f \rightarrow d$; perhaps $s \rightarrow p$ transitions; and 'inverted' electron transfer $\gamma_5 \rightarrow$empty π orbitals of the ligands [22, 42]) and in other cases to a smaller average distance of the electron from the nucleus of the central ion (the electron transfer bands discussed here).

Experimental. The absorption spectra between 800 and 200 mμ were measured on a Cary MS 11 spectrophotometer. The reflection spectra (and the spectra of solutions above 800 mμ) were measured on a Beckman DU spectrophotometer.

Ru; Rh; $Na_3RhCl_6, 12H_2O$; K_2PdCl_6; $KReO_4$; Os; OsO_4; Ir; $K_3IrCl_6, 3H_2O$; $Na_2IrCl_6, 6H_2O$ were supplied by Dansk Hollandsk Ædelmetal (H. Drijfhout & Zoon, Amsterdam). The preparations of some Ru, Ir and Pt complexes have been previously discussed [20].

Ru(III) was found to have considerably different spectra in 4 M and 12 M HCl; the latter, which resembles $IrCl_6^{-}$ closely, probably represents $RuCl_6^{-3}$. $RuBr_6^{-3}$ was measured in 1 M HBr, 5 M NaBr and made by boiling Professor Charonnat's $K_2RuCl_5(H_2O)$ in this solution. Dr. J. L. Woodhead, A.E.R.E., Harwell, was so kind as to inform me that $RuCl_6^{--}$ has another spectrum (characterized by the shoulder at 17·2 kK and the absence of a strong band at 26·0 and 27·7 kK) than $Cl_5RuORuCl_5^{-4}$, as indicated by the measurements of Wehner and Hindman [43] on Ru(IV) in 10 M HCl, kept for 70 days. Actually, the oxo-bridged dimer is very difficult to decompose in HCl, when it is formed from RuO_4, while $RuCl_6^{--}$ is quantitatively formed from Ru(III) and Cl_2.

The variation of the ligand field bands of Rh(III), produced by the slow aquation of $RhCl_6^{-3}$ below 4 M HCl, has been previously discussed [15]. Similar effects are observed of the strong band, which is shifted to 44·5 kK in 1 M HCl. The intensity of the band at 39·2 kK increases curiously enough some 50 per cent (ϵ from 21 000 to 34 000) by going from 4 M to 12 M HCl. The intensity of electron transfer bands varies often with the solvent [44]. $RhBr_6^{-3}$ is only stable in strong bromide solutions, e.g. 5 M NaBr, and decomposes in 1 M NaBr to $RhBr_5(H_2O)^{--}$ or lower complexes with a broad band at 38·5 kK.

$PdCl_6^{--}$ is only stable in HCl with a small concentration of free chlorine [45]. $PdCl_4^{--}$ has very strong bands at 35·8 and 44·9 kK, as will be discussed elsewhere, and the spectrum was obtained by adding grains of K_2PdCl_6 to dilute solutions of Cl_2 in 2 M HCl which previously were measured, and corrected for $PdCl_4^{--}$.

K_2SnCl_6 was measured in 12 M HCl, since it aquates at lower HCl concentrations, as does [46] also $SbCl_6^-$. K_2ReI_6 decomposes very quickly in solution, but the spectrum obtained resembles that given by Rulfs and Meyer [47]. The Os complexes prepared here will be described in another note. The oxidation number +3 was obtained in solutions of HCl, HBr, and HI respectively, by reduction with silver powder. However, the pale yellow $OsCl_6^{-3}$, yellow $OsBr_6^{-3}$, and brown OsI_6^{-3} re-oxidize in some ten minutes to yellow $OsCl_6^{--}$, tomato red $OsBr_6^{--}$, and greyish lilac OsI_6^{--}, even in closed absorption cells. The electron configuration d^5 and thus, the trivalency, was indicated by the close analogy of the electron transfer spectra with those of Ir(IV), while Os(II) should have produced a modified d^6 spectrum. Solid K_2OsCl_6 is dark red and much more coloured than the yellow $[N(C_2H_5)_4]_2OsCl_6$ which has nearly the same colour as the solutions of $OsCl_6^{--}$. The shift towards smaller wave-numbers of the absorption edge in the potassium salt is probably caused by interactions between adjacent $OsCl_6^{--}$ groups, while the more dilute salts with larger cations do not show this effect. Similar effects occur in the dark red K_2ReBr_6, compared to yellow $[N(CH_3)_4]_2ReBr_6$, and are not caused by different grain size. $[N(C_2H_5)_4]_2OsI_6$ is very insoluble and precipitates on addition of tetra-ethyl ammonium salts to the warmed solution of OsO_4 (or the aqueous extract of the melt of Os with NaOH and an oxidizing agent such as $NaClO_3$ or $NaBrO_3$) in KI, HI and ascorbic acid. The solution of OsI_6^{--} in dilute $HClO_4$ turns blue-green in some twenty minutes, due to aquation reactions, and evolves bands at 12·9 and 16·3 kK. Even though the highest band of OsI_6^{--} has the same position as that of I^-, it does not seem to be caused solely by aquation, liberating I^-.

$IrCl_6^{--}$ was measured in HCl from 0·2 to 12 M HCl after treatment two days before with Cl_2 (the ultra-violet absorption of Cl_3^- disappears quickly). $IrBr_6^{--}$ was measured from $K_3IrBr_6, 4H_2O$ (kindly given by Professor M. Delépine) in 1 M $HClO_4$ with 0·002 M Br_2. Here, it was necessary to study the ultra-violet absorption of aqueous bromine solutions, which is very dependent on the presence of Br^-.

K_2PtBr_6 can be dissolved in H_2O without quick decomposition, making the observation of the high frequency band possible without interference of Br^-. K_2PtI_6 was prepared and dissolved in cold 0·2 M $HClO_4$. It gives a black precipitate after some minutes and was rather difficult to measure without the addition of iodide ions (cf. previous measurements of Ir(IV) and Pt(IV) [20]).

				λ	σ	$\delta(-)$	ϵ	P
$4d^4$	Ru(IV)	$RuCl_6^{--}$	$\pi \to \gamma_5$ I	583	17·15	1·0	660	600
			,, II	486	20·3	0·9	4400	3600
			,, IIIa	(436)	(22·9)	—	3500	(1000)
			,, IIIb	(406)	(24·6)	—	3000	(2000)
			$\pi \to \gamma_3$?	(278)	(36·0)	3·3	(12000)	(35000)
			,, ?	(244)	(41·0)	—	(18000)	—
		$Cl_5RuORuCl_5^{-4}$	$\pi \to \gamma_5$ II	469	21·35	1·45	4400	5800
			,, IIIa	385	26·0	—	6800	(10000)
			,, IIIb	(357)	(27·7)	—	5800	(5000)
			$\pi \to \gamma_3$	254	39·4	4·4	14400	58000
$4d^5$	Ru(III)	$RuCl_6^{-3}$	$\pi \to \gamma_5$ I	(390)	25·6	—	600	(800)
			,, II	349	28·65	1·3	2160	2500
			,, III	309	32·4	—	1670	(2000)
			$\pi \to \gamma_3$	229	43·6	3·8	16000	55000
		$RuBr_6^{-3}$	?	(610)	(16·4)	—	130	—
			$\pi \to \gamma_5$ I	(518)	(19·3)	—	720	—
			,, IIa	(470)	(21·3)	—	1420	—
			,, IIb	445	22·5	—	1810	—
			,, IIc	435	23·0	—	1800	—
			,, III	397	25·2	—	2220	—
			,, IV	(367)	(27·2)	—	1780	—
			$\pi \to \gamma_3$	(286)	(35·0)	3·4	(14000)	—
$4d^6$	Rh(III)	$RhCl_6^{-3}$	$\pi \to \gamma_3$	255	39·2	2·8(+)3·2	29000	80000
		$RhBr_6^{-3}$	,, I	332	30·1	2·2	9800	20000
			,, II	294·5	33·9	—	15300	30000
	Pd(IV)	$PdCl_6^{--}$	,,	340	29·4	2·7(+)2·6	14000	34000
			$\sigma \to \gamma_3$	240	41·7	2·9	55000	145000
$4d^{10}$	Sn(IV)	$SnCl_6^{--}$	$\pi \to \gamma_1$	223	44·9	3·1	(10000)	(30000)
	Sb(V)	$SbCl_6^-$	$\pi \to \gamma_1$	271	36·9	2·8(+)3·1	(8000)	22000
$5d^0$	W(VI)	WCl_6 in CCl_4	Impurities?	(720?)	(13·9?)	—	(5)	—
			,,	(585)	(17·1)	—	(60)	—
			,,	(514)	(19·45)	—	(170)	—
				(447)	(22·4)	—	(800)	—
				379	26·4	1·5	(3000)	—
				334	29·9	1·6(+)1·9	(8000)	—

				λ	σ	$\delta(-)$	ϵ	P
$5d^3$	Re(IV)	$ReCl_6^{--}$	$\gamma_5 \to \gamma_3$?	(363·5)	(27·45)	0·9	230	200
			$\pi \to \gamma_5$ I	(320)	(31·3)	1·1	2800	2500
			,, IIa	(300)	(33·3)	—	7000	—
			,, IIb	281	35·6	—	12500	12000
			,, III	(256)	(39·1)	(+)1·0	7000	7000
		$ReBr_6^{--}$	$\pi \to \gamma_5$ Ia	(490)	(20·4)	0·7	180	110
			,, Ib	(437)	(22·9)	0·6	1600	(900)
			,, Ic	(420)	(23·8)	—	2300	—
			,, IIa	(381)	(26·2)	—	5200	(5000)
			,, IIb	352·5	28·4	—	9900	(9000)
			,, III	325·5	30·8	—	8600	(7000)
			,, IV	303	33·0	—	4400	(3000)
			,, ?	262·5	38·1	1·3	9700	(12000)
		ReI_6^{--}	$\pi \to \gamma_5$ Ia	860	11·6	0·35	(300)	(100)
			,, Ib	696	14·35	0·8	(2400)	(2000)
			,, Ic	661	15·1	—	(2600)	
			,, IIa	(599)	(16·7)	—	(4800)	(5000)
			,, IIb	573	17·45	—	(5600)	
			,, IIIa	(534)	(18·75)	—	(6800)	(6000)
			,, IIIb	517	19·35	—	(7800)	
			,, IV	481	20·8	—	(5600)	(1000)
			,, Va	(454)	(22·1)	—	(7200)	(8000)
			,, Vb	444	22·55	—	(7800)	
			,, Vc	432	23·15	—	(8100)	
			,, Vd	424	23·6	—	(7900)	
			,, VI	387	25·85	—	(9200)	—
			I_3^- ?	351	28·5	—	(16000)	—
$5d^4$	Os(IV)	$OsCl_6^{--}$	$\pi \to \gamma_5$ I	418	23·9	1·0	1000	800
			,, II	370	27·0	0·9	7300	6000
			,, IIIa	(341)	(29·3)	—	7700	(12000)
			,, III b	333	30·0	(+)1·3	7900	
			$\gamma_5 \to \gamma_3$?	(301)	(33·2)	—	1000	(800)
			,,	(278)	(36·0)	—	700	(500)
			,,	255	39·2	1·4	2000	(2600)
			$\pi \to \gamma_3$	(213)	(47·0)	3·2	(20000)	(60000)
		$OsBr_6^{--}$	$\pi \to \gamma_5$ I	(579)	(17·3)	1·0	1600	(1000)
			,, IIa	(528)	(18·95)	—	3200	(5000)
			,, IIb	(506)	(19·75)	—	4500	
			,, IIc	489·5	20·45	(+)0·7	5600	
			,, III	445	22·6	0·85	7500	(3000)
			,, IVa	423	23·7	—	5300	(1000)
			,, IVb	399	25·05	(+)1·3	5800	(4000)
			$\gamma_5 \to \gamma_3$?	350	28·6	—	(2500)	—
			$\pi \to \gamma_3$ I	280	35·7	2·6	10000	(20000)
			,, II	245	40·8	—	15000	—
		OsI_6^{--}	$\pi \to \gamma_5$ Ia	(862)	(11·6)	0·85	2500	(1500)
			,, Ib	813	12·3	(+)0·45	4000	1600
			,, IIa	(688)	(14·55)	0·4	3800	—
			,, IIb	653	15·3	(+)0·55	6100	3000
			,, IIIa	550	18·2	0·4	4400	2000
			,, IIIb	537	18·6	0·6	4500	
			$\pi \to \gamma_3$ I	373	26·8	2·4	8000	18000
			,, II	333	30·0	—	7800	(15000)
			,, III	281	35·6	—	9200	(20000)
			$\sigma \to \gamma_3$	224	44·6	3·0	41000	115000

				λ	σ	$\delta(-)$	ϵ	P
$5d^5$	Os(III)	$OsCl_6^{-3}$	$\pi\to\gamma_5$ I	(307)	(32·6)	—	—	—
			,, II	282	35·45	1·1	—	—
			,, IIIa	262	38·2	—	—	—
			,, IIIb	(254)	(39·4)	—	—	—
		$OsBr_6^{-3}$	$\pi\to\gamma_5$ I	(465)	(21·5)	—	(400)	—
			,, IIa	(390)	(25·6)	—	(1400)	—
			,, IIb	(365)	(27·4)	—	(2500)	—
			,, IIc	355	28·2	0·4	(3200)	—
			,, IId	347	28·8	—	(3200)	—
			,, III	322·5	31·0	0·6	(4000)	—
			,, IVa	(312·5)	(32·0)	—	(3600)	—
			,, IVb	(298)	(33·6)	—	(4500)	—
		OsI_6^{-3}	$\pi\to\gamma_5$ Ia	540	18·5	—	—	—
			,, Ib	523	19·1	—	—	—
			,, IIa	494	20·25	—	—	—
			,, IIb	(460)	(21·75)	0·4	—	—
			,, IIc	442	22·65	(+)0·45	—	—
			,, IIIa	400	25·0	0·4	—	—
			,, IIIb	386	25·9	—	—	—
$5d^5$	Ir(IV)	$IrCl_6^{--}$	$\pi\to\gamma_5$ I	590	16·95	0·8	410	300
			,, II	487	20·5	1·0	3280	2800
			,, IIIa	434	23·05	—	2560	4000
			,, IIIb	410	24·4	(+)0·9	2410	
			$\gamma_5\to\gamma_3$?	(360)	(27·8)	—	300	300
			,,	306	32·7	1·0	1180	1000
			$\pi\to\gamma_3$	232	43·1	3·4	21600	67000
		$IrBr_6^{--}$	$\pi\to\gamma_5$ I	(860)	(11·6)	0·75	800	500
			,, IIa	(745)	(13·4)	—	1570	2400
			,, IIb	(700)	(14·3)	—	2350	
			,, IIc	673	14·9	(+)0·5	2520	
			,, III	583	17·15	0·5(+)0·4	3220	1300
			,, IVa	545	18·35	—	1780	1500
			,, IVb	509	19·7	(+)0·8	1530	
			$\pi\to\gamma_3$ I	318	31·5	2·9	8000	20000
			,, II	270	37·0	—	17000	45000
$5d^6$	Ir(III)	$IrCl_6^{---}$	$\pi\to\gamma_3$	206	48·5	4·1	28000	105000
		$IrBr_6^{---}$	,, I	272	36·8	2·2	12000	25000
			,, II	243	41·1	—	20000	50000
	Pt(IV)	$PtCl_6^{--}$	$\pi\to\gamma_3$	262	38·2	2·7(+)2·2	24500	57000
		$PtBr_6^{--}$	,, I	(370)	(27·0)	2·2	7000	15000
			,, IIa	315	31·8	1·8	18000	50000
			,, IIb	(300)	(33·3)	(+)1·5	17000	
			$\sigma\to\gamma_3$	226	44·2	2·0(+)2·1	70000	130000
		PtI_6^{--}	$\pi\to\gamma_3$ I	494	20·25	1·6	12800	18000
			,, II	(440)	(22·75)	—	8300	10000
			,, III	343	29·15	1·7(+)1·2	17000	22000
			$\sigma\to\gamma_3$	252	39·8	3·9	40000	150000
			,, ?	230	43·5	—	59000	—

This investigation was supported by the European Research Office, U.S. Department of Army, Frankfurt am Main, under contract number DA–91–508–EUC–247.

On étudie, par les méthodes de la théorie des groupes, les spectres de transfert électronique des complexes chlorés, bromés, et iodés, de Ru(III), Ru(IV), Rh(III), Pd(IV), Sn(IV), Sb(V), W(VI), Re(IV), Os(III), Os(IV), Ir(III), Ir(IV), Pt(IV), et Pb(IV), et on les interprète comme étant dûs à des transitions d'électrons π (et, aux nombres d'onde plus élevés, d'électrons σ), localisés principalement dans les ligands (groupes coordonnés), vers les orbitales disponibles paires γ_5, γ_3, et γ_1, qui représentent surtout des électrons *d*, *d*, et *s*, de l'ion central. La largeur et l'intensité des bandes soutiennent cette identification. La remarquable similitude entre les spectres des systèmes d^4 et d^5, possèdant un même ensemble de ligands, s'explique par la présence d'un seul état excité efficace pour l'ion central. On calcule la variation de la structure attendue, pour le groupe des bandes dues au transfert d'électrons π, en fonction du paramètre de Landé de l'halogène. On compare l'emploi de configurations simples exprimées par des orbitales moléculaires pour une classification commode (mais non pas comme une très bonne approximation de la fonction d'onde) au cas analogue des spectres atomiques. Il est recommandé d'évaluer les énergies des orbitales moléculaires à partir des spectres d'absorption plutôt que d'essayer de les calculer à partir d'approximations sujettes à caution.

Die Spektren der Elektronenübergänge in den Chlor-, Brom- und Jodkomplexen von Ru(III), Ru(IV), Rh(III), Pd(IV), Sn(IV), Sb(V), W(VI), Re(IV), Os(III), Os(IV), Ir(III), Ir(IV), Pt(IV) und Pb(IV) werden untersucht und mit gruppentheoretischen Verfahren interpretiert als Übergänge von π (bei höheren Wellenzahlen auch σ-) Elektronen, die hauptsächlich an den Liganden lokalisiert sind, zu den verfügbaren Zuständen gerader Parität γ_5, γ_3 und γ_1, die überwiegend *d*, *d*, und *s* Elektronen des Zentralions zukommen. Die Halbwertsbreiten, sowie die Intensitäten der Banden stützen die Zuordnung. Die auffallende Ähnlichkeit zwischen den Spektren von d^4 und d^5 Systemen mit den gleichen Liganden wird damit erklärt, dass für das Zentralion nur ein einziger effektiver Anregungszustand existiert. Die Struktur, die für die Bandengruppe von π-Übergängen zu erwarten ist, wird als Funktion des Landéschen Parameters ζ_{np} des Halogens berechnet. Die Benutzung reiner MO-Konfigurationen für eine einfache Klassifizierung (aber nicht als gute Annäherung der Wellenfunktion) wird mit dem entsprechenden Fall der Atomspektroskopie verglichen. Es wird empfohlen, die MO-Energien lieber aus den Absorptionsspektren abzuschätzen, als zu versuchen, sie aus unzuverlässigen Näherungsansätzen zu berechnen.

REFERENCES

[1] TANABE, Y., and SUGANO, S., 1954, *J. phys. Soc. Japan*, **9**, 753 and 766.
[2] JØRGENSEN, C. K., 1956, *Solvay Council of Chemistry* (Bruxelles: Stoops), p. 355.
[3] JØRGENSEN, C. K., 1957, *Energy Levels of Complexes and Gaseous Ions* (Copenhagen: Gjellerup).

Table 1. The absorption bands observed during this study, with wavelength λ in mμ, wave-number σ in the unit kK ($=1000\ \mathrm{cm}^{-1}$), half-width $\delta(-)$ towards lower wave-numbers, also in kK, the molar extinction coefficient ϵ in the maximum (when indicated in parentheses, the molar concentration of the species has not been known exactly, and ϵ is only given in order to show the relative intensities of the bands) and P the oscillator strength in units of 10^{-5}, calculated from $P = 9{\cdot}2 \times 10^{-9} \epsilon \delta$. The λ and σ of shoulders are given in parentheses, and with a question mark, if it is not at all certain that a shoulder exists. ϵ is the actual value, not the result of a curve analysis. In the extraordinary cases, where $\delta(+)$ is easily determined, it is given with (+) in the $\delta(-)$ column. The electron configuration of the gaseous ion of each oxidation state is given in abbreviated form in the first column, followed by the formulae of the species. In the next column, the proposed identification of the excited level is given, cf. the theoretical discussion.

[4] Moffitt, W., and Ballhausen, C. J., 1956, *Annu. Rev. Phys. Chem.*, **7,** 107.

[5] Orgel, E., 1955, *J. chem. Phys.*, **23,** 1004.

[6] Schäffer, C. E., and Jørgensen, C. K., 1958, Proc. Symposium Co-Ordination Compounds in Rome 1957, *Suppl. Ricerca Scient.*, **28,** 143 and *J. inorg. nucl. Chem.*, **8,** 143.

[7] Jørgensen, C. K., 1958, *Acta chem. scand.*, **12,** 903.

[8] Yamada, S., and Tsuchida, R., 1956, *Ann. Rep. scient. Works Fac. Sci. Osaka Univ.* **4,** 79.

[9] Condon, E. U., and Shortley, G. H., 1953, *Theory of Atomic Spectra*, 2nd Ed. (Cambridge: University Press).

[10] Bethe, H., 1929, *Ann. Phys., Lpz.*, **3,** 133.

[11] Herzberg, G., 1950, *Spectra of Diatomic Molecules*, 2nd Ed. (New York: Van Nostrand).

[12] Van Vleck, J. H., 1935, *J. chem. Phys.*, **3,** 803 and 807.

[13] Kimball, G. E., 1940, *J. chem. Phys.*, **8,** 188.

[14] Flodmark, S., 1958, *Electron Distribution and Energy Bands in Crystals of Metal Borides of the Type MB_6*; Table 5 (Stockholm) and *Arkiv Fysik*, 1959, **14,** 513.

[15] Jørgensen, C. K., 1956, *Acta chem. scand.*, **10,** 500.

[16] Jørgensen, C. K., 1956, *Acta chem. scand.*, **10,** 1505.

[17] Orgel, L. E., 1955, *J. chem. Phys.*, **23,** 1824.

[18] Jørgensen, C. K., 1957, *Acta chem. scand.*, **11,** 53.

[19] Stolarczyk, L., 1958, *Acta chem. scand.*, **12,** 1885.

[20] Jørgensen, C. K., 1956, *Acta chem. scand.*, **10,** 518.

[21] Heal, H. G., and May, J., 1958, *J. Amer. chem. Soc.*, **80,** 2374.

[22] Jørgensen, C. K., 1957, *Acta chem. scand.*, **11,** 166.

[23] Wolfsberg, M., and Helmholz, L., 1952, *J. chem. Phys.*, **20,** 837.

[24] Carrington, A., Schonland, D., and Symons, M. C. R., 1957, *J. chem. Soc.*, 659.

[25] Griffith, J. S., 1958, *Disc. Faraday Soc.*, No. 26, 87 and 173.

[26] Linhard, M., and Weigel, M., 1951, *Z. anorg. Chem.*, **266,** 49.

[27] Orgel, L. E., 1956, X *Solvay Council of Chemistry* (Bruxelles : Stoop), p. 289.

[28] Yamatera, H., 1957, *Naturwissenschaften*, **44,** 632.

[29] Hartmann, H., and Buschbeck, C., 1957, *Z. phys. Chem.*, **11,** 120.

[30] Cady, H. H., and Connick, R. E., 1958, *J. Amer. chem. Soc.*, **80,** 2646.

[31] Bostrup, O., and Jørgensen, C. K., 1957, *Acta chem. scand.*, **11,** 1223.

[32] Tanner, K. N., and Duncan, A. B. F., 1951, *J. Amer. chem. Soc.*, **73,** 1164.

[33] Katzin, L. I., 1955, *J. chem. Phys.*, **23,** 2055.

[34] Franck, J., and Scheibe, G., 1928, *Z. phys. Chem.*, A, **139,** 22.

[35] Phillipp, H. R., and Taft, E. A., 1956, *J. Phys. Chem. Solids*, **1,** 159.

[36] Martienssen, W., 1957, *J. Phys. Chem. Solids*, **2,** 257.

[37] Taft, E. A., and Phillipp, H. R., 1957, *J. Phys. Chem. Solids*, **3,** 1.

[38] Overhauser, A. W., 1956, *Phys. Rev.*, **101,** 1702.

[39] Petersen, R., 1957, *J. Phys. Chem. Solids*, **1,** 284.

[40] Moffitt, W., 1951, *Proc. roy. Soc.* A, **210,** 224 and 245.

[41] Kotani, M., Mizuno, Y., Kayama, K., and Ishiguro, E., 1957, *J. phys. Soc. Japan*, **12,** 707.

[42] Williams, R. J. P., 1955, *J. chem. Soc.*, 137.

[43] Wehner, P., and Hindman, J. C., 1952, *J. phys. Chem.*, **56,** 10.

[44] Bjerrum, J., Adamson, R. W., and Bostrup, O., 1956, *Acta chem. scand.*, **10,** 329.

[45] Cohen, A. J., and Davidson, N., 1951, *J. Amer. chem. Soc.*, **73,** 1955.

[46] Neumann, H. M., 1954, *J. Amer. chem. Soc.*, **76,** 2611.

[47] Rulfs, C. L., and Meyer, R. J., 1955, *J. Amer. chem. Soc.*, **77,** 4505.

[48] Ito, K., and Kuroda, Y., 1955, *J. chem. Soc. Japan*, **76,** 542, 762, 766 and 934.

[49] Nakamoto, K., Fujita, J., Kobayashi, M., and Tsuchida, R., 1957, *J. chem. Phys.*, **27,** 439.

[50] Rabinowitch, E., 1942, *Rev. Mod. Phys.*, **14,** 112.

[51] Mulliken, R. S., and Rieke, C. A., 1941, *Rep. Progr. Phys.*, **8,** 231.

[52] Orgel, L. E., 1954, *Quart. Rev.*, **8,** 422.

[53] Linnett, J. W., 1956, *J. chem. Soc.*, 275.

[54] Keyes, R. W., 1958, *J. chem. Phys.*, **29,** 523.

Paramagnetic resonance in phosphorescent aromatic hydrocarbons. I: Naphthalene

by J. H. van der WAALS and M. S. de GROOT
Koninklijke/Shell-Laboratorium, Amsterdam
(Shell International Research Maatschappij N.V.)

(*Received* 24 *April* 1959)

Recently Hutchison and Mangum have observed electron spin resonance in the lowest triplet state of naphthalene. An analysis of their results is given on the basis of spin–spin interaction between the two unpaired electrons. In addition to the lines observed by these authors another transition, which corresponds to $\Delta m = \pm 2$ in the atomic case, must occur at low field strength. This transition has been observed in a mixed crystal as well as in rigid glass solution.

1. Introduction

Recently Hutchison and Mangum [1] have observed electron spin resonance in naphthalene when irradiating a single crystal of a solid solution of naphthalene in durene with ultra-violet light. Their experiments confirm Lewis and Kasha's suggestion [2] that the phosphorescent state of naphthalene is a triplet state. They measured a highly anisotropic spectrum of four lines; a pair of lines could be assigned to each of the two sets of differently oriented naphthalene molecules in the durene crystal. The anisotropy of the splitting was ascribed to spin–spin interaction, with possibly a minor contribution due to spin–orbit coupling.

In the present paper spin–spin interaction in the triplet state of naphthalene is discussed. It appears that, in addition to the two lines observed by Hutchison and Mangum which correspond to transitions between neighbouring sub-levels of the triplet, a third transition must occur between the highest and lowest sub-levels. Experiments are described which confirm the existence of this transition.

2. Theoretical

The problem can be treated effectively with a two-electron Hamiltonian, representing the magnetic interaction of the two unpaired electrons (numbered 1 and 2) with each other and with the constant field $\mathbf{H}$,

$$\mathscr{H} = g\beta \mathbf{H} \,.\, \mathbf{S} + 4\beta^2 \left\{ \frac{(\mathbf{S}_1 \,.\, \mathbf{S}_2)}{r^3} - 3\,\frac{(\mathbf{r} \,.\, \mathbf{S}_1)(\mathbf{r} \,.\, \mathbf{S}_2)}{r^5} \right\}. \tag{1}$$

The spin operators are expressed in units of $h/2\pi$ and $\mathbf{r}$ is the interelectronic distance.

As zero-order spin functions we take the functions suggested by Hameka and Oosterhoff [3],

$$\left.\begin{aligned} T_x(1,2) &= 2^{-1/2}(\beta_1\beta_2 - \alpha_1\alpha_2), \\ T_y(1,2) &= 2^{-1/2} i(\beta_1\beta_2 + \alpha_1\alpha_2), \\ T_z(1,2) &= 2^{-1/2}(\alpha_1\beta_2 + \beta_1\alpha_2); \end{aligned}\right\} \tag{2}$$

each of which forms a basis for an irreducible representation of the point group D_2 and therefore they diagonalize the Hamiltonian (1) when $H=0$. The total zero-order wave functions are products of the type

$$\Psi(1,2)=\psi(\mathbf{r}_1,\mathbf{r}_2)T_i(1,2), \qquad i=x,y,z. \tag{3}$$

The function $\psi(\mathbf{r}_1,\mathbf{r}_2)$ is an antisymmetric function of the spatial coordinates $\mathbf{r}_1, \mathbf{r}_2$ of the two electrons. (Because of this antisymmetry $r=|\mathbf{r}_1-\mathbf{r}_2|$ can never vanish and hence, as pointed out by Oosterhoff, a term for contact interaction need not be included in (1).) For convenience we shall think in terms of the same coordinate system as used by Hutchison and Mangum; the z-axis is perpendicular to the plane of the naphthalene molecule and the x-axis parallel to its central bond.

If the functions (3) are used as a basis the Hamiltonian matrix (1) can be written as†

$$\begin{bmatrix} X & -ig\beta H_z & ig\beta H_y \\ ig\beta H_z & Y & -ig\beta H_x \\ -ig\beta H_y & ig\beta H_x & Z \end{bmatrix}; \tag{4}$$

$X=2\beta^2\langle\psi(\mathbf{r}_1,\mathbf{r}_2)|3x^2/r^5-1/r^3|\psi(\mathbf{r}_1,\mathbf{r}_2)\rangle$ is an integral over the spatial coordinates and Y and Z are similar integrals.

In the absence of a magnetic field H, the functions (2) are the correct spin eigenfunctions belonging to the energies

$$E_1=X, \qquad E_2=Y, \qquad E_3=Z.$$

Each of these three eigenstates corresponds to a situation in which the spin angular momentum vector lies in one of the three symmetry planes of the molecule. Magnetic dipole transitions between any two of the three states are allowed; for a transition $T_i(1,2)\rightarrow T_j(1,2)$ the transition moment is perpendicular to the ij plane (cf. footnote†).

In the presence of a constant magnetic field of such magnitude that electron spin resonance can be observed the dipolar interaction of the spins is of the same order of magnitude as their interaction with the external field. The component $m(h/2\pi)$ of spin angular momentum in the direction of the field is not a constant of the motion and the selection rule $\Delta m=\pm 1$ does not apply.

Suppose the field is along the x-axis: $H_x=H$, $H_y=H_z=0$. The function $T_x(1,2)$ remains an eigenfunction of the system, but $T_y(1,2)$ and $T_z(1,2)$ are mixed through the off-diagonal elements $\pm ig\beta H_x$ in (4). The roots of the secular equation corresponding with the Hamiltonian (4) then are (cf. heavy lines in figure 1)

$$E_1=X, \quad E_{2,3}=\frac{Y+Z}{2}\pm\sqrt{[\tfrac{1}{4}(Y-Z)^2+(g\beta H)^2]}. \tag{5}$$

The transitions 1←→2 and 1←→3 for which the r.f. magnetic field is perpendicular to the x-direction are those observed by Hutchison and Mangum. The transition 2←→3, however, should also be possible, but it is polarized parallel to the constant field. It is clear from figure 1 that for large values of H, where the coupling of the spins to the constant field becomes much stronger than their mutual interaction, the former transitions correspond to $\Delta m = \pm 1$, whereas the latter becomes forbidden since $\Delta m = \pm 2$. Irrespective of the magnitude of H transitions between neighbouring sub-levels of the triplets will henceforth loosely be called 'allowed transitions' and those between the highest and lowest sub-levels 'forbidden transitions'.

---

† For T_x (1, 2) one has, for instance,
$S_xT_x(1,2)=0$; $S_yT_x(1,2)=-iT_z(1,2)$; $S_zT_x(1,2)=iT_y(1,2)$.
$(\mathbf{S}_1\cdot\mathbf{S}_2)\ T_x(1,2)=\frac{1}{4}T_x(1,2)$.
$(\mathbf{r}\cdot\mathbf{S}_1)(\mathbf{r}\cdot\mathbf{S}_2)T_x(1,2)=\frac{1}{4}(-x^2+y^2+z^2)T_x(1,2)-\frac{1}{2}xyT_y(1,2)-\frac{1}{2}xzT_z(1,2)$.

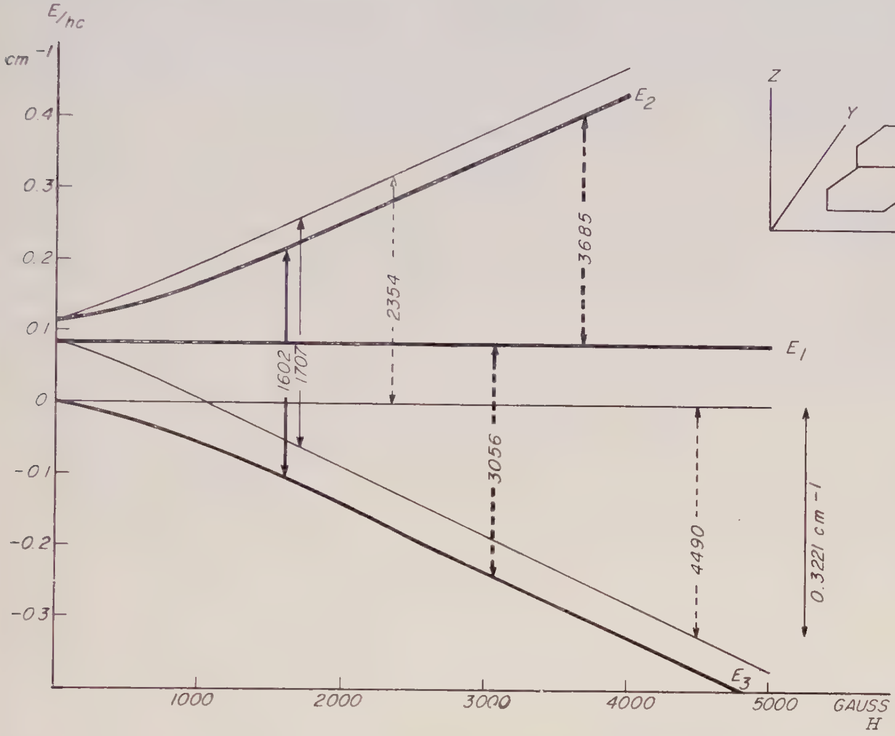

Figure 1. Relative energies of the components of the lowest triplet state of naphthalene as a function of magnetic field strength (derived from the experiments of Hutchison and Mangum).

Heavy lines : magnetic field along x-axis.

Thin lines: magnetic field along z-axis.

The dotted arrows indicate the transitions observed by Hutchison and Mangum, the solid arrows are transitions polarized parallel to the constant field. The length of the arrows corresponds to a frequency of 9654 Mc/s.

If δ is the quantum of energy absorbed in the resonance experiment, $\delta = h\nu$; then it follows from (5) that the transition $2 \leftrightarrow 3$ will occur at a field given by

$$(g\beta H)^2 = \tfrac{1}{4}(E_2 - E_3)^2 - \tfrac{1}{4}(Y-Z)^2 = \tfrac{1}{4}\delta^2 - \tfrac{1}{4}(Y-Z)^2. \qquad (6)$$

The eigen energies then are

$$E_2 = \tfrac{1}{2}(Y+Z) + \tfrac{1}{2}\delta; \qquad E_3 = \tfrac{1}{2}(Y+Z) - \tfrac{1}{2}\delta,$$

while the corresponding eigenfunctions are readily found to be

$$\left.\begin{aligned}\Phi_2(1,2) &= 2^{-1/2}\{\sqrt{[1+(Y-Z)/\delta]}T_y + \sqrt{[1-(Y-Z)/\delta]}iT_z\},\\ \Phi_3(1,2) &= 2^{-1/2}\{\sqrt{[1-(Y-Z)/\delta]}iT_y + \sqrt{[1+(Y-Z)/\delta]}T_z\}.\end{aligned}\right\} \qquad (7)$$

Magnetic dipole transitions are possible when the r.f. field is parallel to the x-axis.

The transition probability

$$\frac{32\pi^3}{3h^2}\beta^2|\langle\Phi_3(1,2)|S_x|\Phi_2(1,2)\rangle|^2$$

on substitution of (7) is found to be proportional to

$$|\langle\Phi_3(1,2)|S_x|\Phi_2(1,2)\rangle|^2=\left(\frac{Y-Z}{\delta}\right)^2. \tag{8}$$

From the results of Hutchison and Mangum it follows that

$$\begin{aligned}(X-Z)/hc&=0{\cdot}0863\ \mathrm{cm}^{-1},\\(Y-Z)/hc&=0{\cdot}1143\ \mathrm{cm}^{-1},\\\delta/hc&=0{\cdot}3221\ \mathrm{cm}^{-1},\\g&=2{\cdot}0133.\end{aligned}$$

Upon substituting these values into (6) and (8) one finds that the forbidden transition should occur at

$$H=H_x=1602\ \text{gauss, with}\ |\langle\Phi_3|S_x|\Phi_2\rangle|^2=0{\cdot}126. \tag{9a}$$

When the constant field is applied along the y- or z-axes one finds in a similar way for the forbidden transitions

$$H=H_y=1650\ \text{gauss},\ |\langle\Phi_3|S_y|\Phi_1\rangle|^2=0{\cdot}072; \tag{9b}$$

$$H=H_z=1707\ \text{gauss},\ |\langle\Phi_1|S_z|\Phi_2\rangle|^2=0{\cdot}008. \tag{9c}$$

In both cases the r.f. magnetic field again is polarized parallel to the constant field. For comparison it may be mentioned that the transitions with transverse polarization observed by Hutchison and Mangum occur at fields between 2354 and 4490 gauss (cf. figure 1) and have calculated intensities of about 0·5 on the present scale.

From these results it is clear that the forbidden transition has an intensity which ranges from 25 per cent (H parallel to the central bond) to 2 per cent (H perpendicular to the molecular plane) of the intensities of the allowed transitions. In addition, the anisotropy of naphthalene for the former transition may be expected to be only one-twentieth of that for the latter. This might render it possible to observe electron spin resonance of triplet states in rigid glass solutions. However, for an assembly of randomly oriented molecules, such as occurs in a glass, one can show that the transition moment is no longer purely polarized parallel to the constant field, but will also have a non-vanishing component perpendicular to this field (cf. ref. [6]).

We have restricted our discussion to spin spin interaction, but in addition there may be spin orbit coupling, which cannot be treated with such a simple two-electron Hamiltonian. If spin–orbit coupling is included it would cause the expressions for the matrix elements X, Y, Z to alter; it would not affect the above numerical predictions, since these are based on experimental values of these elements.

The case of naphthalene has been explicitly considered, but the above treatment is equally applicable to other aromatic molecules with at least one plane of symmetry perpendicular to the plane of the aromatic ring. If the molecule has a 3- or 6-fold symmetry axis (benzene, triphenylene), two of the eigenstates for $H=0$ will form a degenerate pair, since T_x and T_y then belong to a degenerate representation of the point group D_3. When such a molecule is placed perpendicular to the constant field one would expect the parallel transition to be strictly forbidden.

3. Experimental

An experiment was set up in order to detect the transitions (9) for which the r.f. magnetic field is polarized parallel to the constant field.

A Varian V-4500 electron spin resonance spectrometer was employed, which operates at a nominal frequency of 9500 Mc/s. The microwave bridge system of this instrument was connected to a rectangular TE_{102} reflection type cavity constructed for the experiment from a piece of X-band waveguide. An open grid was mounted on one end to permit ultra-violet irradiation whilst the other end was coupled to the feeding waveguide. On both sides there were holes 7 mm in diameter for sample insertion and gold plating served to reduce the effect of wall impurities. The cavity was positioned with the r.f. magnetic field parallel to the external field.

A thin vacuum-jacketed quartz tube, in which the sample was contained, passed through the cavity. Nitrogen gas, at liquid nitrogen temperature, was introduced to provide the necessary cooling.

The light of a 1 kw Philips super-high-pressure mercury arc was focused on the specimen by a quartz lens. In order to prevent overheating of the sample, the light intensity had to be reduced somewhat by means of a diaphragm. A Chance–Pilkington OX7 optical filter was employed to cut off wavelengths above 4000 Å.

Durene, from a commercial source, was distilled *in vacuo*. After this treatment only minute amounts of free radicals could be detected in the solid. Mixed crystals were grown, by the method of McClure [4]. Lumps of single crystal were obtained which contained 0·02 mole per cent of naphthalene. The cleavage plane, the *ab*-plane, was easily found, after which the exact positions of the crystal axes *a*, *b* and *c* could be determined by x-ray analysis. Small specimens of known orientation were cut by the wet string method.

Figure 2 (*a*) shows the spectrum obtained with a durene mixed crystal so oriented that the r.f. magnetic field as well as the constant field were perpendicular to its *ab*-plane. Since the cross-axis of all molecules is tilted away less than 7° from the normal to this plane [5] this means that the magnetic field was very nearly directed along the x-axis of both types of naphthalene molecules. A transition of reasonable intensity and about 10 gauss wide at points of maximum slope is seen to occur at a field of 1564 gauss.

Note that the frequency used here (9425 Mc/s) was slightly less than that given in Hutchison and Mangum's paper (9654 Mc/s). If the correspondingly smaller value $\delta/hc = 0{\cdot}3145\ \mathrm{cm}^{-1}$ for the quantum of r.f. energy is inserted into equation (6) the predicted value of 1602 gauss (9 *a*) is reduced to 1557 gauss, in good agreement with experiment.

The spectrum of figure 2 (*b*) was obtained when the r.f. and the constant magnetic field were parallel to the *ab*-plane and made an angle of 45° with the *a* and *b* crystal axes. For this orientation the magnetic fields were directed approximately parallel to the y molecular axis of one-half of the naphthalene molecules and parallel to the z-axis for the other half. Compared with figure 2 (*a*) the absorption line is weakened in intensity and shifted to a somewhat higher field strength (1605 gauss); its width is increased to about 20 gauss. The experimental conditions do not permit accurate comparison of intensities. Apparently the naphthalene molecules which have their y-axis parallel to the field are responsible for the transition observed; allowing for our lower microwave frequency, the predicted value of the field strength in (9 *b*) is reduced to 1608 gauss. The transition (9 *c*) was too weak to be observed.

It was verified that the signals of figure 2 disappeared with the correct decay time of about 3 sec when the light was switched off.

Finally a rigid glass solution of naphthalene (0·012 mole per cent) in glycerol was subjected to this type of measurement. The asymmetric absorption line

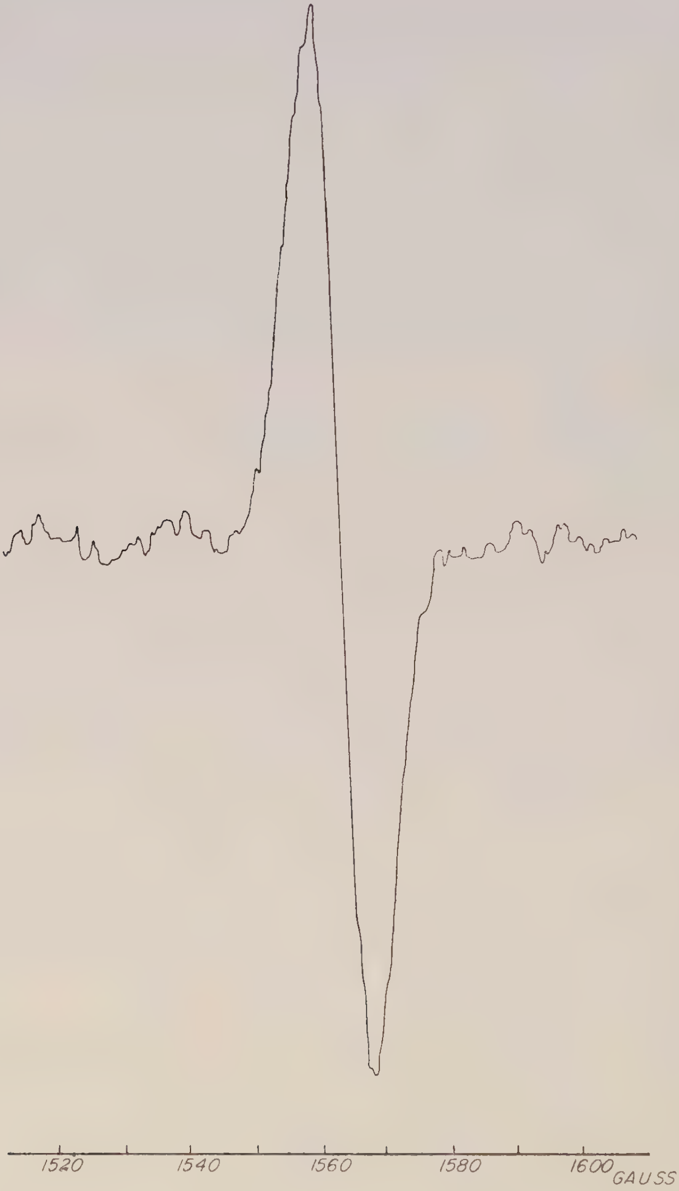

Figure 2 (*a*). Spectrum of phosphorescent naphthalene in durene crystal (0·02 mole per cent; derivative of absorption line). Constant field and r.f. magnetic field perpendicular to *ab*-plane of crystal. Modulation 400 c/s, 7 gauss ; frequency 9425 Mc/s.

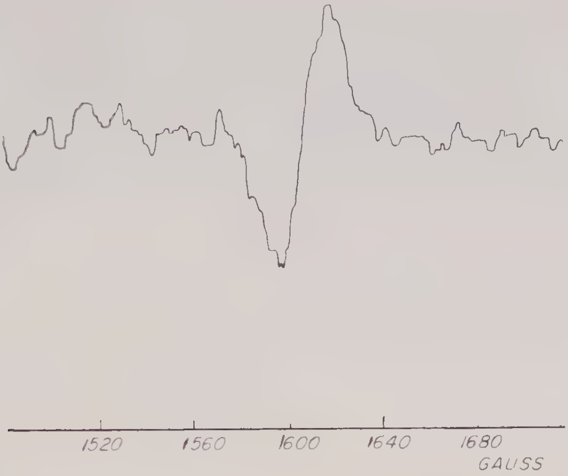

Figure 2 (*b*). Spectrum of phosphorescent naphthalene in durene crystal (0·02 mole per cent; derivative of absorption line). Constant field and r.f. magnetic field parallel to *ab*-plane of crystal under an angle of 45° with *a* and *b* axes. Modulation 400 c/s, 12 gauss; frequency 9425 Mc/s.

of figure 3 was obtained which is in agreement with the situation illustrated in figure 1. A similar signal was observed when performing the experiment in a conventional cavity in which the r.f. magnetic field is perpendicular to the constant field. These results open up a method for investigating the triplet states of other aromatic molecules, for which no suitable crystalline solvent lattices are known.

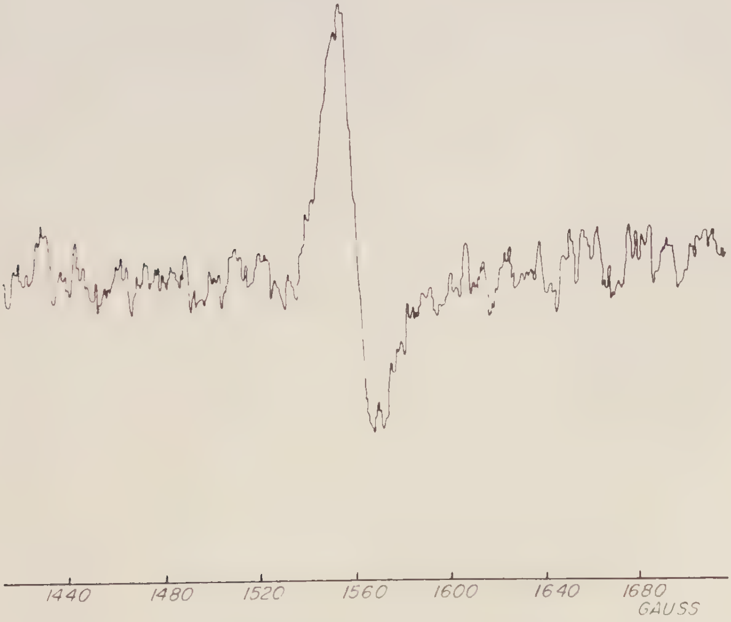

Figure 3. Spectrum obtained from a rigid glass solution of naphthalene (0·012 mole per cent) in glycerol. Modulation 400 c/s, 12 gauss; microwave frequency 9425 Mc/s.

In a subsequent part [6] some results are given for a number of aromatic molecules, with particular reference to those having D_{3h} symmetry. In the latter case it proves possible to derive an exact value of the zero-field splitting from the shape of the absorption curve of a rigid glass solution.

The authors wish to thank Professor L. J. Oosterhoff and Dr. C. MacLean for helpful discussions.

Récemment Hutchison et Mangum ont observé une résonance paramagnétique électronique dans l'état triplet du naphthalène. Dans le présent article on donne une analyse de leurs résultats en se basant sur l'interaction dipolaire des deux électrons à spin parallèle. Il s'ensuit que, en dehors des raies observées par ces auteurs avec un champ magnétique r.f. perpendiculaire au champ magnétique constant, une autre transition doit exister pour les champs faibles, quand les deux champs sont parallèles. Cette dernière transition a été observée dans un cristal mixte et dans une solution rigide.

Hutchison und Mangum haben kürzlich die Elektronen-Spin-Resonanz im niedrigsten Triplettzustand des Naphthalins beobachtet. Ihre Ergebnisse werden als Folge einer Spin-Spin-Wechselwirkung zwischen den beiden ungepaarten Elektronen analysiert. Es wird geschlossen, dass ausser den Linien, die die genannten Autoren bei senkrechter Stellung zwischen hochfrequentem und konstantem Magnetfeld gefunden haben, noch ein weiterer Übergang bei niedriger Feldstärke auftreten sollte, wenn beide Felder parallel stehen. Dieser Übergang wird dann experimentell nachgewiesen.

REFERENCES

[1] HUTCHISON, C. A., and MANGUM, B. W., 1958, *J. chem. Phys.*, **29,** 952.
[2] LEWIS, G. N., and KASHA, M., 1944, *J. Amer. chem. Soc.*, **66,** 2100; 1945, *Ibid.*, **67,** 994.
[3] HAMEKA, H. F., and OOSTERHOFF, L. J., 1958, *Mol. Phys.*, **1,** 358.
[4] MCCLURE, D. S., 1954, *J. chem. Phys.*, **22,** 1668.
[5] ROBERTSON, J. M., 1933, *Proc. roy. Soc.* A, **141,** 594; A, **142,** 659.
[6] DE GROOT, M. S., and VAN DER WAALS, J. H., 1960, *Mol. Phys.*, **3** (to be published as part II).

Electron resonance studies on the kinetics of free radical formation and reaction in the solid phase

by M. FUJIMOTO† and D. J. E. INGRAM‡
University of Southampton

(*Received* 5 *March* 1959)

This paper describes a series of detailed measurements on the electron resonance spectra of U.V. irradiated alcohol–hydrogen peroxide mixtures. The variation of the spectra with both time of irradiation and temperature is followed, and it is concluded that three different radical species are formed in the medium. A quantitative analysis of the growth and decay of these different species is then undertaken and it is shown that there is good agreement with a first-order kinetics of formation and decay.

1. Introduction

In previously reported work [1–3] it has been shown that quite high concentrations of free radicals can be obtained when frozen hydrocarbon glasses are U.V. irradiated. These radicals may either be produced by the initial act of photolysis, if the energy of the incident U.V. quantum is sufficient to break the particular bond, or they may be secondary radicals, formed when the initial photolysis products react with the solvent molecules. One example of the second type of radical is furnished by the various alcohol radicals that can be produced when protons are abstracted by OH radicals, which are themselves formed by the initial photolysis of hydrogen peroxide. Quite a large variety of different alcohol radicals have been prepared and studied in this way [2–3], and in each case a small quantity of hydrogen peroxide was added to the hydrocarbon solvent before freezing and irradiating.

It was noticed in the earlier work [3] that quite often the appearance of the electron resonance spectra changed somewhat with time of radiation, and it was concluded that one or more radical reaction was taking place during the period of irradiation. A systematic survey has therefore been undertaken on the growth and change of the electron resonance spectra obtained from isopropanol and *n*-propanol radicals, and these results are analysed in this paper. It will be seen that three different radical species are formed at different times during the irradiation, and that the growth and decay of these can be followed on a quantitative basis.

2. Experimental

The specimens studied were formed by adding about 10^{-6} to 10^{-5} mol of hydrogen peroxide to the pure alcohols and then deep freezing the solutions to liquid oxygen or nitrogen temperatures. Such concentrations produce electron resonance spectra with the outermost hyperfine components well above the noise level. The quarter-inch diameter specimen tubes were placed centrally in an H_{104} rectangular cavity in such a way that they could be irradiated *in situ* by light from a high pressure mercury lamp [3], which had its main spectral component in the U.V. region at 3650 Å. This wavelength is sufficiently short to dissociate the hydrogen peroxide relatively rapidly but will not photolyze the alcohol molecules to any appreciable extent.

---

† Now at Physics Department, Osaka University, Osaka, Japan.

‡ Now at Physics Department, University College of North Staffordshire, Keele, Staffs.

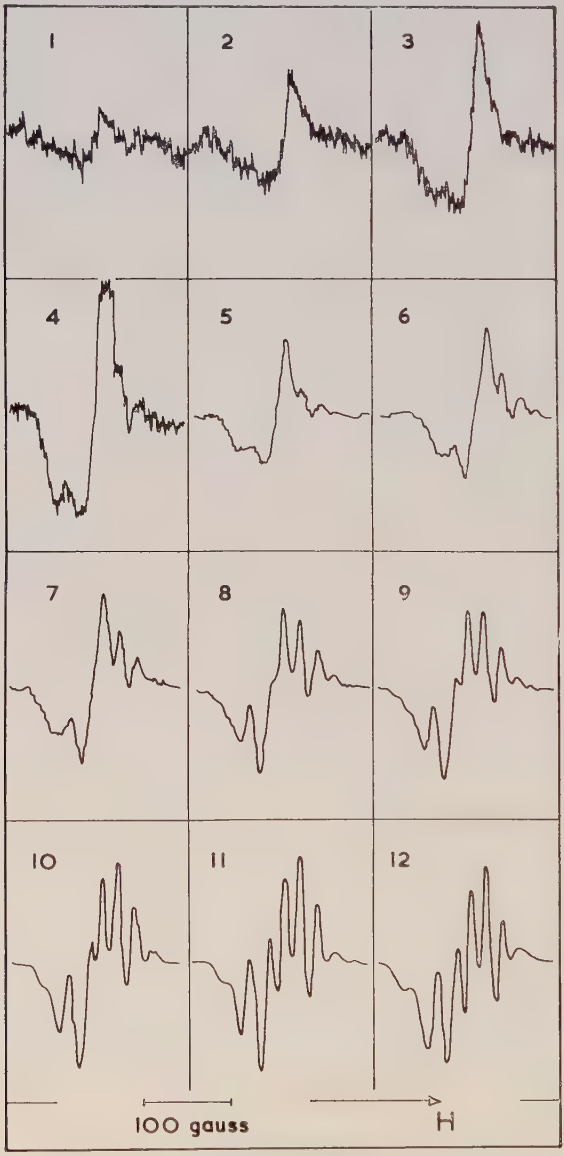

Figure 1. Variation of isopropanol spectra with time of irradiation. Spectra are taken at approximately 10 minute intervals.

The 3 cm wavelength spectrometer employed 100 kc/s magnetic-field modulation and phase-sensitive detection [4], and the resultant spectra were traced out as first derivatives of the absorption by a pen-recorder, as seen in figures 1 and 2. The total absorption due to the specimen was determined by graphical double-integration, and the number of radicals was determined by comparison with a doubly-integrated curve from a standard free-radical sample observed under identical conditions. The standard samples are formed by diluting ground charcoal with an inert filler, and are themselves cross-calibrated with diphenyl picryl hydrazyl.

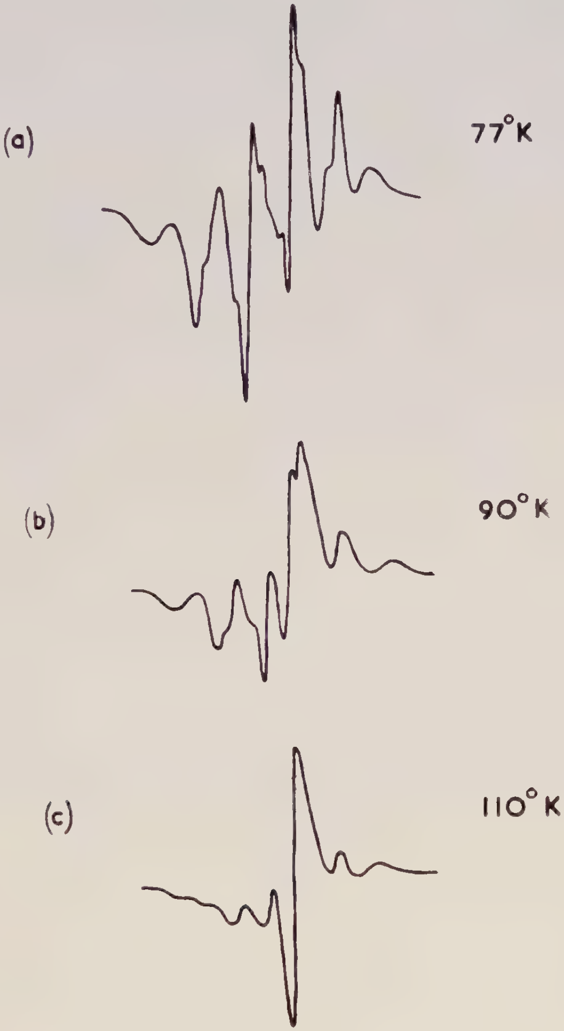

Figure 2. Spectra obtained from *n*-propanol at different temperatures. (*a*) 77°K, (*b*) 90°K, (*c*) 110°K.

The growth of the free-radical spectra and their change with time of irradiation was followed by sweeping through the resonance field value at regular intervals while the sample was continuously irradiated in the cavity at liquid air temperatures. In this way any warm-up due to transfer of the sample from an external irradiation dewar to the cavity can be avoided. Some of the *n*-propanol spectra were obtained by the older method of external irradiation, and the effect of this transient warming was noticeable.

3. RESULTS

The variation of the electron resonance spectrum with both time of irradiation and change of temperature has been studied. The results obtained with continuous irradiation of isopropanol at 110°K are shown in figure 1. These spectra were traced with about 10 min interval between each recording. It is seen that the signal initially appears as a single asymmetrical line (referred to below as type (*a*) spectrum) and then, as this grows in intensity, another more complex pattern appears until finally all the radicals have been converted into the second species with a seven-line spectrum (referred to as type (*b*)). It will be seen in the discussion below that the first species, (*a*), are most likely to be O*H radicals or molecules associated with O*H radicals, whereas the second species, (*b*), are $(CH_3)_2$ C*OH radicals.

If the specimen is then allowed to warm up slightly the seven-line spectrum transforms into a single asymmetrical line of 15 gauss width (referred to as type (*c*) spectrum). This further change on warming is also shown by the *n*-propanol spectra as shown in figure 2. Figure 2 (*a*) is that obtained from the *n*-propanol after prolonged irradiation at 77°K, and this can be interpreted [3] as due to the CH_3 C*H CH_2 OH radical. In this interpretation a different coupling constant is assumed for the CH_3, CH_2 and CH protons as might be expected if one of the CH_2C–H bonds always lies in the plane formed by CH_3 C*H CH_2. On the other hand such complex spectra usually have alternative interpretations, and the exact coupling constants cannot be deduced conclusively at the present stage. If the specimen is warmed up to 110°K however the spectrum changes as shown in figures 2 (*b*) and 2 (*c*), and a single asymmetrical line is seen to grow at the expense of the complex spectrum. It would therefore appear that this is another case in which a type (*b*) spectrum is changing into type (*c*). The possible origin of this last type of spectrum is discussed in detail below. All the spectra will, of course, disappear if the glass is warmed to a temperature near its melting point.

4. DISCUSSION

The possible types of radical reaction can be classified under the three headings of:

(1) *Photo-dissociation of hydrogen peroxide*

$$H_2O_2 + h\nu \rightarrow 2O^*H. \qquad (1)$$

This must be the first act of photolysis with the wavelengths that are employed.

(2) *Hydrogen abstraction by* O*H

$$(RH)OH + O^*H \rightarrow H_2O + R^*OH. \qquad (2)$$

It would appear from chemical evidence, as well as from a large number of electron resonance results, that the hydroxyl radical nearly always removes a proton attached to the carbon atom rather than that of the hydroxyl group.

In this context the term ‘O*H radical’ is used to cover any radical formed by molecular association with the OH radical. Thus, it cannot be categorically stated that the first type of spectrum is due to O*H itself, although it would appear that this simple species is the only one likely to have sufficient mobility in the glass at this temperature.

(3) *Molecular rearrangement*

This may take place as an inter-molecular rearrangement such as

$$\mathrm{R^*OH + (RH)OH \rightarrow (RH)OH + R^*OH}, \tag{3}$$

$$\mathrm{R^*OH + (RH)OH \rightarrow (RH)OH + RHO^*}, \tag{4}$$

or as an intra-molecular rearrangement

$$\mathrm{R^*OH \rightarrow RHO^*}. \tag{5}$$

Since the radicals are trapped in a solid phase of irregular structure these reactions will be restricted to the immediate neighbourhood of the radical, and are not likely to occur at the lower temperatures.

It is seen that the three different radical species $\mathrm{O^*H}$, $\mathrm{R^*OH}$, and $\mathrm{RHO^*}$ are produced by these reactions and it is suggested that these are the three species which give rise to the spectra of types (*a*), (*b*) and (*c*) respectively. It is not possible to say whether the asymmetrical line of the type (*a*) spectrum is due to $\mathrm{O^*H}$ itself or molecularly associated $\mathrm{O^*H}$ radicals. The spectra obtained from $\mathrm{O^*H}$ radicals in γ-irradiated solids [5] has a resolved hyperfine doublet, but the different trapping conditions may account for the broadened spectra in the present case. The asymmetry indicates that the electron is moving in an axially symmetric field and the resultant g-value variation and line width may smear out the hyperfine doublet due to the proton.

There is very little doubt that the type (*b*) spectrum is in fact due to the $\mathrm{R^*OH}$ radical and the seven-line spectrum with binomial intensity distribution clearly indicates an interaction with the six equally coupled protons of the two methyl groups [3]. The single symmetrical line of the type (*c*) spectra, which occurs at comparatively high temperatures, indicates that the unpaired electron is either localized at a position where there are no magnetic nuclei in its vicinity, or that molecular motion or electron transfer is taking place so rapidly that the hyperfine interaction is averaged to zero. The latter explanation appears to be unlikely in the solid phase and it would appear that the type (*c*) spectra are due to $\mathrm{RHO^*}$ type radicals. In this case the electron may be trapped in a relatively deep potential well at the oxygen atom, and this may also be responsible for the bleachable colour centre formed in these glasses and discussed by Livingston [6]. On the other hand it is possible that *inter*-molecular rearrangements can still take place at these temperatures, and it is impossible to rule out these effects completely on the basis of the present results.

If the temperature of the trapping medium is kept sufficiently low, however, the molecular rearrangements will not take place and only spectra of types (*a*) and (*b*) will be obtained. It is then possible to deduce quantitative expressions for the rate of radical formation and decay for the two species, and compare these predictions with those observed experimentally. This analysis is summarized below and compared with the isopropanol results shown in figure 1.

5. KINETIC ANALYSIS OF ISOPROPANOL RESULTS

If the number of hydrogen peroxide molecules initially added to the specimen is n_0, and n is the number at any time t after the start of the irradiation, the rate of decrease of the hydrogen peroxide molecules will be given by

$$-\frac{dn}{dt} = kn \tag{6}$$

where k is a constant of the photo-dissociation and depends on such parameters as the light intensity, geometry of the specimen in the cavity, and the like. The number of hydrogen peroxide molecules left after time t is therefore

$$n_{(t)} = n_0 \exp(-kt) \tag{7}$$

and the number of O*H radicals formed (n_a'), will be

$$n_a' = 2n_0[1 - \exp(-kt)]. \tag{8}$$

At the given time, t, a certain number of these will have reacted to form isopropanol radicals. Let this number be n_b, and hence the actual number of hydroxyl radicals present at the time t is $(n_a' - n_b)$. If the radical concentration is not high, so that radical–radical interaction is unlikely, the rate of formation of new isopropanol radicals can be taken as proportional to the number of hydroxyl radicals existing at that time, i.e. $(n_a' - n_b)$. Hence

$$\frac{dn_b}{dt} = k'(n_a' - n_b). \tag{9}$$

The constant k' of the reaction will probably vary somewhat depending on the detailed structure of each radical-trapping site, but to a first approximation an average value may be taken over all sites. Integration then gives

$$n_b = 2n_0 - \frac{2n_0}{k' - k} \cdot [k' \exp(-kt) - k \exp(-k't)] \quad \text{for} \quad k' \neq k \tag{10}$$

and

$$n_b = 2n_0 - 2n_0(1 + kt) \exp(-kt) \quad \text{for} \quad k' = k. \tag{11}$$

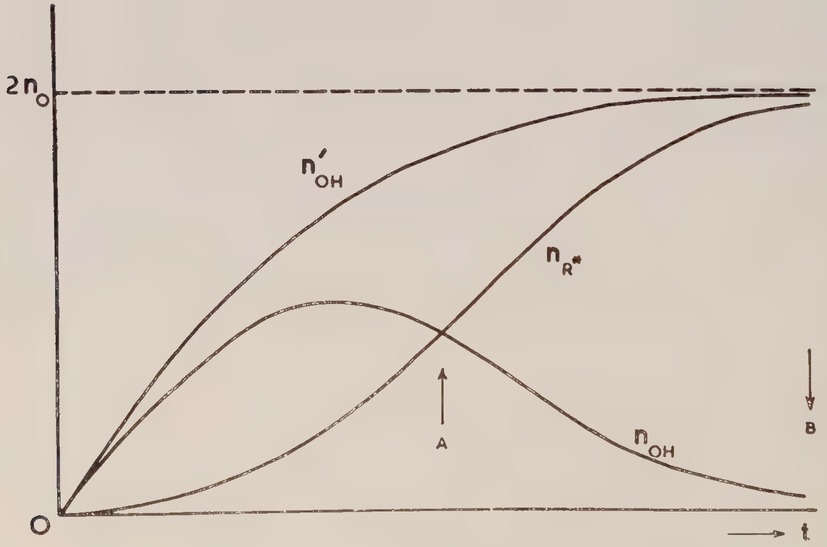

Figure 3. Variation of free-radical concentrations with time of irradiation, as predicted by first-order kinetics.

The predictions of these equations are summarized in figure 3 where the variation of n_a', n_b, and the actual number of OH radicals $n_a = (n_a' - n_b)$, are plotted against time. The actual units along the axes will depend on the values of k and k' for the particular experiment. These values may be determined in this instance by plotting the observed variation of n_a and n_b with time, and then making a best fit of the curves of figure 3 with that obtained experimentally.

In practice the intensity of the type (*b*) spectra can be measured more accurately since there is no overlap of its outer hyperfine peaks on the high field side with the type (*a*) spectrum. The intensity of these peaks may therefore be taken as proportional to the concentration of R*OH radicals present. The analysis of the results of figure 1 in this way is summarized in figure 4, where the intensity of the type (*b*) spectrum is plotted against time. Different values for k and k' are then substituted into the theoretical equations (10) or (11) and a best fit between the curves for n_b of figures 3 and 4 is obtained. The predicted curve for which $k' = 0{\cdot}04$ and $k = 0{\cdot}03\ \text{min}^{-1}$ is found to have a shape very close to that observed experimentally, but with a slight shift along the time axis, which is probably due to initial warm up period of the lamp. It would therefore appear that a simple theory based on first-order kinetics is a good approximation for free-radical formation in such frozen media. It would also appear that free radicals of the type R*OH can be studied in a very pure state if the irradiation is carried out for a sufficiently long time and the specimen is kept at a low enough temperature.

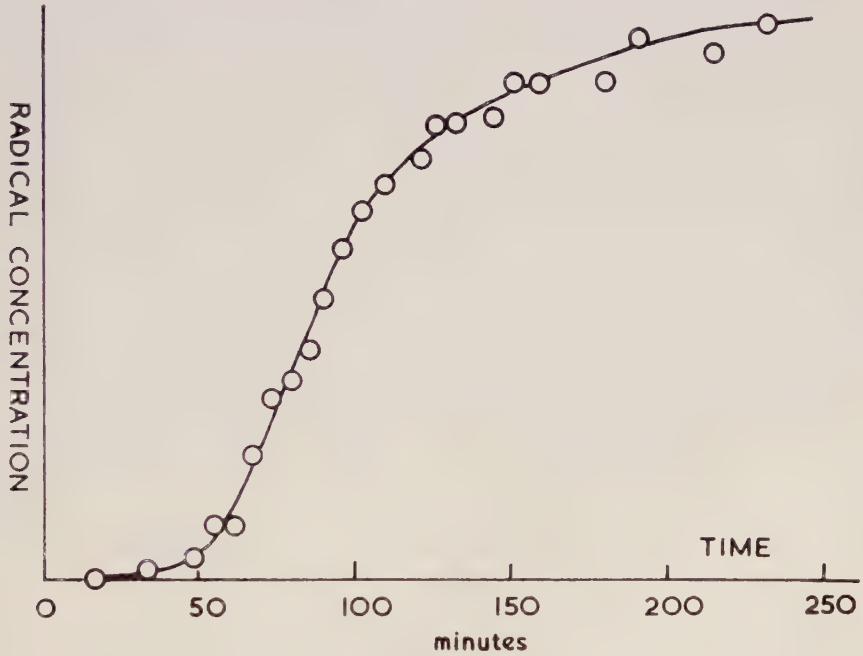

Figure 4. Experimentally observed variation of isopropanol radical concentration with time.

One of us (M. F.) would like to thank the British Council for the award of a scholarship during the time in which this work was carried out.

Le présent article décrit une série de mesures détaillées faites sur les spectres de résonance électronique de mélanges alcool-eau oxygénée irradiés par la lumière ultra-violette. On suit le changement dans les spectres avec le temps d'irradiation ainsi qu'avec la température, et on conclut que trois différents types de radicaux sont produits dans le milieu. On entreprend ensuite une analyse quantitative de l'apparition et de la disparition de ces différents corps et il est montré qu'il existe un bon accord avec un cinétique d'apparition et de disparition du premier ordre.

Eine Reihe ausführlicher Messungen der Elektronen-Resonanzspektren von Alkohol-Wasserstoffperoxyd-Gemischen bei UV-Bestrahlung wird beschrieben. Die Änderung der Spektren als Folge der Bestrahlungszeit, sowie der Temperatur wird verfolgt; und es wird geschlossen, dass drei verschiedene Radikalspezies auftreten. Die Bildung und der Zerfall der verschiedenen Spezies werden quantitativ analysiert; dabei wird gezeigt, dass die Kinetik von Bildung und Zerfall mit einem Geschwindigkeitsgesetz nach der ersten Ordnung gut übereinstimmt.

REFERENCES

[1] Ingram, D. J. E., Hodgson, W. G., Parker, C. A., and Rees, W. T., 1955, *Nature Lond.*, **176,** 1227.

[2] Gibson, J. F., Ingram, D. J. E., Symons, M. C. R., and Townsend, M. G., 1957, *Trans. Faraday Soc.*, **53,** 914.

[3] Fujimoto, M., and Ingram, D. J. E., 1958, *Trans. Faraday Soc.*, **54,** 1304.

[4] Ingram, D. J. E., 1958, *Free Radicals as studied by Electron Spin Resonance* (London: Butterworths), p. 81.

[5] Matheson, M. S., and Smaller, B., 1955, *J. chem. Phys.*, **23,** 521.

[6] Livingston, R., 1958, *Free Radical Stabilization* (Faraday Society Informal Discussion), p. 26.

Nuclear resonance spectrum of ortho bromoaniline

by S. CLOUGH†

Imperial Chemical Industries Limited, Dyestuffs Division, Hexagon House,
Blackley, Manchester, 9

(*Received* 22 *April* 1959)

The changes produced in the nuclear magnetic resonance spectrum of the ring protons of o-bromoaniline by the addition of acetone are found to be associated almost entirely with the decreased shielding of the proton ortho to the amino group. A series of spectra obtained with different amounts of acetone enables the spectral lines due to the individual protons to be identified and approximate values of the chemical shift and spin–spin coupling parameters to be deduced. These are used as a basis for a series of calculated spectra which progressively yield more accurate values of the parameters and finally a close agreement with the experimental spectrum. The dependence of the varying chemical shift upon acetone concentration is measured and discussed.

1. Introduction

Methods of analysis of high-resolution nuclear magnetic resonance spectra have been described for a number of arrangements of interacting nuclei [1, 2]. In most of the cases treated, features of molecular symmetry allow of some simplification. The ring proton spectrum of o-bromoaniline is representative of a more general type of problem. In this example four distinguishable ring protons are involved, each interacting with the other three.

With each proton may be associated a characteristic frequency $\nu_K = (\gamma H_0/2\pi)(1-\sigma_K)$ where γ is the proton gyromagnetic ratio, H_0 the applied magnetic field and σ_K the magnetic shielding constant of proton K. ν_K is the frequency at which proton K would resonate in the absence of spin interaction with other protons and it differs from the resonant frequency of a free proton by the chemical shift $(\gamma H_0/2\pi)\sigma_K$. There are six spin–spin interaction constants, J_{ij} being the magnitude of the interaction between protons i and j. Thus ten parameters are necessary to describe the spectrum completely.

The spin coupling constants connecting benzene ring protons are only slightly affected by substituents [3] and approximate values are

$$J_{\text{ortho}} = 8\text{ c/s} \quad J_{\text{meta}} = 2\text{ c/s} \quad J_{\text{para}} < 0{\cdot}5\text{ c/s}.$$

The main problem then is to find the four characteristic frequencies ν_K. However, the appearance of the spectrum depends on the relative magnitudes of the ν_K's only and so, in fact, only three parameters are involved.

There are two approaches. A general method [4] involves the measurement of the moments of the spectrum from which relationships connecting the characteristic frequencies ν_K are derived. Depending as it does on the precise measurement of areas beneath spectral lines, it is difficult to apply accurately, but it provides some information for the most intractable problem. For a complete solution, some more information is normally required leading to the assignment of at least some of the spectral lines to specific transitions. When this has been done, fairly accurate values of the characteristic frequencies and spin coupling constants may be obtained at once. With the resulting trial set of parameters the spectrum may be calculated and compared with the experimental spectrum. Further trial calculations with suitably adjusted parameters may be required before a satisfactory fit is achieved. The crucial step is the correlation of lines and transitions which depends upon correct interpretation of the basic pattern.

---

† Now at Physics Department, University College of North Wales, Bangor.

In the work described here, use has been made of the changes in the spectrum induced by the addition of acetone. These changes can be explained as a progressive modification of the magnetic shielding of the proton ortho to the NH_2 group. A similar solvent effect has been observed for pyridine [2], the lines of the α protons moving relative to those of the β and γ protons on dilution in carbon tetrachloride. In this case though, the groups of lines were already well separated and the effect did not contribute to the understanding of the spectrum.

2. EXPERIMENTAL

The spectra were obtained at room temperature using a high resolution spectrometer type V4300B made by Varian Associates, operating at 40 Mc/s.

The high resolution spectrum of the ring protons of o-bromoaniline is shown in the upper part of figure 1. On the addition of acetone the spectrum changes. A number of spectra with differing amounts of acetone were obtained; figures 2 and 3 are representative examples.

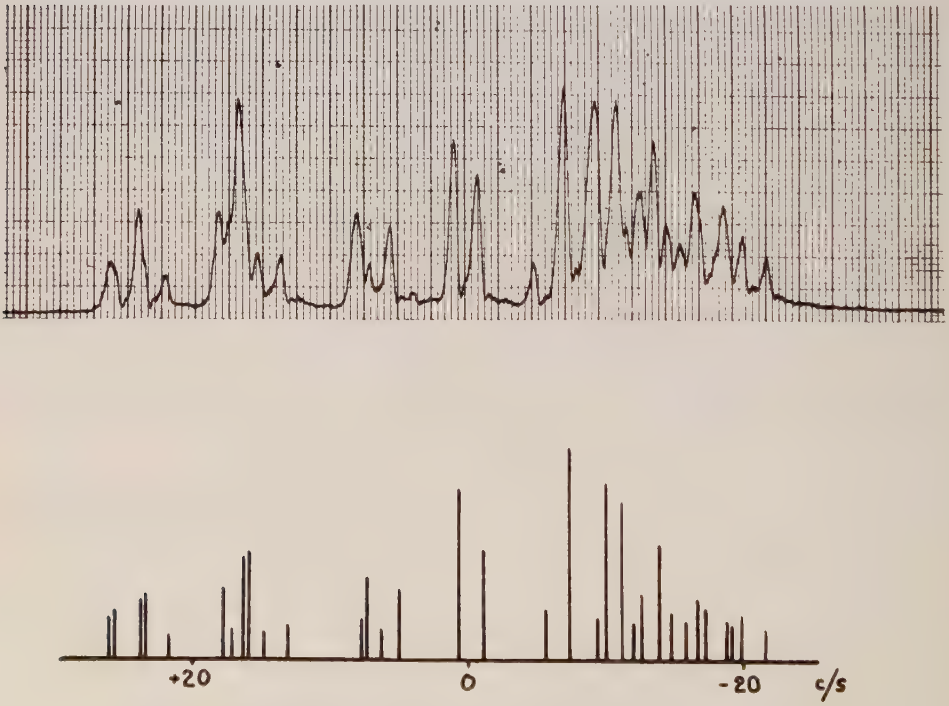

Figure 1. The ring proton spectrum of pure o-bromoaniline.

2.1. *Interpretation*

Let the ring protons be labelled cyclically A, B, C, D, denoting that proton ortho to the NH_2 group by A. Measurements on other benzene derivatives suggest that the effect of a substituent on the chemical shifts of ring protons is to influence an ortho proton rather more strongly than a para proton, and that an amino group tends to increase the shielding of ring protons whilst a bromine atom reduces the shielding. Consequently we may surmise that $\nu_A < \nu_C < \nu_B < \nu_D$. It is difficult, from figure 1 alone to proceed beyond this tentative step to the allocation of the lines to transitions.

The main features of the change illustrated by figures 2 and 3 can be explained on the assumption that only one parameter ν_A, is affected. This is plausible since the interaction between the o-bromoaniline and the acetone probably occurs at the NH_2 group. Once this is understood, figures 2 and 3 provide the necessary extra information for the interpretation of the spectra.

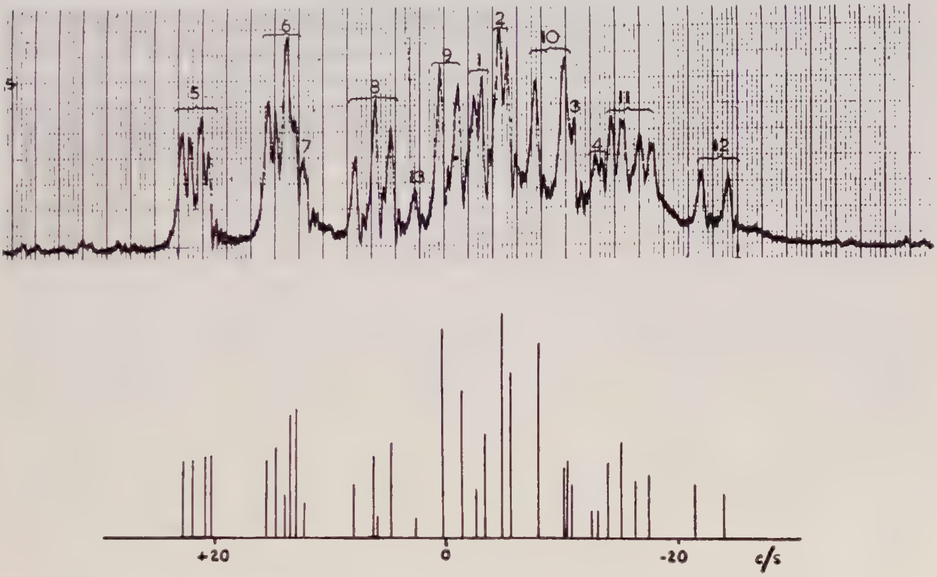

Figure 2. The ring proton spectrum of an acetone o-bromoaniline mixture: molar ratio = 0·6 : 1.

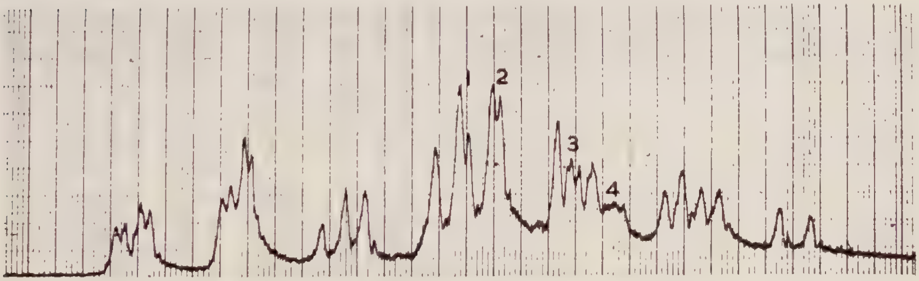

Figure 3. The ring proton spectrum of an acetone o-bromoaniline mixture: molar ratio = 0·9 : 1.

The value of ν_A can be varied over a range of about 12 c/s and the A lines, i.e. those lines which in first order correspond to inverting the spin of the A nucleus can easily be identified. Furthermore, the movement of the A lines uncovers other lines and by increasing the difference between ν_A and ν_C provides conditions under which the spectrum approaches more nearly to a first-order pattern. It then becomes possible to assign all the lines. This procedure can be followed from figure 2.

1. The lines marked 1, 2, 3, 4 in figure 2 can be seen to have moved against a more slowly changing background as the acetone concentration was varied. This is further illustrated by figure 3 which shows the effect of adding more acetone. The doublet 1 now overlaps the right-hand member of doublet 9 while doublet 3, which in figure 2 is partly obscured by one of the components of group 10, is now clear. The lines 1, 2, 3, 4 are therefore A lines. Corroboration of this assignment comes from the arrangement of the lines which is a recognizable approximation to the pattern expected on first-order considerations, although the relative intensities are very different. In addition the integrated intensity is measured to be approximately one quarter of that of the whole spectrum.

2. In figure 2 the groups 5 and 6 are revealed as D lines. The simplification of the spectrum of proton D compared with figure 1 is a consequence of the increase in the difference between ν_A and ν_C.

3. The allocation of the remaining lines is now clear, groups 7, 8 and 9 belonging to proton B and 10, 11 and 12 to proton C.

4. A first approximation for the characteristic frequency of each of the four nuclei is obtained by locating the centre of gravity of the corresponding spectral lines [4].

5. That more than two lines are resolved in group 8 indicates that proton B is not equally coupled to A and C. Approximately, $J_{AB}-J_{BC}=\pm 0{\cdot}5$ c/s. In the same way, the resolution of four lines in group 11 implies that $J_{BC}-J_{CD}=\pm 1$ c/s. The resolution of eight lines for both A and D enables J_{AD} to be measured. $J_{AD}=0{\cdot}3$ c/s.

With approximate values of all the parameters obtained from figure 2 and similar spectra with differing amounts of acetone, trial calculations were made until the spectra shown in the lower halves of figures 1 and 2 were obtained.

2.2. *Calculation of the spectra*

The calculation of the spectra follows upon well-established lines. The unknown eigenfunctions are expanded in terms of products of the individual nuclear spin functions. In the resulting secular determinant off-diagonal elements connecting product functions of different total spin are zero and in consequence it factorizes into two first-order, two fourth-order and one sixth-order determinants. The numerical solution of these determinants is a simple problem for a digital computer. In this work a Pegasus computer made by Ferranti Ltd. was used with a standard programme developed by Ferranti Ltd. for finding latent roots and vectors of matrices.

The centre of gravity of the complete spectrum is unaffected by spin coupling [4] and occurs at

$$\bar{\nu}=\frac{\nu_A+\nu_B+\nu_C+\nu_D}{4}.$$

The relative chemical shifts may be defined by the parameters

$$\delta_{BD}=\nu_B-\nu_D,$$

$$\delta_{AC}=\nu_A-\nu_C,$$

$$\delta=\frac{\nu_B+\nu_D}{2}-\frac{\nu_A+\nu_C}{2}.$$

Product function		Diagonal matrix elements H_{mm}	Off-diagonal elements H_{nm}
1_2	αααα	$2\bar{\nu}+\frac{1}{4}(J_{AB}+J_{AC}+J_{BC}+J_{AD}+J_{BD}+J_{CD})$	—
1_1	αααβ	$\bar{\nu}-\frac{1}{2}(\delta+\delta_{BD})+\frac{1}{4}(J_{AB}+J_{AC}-J_{AD}+J_{BC}-J_{BD}-J_{CD})$	$H_{12}=\frac{1}{2}J_{CD}$ $H_{13}=\frac{1}{2}J_{BD}$ $H_{14}=\frac{1}{2}J_{AD}$ $H_{23}=\frac{1}{2}J_{BC}$ $H_{24}=\frac{1}{2}J_{AC}$ $H_{34}=\frac{1}{2}J_{AB}$
2_1	ααβα	$\bar{\nu}+\frac{1}{2}(\delta-\delta_{AC})+\frac{1}{4}(J_{AB}-J_{AC}+J_{AD}-J_{BC}+J_{BD}-J_{CD})$	
3_1	αβαα	$\bar{\nu}-\frac{1}{2}(\delta-\delta_{BD})+\frac{1}{4}(-J_{AB}+J_{AC}+J_{AD}-J_{BC}-J_{BD}+J_{CD})$	
4_1	βααα	$\bar{\nu}+\frac{1}{2}(\delta+\delta_{AC})+\frac{1}{4}(-J_{AB}-J_{AC}-J_{AD}+J_{BC}+J_{BD}+J_{CD})$	
1_0	ααββ	$-\frac{1}{2}(\delta_{AC}+\delta_{BD})+\frac{1}{4}(J_{AB}-J_{AC}-J_{AD}-J_{BC}-J_{BD}+J_{CD})$	$H_{12}=\frac{1}{2}J_{BC}$ $H_{13}=\frac{1}{2}J_{AC}$ $H_{14}=\frac{1}{2}J_{BD}$ $H_{15}=\frac{1}{2}J_{AD}$ $H_{16}=0$ $H_{23}=\frac{1}{2}J_{AB}$ $H_{24}=\frac{1}{2}J_{CD}$ $H_{25}=0$ $H_{26}=\frac{1}{2}J_{AD}$ $H_{34}=0$ $H_{35}=\frac{1}{2}J_{CD}$ $H_{36}=\frac{1}{2}J_{BD}$ $H_{45}=\frac{1}{2}J_{AB}$ $H_{46}=\frac{1}{2}J_{AC}$ $H_{56}=\frac{1}{2}J_{BC}$
2_0	αβαβ	$-\delta\quad+\frac{1}{4}(-J_{AB}+J_{AC}-J_{AD}-J_{BC}+J_{BD}-J_{CD})$	
3_0	βααβ	$-\frac{1}{2}(\delta_{BD}-\delta_{AC})+\frac{1}{4}(-J_{AB}-J_{AC}+J_{AD}+J_{BC}-J_{BD}-J_{CD})$	
4_0	αββα	$+\frac{1}{2}(\delta_{BD}-\delta_{AC})+\frac{1}{4}(-J_{AB}-J_{AC}+J_{AD}+J_{BC}-J_{BD}-J_{CD})$	
5_0	βαβα	$+\delta\quad+\frac{1}{4}(-J_{AB}+J_{AC}-J_{AD}-J_{BC}+J_{BD}-J_{CD})$	
6_0	ββαα	$+\frac{1}{2}(\delta_{AC}+\delta_{BD})+\frac{1}{4}(J_{AB}-J_{AC}-J_{AD}-J_{BC}-J_{BD}+J_{CD})$	
1_{-1}	βββα	$-\bar{\nu}+\frac{1}{2}(\delta+\delta_{BD})+\frac{1}{4}(J_{AB}+J_{AC}-J_{AD}+J_{BC}-J_{BD}-J_{CD})$	$H_{12}=\frac{1}{2}J_{CD}$ $H_{13}=\frac{1}{2}J_{BD}$ $H_{14}=\frac{1}{2}J_{AD}$ $H_{23}=\frac{1}{2}J_{BC}$ $H_{24}=\frac{1}{2}J_{AC}$ $H_{34}=\frac{1}{2}J_{AB}$
2_{-1}	ββαβ	$-\bar{\nu}-\frac{1}{2}(\delta-\delta_{AC})+\frac{1}{4}(J_{AB}-J_{AC}+J_{AD}-J_{BC}+J_{BD}-J_{CD})$	
3_{-1}	βαββ	$-\bar{\nu}+\frac{1}{2}(\delta-\delta_{BD})+\frac{1}{4}(-J_{AB}+J_{AC}+J_{AD}-J_{BC}-J_{BD}+J_{CD})$	
4_{-1}	αβββ	$-\bar{\nu}-\frac{1}{2}(\delta+\delta_{AC})+\frac{1}{4}(-J_{AB}-J_{AC}-J_{AD}+J_{BC}+J_{BD}+J_{CD})$	
1_{-2}	ββββ	$-2\bar{\nu}+\frac{1}{4}(J_{AB}+J_{AC}+J_{AD}+J_{BC}+J_{BD}+J_{CD})$	—

Table 1. Matrix for the four proton system,

Rules for the calculation of matrix elements are given [1, 2]; the complete matrix for the A, B, C, D system is shown in table 1. The product functions are given in the order A, B, C, D, i.e. $\alpha\beta\beta\alpha$ stands for $A(\alpha)B(\beta)C(\beta)D(\alpha)$. They are numbered arbitrarily with suffixes to indicate the total spin quantum number.

The numerical solution of the secular determinant yields the energy levels and wave functions for the system, the latter being linear combinations of the product functions. All transitions are permitted for which the change in the total spin quantum number is one, giving fifty-six transitions in all. However, combination transitions for which the corresponding product functions for the two states differ in the spins of more than one nucleus are likely to be weak and can for most purposes be neglected. This leaves thirty-two transitions.

The intensity of a transition between states ψ_1 and ψ_2 may be written $[\psi_1 S \psi_2]^2$ where $S=1$ for terms involving a pair of product functions differing in the spin of one nucleus only, and is otherwise zero. The intensities are connected by certain simple relationships. Thus the total intensity of transitions from a spin $=1$ state to the six spin $=0$ states exceeds the intensity of the transition from 1_2 to the spin $=1$ state by 2 units. Since normally only three of the possible six above mentioned transition intensities are calculated, the remaining three being combination transitions, this relationship provides a check that the combination lines can be neglected. In both of the spectra presented here one combination line has a measurable intensity and is included in the calculations.

In general the intensities of lines change more slowly than the positions as chemical shift parameters are varied. Also, measurement of the intensities is less reliable. It is therefore unnecessary to calculate the intensities more than twice—with the original approximate set of parameters and again when the adjusted parameters give a satisfactory set of frequencies.

3. RESULTS

The relative chemical shifts of the four protons and the spin coupling constants are given in table 2. The former are expressed in terms of ν rather than σ so that the same units as are used for J may be employed. They may be transformed to field independent σ values expressed in p.p.m. by dividing by -40.

Molar ratio acetone : bromoaniline	$(\nu_A-\nu_C)$ c/s	$(\nu_B-\nu_C)$ c/s	$(\nu_D-\nu_C)$ c/s
0	−0·6	18·2	33·0
0·05	+0·5	18·5	32·5
0·2	+3·8	19·0	32·5
0·6	+7·6	19·2	32·0
0·9	+9·0	19·2	32·0
1·8	+10·8	19·2	32·0
2·5	+11·5	19·2	32·0

J c/s: $J_{AB}=7{\cdot}6$; $J_{BC}=7{\cdot}0$; $J_{CD}=7{\cdot}9$; $J_{AC}=1{\cdot}7$; $J_{BD}=1{\cdot}7$; $J_{AD}=0{\cdot}3$.

Table 2. Parameters for o-bromoaniline.

4. DISCUSSION

The variation of $(\nu_A - \nu_C)$ with the constitution of the mixture is expected to throw some light on the nature of the molecular interaction responsible for the change. When a proton alternates rapidly between two environments, in this case between bromoaniline in the free state and in interaction with acetone then the observed frequency is

$$\nu = \nu_X \cdot \frac{X}{Y} + \nu_Y \cdot \frac{Y-X}{Y} \tag{1}$$

where Y is the total number of moles of o-bromoaniline present and X/Y is the fraction interacting with acetone and where ν_X and ν_Y are frequencies characteristic of the free and complexed states. The consistency of (1) in this case was checked by measuring the shift of the NH_2 line, which followed within the limits of experimental error, a precisely similar variation to that of $(\nu_A - \nu_C)$ with an increase in magnitude of 2·5 times. The form of this variation may be used with (1) to check the validity of assumptions made about the equilibrium.

The simplest assumption—that the equilibrium involves a 1 : 1 complex—predicts a variation of frequencies which cannot be reconciled with the observations. Rather it is necessary to assume that each molecule of acetone may interact with at least two molecules of o-bromoaniline simultaneously. If interaction with a second molecule of bromoaniline occurs with the same facility as interaction with the first, the equilibrium constant may be defined by

$$k = \frac{2X(Z+Y-X)}{(2Z-X)(Y-X)} \tag{2}$$

where Z is the number of moles of acetone.

The closest agreement with the experimental results is obtained on this simple picture by choosing the values $k = 2{\cdot}5$ and $\nu_X - \nu_Y = 18$ c/s for insertion in equations (1) and (2). In order to check that the interaction did occur at the carbonyl group the experiment was repeated using pinacolin in place of acetone. The results were identical.

Les changements produits dans le spectre de résonance magnétique nucléaire des protons du cycle de l'o-bromoaniline, par addition d'acétone, sont presque entièrement associés à une diminution croissante de l'effet d'écran sur le proton en ortho du groupement NH_2. Grâce à une série de spectres obtenus pour des quantités différentes d'acétone, on a pu identifier les lignes spectrales individuelles des protons, et déduire la valeur approximative des paramètres de déplacement chimique et de couplage spin–spin. On les utilise comme base d'un calcul d'une série de spectres qui fournissent progressivement des valeurs de plus en plus précises des paramètres finalement en bon accord avec le spectre expérimental. On mesure la variation du déplacement chimique en fonction de la concentration en acétone et on la discute.

Das Kernresonanzspektrum der Ringprotonen in o-Bromanilin wird durch Zugabe von Azeton geändert. Es wird gefunden, dass diese Änderungen fast ausschliesslich auf die verringerte Abschirmung des zur Aminogruppe orthoständigen Protons zurückzuführen sind. Eine Reihe von Spektren mit verschiedenen Azetonmengen gestattet es, die Linien der einzelnen Protonen zu identifizieren und Näherungswerte für den Parameter der chemischen Verschiebung und der Spin–Spin-Koppelung abzuleiten. Diese Werte werden der Berechnung einiger Spektren zugrunde gelegt, wobei sich stets genauere Werte für die Parameter ergeben, bis schliesslich eine genaue Übereinstimmung mit dem gemessenen Spektrum erreicht wird. Die Abhängigkeit der veränderlichen chemischen Verschiebung von der Azetonkonzentration wird gemessen und diskutiert.

REFERENCES

[1] McCONNELL, H. M., McLEAN, A. D., and REILLY, C. A., 1955, *J. chem. Phys.*, **23**, 1152.
[2] BERNSTEIN, H. J., POPLE, J. A., and SCHNEIDER, W. G., 1957, *Canad. J. Chem.*, **35**, 65, 1060, 1487; 1958, *Ibid.*, **36**, 1302.
[3] RICHARDS, R. E., and SCHAEFER, T., 1958, *Trans. Faraday Soc.*, **54**, 1280.
[4] ANDERSON, W., and McCONNELL, H. M., 1957, *J. chem. Phys.*, **26**, 1496.

Ion-pair formation in thallous solutions: III

by R. P. H. GASSER and R. E. RICHARDS
Physical Chemistry Laboratory, South Parks Road, Oxford

(*Received* 13 *July* 1959)

Chemical shifts and spin–lattice relaxation times have been measured for the thallium resonance in solutions of thallous salts containing ferricyanide ions, and citrate ions. The results provide strong evidence that the ion-pairs which are formed in these strong solutions are of a predominantly electrostatic character.

1. INTRODUCTION

In an earlier paper [1] the chemical shifts of the nuclear resonance of the thallous ion in various solutions were described. The shifts were interpreted in terms of the formation of ion-pairs and some evidence was obtained that in the ion-pair, the thallous atom is predominantly ionic.

A more sensitive method of detecting covalency in these ion-pairs is to study the chemical shifts of the thallium resonance when the anion is paramagnetic. In this case, if there is any appreciable covalency in the ion-pair, some unpairing of the thallous electrons would occur, causing its magnetic shielding to be greatly reduced and the resonance to shift strongly to lower applied fields. This effect on a chemical shift has been found by Shulman and Jaccarino [2] in crystalline manganous fluoride. The fluorine resonance is strongly shifted (by about 8 per cent) to lower applied fields, because some electron transfer occurs from the fluoride ion to the manganous ion, causing partial unpairing of the fluoride electrons and so transferring to the fluorine some paramagnetic influence. The shifts observed in this compound are about 100 times greater than the chemical shifts found in diamagnetic fluorine compounds [3]. Chemical shifts of ^{205}Tl resonance in solutions containing thallous ions and ferricyanide or citrate ions have therefore been recorded. The spin–lattice relaxation times also provide further information about the ion-pairs.

2. EXPERIMENTAL

The spectra were obtained with the apparatus described previously [4], but using a Varian 12 in. electromagnet. The magnetic field homogeneity was such as to give a thallium resonance line width over the sample volume used of about 50 c/s. With these relatively narrow lines the instrument was operated so that the phase sensitive detector output recorded the absorption curves directly from the modulation side bands, the centre resonance being suppressed [5].

The relaxation times were obtained by the method of progressive saturation using the calibrator with the Pound Watkins spectrometer. The H_1 field was calibrated assuming that $T_1 = T_2$ in the solutions for which the line widths were greater than the magnetic field inhomogeneity.

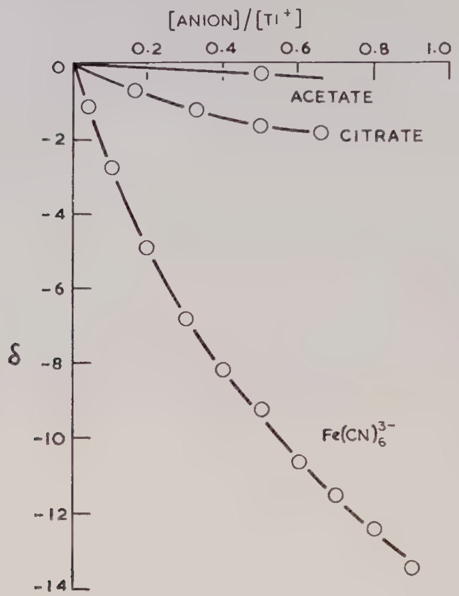

Figure 1.

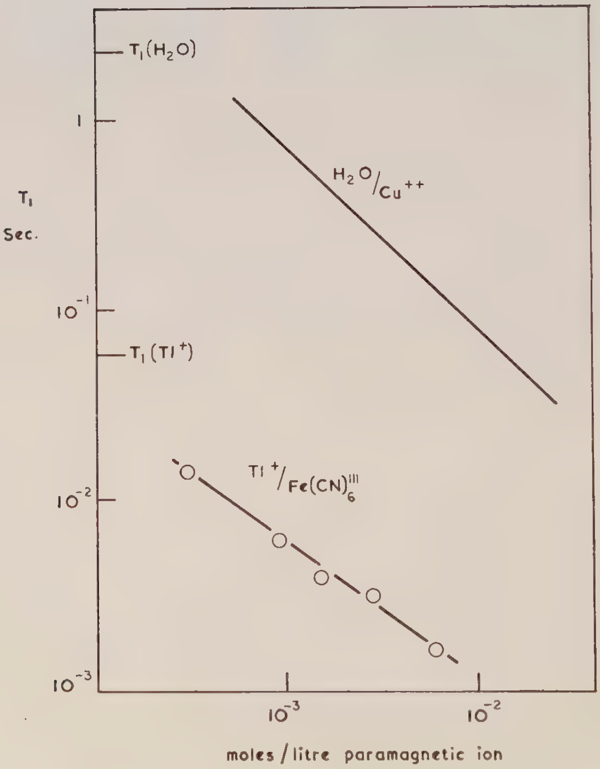

Figure 2.

3. Results

The results of the chemical shift measurements are shown in figure 1. The thallous concentration was maintained at 0·3M and the chemical shift, δ, is defined as

$$\delta = \frac{H_{\text{samp.}} - H_{\text{ref.}}}{H_{\text{ref.}}} \times 10^4 \dagger$$

where $H_{\text{samp.}}$ is the field of the sample resonance at a frequency of 22·6000 Mc/s and $H_{\text{ref.}}$ is the resonant field at the same frequency of a 0·3 M solution of thallous nitrate. Unfortunately thallous ferrocyanide is too insoluble for a comparison to be made.

The values of the spin–lattice relaxation times of the thallium resonances in the solutions containing ferricyanide ions are given in figure 2.

4. Discussion

4.1. *Chemical shifts*

The chemical shifts produced by addition of ferricyanide ions are larger than for the other anions studied previously, by a factor of about 20. This greater effect is probably due mainly to the stronger electric field set up at the thallous ion by the triply charged ferricyanide ion; it is not as great as would be expected for a significant covalency between the thallous and ferricyanide ions. The effect of the citrate ion on the thallous chemical shift is about five times as large as for the acetate, and it would certainly be expected that the ferricyanide ion would produce a much greater shift than this. The observed effects of addition of paramagnetic ferricyanide ions cannot therefore be regarded as significantly greater than would be expected for a similar diamagnetic anion.

4.2. *The ion-pair equilibrium*

The quantitative interpretation of the chemical shifts of the thallium resonance in 0·3 M thallous solutions to which potassium ferricyanide is added, is rather different from that used to explain the earlier experiments. In this case there are present in the solution as well as thallous and ferricyanide ions, not only thallous ferricyanide ion pairs, but also potassium ferricyanide ion pairs [6]. The concentration of thallous ferricyanide ion pairs therefore depends on the relative values of the constants K_1 and K_2 for the equilibria

$$\mathrm{Tl}^+ + \mathrm{Fe(CN)_6}''' \rightleftharpoons \mathrm{TlFe(CN)_6}'', \tag{1}$$

$$\mathrm{K}^+ + \mathrm{Fe(CN)_6}''' \rightleftharpoons \mathrm{KFe(CN)_6}''. \tag{2}$$

The value of K_2 has been found by James and Monk [6] to be 16·6. The concentration of the ion pair $\mathrm{TlFe(CN)_6}''$ in the solutions studied can be calculated as a function of the molar ratio of total ferricyanide to thallous for various assumed values of K_1. In figure 3 this result is illustrated for various values of K_1/K_2 and the values of δ for the thallium resonances are plotted on the same graph. The value of K_1/K_2 is therefore found to be about 4, so that K_1 has the approximate value of 68. In these calculations, the activity coefficients have been assumed to be constant because according to Davies' equation [7] the activity coefficient of a given ion varies only slightly over the concentration range used.

---

† Note that the sign convention used in this paper for chemical shift is opposite to that used in Paper I [1].

The chemical shifts in the solutions of thallous and ferricyanide can therefore be explained plausibly in terms of the formation of ion pairs in which there is no significant covalency.

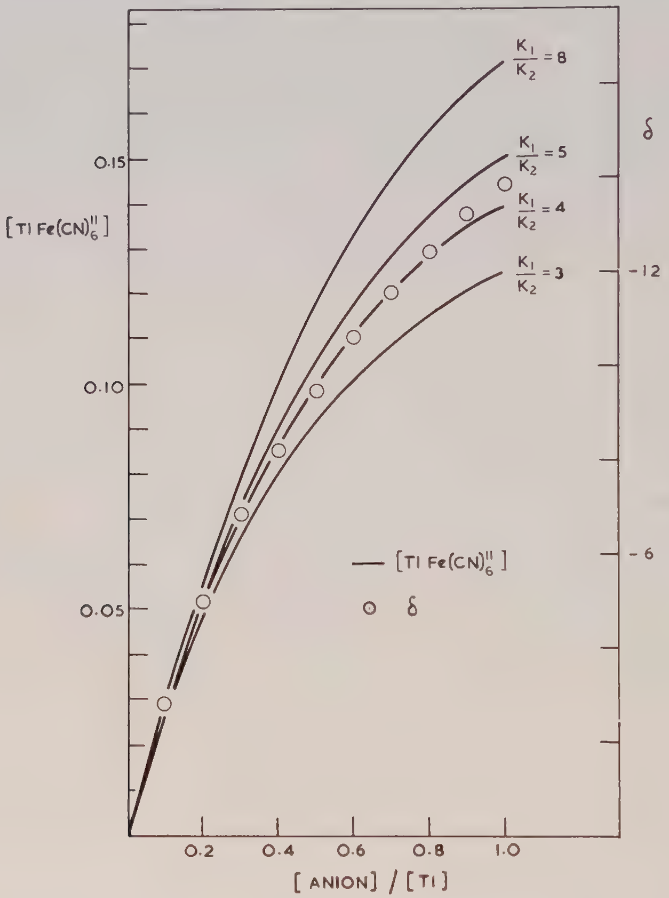

Figure 3.

4.3. *Spin–Lattice relaxation*

Still further evidence is provided by the spin lattice relaxation times of the thallium nuclei in some of these solutions. In figure 2 the values of T_1 obtained for the thallous solutions are plotted against the molar concentration of added paramagnetic ion and compared with the results obtained by Bloembergen, Purcell and Pound [8] for the spin lattice relaxation times of the protons in solutions of cupric ions. The behaviour of the cupric solutions was explained by Bloembergen, Purcell and Pound without invoking any electron transfer, and it is clear that the variation of the spin–lattice relaxation time in the thallous solutions is closely similar. If any significant electron exchange did occur, very much larger changes in the spin lattice relaxation times would be expected. In the case of the copper resonance in the cuprochloride ion [9] addition of the paramagnetic cuprichloride ion causes a large change in the relaxation times. McConnell and Weaver [9] estimate that the contribution of electron exchange between cuprous and cupric ions to the spin–spin relaxation time is about 2×10^{-5} sec when the molar concentration of cupric ion is 10^{-3}. This effect is very much greater than is observed for the thallous solutions described above.

5. Conclusion

These further experiments give no indication that there is any covalency in the thallous ion-pairs studied. The forces holding the ions together must therefore be predominantly electrostatic.

We are grateful to Dr. P. A. H. Wyatt for many helpful discussions. We also thank the Department of Scientific and Industrial Research, the Hydrocarbon Research Group of the Institute of Petroleum, and the National Coal Board for grants in aid of apparatus. We are grateful to the Department of Scientific and Industrial Research for a maintenance grant to one of us (R. P. H. G.).

On a mesuré les déplacements chimiques et les temps de relaxation spin-réseau dans la résonance nucléaire du thallium pour des solutions de sels thalleux contenant des ions ferricyanure et des ions citrate. Les résultats indiquent fortement que les paires d'ions qui se forment dans ces solutions concentrées ont surtout un caractère électrostatique.

Chemische Verschiebungen und Spin-Gitter-Relaxationszeiten wurden für die Thalliumresonanz in Thallosalzlösungen bestimmt, die Ferrizyanid- und Zitrationen enthielten. Die Ergebnisse lassen es als sehr wahrscheinlich erscheinen, dass die in diesen starken Lösungen gebildeten Ionenpaare üperwiegend elektrostatischen Charakter besitzen.

References

[1] Freeman, R., Gasser, R. P. H., Richards, R. E., and Wheeler, D. H., 1959, *Mol. Phys.*, **2,** 75.
[2] Shulman, R. G., and Jaccarino, V., 1957, *Phys. Rev.*, **108,** 1219.
[3] Connick, R. E., and Poulson, R. E., 1959, *J. Phys. Chem.*, **63,** 568.
[4] Freeman, R., Murray, G., and Richards, R. E., 1957, *Proc. roy. Soc.* A, **242,** 455.
[5] Pound, R. V., 1957, *Rev. sci. Instrum.*, **28,** 966; Primas, H., 1958, *Helv. phys. Acta*, **31,** 17.
[6] James, J. C., and Monk, C. B., 1950, *Trans. Faraday Soc.*, **46,** 1041.
[7] Davies, C. W., 1938, *J. chem. Soc.*, p. 2093.
[8] Bloembergen, N., Purcell, E., and Pound, R. V., 1948, *Phys. Rev.*, **73,** 679.
[9] McConnell, and Weaver, 1956, *J. chem. Phys.*, **25,** 307.

The Jahn–Teller effect in manganic acetylacetonate

by A. FORMAN and L. E. ORGEL
Department of Theoretical Chemistry, University Chemical Laboratory,
Lensfield Road, Cambridge

(*Received* 7 *June* 1959)

The infra-red spectra of the tris-acetylacetonates of chromium, manganese, iron and aluminium have been measured as far as 400 cm^{-1}. The nature of the bands due to vibrations involving motion of the oxygen atoms relative to the metal is consistent with the operation of the Jahn–Teller mechanism in the manganic compound.

1. Introduction

The molecular point group of a simple tris-acetylacetonate complex (figure 1) is D_3; that is such a complex has much less symmetry than a regular octahedral complex. In the group D_3 the t_{2g} d orbitals of an octahedrally coordinated metal ion split into two groups, one doubly degenerate and the other non-degenerate, while the e_g orbitals are not split. In our discussion we shall neglect the splitting, and the mixing of the two doubly degenerate orbitals, and continue to refer loosely to the t_{2g} and e_g orbitals, meaning by this the d_{xy}, d_{xz} and d_{yz} orbitals on the one hand and the $d_{x^2-y^2}$ and d_{z^2} orbitals on the other [1]. The justification for this is that the arrangement of oxygen atoms around the metal is known to be quite close to regular octahedral in ferric acetylacetonate [2], and hence the deviations of the true orbitals from those given here should not be very great.

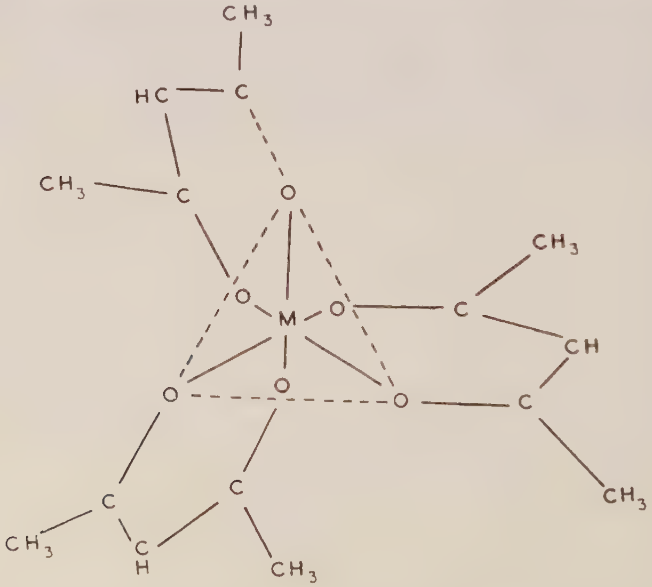

Figure 1. Structure of a metal tris-acetylacetonate emphasizing the threefold axis.

The electronic configurations of the acetylacetonates of Cr^{3+}, Mn^{3+} and Fe^{3+} are known to be of high-spin type from magnetic susceptibility studies [3]. The electron assignments are therefore $(t_{2g})^3$, $(t_{2g})^3(e_g)^1$ and $(t_{2g})^3(e_g)^2$ respectively. The Jahn–Teller theorem shows that of these ions the Mn^{3+} alone is susceptible to appreciable Jahn–Teller distortion. Analogy with octahedral compounds of Cr^{3+}, Mn^{3+} and Fe^{3+} suggests that the Cr^{3+} and Fe^{3+} compounds will have the undistorted D_3 structure while Mn^{3+} might be strongly distorted [4] perhaps, but not necessarily, to give four short bonds in a plane. Furthermore since the e_g orbital is antibonding, we may expect the Fe–O bonds to be substantially weaker than the Cr–O bonds, and the average Mn–O bond strength to be intermediate between these extremes.

Since the acetylacetonates are neutral complexes which form molecular crystals and are readily soluble in organic solvents they provide an unusually favourable system in which to look for evidence of Jahn–Teller distortions by means of infra-red spectroscopy.

2. Results

The infra-red spectra of the acetylacetonates of Cr^{3+}, Mn^{3+}, Fe^{3+} and Al^{3+} are very similar in the region above 650 cm^{-1}, except that the bands of the Mn^{3+} compound tend to be a little broader than those of the others. In the region below 650 cm^{-1} there are substantial differences [5], as may be seen both from the crystal spectra (figures 2–3) and the solution spectra (figures 4–5).

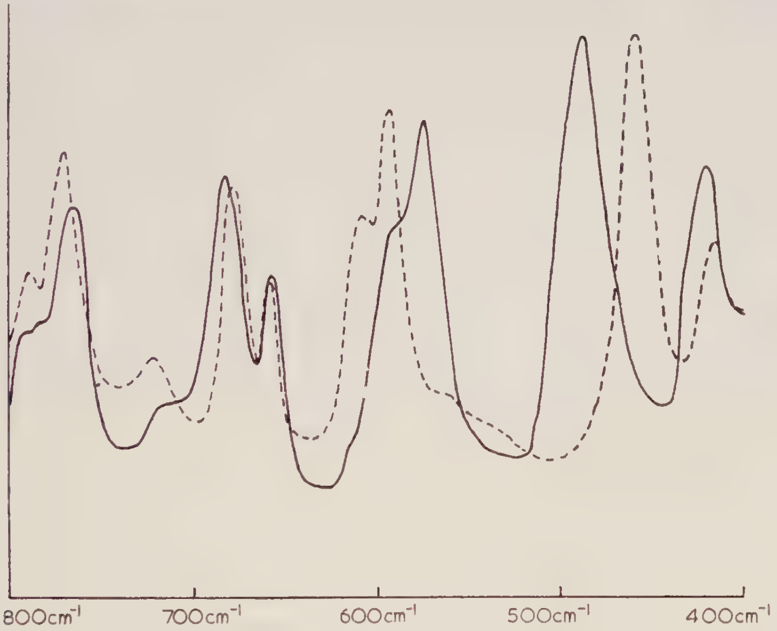

Figure 2. The infra-red spectra of aluminium acetylacetonate (solid line); chromium acetylacetonate (dotted line).

In the region close to 600 cm^{-1} the chromic compound has a sharp peak at 593 cm^{-1} with a shoulder at 607 cm^{-1}, while the ferric compound has a sharp doublet of 559 cm^{-1} and 550 cm^{-1}. The manganic complex has two much

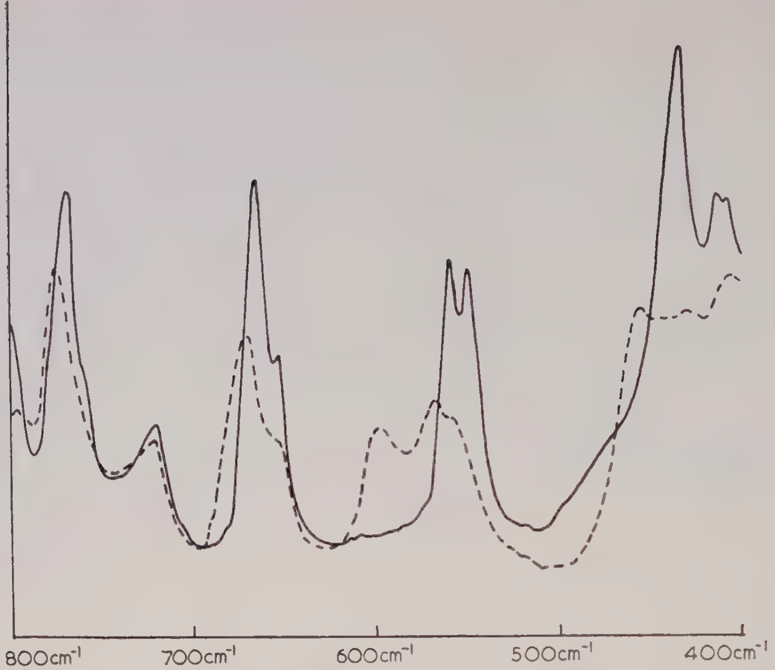

Figure 3. The infra-red spectra of ferric acetylacetonate (solid line); manganic acetylacetonate (dotted line).

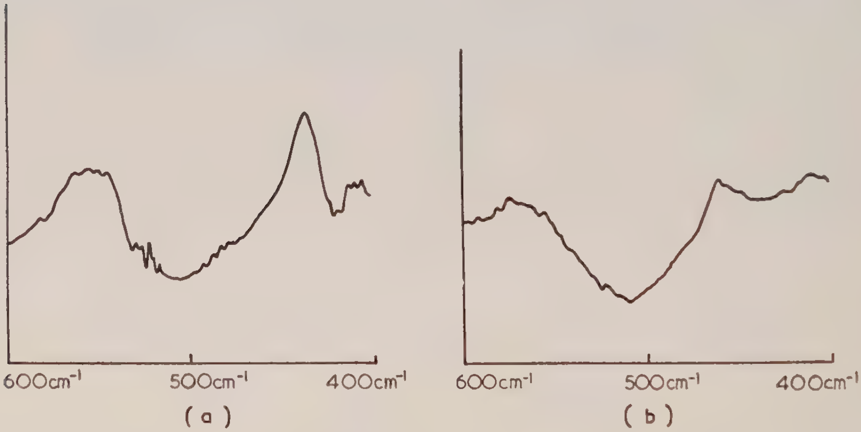

(a)

(b)

Figure 4. The infra-red spectra of CCl_4 solutions of (*a*) ferric acetylacetonate; (*b*) manganic acetylacetonate.

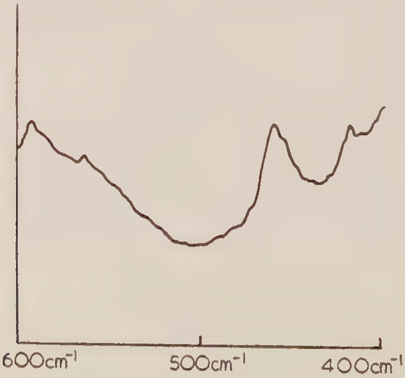

Figure 5. The infra-red spectrum of a CCl_4 solution of chromic acetylacetonate.

broader peaks with maxima at 600 cm^{-1} and 570 cm^{-1}. The aluminium complex has a corresponding band at 585 cm^{-1}.

At somewhat lower wave-numbers the Cr^{3+} and Fe^{3+} compounds have peaks at 458 and 435 cm^{-1} respectively, followed by somewhat weaker peaks at 415 cm^{-1} and 420 cm^{-1}, respectively. The Mn^{3+} compound has quite a different spectrum with strong, almost continuous, absorption from about 460–400 cm^{-1} with slight peaks at 457 cm^{-1}, 432 cm^{-1} and 407 cm^{-1}. The corresponding bands of the Al^{3+} compound are at 487 and 418 cm^{-1}.

3. DISCUSSION

The only bands in the infra-red spectrum which are markedly different in the Fe^{3+} and Cr^{3+} acetylacetonates are the doublets at 550–600 cm^{-1} and the single peaks at about 450 cm^{-1}. In both cases they are at higher frequencies in the Cr^{3+} than in the Fe^{3+} compounds, as would be expected if they involve motions of the oxygen atoms relative to the metal. The exact nature of the transitions however is by no means obvious for they might correspond to either metal–oxygen stretching motions or to bending motions of the six-membered rings which change the O–M–O bond angles. The former assignment has been proposed for the 487 cm^{-1} band of aluminium acetylacetonate [5].

We do not feel able to make any definite assignment of these bands, but think that the balance of the evidence favours the view that the 450 cm^{-1} transition does indeed contain a large contribution from the metal–oxygen stretching frequency. (The most important evidence is the occurrence of the corresponding band in the Al^{3+} compound at higher frequencies than in the Cr^{3+} compound. Since the bond is hardly likely to be stronger we feel that this high frequency must be due in part to the lower mass of the Al^{3+} ion. In the case of the band at about 550 cm^{-1} the Al^{3+} compound is intermediate between those of Cr^{3+} and Fe^{3+}. If these interpretations are correct the frequency of the stretching vibration is less sensitive to the nature of the metal than is the frequency of the bending motion. This is rather surprising, but perhaps we are over-simplifying in trying to assign the bands to independent stretching and bending motions, for the normal modes may involve both types of motion.)

Whatever the detailed interpretation of the two metal-sensitive regions, the consequences of an appreciable Jahn–Teller effect in the Mn^{3+} compound should be to complicate this part of the spectrum. In fact the spectrum of the crystalline Mn^{3+} compound is remarkably like a superposition of the Cr^{3+} and Fe^{3+} spectra, a finding which is completely consistent with the operation of the Jahn–Teller mechanism, but which could not have been predicted from it.

In Cr^{3+} the antibonding e_g orbitals are unoccupied whereas in Fe^{3+} they are half filled, resulting in the Fe–O bonds being weaker than the Cr–O bonds. In Mn^{3+} there is only one electron in the two antibonding orbitals. If these are split by a Jahn–Teller distortion then four of the bonds will be as strong as in Cr^{3+} and the remaining two weak as in Fe^{3+} (or vice versa with two strong and four weak depending on the direction of the distortion), since the antibonding electron is in one of the orbitals only. For a large Jahn–Teller splitting the Mn^{3+} infra-red spectrum should therefore resemble closely a superposition of the spectra of Cr^{3+} and Fe^{3+}.

The Jahn–Teller splitting in the crystal could arise either from an intrinsic instability of manganic acetylacetonate molecules to distortion or, alternatively, from a cooperative interaction between otherwise stable manganic acetylacetonate molecules which reveals a latent tendency to distortion. That the former is the case is suggested by the comparison of the solution spectra in figures 4–5 with the crystal spectra. Unfortunately the solution spectra are insufficiently resolved to settle this point unambiguously.

4. EXPERIMENTAL

Chromic [6], manganic [7] and aluminium [8] tris-acetylacetonates were prepared by methods described in the literature. The same method was used for the preparation of the ferric tris-acetylacetonate as that used for aluminium tris-acetylacetonate.

Analyses

	Calc.		Found	
$AlC_{15}H_{21}O_6$	C 55·55	H 6·49	C 55·51	H 6·36
$CrC_{15}H_{21}O_6$	C 51·57	H 6·02	C 52·1	H 6·38
$MnC_{15}H_{21}O_6$	C 51·15	H 5·97	C 51·22	H 5·99
$FeC_{15}H_{21}O_6$	C 51·01	H 5·97	C 51·47	H 6·20

Infra-red spectra were run in nujol mulls for the solids and in carbon tetrachloride solution using a Perkin Elmer Model 21 spectrophotometer with KBr optics.

On a mesuré les spectres infra-rouges des tris-acetylacétonates de chrome, manganèse, fer, et aluminium, jusqu'à 400 cm^{-1}. Dans le composé manganique, la nature des bandes dues aux vibrations qui mettent en jeu le mouvement des atomes d'oxygène par rapport au metal est en accord avec l'existence d'un mécanisme de Jahn et Teller.

Die Infrarotspektren der Tris-Azetylazetonate von Chrom, Mangan, Eisen und Aluminium wurden bis zu 400 cm^{-1} vermessen. Die Art derjenigen Banden, die von solchen Schwingungen herrühren, bei denen sich die Sauerstoffatome relativ zum Metall bewegen, ist mit der Wirkung eines Jahn–Teller-Mechanismusses in der Manganverbindung vereinbar.

REFERENCES

[1] GRIFFITH, J. S., and ORGEL, L. E., 1957, *Quart. Rev.*, **11**, 381.
[2] ROOF, R. B., 1956, *Acta Cryst.*, **9**, 791.
[3] JARRETT, H. S., 1957, *J. chem. Phys.*, **27**, 1928.
[4] DUNITZ, J. D., and ORGEL, L. E., 1957, *J. Phys. Chem. Solids*, **3**, 20.
[5] NAKAMOLO, P. J., MCCARTHY, P. J., and MARTELL, A. E., 1959, *Nature, Lond.*, **183**, 459.
[6] MOELLER, T., 1957, *Inorganic Syntheses*, **5**, 130 (New York: McGraw-Hill).
[7] CARTLEDGE, J. S., U.S. Pat. No. 2556316.
[8] FERNELIUS, F. C., 1946, *Inorganic Syntheses*, **2**, 25 (New York: McGraw-Hill.)

A determination of the electronegativity parameter in molecular orbital calculations on heteronuclear molecules containing nitrogen

by ALF LOFTHUS

Department of Physics, University of Oslo, Blindern, Oslo, Norway

(*Received* 1 *June* 1959)

Using the semi-empirical LCAO molecular orbital method, the electronegativity parameter δ for nitrogen has been chosen to give reasonable fit between computed and 'correct' bond orders for a series of heterocyclic molecules. A δ-value of about 0·9–1·0 has been found for nitrogen in six-membered rings, and about 1·8–2·0 for pyrrole.

1. INTRODUCTION

Whereas the semi-empirical LCAO molecular orbital method has successfully been applied to conjugated hydrocarbons, this has not always been the case for heteronuclear molecules. One of the main problems in using this method to heteronuclear molecules is how to make reliable estimates of the dependence of the Coulomb integral on the particular type of heteroatom under consideration. This dependence is usually expressed by

$$\alpha = \alpha_0 + \delta\beta_0$$

where α_0 is a standard Coulomb integral (usually for carbon), and β_0 the resonance integral for some standard bond (usually CC), here used as energy unit, and δ the parameter here referred to as the 'electronegativity parameter'. The problem is then reduced to that of finding consistent δ-values for the heteroatoms for as many molecules as possible.

One way of doing this is to make guesses based on considerations of some atomic electronegativity scale, for instance the Pauling scale [1]. δ-values from 0·5 to 2·0 have thus been proposed [2–5]. Another way of doing it is to choose parameters to give reasonable fit between computations and some measurable quantity. Thus δ-values from 0·6 to 1·0 have been found to reproduce the observed dipole moment of pyridine [6–7].

The purpose of the present investigation is, by using the semi-empirical LCAO molecular orbital method including overlap, to try to choose a value for the electronegativity parameter δ for nitrogen such as to give reasonable fit between calculated and 'correct' bond orders for the heterocyclic series pyridine, pyridazine, pyrimidine, pyrazine, triazine and pyrrole. Such an investigation might be possible due to the recent high precision bond distance measurements of several important organic molecules, giving better bond order/bond length relations.

Because the results to some extent must be dependent on the particular way of using the LCAO molecular orbital method, and on the assumptions made in the course of calculations, we shall first outline in some detail the method as it is used here, and make out the choice of other parameters.

2. METHOD OF CALCULATION

The present calculations are restricted to the π-electron system only. Each of the π-electrons of the conjugated molecule is supposed to move in a molecular orbital ψ of the type

$$\psi = \sum_i c_i \phi_i$$

where the ϕ_i's are the atomic 2pπ orbitals. The energies of the electron levels are then given by the roots of the secular equation

$$|H_{ij} - S_{ij}E| = 0,$$

where

$$E = \int \psi^* H \psi \, d\tau; \quad H_{ii} = \int \phi_i^* H \phi_i \, d\tau = \alpha_{ii};$$

$$H_{ij} = H_{ji} = \int \phi_i^* H \phi_j \, d\tau = \gamma_{ij};$$

$$S_{ij} = S_{ji} = \int \phi_i^* \phi_j \, d\tau; \quad S_{ii} = 1.$$

Introducing the quantities

$$\beta_{ij} = \gamma_{ij} - \tfrac{1}{2} S_{ij} (\alpha_{ii} + \alpha_{jj}),$$
$$x_{ij} = \tfrac{1}{2}(\alpha_{ii} + \alpha_{jj}) - E,$$

such that

$$\gamma_{ij} - S_{ij}E = \beta_{ij} + S_{ij}x_{ij},$$

the secular equation then takes the form

$$|\beta_{ij} + S_{ij}x_{ij}| = 0.$$

In order to take into account the dependence of β_{ij} on bond lengths, we assume $\beta_{ij} = \rho_{ij}\beta_0$, where the parameter ρ_{ij} is supposed to be of the form [8]

$$\rho_{ij}(r) = S_{ij}(r)/S_0(1{\cdot}397),$$

where $S_{ij}(r)$ is the overlap integral between two atoms of arbitrary distance, $S_0(1{\cdot}397)$ the overlap integral for a CC bond in benzene, and β_0 the resonance integral for the same bond.

The different electronegativities for various atoms are accounted for by introducing the parameter δ defined by the expression

$$\alpha_{kk} = \alpha_0 + \delta_{kk}\beta_0$$

such that

$$\begin{aligned} x_{ij} &= \tfrac{1}{2}(\alpha_{ii} + \alpha_{jj}) - E \\ &= \tfrac{1}{2}(\alpha_0 + \delta_{ii}\beta_0 + \alpha_0 + \delta_{jj}\beta_0) - E \\ &= x_0 + \tfrac{1}{2}(\delta_{ii} + \delta_{jj})\beta_0 \end{aligned}$$

where

$$x_0 = \alpha_0 - E.$$

In these calculations we have assumed that α has the same value for all carbon atoms in the system; i.e. $\delta_C = 0$, but that α for the nitrogen atom is equal to, or larger than that of carbon, i.e. $\delta_N \geqslant 0$ (nitrogen is electronegative with respect to carbon). The calculations were performed for three values of δ, namely, 0, 1·0 and 2·0.

Slater atomic orbitals were used, and the appropriate values of the overlap integrals were taken from existing tables [9]. Overlap between non-neighbour atoms only was neglected.

Bond type	Bond order	Bond distance
C–C	1	1·543 [11]
C=C	2	1·335 [12]
C≡C	3	1·207 [13]
CC (benzene)	5/3	1·397 [14]
C–N	1	1·474 [15]
C=N	2	1·274 †
C≡N	3	1·157 [16]
N–N	1	1·47 [17]
N=N	2	1·25 [17]
N≡N	3	1·098 [18]

† Assumed.

Table 1. Reference points for bond order curves.

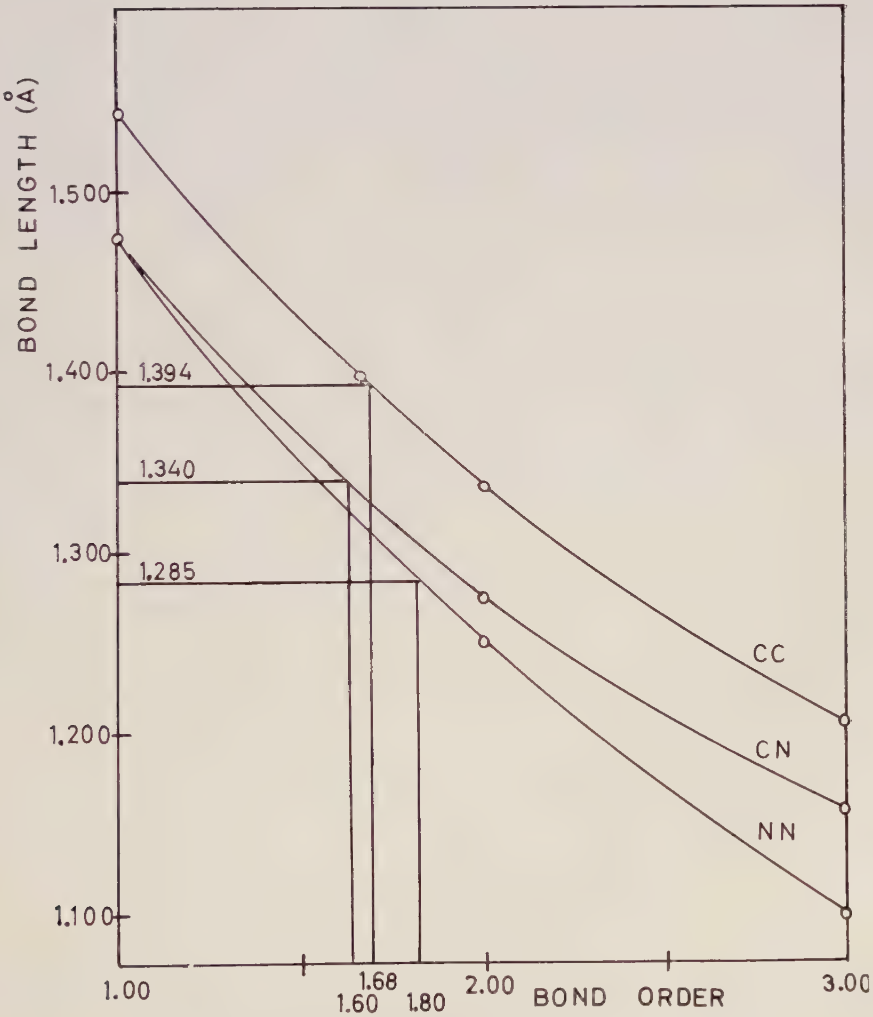

Bond order/bond length curves for CC, CN and NN bonds.

Having found the energy values, the coefficients c_i of the MO's can readily be evaluated from the formula

$$\sum_j c_i(H_{ij} - S_{ij}E) = 0, \qquad j = 1, 2, 3, \ldots, n.$$

Since heteroatomic molecules are considered, it is found that the Chirgwin–Coulson [10] definition of the total bond order is the appropriate one to use:

$$P_{ij} = 1 + \tfrac{1}{2} \sum_{\nu} n_{\nu}(c_{\nu i}y_{\nu j} + c_{\nu j}y_{\nu})$$

where

$$y_{\nu i} = \sum_j S_{ij}c_{\nu j} \quad (\nu \text{ indicates a MO}).$$

3. Results

On the basis of the reference points given in table 1, bond order/bond length curves have been constructed for CC, CN, and NN bonds (figure 1). From these curves the 'correct' bond orders listed in table 2 were found.

	Bond type	Bond distance [19]	'Correct' bond order	Calculated bond order		
				$\delta = 0$	$\delta = 1$	$\delta = 2$
Pyridine						
	CN	1·340	1·60	1·661	1·613	1·511
	C(2)C(3)	1·394	1·68	1·691	1·686	1·696
	C(3)C(4)	1·394	1·68	1·661	1·662	1·655
Pyridazine						
	NN	1·285	1·80	1·667	1·780	1·829
	CN	1·340	1·60	1·663	1·556	1·495
	C(3)C(4)	1·394	1·68	1·677	1·723	1·739
	C(4)C(5)	1·394	1·68	1·652	1·629	1·624
Pyrimidine						
	N(1)C(2)	1·340	1·60	1·672	1·627	1·542
	N(3)C(4)	1·340	1·60	1·656	1·600	1·489
	C(4)C(5)	1·394	1·68	1·672	1·670	1·668
Pyrazine						
	CN	1·340	1·60	1·655	1·643	1·593
	CC	1·394	1·68	1·689	1·623	1·525
Triazine						
	CN	1·340	1·60	1·667	1·613	1·518
Pyrrole						
	CN	1·379	1·40	1·615	1·496	1·385
	C(2)C(3)	1·367	1·83	1·702	1·788	1·841
	C(3)C(4)	1·446	1·40	1·590	1·531	1·486

The NN distance 1·285 Å in pyridazine is assumed. The CN and CC distances in the rest of the series are assumed to be the same as in pyridine except for pyrrole.

Table 2. 'Correct' and calculated bond orders for various values of the electronegativity parameter δ.

The calculated bond orders for various values of δ are also listed in table 2. It is seen that the best fit with the 'correct' bond orders for a δ-value of about 1·0 for six-membered rings, and about 2·0 or a little less for pyrrole.

It must be noted that the present results are found using β_0 as the resonance integral for a CC bond in benzene as standard (1·397 Å). If another bond is used as standard, the present δ-values must be multiplied by $S(1{\cdot}397)/S_0(r)$. Thus, if the pure double bond is taken as standard ($r = 1{\cdot}335$ Å), this factor becomes 0·9. In this case the electronegativity parameter will be 0·9 instead of 1·0.

En employant la méthode des orbitales moléculaires LCAO semi-empirique, on a choisi le paramètre d'electronegativité δ de l'azote afin d'obtenir un accord raisonnable entre les indices de liaison calculés et les indices ' corrects ' pour une série de molécules hétérocycliques. On trouve une valeur δ d'environ 0,9–1,0 pour l'azote dans les cycles à six atomes, et d'environ 1,8–2,0 pour le pyrrole.

Mit Hilfe der halbempirischen LCAO Methode zur Berechnung von Molecular Orbitals wird der Elektronegativitätsparameter δ für Stickstoff so angepasst, dass die abgeschätzten Bindungsordnungen für eine Reihe heterozyklischer Molekeln gut mit den ' richtigen ' Bindungsordnungen übereinstimmen. Für Stickstoff in sechsgliedrigen Ringen wird ein δ-Wert von etwa 0,9–1,0 gefunden, für Pyrrol 1,8–2,0.

REFERENCES

[1] PAULING, L., 1948, *The Nature of the Chemical Bond.* (Ithaca, N.Y.: Cornell University Press).

[2] WHELAND, G. W., and PAULING, L., 1935, *J. Amer. chem. Soc.*, **57**, 2086.

[3] LONGUET-HIGGINS, H. C., and COULSON, C. A., 1947, *Trans. Faraday Soc.*, **43**, 87.

[4] NORDHEIM, G. P., and SPONER, H., 1952, *J. chem. Phys.*, **20**, 285.

[5] JAFFÉ, H. H., 1955, *J. Amer. chem. Soc.*, **77**, 4448.

[6] ORGEL, L. E., COTTRELL, T., DICK, W., and SUTTON, L., 1951, *Trans. Faraday Soc.*, **47**, 113.

[7] LÖWDIN, P. O., 1951, *J. chem. Phys.*, **19**, 1333.

[8] MULLIKEN, R. S., 1949, *J. Chim. phys.*, **46**, 675.

[9] MULLIKEN, R. S., RIEKE, C. A., ORLOFF, D., and ORLOFF, H., 1949, *J. chem. Phys.* **17**, 1248.

[10] CHIRGWIN, B. H., and COULSON, C. A., 1939, *Proc. roy. Soc.* A, **169**, 413.

[11] HANSEN, G. E., and DENNISON, D. M., 1952, *J. chem. Phys.*, **20**, 215.

[12] BARTELL, L. S., and BONHAM, R. A., 1957, *J. chem. Phys.*, **27**, 1414.
ALLEN Jr., H. C., and PLYLER, E. K., 1958, *J. Amer. chem. Soc.*, **80**, 2673.

[13] CALLOMON, J. H., and STOICHEFF, B. P., 1957, *Canad. J. Phys.*, **35**, 373.

[14] LANGSETH, A., and STOICHEFF, B. P., 1956, *Canad. J. Phys.*, **34**, 350.

[15] LIDE, D. R., 1957, *J. chem. Phys.*, **27**, 343.
COX, E. G., and JEFFREY, G. A., 1951, *Proc. roy. Soc.* A, **207**, 110.

[16] WESTENBERG, A. A., and WILSON, E. B., 1950, *J. Amer. chem. Soc.*, **72**, 199.

[17] ORVILLE-THOMAS, W. J., 1957, *Chem. Rev.*, **57**, 1179.

[18] LOFTHUS, A., 1956, *Canad. J. Phys.*, **34**, 780.

[19] Pyridine: BAK, B., HANSEN-NYGAARD, and RASTRUP-ANDERSEN, J., 1958, *J. mol. Spectroscopy*, **2**, 361.
Pyrrole: BAK, B., CHRISTENSEN, D., HANSEN, L., and RASTRUP-ANDERSEN, 1956, *J. chem. Phys.*, **24**, 720.
Triazine: LANCASTER, J. E., and STOICHEFF, B. P., 1956, *Canad. J. Phys.*, **34**, 1016.

Application of the principle of corresponding states to the viscosity and diffusion of pure liquids and mixtures

by G. THOMAES and J. VAN ITTERBEEK
Faculty of Science, University of Brussels, Belgium

(*Received* 17 *January* 1959)

An attempt is made to establish a theorem of corresponding states for the viscosity and diffusion of pure liquids and solutions, based on Prigogine's theory of solutions. The agreement between theory and the little available experimental data is satisfactory.

---

1. INTRODUCTION

The coefficient of viscosity binding the pressure tensor to the velocity gradient has the dimension $M^{1/2}E^{1/2}L^{-2}$. The coefficient of isothermal diffusion binding the flow of matter to the concentration gradient has the dimension $M^{-1/2}E^{1/2}L$.

We shall use the following assumptions:

(1) the molecules are simple: monatomic or spherical,

(2) the potential energy of a pair of molecules can be represented by means of a universal function ϕ together with two parameters ϵ^* and r^*:

$$\epsilon(r)=\epsilon^*\phi(r/r^*)$$

where ϵ^* and r^* are the coordinates of the interaction curve minimum,

(3) the molecular species is characterized only by the three parameters ϵ^*, r^* and the mass m, without the introduction of internal parameters.

Then we can reduce the coefficient of viscosity and diffusion by means of ϵ^*, r^* and m to obtain quantities which are independent of the chemical nature of the molecule. The reducing factors are:

$$\text{for } \eta: \quad Z=(m\epsilon^*)^{1/2}r^{*-2},$$
$$\text{for } D: \quad \kappa=\epsilon^{*1/2}r^*m^{-1/2}.$$

The reduced functions $\tilde{\eta}=\eta Z^{-1}$ and $\tilde{D}=D\kappa^{-1}$, being dimensionless functions, can only depend on dimensionless quantities. In the case of very simple liquids —monatomic molecules and globular substances—we can suppose that

$$\tilde{\eta}=\tilde{\eta}(\tilde{p},\tilde{v},\tilde{T}) \quad \text{and} \quad \tilde{D}=\tilde{D}(\tilde{p},\tilde{v},\tilde{T})$$

where

$$\left.\begin{aligned} \tilde{p}&=pr^{*3}/\epsilon^*,\\ \tilde{v}&=vr^{*-3},\\ \tilde{T}&=kT/\epsilon^*. \end{aligned}\right\} \tag{3}$$

If we assume that the liquids are described by an equation of state $\tilde{v}=\tilde{v}(\tilde{p},\tilde{T})$, we can reduce the number of variables to two, for example $\tilde{p}$ and $\tilde{T}$.

Furthermore, since the experiments are carried out at saturation pressure, we have a relation between $\tilde{p}$ and $\tilde{T}$. Hence

$$\tilde{\eta}=\tilde{\eta}(\tilde{T}) \quad \text{and} \quad \tilde{D}=\tilde{D}(\tilde{T}). \tag{4}$$

Thus, we can hope to check these relations by computing the molecular parameters from the experimental data.

2. DETERMINATION OF THE MOLECULAR PARAMETERS FROM THE EXPERIMENTAL DATA

Very few experiments have been carried out with liquids which fulfil the theorem of corresponding states for the viscosity of simple liquids.

First, we notice that

$$\frac{1}{T}\frac{d\ln\eta}{d(1/T)}=\frac{1}{\tilde{T}}\frac{d\ln\tilde{\eta}}{d(1/\tilde{T})}. \tag{5}$$

For simple liquids, we have to a first approximation

$$d\ln\eta/d(1/T)\simeq\text{constant } C \tag{6}$$

then $C/T=\tilde{C}/\tilde{T}$ where $\tilde{C}$ is a universal constant

$$\tilde{C}=Ck/\epsilon^*. \tag{7}$$

For two liquids A and B, taking A as the reference compound, we have

$$\frac{C_{\mathrm{AA}}}{C_{\mathrm{BB}}}=\frac{\epsilon_{\mathrm{BB}}{}^*}{\epsilon_{\mathrm{AA}}{}^*}=1+\delta\dagger \tag{8}$$

in which $\epsilon_{\mathrm{AA}}{}^*=$ minimum of the interaction curve A–A,
$\epsilon_{\mathrm{BB}}{}^*=$,, ,, ,, ,, ,, B–B,

and

$$\delta=\frac{\epsilon_{\mathrm{BB}}{}^*-\epsilon_{\mathrm{AA}}{}^*}{\epsilon_{\mathrm{AA}}{}^*}. \tag{9}$$

Furthermore,

$$\eta_{\mathrm{AA}}(T_{\mathrm{AA}})=Z_{\mathrm{AA}}\tilde{\eta}_{\mathrm{AA}}(\tilde{T}_{\mathrm{AA}}). \tag{10}$$

At the same reduced temperature

$$\tilde{T}_{\mathrm{AA}}=\tilde{T}_{\mathrm{BB}} \quad \text{or} \quad T_{\mathrm{BB}}=T_{\mathrm{AA}}(1+\delta) \tag{11}$$

we obtain

$$\frac{\eta_{\mathrm{BB}}[T_{\mathrm{AA}}(1+\delta)]}{\eta_{\mathrm{AA}}(T_{\mathrm{AA}})}=\left(\frac{m_{\mathrm{B}}}{m_{\mathrm{A}}}\right)^{1/2}(1+\delta)^{1/2}(1+\rho)^{-2} \tag{12}$$

with

$$\rho=(r_{\mathrm{BB}}{}^*-r_{\mathrm{AA}}{}^*)r_{\mathrm{AA}}{}^{*-1}. \tag{13}$$

Then

$$1+\rho=\frac{r_{\mathrm{BB}}{}^*}{r_{\mathrm{AA}}{}^*}=\left\{\frac{\eta_{\mathrm{AA}}(T_{\mathrm{AA}})}{\eta_{\mathrm{BB}}[T_{\mathrm{AA}}(1+\delta)]}\right\}^{1/2}\left(\frac{m_{\mathrm{B}}}{m_{\mathrm{A}}}\right)^{1/4}(1+\delta)^{1/4}. \tag{14}$$

We notice that the determination of the parameters $\epsilon_{\mathrm{BB}}{}^*/\epsilon_{\mathrm{AA}}{}^*$ can be made at once, while $(1+\rho)$ depends on the choice of $(1+\delta)$. If $(d\ln\eta/d(1/T))$ is not a constant, but a function of T, $f(T)$, we can expand it in powers of T and if we restrict ourselves to first-order terms, we obtain

$$\delta=[f_{\mathrm{BB}}(T_{\mathrm{AA}})/f_{\mathrm{AA}}(T_{\mathrm{AA}})-1]\left[1-\left(\frac{\partial f}{\partial T}\right)_{T_{\mathrm{BB}}}\frac{T_{\mathrm{A}}}{f_{\mathrm{AA}}(T_{\mathrm{AA}})}\right]^{-1}. \tag{15}$$

Tables 1 and 2 summarize the results obtained from (8) for some simple liquids, taking argon as the reference compound for liquefied gases, and cyclohexane for more complex substances. For comparison, we give the same parameters computed from critical data.

---

† In the following, we adopt the notation of I. Prigogine (*Molecular Theory of Solutions*, North-Holland Publishing Company, Amsterdam: 1957) in which the quantities like X_i refer to the component i in solution and X_{ii} to the pure component i.

	From (8)	From critical data and $B(T)$
A	1·00	1·00
CO	0·91	0·89
N_2	0·91	0·84
O_2	0·83	0·97
CH_4	1·01	1·20

Table 1. Molecular parameters $\epsilon_{BB}^*/\epsilon_{AA}^*$. Reference compound: argon.

	From (8)	From critical data and $B(T)$
C_6H_{12}	1·00	1·00
CCl_4	0·83	1·00
$C(CH_3)_4$	0·82	0·77
C_6H_6	0·84	1·02
CH_4	0·20	0·30

Table 2. Molecular parameters $\epsilon_{BB}^*/\epsilon_{AA}^*$. Reference compound: cyclohexane.

Tables 3 and 4 show several determinations of $(1+\rho)$: the results in the first column are obtained from (8) and (14), those in the second column from (14) and the value of $(1+\delta)_{crit}$.

	From (8) and (14)	From (14) and $(1+\delta)_{crit}$	From $B(T)$
A	1·00	1·00	1·00
N_2	1·15	1·03	1·08
CO	1·05	1·02	1·10
O_2	0·85	1·04	1·05

Table 3. Molecular parameters r_{BB}^*/r_{AA}^*. Reference substance: argon.

	From (8) and (14)	From (14) and $(1+\delta)_{crit}$	From $B(T)$
C_6H_{12}	1·00	1·00	1·00
CCl_4	0·73	1·09	0·97
$C(CH_3)_4$	1·13	0·99	1·17
C_6H_6	0·75	1·16	0·87

Table 4. Molecular parameters r_{BB}^*/r_{AA}^*. Reference substance: cyclohexane.

Those in the third column are deduced from the second virial coefficient $B(T)$. We conclude that simple compounds (except for methane) satisfy roughly the principle of corresponding states. It would be interesting to verify these relations by more precise measurements carried out under the conditions required by the theory.

In the case of isothermal diffusion, the molecular parameters of the mixture ϵ_i^* and r_i^* are the measured quantities, even for self-diffusion.

We obtain $\epsilon_A^*/\epsilon_B^* = C_A'/C_B'$ where C_A' and C_B' are the slopes of the curve $\ln D$ versus $1/T$, and

$$\frac{r_A^*}{r_B^*} = \frac{D_B[T_A\,\epsilon_B^*/\epsilon_A^*]}{D_A[T_A]}\left(\frac{\epsilon_A^*}{\epsilon_B^*}\right)^{1/2}\left(\frac{m_B}{m_A}\right).$$

ϵ_A^*, ϵ_B^*, r_A^* and r_B^* are evaluated from the molecular theory of solutions

$$\left.\begin{aligned}
\epsilon_A^*/\epsilon_{AA}^* &= 1 + x_B(-\delta^2/8 + \delta/2 - 9\rho^2 x_A),\\
\epsilon_B^*/\epsilon_{AA}^* &= 1 + \delta + x_A(-\delta^2/8 - \delta/2 - 9\rho^2 x_B),\\
r_A^*/r_{AA}^* &= 1 + \tfrac{1}{2}\rho x_B[1 + (-\delta^2/8 + \delta/2)x_A + 17/4\ \rho x_A],\\
r_B^*/r_{BB}^* &= 1 + \rho - \tfrac{1}{2}\rho x_A[1 + (-\delta^2/8 - \delta/2)x_B - 17/4\ \rho x_B],
\end{aligned}\right\} \tag{16}$$

where x_i is the mole fraction of the component i.

3. THE VISCOSITY OF MIXTURES

Here, we need a kinetic scheme to establish the law of the viscosity of the mixtures. From Eyring's scheme,

$$\eta = \frac{fd}{k_\tau \bar{\lambda}} \tag{17}$$

where d = mean distance between two layers, $\bar{\lambda}$ = mean distance between two equilibrium positions, k_τ = the number of times a molecule crosses the potential barrier, f = force per cm^2.

If $d \simeq \bar{\lambda}$ then $\eta = f/k_\tau = v^{-2/3}(2\pi mkT)^{1/2}\exp(\Delta F^*/RT)$. If we assume that the displacements of the molecules A and B are independent, the fluidity of the mixture is

$$\varphi_m = \frac{k_{\tau_A} x_A}{f} + \frac{k_{\tau_B} x_B}{f} = x_A v_A^{2/3}(2\pi m_A kT)^{-1/2}\exp(-\Delta F_A^*/RT)$$
$$+ x_B v_B^{2/3}(2\pi m_B kT)^{-1/2}\exp(-\Delta F_B^*/RT) = x_A\varphi_A + x_B\varphi_B, \tag{18}$$

where φ_A = fluidity of A in the mixture, φ_B = fluidity of B in the mixture. For a pure liquid A, we have

$$\varphi_{AA}(T_{AA}) = Z_{AA}^{-1}\tilde{\phi}(\tilde{T}_{AA}) \quad \text{where} \quad Z_{AA} = \frac{(m_A\epsilon_{AA}^*)^{1/2}}{r_{AA}^{*2}}. \tag{19}$$

On the other hand, for the same compound in a mixture, we have

$$\varphi_A(T_A) = Z_A^{-1}\tilde{\varphi}(\tilde{T}_A) \quad \text{where} \quad Z_A = \frac{(m_A\epsilon_A^*)^{1/2}}{r_A^{*2}} \tag{20}$$

then

$$\varphi_A = \varphi_{AA}\,\frac{Z_{AA}}{Z_A}\,\frac{\tilde{\varphi}(\tilde{T}_A)}{\tilde{\varphi}(\tilde{T}_{AA})}. \tag{21}$$

At the same reduced temperature $\tilde{T}_A = \tilde{T}_{AA}$, we obtain

$$\varphi_A = \left(\frac{\epsilon_{AA}^*}{\epsilon_A^*}\right)^{1/2}\left(\frac{r_A^*}{r_{AA}^*}\right)^2 \varphi_{AA}(T_{AA}) \quad \text{where} \quad T_{AA} = T_A\,\epsilon_{AA}^*/\epsilon_A^*. \tag{22}$$

We conclude that the partial fluidity of A in a solution at temperature T is equal to the fluidity of the pure component A at a temperature T_{AA} times a factor determined by the theory of solutions.

The parameters ϵ_i^* and r_i^* are functions of the parameters δ and ρ, and the mole fraction. By means of (18–22) we thus can calculate the viscosity of a solution from the knowledge of the viscosities of the pure components [1].

We have checked these relations for the following solutions: C_6H_{12}–CCl_4, C_6H_6–CCl_4 and C_6H_{12} C_6H_6 [2], and CCl_4–$C(CH_2)_4$ [3]. Tables 5 and 6 give the values of the partial fluidity calculated from (22) and the values $(\varphi_m - \varphi_m^*)$ which is the difference between experimental (or theoretical) values and the linear expression

$$\varphi_m^* = \varphi_{AA} x_A + \varphi_{BB} x_B.$$

$A(C_6H_{12})$–$B(CCl_4)$

$(1+\delta)=1{\cdot}00$, $(1+\rho)=0{\cdot}98$, $T=298{\cdot}2°K$

x_A	$\varphi_{exp.}$	$\varphi_{th.}$	φ_A	φ_B	$(\varphi-\varphi^*)_{exp.}$	$(\varphi-\varphi^*)_{th.}$
0·000	1·108	1·111	—	1·111	0·000	0·00
0·230	1·153	1·145	1·284	1·111	+0·040	+0·03
0·471	1·167	1·113	1·091	1·133	+0·049	+0·02
0·728	1·165	1·118	1·113	1·133	+0·042	+0·01
1·000	1·129	1·113	1·113	—	0·000	0·00

$A(CCl_4)$–$B(C_6H_6)$

$(1+\delta)=1{\cdot}02$, $(1+\rho)=0{\cdot}96$, $T=298{\cdot}2°K$

x_A	$\varphi_{exp.}$	$\varphi_{th.}$	φ_A	φ_B	$(\varphi-\varphi^*)_{exp.}$	$(\varphi-\varphi^*)_{th.}$
0·000	1·668	1·659	—	1·659	0·000	0·00
0·235	1·503	1·509	1·024	1·659	−0·033	−0·01
0·483	1·360	1·400	1·089	1·692	−0·035	0·00
0·777	1·206	1·264	1·111	1·799	−0·025	+0·03
1·000	1·109	1·111	1·111	—	0·000	0·00

$A(C_6H_{12})$–$B(C_6H_6)$

$(1+\delta)=1{\cdot}02$, $(1+\rho)=0{\cdot}92$. $T=298{\cdot}2°K$

x_A	$\varphi_{exp.}$	$\varphi_{th.}$	φ_A	φ_B	$(\varphi-\varphi^*)_{exp.}$	$(\varphi-\varphi^*)_{th.}$
0·000	1·667	1·659	—	1·659	0·000	0·00
0·215	1·742	1·555	1·046	1·695	+0·191	+0·01
0·451	1·663	1·522	1·068	1·894	+0·239	+0·11
0·756	1·405	1·392	1·218	1·930	+0·145	+0·15
1·000	1·129	1·113	1·113	—	0·000	0·00

Table 5.

Examination of the tables shows that in most cases the agreement is fairly satisfactory, if one keeps in mind the uncertainty of the experimental data. Indeed, the lack of precise measurements on simple solutions studied under the above conditions makes it difficult to state the validity of such a theorem applied to the liquid phase. This is the reason why in Brussels we have started the study of the viscosity of systems of liquefied gases with simple structure.

A(CCl_4)–B($C(CH_3)_4$)

$(1+\delta)=0{\cdot}77,\ (1+\rho)=1{\cdot}04,\ T=293{\cdot}2$°K

x_A	$\varphi_{exp.}$	$\varphi_{th.}$	φ_A	φ_B	$(\varphi-\varphi^*)_{exp.}$	$(\varphi-\varphi^*)_{th.}$
0·000	3·717	4·048	—	4·048	0·000	0·00
0·253	2·680	3·196	1·816	3·745	−0·355	−0·15
0·518	1·923	2·185	1·612	2·791	−0·400	−0·30
0·623	1·675	1·884	1·339	2·785	−0·368	−0·29
0·832	1·288	1·321	1·135	2·269	−0·193	−0·20
1·000	1·029	1·035	1·035	—	0·000	0·00

A(CCl_4)–B($C(CH_3)_4$)

$T=273{\cdot}2$°K

x_A	$\varphi_{exp.}$	$\varphi_{th.}$	φ_A	φ_B	$(\varphi-\varphi^*)_{exp.}$	$(\varphi-\varphi^*)_{th.}$
0·000	2·747	3·048	—	3·048	0·000	0·00
0·253	2·000	2·375	1·269	2·750	−0·240	−0·19
0·518	1·420	1·620	1·225	2·045	−0·287	−0·26
0·623	1·237	1·363	1·002	1·960	−0·260	−0·24
0·832	0·939	0·996	0·833	3·871	−0·139	−0·14
1·000	0·740	0·752	0·752	—	0·000	0·00

A(CCl_4)–B($C(CH_3)_4$)

$T=262{\cdot}2$°K

x_A	$\varphi_{exp.}$	$\varphi_{th.}$	φ_A	φ_B	$(\varphi-\varphi^*)_{exp.}$	$(\varphi-\varphi^*)_{th.}$
0·000	2·283	2·511	—	2·511	0·000	0·00
0·253	1·652	1·943	1·075	2·244	−0·204	−0·09
0·518	1·170	1·294	1·035	1·583	−0·241	−0·24
0·622	1·018	1·111	0·829	1·579	−0·217	−0·22
0·832	0·767	0·785	0·689	1·264	−0·116	−0·15
1·000	0·600	0·617	0·617	—	0·000	0·00

Table 6.

4. CALCULATION OF THE ISOTHERMAL DIFFUSION COEFFICIENT

In the case of diffusion, by a similar treatment, one can predict the diffusion coefficient of a substance in a solvent when the coefficient of another substance in the same solvent is known. For instance, let us consider a solution A–B, where B is the solvent. From (2), we have

$$\tilde{D}(\tilde{T}_A)=D_A(T_A)\kappa_A^{\ \ 1}$$

where

$$\kappa_A=\frac{\epsilon_A^{*1/2}r_A^*}{m_A^{1\ 2}}$$

is a function of the mole fraction through ϵ_B^* and r_A^*. For a solution of C in B, we shall have

$$\tilde{D}(\tilde{T}_C)=D_C(T_C)\kappa_C^{\ \ 1}\quad \text{where}\quad \kappa_C=\frac{\epsilon_C^{*1/2}r_C^*}{m_C^{1\ 2}}.$$

At the same reduced temperature

$$T_A = \tilde{T}_C = \tilde{T}, \quad \tilde{D}(\tilde{T}_A) = \tilde{D}(\tilde{T}_C), \quad \text{and} \quad T_C = T_A \epsilon_C^*/\epsilon_A^*,$$

from which we obtain the relation

$$D_A(T_A) = D_C(T_A \epsilon_C^*/\epsilon_A^*) \left(\frac{m_C}{m_A}\right)^{1/2} \left(\frac{\epsilon_A^*}{\epsilon_C^*}\right)^{1/2} \left(\frac{r_A^*}{r_C^*}\right).$$

This relation must now be tested for reasonably simple solutions.

We would like to express our gratitude to Professor I. Prigogine for his suggestion of this research as well as his aid and advice in many of the matters discussed in this paper.

On essaye d'établir, en se basant sur la théorie des solutions de Prigogine, un théorème des états correspondants pour la viscosité et la diffusion des liquides purs et des solutions. L'accord entre la théorie et les rares données expérimentales disponibles est satisfaisant.

Ausgehend von der Prigogine'schen Theorie der Lösungen wird versucht, für die Viskosität und die Diffusion reiner Flüssigkeiten und Lösungen ein Theorem der übereinstimmenden Zustände zu begründen. Die Übereinstimmung zwischen der Theorie und den spärlichen verfügbaren experimentellen Daten ist befriedigend.

REFERENCES

[1] RUDENKO, N. S., and SHUBNIKOV, L. W., 1934, *Phys. Z. Sowjet.*, **6**, 470; 1953, *Selected Values of Physical and Thermodynamic Properties of Hydrocarbons and Selected Compounds*, American Petroleum Institute (Pittsburgh: Carnegie Press).
[2] GRUNBERG, L., 1954, *Trans. Faraday Soc.*, **50**, 1293.
[3] VAN ITTERBEEK, J., 1956, unpublished measurements, Brussels.

Thermal diffusion and the approach to the steady state in gases: II †

by S. C. SAXENA‡ and E. A. MASON
Institute for Molecular Physics, University of Maryland, College Park

(*Received* 1 *June* 1959)

The theory of the rate of approach to the steady state in themal diffusion is tested experimentally on the systems He–Ar, He–CO_2, H_2–CO_2, and D_2–CO_2 over a temperature range of about −78°C to 325°C. The course of the diffusion has been followed by means of the radioactive tracers ^{37}Ar and $^{14}CO_2$. The theory appears to be verified, and the results are used to calculate ordinary diffusion coefficients, which are in reasonable accord with previous measurements by other techniques. The thermal diffusion factors, which are obtained from the same measurements, also appear to have reasonable accuracy. The experimental method therefore appears to have promise as a sensitive method for the determination of forces between unlike molecules.

1. INTRODUCTION

Forces between unlike molecules are best investigated experimentally by measurements of those properties of mixtures which are most sensitive to the unlike molecular interactions, and only weakly dependent on the like molecular interactions. For this purpose the best properties to use are gaseous ordinary diffusion and gaseous thermal diffusion, and an experiment in which both properties can be determined at the same time is accordingly very attractive. The rate of separation of a mixture under the influence of a temperature gradient depends on the ordinary diffusion coefficient D, and the final steady-state separation depends on the thermal diffusion factor α_T. Both quantities can therefore be determined from a single experiment in which both the steady-state separation and the rate of approach to the steady state are observed.

Unfortunately, the theory of the rate of approach to the steady state in thermal diffusion has usually involved a number of unrealistic assumptions, so that the results have been of dubious quantitative value. Nettley [1] was apparently the first to perform careful experiments on the rate of approach to the steady state. He attempted to observe only the variation of the diffusion coefficient with the composition in H_2–N_2 mixtures, in order to work in terms of relative measurements in the hope of avoiding the obvious faults of the theory. Lonsdale and Mason [2] were able to remove some, but not all, of the unrealistic assumptions involved, and attempted to measure both the absolute value of D and its variation with temperature for H_2–CO_2 and He–CO_2. Their results showed that the method had promise, but were still uncertain because of the assumptions remaining and because of somewhat non-ideal apparatus geometry.

---

† This research was supported in part by the U.S. Atomic Energy Commission.

‡ Present address: Atomic Energy Establishment, Apollo Pier Road, Bombay-1, India.

We have recently reconsidered the theory of the rate of approach to the steady state, and removed all but one important assumption [3]. The present paper reports measurements designed to test the theory and to obtain values of diffusion coefficients over a range of temperature. The values of the thermal diffusion factor are also obtained from the same experiments. The apparatus is basically that used by Lonsdale and Mason, but has been rebuilt with more uniform and precisely known geometry in order to remove ambiguity. The measurements have been performed with radioactive tracers, the radioactive component being present in vanishingly small concentrations. This technique has advantages both in the interpretation of the experiments themselves and in their subsequent analysis to obtain the forces between unlike molecules [2].

Measurements are reported for the systems He–^{37}Ar, He–$^{14}CO_2$, H_2–$^{14}CO_2$, and D_2–$^{14}CO_2$ over a temperature range of about −78°c to 325°c. The theory of the rate of approach to the steady state appears to be verified, and values of D and α_T are obtained which are consistent with previous measurements on these systems. Analysis of the final results in terms of forces between unlike molecules will be reported in a subsequent paper.

2. Experimental

The apparatus is essentially that of Lonsdale and Mason [2], rebuilt to improve precision of both measurement and interpretation. The apparatus consists of two cylindrical bulbs of volume V_1 and V_2, held at temperatures T_1 and T_2, respectively, and connected by a long, narrow tube of length L and cross-sectional area A. The connecting tube contains a metal stopcock, of the same bore as the tube, for isolation of the bulbs during filling. The apparatus is mounted vertically, with the hot bulb uppermost, to avoid convection. The bulb V_1 is constructed as an ionization chamber in order to follow the radioactive tracer component of the gas mixture. The measuring circuit has been previously described [2], and has a precision of about 0·1 per cent. For the systems studied, voltages from −67 to −180 volts were used on the collecting electrode, and were sufficient to collect essentially all ions formed without starting any secondary ionization. The apparatus is constructed with V_1 much smaller than V_2 to secure sensitivity, since the composition changes in the bulbs are approximately in the inverse ratio of the bulb volumes [4].

The ionization chamber and associated critical electrical components are always maintained near room temperature (usually about 30°c) for ease of operation, and it was therefore convenient to construct two apparatuses, one for operation below room temperature ($T_1 > T_2$), and the other for operation above room temperature ($T_1 < T_2$). Use of the two apparatuses also has the advantage of permitting the geometry to be varied in a systematic way in order to test the theory of the rate of approach to the steady state. The geometrical constants of the two apparatuses were carefully determined, usually by two independent methods, and are as follows:

(1) Low-temperature apparatus: $V_1 = 11{\cdot}21$ cm^3, $V_2 = 535{\cdot}9$ cm^3, $L = 15{\cdot}87$ cm, $A = 0{\cdot}243$ cm^2.

(2) High-temperature apparatus: $V_1 = 14{\cdot}98$ cm^3, $V_2 = 750{\cdot}5$ cm^3, $L = 23{\cdot}80$ cm, $A = 0{\cdot}126$ cm^2.

These constants refer to a temperature of 20°c, and small corrections for their temperature dependence have been made where necessary.

The major change in apparatus design, aside from better geometry, is in the construction of the connecting tubes to secure a stable temperature distribution which can be measured precisely. As shown previously [2, 3], knowledge of this temperature distribution is necessary for the determination of diffusion coefficients from measurements of the rate of approach to the steady state. A connecting tube is constructed of brass with $\frac{1}{4}$ in. wall thickness; eight small recesses are drilled radially into the wall, a thermocouple securely fastened in each, and the whole tube well insulated with asbestos. Temperature distributions can thus be determined at ten points along the connecting tube, including the two ends, and were always found to be very nearly linear. Minor apparatus changes include rebuilding the metal stopcocks with provision for more accurate lining-up of the bore of the stopcock with that of the rest of the connecting tube when the stopcock is opened to start a run, and construction of new large bulbs (V_2) from very heavy-walled copper in order to achieve more uniform temperature. The large hot bulb of the high-temperature apparatus is plated on the outside with rhodium to resist oxidation.

The temperature T_1 was maintained by a conventional stirred oil bath and read on a sensitive mercury thermometer which had previously been calibrated against a platinum resistance thermometer. The values of the temperature T_2 were maintained by fixed points: the sublimation temperature of carbon dioxide (-78°c), and the melting temperatures of chloroform (-63°c), chlorobenzene (-45°c), *o*-dichlorobenzene (-18°c), and water (0°c). These temperatures were monitored with a thermocouple, and were determined during a run to an accuracy of about 0·05°c. The constancy of the temperature was usually better than this except in the case of the chloroform point, which had a tendency to drift. High values of the temperature T_2 were maintained by a specially built oven with one main heater winding and two auxiliary windings. Four smaller auxiliary heaters were distributed over the hot bulb V_2 to help smooth out temperature irregularities. The temperature T_2 was monitored by four thermocouples distributed over the surface of the hot bulb and in mechanical contact with it. Constancy of temperature during a run is much more important than uniformity of temperature over the bulb, which has only a very small effect on the results. Constancy was obtained by supplying regulated voltage to the oven heaters and controlling the room temperature. The maximum drift during a run was about 1°c, and was much less for most runs.

All thermocouples used were chromel alumel, calibrated at the previously mentioned low-temperature fixed points, at the transition temperatures of sodium sulphate (32·383°c) and of manganous chloride (58·089°c), and at the melting points of U.S. National Bureau of Standards samples of tin, lead, and zinc.

The gases used in the experiment were inert helium (99·99 per cent pure), inert hydrogen (99·99 per cent pure after removal of water vapour), inert deuterium (>99·5 per cent pure D_2), radioactive ^{37}Ar (carrier-free), and radioactive $^{14}CO_2$. The only important impurity in the deuterium was HD, which introduces only a small error into the final results. The $^{14}CO_2$ was generated [5] from barium carbonate containing about 20 per cent $Ba^{14}CO_3$. The inert CO_2 thus introduced acts as an impurity of a few parts per thousand in the gas mixtures. Since the possible error in the final results caused by this impurity is just on the borderline of the overall experimental reproducibility, no attempt has been made to apply a correction.

The procedure followed in making a run was essentially as follows. A small amount of radioactive tracer was thoroughly mixed with a large quantity of inert gas, and the mixture introduced into the two bulbs of the apparatus, which had been previously evacuated and brought to a steady temperature. The pressures were made equal by connecting the two bulbs externally for a moment. The pressure was measured to 0·05 mm by means of a mercury manometer and cathetometer. The initial ionization current was measured, the stopcock opened, and ionization current measured as a function of time until the final steady-state separation was attained.

3. THEORY OF THE EXPERIMENT

The equation of diffusion for one component in the connecting tube is [6],

$$J=-nD\left[\frac{\partial x}{\partial z}+x(1-x)\alpha_T\frac{\partial \ln T}{\partial z}\right], \tag{1}$$

where J is the flux density of the component, x is its mole fraction, n is the total number of both kinds of molecules per unit volume, and z is the distance along the connecting tube. For the radioactive tracer component, we have $x \ll 1$. At the steady state we have $J=0$, and equation (1) can be integrated to yield

$$\ln q(\infty)=\int_{T_1}^{T_2}\alpha_T d\ln T, \tag{2}$$

where $q(\infty)=x_1(\infty)/x_2(\infty)$ is the separation factor. The subscripts 1 and 2 refer to the two bulbs and the infinity refers to the steady state. The value of α_T in equation (2) depends on the temperature but not on the composition, which is fixed at effectively $x=0$, and α_T can be determined from equation (2) by either of two methods. The simplest method is to calculate an average thermal diffusion factor, $\bar{\alpha}_T$, for the temperature range T_1 to T_2,

$$\bar{\alpha}_T=\frac{\ln q(\infty)}{\ln(T_2/T_1)}. \tag{3}$$

This average value can then be identified with the actual value of α_T at some average temperature $\bar{T}$ between T_1 and T_2 [7]. A better procedure is to make a series of measurements at different values of T_2 and a fixed value of T_1, and then determine α_T by differentiation,

$$\alpha_T=\frac{d\ln q(\infty)}{d\ln(T_2/T_1)}, \quad T_1 \text{ constant}, \tag{4}$$

so that α_T at any temperature T_2 is the slope of the $\ln q(\infty)$ *vs.* $\ln(T_2/T_1)$ curve at the point corresponding to T_2. Equation (4) gives more unambiguous results than equation (3), and also permits α_T to be determined over a larger temperature range, but it throws considerable strain on the precision of the measurements because of the differentiation. Both methods have been examined in the present work, and the final results have been obtained according to (4).

In the present apparatus only x_1 can be measured, but $x_2(\infty)$ can be calculated from a consideration of the conservation of the number of molecules in the apparatus [4]. The result is

$$q(\infty)=\frac{x_1(\infty)}{x(0)}\left[1+\frac{V_1T_2}{V_2T_1}\left(1-\frac{x_1(\infty)}{x(0)}\right)+\Delta\right]^{-1}, \tag{5}$$

where $x(0)$ is the composition at zero time (uniform gas mixture), and Δ is a small correction for the gas contained in the connecting tube. For a linear temperature distribution along the connecting tube, Δ is given by the expression [2],

$$\Delta = \frac{AL}{V_2}\left[1 - \frac{x_1(\infty)}{x(0)}\frac{q(\infty)-1}{\ln q(\infty)}\right]\left(\frac{T_2}{T_2-T_1}\right)\ln\left(\frac{T_2}{T_1}\right). \tag{6}$$

The rate of approach to the steady state can be derived on the basis of a sort of quasi-stationary state assumption. The most general form of the result can be written as follows [3]:

$$S(t) = S(\infty)\{1-\exp[-t(1+\delta)/\tau]\}, \tag{7}$$

where $S = x_1 - x_2$ is the separation, t is the time, δ is a small correction term, and τ is a relaxation time, given by

$$\tau = K\frac{L}{A}\left(\frac{T_1}{V_1}+\frac{T_2}{V_2}\right)^{-1}\left\langle\frac{T}{D}\right\rangle_{\text{av}}, \tag{8}$$

$$\left\langle\frac{T}{D}\right\rangle_{\text{av}} = \frac{1}{L}\int_0^L \frac{T}{D}\,dz. \tag{9}$$

It is seen that a peculiar kind of average diffusion coefficient can be obtained from τ. This average diffusion coefficient can, however, be identified with the actual value of D at some average temperature between T_1 and T_2 [2]. The quantity K in equation (8) represents the ratio of two average flux densities, as follows:

$$K = \bar{J}/\bar{J}', \tag{10}$$

where

$$\bar{J} = \int_0^L J(T/D)\,dz \Big/ \int_0^L (T/D)\,dz, \tag{11}$$

$$\bar{J}' = \left(J_1\frac{T_1}{V_1} + J_2\frac{T_2}{V_2}\right)\Big/\left(\frac{T_1}{V_1}+\frac{T_2}{V_2}\right), \tag{12}$$

and J_1 and J_2 are the flux densities at the entrances to V_1 and V_2, respectively. The strict quasi-stationary state assumption requires that J be constant along the connecting tube, in which case $K = 1$. It is possible, however, that a much weaker assumption is a good approximation, namely that the ratio of the average fluxes is a constant, but not necessarily equal to unity. One of the purposes of the present work is to test this possibility quantitatively by considering K as an apparatus constant and studying its behaviour under different conditions.

The conversion of equation (7) into a form involving only quantities measurable in the present apparatus is straightforward, and yields the result

$$\left[\frac{x_1(t)}{x_1(\infty)} - 1\right] = \left[\frac{1-q(\infty)}{(1+\Delta')q(\infty)}\right]\exp[-t(1+\delta)/\tau], \tag{13}$$

where $q(\infty)$ is given by (5), and Δ' is a small time-independent correction for the composition changes in V_2 and in the connecting tube, given approximately by

$$\Delta' \approx \frac{V_1T_2 + AL\bar{T}}{V_2T_1}, \tag{14}$$

where $\bar{T}$ is an average temperature. The small correction term δ appearing in (7) and (13) takes into account the variation with time of the thermal diffusion ratio, $k_T = x(1-x)\alpha_T$, and for the present case of $x \ll 1$ takes on the simple form

$$\delta = \left[1 - q(\infty) + \frac{x(0)}{x_1(\infty)} q(\infty) \ln q(\infty)\right]\left[q(\infty) - 1\right]^{-1}. \tag{15}$$

According to (13), a suitable semi-logarithmic plot should yield a straight line whose slope gives τ. A typical plot of this sort is shown in figure 1, and is seen to yield a good straight line except for a brief transient at the beginning of the run. This transient is probably caused by the thermal separation which occurs between the bulb V_2 and its portion of the connecting tube, before the stopcock is opened. The resulting concentration gradient when the stopcock is opened causes an additional diffusion, and slightly disturbs the exponential approach to the steady state. The effect can also be thought of as a perturbation in the time, such that the time of opening the stopcock to start the run is not the true zero time, but a somewhat later time because some separation has already occurred. The existence of the transient means that the extrapolation of the linear plot to zero time gives an intercept which is not in agreement with the value of $x(0)$ measured before the stopcock is opened. This has two unfortunate consequences. First, one check for internal consistency is lost. Second, if the initial conditions for a run were slightly off, the extrapolated value of $x(0)$ could be used instead of the directly measured, but slightly incorrect, value of $x(0)$, except for the presence of the transient. In actual practice it is surprisingly

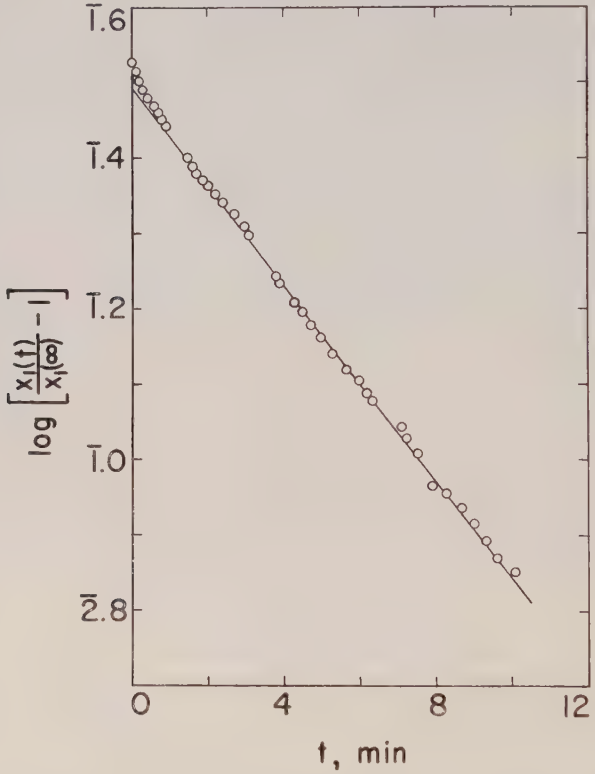

Figure 1. Typical measurements of the rate of approach to the steady state (actually a He–^{37}Ar run with $T_1 = 304{\cdot}2$°K, $T_2 = 195{\cdot}5$°K, $p = 225{\cdot}25$ mm).

difficult to secure an ideal filling of the apparatus such that the measured $x(0)$ really corresponds to the perfectly uniform gas mixture. A theoretical correction for the initial transient is thus useful, and one is given in the appendix.

4. RESULTS

4.1. *Diffusion coefficients*

The fact that the observed rate of approach to the steady state is indeed exponential, as has been illustrated in figure 1, provides some verification of the theory of the rate of approach. This is rather weak verification, unfortunately, since much simpler theories also predict an exponential rate of approach [1–3]. These simple theories, however, do not yield very good values of diffusion coefficients, so the most important test of the theory is its ability to yield reliable absolute values of diffusion coefficients. In the present work this test is carried out by treating the quantity K in (8) as an apparatus constant and checking whether absolute values of diffusion coefficients can be obtained in this way under different conditions of pressure, temperature, gas pairs, and apparatus geometry.

On rather general grounds one might expect that K would depend on the apparatus geometry through the parameters V_1, V_2, L, A, and on the temperature distribution along the connecting tube, but not on other parameters such as the pressure, the masses of the diffusing molecules, and the forces between the molecules. The reason K would be independent of the latter parameters is that these only affect the value of D. In the original differential equations describing the diffusion process, D always occurs as the product Dt, and therefore a change in D is in effect only a change in the time scale, and should not be a fundamental change in the problem of obtaining an approximate solution to the differential equations. Thus, since τ is observed to be independent of t, K is also independent of t, and therefore also presumably independent of D as well.

Actually, the present apparatus is arranged so that the dependence of K on apparatus geometry and temperature would be expected to be greatly simplified. First of all, the temperature distribution has practically the same form regardless of the values of T_1 and T_2 (the distribution is nearly linear). Second, V_2 is large enough compared to V_1 and AL that it can be considered as an almost infinite reservoir. Third, the lengths of the connecting tubes are much greater than their diameters. Thus it is at least reasonable to expect K to be essentially independent of temperature and to depend only on the quantity AL/V_1, with K approaching unity as AL/V_1 approaches zero. The present results appear to verify this expectation. In particular, systematic variation of the following quantities had the expected effect on K:

(*a*) Pressure of the gas mixture.

(*b*) Molecular masses and forces. The masses were varied independently of the forces by studying the systems H_2–$^{14}CO_2$ and D_2–$^{14}CO_2$.

(*c*) Temperature.

(*d*) Apparatus geometry.

Determination of numerical values of K requires that the absolute value of D be known independently at some temperature within the range of the apparatuses. Absolute values of D were obtained by placing the high-temperature apparatus at constant temperature (regulated room temperature) and performing an ordinary diffusion experiment, in which one bulb is filled with inert gas plus radioactive tracer and the other bulb is filled with inert gas alone. The theory of such a two-bulb ordinary diffusion experiment is well understood [8, 9] and permits the evaluation of absolute values of D. As a check, several ordinary diffusion runs were also made in the low-temperature apparatus with H_2–$^{14}CO_2$. A small correction is necessary to allow for the fact that the fluxes may extend somewhat beyond the ends of the connecting tube. This end correction is made by increasing the length of the tube at each end by an amount $0{\cdot}82r$, where r is the tube radius [8, 9]. The correction was consistently made for all runs. It is unimportant for the thermal diffusion runs since it could just as easily have been absorbed into the numerical value of K, but it is important for the ordinary diffusion runs.

Average values of the experimental relaxation times,

$$\tau_{\mathrm{exp}} = \tau/(1+\delta), \tag{16}$$

are given in table 1. The uncertainties shown are the average absolute deviations for a number of duplicate runs, and are given just to indicate the experimental reproducibility and not our estimate of the probable absolute error. Duplicate runs were not always at exactly the same temperature, but were converted to a common temperature basis before averaging to give the results in table 1. According to (8) and (15), τ_{exp} should vary directly with pressure, since D varies inversely with the pressure and δ is independent of pressure. This expected pressure dependence was tested experimentally and found to be true within the experimental reproducibility. All results in table 1 are therefore reported on the basis of a standard pressure of 1 atmosphere, although the actual measurements were made at various pressures between 90 and 340 mm. The large difference in magnitudes of τ_{exp} at low and at high temperatures is a result of the different geometries of the two apparatuses. Runs could not be made at very high temperatures with H_2–CO_2 and D_2–CO_2 because of chemical reduction of the CO_2. Even with He–CO_2 some chemical action appeared to occur at high enough temperatures.

The appropriate values of the correction term δ, given by (15), are also included in table 1, and it is seen that this correction can be quite substantial. Neglect of δ would yield not only erroneous absolute values of τ, but also an erroneous temperature dependence, since δ itself is obviously temperature dependent.

It was found that all the measurements in table 1 could be correlated by means of a constant apparatus factor K, essentially independent of pressure, gas pair, or temperature. The values used for K are based on the requirements that the diffusion coefficients calculated from relaxation times be concordant between the two apparatuses and the different gas pairs, and consistent with the ordinary diffusion measurements. The values are as follows: $K = 1{\cdot}37$ for the low-temperature apparatus; $K = 1{\cdot}12$ for the high-temperature apparatus. These values also correlate well with apparatus geometry, and are given within $0{\cdot}4$ per cent by the equation

$$K = 1 + 3{\cdot}1(AL/V_1)^2. \tag{17}$$

Equation (17) is only empirical, but it can be used to indicate the sort of geometry necessary for the strict quasi-stationary state assumption to apply. Thus for K to be equal to unity within 1 per cent requires that the small bulb have a volume

System	T_1, °K	T_2, °K	τ_{exp}†, min	δ	$q(\infty)$
He–^{37}Ar	304·2	195·3	22·3 ± 0·2	0·151	0·7479 ± 0·0057
	304·2	202·8	21·8 ± 0·3	0·133	0·7679 ± 0·0001
	304·2	226·6	21·3 ± 0·3	0·096	0·8216 ± 0·0005
	304·2	250·7	20·7 ± 0·3	0·064	0·8775 ± 0·0005
	304·2	273·2	21·1 ± 0·3	0·035	0·9310 ± 0·0001
	308·0	363·2	68·6 ± 1·3	−0·049	1·1110 ± 0·0008
	308·7	379·8	68·0 ± 0·8	−0·060	1·1438 ± 0·0008
	314·3	408·8	63·5 ± 0·2	−0·078	1·1899 ± 0·0013
	313·8	447·0	63·3 ± 0·2	−0·099	1·2468 ± 0·0007
	313·2	453·8	61·5 ± 0·2	−0·108	1·2713 ± 0·0004
	314·2	512·3	64·0 ± 0·4	−0·147	1·4001 ± 0·0010
	314·3	558·5	61·8 ± 0·2	−0·166	1·4746 ± 0·0007
	314·3	598·0	62·3 ± 0·1	−0·184	1·5423 ± 0·0022
He–^{14}CO$_2$	303·1	194·0	—	—	0·6962 ± 0·0027‡
	304·2	194·9	29·8 ± 1·0	0·199	0·6764 ± 0·0019
	304·2	204·6	28·6 ± 0·3	0·169	0·7166 ± 0·0048
	304·2	226·3	28·3 ± 0·6	0·126	0·7771 ± 0·0014
	304·2	250·8	28·1 ± 0·3	0·076	0·8487 ± 0·0041
	304·2	273·2	26·7 ± 0·2	0·045	0·9117 ± 0·0042
	304·3	345·5	93·2 ± 4·4	−0·051	1·1194 ± 0·0022
	307·2	389·5	85·2 ± 1·8	−0·090	1·2233 ± 0·0031
	303·1	422·1	—	—	1·3455 ± 0·0001‡
	314·6	431·6	84·1 ± 0·0	−0·122	1·3149 ± 0·0012
	315·4	475·9	86·8 ± 0·2	−0·162	1·4497 ± 0·0004
	315·7	537·1	82·8 ± 0·7	−0·202	1·6112 ± 0·0011
H$_2$–^{14}CO$_2$	303·1	194·2	—	—	0·8271 ± 0·0015‡
	303·1	194·2	—	—	0·8127 ± 0·0013§
	303·9	195·2	26·6 ± 0·2	0·103	0·8098 ± 0·0072
	325·2	195·2	24·3 ± 0·4	0·104	0·7891 ± 0·0024
	304·2	203·8	26·8 ± 1·6	0·096	0·8260 ± 0·0028
	304·2	226·6	25·4 ± 1·3	0·070	0·8645 ± 0·0032
	304·2	251·3	24·4 ± 0·4	0·051	0·9019 ± 0·0008
	304·2	273·2	22·9 ± 1·6	0·029	0·9404 ± 0·0016
	308·7	364·2	66·9 ± 0·6	−0·049	1·1120 ± 0·0023
	309·2	400·2	70·9 ± 2·5	−0·072	1·1728 ± 0·0020
	303·1	422·1	—	—	1·2029 ± 0·0029‡
	316·6	441·6	73·7 ± 1·2	−0·097	1·2430 ± 0·0009
D$_2$–^{14}CO$_2$	304·2	195·4	37·6 ± 1·2	0·103	0·8109 ± 0·0022
	304·2	203·7	35·3 ± 1·1	0·090	0·8348 ± 0·0021
	304·2	225·7	36·3 ± 0·4	0·072	0·8649 ± 0·0013
	307·7	392·0	105·0 ± 1·3	−0·058	1·1349 ± 0·0019
	315·6	440·3	101·7 ± 0·3	−0·083	1·2015 ± 0·0007

† Converted to 1 atmosphere.
‡ Reference [22].
§ Reference [21].

Table 1. Measured relaxation times and separation factors.

almost twenty times that of the connecting tube. An experimental check with this type of apparatus geometry would be very interesting. Of course it is also still necessary that V_2 be very large and that the length of the connecting tube be much greater than the diameter.

System	$\bar{T}$, °K	$\bar{D}$, cm^2/sec	System	$\bar{T}$, °K	$\bar{D}$, cm^2/sec
He–Ar	251	0·544	H_2–CO_2	250	0·481
	259	0·583		258	0·502
	269	0·639		257	0·488
	280	0·703		267	0·548
	289	0·731		279	0·606
	296·0	0·744†		288	0·680
	328	0·851		296·5	0·635‡
	337	0·889		296·6	0·662†
	354	1·000		332	0·885
	366	1·060		348	0·893
	372	1·122		368	0·991
	387	1·165			
	405	1·288			
	418	1·344			
He–CO_2	250	0·392	D_2–CO_2	250	0·337
	259	0·433		256	0·370
	268	0·469		267	0·383
	280	0·515		297·0	0·494†
	288	0·576		346	0·594
	298·4	0·600†		372	0·660
	321	0·626			
	342	0·752			
	365	0·821			
	382	0·867			
	404	1·005			

† From ordinary diffusion runs, high-temperature apparatus.
‡ From ordinary diffusion runs, low-temperature apparatus.

Table 2. Average diffusion coefficients at 1 atmosphere.

Values of the diffusion coefficients calculated from the measured relaxation times and from the ordinary diffusion measurements are given in table 2. The order of the entries is the same in tables 1 and 2. The calculation of the average temperature $\bar{T}$ from the measured temperature distribution along the connecting tube involves numerical integration and is somewhat tedious, but is straightforward and has previously been outlined in detail [2]. The diffusion coefficients have been corrected slightly to refer to Ar and CO_2 rather than to $^{37}\mathrm{Ar}$ and $^{14}\mathrm{CO}_2$. This correction is less than 0·5 per cent in all cases.

The results of the present measurements of D are shown in figures 2 and 3, together with previous measurements [10–19]. The present results can all be represented within the experimental scatter by equations of the form,

$$D = D_0 T^s, \tag{18}$$

where D_0 and s are constants which were determined by least squares and are given in table 3. These equations are shown as the solid lines in figures 2 and 3. The

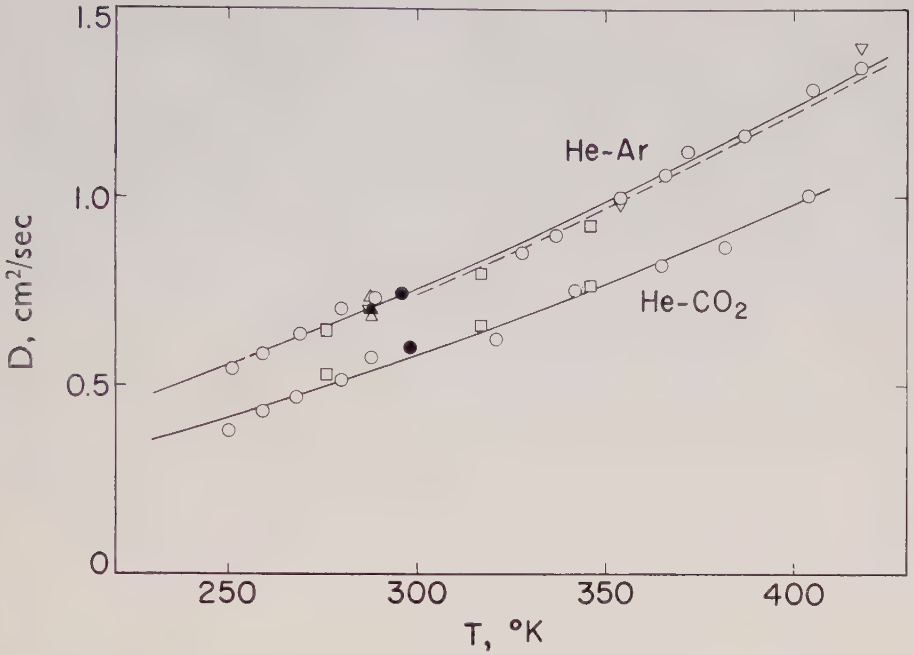

Figure 2. Diffusion coefficients of He–Ar and He–CO_2 as a function of temperature. The solid lines represent the present results according to (18), and the dashed line represents the experimental results of Walker and Westenberg. The points are: ○ present results, thermal diffusion; ● present results, ordinary diffusion; ▲ Schmidt; △ Lonius; ▽ Strehlow; □ Holsen.

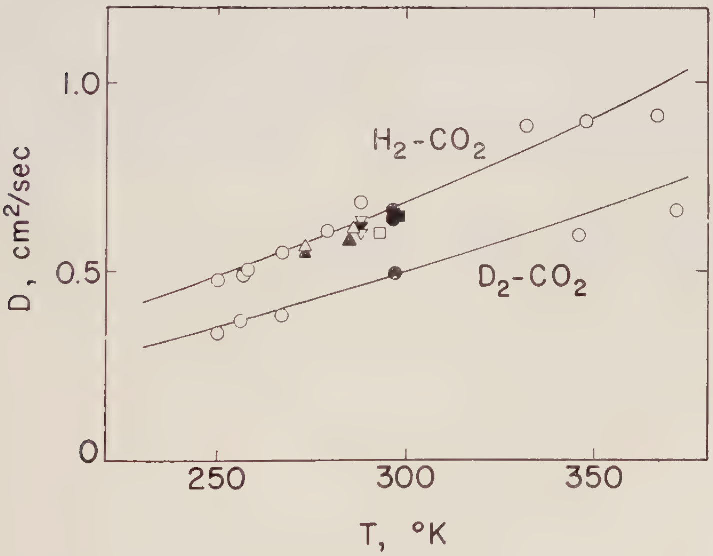

Figure 3. Diffusion coefficients of H_2–CO_2 and D_2–CO_2 as a function of temperature. The solid lines represent the present results according to (18). The points are: ○ present results, thermal diffusion; ● present results, ordinary diffusion; △ Loschmidt; ▲ von Obermayer; ▽ Lonius; ▼ Boardman and Wild; □ Waldmann ■ Boyd, Stein, Steingrimsson, and Rumpel.

average absolute deviations of the present measured values from the curves are: He–Ar, 1·9 per cent; He–CO$_2$, 3·0 per cent; H$_2$–CO$_2$, 3·4 per cent. The curve for D$_2$–CO$_2$ was not calculated from the measurements on D$_2$–CO$_2$, but from the measurements on H$_2$–CO$_2$ together with the theoretical mass correction factor. The fact that substantial agreement is obtained (average absolute deviation, 4·5 per cent) provides some verification of the experimental method and its theoretical interpretation. A more direct procedure is to calculate the diffusion coefficient ratio of H$_2$–CO$_2$ to D$_2$–CO$_2$ on a point-by-point basis. The result averages 1·400, in good agreement with the theoretical ratio of 1·384, based on the reduced masses.

System	D_0 cm^2/(sec. $^\circ$K^s)	s
He–Ar	$4{\cdot}41 \times 10^{-5}$	1·71
He–CO$_2$	$1{\cdot}60 \times 10^{-5}$	1·84
H$_2$–CO$_2$	$1{\cdot}87 \times 10^{-5}$	1·84
D$_2$–CO$_2$	$1{\cdot}35 \times 10^{-5}$	1·84

Table 3. Parameters of equation (18).

The present measurements are further seen to be in essential agreement with previous measurements, showing that the absolute accuracy of the present method is reasonable. All the previous measurements refer to bulk mixtures except those of Walker and Westenberg, who used a trace technique in a flow system [20]. Their results for He–Ar cover the range 300–1100°K and for helium as the trace gas are represented with a standard deviation of ±1 per cent by an equation of the form of (18), with $s = 1{\cdot}746$ and $D_0 = 3{\cdot}61 \times 10^{-5}$ cm^2/(sec. $^\circ$K^s). According both to kinetic theory and to their own measurements [18], D for argon as the trace gas would be about 3 per cent smaller, and the dashed line in figure 2 was obtained on that basis. The agreement with the present results as to the temperature dependence of D for He–Ar is especially gratifying.

A comparison with Lonsdale and Mason's previously reported measurements [2] on the rate of approach to the steady state in H$_2$–CO$_2$ and He–CO$_2$ is also of interest. No direct comparison is possible because the value of K is not known for these previous measurements, nor can a value be estimated from the present results because of somewhat different apparatus geometries and greatly different temperature distributions along the connecting tubes. Nevertheless, the *relative* values of the measured relaxation times should agree, provided the correction given by δ is taken into account, since K will cancel out on taking ratios. According to Lonsdale and Mason's measurements,

$$\tau(\text{He–CO}_2)/\tau(\text{H}_2\text{–CO}_2) = 1{\cdot}10 \pm 0{\cdot}04.$$

According to table 3, the present measurements yield the ratio 1·17 ± 0·05, in fair agreement.

The present measurements of D thus appear to have an absolute accuracy of 2–4 per cent, as estimated on the basis of reproducibility, smoothness as a function of temperature, and agreement with previous results. Better accuracy is associated with those systems having greater thermal separations, and thus a larger effect to be measured. We believe this accuracy constitutes good evidence for the essential correctness of the theory of the rate of approach to the steady state.

4.2. *Thermal diffusion factors*

Values of the experimental separation factors are given in table 1, and have all been checked for consistency according to the theory of the initial transient outlined in the Appendix. Also shown are the results of some earlier less extensive measurements in similar apparatuses by Reisfeld [21] and by Lonsdale [22]. These results have also been corrected for the initial transient. The uncertainties shown are absolute average deviations for several duplicate runs, and are given to indicate only reproducibility and not the probable absolute error. According to kinetic theory ,α_T and $q(\infty)$ are predicted to be independent of pressure, and the present results confirm this within the experimental error.

Values of α_T have been obtained from the measured values of $q(\infty)$ by the methods outlined in § 3. They are well represented by the following equations:

$$\text{He–Ar:} \quad \alpha_T = (0{\cdot}687 \pm 0{\cdot}011) - \frac{(1{\cdot}44 \pm 1{\cdot}09) \times 10^3}{T^2}, \quad 200° \leqslant T \leqslant 590°\text{K}; \quad (19)$$

$$\text{He–CO}_2: \quad \alpha_T = (0{\cdot}918 \pm 0{\cdot}017) - \frac{(4{\cdot}70 \pm 1{\cdot}32) \times 10^3}{T^2}, \quad 200° \leqslant T \leqslant 530°\text{K}; \quad (20)$$

$$\text{H}_2\text{–CO}_2: \quad \alpha_T = (0{\cdot}995 \pm 0{\cdot}032) - \frac{128{\cdot}8 \pm 7{\cdot}1}{T}, \quad 200° \leqslant T \leqslant 440°\text{K}. \quad (21)$$

These equations have all been determined by least squares, and the uncertainties indicated are the usual standard errors as calculated from the least squaring procedure [23]. Typical resulting standard errors in α_T are 2·4 per cent for He–Ar, 2·6 per cent for He–CO_2, and 7·1 per cent for H_2–CO_2 at 300°K. All the separation factors listed in table 1 have been used in calculating (19)–(21) except those given by Lonsdale for H_2–CO_2, which are definitely discordant both with the present results and with Reisfeld's older measurements. No very definite reason for the discrepancy is apparent, although it might have been caused by systematic errors in the filling of the apparatus. The present values of α_T for H_2 CO_2 are thus nearly 12 per cent larger than those given in reference [2]. On the other hand, the agreement for He-CO_2 is good, the absolute average deviation of the values of α_T in reference [2] from the present results being only 3·9 per cent.

The expressions (19) (21) for α_T have been corrected slightly to refer to Ar and CO_2 instead of ^{37}Ar and $^{14}CO_2$. Such a correction is not in general possible without knowledge of the intermolecular forces, but for the present mixtures, consisting of a trace of heavy gas in a light gas, the correction is almost entirely dependent on the molecular masses and is very insensitive both to temperature and to the intermolecular forces. The corrections used were 1·013 for He–Ar, 0·994 for He–CO_2 and 0·997 for H_2 CO_2, calculated from the theoretical first approximation for α_T.

The measured separation factors for D_2 $^{14}CO_2$ have not been treated by the same methods used in obtaining (19) (21), but instead are compared in figure 4 with the results from H_2–$^{14}CO_2$, corrected for the effect of the different masses of H_2 and D_2. The curve shown corresponds to equation (21), and is seen to represent the D_2–$^{14}CO_2$ measurements adequately. This supplies a useful check on the experimental procedure and its interpretation. The factor used for converting H_2–$^{14}CO_2$ results to D^2–$^{14}CO_2$ results was calculated from the theoretical first approximation for α_T and found to be equal to 1·077, constant within 0·2 per cent for any temperature in the experimental range and any reasonable choice of intermolecular force laws. The thermal diffusion factor for D_2–CO_2 obtained from (21) is thus:

$$D_2\text{–}CO_2: \quad \alpha_T = (0{\cdot}921 \pm 0{\cdot}030) - \frac{119{\cdot}2 \pm 6{\cdot}6}{T}, \qquad 200° \leqslant T \leqslant 440°\text{K}. \qquad (22)$$

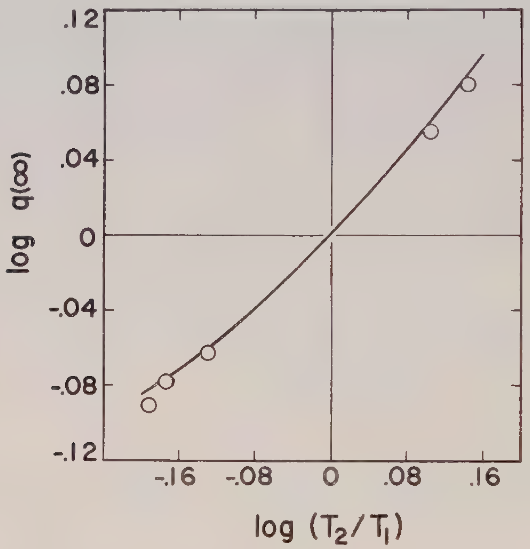

Figure 4. Separation factors for D_2–$^{14}CO_2$. The curve has been calculated from the results for H_2–$^{14}CO_2$.

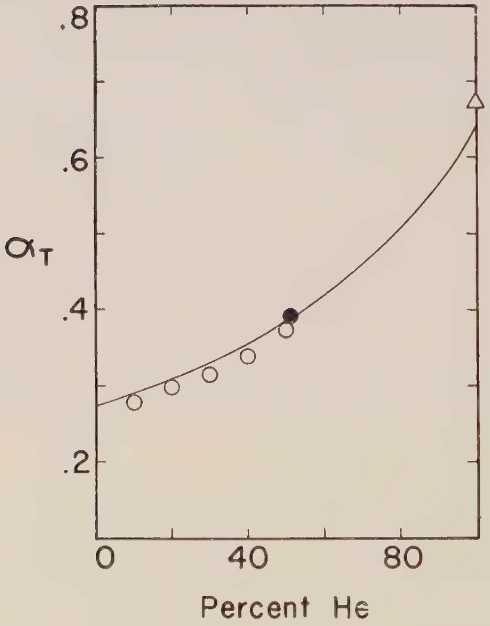

Figure 5. Comparison of present measurements (△) with previous measurements by Atkins, Bastick, and Ibbs (○) and by Grew (●) on He–Ar at 327°K. The curve is a theoretical first approximation.

Comparison of the present measurements of α_T with previous measurements must be somewhat indirect because of the strong composition dependence of α_T, and is made by means of a plot of α_T as a function of composition. In figure 5 the present results for He–Ar are compared with the results obtained by Atkins, Bastick, and Ibbs [24] and by Grew [25] at a mean temperature of 327°K. The curve shown is not of high accuracy and is included only to indicate the expected trend of the results. It was calculated according to Kihara's first approximation, using tabulated exp-six potential parameters [26]. The present results are seen to be at least consistent with the earlier work. For He–CO_2, Lonsdale and Mason have previously shown that there is consistency with earlier measurements. They have also made comparisons for H_2–CO_2, but these must now be repeated, inasmuch as the present results are appreciably different. Figure 6 shows a comparison with the measurements of Ibbs and Underwood [27] on H_2–CO_2 at a mean temperature of 324°K. The curve shown is only a first approximation, calculated with Lennard-Jones (12–6) potential parameters ($\epsilon_{12}/k = 79{\cdot}5$°K, $\sigma_{12} = 3{\cdot}482$ Å) [28]. Because this potential is not so satisfactory for H_2 and CO_2, experimental viscosities and diffusion coefficients were used in place of theoretical collision integrals where possible [29]. The present results are seen to be reasonably consistent with Ibbs and Underwood's measurements. They are also reasonably consistent with similar measurements by Clusius and Huber [2, 30] at somewhat different temperatures.

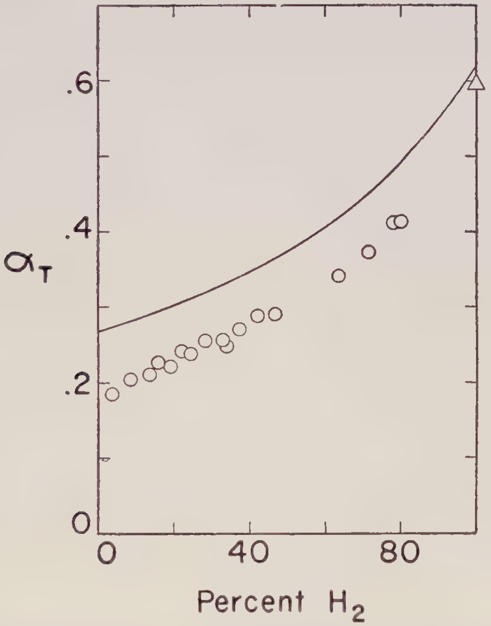

Figure 6. Comparison of present measurements (△) with previous measurements by Ibbs and Underwood (○) on H_2–CO_2 at 324°K. The curve is a theoretical first approximation.

5. CONCLUSIONS

The present results appear to verify the theory of the rate of approach to the steady state, and show that the experimental method can be used to obtain absolute values of diffusion coefficients of reasonable accuracy. The results also indicate the apparatus geometry conditions necessary for the strict quasi-stationary state assumption to hold. The accuracy of the thermal diffusion factors obtained at the same time is also reasonably good. It thus appears that the experimental method has considerable potential for the experimental investigation of forces between unlike molecules.

The authors wish to thank Dr. S. Weissman for his help with some of the calculations, especially the treatment of the initial transient, and for making several check runs. They wish to thank Mr. K. P. McCarty for his assistance in taking many of the observations. They are also grateful to Dr. R. E. Walker and Dr. A. A. Westenberg of the Johns Hopkins University Applied Physics Laboratory, and to Professor J. N. Holsen of Washington University of St. Louis for their kindness in communicating results of their diffusion measurements before publication. Thanks are also due to the General Research Board of the University of Maryland for a grant for the purchase of some equipment.

Appendix

Determination of initial transient

The purpose of studying the initial transient is to obtain a correlation between the measured composition at zero time, $x(0)$, and the zero-time intercept of the idealized equation (13) for the rate of approach to the steady state. Such a correlation permits a check to be made on the measured value of $x(0)$. Equation (13) can be rewritten in the form

$$\left[\frac{x_1(t)}{x_1(\infty)}-1\right]=\left[\frac{x_1(i)}{x_1(\infty)}-1\right]\exp\left(-t/\tau_{\text{exp}}\right), \tag{23}$$

where $x_1(i)$ is the zero-time intercept and τ_{exp} is given by (16). Since $x_1(i)$ and $x(0)$ are never very different, a fairly crude treatment of the initial transient is sufficient. The procedure adopted is as follows. First the composition gradient in the connecting tube is calculated before the stopcock is opened, assuming a steady state exists between the connecting tube and V_2. Next, the change in composition in V_1 required to even out this composition gradient by ordinary diffusion between V_1 and the connecting tube after the stopcock is opened is calculated by a simple material balance. The result is assumed to represent the value of x_1 at the point where the transient joins the quasi-steady-state curve at a time t_s after the stopcock is opened, and is approximately

$$\frac{x_1(t_s)}{x(0)}=1-\frac{AL}{V_1}\frac{T'}{T_2}\left[1-\frac{q(\infty)-1}{\ln q(\infty)}\right]\left[1+\frac{AL}{V_1}\frac{T'}{T_2}\right]^{-1}, \tag{24}$$

where

$$T'=\frac{T_1T_2}{T_2-T_1}\ln\left(\frac{T_2}{T_1}\right). \tag{25}$$

The initial variation of the transient with time is then approximated by the result for ordinary diffusion with constant diffusion coefficient [31],

$$\frac{x_1(t)}{x(0)}=1-2g\frac{A}{V_1}\left[1-q(\infty)\right]\left(\frac{Dt}{\pi}\right)^{1/2}, \tag{26}$$

where g is a geometry factor which should lie between $\frac{1}{2}$ and 1. Rather than determine the value of g from apparatus geometry, however, we allow g to be a disposable parameter to compensate to some extent for the crudity of the various assumptions.

The desired relationship between $x(0)$ and $x_1(i)$ is then obtained by requiring that (23), (24), and (26) all give the same result at $t = t_s$. The procedure is to calculate $x_1(t_s)$ from (24), substitute this value into (26) to obtain t_s, and finally substitute both $x_1(t_s)$ and t_s into (23) to yield a relation between $x_1(i)$ and $x(0)$. This relation then serves as a consistency check among different runs, since only one disposable parameter, g, is involved. It also turns out that t_s reduced to a standard pressure is essentially a constant for a given system and apparatus, and that values of t_s for different systems in the same apparatus are in the inverse ratio of the diffusion coefficients for the systems, as would be expected from (26).

On examine expérimentalement la théorie de la vitesse d'approche vers l'état stationnaire dans la diffusion thermale pour les systèmes He–Ar, He–CO_2, H_2–CO_2, et D_2–CO_2, dans l'intervalle de température (−78°c, 325°c). On a suivi la marche de la diffusion grâce aux indicateurs radioactifs ^{37}Ar et $^{14}CO_2$. La théorie semble être vérifiée, et on utilise les résultats pour calculer des coefficients de diffusion ordinaires; ceux-ci sont en accord raisonnable avec des mesures antérieures faites par d'autres techniques. Les facteurs de diffusion thermale, qui sont obtenus à partir des mêmes mesures, semblent aussi être raisonnablement précis. La méthode expérimentale promet donc, semble-t-il, de devenir une méthode sensible de détermination des forces entre molécules dissemblables.

Die Theorie der Geschwindigkeit der Annäherung an den stationären Zustand bei thermischer Diffusion wurde in den Systemen He–Ar, He–CO_2, H_2–CO_2, und D_2–CO_2 im Temperaturgebeit zwischen −78°c und 325°c experimentell überprüft. Der Verlauf der Diffusion wurde mit Hilfe der Radioisotopen ^{37}Ar und $^{14}CO_2$ verfolgt. Die Theorie wird anscheinend bestätigt und die Ergebnisse werden zur Berechnung gewöhnlicher Diffusionskoeffizienten benutzt, die mit früheren Messergebnissen nach anderen Verfahren vernünftig übereinstimmen. Die Thermodiffusionsfaktoren, die aus den gleichen Messungen bestimmt werden, erweisen sich ebenfalls als recht genau. Die Versuchsmethode verspricht somit, sich als empfindliches Verfahren zur Bestimmung von Kraftwirkungen zwischen ungleichen Molekeln zu eignen.

REFERENCES

[1] NETTLEY, P. T., 1954, *Proc. phys. Soc. Lond.*, B, **67**, 753.
[2] LONSDALE, H. K., and MASON, E. A., 1957, *J. phys. Chem.*, **61**, 1544. This is Paper I.
[3] SAXENA, S. C., and MASON, E. A., 1959, *Mol. Phys.*, **2**, 264.
[4] GREW, K. E., and IBBS, T. L., 1952, *Thermal Diffusion in Gases* (Cambridge : University Press), p. 37.
[5] ZWIEBEL, N., TURKEVICH, J., and MILLER, W. W., 1949, *J. Amer. chem. Soc.*, **71**, 376.
[6] See ref. [4], p. 23.
[7] BROWN, H., 1940, *Phys. Rev.*, **58**, 661; or see ref. [4], p. 126.
[8] NEY, E. P., and ARMISTEAD, F. C., 1947, *Phys. Rev.*, **71**, 14.
[9] PRESENT, R. D., 1958, *Kinetic Theory of Gases* (New York: McGraw-Hill), p. 197.
[10] LOSCHMIDT, J., 1870, *S.B. Akad. Wiss. Wien*, **62**, 468.
[11] VON OBERMAYER, A., 1880, *S.B. Akad. Wiss. Wien*, **81**, 1102.
[12] SCHMIDT, R., 1904, *Ann. Phys., Lpz.*, **14**, 801.
[13] LONIUS, A., 1909, *Ann. Phys., Lpz.*, **29**, 664.
[14] BOARDMAN, L. E., and WILD, N. E., 1937, *Proc. roy. Soc.* A, **162**, 511.
[15] WALDMANN, L., 1944, *Naturwissenschaften*, **32**, 223.
[16] BOYD, C. A., STEIN, N., STEINGRIMSSON, V., and RUMPEL, W. F., 1951, *J. chem. Phys.*, **19**, 548.

[17] Strehlow, R. A., 1953, *J. chem. Phys.*, **21,** 2101.
[18] Walker, R. E., and Westenberg, A. A., 1959, *J. chem. Phys*, **31,** 519.
[19] Holsen, J. N., private communication.
[20] Walker, R. E., and Westenberg, A. A., 1958, *J. chem. Phys.*, **29,** 1139, 1147.
[21] Reisfeld, M. J., 1955, Thesis, Pennsylvania State University.
[22] Lonsdale, H. K., 1957, Thesis, Pennsylvania State University.
[23] Deming, W. E., 1943, *Statistical Adjustment of Data* (New York: John Wiley).
[24] Atkins, B. E., Bastick, R. E., and Ibbs, T. L., 1939, *Proc. roy. Soc.* A, **172,** 142.
[25] Grew, K. E., 1947, *Proc. roy. Soc.* A, **189,** 402.
[26] Mason, E. A., 1955, *J. chem. Phys.*, **23,** 49.
[27] Ibbs, T. L., and Underwood, L., 1927, *Proc. phys. Soc. Lond.*, **39,** 227.
[28] Hirschfelder, J. O., Curtiss, C. F., and Bird, R. B., 1954, *Molecular Theory of Gases and Liquids* (New York: John Wiley), p. 1110.
[29] Amdur, I., and Mason, E. A., 1958, *Phys. Fluids*, **1,** 370.
[30] Clusius, K., and Huber, M., 1955, *Z. Naturf.*, **10 a,** 230.
[31] Crank, J., 1956, *The Mathematics of Diffusion* (Oxford: Clarendon Press), Chap. 2.

Steric forces in halogen-substituted benzenes

by C. A. COULSON and D. STOCKER
Mathematical Institute, Oxford

(*Received* 2 *March* 1959)

Theoretical calculations are made of the non-bonded repulsion energies between the halogen atoms in the hexa-halogeno-benzenes. The theoretical conclusions are compared with the available experimental evidence.

1. INTRODUCTION

The hexa-substituted benzenes C_6X_6, in which X is a halogen atom, provide important situations in which to look for the influence of steric forces between non-bonded atoms. This is because, with the exception of C_6F_6, all these molecules are such that the X...X distance ($r_{X\,..X}$) is less than twice the van der Waals radius ($r_{v.d.w.}$) of the halogen. Using the notation of figure 1 the table below shows how serious this overcrowding is for the heavier substituents.

Molecule	$r_{X...X}\,(=a+b)$	$2r_{v.d.w.}$	Conclusion
C_6F_6	2·79	2·70	Not overcrowded
C_6Cl_6	3·12	3·60	Overcrowded
C_6Br_6	3·27	3·90	Overcrowded
C_6I_6	3·54	4·30	Overcrowded

N.B.—All distances are in Å.

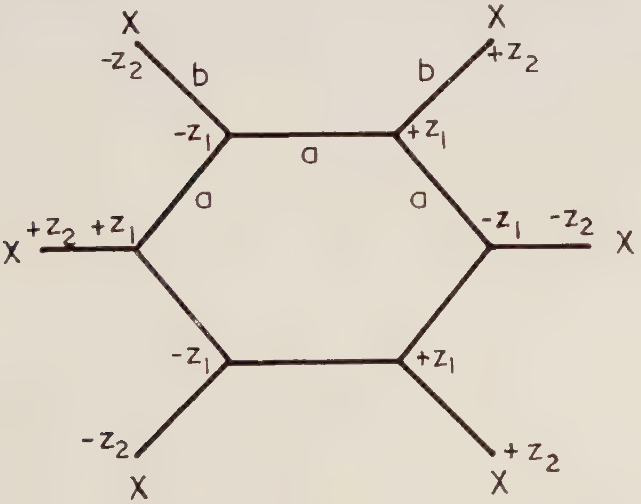

Figure 1. Out-of-plane displacements z_1, z_2 in C_6X_6.

Now the mere fact that $r_{\mathrm{x...x}}$ is less than $2r_{\mathrm{v.d.w.}}$ is no guarantee that the molecule will distort. But since the repulsive forces associated with atomic separations in which the van der Waals spheres overlap, rapidly increase with approach of the atoms, it is likely that at a certain stage the molecule extricates itself from the strain by buckling in such a way that alternate X atoms are displaced symmetrically above and below the mean plane. These X-displacements will presumably carry the attached carbon atoms through smaller displacements, leading to a corrugated appearance of the molecule.

The experimental evidence concerning these molecules is confused. Thus C_6Cl_6 has recently been shown to be exactly, or closely, planar in the solid state [1], and since C_6Br_6 and C_6Cl_6 are isomorphous, we may expect a similar situation in C_6Br_6. On the other hand some early electron-diffraction studies by Bastiansen and Hassel [2] suggested a corrugated model for C_6Cl_6. A more recent unpublished study by Bastiansen, however, seems to confirm the planar arrangement. Spectroscopic evidence [3] favours a little bending in the gas phase of C_6Cl_6, and so does some nuclear quadrupole resonance work [4]. Now it is just conceivable that packing forces in the solid might be sufficient to cause planarity—as seems to be probable in the case of diphenyl. And Ali and Coulson [5] have recently shown that intermolecular forces in the solid state are sufficiently large to cause certain small deformations away from planarity in the case of some polynuclear hydrocarbons. But it seems unlikely that large deformations would occur in this way. It is, of course, conceivable that the planar configuration is the most stable, but that large out-of-phase displacements occur in the course of internal molecular vibration. Such a situation might simulate a type of corrugation, as suggested by Harnik *et al.* [6]. Professor Schmidt [7] claims that, despite the large degree of overcrowding implied in the earlier table, both C_6Br_6 and C_6I_6 are planar molecules in the solid. However, it is possible that puckering may occur at some temperatures and not at others. Thus in the hexamethyl compound C_6Me_6, Wolf [8] finds a change of state at about 110°K, and Schnepp [9] pictures a situation in which, at low temperatures, all twelve carbon atoms are coplanar, with the methyl groups oriented in such a way that all six are geared to each other. As the temperature increases, the methyl groups appear to rotate without slipping gears, since the entropy change is just about R. But at higher temperatures, when slipping of the gears takes place, we must replace each methyl group by a van der Waals sphere, and then, since there is no room for all six methyls, the whole molecule becomes puckered. Now the van der Waals radius for chlorine is about the same as for methyl. It is clear, therefore, that steric forces must play a very critical rôle in determining planarity or puckering.

In view of all this, we have thought it worth while to see how much can be argued about these steric forces, on a theoretical basis.

2. THE REPULSIVE X...X POTENTIAL

A simple calculation shows how the steric forces X...X affect the molecular geometry. Let us suppose (figure 1) that the carbon atoms are kept fixed, in a regular coplanar hexagon, but that alternate C—X bonds are rotated, through an angle $\pm\theta$ out of the plane. Then if R denotes the distance X...X and $V(R)$ is the interatomic potential between any two adjacent X atoms, the change in potential energy due to the X...X forces is $\Delta V = 6\,(dV/dR)\,\delta R$. But simple geometry shows that $2R\,\delta R=(3b^2-ab)\,\theta^2$, so that (putting $R=a+b$)

$$\Delta V=\frac{3b(3b-a)}{(a+b)}\frac{dV}{dR}\,\theta^2.$$

Thus the X...X repulsive forces are equivalent to a contribution to the force constant for this motion, whose magnitude is

$$\frac{3b(3b-a)}{2(a+b)}\frac{dV}{dR}. \tag{1}$$

Since dV/dR is the slope of the X...X potential curve, it is negative for fairly close distances. Thus the X...X forces reduce the 'true' angular force constant by the amount (1). If the slope of the $V(R)$ curve is great enough as to make (1) exceed the unhindered force constant, the molecule will become puckered: otherwise it will stay planar, though the force constants for the corrugation-vibration and the in-phase 'umbrella' vibration should be strongly dependent on dV/dR. When the force constants for a series of C_6X_6 molecules have been determined experimentally, we may expect to throw light on this.

In calculating (1) no allowance has been made for corrugations of the carbon hexagon. These allowances can be introduced. But they only cause small alterations in (1), and will not therefore be described in detail. It is clear from (1) that the only new quantity to be calculated is dV/dR. In the following paragraphs we shall consider various contributions to V, and so to dV/dR. These include electrostatic forces due to (*a*) formal charges on C and X, (*b*) bond dipoles in C—X; conventional kinetic theory van der Waals forces; and exchange forces of a kind that we shall call pseudo-valence forces.

However, before calculating the effects of these forces we must consider the rest of the potential function for C_6X_6. Let us write this as

$$W=6V+U \tag{2}$$

where V is the X...X potential already discussed, and U is a conventional function of the internal coordinates. Since no complete treatment seems to be available for any of these molecules, we have represented U in the same way as Coulson and Senent [10] in their discussion of the steric deformation of seriously overcrowded polynuclear hydrocarbons such as 3 : 4-benzphenanthrene. This is the sum of (1) a set of non-planarity terms, governed by a force constant k_1, and having one such term for every carbon atom at which the directions of the three bonds are not coplanar; and (2) a set of torsion terms, governed by a force constant k_2, and having one such term for every C—C bond around which any torsion occurs. In the case of C_6X_6 we have chosen for the torsion constant k_2 the same value as Coulson and Senent obtained with benzene ($k_2=0{\cdot}0553\times10^5$ dynes cm^{-1}). There seems no definite knowledge of k_1, except of course for benzene. So we have used the same method as Westheimer [11], who also wanted to estimate some unknown force constants. In effect he compared force constants for saturated and unsaturated molecules, and then, using the known values for most of these, he could make plausible guesses for the others. The final values which we chose as a result of this procedure, were Cl, $k_1=0{\cdot}606$; Br, $k_1=0{\cdot}646$; I, $k_1=0{\cdot}740$, all in units of 10^5 dynes cm^{-1}. But we shall consider briefly the effect of varying k_1 from these values.

The explicit form of W in equation (2) now depends on the displacements of the carbon and halogen atoms away from their mean coplanar sites. If we call these z_1 and z_2 respectively, as in figure 1, W may be regarded as a function simply of z_1 and z_2. We look for the values of z_1 and z_2 that make W a minimum. The values $z_1 = z_2 = 0$ always lead to a stationary value of W. If it is a minimum the planar shape is stable, and the potential energy curve in this vibration is as in figure 2 (*a*). If it is a maximum, the planar shape is unstable, and the potential energy curve is as in figure 2 (*b*).

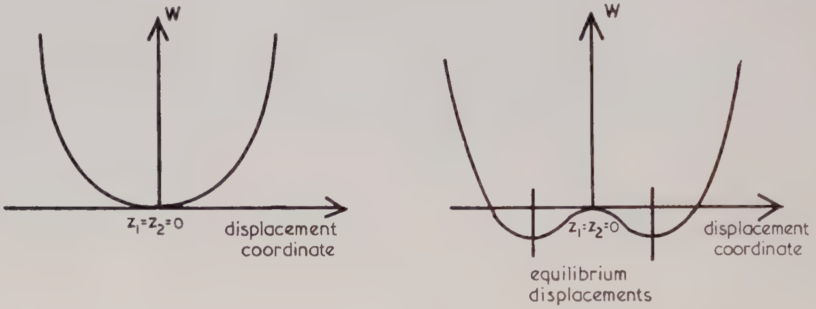

(*a*) (*b*)

Figure 2. Potential energy curves for C_6X_6. (*a*) case when equilibrium configuration is planar, (*b*) case when equilibrium configuration is corrugated.

3. Electrostatic forces

In molecules like C_6X_6 there will be electrostatic forces between the X atoms as a result of the polarity of the C—X bonds. If we write this as C^{+q}—X^{-q}, where $\pm q$ represents the formal charges on C and X, we may estimate the total X...X interaction (V in equation (1)) by considering all the Coulomb forces between the six charges $+q$ and the six charges $-q$. The value of q is to be estimated from the bond dipole moment, taken to be $\mu_{C-X} = bq$. In the case of C—Cl, this gives $b = 1{\cdot}72$ Å, $q = 0{\cdot}907 \times 10^{-10}$ e.s.u.

We have to find the values of z_1 and z_2 for which $\partial W/\partial z_1 = 0 = \partial W/\partial z_2$. When numerical values are inserted, it appears that the condition $\partial W/\partial z_1 = 0$ leads to an equation

$$\alpha z_1 + \beta z_2 = \text{terms of order } 1/200 \text{ of } \alpha z_1 \text{ and } \beta z_2.$$

Thus, to a high degree of accuracy $\alpha z_1 + \beta z_2 = 0$. Similarly $\partial W/\partial z_2 = 0$ leads to another equation $\gamma z_1 + \delta z_2 = 0$ where there is no proportionality between α, β, γ and δ. It follows that the solution is $z_1 = z_2 = 0$. Indeed, these forces lead to planar molecules for all four hexahalogenobenzenes.

An alternative calculation of V can be made by treating each C—X bond as a point dipole, localized at some place along the bond axis. But since the precise place at which the dipole should be located, is not quite certain, and since the magnitudes of the forces are of the same order as in the previous calculation, we have not carried these calculations any further. Our conclusion is that electrostatic forces do not lead to buckling of the molecule.

4. Kinetic Theory Van der Waals Forces

Terrell L. Hill [12] has given expressions for the interaction energy between two halogen atoms at a distance R apart. These are obtained from kinetic theory and viscosity data. He uses an inverse sixth power-exponential law of the form

$$V(R) = -2{\cdot}25\epsilon\left(\frac{R^*}{R}\right)^6 + 8{\cdot}28 \times 10^5 \epsilon \exp\left(\frac{-R}{0{\cdot}0736R^*}\right) \tag{3}$$

where the values of ϵ and R^* are given below:

$X=$	Cl	Br	I
$R^*=$	3·7	3·9	4·3
$10^{15}\epsilon=$	21·8	30·6	89·2

V and ϵ are in ergs/molecule, and R^* is in Å.

Using this form of $V(R)$ and the Coulson-Senent form of $U(R)$, it was found that the coplanar situation was the most stable one for C_6Cl_6 and C_6Br_6, but that in C_6I_6 a minimum of the total energy W occurred when

$$z_1 = 0{\cdot}050\,\text{Å}, \quad z_2 = 0{\cdot}403\,\text{Å}. \tag{4}$$

If we let θ be the angle which the C—X bond makes with the mean plane of the molecule, then in C_6I_6, $\theta = 9°$. We found by repeating these calculations for a variety of values of the fundamental force constant k_1, that the values in (4) were not strongly dependent on k_1. Since neither k_1 nor ϵ and R^* in (3) are known exactly, our conclusions from this calculation are that the best kinetic theory form of the van der Waals force leads to corrugation only in the hexaiodocompound.

5. PSEUDO-VALENCE FORCES

There is an alternative way of estimating $V(R)$, which makes use of purely spectroscopic data. It was originally proposed by Eyring [13] when studying hindered rotation in ethane, that there were exchange forces between the non-bonded hydrogen atoms attached to separate carbons. These arise because their spins are oriented randomly relative to each other. If the spins are anti-parallel, we have a singlet stage ${}^1\Sigma_g$ with energy ${}^1E(R)$. If they are parallel, we have a triplet state ${}^3\Sigma_u$ with energy ${}^3E(R)$. But if the spins are random the mutual energy is

$$E(R) = \tfrac{1}{4} \times {}^1E(R) + \tfrac{3}{4} \times {}^3E(R). \tag{5}$$

If spectroscopic measurements have been made of the two energy curves, it is thus possible to deduce $E(R)$. And if we may suppose that the electronic distribution around the H atoms in ethane (or in benzene) is the same as in a hydrogen molecule with its H atoms suitably separated, then (5) is the appropriate H...H energy. A calculation† for benzene (C_6X_6, with X = H) leads to an effective force constant (1) for puckering, whose numerical value is $0{\cdot}0009 \times 10^5$ dynes cm^{-1}. This is only a small fraction of the Coulson Senent force constant k_1, so that we feel confident in saying that H...H forces in benzene play only a relatively small part in determining these out-of-plane vibrations. This is not surprising in the case of C_6H_6 where the H...H distance (2·48 Å) is almost equal to twice the van der Waals radius for H, so that there is no overcrowding. But, as Adrian [14] has recently shown, this is not the case with overcrowded systems such as diphenyl. Here these pseudo-valence forces are of prime importance in determining the angle of mutual rotation of the two phenyl groups. Some other applications are described in a review article by one of us [15].

There are more serious objections to the use of (5) in the halogen molecules C_6X_6. For there are polarity effects in the C—X bonds and there is also the polarization of the bonding $p\sigma$ electrons as revealed by hybridization calculations. Both these effects are small or non-existent in C_6H_6. However, we have seen in § 3 that electrostatic effects do not suffice to cause buckling. We may therefore

† We are grateful to Miss Judith Westwood for making this calculation for us.

hope that the use of equation (5) for the halogen substituted benzenes may not be very inaccurate. In both C_6H_6 and C_6X_6, of course, the use of (5) pays no attention to any directional properties in the bonding orbitals.

We require $E(^1\Sigma_g)$ and $E(^3\Sigma_u)$. The potential functions for the ground states $^1\Sigma_g$ of the halogen molecules are given by Hulbert and Hirschfelder [16] in terms of the Morse function

$$E=D\,[1-\exp(-x)]^2, \quad x=2\beta\left(\frac{r-r_e}{r_e}\right)$$

where r is the X. . .X distance and the other parameters have the following values:

Molecule	D (cm^{-1})	2β	r_e
Cl_2	20298	4·015	1·989
Br_2	16063	4·482	2·284
I_2	12553	4·950	2·667

For the lowest-lying $^3\Sigma_u$ states, we found graphs [17] in the literature, and fitted them, over the important range of internuclear distances (3–4 Å) with equations of the form

$$E(r)=\left(\frac{c}{r-s}\right)^n+t,$$

where the parameters c, s, t and n have the following values:

Molecule	c	s	t	n
Cl_2	46·9	2·00	21800	2·16
Br_2	58·6	2·00	23000	1·82
I_2	609	2·30	12400	1·40

Since there appears to be still some uncertainty in the identification of these electronic levels, particularly for I_2 whose spin–orbit coupling may be important, we do not wish to claim a very great confidence in these values. But if we use them, and then combine the singlet and triplet energies according to equation (5) we can discuss possible steric deformations. Detailed calculations show that in all three cases no deformation would be expected, and all C_6X_6 molecules should be coplanar.

6. A POSSIBLE NEW CALCULATION OF $V(R)$

We have seen in § 3·5 that the shape of the $V(R)$ curve is crucial. But this curve is not well established, and we therefore considered four possible ways of estimating it. We now want to suggest a fifth way, which we shall illustrate for the hexachloro compound.

We begin with CCl_4 molecules. The law of force between these is well known [18]. If it is of the form

$$U(r)=4\epsilon[(\sigma/r)^{12}-(\sigma/r)^6] \qquad (6)$$

with $\epsilon = 327\,k\,^\circ\mathrm{K}$, $\sigma = 5{\cdot}881\,\text{Å}$. We may regard this interaction (figure 3) as the sum of all $C_1 \ldots Cl_2$ and $Cl_1 \ldots Cl_2$, etc. forces. The greater part will come from those $Cl_1 \ldots Cl_2$ interactions due to the closest Cl atoms in the two molecules. Let us therefore only consider $Cl_1 \ldots Cl_2$ forces and suppose that $U(r)$ in (6) is the statistical mean of all possible orientations of the two molecules. If the molecules are not too close together (no actual collision of atoms!) we may treat them as spherical, and then (figure 4)

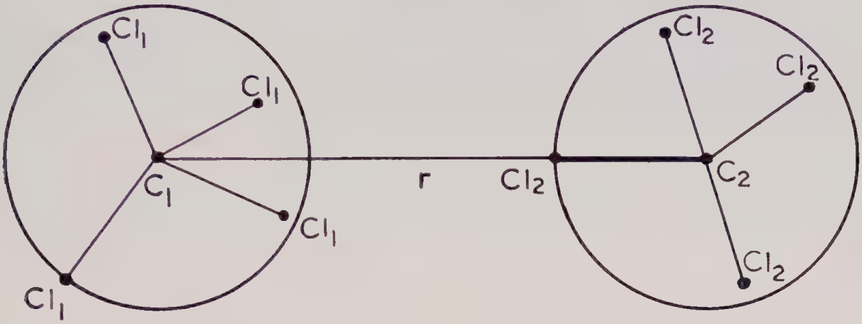

Figure 3. Two CCl_4 molecules with centres a distance r apart.

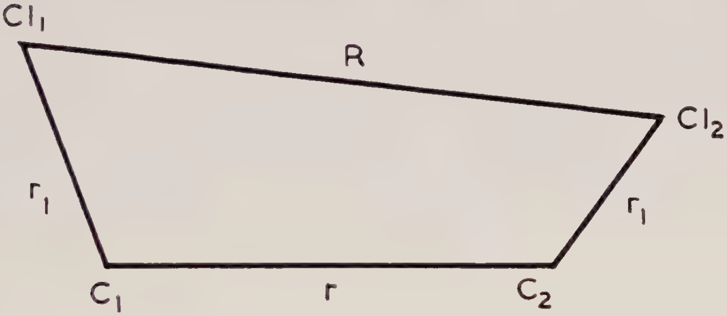

Figure 4.

$$U(r) = 16 \times \iint V(R) \frac{d\omega_1}{4\pi} \frac{d\omega_2}{4\pi} \tag{7}$$

where R is the Cl_1—Cl_2 distance, and $V(R)$ is the $Cl_1 \ldots Cl_2$ interaction energy; the integrations are over both solid angles ω_1 and ω_2. Our object now is to invert this last equation so that the experimental knowledge (6) of $U(r)$ may lead to a knowledge of $V(R)$. We tried several forms for $V(R)$, but finally came to the conclusion that the best one was of the form

$$V(R) = \frac{D_1}{R^3} + \frac{D_2}{R^4} + \frac{D_3}{R^5} + \frac{D_4}{R^6}, \tag{8}$$

where the coefficients $D_1 \ldots D_4$ had to be obtained by completing the integrations in (7) and then making the closest fit with (6) over the range of importance. It may be worth reporting that we found the form (8) far better than the conventional van der Waals' type energy $A/R^6 + B/R^{12}$. This is, perhaps, not very surprising, when it is realized that our device for determining the interaction energy does make some sort of allowance for polarity effects. This would lead us to expect lower powers of

$1/R$ than $1/R^6$. By fitting the value of the $U(r)$ obtained from the integration (7) to the observed $U(r)$ in (6) at $r = 3{\cdot}75$, $4{\cdot}25$, $4{\cdot}75$ and $5{\cdot}25$ Å, we found that in equation (8)

$$D_1 = 2{\cdot}00 \times 10^{-13},\ D_2 = -6{\cdot}390 \times 10^{-11},\ D_3 = 5{\cdot}802 \times 10^{-10},\ D_4 = -1{\cdot}088 \times 10^{-10} \tag{9}$$

when V is in ergs/molecule, and R is in Å.

This law of force may now be inserted in the equations to determine z_1 and z_2. The result is a corrugation of C_6Cl_6 defined by

$$z_1 = 0{\cdot}050\,\text{Å},\quad z_2 = 0{\cdot}332\,\text{Å},\quad \theta = 9^\circ. \tag{10}$$

We made an alternative calculation, fitting $U(r)$ at four other values of r. This led to a different set of coefficients (9), and to larger deflections (10). We have not reported these, because it is almost certain that this method overestimates $V(r)$. This is because we have neglected all interactions between two CCl_4 molecules which arise from the carbon atoms, and we have not fully allowed for the fact that, so far as possible, adjacent $C\,Cl_4$ molecules will tend to align themselves so that two chlorine atoms are not directly on the C...C line. If we were to reduce the $V(R)$ values by a factor of 2, the displacements in (10) would themselves be much reduced (perhaps by a factor of 4). If the $V(R)$ were reduced by a factor of about 4, there is no displacement at all.

We have verified that this method, when applied to CF_4 molecules, leads to an expected planar C_6F_6 molecule.

We also tried to estimate Cl...Cl forces by considering the interaction energy between two Cl_2 molecules. No satisfactory reversal of the integration in (7) seemed to be possible, presumably because, on account of the lack of spherical character in a single Cl_2 molecule, the interaction energy $U(r)$ should have angular terms, dependent on the mutual orientation of the two Cl_2 molecules. This method was therefore abandoned.

7. *o*-DISUBSTITUTED BENZENES

It is interesting to speculate on the situation in ortho-disubstituted benzenes. Here it is possible to relieve strain either by out-of-plane displacements, or by opening out the XCCX region, but still keeping the molecule planar (figure 5).

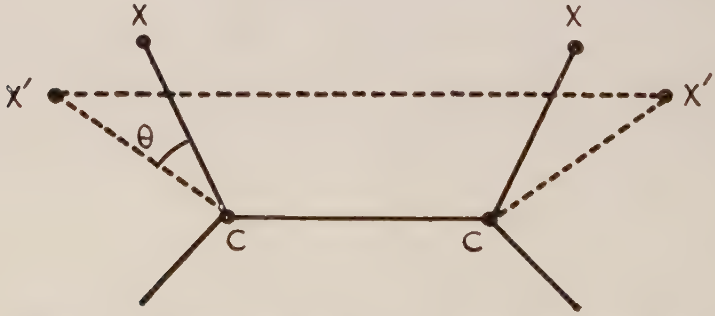

Figure 5. In-plane distortions in ortho-substituted molecules

In this latter case we suppose that the two X atoms move from X to X′, and the CX direction turns through an angle θ. The potential energy of the molecule is given by

$$W = V(R) + U$$

where $V(R)$ is the X...X interaction energy, U is the energy corresponding to the deformation θ, and we neglect H...Cl forces as being much smaller than Cl...Cl forces. For chlorine atoms

$$U = 2 \times \tfrac{1}{2} k b^2 \theta^2$$

where k is the in-plane wagging force constant given by $k = 0{\cdot}963 \times 10^5$ dyne cm^{-1}. When the expression (8) is used for $V(R)$ it is found that the equilibrium displacement is about $\theta = 4°$, and, further, that this is not modified by also allowing out-of-plane displacements. We conclude therefore that the ortho compounds should remain planar. This is just what is found for 1:2–4:5 tetra bromobenzene [19]. It is almost certainly also true for 1:2-4:5 tetrachlorobenzene. In the case of the bromo-compound, the observed value of θ is $1\frac{1}{2}°$, but the accuracy of this displacement is not sufficiently great to justify a comparison with the theoretical value. In the case of $C_6H_2Cl_4$ Dean *et al.* [20] obtain an experimental $\theta = 1\frac{1}{2}°$, approximately the same as in $C_6H_2Br_4$.

8. Steric repulsion energies

If our analysis is correct, there are evidently large forces between non-bonded atoms. Fortunately there is other evidence for the existence of these large forces. For example Baughan [21] from a careful comparison of bond energies and lengths, has estimated that in CCl_4 the C—Cl bond is about 0·128 Å longer than it would be, if these Cl...Cl repulsive forces could be neglected. Heath and Linnett [22] claim that this increase may even be as large as 0·49 Å, though a value in the region of 0·13 Å seems more likely. However, even the smaller value leads to substantial total energies. The use of a Urey-Bradley field for CCl_4 leads to a total Cl...Cl energy [23] of about 100 kcal. mole^{-1}. Our own law of force (8) leads to 162 kcal. mole^{-1}. (This is further evidence that (8) is about twice too large.) Similarly, our law of force leads to a barrier to internal rotation in hexachloroethane of about 35 kcal. mole^{-1}, to be compared with the experimental value [24] of 12 ± 2 kcal. mole^{-1}. These large values of steric energy will not normally be noticed (except of course when measuring the height of internal barriers to rotation), since as (1) shows, it is the rate of change of this energy rather than its absolute value, which affects steric deformation. It might have been expected that in the case of the series CH_nCl_{4-n} ($n = 0, 1, 2, 3, 4$) we should have detected it from a study of bond energies. But this may not be possible, since as van Vleck [25] showed several years ago, even in methane the H...H repulsion energy amounts to as much as 57 kcal. This is of the same order as the Cl...Cl energies. Until both of these terms are known with more certainty than at present, it is probably unprofitable to speculate on their difference. Our conclusion is that steric forces between non-bonded atoms really are large, and that, although we have no present way of calculating them at all exactly, our own values for the particular cases discussed in this paper are probably of the right order of magnitude.

On fait des calculs théoriques sur les énergies de répulsion entre atomes non liés pour les atomes d'halogène des hexa-halogéno-benzènes. On compare les conclusions théoriques avec les résultats expérimentaux disponibles.

Für die Abstossungsenergien zwischen den Halogenatomen in den Hexa-Halogenbenzolen werden theoretische Berechnungen durchgeführt. Die aus der Theorie gezogenen Schlussfolgerungen werden mit den zur Verfügung stehenden Messwerten verglichen.

References

[1] Tulinsky, A., and White, J. G., 1958, *Acta Cryst.*, **11,** 7.

[2] Bastiansen, O., and Hassel, O., 1947, *Acta chem. Scand.*, **1,** 489.

[3] Schnepp, O., and Kopelman, R., 1959, *J. chem. Phys.*, **30,** 868.

[4] Bray, P. J., Barnes, R. G., and Bersohn, R., 1956, *J. chem. Phys.*, **25,** 813.

[5] Ali, M. A., and Coulson, C. A., 1959, *J. chem. Soc.*, p. 1558.

[6] Harnik, E., Herbstein, F. H., Schmidt, G. M. J., and Hirschfeld, F. L., 1954, *J. chem. Soc.*, p. 3288.

[7] Schmidt, G. M. J. (private communication).

[8] Wolf, H. C., 1958, *Z. Naturf.* A, **13,** 336.

[9] Schnepp, O., 1958, *J. chem. Phys.*, **29,** 56.

[10] Coulson, C. A., and Senent, S., 1955, *J. chem. Soc.*, p. 1813.

[11] Westheimer, F. H., 1947, *J. chem. Phys.*, **15,** 252.

[12] Hill, T. L., 1948, *J. chem. Phys.*, **16,** 399.

[13] Eyring, H., *J. Amer. chem. Soc.*, **54,** 3191.

[14] Adrian, F. J., 1958, *J. chem. Phys.*, **28,** 608.

[15] Coulson, C. A., 1958, *Theoret Org. Chem. Papers, Kekulé Symposium*, p. 49.

[16] Hulbert, H. M., and Hirschfelder, J. O., 1941, *J. chem. Phys.*, **9,** 61.

[17] (*a*) Cl_2, Venkateswarlu, P., 1947, *Proc. Indian Acad. Sci.*, **26,** 22. (*b*) Br_2, *Ibid.*, **25** 138. (*c*) I_2, Mathieson, L., and Rees, A. L. G., 1956, *J. chem. Phys.*, **25,** 753.

[18] Hirschfelder, J. O., Curtiss, C. F., and Bird, R. B., 1954, *Molecular Theory of Gases and Liquids* (Wiley), p. 1114.

[19] Gafner, G., and Herbstein, F. H., 1958, *Mol. Phys.*, **1,** 412.

[20] Dean, C., Pollak, M., Craven, B. M., and Jeffrey, G. A., 1958, *Acta Cryst.*, **11,** 710.

[21] Baughan, E. C., 1953, *Quart. Rev.*, **7,** 103.

[22] Heath, D. F., and Linnett, J. W., 1948, *Trans. Faraday Soc.*, **44,** 561, 878.

[23] Urey, H. C., and Bradley, C. A., 1931, *Phys. Rev.*, **38,** 1969.

[24] Luft, N. W., 1955, *J. phys. Chem.*, **59,** 92.

[25] van Vleck, J. H., 1934, *J. chem. Phys.*, **2,** 20.

An analysis of the fluorescence spectrum of europium ethyl sulphate

by B. R. JUDD†
The Clarendon Laboratory, Oxford

(*Received* 20 *February* 1959)

A theoretical analysis is made of the splittings induced in the levels $^7F_1$, $^7F_2$, $^7F_3$, $^7F_4$, $^7F_5$, $^7F_6$ of the ion Eu^{3+} by the electric field of the ethyl sulphate lattice. Four parameters are used to fit the data, and it is found that very good agreement can be established between experiment and theory in the great majority of cases. The parameters are compared to the corresponding ones for other rare earth ethyl sulphates. A reason is given for the absence of a magnetic dipole character in the transition $^5D_1 \rightarrow {}^7F_1$.

1. Introduction

The fluorescence spectra of crystals containing Eu^{3+} ions have been of interest for some time now. Early work was carried out by Gobrecht [1], Lange [2], and Deutschbein [3]. More recently Sayre and Freed [4] have examined in detail the spectrum of europium ethyl sulphate, $Eu(C_2H_5SO_4)_3 . 9H_2O$, and the present paper is based on the experimental results they give. The ground term of Eu^{3+} is ^7F, which under the influence of spin–orbit coupling breaks up into seven levels ^7F_J, where $J=0, 1, 2, \ldots, 6$. The fluorescence corresponds to transitions to these levels from two excited levels, which Sayre and Freed designate X_1 and X_0; there seems to be no doubt, however, that these levels are in fact $^5D_1$ and $^5D_0$ [5, 6], and the latter descriptions will be used here. Owing to the electric field produced at a europium ion by the crystal lattice, the $(2J+1)$-fold degeneracy of a level is wholly or partially lifted, and as a consequence the spectrum shows a fine structure. The spacings of the levels are such that $^5D_1 \rightarrow {}^7F_4$ overlaps $^5D_0 \rightarrow {}^7F_2$, while $^5D_1 \rightarrow {}^7F_5$ and $^5D_1 \rightarrow {}^7F_6$ nearly coincide with $^5D_0 \rightarrow {}^7F_3$ and $^5D_0 \rightarrow {}^7F_4$ respectively [4]. One of the features of the investigation of Sayre and Freed was that they were able to separate these transitions and give fairly complete energy level schemes for all the levels.

Several detailed analyses of the crystal splittings of levels in rare earth ions have already been carried out [7, 8], and the treatment given here will follow the previous pattern. The detailed theory is based on the work of Stevens [9] and Elliott *et al.*. [10]. The Hamiltonian for an ion Eu^{3+} in the ethyl sulphate lattice is assumed to be the same as that for a free ion to which the terms

$$\begin{aligned} V = A_2^0\sum(3z^2-r^2) + A_4^0\sum(35z^4-30z^2r^2+3r^4) \\ + A_6^0\sum(231z^6-315z^4r^2+105z^2r^4-5r^6) \\ + A_6^6\sum(x^6-15x^4y^2+15x^2y^4-y^6) \end{aligned} \quad (1)$$

are added. The summations run over the six $4f$-electrons that the europium ion possesses. The quantities A_n^m are characteristic of the lattice and always occur in the analysis in conjunction with the corresponding quantities $\langle r^n \rangle$, the mean value of r^n for a single $4f$-electron. The products $A_n^m\langle r^n \rangle$ are called the crystal field parameters, and the problem is to fit the crystal splittings of the levels ^7F_J treating these parameters as adjustable constants.

---

† Present Address: The Radiation Laboratory, University of California, Berkeley.

2. Method of analysis

The crystal splittings of the levels are of the order of 100 cm^{-1}, whereas the spacings between the levels are in the region of 1000 cm^{-1}. It is therefore convenient to set up the problem in which the states are labelled by the quantum numbers $LSJJ_z$ and then use perturbation theory to find the effect of V. The matrix elements of the various components of V between states possessing the same value of J are easily found by means of the equivalences

$$\sum(3z^2-r^2)\equiv \alpha\langle r^2\rangle[3J_z^2-J(J+1)],$$

$$\sum(35z^4-30z^2r^2+3r^4)\equiv \beta\langle r^4\rangle[35J_z^4-30J(J+1)J_z^2+25J_z^2 -6J(J+1)+3J^2(J+1)^2],$$

$$\sum(231z^6-315z^4r^2+105z^2r^4-5r^6)\equiv \gamma\langle r^6\rangle[231J_z^6-315J(J+1)J_z^4+735J_z^4 +105J^2(J+1)^2J_z^2-525J(J+1)J_z^2 +294J_z^2-5J^3(J+1)^3+40J^2(J+1)^2 -60J(J+1)],$$

$$\sum(x^6-15x^4y^2+15x^2y^4-y^6)\equiv \tfrac{1}{2}\gamma\langle r^6\rangle[(J_x+iJ_y)^6+(J_x-iJ_y)^6],$$

which are given by Stevens [9] and Elliott and Stevens [11]. Values of α, β and γ have been calculated for all the levels of the ground multiplet, and they are set out in table 1.

Level	α	β	γ
$^7F_6$	1/99	−2/11 . 15 . 99	1/11 . 189 . 429
$^7F_5$	1/135	2/99 . 105	−1/189 . 429
$^7F_4$	1/385	23/15 . 33 . 77	2/77 . 429
$^7F_3$	−1/135	1/33 . 45	−2/27 . 429
$^7F_2$	−11/315	−2/189	0
$^7F_1$	−1/5	0	0
$^7F_0$	0	0	0

Table 1. Operator equivalent factors for the ground multiplet of Eu^{3+}.

With a knowledge of the operator equivalent factors α, β and γ, the first-order splittings of the levels may be quickly found. The influence of neighbouring levels, for example, corrections to $\langle {}^7F_J, J_z|V|{}^7F_J, J_z\rangle$ of the type

$$\langle {}^7F_J, J_z|V|{}^7F_{J'}, J_z'\rangle\langle {}^7F_{J'}, J_z'|V|{}^7F_J, J_z\rangle/W, \tag{2}$$

where W is the energy separation of $^7F_{J'}$ and ^7F_J, involves knowing the matrix elements of V between states possessing different values of J. The method described by Judd [12] was used here.

In an earlier paper [13] the author showed that the centres of gravity of the levels ^7F_J are seriously displaced by intermediate coupling effects. Thus $^7F_1$ is depressed by 1150 cm^{-1} due to the mechanism

$$\langle {}^7F_1|\sum \mathbf{l}\cdot\mathbf{s}|{}^5D_1\rangle\langle {}^5D_1|\sum \mathbf{l}\cdot\mathbf{s}|{}^7F_1\rangle/E, \tag{3}$$

where E is the energy of $^5D_1$ above $^7F_1$ (18 700 cm^{-1}). The symbol J_z is omitted from the matrix elements since they are independent of this quantum number. It is natural to anticipate serious corrections to the splitting of $^7F_1$; i.e. corrections to $\langle {}^7F_1, J_z|V|{}^7F_1, J_z\rangle$ of the type

$$\langle {}^7F_1, J_z|\sum \mathbf{l}\cdot\mathbf{s}|{}^5D_1, J_z\rangle\langle {}^5D_1, J_z|V|{}^5D_1, J_z\rangle\langle {}^5D_1, J_z|\sum \mathbf{l}\cdot\mathbf{s}|{}^7F_1, J_z\rangle/E^2.$$

However, a detailed study of the effect of terms of the type ^5D, ^5F and ^5G (which will certainly make the most important contribution) on the ground term ^7F by Mr. Loudon (privately communicated) reveals that their effect is in fact extremely small, even compared to second-order crystal field effects as exemplified by (2), and they may safely be neglected. We see therefore that the effect of the partial breakdown of Russell–Saunders coupling is to depress the centres of gravity of the levels by large amounts without altering their splittings. Since in this paper we are concerned only with the latter effect, the centres of gravity will be treated as adjustable parameters; fitting these parameters to a theory will of course be independent of crystal field effects. A theory carried to second order in the spin-orbit coupling (i.e. involving perturbation mechanisms of the type (3)) has already been given [13], and the present results for the centres of gravity of the levels are essentially the same as the values used in that paper, which were obtained from other europium crystals.

The method for finding the values of the crystal field parameters which best reproduce the experimental results follows a process of successive approximation. Neglecting second-order effects of the type (2), the structure of $^7F_1$ gives at once a preliminary value for $A_2^0\langle r^2\rangle$. Consideration of $^7F_2$, $^7F_3$ and $^7F_4$ enables values of the other parameters to be obtained, and from these the second-order corrections (which are of the order of 10 cm^{-1}) can be calculated. These results lead to better estimates of the parameters, and a set is obtained which is the most satisfactory. The levels $^7F_5$ and $^7F_6$ were purposely excluded from the initial analysis because experimentally their crystal splittings are the most difficult to obtain accurately; hence if any inconsistencies had arisen through using data on these levels (and it will later be seen that this would have happened), these data would be discarded rather than data on $^7F_1$, $^7F_2$, $^7F_3$ or $^7F_4$. The crystal splittings of $^7F_5$ and $^7F_6$ that will subsequently be given are therefore predicted on the basis of the analysis of the other levels.

3. COMPARISON WITH EXPERIMENT

The point symmetry at a rare earth ion in the ethyl sulphate lattice is of the type C_{3h} [14], though the nine waters of crystallization which cluster around the ion exhibit the slightly higher symmetry D_{3h}. The distinction between these two symmetries enters the theory through the contributions to V of odd parity, for whereas in the case of C_{3h} symmetry terms such as

$$A_3^3\sum[a(x+iy)^3+b(x-iy)^3]$$

are included in the complete expression for V, the corresponding contribution for D_{3h} symmetry must satisfy $a=\pm b$. However, the matrix elements of terms of odd parity between states built from the configuration f^6 are zero, and since the present analysis is restricted to such states, expressions of odd parity need not be included in V. Thus, if configurational interaction is neglected, the energy levels may be labelled by the irreducible representations of D_{3h} in spite of the fact that the true point symmetry is C_{3h}. In some cases, Sayre and Freed [4] were able to show that such a classification is more appropriate than a classification according to the irreducible representations of C_{3h}, a result perhaps of the local symmetry about a europium ion. The four one-dimensional irreducible representations of D_{3h} can be spanned by any linear combinations of the kets (defined by values of J and J_z) set out below:

$$\begin{array}{ll} A_1' & |0,0\rangle,\ |2,0\rangle,\ |4,0\rangle,\ |6,0\rangle,\ \sqrt{\tfrac{1}{2}}|6,6\rangle+\sqrt{\tfrac{1}{2}}|6,-6\rangle. \\ A_2' & |1,0\rangle,\ |3,0\rangle,\ |5,0\rangle,\ \sqrt{\tfrac{1}{2}}|6,6\rangle-\sqrt{\tfrac{1}{2}}|6,-6\rangle. \\ A_1'' & \sqrt{\tfrac{1}{2}}|J,3\rangle+(-1)^J\sqrt{\tfrac{1}{2}}|J,-3\rangle. \\ A_2'' & \sqrt{\tfrac{1}{2}}|J,3\rangle-(-1)^J\sqrt{\tfrac{1}{2}}|J,-3\rangle. \end{array}$$

The pairs of kets, any linear combinations of which span the two two-dimensional irreducible representations of D_{3h}, are as follows:

$$\begin{array}{ll} E' & |J,\pm 2\rangle,\ \ |J,\mp 4\rangle. \\ E'' & |J,\pm 1\rangle,\ \ |J,\mp 5\rangle. \end{array}$$

The reduction $D_{3h}\rightarrow C_{3h}$ is accomplished very simply by eliminating the subscripts on the symbols for the irreducible representations of D_{3h}.

The set of parameters which were used in the last stages of the analysis and which were felt to give the best account of the experimental results are as follows:

$$\begin{array}{ll} A_2^0\langle r^2\rangle=80, & A_6^0\langle r^6\rangle=-38{\cdot}6, \\ A_4^0\langle r_4\rangle=-63{\cdot}1, & A_6^6\langle r^6\rangle=510\ \text{cm}^{-1}. \end{array}$$

The splittings of the levels which are calculated on the basis of these parameters, taking interactions between levels into account, are set out in table 2. The deviations between columns (b) and (e) for the levels ${}^7F_1$, ${}^7F_2$ and ${}^7F_3$ are in all cases not greater than 1 cm^{-1}. Six energy spacings are being fitted to four parameters, and the excellent agreement between experiment and theory gives one a great deal of confidence in applying the theory to the other levels. It should be mentioned that in their paper, Sayre and Freed interchange the symbols A_1' and E'' for the components at 1106 and 1015 cm^{-1}, but it is clear that this is a trivial slip in interpreting their own data. The polarization of the fluorescence lines points directly to the designations given in table 2.

The agreement between experiment and theory in the case of ${}^7F_4$ is quite satisfactory, and it is not until the next level is examined that serious discrepancies arise. Components of the type A' are only observed if the transition involved is magnetic dipole in character, and the absence of an energy level in the vicinity of 3826 cm^{-1} is not significant. (For similar reasons the A' components of ${}^7F_4$ and ${}^7F_6$ are not observed.) The main cause for disquiet lies in the inversion of the order in which A_2'' and E' occur in column (c) compared to (d). In a private communication, Professor Sayre has commented on this discrepancy, and considers that the experimental evidence for the energies 4021 and 3997 is definite in both the transitions ${}^5D_0\rightarrow{}^7F_5$ and ${}^5D_1\rightarrow{}^7F_5$. The present writer has checked the calculations, and finds it difficult to see how such a result can be incorporated into the theory. If the analysis is correct, the only solution to this problem involves both the presence of spurious lines and the absence of expected ones. The matter must rest at present in this unsatisfactory position.

In the case of ${}^7F_6$, only the two E'' components show appreciable deviations from the experimental scheme. The evidence for these comes from the transition ${}^5D_1\rightarrow{}^7F_6$ alone, and Professor Sayre considers that it is possible that the energy level at 4915 is spurious. Thus in this case the discrepancies between experiment and theory are not so disconcerting as for ${}^7F_5$.

Level	(a)	(b)	(c)	(d)	(e)
$^7F_6$	103·6	5105	A_2'		
	101·9	5103	A_1'		
	33·3	5034	E''		
	23·6	5025	A_1'		
	6·4	5007	E''	E''	4996
	−6·5	4996	E'	E'	4992
	−25·1	4976	A_1''	A''	4976
	−44·5	4957	E'	E'	4958
	−64·9	4936	A_2''	A''	4937
				E''	4915
$^7F_5$	138·7	4061	A_2''	E'	4021
	80·3	4003	E'	A''	3997
	31·7	3954	E''	E''	3955
	13·5	3936	A_1''	A''	3937
	−46·9	3876	E'	E'	3880
	−64·4	3858	E''	E''	3858
	−96·4	3826	A_2'		
$^7F_4$	169·8	3050	A_1''	A_1''	3056
	14·0	2894	E'	E'	2893
	11·5	2892	A_2''	A_2''	2890
	10·0	2890	A_1'		
	−34·7	2845	E''	E''	2841
	−98·4	2782	E'	E'	2782
$^7F_3$	17·0	1928	E''	E''	1929
	2·7	1914	A_1''	A_1''	1913
	−6·8	1904	E'	E'	1903
	−32·5	1878	A_2'		
	−54·0	1857	A_2''	A_2''	1856
$^7F_2$	60·2	1105	A_1'	A_1'	1106
	−15·9	1031	E'	E'	1031
	−31·4	1016	E''	E''	1015
$^7F_1$	22·5	399	A_2'	A_2'	398
	−21·0	356	E''	E''	356
$^7F_0$	−6·6	0	A_1'	A_1'	0

Column (a) gives the calculated energy of a component relative to the centre of gravity of the level in the free ion Eu^{3+}. The irreducible representation of D_{3h} describing the component is given in (c). The energy level scheme and the types of the components which Sayre and Freed [4] observed are set out in (e) and (d). Column (b) repeats column (a) except that all the components of a level are given an identical displacement to bring the theoretical scheme as close as possible to (e). All energies are measured in cm^{-1}.

Table 2. A comparison between theory and experiment.

4. THE TRANSITION $^5D_1 \to {}^7F_1$

The selection rules for magnetic dipole radiation are $\Delta J = 0, \pm 1$, where ΔJ is the difference in the two values of J for the levels concerned. The transition $J = 0 \to J = 0$ is excluded. Sayre and Freed [4] find that the transitions $^5D_1 \to {}^7F_0$, $^5D_1 \to {}^7F_2$, and $^5D_0 \to {}^7F_1$ are all magnetic dipole in origin, but that $^5D_1 \to {}^7F_1$ occurs as electric dipole only. The absence of the anticipated magnetic dipole character of this transition has a fairly simple explanation. The level labelled $^7F_1$ is not built from pure $^7F_1$ states, but, owing to off-diagonal matrix elements of the spin–orbit coupling, contains small amounts of other levels with $J = 1$, principally $^5D_1$ and $^5F_1$. Similarly, the $^5D_1$ level contains small admixtures of $^7F_1$, $^5P_1$, $^5F_1$, $^3P_1$ and $^3D_1$. If quantities which can contribute to the first order in smallness only are retained in finding the matrix element of a component $L_i + 2S_i$ of the magnetic dipole operator between the impure $^5D_1$ and $^7F_1$ states, one obtains the expression

$$[\langle {}^7F_1, J_z| + x\langle {}^5D_1, J_z|](L_i + 2S_i)[|{}^5D_1, J_z'\rangle - x|{}^7F_1, J_z'\rangle]$$

for the matrix element which determines the transition probability. It can be immediately written as

$$x\langle J_z|J_i|J_z'\rangle[g({}^5D_1) - g({}^7F_1)],$$

where, in the usual way,

$$g({}^{2S+1}L_J) = 1 + \frac{J(J+1) - L(L+1) + S(S+1)}{2J(J+1)}.$$

However, it is easily seen that $g({}^5D_1) = g({}^7F_1) = 3/2$, so the matrix element vanishes, and in this approximation the transition probability for $^5D_1 \to {}^7F_1$ is zero. The argument has been simplified by neglecting the two other $^5D_1$ levels which exist in f^6; but they lie far away in the ultra-violet and play only a small rôle in the calculation. The corresponding matrix elements do not vanish in those cases where $J = \pm 1$, and hence the absence of magnetic dipole character in the transition $^5D_1 \to {}^7F_1$ is accounted for.

5. DISCUSSION

Many rare earth ions in the ethyl sulphate sulphate lattice show a paramagnetic resonance. The experimental results for ions containing an odd number of electrons, i.e. possessing an energy level structure consisting entirely of Kramers doublets, have been examined in great detail by Elliott and Stevens [11]. More recently, Baker and Bleaney [15] have studied salts of ions containing an even number of electrons. These analyses give information about the crystal field parameters $A_n^m\langle r^n\rangle$ for ions in the ethyl sulphate lattice, though in many cases it is impossible to obtain their values uniquely. Interpolation techniques are used least in the first half of the rare earth series, and the various values of the parameters that these two sources give are set out in table 3. For completeness, the values for Eu^{3+} obtained in the present paper are included.

The general trends of the parameters $A_6^6\langle r^6\rangle$ and $A_6^0\langle r^6\rangle$ are apparent, but $A_4^0\langle r^4\rangle$ shows some irregularities, and there appears to be little pattern to the value of $A_2^0\langle r^2\rangle$ as one proceeds along the rare earth series. The striking difference between the values of $A_2^0\langle r^2\rangle$ for PrCl$_3$ and NdCl$_3$ has been discussed elsewhere [8], and the large value of $A_2^0\langle r^2\rangle$ for europium ethyl sulphate, an outstanding feature of table 3, is a result of the same kind. There is a slight suggestion that the value of $A_2^0\langle r^2\rangle$ depends on whether the ion has an odd or an even number of electrons. Elliott and Stevens [11], in their analysis of ions of the first kind, found that a small negative value of $A_2^0\langle r^2\rangle$ is satisfactory for Ce^{3+} and Nd^{3+} and were able to take it to be zero for other ions; whereas Baker and Bleaney [15] give positive values for Pr^{3+} and Tb^{3+}, and it is positive also for Eu^{3+}. However, it would probably be premature, and in any case out of place in the present paper, to examine this idea in any further detail.

Ion	Ce^{3+}	Pr^{3+}	Nd^{3+}	Pm^{3+}	Sm^{3+}	Eu^{3+}	Gd^{3+}
$A_2^0\langle r^2\rangle$	−15	50	−15	—	0	80	—
$A_4^0\langle r^4\rangle$	−40	−100	−35	—	−30	−63	—
$A_6^0\langle r^6\rangle$	−92	−48	−60	—	−54	−39	—
$A_6^6\langle r^6\rangle$	1150	660	640	—	590	510	—

All entries are in cm^{-1}.

Table 3. Values of the crystal field parameters.

6. CONCLUSION

A consistent treatment has been given of the crystal splittings of the ground multiplet of the ion Eu^{3+} in the ethyl sulphate lattice. Apart from a few discrepancies in the cases of $^7F_5$ and $^7F_6$, the agreement between experiment and theory is highly satisfactory. The theory of the ^7F multiplet in Tb^{3+} would follow a very similar pattern; the multiplet is inverted, and the operator equivalent factors are opposite in sign to those given in table 1. It is interesting to note that the present theory for Eu^{3+} gives two close components A_2' and A_1' uppermost in the multiplet: if the crystal field parameters for Tb^{3+} are similar to those for Eu^{3+}, this pair of components would be expected to come lowest in terbium ethyl sulphate. In fact, Baker and Bleaney [15] observed paramagnetic resonance between two components of this kind, the zero-field separation between them being only 0·387 cm^{-1}. The greater separation between the corresponding pair in europium ethyl sulphate, namely 1·7 cm^{-1}, indicates that $A_6^6\langle r^6\rangle$ is greater for this salt—for this parameter alone is responsible for the splitting.

Finally, it should be mentioned that Gruen *et al.* [16] have observed fluorescence in crystals of $LaCl_3$ containing small amounts of Am^{3+}. This ion is the analogue of Eu^{3+}, the ground state being $5f^6\,{}^7F_0$ instead of $4f^6\,{}^7F_0$. It would be of considerable interest to discover whether a theory based on a static crystalline electric field would be adequate to account for the experimental results, and it is to be hoped that the fluorescence lines which have been observed can eventually be interpreted in terms of an energy level scheme.

I wish to thank Professor E. V. Sayre for his comments and Mr. R. Loudon for communicating to me the results of his calculation on the deviations from Russell–Saunders coupling.

On fait une analyse théorique des dédoublements induits par le champ électrique du réseau du sulfate d'éthyle dans les niveaux, $^7F_1$, $^7F_2$, $^7F_3$, $^7F_4$, $^7F_5$, et $^7F_6$ de l'ion Eu^{3+}. Quatre paramètres sont employés pour l'ajustement aux données expérimentales, et on trouve qu'un très bon accord peut être établi, dans la grande majorité des cas, entre l'expérience et la théorie. On compare les paramètres aux valeurs correspondantes pour les sulfates d'éthyle d'autres terres rares. On fournit une explication de l'absence de caractère dipolaire magnétique dans la transition $^5D_1 \rightarrow {}^7F_1$.

Durch das elektrische Feld des Äthylsulfatgitters werden die Niveaus $^7F_1$, $^7F_2$, $^7F_3$, $^7F_4$, $^7F_5$, $^7F_6$ des Eu^{3+} Ions gespalten; diese Aufspaltungen werden theoretisch analysiert. Zur Anpassung der Messwerte werden vier Parameter benutzt, mit deren Hilfe es gelingt, in der überwiegenden Mehrzahl der Fälle eine gute Übereinstimmung zwischen Experiment und Theorie zu erreichen. Die Parameter werden mit den entsprechenden Werten für die Äthylsulfate anderer seltener Erdmetalle verglichen. Die Abwesenheit eines magnetische Dipolcharakters im Übergang $^5D_1 \to {}^7F_1$ wird begründet.

REFERENCES

[1] GOBRECHT, H., 1937, *Ann. Phys.*, **28,** 673.
[2] LANGE, H., 1938, *Ann. Phys.*, **32,** 361.
[3] DEUTSCHBEIN, O., 1939, *Ann. Phys.*, **36,** 183.
[4] SAYRE, E. V., and FREED, S., 1956, *J. chem. Phys.*, **24,** 1213.
[5] HELLWEGE, K. H., and KAHLE, H. G., 1951, *Z. Phys.*, **129,** 62.
[6] HELLWEGE, K. H., and KAHLE, H. G., 1951, *Z. Phys.*, **129,** 85.
[7] JUDD, B. R., 1957, *Proc. roy. Soc.* A, **241,** 414.
[8] JUDD, B. R., 1959, *Proc. roy. Soc.* A, **251,** 134.
[9] STEVENS, K. W. H., 1952, *Proc. phys. Soc. Lond.*, A, **65,** 209.
[10] ELLIOTT, J. P., JUDD, B. R., and RUNCIMAN, W. A., 1957, *Proc. roy. Soc.* A, **240,** 509.
[11] ELLIOTT, R. J., and STEVENS, K. W. H., 1953, *Proc. roy. Soc.* A, **219,** 387.
[12] JUDD, B. R., 1955, *Proc. roy. Soc.* A, **227,** 552.
[13] JUDD, B. R., 1956, *Proc. phys. Soc. Lond.*, A, **69,** 157.
[14] KETELAAR, J. A. A., 1937, *Physica*, **4,** 619.
[15] BAKER, J. M., and BLEANEY, B., 1958, *Proc. roy. Soc.* A, **245,** 156.
[16] GRUEN, D. M., CONWAY, J. G., MCLAUGHLIN, R. D., and CUNNINGHAM, B. B., 1956, *J. chem. Phys.*, **24,** 1115.

Environmental perturbations on foreign atoms and molecules in solid argon, krypton and xenon†

by MACLYN McCARTY, Jr. and G. WILSE ROBINSON‡
Department of Chemistry, The Johns Hopkins University, Baltimore, Maryland

(*Received* 4 *August* 1959)

Perturbations which are responsible for the shifts of electronic and vibrational spectra of species trapped in a solid are considered in terms of the intermolecular potential which describes interactions between these species and neighbouring atoms. It is shown that in certain instances London's theory can give an adequate approximation to the dispersion energy between an electronically excited species and a rare gas atom. The experimental shifts in the electronic absorption spectra of Hg, NH and C_2 at lattice sites in rare gas crystals at 4·2°K are explained quantitatively on the basis of a Lennard-Jones (6–12) or (6–8–12) potential between the trapped species and the rare gas atoms. The theory does not adequately explain the shifts in those cases where strong angular dependent forces differing appreciably in the two electronic states are present, data on trapped NH_2 free radicals being presented as a case in point. The interaction of sodium atoms with argon at 4·2°K is very complex, the data being consistent with multiple trapping sites for the atoms, a large repulsive interaction between the excited state of sodium and the rare gas, and apparent removal of the three-fold orbital degeneracy in the excited state by the environmental perturbation. The three-fold orbital degeneracy in the $^3P_1$ state of mercury was found also to be removed. The blue shift of 1281 cm^{-1} for the $^3P_1 \leftarrow {}^1S_0$ transition of mercury in solid argon at 4·2°K corresponds almost exactly with the position of one of the two prominent features in the spectrum of mercury in argon gas at comparable densities and illustrates the similarity of structure in the two physical states. The interesting perturbations on the vibrational states of NH and C_2 suggest a close similarity to the effect which causes environmental variations of coupling constants for hyperfine interactions in trapped hydrogen atoms.

1. INTRODUCTION

Because of the recent interest in the study of simple atoms and free radicals trapped in inert solids at low temperatures, a number of interesting experimental results have emerged concerning the effects of environmental perturbations on the trapped species. The perturbations may divulge themselves through changes in the vibrational structure of a trapped molecule, changes in the coupling between electron spins and nuclear spins as evidenced through electron spin resonance studies and finally by shifts in the electronic spectra of the trapped species. These three effects are all caused by perturbations on the electronic eigenstates, and for this reason the latter, where the effects are relatively large, is perhaps the most direct way of studying them. This paper attempts to explain the shifts as well as some of the other interesting features in the electronic spectra of trapped Hg, NH, NH_2, C_2 and Na on the basis of a very simple model using Lennard-Jones (6–12) and (6–8–12) potential functions to describe the interactions between trapped species and rare gas atoms in a rare gas crystal at 4·2°K.

---

† Work supported in part by Office of Ordinance Research, U.S. Army and the National Science Foundation.

‡ Present address: Gates and Crellin Laboratories of Chemistry, California Institute of Technology, Pasadena, California.

2. The intermolecular potential

An intermolecular pair potential function ϕ_{ab} for non-valence interactions between two non-polar species a and b can usually be described as a small perturbation upon the zero-order system defined when the two species approach infinite separation. The perturbation Hamiltonian for the interaction contains purely electrostatic terms due to the repulsion of electrons and nuclei of one species by those of the other, and attractive terms arising from electron-nuclear interactions. If there is no angle dependence the perturbation Hamiltonian is [1]

$$H_{ab}=\frac{Z_aZ_be^2}{r_{ab}}+\sum_{i=1}^{n_a}\sum_{j=1}^{n_b}\frac{e^2}{r_{ij}}-\sum_{i=1}^{n_a}\frac{Z_be^2}{r_{bi}}-\sum_{j=1}^{n_b}\frac{Z_ae^2}{r_{aj}} \tag{1}$$

for atoms having nuclear charges Z_a and Z_b and n_a and n_b electrons respectively.

The zero-order wave functions are taken to be products of the unperturbed atomic wave functions properly antisymmetrized with respect to permutations among all (n_a+n_b) electrons, and ϕ_{ab} is then calculated as first- and second-order perturbation corrections, $\phi_{ab}{}^{\mathrm{I}}$ and $\phi_{ab}{}^{\mathrm{II}}$, to the energy at infinite separation. In the first-order calculation coulomb terms arise which are analogous to classical interactions among spherical charge distributions and positive point charges. In addition there are exchange terms present which arise because of the antisymmetrization, and these are characterized by the usual sign reversal associated with Fermion eigenfunctions. Calculations of neon–neon [2] and argon–argon [3] interactions show the exchange contributions, which because of the sign reversal are repulsive, to be about six times larger than the coulomb contributions for which attractive terms dominate.

Second-order theory takes into account to some extent the distortion of the electronic wave functions of the interacting species as a result of the perturbation. This part of the calculation is normally carried out by expanding [4] the interaction Hamiltonian in inverse powers of the intermolecular separation. Since exchange terms fall off very rapidly with distance they are not important in the second-order calculations except at intermediate distances. The second-order coulomb terms are responsible for the usual London [5] dispersion forces and are generally but not always attractive. For atoms in S-states the first non-vanishing term in the expansion yields the well-known inverse sixth-power dependency of intermolecular force on separation. For intermediate distances higher order terms of the type, $-C_8/r^8$, $-C_{10}/r^{10}\ldots$, become important. Little is known experimentally about these contributions but for the rare gases theoretical calculations [6] show the magnitude of the eighth-power term to be about one-third the magnitude of the sixth-power term at a distance corresponding to the minimum in the pair potential function. The tenth-power term gives a much smaller contribution at these distances. For atoms not in S-states the atomic quadrupole moments must be considered.

The inverse sixth-power term given by the results of the second-order theory is [5]

$$\phi_{ab}^{\text{II}}(k_a, k_b) = \frac{1}{r_{ab}^6}\left(\frac{3e^4\hbar^4}{2m^2}\right) \times \sum_{k_a', k_b'} \frac{f_a(k_a, k_a')f_b(k_b, k_b')}{(E_{k_a}-E_{k_a'})(E_{k_b}-E_{k_b'})(E_{k_a}+E_{k_b}-E_{k_a'}-E_{k_b'})} \tag{2}$$

where m is the mass of the electron, the k's label electronic eigenstates having energies E, and the f's are oscillator strengths for transitions between eigenstates. It is important to note that, since by definition [7] $f(k, k')$ has the same sign as $(E_k - E_{k'})$, the sign of each term depends solely on the sign of the third term in the denominator. Thus, if k_a, k_b are ground states, this term is always negative and the potential is attractive, but for excited states the potential can be repulsive. Equation (2) is known to give reasonable results only for very light atoms or molecules. For other systems the experimental dispersion energies are roughly twice the calculated ones [8].

3. SPECTRAL SHIFTS

For the purposes of the most elementary discussion of intermolecular forces in the solid, a Lennard-Jones (6–12) function

$$\phi_{ab} = 4\epsilon_{ab}\left[\left(\frac{\sigma_{ab}}{r_{ab}}\right)^{12} - \left(\frac{\sigma_{ab}}{r_{ab}}\right)^{6}\right] \tag{3}$$

is a convenient and fairly good approximation to the intermolecular potential between two non-polar spherically symmetric species a and b. The expression suffers from the fact that the repulsive energy is represented by an inverse twelfth-power term instead of an exponential which is indicated theoretically. In equation (3), σ is a measure of the molecular size since it is the distance at which attractive and repulsive forces are equal, and ϵ is the intermolecular well-depth. The use of combining laws for the force constants in the intermolecular potential between two different species allows the number of unknown parameters in the treatment to be reduced if the force constants for the matrix gas are known. The usual relationships

$$\sigma_{ab} \approx \tfrac{1}{2}(\sigma_a + \sigma_b) \tag{4}$$

and

$$\epsilon_{ab} \approx \sqrt{(\epsilon_a \epsilon_b)} \tag{5}$$

are difficult to justify from the first- and second-order perturbation results unless $\sigma_a \approx \sigma_b$ and also $\epsilon_a \approx \epsilon_b$. For excited states, with which we are dealing here, such approximations are expected to be rather poor.

A more reasonable combining law which can be better justified from equation (2) and is preferable for excited states since it is less sensitive to differences between the force constants is

$$\epsilon_{ab}\sigma_{ab}^6 \approx (\epsilon_a \sigma_a^6)^{1/2}(\epsilon_b \sigma_b^6)^{1/2}. \tag{6}$$

Assuming the potential of a trapped species in a rare gas crystal to be given by a sum over pair potentials between all the neighbours we have for a close-packed structure at a lattice site [9]

$$\phi_{ab} \approx 4\epsilon_{ab}\left[12{\cdot}13\left(\frac{\sigma_{ab}}{d_{ab}}\right)^{12} - 14{\cdot}45\left(\frac{\sigma_{ab}}{d_{ab}}\right)^{6}\right] \tag{7}$$

where d_{ab} is the nearest neighbour distance. Equation (7) will be approximately valid even if d_{ab} is different from d_0 of the pure matrix crystal. It can be easily shown that the most stable trapping site is at a substitutional position rather than an interstitial position. This is true because of the large space requirements for van der Waals' binding, and the fact that at a lattice site the number of nearest neighbours is a maximum which is energetically favourable since the potential sum is carried out over all neighbours. Previous experimental results concerning the electronic spectra of trapped NH_2 [10], NH [11] and Hg [12] in rare gases show that there is only one major trapping site in these cases. The fact that the spectral lines are sharp but considerably shifted from the gas phase positions shows further that the trapped species experience a highly reproducible perturbation throughout the matrix and thus rules out surface trapping or intercrystal trapping. This does not mean that there are no species trapped in such sites, but their spectra would be very broad and therefore not detectable by the experimental technique. The presence of nearly free rotation which was demonstrated in the cases of NH_2 and NH also helps to bear out the contention that the species are trapped at lattice sites rather than in interstitial positions.

The matrix shift $\Delta\phi_{ab}$ in the energy of an electronic absorption transition between the ground and an excited state of a trapped species is simply the difference between ϕ_{ab} for the two states. According to equations (6) and (7)†,

$$\frac{\Delta\phi_{ab}d_{ab}^6}{57\cdot 8\sqrt{(\epsilon_a\sigma_a^6)}} \approx \frac{0\cdot 84\sigma_a^3}{d_{ab}^6}\Delta\sqrt{(\epsilon_b\sigma_b^{12})}-\Delta\sqrt{(\epsilon_b\sigma_b^6)} \tag{8}$$

where the Δ's refer to the excited state function minus the ground-state function Henceforth $\Delta\sqrt{(\epsilon_b\sigma_b^{12})}$ and $\Delta\sqrt{(\epsilon_b\sigma_b^6)}$ will be designated Δ_{12} and Δ_6 respectively. This gives an approximate linear relationship from which the trapped species difference parameters, Δ_{12} and Δ_6, can be estimated. In actual practice deviations from the linear relationship occur because of defects of the (6–12) potential and especially uncertainties in the tabulated rare gas force constants, the approximate nature of the first- and second-order perturbation results and the combining law relationship, the uncertainty in d_{ab}, slight non-additivity of the pair potentials, and zero-point effects.

The value of d_{ab} is expected to be not quite the same as it is for the pure matrix crystal but will be smaller for 'small' trapped species and larger for 'large' ones. Since the strong crystal forces will not allow too much distortion of d_{ab}, this quantity as a first approximation can be taken to be the same as the nearest neighbour distance d_0 for the pure crystal. Because of the Franck-Condon effect the instantaneous value of d_{ab} in the excited state for the most intense transition must be identical to that of the ground state. Differences in equilibrium values of d_{ab} in ground and excited states will merely show up as a difference in energy of emission and absorption lines, such shifts having already been observed in the case of C_2 [12]. For a close-packed lattice held together by (6–12) interactions, $d_0 = 1\cdot 0902\sigma$, neglecting zero-point motions.

---

† For a (6–14) potential this relationship is

$$\frac{\Delta\phi d_{ab}^6}{47\cdot 7\sqrt{(\epsilon_a\sigma_a^6)}} \approx \frac{0\cdot 83\sigma_a^4}{d_{ab}^8}\Delta\sqrt{(\epsilon_b\sigma_b^{14})}-\Delta\sqrt{(\epsilon_b\sigma_b^6)}.$$

The effect of changing the power dependence of the repulsive term is small compared with the effects of uncertainties in the rare gas force constants.

4. INCLUSION OF $-C_8r^{-8}$ TERM

Without introducing any new parameters, it is a simple matter to estimate the effects of higher order terms in the dispersion energy. In the vicinity of the potential minimum, which is just the region in which we are interested, the $-C_8r^{-8}$ terms contribute substantially [6] to the intermolecular potential even for closed shell atoms and molecules, C_8/C_6 being about 3×10^{-16} cm²†.

We may write for the pair potential,

$$\phi_{ab} = 4\epsilon_{ab}\left[\left(\frac{\sigma_{ab}}{r_{ab}}\right)^{12} - \left(\frac{\sigma_{ab}}{r_{ab}}\right)^{6} - \gamma\left(\frac{\sigma_{ab}}{r_{ab}}\right)^{8}\right] \tag{9}$$

where $\gamma = (C_8/C_6\sigma_{ab}^2)$ and for convenience it may be assumed that C_8/C_6 is exactly 3×10^{-16} cm². In order not to alter the observed well depth and 'size', the parameters in equation (9) must be related to the parameters in the (6–12) potential in the following way:

$$\sigma(6\text{–}8\text{–}12) \approx (1+\gamma)^{1/6}\sigma(6\text{–}12) \tag{10}$$

and

$$\epsilon(6\text{–}12) \approx [(1+4a)(1+2a)]\epsilon(6\text{–}8\text{–}12) \tag{11}$$

where $a = (\gamma\sigma^2 r_m^{-2}\ 3)$ and r_m is the intermolecular distance at the pair potential minimum. The values of ϵ and σ for the (6–8–12) potential do not have the same physical significance as those for the (6–12) potential.

When the potentials are properly summed the relationship between the matrix shifts and the parameters for the (6–8–12) potential is given by

$$\frac{\Delta\phi d_{ab}^{8}}{57{\cdot}8\sqrt{(\epsilon_a\sigma_a^6)}\left(d_{ab}^2 + \dfrac{0{\cdot}886C_8}{C_6}\right)} = \frac{0{\cdot}84\sigma_a^3}{d_{ab}^4\left(d_{ab}^2 + \dfrac{0{\cdot}886C_8}{C_6}\right)}\Delta_{12} - \Delta_6 \tag{12}$$

where the parameters are those for the (6–8–12) potential. It is seen that the linear relationship is preserved.

Parameters obtained from equation (8) or equation (12) of course must be considered as effective parameters for the true potential which has been force-fitted to a mathematically convenient function‡.

5. RARE GAS CONSTANTS

Perhaps the greatest source of error in this treatment lies in the choice of rare gas force constants and unit cell dimensions. Reported values for the force constants [13, 14] may differ by greater than 10 per cent for $\epsilon\sigma^6$ and X-ray values [15] of d_0 vary with temperature and appear to be uncertain by nearly 0·1 Å. Since the potentials vary as high powers of σ and d_0 it is important to be as consistent as possible in the choice of these parameters. Consistency is attained by assuming a reasonable set of (6–12) force constants and calculating from them $d_0 = 1{\cdot}0902\sigma$ and the (6–8–12) constants. The d_0 so obtained is not quite equal to the available experimental values which are averages over lattice vibrations at the temperature of the experiment, but is the minimum of the many-body potential function. Slight errors are thus introduced by this procedure because of lattice motions at 4·2°K.

† For the alkali metals which have low-lying resonance transitions C_8/C_6 is about seven times this great and at distances comparable to the potential minimum it is questionable whether the expansion converges in these cases.

‡ It will be seen later that there is little to be gained from using equation (12). The higher contributions can be more easily included if equation (8) is used with the understanding that there is an effective parameter, $C_6' = C_6 + C_8/\sigma^2 + C_{10}/\sigma^4 + \ldots$.

Table 1 lists the rare gas force constants used. It is not claimed that these are the best, but they are reasonable and serve to illustrate the method of calculation. Since the force constants for krypton are particularly uncertain, reasonable values of σ and ϵ for this atom were chosen so as to best explain our data. The use of these krypton parameters, which are not much different from some literature values, we feel is partly justified since they improve the agreement between theory and experiment in the two cases where the data are complete.

	σ(6–12)	ϵ/k	ϵ(6–12)	d_0 (calc.)	σ(6–8–12)	ϵ(6–8–12)
A	3·46 Å	119°K	82·7 cm^{-1}	3·772 Å	3·59 Å	57·6 cm^{-1}
Kr†	3·62	146	101·6	3·947	3·75	72·9
Xe	3·98	229	159·2	4·339	4·10	120·5

† Published values ϵ(6–12) = 158–190°K, σ(6–12) = 3·59–3·61 Å.

Table 1. Rare gas force constants [14].

	(6–12)		(6–8–12)	
	M	N	M	N
A	0·1323 $(\mathrm{cm}^{-1})^{1/2}$ $\mathrm{Å}^3$	0·01207 $\mathrm{Å}^{-3}$	0·1195 $(\mathrm{cm}^{-1})^{-1/2}$ $\mathrm{Å}^3$	0·01137 $\mathrm{Å}^{-3}$
Kr	0·1367	0·01054	0·1172	0·00999
Xe	0·1451	0·00793	0·1343	0·00763

Table 2. The coefficients M and N.

Table 2 gives the calculated values of coefficients M and N in relationships (8) and (12), these quantities being defined such that

$$M\Delta\phi = N\Delta_{12} - \Delta_6, \tag{13}$$

and where d_{ab} is taken to be d_0 (calc.).

These parameters will now be used to discuss the shifts in the electronic absorption spectra of Hg, NH, NH_2, C_2 and Na in rare gas lattices.

6. EXPERIMENTAL

For the study of resonance transitions of mercury and sodium, the rare gas at a moderately low pressure (~200 μ) is passed over the metal at a temperature such that its vapour pressure is about 10^{-3} to 10^{-4} of the rare gas pressure. The temperature used for mercury was −5°C (v.p. = 0·1 μ) and for sodium, +190°C (v.p. = 0·1 μ). The ratio of rare gas to metal atoms is thus greater than 1000 : 1 so that the tendency for dimer or polymer formation in the solid during the cooling down process is highly reduced. The equilibrium dimer concentration [16] in gaseous sodium at 190°C is about 0·5 per cent of the monomer concentration and is also negligible. Mercury is known [17] to exist as primarily monomer in the vapour phase. The vapour mixture is leaked through a 1 mm diameter hole into a high-vacuum (10^{-4} mm Hg) chamber and a small fraction of it condenses on a liquid helium cooled quartz tube through which the spectra can be observed.

The remainder of the gas is removed by two 60 l/sec diffusion pumps. Naturally, in the case of sodium, the oven must extend into the high-vacuum chamber to prevent premature condensation of the metal on the walls. Deposit rates much faster than the ones used are difficult to control and cause too intense absorption after a very short period of time for these metals whose transitions have fairly large oscillator strengths.

The free radicals NH, NH_2 and C_2 were trapped in the rare gas lattice by a technique which has been previously described in the literature [10]. Table 3 shows the experimental data for Hg, NH, NH_2, C_2 and Na. Experiments are continuing which will give a more complete set of data for C_2 and Na.

	Gas	A	Kr	Xe
$Hg(^3P_1 \leftarrow {}^1S_0)$†	39 412 cm^{-1}	+1281 cm^{-1}	+796 cm^{-1}	+30 cm^{-1}
$NH(A^3\Pi \leftarrow X^3\Sigma^-)$‡	29 773	−192	−264	−370
$NH_2(^2A_1 080 \leftarrow {}^2B_1)$	15 902·3	+28·7	−15·8	−40·3
$C_2(A^3\Pi_g \leftarrow X^3\Pi_u)$‡	19 380	−180	—	−410
$Na(^2P_{3/2,\ 1/2} \leftarrow {}^2S_{1/2})$†	16 965	+60, +1400	—	—

† Removal of orbital degeneracy observed.
‡ 0–0 band.

Table 3. Experimental matrix shifts (M–G) for Hg, NH, NH_2, C_2 and Na in rare gases.

7. MERCURY IN ARGON, KRYPTON AND XENON

In order to understand the shifts it is best to start with the simplest system possible, and this would appear to be the case of an atom trapped in a rare gas. Unfortunately most detectable absorption transitions of the simple atoms lie in the vacuum ultra-violet and only recently [18] has this region come under study in trapped atom spectroscopy. Low-lying strong resonance transitions in some atoms take place in more accessible regions of the spectrum but as we shall see in the case of the alkali metals, the nature of the interaction need not be simple if the low-lying transition has a high oscillator strength and if there is orbital degeneracy which can be removed by the lattice perturbation. The $^3P_1 \leftarrow {}^1S_0$ transition at 2537 Å in mercury, except for the removal of the orbital degeneracy in the P state, can be considered to be a particularly simple illustration of the problem.

Figure 1 shows the results of applying equations (8) and (12) to the Hg data in table 3. From the intercepts and the slopes of the approximately straight lines it is found that $\Delta_6(Hg) = +3{\cdot}12 \times 10^2$ and $+3{\cdot}00 \times 10^2\ (cm^{-1})^{1/2}\ Å^3$ using the (6–12) and (6–8–12) potentials respectively, and that $\Delta_{12}(Hg) = +3{\cdot}99 \times 10^4\ (cm^{-1})^{1/2}\ Å^6$ for both potentials. The positive sign of the change of the attractive constant is predicted from equation (2) since the most intense transitions from the $^3P_1$ state lie to higher energy, and such states are relatively close to the $^3P_1$ state compared with the states which can mix with the ground state. This can be seen by examination of the energy level diagram of mercury [19] which shows that the most important states mixing with the ground state lie above the ground state by at least 54 000 cm^{-1} while there are a number of states lying within 35 000 cm^{-1} which can mix with the $^3P_1$ state.

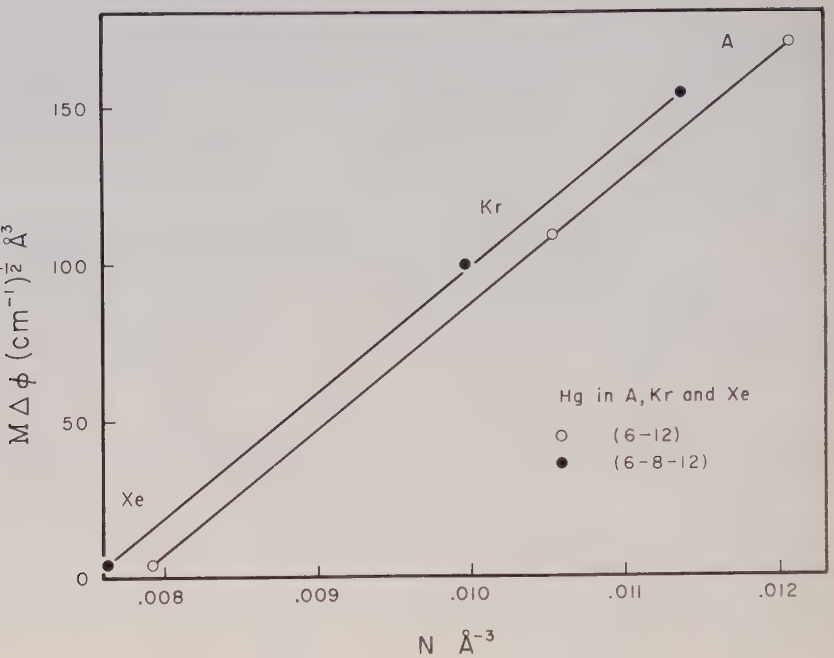

Figure 1. $M\Delta\phi$ *vs.* N for Hg in A, Kr and Xe.

Mercury–mercury interactions of course are actually much different from those caused by dispersion forces as evidenced by the magnitudes of the experimental force constants, $\sigma = 2{\cdot}898$ Å and $\epsilon/k = 951$°K, obtained from the viscosity of liquid mercury [20]. On the other hand, mercury–rare gas interactions are expected to be more of the 'dispersion type'†. London [5] has calculated the value of $C_6(^1S_0)$ for ground state Hg–Hg dispersion interactions to be 129×10^4 cm^{-1} Å^6 (256×10^{-60} erg cm^6). More recently Heller [21] has treated the same problem using effective oscillator strengths and transition energies which give the correct dispersion formula and including terms to r^{-12} by use of Margenau's harmonic oscillator model [6]. The calculations give a value of 147×10^4 cm^{-1} Å^6 (292×10^{-60} erg cm^6) for $C_6' = C_6 + C_8/\sigma^2 + C_{10}/\sigma^4 + C_{12}/\sigma^6$ using $\sigma_{\mathrm{Hg}} = 5{\cdot}04$ Å (*vide infra*). These values should be multiplied by a factor of about two to be compared with experimental data. Remembering that $C'_6 = 4\epsilon\sigma^6$ and using the value 294×10^4 cm^{-1} Å^6 for $C_6'(^1S_0)$, $C'_6(^3P_1)$ is found from the Δ_6(Hg) value for the (6–12) potential to be 547×10^4 cm^{-1} Å^6 (1086×10^{-60} erg cm^6). This appears to be quite reasonable in view of the fact that C_6 (and approximately C'_6) varies as the inverse third power of the transition energy and that the total oscillator strength (which enters as the square) for transitions from the $^3P_1$ state has a weight of roughly one-third. If 80 000 cm^{-1} were chosen as an average transition energy of states mixing with the ground state the average energy to states mixing with the $^3P_1$ state is found to be 31 300 cm^{-1}. This is nearly equivalent in energy to the strong transitions from the $^3P_1$ state of mercury exactly as expected. Thus it appears as if the London theory might give a reasonable estimate for dispersion forces in the excited state of mercury, and conversely it appears as if our model based on the very simple two-constant potential function is adequate for the explanation of the matrix shifts in this case.

---

† Comparatively weak interactions for which second order perturbation theory is adequate.

This point is further illustrated by the fact that the quantity $(\Delta_{12}/\Delta_6)^{1/3}$ gives an approximate value for σ_{Hg} if the van der Waals radius does not change appreciably from ground to excited state. The calculation gives $\sigma_{\mathrm{Hg}} \approx 5{\cdot}04$ Å which is a reasonable value for this parameter.

The magnitude of σ is primarily dependent on exchange forces and these may be larger or smaller in the excited state depending on the 'size' of the electron orbitals. Let $\sigma' = \sigma'' + \delta$, where δ is small. Then,

$$\sigma'' \approx \left[\frac{(\Delta_{12}/\Delta_6)}{1 + \dfrac{3\delta/\sigma''}{1 - \sqrt{\epsilon''}/\sqrt{\epsilon'}}} \right]^{1/3}. \tag{14}$$

Since $\sqrt{\epsilon''}/\sqrt{\epsilon'}$ is probably of the order of 0·7 to 0·9, a change of 0·1 Å (which is no doubt an upper limit) in σ in the excited state would cause for positive δ,

$$\sigma'' \approx 0{\cdot}8(\Delta_{12}/\Delta_6)^{1/3}. \tag{15}$$

For this reason the Δ_{12} and Δ_6 parameters are considered to have more significance than do their individual parts.

8. RELATION BETWEEN THE SOLID AND THE HIGH DENSITY GAS

Robin and Vodar [22, 23] have studied the 2537 Å absorption line of mercury in gaseous argon at densities approaching that of solid argon. At densities greater than 150 amagats a broad peak (labelled S_1) which is blue shifted from 2537 Å is observed. As the pressure is increased the shift becomes greater, and at densities greater than 600 amagats another peak (labelled S_2) further to the blue becomes apparent. The position of S_2 is also pressure dependent and by a short extrapolation of the data the shift at the solid argon density ($\sim$ 924 amagats) is found to be 1290 cm^{-1}. The shift in solid argon is 1281 cm^{-1}, hence the two values agree quite well. This is not unreasonable since the short-range order in the gas at this high density must be very similar to that of the solid. By assuming a uniformly expanding gas, using the parameters obtained from the solid, and calculating the shift of the Hg 2537 Å line at densities less than the solid density it is found that the predicted blue shifts are much less than the observed ones. This is experimental evidence that the gas at moderately high densities does not uniformly expand but is composed of clusters and holes, where the average internuclear distance in the clusters is much less than that calculated from the average density of the whole gas.

The origin of the S_1 peak which is most prominent at intermediate densities is not clear. It is likely that it corresponds to a structure or structures having less close-packing, but the Hg–A intermolecular potential is not sufficiently good to make a definite statement about this at the present time.

9. NH AND C_2 IN RARE GASES

Although NH and C_2 are not atoms it is expected that to a good approximation a Lennard-Jones potential can be used to express interactions of these species with a rare gas. Contributions due to asphericity and thus angular dependent forces are probably not too large for a small hydride, and those present should be very nearly the same in the two electronic states considered here. This is expected for example on the basis of the NH electronic spectrum [24] which reveals a great similarity of bonding in the $X^3\Sigma^-$ and $A^3\Pi$ states. In C_2 there are a number of very low-lying electronic states [25], transitions to which are moderately weak, but which nevertheless, because of their proximity, are expected to contribute rather significantly to the dispersion energies of the states considered here. There can be no permanent dipole moment in C_2 so that, except possibly for the low-lying electronic states, the molecule should present a fairly well-behaved case where the theory applies. Figure 2 shows the results of plotting $M\Delta\phi$ *vs.* N for the NH($A^3\Pi \leftarrow X^3\Sigma^-$) shifts in A, Kr and Xe. For $C_2(A^3\Pi_g \leftarrow X^3\Pi_u)$ the data at present exist only for A and Xe so that no plot is given to illustrate a straight line relationship. The data for NH and C_2 can be treated in an exactly identical fashion as those for Hg and table 4 gives the results for all three of these cases.

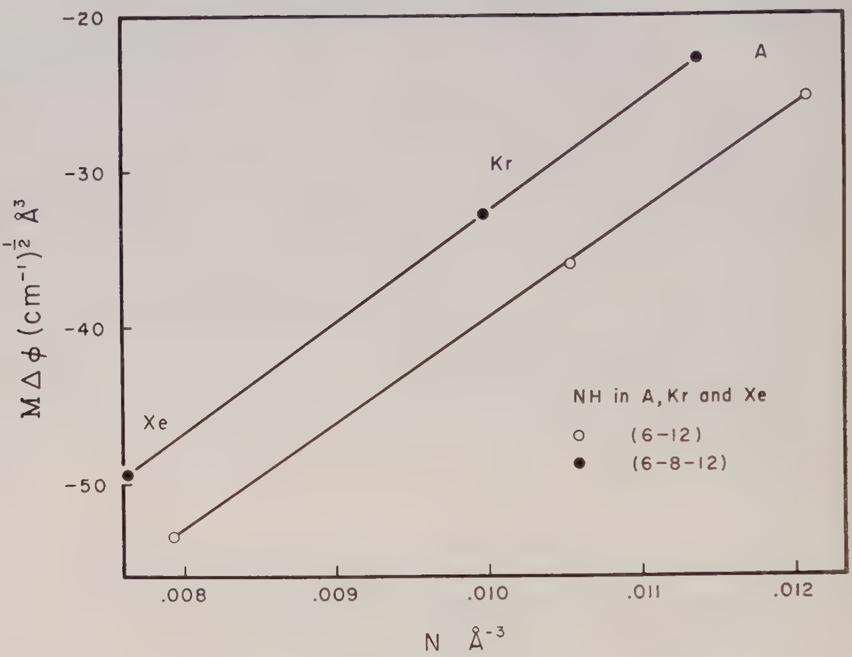

Figure 2. $M\Delta\phi$ *vs.* N for NH in A, Kr and Xe.

	$\Delta_6 (cm^{-1})^{1/2}\ Å^3$		$\Delta_{12} (cm^{-1})^{1/2}\ Å^6$		σ Å
	6–12	6–8–12	6–12	6–8–12	6–12
Hg	$3{\cdot}12 \times 10^2$	$3{\cdot}00 \times 10^2$	$3{\cdot}99 \times 10^4$	$3{\cdot}99 \times 10^4$	5·04
NH	$1{\cdot}07 \times 10^2$	$1{\cdot}04 \times 10^2$	$6{\cdot}80 \times 10^3$	$7{\cdot}11 \times 10^3$	3·99
C_2	$1{\cdot}27 \times 10^2$	$1{\cdot}23 \times 10^2$	$8{\cdot}58 \times 10^3$	$8{\cdot}93 \times 10^3$	4·07

Table 4. Observed trapped species parameters.

The theory appears to give a partially satisfactory explanation of the spectral shifts for NH. The rather large σ_{NH}, which predicts that NH at a rare gas lattice site interacts on the repulsive part of the intermolecular potential, is expected to be fictitious if, as discussed earlier, σ_{NH} changes appreciably in the excited state or if the separation of this term from the ϵ term in C_6' has no meaning. Experimental evidence that the interaction *does* take place on the attractive rather than the repulsive side of the potential is furnished by the vibrational perturbations discussed in the next section.

The results for the C_2 molecule appear to be very reasonable except again the calculated σ seems slightly high when it is compared with the values for N_2, O_2, NO and CO [26]. One should not forget the presence of the low-lying electronic states in C_2 which makes comparison with some of the other diatoms more difficult. The direction of the vibrational perturbations discussed in the next section does indicate that C_2 is fairly large and interacts primarily on the repulsive side of the intermolecular potential.

10. VIBRATIONAL PERTURBATIONS

While it is not the purpose of this paper to dwell on the subject of vibrational perturbations in the solid, some results pertaining to the NH and C_2 molecules are worthy of mention at this time. Table 5 illustrates the vibrational perturbations arising in the cases of NH($A^3\Pi$) in argon, and C_2($A^3\Pi_g$ and $X^3\Pi_u$) in xenon. The results were obtained from absorption as well as fluorescence spectra† of these species at 4·2°K. The salient features of table 5 are the smaller $\Delta G_{1/2}$ for NH in argon than in the gas, the remarkably larger ΔG values for trapped C_2 in both the lower and excited electronic states, and the negative or near zero anharmonicity in the lower state (and no doubt the excited state also) of C_2. These effects can be explained on the basis of interaction on the attractive part of the potential in the case of NH but on the steeply repulsive part of the potential in the case of C_2. If the interaction is attractive this means that the electrons of the species and also of the lattice are slightly delocalized into the 'intermolecular bond'. This effect follows by the usual description of dispersion interactions or by merely considering the electrons of the trapped species to be in the presence of a polarizable medium in which case they will be attracted by an induction contribution of the approximate form

	$\Delta G_{1/2}$	$\Delta G_{3/2}$
NH($A^3\Pi$) in argon	2979 cm^{-1}	
gas [24]	3034	
C_2($X^3\Pi_u$) in xenon	1720	1740
gas [32]	1618	1595
C_2($A^3\Pi_g$) in xenon	1940	
gas [32]	1755	

Table 5. Vibrational perturbations in NH and C_2.

$$\phi = -\frac{e^2\alpha}{2r^4}, \tag{16}$$

---

† The C_2 fluorescence lines are shifted 50 cm^{-1} to the red of the absorption lines. Using the experimental parameters it can be deduced from the Franck–Condon principle that this shift corresponds to a change of less than 0·05 Å in equilibrium lattice distance in going from the lower to the excited state of the trapped species. It is interesting that d_{ab} is thus measurably dependent upon the intermolecular force constants between the impurity and the rare gas atoms. This fact shows that our previous approximation which took d_{ab} to be equal to d_0 for the pure crystal introduces errors into the treatment.

where α is the polarizability of a spherically symmetric medium whose centre lies a distance r from the charge e. The presence of this type of interaction causes the electron density in the molecular bond to decrease, thus reducing the force constant and the vibrational frequency.

A repulsive interaction between the trapped species and the solid, as was mentioned earlier, is primarily caused by exchange forces. Physically this means that an electron of the trapped species will meet strong resistance if it attempts to crowd into the already filled orbitals of the rare gas simply because of the Pauli exclusion principle. The situation at small intermolecular separations is then likened to the problem of an electron in a fairly rigid box to which a Hartree field has been added at its centre. As the box becomes smaller the near-vanishing electronic wave functions at the boundaries of the box must be compensated for, because of normalization, by greater electron density in the centre of the box, in this case in the molecular bond. The force constant and vibrational frequency are accordingly increased.

These aspects of intermolecular interactions in the solid are very analogous to the situation which exists when hydrogen atoms are trapped in various interstitial and lattice sites in rare gas crystals [27]. The electron density at the proton as determined from the magnitude of the coupling constant for hyperfine interactions is larger for the less stable and therefore more repulsive sites. The study of vibrational force constants therefore appears to be an alternative way of studying these effects in molecules.

11. ANGULAR DEPENDENT FORCES—NH_2

The plot of $M\Delta\phi$ *vs.* N (figure 3) for the $(0,8,0)^2A_1\Pi \leftarrow (0,0,0)^2B_1$ vibronic transition of NH_2 does not give a straight line. This deviation is likely to be caused by a dipole-induced dipole interaction which is neglected in this treatment.

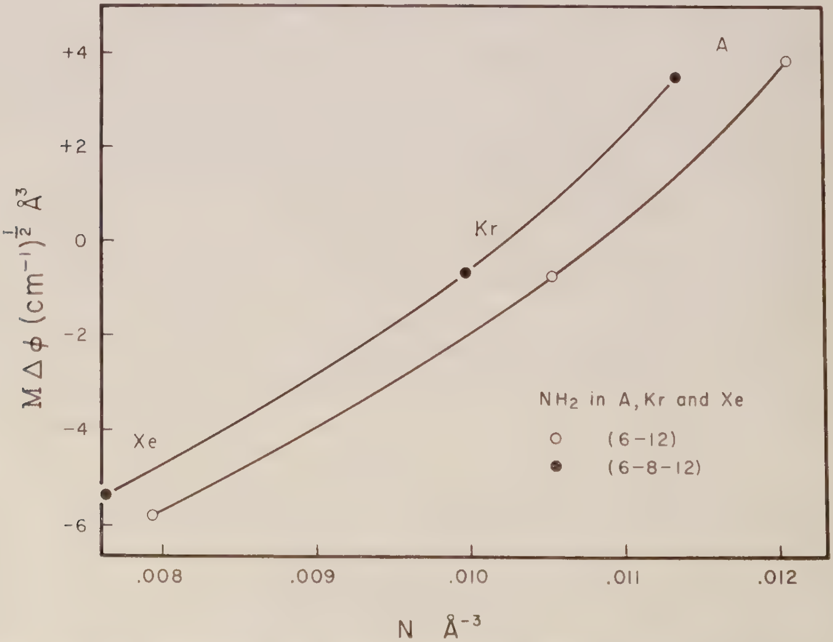

Figure 3. $M\Delta\phi$ *vs.* N for NH_2 in A, Kr and Xe showing effect of angular dependent forces.

NH_2 [28] is bent in its ground state with an H–N–H angle of 102° while it is linear in the excited state so that there is a dipole moment change which may be of the order of 1 Debye. The effect of the dipole-induced dipole interaction in the ground state, which vanishes in the excited state, is to contribute a blue shift opposing the usual dispersion red shift. This is qualitatively in agreement with the experimental results which show a dominant dipole-induced dipole term in argon, but a dominant dispersion term in xenon. In krypton the two contributions approximately cancel.

An attempt to include the dipole-induced dipole interaction

$$\phi = -\sum_{\text{all sites}} \mathrm{f}(\theta) \frac{\mu_a{}^2 \alpha_b}{d_0{}^6} \approx -14 \frac{\mu_a{}^2 \alpha_b}{d_0{}^6} \tag{17}$$

was not completely successful probably due to the non-applicability of the point dipole expression at these intermolecular distances. Equation (17) alone predicts about a 40 cm^{-1} blue shift in all three instances for a change of dipole moment in NH_2 of 1·0 Debye.

12. Sodium in argon

Except for possible slow convergence of the Hamiltonian expansion, the sodium–argon attractive interaction would appear to be easy to calculate from equation (2) considering the fact that only a few transitions need be considered for sodium [29]. Using oscillator strengths and average transition energies for argon [6] one finds $C_6(^2S_{1/2}) = 91 \times 10^4\,cm^{-1}\,Å^6$ (181×10^{-60} erg cm^6) and $C_6(^2P_{3/2,1/2}) = 265 \times 10^4\,cm^{-1}\,Å^6$ (526×10^{-60} erg cm^6) for the sodium–argon interaction. These should be compared with the calculated C_6 value $53 \times 10^4\,cm^{-1}\,Å^6$ (105×10^{-60} erg cm^6) for the mercury ($^1S_0$) argon interaction [21]. It is seen that the C_6 interaction constant is at least double that for interactions between Hg and argon. When the large C_8, $C_{10}\ldots$ terms are taken into account the total interaction for sodium and a rare gas is expected to be even larger than indicated by the C_6 term alone. Furthermore σ may change to a greater extent than in any of the other cases considered here.

Figure 4 shows the spectrum of Na in A near 6000 Å and table 6 lists the measurements for these six lines as well as for some of the weaker ones. The spectrum is not simple. The shifts are to the blue indicating that repulsive interactions dominate the attractive ones. This might be expected since the electron on sodium is very loosely bound in the ground state and much less so in the excited state, and any 'squeezing effect' caused by the argon cage will tend to send the transitions to higher energy. The ionization potential of Na in argon is expected to be appreciably larger than that for the free atom.

Figure 4 shows the presence in the $3p^2P_{1/2,3/2}$ state of what appears to be two prominent triplets with splitting of about 320 cm^{-1}. The weaker triplet to the red of the intense one may be caused by sodium atoms in a less repulsive environment, but experimental evidence in support of this is lacking. Considerably more experimental work must be done before very much can be said quantitatively about these interesting alkali metal rare gas interactions. That the interactions are large is evident from the calculations as well as from these preliminary experimental results.

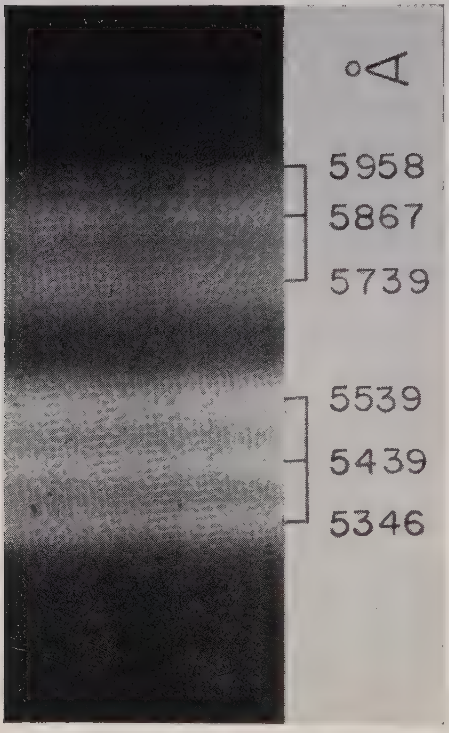

Figure 4. Spectrum near 6000 Å of Na in argon at 4·2°K.

Transition and free atom energy	Transition in argon (cm^{-1})
3p $^2P_{1/2,\,3/2} \leftarrow {}^2S_{1/2}$ 16964 cm^{-1}	16780 ± 30 broad, weak 17040 ± 30 broad, weak 17420 ± 30 broad, weak 18050 ± 30 broad, strong 18380 ± 30 broad, strong 18700 ± 30 broad, strong
?	19204 ± 5 sharp, weak 20393 ± 5 sharp, weak
4p $^2P_{1/2,\,3/2} \leftarrow {}^2S_{1/2}$ 30269 cm^{-1}	30280 ± 20 fairly sharp, very weak 31020 ± 20 fairly sharp, very weak 32190 ± 20 fairly sharp, weak

Table 6. Sodium in argon.

13. REMOVAL OF ORBITAL DEGENERACY BY THE PERTURBATION

The electronic transitions observed for Hg and Na involve excited states which are respectively $^3P_1$ and $^2P_{1/2,\,3/2}$. In each instance the three-fold orbital degeneracy appears to be removed in the solid phase. The observed triplet splitting for Hg is 120 ± 15 cm^{-1} in all three rare gases. It was seen that the splitting for sodium in argon is about 320 cm^{-1}. Since these systems can be considered to be loosely coupled molecules in orbitally degenerate states, the Jahn-Teller [30] effect requires that the lattice distorts to remove the degeneracy. The distorted lattice in the vicinity of the trapped species must have no higher than orthorhombic symmetry if the degeneracy is to be completely removed. It is puzzling however why the splitting should be approximately the same for Hg in the three different rare gases.

The situation in the case of sodium is somewhat reminiscent of the much smaller effects observed in alkali metal spectra in rare gases at moderate densities (< 100 amagats) [31]. The solid phase spectra discussed here, however, would more nearly correspond, except for the absence of cluster fluctuations, to the situation in the gas phase at densities of the order of the solid density (~ 1000 amagats). At such densities a statistical theory becomes difficult to apply and should be abandoned in favour of a cluster theory of the type proposed here. The experimental work on Hg in the gas combined with this theory indicates, furthermore, that large clusters may be important at densities as low as 100 amagats, and that two different cluster configurations may be present together, their relative importance being dependent upon density.

On considère les perturbations auxquelles sont dues les déplacements de fréquence dans les spectres électroniques et vibrationnels d'espèces emprisonnées dans un solide, en fonction du potential intermoléculaire qui représente les interactions entre ces espèces et les atomes voisins. On montre que dans certains cas la théorie de London donne une approximation convenable pour l'énergie de dispersion entre une espèce excitée électroniquement et un atome de gaz rare. On explique quantitativement les déplacements expérimentaux dans les spectres d'absorption electronique, à 4,2°K, de Hg, NH, et C_2, se trouvant aux noeuds des reseaux dans des cristaux de gaz rare, en se basant sur un potentiel d'interaction de Lennard-Jones (6–12) or (6–8–12), entre l'espèce emprisonnée et les atomes du gaz rare. La théorie n'explique pas de façon satisfaisante les déplacements dans le cas où des forces à forte dépendence angulaire, et qui varient de façon appréciable entre les deux états électroniques, sont présentes; on présente des données sur les radicaux libres NH_2 emprisonnés comme exemple de ce cas. L'interaction d'atomes de sodium avec l'argon à 4,2°K est très complexe, les données expérimentales étant compatibles avec de nombreux points d'emprisonnement pour les atomes, une large interaction répulsive entre l'état excité du sodium et le gaz rare, et la disparition manifeste de la dégénérescence triple des orbitales dans l'état excité par la perturbation par l'entourage. La dégénérescence triple des orbitales dans l'état $^3P_1$ du mercure est supprimée aussi. Le déplacement de 1281 cm^{-1} vers le bleu, pour la transition $^3P_1 \leftarrow {}^1S_0$ du mercure dans l'argon solide à 4,2°K, correspond presque exactement à la position d'un des deux traits saillants du spectre du mercure dans l'argon gazeux à des densités comparables, et démontre la ressemblance de structure des deux états physiques. Les perturbations intéressantes des états vibrationnels de NH et C_2 suggèrent une forte ressemblance avec l'effet auquel est due la variation des constantes de couplage pour les interactions spin électronique-spin nucléaire d'atomes d'hydrogène emprisonnés.

Für Spezies, die in einem Festkörper eingefangen sind, werden die Störungen betrachtet, die für die Verschiebungen in den Elektronen- bzw. Schwingungsspektren verantwortlich sind. Hierzu wird das zwischenmolekulare Potential herangezogen, das Wechselwirkungen zwischen den genannten Spezies und ihren Nachbaratomen beschreibt. Gezeigt wird, dass die London'sche Theorie in bestimmten Fällen eine angemessene Näherung der Dispersionsenergie zwischen einer elektronisch angeregten Spezies und einem Edelgasatom ermöglicht. Die experimentellen Verschiebungen in den elektronischen Absorptionsspektren von Hg, NH und C_2 auf Gitterplätzen in Edelgaskristallen bei 4,2°K werden quantitativ erklärt auf Grund eines Lennard-Jones'schen (6–12)- bzw. (6–8–12)-Potentials zwischen den eingefangenen Spezies und den Edelgasatomen. Die Theorie gibt für die Verschiebungen in solchen Fällen keine angemessene Erklärung, wo starke vom Winkel

abhängige Kräfte auftreten, die in den beiden Elektronenzuständen merklich verschieden sind. Als Beispiel hierzu werden Daten über eingefangene freie NH_2-Radikale angeführt. Die Wechselwirkung von Natriumatomen mit Argon bei 4,2°K ist sehr verwickelt, die Daten sind vereinbar mit der Annahme mehrfacher Einfangplätze für die Atome, grosser Abstossung zwischen dem angeregten Zustand von Natrium und dem Edelgas, sowie einer Aufhebung der dreifachen Bahn-Entartung im angeregten Zustand infolge einer Umgebungsstörung. Die dreifache Bahn-Entartung im $^3P_1$-Zustand von Quecksilber verschwindet ebenfalls. Die Blauverschiebung von 1281 cm^{-1} für den $^3P_1 \leftarrow {}^3S_0$ Übergang von Quecksilber in festem Argon bei 4,2°K entspricht fast genau der Lage einer der beiden auffallenden Gebilde im Spektrum von Quecksilber in Argongas bei vergleichbaren Dichten. Hierdurch wird die strukturelle Ähnlichkeit in den beiden physikalischen Zuständen illustriert. Die interessanten Störungen der Schwingungszustände von NH und C_2 lassen eine grosse Ähnlichkeit mit dem Effekt vermuten, der Änderungen der Kopplungskonstanten für Nachbar-Wechselwirkungen zwischen Elektronspin und Kernspin in eingefangenen Wasserstoffatomen verursacht.

REFERENCES

[1] HIRSCHFELDER, J. O., CURTISS, C. F., and BIRD, R. B., 1954, *Molecular Theory of Gases and Liquids* (New York: John Wiley and Sons, Inc.), p. 922.
[2] BLEICK, W. E., and MAYER, J. E., 1934, *J. chem. Phys.*, **2,** 252.
[3] KUNIMUNE, M., 1950, *Progr. theor. Phys., Japan*, **5,** 412.
[4] See, for example, ref. [1], p. 923.
[5] LONDON, F., 1930, *Z. phys. Chem.* B, **11,** 222.
[6] MARGENAU, H., 1938, *J. chem. Phys.*, **6,** 896.
[7] CONDON, E. U., and SHORTLEY, G. H., 1935, *Theory of Atomic Spectra* (Cambridge: University Press), p. 108.
[8] Ref. [1], p. 966.
[9] KIHARA, T., and KOBA, S., 1952, *J. phys. Soc. Japan*, **7,** 348.
[10] ROBINSON, G. W., and MCCARTY, Jr., M., 1959, *J. chem. Phys.*, **29,** 999.
[11] MCCARTY, Jr., M., and ROBINSON, G. W., 1959, *J. Amer. chem. Soc.*, **81,** 4472.
[12] MCCARTY, Jr., M., ROBINSON, G. W., 1959, 9th Annual Meeting, Société de Chemie Physique, Paris, 26–29 May, to be published in *J. Chim. phys.*
[13] Ref. [1], p. 1110.
[14] PRESENT, R. D., 1958, *Kinetic Theory of Gases* (New York: McGraw-Hill), p. 253.
[15] DONNAY, J. D. H., and NOWACKI, W., 1954, *Crystal Data* (New York: Geological Society of America).
[16] SITTIG, M., 1956, *Sodium—Its Manufacture Properties and Uses* (New York: Reinhold Publishing Co.), p. 478.
[17] MELLOR, J. W., 1923, *Inorganic and Theoretical Chemistry*, Vol. IV (London: Longmans, Green and Co.), p. 713.
[18] DRESSLER, K., and SCHNEPP, O. (private communication).
[19] HERZBERG, G., 1944, *Atomic Spectra* (New York: Dover Publications), p. 202.
[20] EPSTEIN, L. F., and POWERS, M. D., 1953, *J. phys. Chem.*, **57,** 336.
[21] HELLER, R., 1941, *J. phys. Chem.*, **9,** 154.
[22] ROBIN, J., and VODAR, B., 1956, *Comp. rend.*, **242,** 2330.
[23] ROBIN, J., BERGEON, R., GALATRY, L., and VODAR, B., 1956, *Disc. Faraday Soc.*, **22,** 30.
[24] DIXON, R. N., 1959, *Canad. J. Phys.*, **37,** 1171.
[25] BALLIK, E. A., and RAMSAY, D. A., 1958, *J. chem. Phys.*, **29,** 1418.
[26] Ref. [1], p. 1111.
[27] COCHRAN, E. L., BOWERS, V. A., FONER, S. N., and JEN, C. K., 1957, *Phys. Rev. Letters.*, **2,** 43.
[28] RAMSAY, D. A., 1957, *Mém. Soc. Sci. Liége*, **18,** 471.
[29] Ref. [7], p. 149.
[30] JAHN, H. A., and TELLER, E., 1937, *Proc. roy. Soc.* A, **161,** 220.
[31] KLEIN, L., and MARGENAU, H., 1959, *J. chem. Phys.*, **30,** 1556.
[32] HERZBERG, G., 1950, *Spectra of Diatomic Molecules* (New York: D. van Nostrand Co. Inc.), 2nd ed., p. 513.

RESEARCH NOTE

Photo-ionization of aromatic hydrocarbons in boric acid glasses

by P. BENNEMA, G. J. HOIJTINK, J. H. LUPINSKI,
L. J. OOSTERHOFF, P. SELIER and J. D. W. VAN VOORST
Chemical Laboratory of the Free University, Amsterdam; Laboratory for
Theoretical Organic Chemistry, University of Leiden

(*Received* 19 *May* 1959)

Some years ago Evans [1] reported that on irradiation of triphenylene in boric acid glass a permanent blue colour is observed, which he ascribed to the formation of free radicals ($S = \frac{1}{2}$). This agrees with the result that, after irradiation, the paramagnetism maintains a finite value. Similarly Hubert-Habart and Muel [2] observed that on irradiation of 3, 4-benzpyrene in boric acid the glass becomes permanently red coloured.

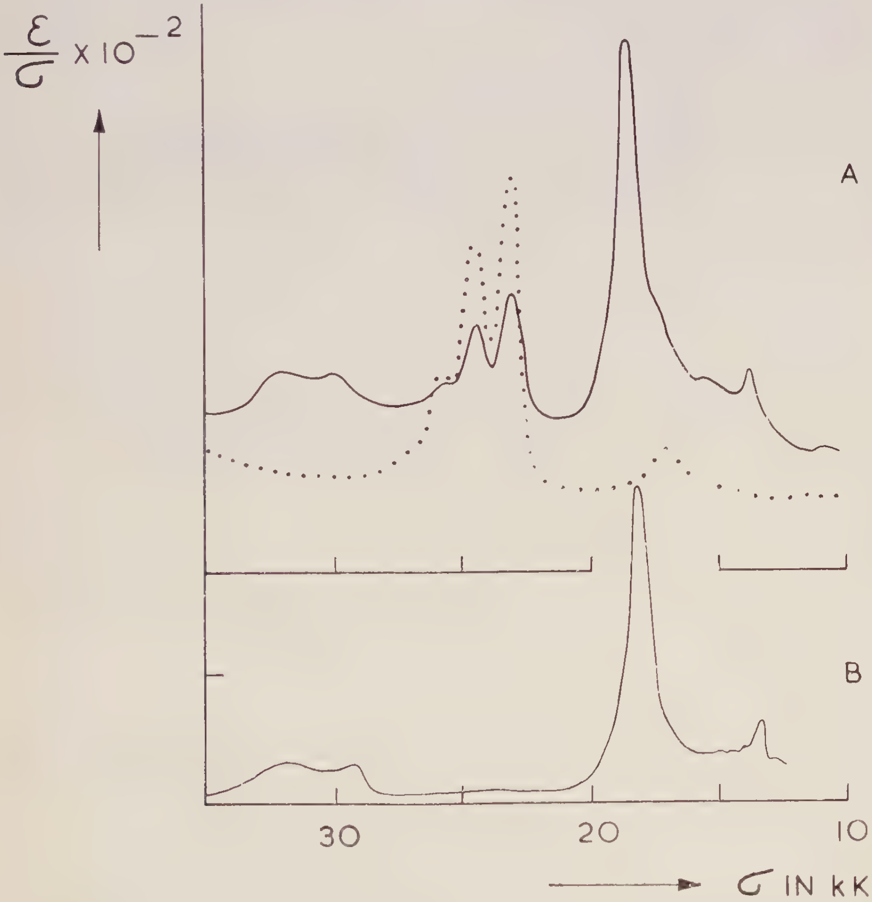

Figure 1.
A: Absorption spectra of perylene in boric acid glass before . . . . and after ——— irradiation.
B: Absorption spectrum of perylene mono-positive ion [3].

The formation of these coloured photo products has now been investigated in more detail. For that purpose we have measured the electron spin resonance and the electronic absorption spectra of various aromatic hydrocarbons in boric acid, before and after exposure to the ultra-violet light of a high-pressure mercury arc.

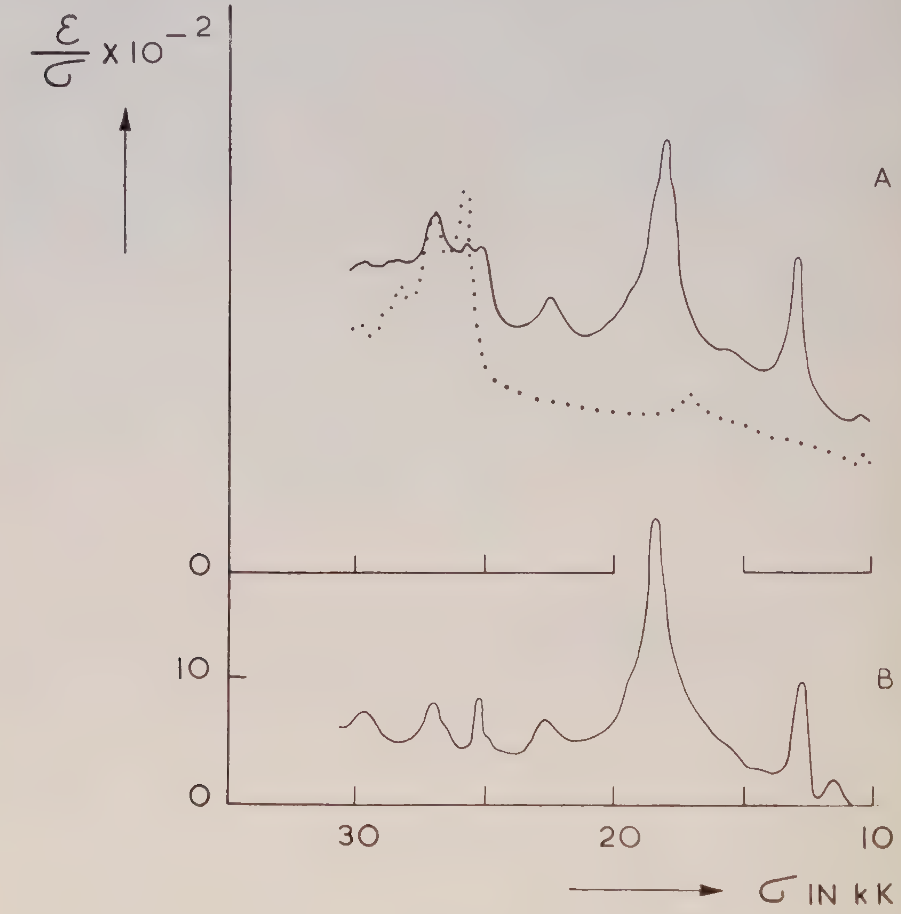

Figure 2.

A: Absorption spectra of 3, 4-benzpyrene in boric acid glass before . . . . and after ——— irradiation.

B: Absorption spectrum of 3, 4-benzpyrene mono-positive ion [3].

The irradiated solutions of diphenyl, phenanthrene, triphenylene, tetracene, pyrene, perylene and coronene in boric acid displayed electron spin resonance, suggesting the formation of free radicals, which is further confirmed by a study of the electronic absorption spectra.

Some of the absorption spectra of the plane parallel polished glass plates are shown in the figures 1 to 5. From the figures 1 and 2 it becomes clear that the spectra of perylene and 3, 4-benzpyrene, after irradiation of the glass, resemble very closely those of the mono-positive ions recently reported [3]. Apparently on irradiation of the hydrocarbons in boric acid glass photo-ionization takes place, the electrons being captured in the glass.

The spectra of the mono-positive ions of triphenylene, quaterphenyl and coronene drawn in the figures 3, 4 and 5 were hitherto unknown. On theoretical grounds one may expect the spectra of the mono-positive and mono-negative ions of alternant hydrocarbons to be very similar [4, 6]. For that reason the spectra of the latter solutions are compared with those of the corresponding hydrocarbon mono-negative ions [5, 6]. From the figures it appears that the correspondence is very striking.

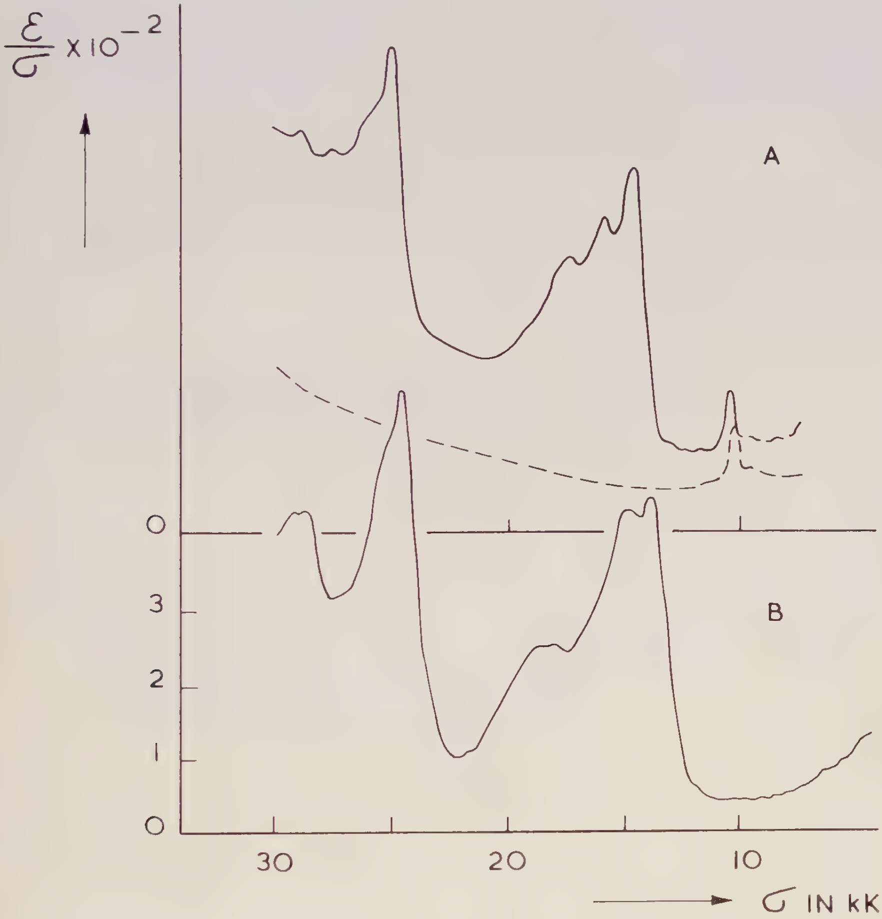

Figure 3.

A: Absorption spectra of triphenylene in boric acid glass before . . . . and after ——— irradiation.

B: Absorption spectrum of triphenylene mono-negative ion [6].

Apart from the absorption bands of the hydrocarbon molecules, the spectra of perylene and 3, 4-benzpyrene before irradiation display an absorption band in the 15–20 kK region, which in the light of recent studies [3] may be ascribed to the formation of co-valent complex of the hydrocarbon with boric acid.

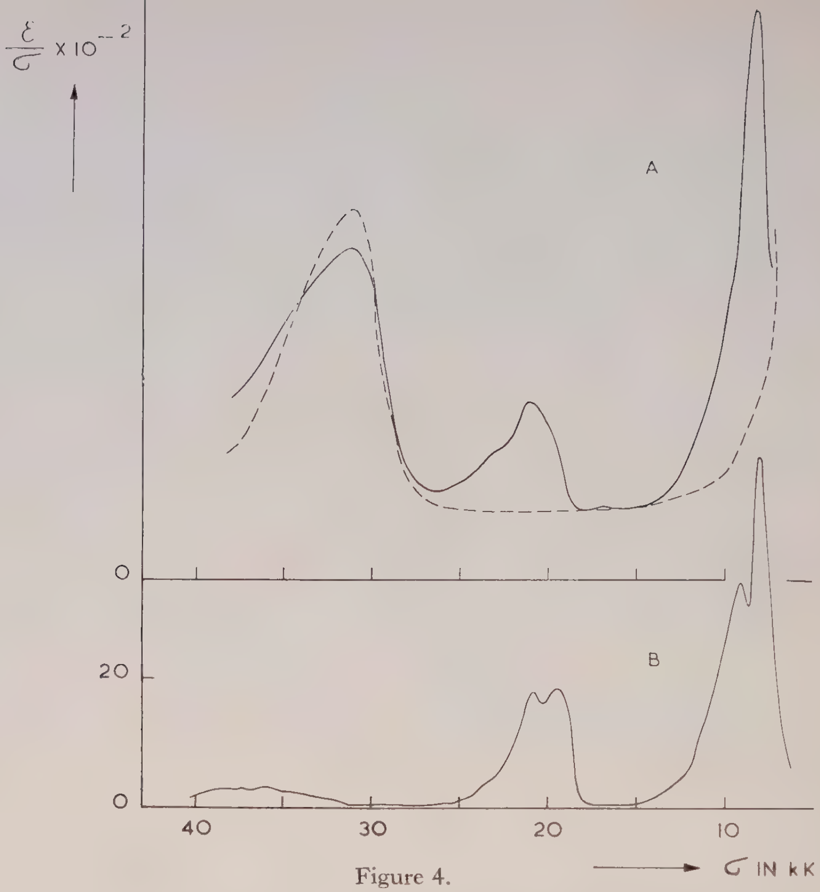

Figure 4.

A: Absorption spectra of quaterphenyl in boric acid glass before . . . . and after ——— irradiation.

B: Absorption spectrum of quaterphenyl mono-negative ion [5].

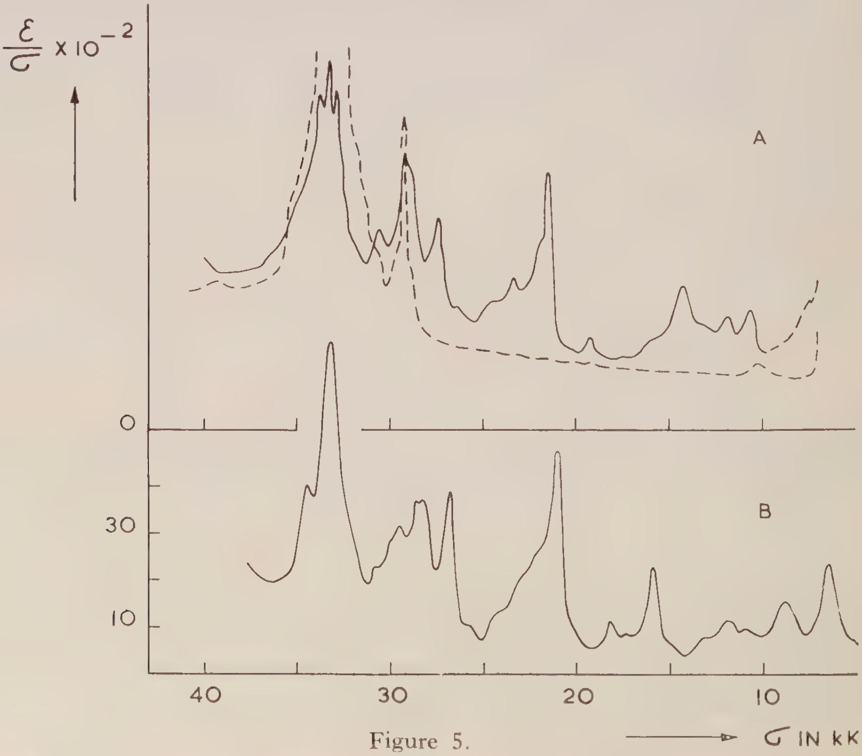

Figure 5.

A: Absorption spectra of coronene in boric acid glass before . . . . and after ——— irradiation.

B: Absorption spectrum of coronene mono-negative ion [6].

The present results are strongly similar to those obtained by Lewis and Lipkin [7] and by Linschitz *et al.* [8] who investigated the photo-ejection of electrons in rigid solutions of easily oxidized organic molecules. Just like these authors we found that on slowly heating the coloured glasses the colour disappears under phosphorescence emission of the hydrocarbon molecule.

REFERENCES

[1] EVANS, D. F., 1955, *Nature, Lond.*, **176,** 777.

[2] HUBART-HABART, M., and MUEL, B., 1958, *J. Chim. phys.*, **55,** 377.

[3] AALSBERSBERG, W. IJ., HOIJTINK, G. J., MACKOR, E. L., and WEIJLAND, W. P., *J. chem. Soc.* (to be published).

[4] WEIJLAND, W. P., 1958, Thesis, Free University, Amsterdam.

[5] BALK, P., HOIJTINK, G. J., and SCHREURS, J. W. H., 1957, *Rec. Trav. chim. Pays-Bas*, **76,** 813.

[6] HOIJTINK, G. J., 1959, *Mol. Phys.*, **2,** 85.

[7] LEWIS, G. N., and LIPKIN, D., 1942, *J. Amer. chem. Soc.*, **64,** 2801.

[8] LINSCHITZ, H., BERRY, M. G., and SCHWEITZER, D., 1954, *J. Amer. chem. Soc.*, **76,** 5833.

ERRATA

The singularities of the integrals in Mayer's ionic solution theory

by HAROLD L. FRIEDMAN†

Department of Chemistry, University of Southern California, Los Angeles 7, California

In a recent paper [1] there is an error in the last member of equation (3.24), which should read

$$\tilde{f}_1(L,R)=[\exp(-\kappa R)/64\pi^2\kappa R][\log(3)-E_1(\kappa R)+\exp(2\kappa R)E_1(3\kappa R)+\ldots].$$

The second factor in square brackets is now $O(\kappa R\log(\kappa R))$, rather than $O(\kappa^0)$. This necessitates the following changes in the paper.

1. Replace the two sentences following equation (3.24) by “ The transform of this bond function is ” and replace equation (3.25) by
$$\tilde{F}_1=F_1F_2.$$
2. In figure 2 replace $q=1$ by $q=0$ for H', i' and j', and delete the words “ and the fact . . . as $f(L, R)$ ”, at the end of the legend.
3. Delete the last paragraph beginning on p. 201.
4. Replace equation (5.2) by
$$K_3(\alpha')\propto\int_0^L \Phi''_{ik}(R)\exp(-\kappa R)\log(\kappa R)\,R^2\,dR$$
$$=\int_0^L \Phi''_{ik}\exp(-\kappa R)\log(R)\,R^2\,dR+[\log\kappa]\int_0^L \Phi''_{ik}\exp(-\kappa R)\,R^2\,dR.$$
5. Delete the last sentence of § 5.
6. The entry in the table in § 6 for $u=3$, $\mu_3=0$ should be $c^3\log c$.

Another error was made in the two sentences following equation (A 5). These should be replaced by: “The use of these equations is illustrated by considering the integral of interest ”.

After the necessary change in equation (3.25) the derivations of equations (3.26) and (3.27) become rather difficult although the results are unchanged. The details will be furnished by the author upon request.

Reference

[1] Friedman, H. L., 1959, *Mol. Phys.*, **2**, 190.

---

† Present address: I.B.M. Research, P.O. Box 218, Yorktown Heights, N.Y.

INDEX OF AUTHORS (WITH THE TITLES OF PAPERS)

Andersen, W. H., and Hornig, D. F.: The structure of shock fronts in various gases, 49

Babloyantz, Agnessa: Rotational effect on the thermodynamic properties of isotopes, 39
Babloyantz, Agnessa, *see* Bellemans, A.
Bak, Thor A., Goche, M., and Henin, F.: On the motion of a particle coupled to lattice vibrations, 181
Ballhausen, C. J., and Liehr, A. D.: Intensities in inorganic complexes. III. Octahedral complexes of Ni(II) and V(III), 123
Ballinger, R. A.: The electronic structure of hydrogen fluoride, 139
Bellemans, A., and Babloyantz, Agnessa: Statistical mechanics of solid and liquid mixtures of ortho and para-hydrogen, 169
Bennema, P., Hoijtink, G. J., Lupinski, J. H., Oosterhoff, L. J., Selier, P., and van Voorst, J. D. W.: Photo-ionization of aromatic hydrocarbons in boric acid glasses, 431
Berthier, G.: A self-consistent field for the H_2 molecule, 225
Brown, R. D., and Coller, B. A. W.: Molecular-orbital treatment of a new type hetero-aromatic compound, 158

Clough, S.: Nuclear resonance spectrum of ortho bromoaniline, 349
Coller, B. A. W., *see* Brown, R. D.
Coulson, C. A., and Stocker, D.: Steric forces in halogen-substituted benzenes, 397

Dickens, P. G.: Calculation of vibrational relaxation times in gaseous cyanogen, 206
Dickens, P. G., and Linnett, J. W.: Efficiencies of third bodies in the reaction $H+O_2+M=HO_2+M$, 259

Forman, A., and Orgel, L. E.: The Jahn–Teller effect in manganic acetylacetonate, 362
Fred, M., *see* Moffitt, W.
Freeman, R., Gasser, R. P. H., Richards, R. E., and Wheeler, D. H.: Chemical shifts of thallium resonance spectra in solutions of thallous salts, 75
Freeman, R., Gasser, R. P. H., and Richards, R. E.: Thallium nuclear resonance spectra, Part II, 301
Friedman, H. L.: On Mayer's ionic solution theory, 23
Friedman, H. L.: The singularities of the integrals in Mayer's ionic solution theory, 190
Friedman, H. L.: The singularities of the integrals in Mayer's ionic solution theory (Errata), 436
Fujimoto, M., and Ingram, D. J. E.: Electron resonance studies on the kinetics of free radical formation and reaction in the solid phase, 341

Gasser, R. P. H., and Richards, R. E.: Ion-pair formation in thallous solutions, 357
Gasser, R. P. H. *see* Freeman, R.
Ghosh, D. K., and Whiffen, D. H.: The electron spin resonance spectrum of a γ-irradiated single crystal of glycine, 285
Goche, M., *see* Bak, Thor A.
Goodman, C. L., *see* Moffitt, W.
de Groot, M. S., *see* van der Waals, J. H.

Hameka, H. G.: Relationship between proton shielding constants and electric dipole moments in the hydrogen halides, 64
Henin, F., *see* Bak, Thor A.
Hirschfelder, J. O., and Löwdin, P. O.: Long-range interaction of two 1s-hydrogen atoms expressed in terms of natural spin-orbitals, 229

Hoijtink, G. J.: Correlations between the electronic spectra of alternant hydrocarbon molecules and their mono- and di-valent ions. I. Benzene, coronene and triphenylene, 85

Hoijtink, G. J., see Bennema, P.

Hornig, D. F., *see* Andersen, W. H.

Ingram, D. J. E., *see* Fujimoto, M.

van Itterbeek, J., *see* Thomaes, G.

Jørgensen, C. K.: Absorption spectra of actinide compounds, 96

Jørgensen, C. K.: Electron transfer spectra of hexahalide complexes, 309

Judd, B. R.: An analysis of the fluorescence spectrum of europium ethyl sulphate, 407

Liehr, A. D., *see* Ballhausen, C. J.

Linnett, J. W., *see* Dickens, P. G.

Lofthus, Alf: A determination of the electronegativity parameter in molecular orbital calculations on heteronuclear molecules containing nitrogen, 367

Löwdin, P. O., *see* Hirschfelder, J. O.

Lupinski, J. H., *see* Bennema, P.

Mason, E. A. *see* Saxena, S. C.

McCarty, Maclyn (Jr.), and Robinson, G. Wilse: Environmental perturbations on foreign atoms and molecules in solid argon, krypton and xenon, 415

McConnell, H. M., and Strathdee, J.: Theory of anisotropic hyperfine interactions in π-electron radicals, 129

McLachlan, A. D.: The pairing of electronic states in alternant hydrocarbons, 271

McLachlan, A. D.: The signs of the valence bond wave functions in an alternant hydrocarbon, 223

Moffitt, W., Goodman, G. L., Fred, M., and Weinstock, B.: The colours of transition metal hexafluorides, 109

Münster, A.: Zur Theorie der generalisierten Gesamtheiten, 1

Oosterhoff, L. J., *see* Bennema, P.

Orgel, L. E., *see* Forman, A.

Parsonage, N. G., and Staveley, L. A. K.: Thermodynamic properties of clathrates. I. The heat capacity and entropy of argon in argon quinol clathrates, 212

Richards, R. E., *see* Freeman, R.

Richards, R. E., *see* Gasser, R. P. H.

Robinson, G. Wilse, *see* McCarty, Maclyn (Jr.)

Sack, R. A.: Pressure-dependent partition functions, 8

Saxena, S. C., and Mason, E. A.: Diffusion coefficients of gases from the rate of approach to the steady state in thermal diffusion, 264

Saxena, S. C., and Mason, E. A.: Thermal diffusion and the approach to the steady state in gases: II, 379

Selier, P., see Bennema, P.

Staveley, L. A. K., *see* Parsonage, N. G.

Stocker, D., *see* Coulson, C. A.

Strathdee, J., *see* McConnell, H. M.

Thomaes, G., and van Itterbeek, J.: Application of the principle of corresponding states to the viscosity and diffusion of pure liquids and mixtures, 372

van Voorst, J. D. W., *see* Bennema, P.

van der Waals, J. H., and de Groot, M. S.: Paramagnetic resonance in phosphorescent aromatic hydrocarbons. I. Naphthalene, 333

Wassermann, A.: Proton acceptor properties of lycopene, 226

Weinstock, B., *see* Moffitt, W.

Wheeler, D. H., *see* Freeman, R.

Whiffen, D. H., *see* Ghosh, D. K.